TRANSACTIONS
OF THE ASME
Series C

Journal of HEAT TRANSFER

August 1961

RADIATION • CONDUCTION • CONVECTION • COMPLEX SYSTEMS • PHASE CHANGES AND MIXTURES • TRANSIENT PHENOMENA • THERMOPHYSICAL PROPERTIES • EXPERIMENTAL TECHNIQUES • THERMOMETRY • ANALOG METHODS • ANALYTICAL AND NUMERICAL METHODS • APPLICATIONS • DESIGN TECHNIQUES • HEAT EXCHANGERS • INSULATION • ECONOMIC FACTORS BIOTECHNOLOGY • ASTRONAUTICS

Published Quarterly by
THE AMERICAN SOCIETY OF MECHANICAL ENGINEERS

TRANSACTIONS OF THE ASME
Series C

EDITORIAL DEPARTMENT

Editor, J. J. JAKLITSCH, JR.
Consulting Editor, LEO BLODGETT
Production, JEAN NORTH
Production Asst., CARMEN L. CABRANES
Art Editor, HENRY BALFOUR

HEAT TRANSFER DIVISION

Chairman, M. RONSENOW
Secretary, S. OSTRACH
Papers Review, T. F. IRVINE, JR.
Consulting Editor, S. P. KEZIOS

OFFICERS OF THE ASME

President, W. H. BYRNE
Secretary, O. B. SCHIER, II
Treasurer, E. J. KATES
Assistant Treasurer, H. J. BAUER

PUBLICATIONS COMMITTEE

Chairman, HENDLEY N. BLACKMON
R. D. MINDLIN
MARTIN GOLAND
VITO L. SALERNO
F. J. HEINZE

Junior Representatives
J. W. FOLLANSBEE
STEWART H. ROSS

REGIONAL ADVISORY BOARD

Region I, H. M. ROGERS, JR.
Region II, ROBERT E. ABBOTT
Region III, A. F. BOCHENEK
Region IV, FRANCIS C. SMITH
Region V, WM. J. TITZEL
Region VI, C. R. EARLE
Region VII, RALPH L. SCORAH
Region VIII, G. CORRY MCDONALD
Region IX, M. S. UMBENHAUER
Region X, CARL J. ECKHARDT

Published quarterly by The American Society of Mechanical Engineers. Publication office at 20th and Northampton Streets, Easton, Pa. The editorial department is located at the headquarters of the Society, 29 West Thirty-Ninth Street, New York 18, N. Y. Cable address, "Mechaneer," New York. Price $3.00 a copy, $10.00 annually to members, $1.50 a copy, $5.00 annually. Add 50 cents for postage to all countries outside the United States and Canada. Changes of address must be received at Society headquarters seven weeks before they are to be effective on the mailing list. Please send old as well as new address. . . . By-Law: The Society shall not be responsible for statements or opinions advanced in papers or . . . printed in its publications (B13, Par. 4). . . . Second-class mail privileges authorized at Easton, Penna. . . . This publication is authorized to be mailed at the special rates of postage prescribed by Section 132.122 . . . © Copyrighted, 1961, by The American Society of Mechanical Engineers. Reprints from this publication may be made on condition that full credit be given the Transactions of the ASME, Series C—Journal of Heat Transfer, and the author, and that date of publication be stated.

TRANSACTIONS OF THE ASME
is indexed by the Engineering Index, Inc.

Journal of HEAT TRANSFER

VOL. 83 • SERIES C • NO. 3

August 1961

CONTENTS

233 **Pool Boiling in an Accelerating System** (60—HT-22)
Herman Merte, Jr., and J. A. Clark

243 **An Experimental Study of Boiling in Reduced and Zero Gravity Fields** (60—HT-10)
C. M. Usiskin and R. Siegel

254 **Measured Variations in Local Surface Temperatures in Pool Boiling of Water** (60—HT-32)
S. T. Hsu and F. W. Schmidt

261 **Natural-Circulation Tests With Water at 800 to 2000 Psia Under Nonboiling, Local Boiling, and Bulk Boiling Conditions** (60—HT-36)
O. J. Mendler, A. S. Rathbun, N. E. Van Huff, and A. Weiss

274 **Heat Transfer to Laminar Flow Across a Flat Plate With a Nonsteady Surface Temperature** (60—HT-7)
R. D. Cess

281 **Film Cooling With Multiple Slots and Louvers** (60—HT-35)
J. H. Chin, S. C. Skirvin, L. E. Hayes, and F. Burggraf

293 **Velocity Distributions, Temperature Distributions, Effectiveness and Heat Transfer for Air Injected Through a Tangential Slot Into a Turbulent Boundary Layer** (60—HT-31)
J. P. Hartnett, R. C. Birkebak, and E. R. G. Eckert

307 **Two-Phase Slug Flow** (60—HT-28)
Peter Griffith and G. B. Wallis

321 **Dynamic Response of Heat Exchangers Having Internal Heat Sources—Part IV** (60—WA-127)
W. J. Yang, J. A. Clark, and V. S. Arpaci

339 **A Comprehensive Approach to the Analysis of Cooling Tower Performance** (60—WA-85)
Donald R. Baker and Howard A. Shryock

351 **Film-Boiling Heat Transfer From a Horizontal Surface** (60—WA-147)
P. J. Berenson

359 **An Integral Treatment of Two-Phase Boundary Layer in Film Condensation** (60—WA-253)
J. C. Y. Koh

363 **Oscillations in Two-Phase Flow Systems** (60—WA-209)
G. B. Wallis and J. H. Heasley

370 **Film Boiling in a Forced-Convection Boundary-Layer Flow** (60—WA-148)
R. D. Cess and E. M. Sparrow

TECHNICAL BRIEFS

377 **Subcooled Forced-Convection Film Boiling on a Flat Plate**
R. D. Cess and E. M. Sparrow

379 **Flow Visualization and Velocity Measurement in Natural Convection With the Tellurium Dye Method**
R. Eichhorn

382 **Truncation Error Estimates for Numerical and Analog Solutions of the Heat-Conduction Equation**
N. H. Freed and C. J. Rallis

384 **Frictional Pressure Drop in Noncircular Ducts**
R. I. Hodge

385 **A Musical Heat Exchanger**
Robert Lemlich

386 **Transition on a Heated Horizontal Rotating Cylinder**
P. D. Richardson

387 **Free Convection With Blowing or Suction**
E. M. Sparrow and R. D. Cess

389 **On Jenkins Model of Eddy Diffusivities for Momentum and Heat**
C. L. Tien

HERMAN MERTE, JR.
Assistant Professor,
Department of Mechanical Engineering,
Heat Transfer and Thermodynamics
Laboratory, University of Michigan,
Ann Arbor, Mich.

J. A. CLARK
Professor,
Department of Mechanical Engineering,
Professor-in-Charge, Heat Transfer and
Thermodynamics Laboratory, University
of Michigan, Ann Arbor, Mich.
Assoc. Mem. ASME

Pool Boiling in an Accelerating System[1]

A study is reported of the influence of system acceleration (1 to 21 g) on pool boiling heat transfer using distilled water at approximately atmospheric pressure. The acceleration of the system is such that the resulting force field is normal to the heating surface, thereby increasing the buoyant forces acting on the vapor bubbles. Heat-flux rate is varied from approximately 5000 Btu/hr-sq ft (nonboiling) to 100,000 Btu/hr-sq ft. Data are presented for the influence of subcooling with the boiling system under acceleration at the lower values of heat flux. A preliminary analysis is presented for a theoretical description of the process of boiling under the influence of high acceleration, including the simultaneous effect of natural convection.

Introduction

THIS PAPER presents the results of an initial study of the influence of a force field on pool-boiling heat transfer. A force field was utilized which produced accelerations normal to a heated surface in the range 1 to 21 times standard gravity. Although system acceleration different from that due to gravity is not commonly encountered in boiling processes, its role is important as it is the source of the natural convective movement in fluids. With the various new problems encountered in space technology it may be expected that boiling heat transfer will occur in force fields different from that found on earth.

The high rate of heat transfer by boiling has been ascribed to the intense agitation of the liquid at the heating surface by the bubbles [1, 36].[2] Various researchers [2–9] have described the boiling process by means of correlating equations. In some cases the action of the bubbles was considered by the use of dimensional analysis, and in others by the selection and treatment of suitable models. Owing to the inability to describe the bubble action adequately, it was necessary to conduct experiments to determine certain constants which themselves frequently include other factors. Analytical results showing agreement with certain experimental data usually are given but as yet no widely applicable theory exists.

The bubble-growth rate has been described well in terms of liquid superheat by the equations of Plesset and Zwick [10], Forster and Zuber [11], and Griffith [12]. Fritz [13] obtained an expression for the maximum volume of a vapor bubble at departure from a surface based on the work of Bashforth and Adams [14] and Wark [15]. It considers the equilibrium of the surface of curvature separating two phases in the force field, hence is valid only for conditions of equilibrium such as might be present in boiling at low heat-flux rates to a saturated liquid. Although several correlations for boiling [4, 5] utilized this expression, equation (1), it has been verified experimentally only for low heat-flux rates in a force field of one standard gravity [1, 16]:

$$V_{b\max} = (0.0119\phi)^3 \left[\frac{2\sigma g_c}{g(\rho_l - \rho_v)}\right]^{3/2} \tag{1}$$

A relation between the frequency of bubble formation and the bubble diameter at departure from a horizontal heating surface, of the form

$$fD_b = \text{constant} \tag{2}$$

was observed [1, 16, 17] with the boiling of a saturated liquid at low values of heat flux. For methanol, Perkins and Westwater [18] determined that f, D_b, and hence fD_b remained constant up to approximately 80 per cent of the peak heat flux, after which the values increased. However, a horizontal round tube was used for the heating surface and no information was given as to where the measurements were made. Recent experimental work [19]

[1] A publication of the Heat Transfer and Thermodynamics Laboratory, Department of Mechanical Engineering, University of Michigan, Ann Arbor, Mich.

[2] Numbers in brackets designate References at end of paper.

Contributed by the Heat Transfer Division of THE AMERICAN SOCIETY OF MECHANICAL ENGINEERS and presented at the ASME-AIChE Heat Transfer Conference, Buffalo, N. Y., August 15–17, 1960. Manuscript received at ASME Headquarters, May 19, 1960. Paper No. 60—HT-22.

Nomenclature

A = area
a = acceleration
a/g = dimensionless acceleration
f = frequency of bubble formation
g = local gravitational acceleration
g_c = mass-force conversion constant = 32.174 lb_M-ft/lb_f-sec^2
N/A = number of active nucleating sites per unit area
n = unknown constant
q = heat-transfer rate
q/A = heat-flux rate
T = temperature
$T_{t,s}$ = temperatures at thermocouple TC-5 and TC-6, Fig. 1
$T_w - T_{sat}$ = difference between heating-surface temperature and fluid saturation temperature at heating surface
V = volume
Nu = Nusselt number
Gr = Grashof number
Pr = Prandtl number
$\gamma = A_B/A_w$ Equation (7)
σ = surface tension
$\Delta\theta = T_w - T_{sat}$
ϕ = contact angle
ρ = density

Subscripts

b = bubble
B = boiling
c = nonboiling convection
l = liquid
P = peak or maximum
sat = saturation
t = total
v = vapor
w = wall

indicates the bubble diameter at departure decreases with an increase in heat flux.

A relation for the thickness of the superheated liquid boundary layer next to a heated surface was derived by Chang [20] which predicts the thickness increases with heat flux. By using the variation in index of refraction of light in water with temperature the thickness of a "boundary layer" near a horizontal heated surface with pool boiling to a saturated water was measured [21] at low values of heat flux, and was found to decrease with an increase in heat flux. On the other hand, with forced-convection boiling to saturated water, Treshchov [22] measured fluid temperatures within 0.0025 in. of the heating surface and found that at a distance of 0.006 in. the temperature of the water was uninfluenced by large increases in heat flux, up to 1.3×10^6 Btu/hr-sq ft, which suggests the presence of boundary layer in boiling systems.

Jakob [23] observed a linear relationship between heat flux and the number of nucleating sites at low values of heat flux. Recent investigations [19, 21], however, indicate a relationship of the form

$$q/A \propto (N/A)^{1/2} \tag{3}$$

The role of surface defects or crevices as providing preferential sites for the formation of vapor bubbles has been studied experimentally and theoretically [24, 25].

Acceleration of a boiling system directly influences the buoyant force on the vapor bubble. The bubble growth rate also will be influenced if the thickness and temperature distribution within the superheated boundary layer at the heating surface are affected by the acceleration. In general, bubble growth-rate equations have neglected buoyant forces, but it may be anticipated that at certain acceleration this factor will have to be considered. The bubble size at departure probably will decrease with an increased buoyant force. While the mechanism which causes the departure is as yet little understood a plausible cause [12, 26] attributes the motion to the inertia of the surrounding liquid. A recent photographic study of boiling in the absence of gravity [27], however, seems to discount the importance of liquid inertia. The vapor remained adjacent to the heating surface and there was no evidence of bubbles being pushed away from the surface to any appreciable extent during their formation.

The effect of a vortex flow on the peak heat flux was studied by Gambill and Green [28]. Peak heat flux up to 55×10^6 Btu/hr-sq ft was obtained. The high values were attributed to the increased buoyancy on the bubbles due to centrifugal action, although it was not possible in this case to separate the forced-convection contribution to the heat flux associated with the high velocities.

This paper summarizes the results of a research program recently completed in which the influence of system acceleration up to $21g$ on pool-boiling heat transfer was investigated [29]. Continuation of this work is in progress to include a study of accelerations up to $100g$ and higher, maximum heat flux, surface orientation, and the use of cryogenic fluids.

Experimental Apparatus

Centrifugal motion is used to provide a force field producing accelerations of 1 to 21 g's. To isolate the influence of the increase in buoyant force on the bubbles most effectively with nucleate boiling, the orientation of the heater was such that the acceleration is applied normal to the heated surface. The test vessel was pivoted to maintain an approximately uniform depth of liquid and a normal acceleration at all rotational speeds.

Fig. 1 is a sketch of the pivoted test vessel and Fig. 2 shows the over-all assembly.

The heater consists of a cylindrical leaded-copper block 3 in. in diameter and 1 in. long. One end of the cylinder is chromium-plated and serves as the heat-transfer surface. The edge is undercut with a bevel and an undersize stainless-steel mating piece 0.022 in. thick, attached by a shrink fit to provide a continuous surface and to keep heat losses by conduction at a minimum. At the other end of the cylinder 32 parallel slots 0.008 in. wide by $^{6}/_{16}$ in. deep are machined to accommodate 6 ft of chromel-A heater ribbon $^{1}/_{4}$ in. wide by 0.002 in. thick, insulated from the block with mica strips. A guard heater minimizes heat loss from the underside.

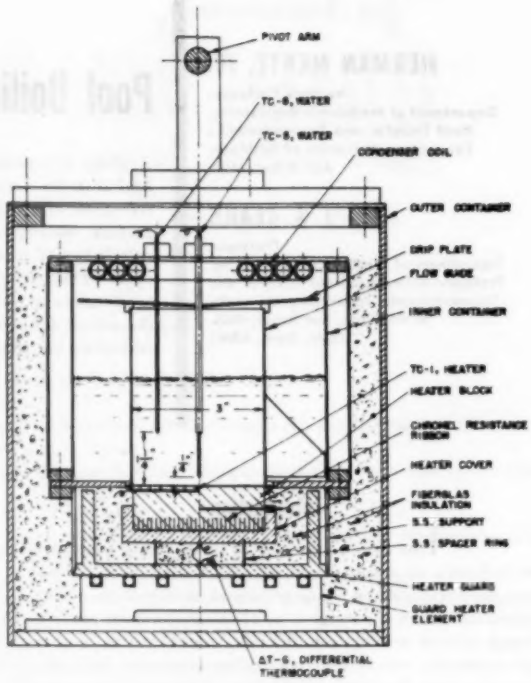

Fig. 1 Test vessel

Power to the main heater is measured with calibrated meters. The largest source of error in the determination of heat flux arises from the heat loss from the stainless-steel heater skirt. This is estimated to vary from 5 per cent at $q/A = 10{,}000$ Btu/hr-sq ft to 1 per cent at $q/A = 100{,}000$ Btu/hr-sq ft.

To eliminate the possible influence of the gross convection currents on the bubbles forming near the edge of the heated section, a flow guide was installed consisting of a cylinder of thin sheet stainless steel open at both ends and slightly larger in diameter than the heater. The effect is that of having a system whose entire bottom surface is heated and essentially isothermal.

Four $^{1}/_{32}$-in-diameter holes are drilled radially in the heater block at four locations for the insertion of thermocouples. Two of the holes are drilled to the center at distances of $^{1}/_{16}$ and $^{7}/_{16}$ in. from the heating surface for purposes of extrapolating measured temperatures to obtain that of the heater surface.

The thermocouples in the heater consist of an insulated 30-gage constantan wire passing through a $^{1}/_{32}$-in-OD copper tube with a capacitor discharge welded junction at the tip. A 30-gage copper wire is welded to the other end of the tube to complete the circuit. This Cu-Cu junction produces negligible thermal emf. Two 30 gage-copper-constantan thermocouples, designated TC-5 and TC-6 in Fig. 1, were encased in $^{1}/_{16}$-in-OD stainless-steel tubing for water-temperature measurements. All thermocouples were

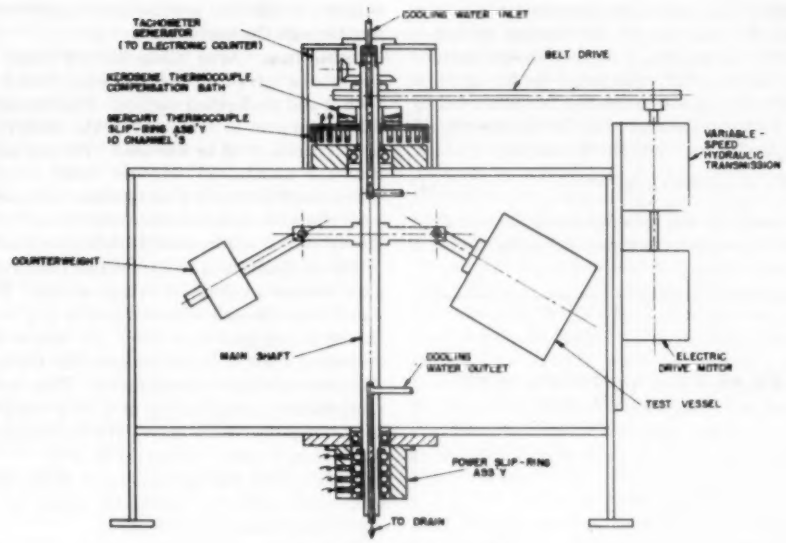

Fig. 2 Centrifuge assembly

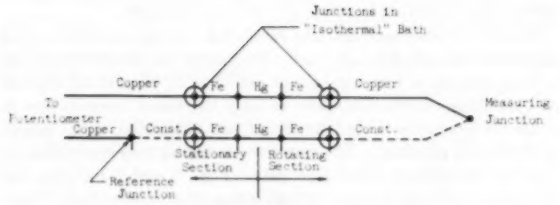

Fig. 3 Equivalent thermocouple circuit

calibrated at the steam point and by comparison with Bureau of Standards calibrated mercury-in-glass thermometers. A Leeds & Northrup type K-3 potentiometer with a mirror-type galvanometer was used throughout.

The measurement of the thermocouple emf from the rotating member was accomplished through the use of liquid-mercury commutators. Ten concentric mercury channels were machined in a plexiglas base which rested on a heavy aluminum block to insure isothermal conditions. To avoid amalgamation with the mercury a pure iron wire served as an intermediate metal between the rotating and stationary copper and constantan wires. Fig. 3 shows the equivalent thermocouple circuit. Extensive tests were conducted to determine the extent of errors in thermal emf introduced by this circuit. Thermocouples were checked at the steam point using a hypsometer under nonrotating conditions, and the emf were identical with those obtained with a direct connection. The emf for the nonrotating and rotating conditions were measured for each of the mercury-channel pairs forming a circuit for no power input to the heater. Changes in emf were observed in each pair which depended upon the rotational speed. Reversing the direction of rotation reversed the polarity of the change. Hence it is believed this emf results from the influence of the earth's magnetic field on the rotating circuit, producing in effect the action of a unipole generator. This effect was reproducible within $\pm 2\ \mu_v$ and the correction at the maximum speed was $10\ \mu_v$ for TC-6 in Fig. 1, $4\ \mu_v$ for TC-5, and zero μ_v for the thermocouples in the heater block. Considering other sources of error, it is estimated that the uncertainty in the level of temperature of any thermocouple on the rotating assembly is ± 0.2 deg F, but that changes in the temperature of the thermocouple are known with an uncertainty of ± 0.1 deg F.

The acceleration at the heating surface is calculated using the measured location of the center of gravity of the test vessel and the blueprint dimensions. The increase in hydrostatic pressure at the heating surface resulting from rotation was computed from the depth of the water and system acceleration. The uncertainty in T_{sat} at the heating surface, employed in the boiling parameter $T_w - T_{sat}$, is estimated to be ± 0.1 deg F. This estimated uncertainty results from the fact that the depth of the boiling fluid was not measured while under rotation. Visual observation of the boiling process at the maximum heat flux of 100,000 Btu/hr-sq ft without rotation indicated that the change in liquid depth due to the bubbles was almost negligible. As will be noted in Fig. 8 the liquid subcooling increases as the system is subjected to acceleration. Hence, under these circumstances, the vapor volume can be expected to be less than under standard gravitational acceleration (no rotation) and the change in depth correspondingly smaller. The test vessel was vented to the atmosphere. The depth of the water was $2^1/_2$ in. in all tests, and its initial resistivity was at least $1.5 \times 10^6\ \Omega$ cm, as measured with a conductivity cell. For the data reported here, the resistivity at the conclusion of a test varied from 0.8×10^6 to $1.1 \times 10^6\ \Omega$ cm.

A cooling coil mounted on the underside of the test-vessel cover serves to condense the vapor formed. At the lower heat-flux rates it is possible to control the temperature of the test water by varying the cooling-water flow rate and thus obtain limited data for boiling of a subcooled liquid.

The rotational speed was obtained from a tachometer-generator generating 60 pulses per revolution. Its output was fed into a Model 522B Hewlett-Packard electronic counter.

Detailed description of the experimental apparatus is given in reference [29].

Results

Nonboiling Data. Several tests were conducted under nonboiling conditions. Fig. 4 indicates how the temperature difference $T_w - T_b$ varies as a function of acceleration. For a given heat flux the presence of the flow guide decreases the temperature difference.

The data are plotted in Fig. 5 using the conventional free-convection moduli where the diameter of the heating surface is taken as the characteristic length and g in the Grashof number is replaced with acceleration. The influence of the flow guide is noted. Included for reference is the correlation recommended by McAdams [30] for a horizontal heated plate facing upward. A correlation which best fits the data with the flow guide is

$$\mathrm{Nu} = 0.0505(\mathrm{GrPr})^{0.338} \tag{4}$$

For one particular test (C-5) the data fell above the best fit of the data. In this case the water was highly subcooled and it is believed this lack of correlation occurs because of increased heat loss through the heater skirt.

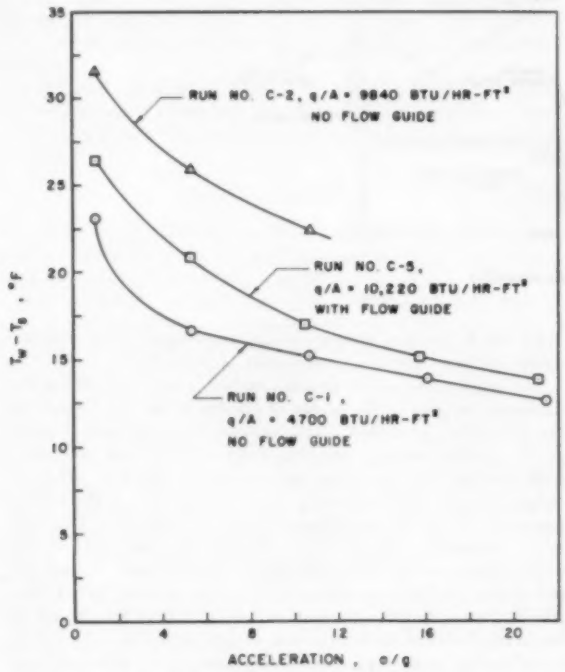

Fig. 4 Plot of ΔT_c versus acceleration for natural convection indicating effect of flow guide

Boiling Data. After filling the test vessel with distilled water, power was turned on and the water boiled vigorously to degas both it and the heating surface. Prior to each run, this was done for a minimum of 4 hr, and in the majority of cases degassing over a period of 16 hr was used. For any particular test the heat flux was maintained constant while acceleration was varied. When conditions such as acceleration and cooling-water flow rates were changed, sufficient time was allowed for the attainment of steady-state conditions before data were taken.

The acceleration rates were varied from 1 to 21.15 times normal gravitational acceleration in 5 to 8 steps. In earlier tests it was noted that the wall temperatures at $a/g = 1$ shifted gradually during a long period of time. To isolate the effect of the acceleration a set of measurements was taken at $a/g = 1$ before and after each higher acceleration. Thus any shift in the surface temperature during boiling at $a = g$ could be compensated by considering the change only. The maximum shift which occurred was 0.8 deg F over a test period of 12 hr.

To determine the reproducibility of the data, several accelerations were duplicated during the course of a specific test. No significant change was detected.

The heater surface was highly polished prior to its chromium plating. No roughness measurements were made, but the heater surface was given a similar treatment prior to each run; it is believed that the roughness was the same for all tests.

Except for one case the data presented are representative of at least two reproducible test runs. Because of the sensitivity of the boiling process at lower values of heat flux to even small degrees of subcooling, it was necessary to vary the water temperature in order to determine when the liquid was saturated, or as nearly saturated as possible. The water temperature was controlled by varying the cooling water flow rate. Figs. 6 and 7 indicate the influence of a limited degree of subcooling at several values of heat flux and acceleration. The asterisk on the data points indicates where the coolant flow was so low that a net quantity of vapor escaped from the atmospheric vent, with an attendant possible increase in pressure.

In Fig. 6 for $q/A = 10{,}870$ Btu/hr-sq ft and $a/g = 5.29$, the heater surface temperature exhibits a pronounced maximum as the subcooling is decreased and becomes constant as the saturation temperature is reached. At $a/g = 10.47$, no maximum in $T_w -$

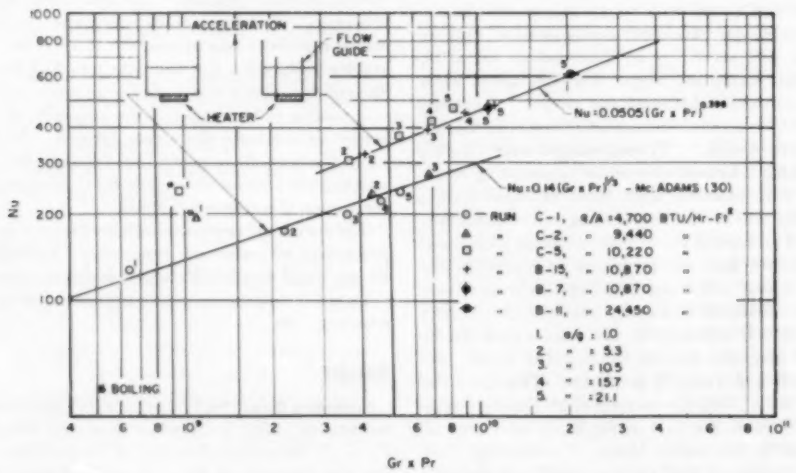
ACCELERATION
FLOW GUIDE
HEATER
Nu = 0.0505 (Gr x Pr)^0.338
Nu = 0.14 (Gr x Pr)^1/3 - Mc ADAMS (30)
RUN C-1, q/A = 4,700 BTU/Hr-Ft²
" C-2, " 9,440 "
" C-5, " 10,220 "
" B-15, " 10,870 "
" B-7, " 10,870 "
" B-11, " 24,450 "
1 a/g = 1.0
2 " = 5.3
3 " = 10.5
4 " = 15.7
5 " = 21.1
BOILING
Nu
Gr x Pr

Fig. 5 Correlation of natural-convection data with acceleration normal to heating surface

T_{sat} is observed, but a long plateau is noted. In Fig. 7 for q/A = 24,450 Btu/hr-sq ft, subcooling was not increased sufficiently to prevent boiling and a maximum could not be observed. The decrease of the heater surface temperature with decreasing subcooling is still present as is the leveling off of $T_w - T_{sat}$ except for the highest acceleration. For values of heat flux up to 50,000 Btu/hr-sq ft it was thus possible to determine when $T_w - T_{sat}$ became independent of the degree of subcooling. This was used as a criterion for defining the existence of "saturated" pool boiling.

Sufficient data are not available at this time to make generalized conclusions as to the role of subcooling or liquid depth with the system under acceleration. It is believed possible that the decrease[3] in T_w with decreasing subcooling is an indication of increased fluid agitation or turbulence within the superheated region near the heated surface. With a reduction in heater surface temperature it seems unlikely that additional nucleating sites are being formed. If so, then the existing ones must be more effective in providing increased agitation either from more rapid bubble-growth rates, increased bubble sizes, increased frequency of formation, or a combination of these.

At nominal heat-flux values of 75,000 and 100,000 Btu/hr-sq ft it was not possible to vary the water temperature with the present system. The water temperature near the heated surface remained subcooled with the system under acceleration. The subcooling occurs because of the large saturation-temperature changes in the water resulting from the large acceleration. Similar phenomena of lesser magnitude have been observed with water [1] and mercury [31] in a gravity field. Fig. 8 shows the profile of the water and saturation temperatures between the heated surface and the vapor interface. The water depth at filling in all cases was 2½ in., and the variation in T_{sat} results solely from the change in hydrostatic pressure with depth. The change in depth under boiling at the various accelerations was not considered great as was discussed earlier. The system accelerations specified are at the heating surface. While this is located approximately 15.4 in. from the center line of rotation, the hydrostatic pressure within the liquid above this surface was computed taking into consideration the small local variation in acceleration.

The relation between the measured water and saturation temperature in Fig. 8 is typical for heat flux between 50,000 and 100,000 Btu/hr-sq ft. A minimum subcooling was obtained at heat flux above 50,000 Btu/hr-sq ft which was a function of acceleration and liquid depth. It is probable that this minimum subcooling (or maximum water temperature) results from the liquid temperature at the vapor interface reaching a maximum; i.e., its saturation value. Data reported at heat flux at 75,000 and 100,000 Btu/hr-sq ft are thus considered to correspond to the same conditions as those at the lower heat flux where subcooling did not influence $T_w - T_{sat}$.

Fig. 9 is a composite plot of $T_w - T_{sat}$ versus acceleration for the various values of heat flux with pool boiling of essentially saturated water. Some deviation of the data with a gravity field did exist, and several of the curves were displaced to bring $T_w - T_{sat}$ at $a/g = 1$ in agreement with the best fit of data from a number of tests conducted at $a/g = 1$, shown in Fig. 10.

The difference between the heater surface temperature T_w and the water saturation temperature T_{sat} at the heating surface decreases with an increase in acceleration at lower values of heat

[3] Occasioned by the decrease in $T_w - T_{sat}$, as T_{sat} at the wall is constant for a given acceleration.

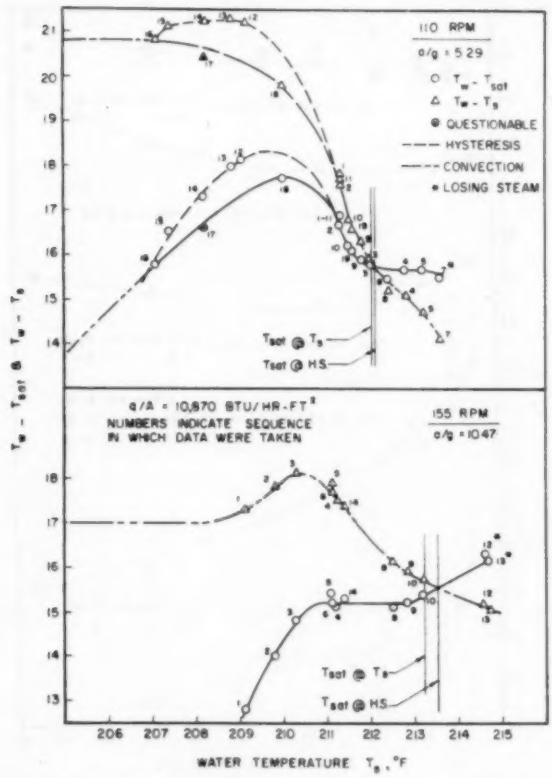

Fig. 6 Run No. B-15. Plot of $T_w - T_{sat}$ and $T_w - T_b$ versus water temperature T_b at 110 and 155 rpm.

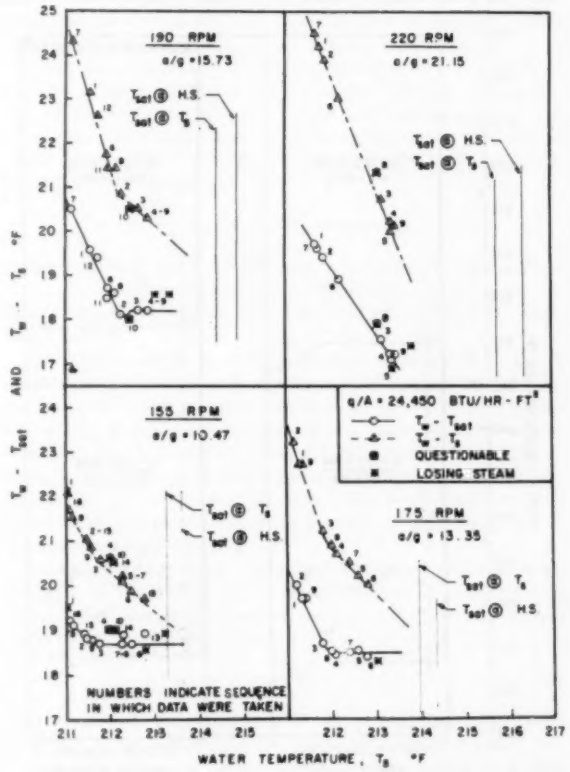

Fig. 7 Run No. B-9. $T_w - T_{sat}$ and $T_w - T_b$ versus water temperature T_b at various accelerations.

flux. This is attributed to the increasing contribution of natural convection (nonboiling) with acceleration. As the heat-flux level increases, the decrease in $T_w - T_{sat}$ becomes smaller, and at the higher values of heat flux $T_w - T_{sat}$ increases with an increase in acceleration. The contribution of natural convection is relatively smaller at the higher heat flux. It is believed that increased system acceleration results in smaller bubble sizes at departure, with an attendant decrease in agitation. To provide for a fixed total heat flux, more nucleating sites then are required, which in turn requires the increased wall temperatures, as observed.

Discussion of Results. Because the quantity of data obtained is not large and is for one Prandtl number over a relatively small range of conditions, it is believed that to attempt a direct correlation of the data either with existing relationships or with ones which might be worked out would be premature, although a start is made in the following text. Further, none of the correlations in the literature which has been examined [e.g., 4, 5, 6, 7, 9, 20] appears capable of predicting the trends shown in Fig. 9 resulting from acceleration of the boiling system. This may be due in part to the inadequacy of the models used to describe heat transfer by boiling or to neglect of the nonboiling contribution.

Under acceleration, the nonboiling free-convection contribution is significant. This is more readily seen in Fig. 11, which is a replotting of the data from Fig. 9. It places the data in the more familiar form of q/A versus $T_w - T_{sat}$. In the lower portion of the curves corresponding to natural convection for the same accelerations are shown using the correlation given in equation (4). The data do not permit determination of the intersection between the nonboiling and boiling curves except for the higher values of heat flux. It is of interest to note, however, that if the boiling curves of constant acceleration are extrapolated, the intersection with the nonboiling curves occurs for $T_w - T_{sat}$ between 14 and 15 F, indicating the possibility that the point of incipient boiling of a saturated liquid is not greatly influenced by a change in the force field. The data also suggest that one result of system acceleration is to widen or delay the transition from nonboiling to fully established boiling, the retention of nonboiling influences being more persistent at the higher accelerations.

The influence of acceleration is greatest in the heat-flux range up to 50,000 Btu/hr-sq ft, where it appears that a transition in the convective mechanism is taking place. Within this range acceleration decreases the temperature difference $T_w - T_{sat}$ required for a given flux. Above this heat-flux range a reversal of the effect of acceleration is observed on the temperature difference, although the total influence is small. The upper range of the curve is extended to $(q/A) = 200{,}000$ Btu/hr-sq ft to include some recent data of Costello [32] for water on a similar configuration for $a/g = 1$ and $a/g = 20$. The general agreement between the two sets of data is quite satisfactory.

With fully established pool boiling in a standard gravitational field, the contribution of nonboiling convection to the total heat transfer is so small that generally it is not separated from the total heat flux in analysis. With the application of an acceleration, however, the nonboiling convection can become quite appreciable, as was indicated by these results. In order to describe the total heat transfer, it is necessary to determine the relative contribution of the bubbles and that not resulting from the bubbles. This was accomplished in effect by Chang [20] by considering the rate of momentum exchange in the liquid near the heating surface to consist of the sum of the molecular diffusivity and the eddy diffusivity. Another method, which is introduced here, is to consider the nonboiling and boiling contributions separately and to weight them in some manner.

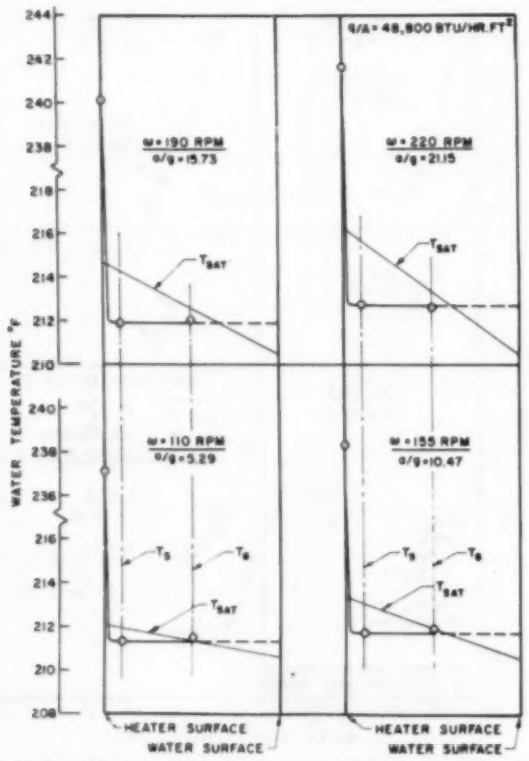

Fig. 8 Run No. B-14. Temperature profile between heater and water surface for various accelerations.

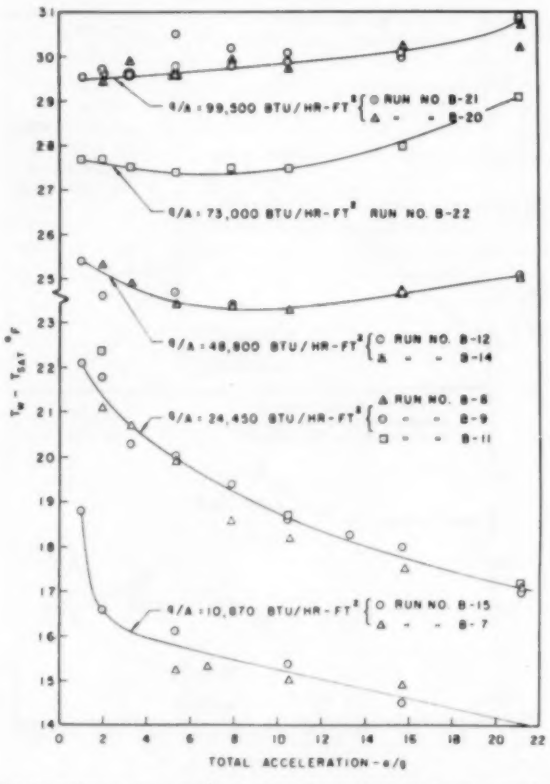
q/A = 99,500 BTU/HR-FT² { ○ RUN NO B-21 △ " " B-20
q/A = 73,000 BTU/HR-FT² RUN NO. B-22
q/A = 48,800 BTU/HR-FT² { ○ RUN NO. B-12 △ " " B-14
q/A = 24,450 BTU/HR-FT² { △ RUN NO. B-6 ○ " " B-9 □ " " B-11
q/A = 10,870 BTU/HR-FT² { ○ RUN NO. B-15 △ " " B-7
T_w - T_SAT °F
TOTAL ACCELERATION - a/g

Fig. 9 Influence of acceleration on $T_w - T_{sat}$ with pool boiling to saturated water

The total heat-transfer rate q_t is

$$q_t = q_c + q_B \tag{5}$$

where q_c is that portion due to nonboiling and q_B is that portion due to boiling and includes the influence of agitation induced by the bubble action. Dividing equation (5) by the total area, A_t, gives

$$\frac{q_t}{A_t} = \frac{q_c}{A_t} + \frac{q_B}{A_t} \tag{6}$$

If A_B represents a time-averaged area projected on the heater surface in which the influence (agitation) of the bubbles is concentrated and A_c ($A_c = A_t - A_B$) is that area in which natural convection is effective, then

$$(q/A)_t = \frac{q_c}{A_c}\frac{A_c}{A_t} + \frac{q_B}{A_B}\frac{A_B}{A_t}$$

$$= (q/A)_c(1 - \gamma) + (q/A)_B\gamma \tag{7}$$

A_B is not the heater surface area covered by the bubbles but is considered differently. It might be designated as an "area of influence" of the bubbles. Fig. 12 is an illustration of this concept.

The fractional effective boiling area γ is found from equation (7) as

$$\gamma = \frac{(q/A)_t - (q/A)_c}{(q/A)_B - (q/A)_c} \tag{8}$$

To evaluate γ as a function of a/g and $(q/A)_t$ it is necessary to make certain assumptions regarding $(q/A)_c$ and $(q/A)_B$. For $(q/A)_c$ it is assumed that the correlation given in equation (4) would be appropriate for its calculation using the experimentally observed value of $T_w - T_b$. Equation (4) is used as it is felt that the convective pattern between bubbles would more closely be represented by this correlation.

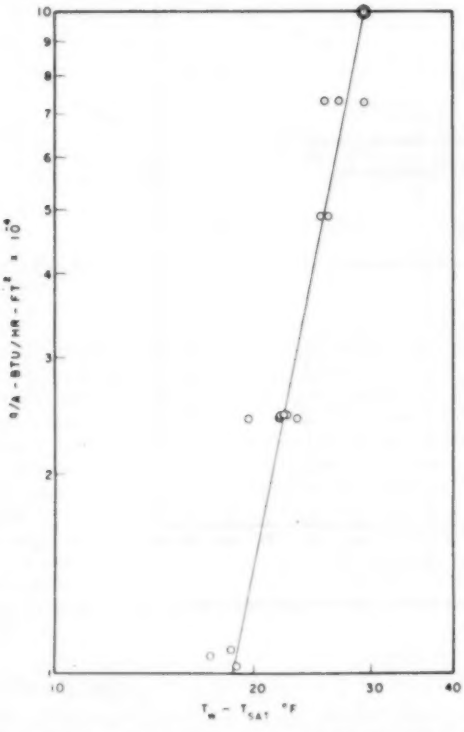

Fig. 10 Plot of q/A versus $T_w - T_{sat}$ for boiling in standard gravitational field

The quantity $(q/A)_B$ is that heat flux which may be associated directly with the micro convection of the bubbles. For fixed acceleration it is assumed that this quantity is a constant. The total heat flux $(q/A)_t$ will vary with $T_w - T_{sat}$, of course, but this results because the number of active sites, hence also γ, varies with $T_w - T_{sat}$. It will be assumed further that not only will $(q/A)_B$ be constant for a given acceleration but that it will be equal to the peak or burnout heat flux at that acceleration. This requires some explanation which follows.

Nishikawa and Urakawa [34] in a study of nucleate boiling in saturated liquids made the following independent observations from their experimental data

$$h \propto \left(\frac{N}{A} D_b^2 f\right)^{1/3} \tag{9}$$

$$\Delta\theta \propto \left(\frac{N}{A}\right)^{-1/4}\left(\frac{q}{A}\right)_t^{2/3} \tag{10}$$

$$\left(\frac{q}{A}\right)_t \propto \left(\frac{N}{A}\right)^{1/2} \tag{11}$$

From these relations it may then be deduced that the quantity $D_b^2 f$, which is proportional to the rate of volume flow of vapor away from the heated surface, is a constant, and is independent of $(q/A)_t$, N/A, and $\Delta\theta$. If true this is a significant result as it has been observed that $D_b f$ is constant [1], equation (2). As mentioned earlier, recent data on methanol [18] indicated that f, D_b, and thus both fD_b and $D_b^2 f$ remained constant up to approximately 80 per cent of the peak heat flux, but other observations [19] suggest that D_b decreases with increase in heat flux.

If the hydromechanics or micro convection of the bubbles is thought to be proportional in its influence ("agitation") to the volume flow of liquid into the surface associated with the rate of volume flow of vapor away from the surface or any exponential power of this flow and that this directly affects the heat flux $(q/A)_B$, then it follows that

$$(q/A)_B \sim (D_b^2 f)^n = \text{constant} \tag{12}$$

Because of this result it was assumed in the foregoing that $(q/A)_B$ is a constant for a given acceleration. This point remains unresolved but the assumption is necessary to this discussion.

The next problem is to find an expression for $(q/A)_B$. It seems reasonable that it should be related in some way to the maximum heat flux. In view of recent studies by DeBortoli and Green [33] it would appear that $(q/A)_B$ might be more closely related to that heat flux at which a significant departure is made from the processes of nucleate boiling, indicating a change in the mechanism of the bubbles. However, this condition is not well understood at present and for the purposes of this paper $(q/A)_B$ will be taken equal to $(q/A)_p$.

Relationships for $(q/A)_p$ have been developed which show an influence of acceleration [3, 4, 35] although none has been confirmed by experiment. However, for application here the following expression of Zuber [35] will be used

$$(q/A)_p = K_2\lambda\rho_v^{1/3}[\sigma g(\rho_l - \rho_v)]^{1/4} \tag{13}$$

The constant K_2 was determined for these calculations from values of $(q/A)_p$ in saturated water at 1 g and found to be 0.146.

Using the foregoing data the corresponding values of γ were computed from equation (8) and are shown in Fig. 13 as a function of dimensionless acceleration a/g and total heat flux.

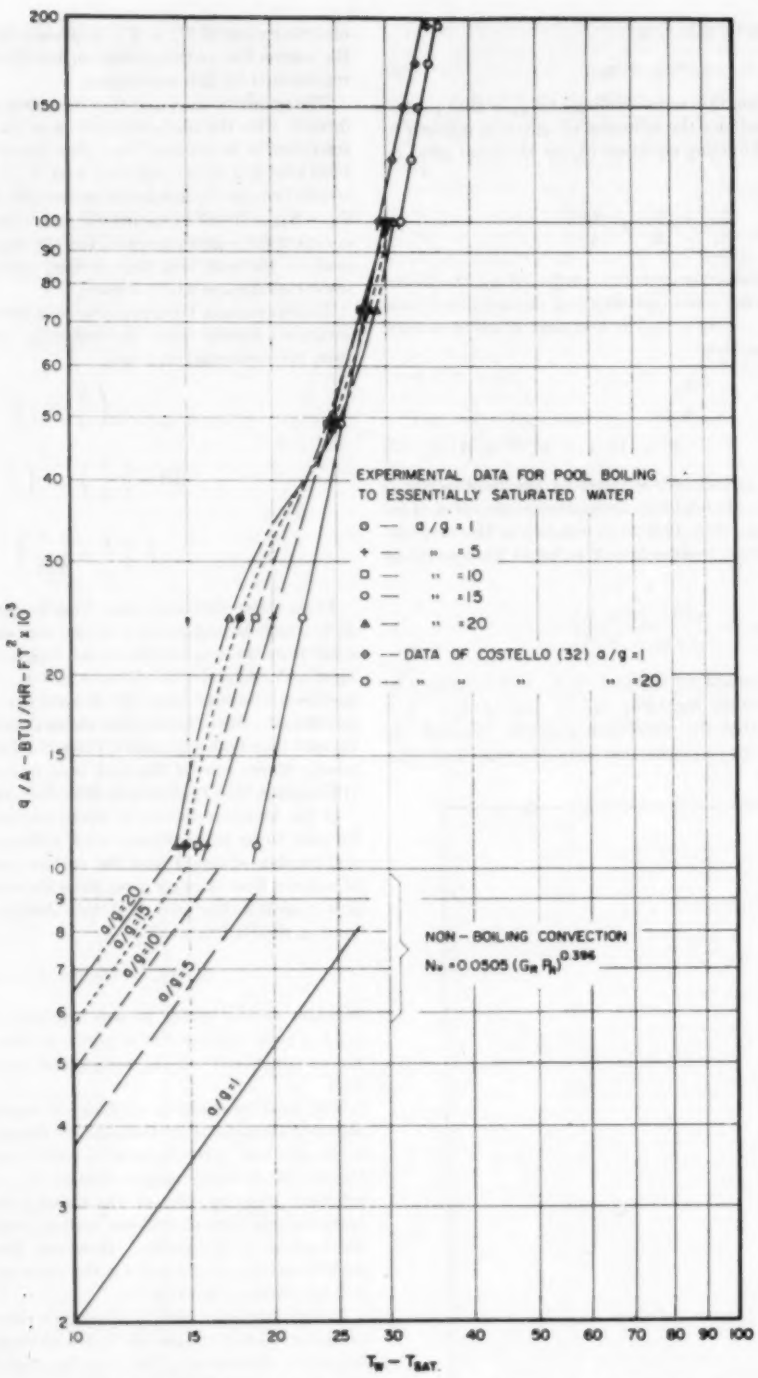
EXPERIMENTAL DATA FOR POOL BOILING
TO ESSENTIALLY SATURATED WATER
o — a/g = 1
+ — " = 5
□ — " = 10
○ — " = 15
△ — " = 20
◇ — DATA OF COSTELLO (32) a/g = 1
○ — " " " " = 20
NON – BOILING CONVECTION
$N_u = 0.0505 (G_R P_R)^{0.396}$
a/g=20
a/g=15
a/g=10
a/g=5
a/g=1
q/A – BTU/HR–FT² x 10⁻³
$T_w - T_{SAT.}$

Fig. 11 Influence of system acceleration normal to heating surface on convection and pool boiling

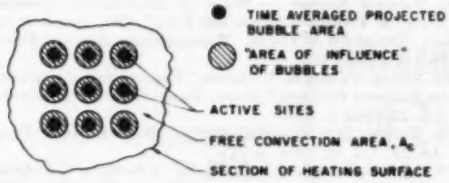
TIME AVERAGED PROJECTED BUBBLE AREA
"AREA OF INFLUENCE" OF BUBBLES
ACTIVE SITES
FREE CONVECTION AREA, A_c
SECTION OF HEATING SURFACE

Fig. 12 Illustration of area of influence of bubble with boiling heat transfer

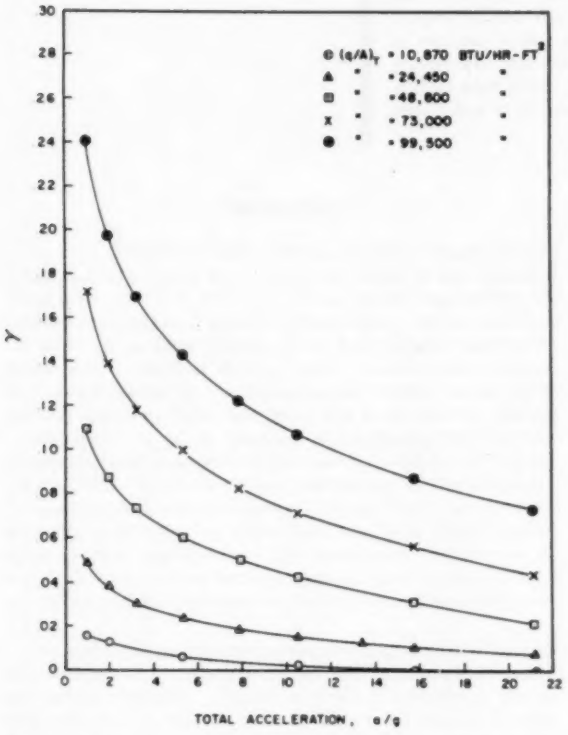

Fig. 13 Calculated values of γ as a function of total heat flux and acceleration

Whether this result is generally applicable for the fractional area of effective boiling has yet to be established although the trend appears reasonable. That is, according to equation (1) D_b is reduced as acceleration is increased which would also reduce the area influenced by the bubble. As seen from the data an increase in acceleration causes a decrease in heated surface temperature (at the lower heat flux) which would reduce the number of nucleating sites for these conditions. At the higher heat flux the decrease in γ results principally from the larger relative increase in $(q/A)_p$ with increased acceleration. It is possible the paramater on the curves should be $(q/A)_t/(q/A)_p$ rather than $(q/A)_f$. This could easily be done but a somewhat different set of curves would result.

Acknowledgment

The assistance of the U. S. Army Ballistic Missile Agency, Huntsville, Alabama, the co-operation of Mr. H. G. Paul and Dr. R. R. Head of that organization, and the aid of the Department of Mechanical Engineering of The University of Michigan in the conduct of this research are gratefully acknowledged.

References

1 M. Jacob, "Heat Transfer, I," John Wiley & Sons, Inc., New York, N. Y., 1949.

2 S. S. Kutateladze, "Hydrodynamic Model of the Crisis of Heat Transfer in a Boiling Liquid With Free Convection," *Journal of Technical Physics*, vol. 20, 1950, p. 1389.

3 V. M. Borishanskii, "An Equation Generalising Experimental Data on the Cessation of Bubble Boiling in a Large Volume of Liquid," *Zhurn. Tekh. Fiz.*, vol. 26, 1956, p. 452; translated in *Soviet Physics-Technical Physics*, vol. 1, American Institute of Physics, New York, N. Y., p. 438.

4 Y. Chang and N. W. Snyder, "Heat Transfer in Saturated Boiling," Preprint 104 presented at Third National Heat Transfer Conference, ASME-AIChE, August, 1959.

5 W. M. Rohsenow, "A Method of Correlating Heat-Transfer Data for Surface Boiling of Liquids," TRANS. ASME, vol. 74, 1952, p. 969.

6 S. Levy, "Generalized Correlation of Boiling Heat Transfer," TRANS. ASME, JOURNAL OF HEAT TRANSFER, Series C, vol. 81, 1959, p. 37.

7 K. Forster and R. Greif, "Heat Transfer to a Boiling Liquid-Mechanism and Correlations," Ibid., p. 43.

8 F. Hirano and K. Nishikawa, "The Phenomena of Boiling—Part 4," *Machinery Research*, Japan, vol. 8, 1959, p. 625.

9 H. K. Forster and N. Zuber, "Dynamics of Vapor Bubbles and Boiling Heat Transfer," *AIChE Journal*, vol. 1, 1955, p. 531.

10 M. S. Plesset and S. A. Zwick, "The Growth of Vapor Bubbles and Superheated Liquids," *Journal of Applied Physics*, vol. 25, 1954, p. 493.

11 H. K. Forster and N. Zuber, "Growth of a Vapor Bubble in a Superheated Liquid," *Journal of Applied Physics*, vol. 25, 1954, p. 474.

12 P. Griffith, "Bubble Growth Rates in Boiling," TRANS. ASME, vol. 80, 1958, p. 721.

13 W. Fritz, "Calculation of the Maximum Volumes of Vapor Bubbles," *Physik Zeitschrift*, vol. 36, 1935, p. 379.

14 F. Bashforth and J. Adams, "Capillary Action," Cambridge University Press, Cambridge, England, 1883.

15 J. W. Wark, "The Physical Chemistry of Flotation," *Journal of Physical Chemistry*, vol. 37, 1933, p. 623.

16 F. Hirano and K. Nishikawa, "The Phenomena of Boiling—Part 2," *Machinery Research*, Japan, vol. 8, 1956, p. 431.

17 F. Hirano and K. Nishikawa, "Boiling of Hard Water," *Trans. Japan Society of Mechanical Engineers*, vol. 19, 1953, p. 33.

18 A. S. Perkins and J. W. Westwater, "Measurements of Bubbles Formed in Boiling Methanol," *AIChE Journal*, vol. 2, 1956, p. 471.

19 R. F. Gaertner and J. W. Westwater, "Populations of Active Sites in Nucleate Boiling Heat Transfer," Preprint 105 presented at Third National Heat Transfer Conference, ASME-AIChE, August, 1959.

20 Y. P. Chang, "A Theoretical Analysis of Heat Transfer in Natural Convection and in Boiling," TRANS. ASME, vol. 79, 1957, p. 1501.

21 F. Hirano and K. Nishikawa, "The Phenomena of Boiling—Part 3," *Machinery Research*, Japan, vol. 8, 1956, p. 521.

22 G. G. Treshchov, "An Experimental Investigation of Heat Exchange Mechanism With Surface Boiling Water," *Teploenergetika*, vol. 4, 1957, p. 44.

23 M. Jakob, "Local Temperature Differences Occurring in Evaporation, Condensation, and in Catalytic Reactions," *Temperature, Its Measurement and Control in Science and Industry*, Reinhold Publishing Corporation, New York, N. Y., 1941, p. 843.

24 C. Corty and A. S. Foust, "Surface Variables in Nucleate Boiling," Chemical Engineering Progress Symposium, series no. 17, vol. 51, 1955, pp. 1–12a.

25 S. G. Bankoff, "Ebullition From Solid Surfaces in the Absence of a Pre-Existing Gaseous Phase," TRANS. ASME, vol. 79, 1957, p. 735.

26 M. Ellion, "A Study of the Mechanism of Boiling Heat Transfer," JPL, Memo 20–88, Pasadena, Calif., March, 1954.

27 R. Siegel and C. Usiskin, "A Photographic Study of Boiling in the Absence of Gravity," TRANS. ASME, Series C, JOURNAL OF HEAT TRANSFER, vol. 81, 1959, p: 230.

28 W. R. Gambill and N. D. Green, "A Study of Burnout Heat Fluxes Associated With Forced-Convection, Subcooled, and Bulk Nucleate Boiling of Water in Source-Vortex Flow," *Chemical Engineering Progress*, vol. 54, 1958, p. 68.

29 H. Merte, Jr., and J. A. Clark, "A Study of Pool Boiling in an

Accelerating System," University of Michigan Research Institute Project No. 2646, November, 1959.

30 W. H. McAdams, "Heat Transmission," third edition, McGraw-Hill Book Company, Inc., New York, N. Y., 1954.

31 C. F. Bonilla, J. S. Busch, A. Stalder, N. S. Shaikhmahmud, and A. Ramachandran, "Pool-Boiling Heat Transfer With Mercury," Reactor Heat Transfer Conference of 1956.

32 C. P. Costello and W. E. Tuthill, "Effects of Acceleration on Nucleate Pool Boiling," personal communication to J. A. Clark, December, 1959.

33 R. A. DeBortoli, S. J. Green, et al., "Forced-Convection Heat Transfer Burnout Studies for Water in Rectangular Channels and Round Tubes at Pressures Above 500 Psia," AEC Research and Development Report WAPD-188, Westinghouse Atomic Power Division, Bettis, June, 1958.

34 K. Nishikawa and K. Urakawa, "Experiment of Nucleate Boiling Under Reduced Pressure," *Trans. Japan Society of Mechanical Engineers*, vol. 23, 1957, p. 935.

35 N. Zuber, "On the Stability of Boiling Heat Transfer," TRANS. ASME, vol. 80, 1958, p. 711.

36 W. M. Rohsenow and J. A. Clark, "A Study of the Mechanism of Boiling Heat Transfer," TRANS. ASME, vol. 73, 1951, p. 609.

An Experimental Study of Boiling in Reduced and Zero Gravity Fields

C. M. USISKIN[1]
R. SIEGEL
NASA, Lewis Research Center, Cleveland, Ohio. Assoc. Mem. ASME

A pool boiling apparatus was mounted on a counterweighted platform which could be dropped a distance of nine feet. By varying the size of the counterweight, the effective gravity field on the equipment was adjusted between zero and unity. A study of boiling burnout in water indicated that a variation in the critical heat flux according to the one quarter power of gravity was reasonable. A consideration of the transient burnout process was necessary in order to properly interpret the data. A photographic study of nucleate boiling showed how the velocity of freely rising vapor bubbles decreased as gravity was reduced. The bubble diameters at the time of breakoff from the heated surface were found to vary inversely as gravity to the 1/3.5 power. Motion pictures were taken to illustrate both nucleate and film boiling in the low gravity range.

Introduction

One of the most important environmental changes which man encounters as he leaves the earth is the change in the gravity field. In free space or in an orbiting satellite the gravitational field may closely approach zero. On the surface of the moon or the inner planets of our solar system, the gravitational field is less than that on earth. Heat-transfer processes such as free convection, condensation, and boiling depend on the gravitational body force, and hence will be affected by this new environment. As yet, to the authors' knowledge, there has been no experimental heat-transfer information available for reduced gravity fields. Hence any design calculations for this range must be based upon an extrapolation of theories which have included a gravity parameter, but which have only been checked experimentally at normal gravity. The importance of gravity in the pool boiling mechanism has been demonstrated by the authors in a previous photographic study of boiling in the absence of gravity [1].[2]

The goal of the present work is to provide quantitative information on how reducing the gravity field affects boiling heat transfer and bubble dynamics. The latter is of some interest in connection with void formation in water-moderated nuclear reactors. Two recent semitheoretical correlations which have been proposed for nucleate boiling are those of Rohsenow and co-workers and of Forster and Zuber [2]. The correlation of Rohsenow takes the velocity of a bubble at the instant of breakoff from the surface as being the most meaningful velocity in the heat-transfer mechanism. Since this velocity depends on the buoyancy force of the bubble, it is not surprising that the heat-transfer coefficient is a function of gravity. However, in the theoretical correlation, gravity appears to only a small power. On the other hand, Forster and Zuber feel that the radial growth velocity of the bubbles, while they are still close to the surface, is more significant in governing the heat-transfer process. As a result, their heat-transfer correlation is independent of the gravity field. Hence the theories are not in agreement as to the role of gravity in nucleate boiling.

The theories for nucleate boiling do not predict the critical heat flux. An analysis of Zuber [3] on transition boiling gives a prediction of the critical heat flux. The theory is based on a hydrodynamic instability between the liquid and vapor motions near the heated surface. These motions are gravity dependent, and hence gravity appears in the final expressions. A few other theories which are summarized by Cole [4] also predict that the critical heat flux will be a function of gravity. This dependence is investigated experimentally in the present work.

The apparatus used in the present investigation was a modification of that employed in reference [1]. The boiling equipment was placed on a platform which could be hoisted and then dropped a distance of nine feet. A counterweight was attached to the platform to slow its downward acceleration and thereby provide gravity fields between zero and one. A high-speed motion-picture camera was mounted on the platform so that boiling could be photographed for various gravity fields and heat fluxes. The motion pictures in the nucleate boiling regime were analyzed to determine the effect of gravity on bubble sizes and rise rates. Color pictures were taken of film boiling from a red hot surface for a few different low gravity fields. The equipment was instrumented so that a study could be made of the variation of the critical heat flux with gravity field. The critical heat flux data for each experimental run were recorded while the platform was falling through the air. Since the fall lasted only about 1 sec, a proper interpretation of the data required a knowledge of the transients involved in the burnout[3] phenomenon. Hence a brief investigation of transient boiling for conditions slightly above the critical heat flux was carried out to provide a better understanding of the experimental results.

[1] Present address: Radio Corporation of America, Astro-Electronic Products Division, Princeton, N. J.

[2] Numbers in brackets designate References at end of paper.

Contributed by the Heat Transfer Division of The American Society of Mechanical Engineers and presented at the ASME-AIChE Heat Transfer Conference, Buffalo, N. Y., August 15–17, 1960. Manuscript received at ASME Headquarters, April 14, 1960. Paper No. 60—HT-10.

[3] Since the platinum wire test sections, which were used for this study, failed by melting when the critical heat flux was reached, the terms "critical heat flux" and "burnout" are used interchangeably throughout the paper.

Nomenclature

A = surface area of heated test section
g = gravity field
g_n = normal earth gravity field
Q = total heat dissipation from test section
t_s = surface temperature of test section
t_{sat} = saturation temperature of water
Δt = temperature difference, $t_s - t_{sat}$

Experimental Equipment

A schematic representation of the apparatus is shown in Fig. 1. This is a modification of the equipment used in reference [1], and hence only a brief description of the basic apparatus will be given here along with a more detailed description of the additions which were made. A cross shaped platform was constructed which was free to move in the vertical direction. A Fastex motion-picture camera, capable of taking up to 5000 frames per sec, was mounted on the platform along with a rectangular tank ($3^1/_2$ in. $\times$ $5^3/_4$ in. $\times$ $5^1/_2$ in. deep) in which the boiling took place. A cable ran from the platform, over pulleys attached to the ceiling, and then down to a counterweight. By changing the size of the counterweight, the downward acceleration of the platform could be varied, and hence experimental runs could be taken at any gravity field in the range between zero and unity. When making a run, the counterweight was pulled down to the floor which raised the platform to the ceiling. The bottom end of the counterweight was grasped by a solenoid operated grapple bolted to the floor. Opening the grapple allowed the platform to fall nine feet before contacting a sand bed which was used as a braking device. For zero gravity conditions, the platform fell freely after being released from a grapple at the ceiling.

Test Sections. An electrically heated element was supported in a brass tank having lucite windows in the front and back faces. The other surfaces of the tank were covered with insulation to help maintain the water uniformly at the saturation temperature. A copper electrode $^1/_2$ in. in diameter was brought through each end of the tank and supported on the outside by a Teflon flange which insulated it from the tank. Different test sections could be easily clamped to the electrodes. Three types of test sections, which were used for different purposes, will now be described.

The tests to determine the variation of burnout heat flux with gravity were conducted with platinum wires 0.0453 in. in diameter. In reference [5] the boiling curve at high heat fluxes was not influenced when the platinum wire test section was changed from 0.016 to 0.024 in. in diameter. Hence it was hoped that the wires used here would be of sufficiently large diameter so as not to limit the generality of the results. The ends of the wires were soft soldered to copper blocks which were spaced $2^1/_2$ in. apart. Voltage taps were drilled into the copper blocks as close as possible to the platinum wire so that the voltage drop across the wire could be accurately determined. The copper blocks were then bolted to the two electrodes. Some of the wires were calibrated by the instrumentation section of the laboratory so that they could be used as resistance thermometers and an average wire temperature determined.

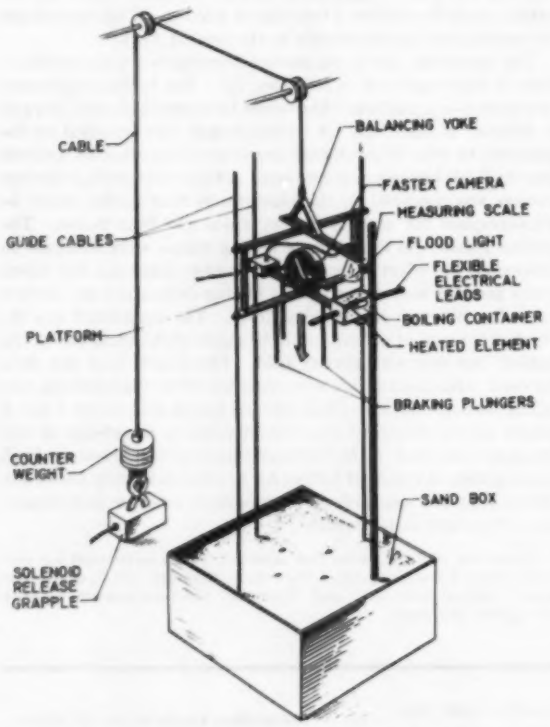

Fig. 1 Schematic diagram of the counterweighted platform

The photographic studies to determine bubble sizes and rise rates in the nucleate boiling range, were made using flat nickel ribbons, 0.2 in. wide and 0.010 in. thick. These ribbons were also soldered to copper blocks spaced $2^1/_2$ in. apart, and then their bottom sides were insulated by cementing them to bakelite strips $^1/_4$ in. thick. Boiling then occurred from only the top surface, and this provided a relatively simple configuration for making bubble measurements.

For photographic studies of film boiling, the test sections were fabricated from stainless-steel tubing with an outside diameter of 0.157 in. The ends of the tubing were flattened and clamped between copper blocks $2^1/_2$ in. apart which were bolted to the electrodes. The stainless steel could remain red hot under water for several minutes without burning out.

Power Supply. Power was supplied by a 3-phase Mallory rectifier unit which could provide up to 500 amps dc with about 5 per cent ripple. The power was controlled by a system of Powerstats on the 220 volt a-c line which supplied the rectifier. The d-c current flow was measured by reading the voltage drop across a 0.001 ohm Leeds and Northrup precision resistor placed in series in the circuit. Large loops of flexible woven welding cable, which could fall freely with the platform, were used to carry the current to the electrodes in the boiling container.

Instrumentation. The voltage across the calibrated resistor and the voltage across the heated test section were both measured with a Rubicon potentiometer and light beam galvanometer. The current in the circuit could be determined within ± 0.2 amp at 100 amp and the voltage across the test section read within 0.002 volt at 1 volt. Although this instrument was quite sensitive, there were slight current and voltage fluctuations during the boiling process, and hence the heat dissipation could be in error a few per cent. The potentiometer readings were taken just before the equipment was dropped. To read the transient current and voltage while the equipment was descending, a dual beam oscilloscope (Tektronix Type 535) was used. The bias settings on the two preamplifiers were made to center the initial voltage and current signals, and the gains were set as high as possible so that small changes from the initial values could be observed. Transient temperature changes of the test section were evident if they exceeded about 6 deg F. While the apparatus fell, the signals made a single sweep at 5 cm/sec and were recorded with a Polaroid camera. The 5 per cent ripple from the power supply caused a corresponding ripple in the oscilloscope signals, and this had to be filtered out since it was of the same order of magnitude as the changes to be observed. This was done with a low band pass filter which reduced a 60 cps signal by a factor of 20, but allowed a signal with a frequency of less than 12 cps to pass unaffected. For a step function pulse, the filter gave a full response within 1/20th of a second, and hence would adequately follow the signals to be observed. To eliminate spurious signals, the wires in the circuitry were carefully shielded.

The temperature of the boiling water was measured with two copper-constantan thermocouples immersed in the tank and read with a Rubicon potentiometer.

Experimental Procedure

Due to the dependence of the boiling process on many parameters, a great deal of care had to be taken to try to keep conditions the same during successive experimental runs. A learning period of several weeks was necessary before a good experimental technique was achieved. In order to provide a basis for critical evaluation of the work, and to aid any future workers who may use this type of apparatus, a detailed description of a typical burnout test will follow.

Several platinum test sections were fabricated in an identical way, and one was attached between the electrodes in the boiling container. The tank was then filled with boiled distilled water and a 350-w stainless-steel jacketed immersion heater was inserted to bring the water to the saturation temperature. During this time the d-c power was turned on and a moderate current passed through the platinum wire. When the saturation temperature was reached, as indicated by the thermocouples as well as by normal boiling conditions, the immersion heater was removed and the burnout heat flux of the wire was checked. This was accomplished by slowly raising the power in the circuit while watching an ammeter connected into the output of the d-c power supply. At the onset of burnout the increase in temperature of the heated wire caused an increase in resistance in the circuit and hence a decrease in current. As soon as a reduction in current began, the power was immediately shut off. It was found that sometimes the wire could boil normally for a few minutes at a given power setting and then suddenly burn out, and hence the power was raised slowly to provide ample time for the boiling to adjust properly. The transients involved in initiating burnout will be discussed in a later section.

In the instant that the wire started to burn out before the power was shut off, the wire would usually begin to glow slightly in one local region, but no physical damage could be observed. However, when the power was restored, and boiling resumed, it was noted that the region which had started to burn out was deficient in nucleation centers, possibly due to the high temperature which had been reached at that location. This phenomenon has been observed before by McAdams, et al. [5]. If the heat flux was immediately brought up again, the burnout flux was much lower, apparently due to the lack of efficient boiling over part of the wire surface. However, if a period of 2 to 5 minutes was allowed, then the nucleation centers would be restored, and the burnout flux would return close to its former value.

After the burnout check, several minutes were allowed for the nucleation centers to become re-established. Then the power was set at the desired value for the low gravity test, and a counterweight corresponding to the required gravity field was placed at the end of the hoisting cable. The platform was then raised to the ceiling and the cable secured by the solenoid grapple. Potentiometer readings of the voltage and current in the test section were recorded, and the thermocouple readings for the water temperature were taken. Upon depressing a switch the following sequence of events took place. The oscilloscope was triggered and began a two-second sweep. The high-speed motion-picture camera was started to record the initial boiling state before the platform fell. From 0.3 to 0.5 sec later, according to the setting on a timer, the solenoid grapple opened and the platform began to fall. As soon as the drop was complete the power was cut off to prevent the test section from melting in the event that burnout had been initiated while the low gravity environment existed. The existence of burnout during the drop was shown by oscillograph traces of the current and voltage. These showed an increase in voltage drop across the heated wire and a decrease in the current flow due to the increase in wire resistance as the temperature increased. Fig. 2 shows a typical record of the transient current and voltage when burnout occurred. Depending on whether burnout did or did not occur during the drop, the power was decreased or increased by about 5 per cent and another run taken. This procedure was continued until two runs were obtained, one where burnout occurred, and one at a power about 5 per cent lower where burnout did not occur. After these two runs were achieved, the burnout heat flux was checked again at normal gravity for comparison purposes. This procedure was repeated for several different gravity fields and with several platinum wire test sections.

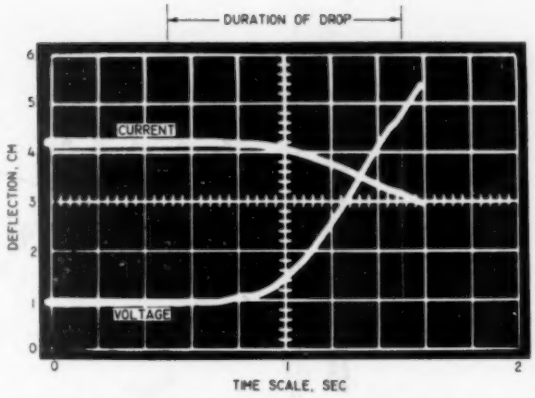

Fig. 2 Behavior of voltage and current in a typical drop test with burnout occurring. (Deflection scales: 0.072 cm/amp, 8.5 cm/volt.)

The effective gravity field for a given counterweight size was determined by measuring the rate of descent of the platform. This was accomplished by placing a stationary vertical measuring scale in the viewing field of the falling motion-picture camera to provide a continuous record of platform height on the film. In addition, an argon timing lamp in the camera placed a mark on the film every 1/120th of a second. From the data of distance and time, the acceleration of the platform could be determined.

Effect of Gravity on Burnout

For each series of drop tests at a particular gravity, a heat flow per unit area just above and below the apparent burnout point was computed from the current and voltage measurements. These values were then divided by the burnout flux at normal gravity for that particular test section. The effect of gravity on the burnout heat flux is shown by the data in Fig. 3. It is seen that there is a considerable scatter in the data at each gravity. This is believed to be due to the transients involved in the burnout process, and some experimental results to explain this will be discussed in the next section. In spite of the scatter, the data do indicate a definite trend. For example, at 5.5 per cent gravity the burnout flux has been reduced to about 65 per cent of the value at normal gravity. At 47.5 per cent gravity the wire would not burn out during the drop even for heat fluxes within 7 per cent of the normal gravity burnout limit. Also shown on the curve is a line of $(g/g_n)^{1/4}$ variation. This variation for the critical heat flux has been predicted by a number of investigators as discussed, for example, in reference [4]. The curve appears to provide a reasonable lower limit for the data. The results for zero gravity will be considered in more detail in connection with the discussion in the next section.

Transient Burnout Studies

The data in these experiments were obtained during a time interval on the order of a second while the heated surface was being subjected to a decreased gravity field. The question then

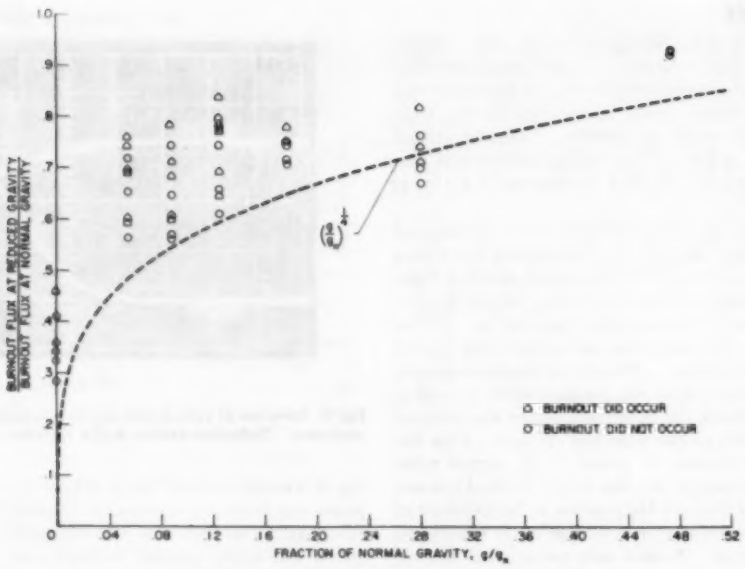

Fig. 3 Effect of reduced gravity on burnout heat flux

arises as to how rapidly the system will respond and indicate a burnout condition after a sudden change in gravity field. For example, if the power were set at the burnout flux corresponding to a certain low gravity, and then the test section were subjected to that gravity, how long would it take for a burnout condition to be indicated? It was necessary to investigate this transient response in order to properly interpret the burnout data.

For this investigation a resistor and a switch were placed in parallel across the heated wire. When the switch was closed, part of the current would go through the resistor. When the switch was opened, the wire received a step increase in power. Using the same instrumentation as in the drop tests, the experiments were carried out as follows: First, the power was slowly raised to determine the burnout flux for the test section. Then the switch on the parallel resistor was closed, and the total current flow was increased so that when the switch was opened the heat flux in the test section would be a certain percentage above the burnout value. Just before the switch was opened, the oscilloscope was triggered on a ten-second sweep to record the current flow and voltage drop across the test wire. From a photograph of the traces, the time from the step in power to the onset of burnout could be measured.

In order to obtain good statistical data on the transient time required for burnout, a large number of tests are necessary. The same test section should be repeatedly subjected to the same power pulse until a good distribution curve is obtained which gives the probability for burnout to occur within a given time. The manual power shutoff which was used to prevent destruction of the test wire was a limitation in this experiment, since it was not rapid enough to prevent the wire from glowing slightly red for each test. After a dozen or so tests this would cause changes in the wire, and the burnout limit would decrease so that the data would become inconsistent. Despite this limitation we can say that for a step in power to 10 per cent above the burnout flux, only about 30 per cent of the burnouts occurred in less than one second. The remaining 70 per cent took from 1 to 5 sec. However, when the power was pulsed to about 25 per cent above burnout, all of the burnouts took place within a second and many of them were essentially instantaneous.

These transient tests could only be performed under normal gravity conditions. However, it is reasonable to assume they apply qualitatively for reduced gravity. The results of these tests offer a possible explanation for the scatter which was observed in Fig. 3. Let us say that a series of drop tests were being made in which the power was increased in increments until burnout occurred. When the power was just above the burnout flux for the gravity field under consideration, there was a fairly small probability that burnout would occur during the short duration of the test, and hence a burnout would only be observed at this power setting in some instances. Most likely the power would have been increased and another test performed. Hence burnout would finally be observed at some higher value where there was a greater probability of the instability taking place within one second. As a consequence, the burnout data would generally be too high, but not by over 25 per cent since at this excess power, burnout within one second would be expected. The very lowest data points at a given gravity would be near the true burnout limit and would be the result of a highly improbable event occurring.

Although there is no experimental evidence on local surface temperature fluctuations in boiling (reference [2]) there is a possibility that these would account for the randomness in the transient burnout behavior. When part of the wire reaches a certain critical temperature the process becomes unstable and burnout occurs. As the mean temperature level of the wire is raised, the probability is increased that locally the burnout temperature could be exceeded in a given time interval. For a power setting which would cause the average temperature of the entire wire to be above the critical value, burnout would occur almost instantaneously.

The transient considerations are especially important for the zero gravity case. In this instance, the theories for the critical heat flux indicate that the burnout flux would go to zero. This, of course, neglects the heat removal that would actually occur by radiation and conduction when the heated surface is completely surrounded by vapor. If the liquid is at the saturation temperature, the vapor cavity may keep increasing in size as time proceeds. For a proper evaluation it would be desirable to have experimental information for periods of zero gravity which are longer than those in the present investigation.

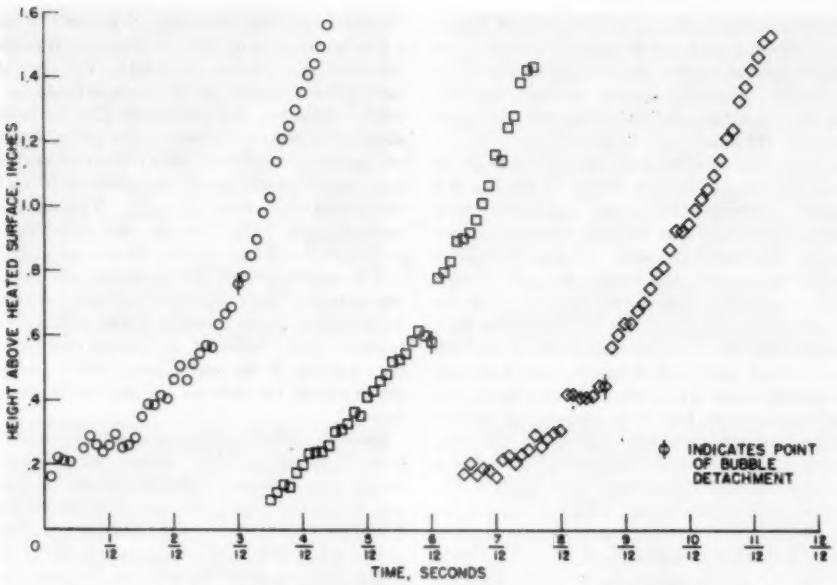

Fig. 4(a) The rise of individual bubbles in 5.5 per cent of normal gravity

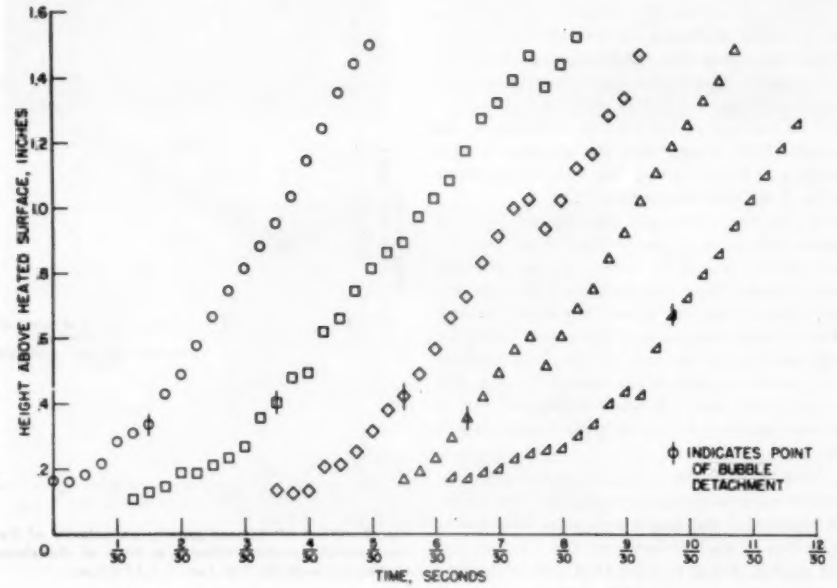

Fig. 4(b) The rise of individual bubbles in 28.2 per cent of normal gravity

Nucleate Boiling at Low Gravity

Photographic Study. A photographic study was made at several gravity fields of boiling from a flat horizontal nickel ribbon with boiling from only the upper surface. The ribbon heat fluxes for the films were all within a few per cent of 91,000 Btu/(hr)(ft²). The motion pictures were placed in a viewer and measurements were taken on about 15 different bubbles for each gravity field. The number of bubbles measured was limited by the low gravity runs where relatively few bubbles are formed because vapor removal is so poor. As soon as a bubble could be distinguished on the ribbon, measurements were taken every 1/120th of a second of the height of its center of gravity above the ribbon. These measurements were taken until the bubble had traveled about 1.5 in. upward from the heated surface. The center of gravity was estimated at the center of the area of the bubble when it was attached, and at the intersection of the major and minor axes when the bubble was detached. The values of the major and minor diameters were recorded at about six successive 1/120 second time increments immediately following breakoff from the surface.

It was found that in the low gravity range, the bubbles would become quite irregular and poorly defined while attached to the surface. This was due to the poor removal of vapor which would

cause small bubbles to coalesce and form a larger film of vapor. For this reason, the bubbles attached to the surface were very irregular, and hence an average bubble size for attached bubbles could not be determined. Shortly after the bubbles detached, they became much more distinct, and hence diameter measurements could be made for the detached condition.

Bubble Rise Rates. Figs. 4(*a*) and (*b*) show typical curves of the heights of the bubble centers as a function of time for 5.5 and 28 2 per cent gravity fields. Although the bubbles had a fairly wide variation in diameters, it is seen that the rise rates for the detached bubbles are all very much the same for a given gravity field. This is in agreement with the results for high bubble Reynolds numbers in reference [6] where the rise rate of bubbles was found to be independent of size. The bubble paths have some irregularities probably due to the stirring action of the boiling process. The resulting convection currents have increased importance at low gravity fields where the buoyancy forces become small. When looking at the films it was noted that bubbles would move downward at times due to the convection currents.

Plots similar to those in Fig. 4 were prepared for each gravity field including the normal one gravity condition. For each bubble path two straight lines were then drawn. One line went in an average way through all the points after the bubble had detached, and hence its slope gave an average bubble velocity for about one in. of rise away from the heated surface. The other line was drawn tangent to curve of the data at the point of detachment, and the slope of this line gave the bubble velocity at the time of breakoff from the surface. An arithmetic average of each of these two rise rates was then computed using all the bubble paths for each gravity field, and these were divided by the corresponding rise rates for normal gravity. Fig. 5 shows the rise rates relative to those for normal gravity, as a function of the gravity field. For normal gravity the average of the bubble velocities at the time of detachment was 0.98 ft/sec, while the average velocity over one in. of rise was 1.17 ft/sec. Except for very low gravities the data points in Fig. 5 fall close to a straight line.

The magnitude of the rise rates and their dependence on gravity did not agree with those of gas bubbles rising through liquids as given in references [6 and 7]. The rise rate measured for normal gravity was higher than that predicted from the gas bubble correlations. Even larger rise rates have been observed in reference [4]. The bubble velocities may have been influenced by cellular convective motions in the tank, which would produce an upward circulation in the vicinity of the heated element, and a downward motion along the sides. In view of these motions it is not known if the calculation of bubble drag coefficients would be very meaningful.

Bubble Diameters. Since most of the bubbles were not spherical, an assumption had to be made to obtain an average bubble diameter from the measurements of the major and minor diameters. Since the third dimension of each bubble into the plane of the photograph was not known, it was decided that any refinement beyond a simple arithmetic average bubble diameter was not warranted. For each bubble, the diameter at detachment was taken as the arithmetic average of several readings taken at successive 1/120 sec intervals immediately following detachment. Then an average was taken of all the bubbles for a given gravity field.

For comparison, information on bubble diameters for the normal gravity condition was needed. This was obtained by starting the motion-picture camera about one quarter of a second before the platform was released. The bubble rise rates for normal gravity did not vary appreciably from run to run, but the bubble diameters could vary by several per cent. This variation in bubble size was possibly due to small differences in water temperature for different runs. Hence the data on bubble diameter for each gravity field was compared with the normal gravity condition observed immediately before the drop. Fig. 6 shows a plot of the ratio of bubble diameter to normal gravity bubble diameter, as a function of gravity. For normal gravity the average bubble diameter for all runs was 0.245 in. As expected, the bubble diameter increases as the gravity field is reduced. The slope of the line on the logarithmic plot is about 1/3.5. This does not agree very well with theory which indicates (see reference [3] for example) that, for bubbles departing from a horizontal surface, the diameters increase as $1/\sqrt{g}$. This assumes that the bubble contact angle, which also appears in the theoretical expression, is independent of gravity at the instant of bubble breakoff.

A rough comparison of bubble sizes can be seen in Fig. 7 which shows typical photographs of bubbles for five different gravity fields with the same heat flux at the surface. In the pictures, the bubbles appear fairly evenly spaced (the photograph for 13 per cent gravity is especially good) which indicates that in low gravity fields the bubbles continue to be generated in a regular fashion.

Comments on Nucleate Boiling Data. It was thought that, in the nucleate boiling range, a decrease in the gravity field might be reflected in a poorer heat transfer due to the accumulation of vapor near the heated surface. This would require a higher surface temperature to dissipate the same heat flux. Hence during a drop test the oscilloscope traces might show a higher voltage drop and a lower current flow due to the resistance increase of the platinum wire. However, in drop tests where burnout was not

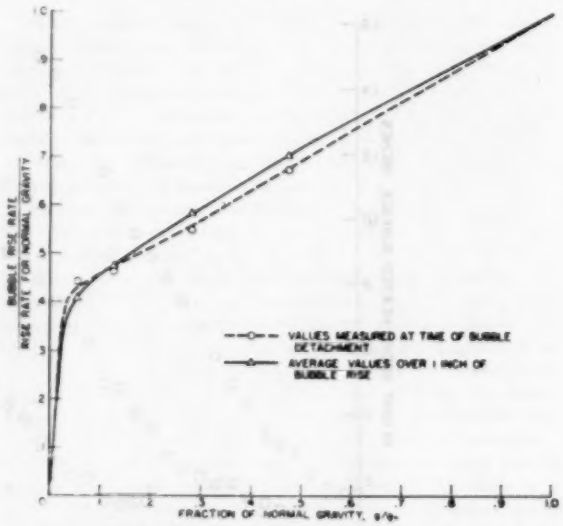
BUBBLE RISE RATE
RISE RATE FOR NORMAL GRAVITY
VALUES MEASURED AT TIME OF BUBBLE DETACHMENT
AVERAGE VALUES OVER 1 INCH OF BUBBLE RISE
FRACTION OF NORMAL GRAVITY, g/g0

Fig. 5 Effect of reduced gravity on velocity of freely rising bubbles. For normal gravity: Velocity at time of detachment = 0.98 ft/sec, average velocity for 1 in. rise = 1.17 ft/sec.

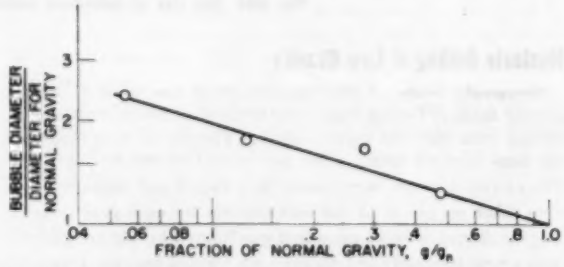

Fig. 6 Effect of reduced gravity on diameter of bubbles at the time of detachment from the surface. Average bubble diameter for normal gravity = 0.245 in.

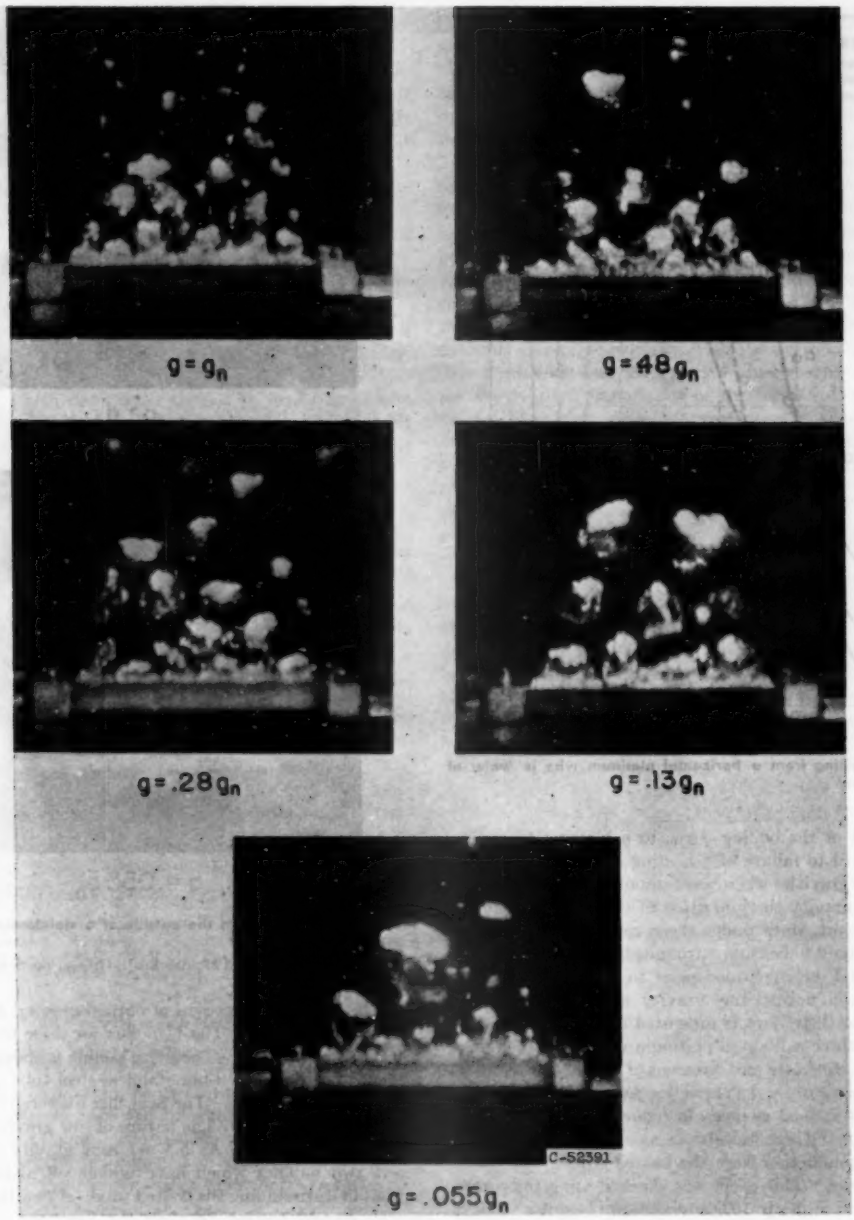

Fig. 7 Nucleate boiling from the top surface of a nickel ribbon for five different gravity fields

Heat flux = 91,000 Btu/hr-ft², g_n earth gravity

present, the traces went straight across the screen and no surface temperature change could be detected. It should be noted, however, that a change could only be clearly detected if it were at least 6 deg F, so that a shift in the boiling curve of Q/A as a function of $t_s - t_{sat}$ could have taken place of less than this magnitude. These results can be justified in terms of the analysis of Forster and Zuber (see reference [2]) which yields a heat-transfer coefficient independent of gravity. Their analysis shows that the "stirring action" of the bubbles, as indicated by the product of the bubble radius and the change in radius with time, is independent of the size of the bubbles. Hence the large bubbles obtained in low gravity fields may be just as effective in promoting good heat transfer. The results of Rohsenow [2] do contain a gravity parameter, but it is to a small power. If Q/A is constant, then Δt is proportional to $(g_n/g)^{1/4}$. For example, if a drop test is performed where g is reduced suddenly to 20 per cent of normal gravity, than Δt would be increased by about 30 per cent. Since the Δt for these tests is on the order of 25 deg F, a 30 per cent change would just be detectable. Hence with our instrumentation, a shift in the boiling curve would only be detected for gravities less than about 1/5 of normal. In this range we still did not observe any change in wire temperature during the experiments.

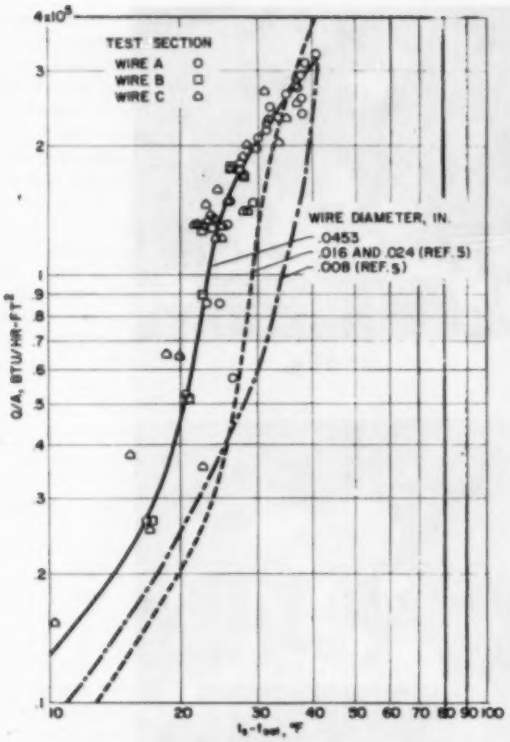

Fig. 8 Nucleate boiling from a horizontal platinum wire in water at atmospheric pressure

The possible shift of the boiling curve to a higher Δt is unimportant with regard to failure of a heating element by melting, except at very low gravities where a continuous vapor film may be formed. At zero gravity the limitation of the short duration of the test is significant, since under these conditions the surface would eventually tend to become surrounded by vapor.

The experimental data recorded prior to each drop test provide information on normal one gravity nucleate boiling. A boiling curve using these data is presented in Fig. 8. The data were taken using three calibrated platinum wires with diameters of 0.0453 in. The resistance measurement of the wire provides an average wire temperature, and a correction for the radial temperature variation was applied as given in reference [5] to yield the surface temperature. There was also an axial temperature variation due to heat conduction from the heated wire to the cooler supporting electrodes. This effect was checked using the results of Callendar (reference [8], p. 152) and found to be quite small so no correction was needed. The figure also shows how the data are located relative to those for smaller diameter wires given in reference [5]. Near the critical heat flux, the data fall in the same range as those for smaller wires. Hence it is felt that the influence of wire diameter is probably unimportant for the burnout data given here.

Motion-Picture Film

A 16-mm narrated color film has been prepared and is available on loan from the NASA, Lewis Research Center. The number of the film is C208 and it is entitled "Boiling in Reduced Gravity," by C. M. Usiskin and R. Siegel. The film shows the experimental equipment and illustrates its operation. Nucleate boiling of water from a horizontal platinum wire is shown for three gravity fields, 28, 5.5, and 0 per cent of normal gravity, and is compared with normal boiling. The heat flux for these three sequences is 230,000 Btu/(hr)(ft²). Then film boiling is shown from the outside of a horizontal, red-hot stainless-steel tube at 5.5 and 0 per cent of normal gravity. The heat flux for these two sequences is 175,000 Btu/(hr)(ft²). The nature of low gravity film boiling is illustrated in Fig. 9. At 5.5 per cent gravity the photograph shows two bubbles which have broken off at each end of the vapor film surrounding the heated tube. A new bubble is growing in the central section between the locations from which the previous bubbles have departed. The formation of bubbles at alternately spaced locations is a well-known characteristic of film boiling and evidently persists for low gravity fields.

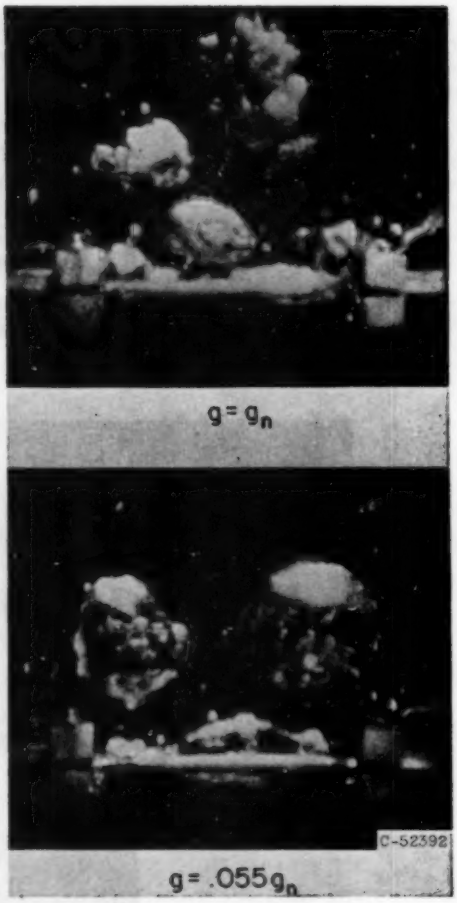

Fig. 9 Film boiling from the outside of a stainless-steel tube for two gravity fields

Heat flux = 127,000 Btu/hr-ft², g_n earth gravity

Conclusions

The burnout heat flux decreases with decreased gravity as expected from the trend predicted by theory. The theoretical curve which gives the burnout flux varying as gravity to the one quarter power appears to be a reasonable lower limit for the data. If the heat flux is suddenly raised above the burnout limit an interval of time is required before burnout actually occurs. This transient time decreases as the magnitude of the step in power is increased beyond the burnout limit. Because the data in this work were all obtained during drop tests which only lasted

about a second, the transient phenomenon is significant in accounting for the scatter of the burnout data.

The photographic study of nucleate boiling indicates how the velocity of freely rising bubbles decreases as gravity is reduced. The bubble diameters increase as gravity is decreased approximately as gravity to the 1/3.5 power. At zero gravity, film and nucleate boiling take on a similar appearance.

For nucleate boiling, within the limitations of the present experimental equipment, the surface temperature of the test section for a fixed heat dissipation was not influenced by the reduction in gravity field.

Acknowledgment

The authors wish to express sincere thanks for the help and ideas received from other members of the Lewis Research Center. The staff of the photo lab helped us considerably to obtain clear motion pictures. Particular thanks are due to Royal Boyd who fabricated the equipment and assisted during its operation, and Eileen Norris, Marcelle Jordan, and Eileen Cox who helped analyze the photographic data.

References

1 R. Siegel and C. M. Usiskin, "A Photographic Study of Boiling in the Absence of Gravity," JOURNAL OF HEAT TRANSFER, TRANS. ASME, Series C, vol. 81, 1959, pp. 230–236.

2 J. W. Westwater, "Boiling of Liquids," Advances in Chemical Engineering, vol. I, Academic Press, Inc., New York, N. Y., 1956, pp. 1–76.

3 N. Zuber, "Hydrodynamic Aspects of Boiling Heat Transfer," PhD thesis, University of California, Los Angeles, Calif., June, 1959.

4 R. Cole, "A Photographic Study of Pool Boiling in the Region of the Critical Heat Flux," Paper No. 21, Fourth National Heat Transfer Conference, Buffalo, N. Y., August, 1960, submitted for publication in the *AIChE Journal*.

5 W. H. McAdams, J. N. Addoms, P. M. Rinaldo, and R. S. Day, "Heat Transfer From Single Horizontal Wires to Boiling Water," *Chemical Engineering Progress*, vol. 44, 1948, pp. 639–646.

6 F. N. Peebles and H. J. Garber, "Studies on the Motion of Gas Bubbles in Liquids," *Chemical Engineering Progress*, vol. 49, 1953, p. 88.

7 D. W. Moore, "The Rise of a Gas Bubble in a Viscous Liquid," *Journal of Fluid Mechanics*, vol. 16, part I, July, 1959, pp. 113–130.

8 H. S. Carslaw and J. C. Jaeger, "Conduction of Heat in Solids," second edition, Clarendon Press, Oxford, England, 1959.

DISCUSSION

Marvin Adelberg[4] and Kurt Forster[5]

We are fortunate to have, in the present paper, one of very few experimental investigations on the influence of gravity upon heat transfer to a boiling liquid. The authors feel that their results, which showed no significant influence of gravity, substantiated the correlations of Forster and co-workers as contrasted with the correlations of Rohsenow and co-workers. We wish to note, however, that the fact that g does not appear *explicitly* in the correlations of Forster and co-workers does not imply that this correlation is independent of g. The correlation constant C in that correlation was obtained by reference to experiments performed under normal gravity ($g/g_n = 1$); for example, had C for the correlation been determined by reference to experiments performed on the moon ($g/g_n = 1/6$), then the influence of g would have been manifested in a new value of C.

To elaborate on this point, by reasoning from dimensional analysis: Assuming four primary dimensions (time, temperature, mass, and length) and noting the large number of significant and independent variables which appear in the various correlations, it is evident that more than three Π terms are required for a complete set. Thus the additional Π terms which do not appear explicitly are incorporated in the constant C. Should g be a significant independent variable, then at least one of these additional Π terms in C contain g.

We want to take this opportunity to present some physical considerations concerning the relative importance of gravity in the transfer of heat from a heated surface to a boiling liquid. The main function of gravity in this process is the removal of the vapor bubbles from the heated surface. Apart from gravity, the vapor bubbles can be removed from the surface also by forced convection (shear) forces and/or by the flow field induced by the dynamics of the growing bubble. Let us estimate the dynamic force F_d associated with the growing bubble and compare it with the buoyancy force F_b in order to obtain a criterion for the relative importance of the latter. Consider a hemispherical cavity of radius $R(t)$ growing on a flat surface in a liquid of density ρ; its apparent mass is of the order $^2/_3\rho R^3\pi$, and its velocity is of the order $\dot{R}$. We set the dynamic force F_d associated with this mass flow proportional to the momentum change

$$F_d \propto \frac{d}{dt}\left(\frac{2}{3}\,\rho\pi R^3\dot{R}\right) = 2\rho\pi\left(R^3\dot{R}^2 + \frac{1}{3}\,R^3\ddot{R}\right) \tag{1}$$

and we submit that in a system in which the buoyancy force dominates, the ratio F_d/F_b is small and that when this ratio is large, the system will be essentially independent of gravity as far as removal of vapor from the heating surface is concerned. We therefore form this ratio, which is of the nature of a Froude number,

$$\Pi = \frac{2\rho\pi\left(R^3\dot{R}^2 + \frac{1}{3}\,R^3\ddot{R}\right)}{\frac{2}{3}\,\rho\pi R^3 g} \tag{2}$$

It is well known that, for a bubble growing in either a saturated or a subcooled liquid, $\ddot{R}$ is negative and, inasmuch as the present is a consideration in orders of magnitude, we neglect the second term in equation (2) and we approximate $\dot{R}$ by the mean value theorem

$$\dot{R} \approx \frac{R_{max}}{t_{max}} \tag{3}$$

in terms of the maximum radius R_{max} and the time t_{max} at which this maximum radius occurs. Hence

$$\Pi = \frac{3R_{max}}{gt^2_{max}} \tag{4}$$

The problem for the designing engineer is to develop a system under normal ($g/g_n = 1$) conditions such that he can predict its performance for other gravity levels. Equation (4) indicates that the important ratio is that of R/t^2 versus g. For saturated boiling at $g/g_n = 1$, significant times for detachment of the vapor bubbles are of the order of 3×10^{-2} seconds and the corresponding maximum radius is about 0.4 cm. For this condition Π, from equation (4), is seen to be about unity. Without resorting to new experiments, we can take advantage of the fact that, for a subcooled liquid, in which the bubbles collapse due to condensation (rather than being detached by gravity), the boiling mechanism should not be significantly influenced by gravity. We might conclude from this that values of Π corresponding to the subcooled case indicate a system which is insensitive to changing conditions of gravity. To obtain a feeling for the magnitude of Π under such

[4] Member, Technical Staff, Space Technology Laboratories, El Segundo, Calif.

[5] Professor of Engineering, University of California, Los Angeles, Calif.

onditions, we tabulate below some experimental data reported by Ellion[6] for water:

Table 1 Effect of subcooling upon the ratio Π

Liquid temp T_L-deg F	R_{max} cm $\times 10^{-2}$	t_{max} sec $\times 10^{-3}$	Π [Equation (4)]
[212	40	30	1.3]
170	5.3	1.1	130
120	4.4	0.83	190
60	3.4	0.50	410

We conclude that a system which is characterized at $g/g_n = 1$ by a value for Π greater than, say, one hundred is essentially insensitive to change of gravity. The relatively very low value of Π in the first row of the foregoing table suggests that a system designed for pool boiling of a saturated liquid at $g/g_n = 1$ will fail at low g levels. This is so for the following reason: In order to produce sizable dynamic forces of the growing vapor bubbles in a saturated liquid, the superheat would have to be extremely high; but superheat is limited to low values by the occurrence of "burnout." Deeper insight into these questions might be obtained by the experiment suggested below.

The authors stress the desirability of experimental investigation of extended duration to minimize transient effects. We would appreciate the authors' comments on some experiments, proposed by one of us a few years ago, intended to yield design criteria for heat-transfer components to operate independently of the level of gravity. Essentially, the designer needs to know two criteria regarding the boiling process, for his system designed under $g/g_n = 1$ conditions, to remain largely unaffected by reduction in gravity: (1) The level of subcooling and/or superheat at which the bubble *dynamic forces* dominate and are sufficient to insure removal of the bubbles from the heating surface. (2) The velocity in forced convection at which the *shear forces* near the heating surface dominate and are sufficient to remove the vapor from the heating surface. A simple experiment which will yield the foregoing design criteria and which permits the observation of the phenomena in the steady state is the following: Consider a system with a flat heating surface on top of and in contact with the liquid. In this case gravity tends to keep the bubbles attached to the heating surface instead of aiding their removal (as takes place in the "heating from below" condition); in this manner one can observe a system in which g/g_n is effectively -1, and one can obtain experimentally the relation between boiling heat transfer and the usual parameters (superheat, subcooling, convective velocity, and so on). The desired above-mentioned criteria would be established for the range $-1 < g/g_n < +1$ when superheat, subcooling, and convective velocities were found such that the resulting heat flux in this "heating from above" case approximates the heat flux obtained by "heating from below." In this manner, criteria for sufficient conditions for proper heat-transfer design at low gravity can be established conveniently (at rest) by observing the operation at $g/g_n = -1$.

C. P. Costello[7]

This writer wishes to congratulate the authors not only on obtaining significant data but also on presenting the information clearly and completely so as to facilitate appraisal of the data.

The use of a 0.0453 in. diameter wire for burnout studies should give slightly low values of burnout heat flux according to Bernath.[8] He has accumulated data for nonaccelerating pool boiling systems which show that heater diameters up to roughly 0.1 in. are influential in determining burnout. The peak heat flux for a wire of 0.0453 in. diameter appears to be roughly 85 per cent of that obtainable with heaters above 0.1 in. diameter.

The fact that no changes of $t_s - t_{sat}$ with various accelerations were observed is understandable. Costello and Tuthill[9] observed that acceleration up to 40 times the local acceleration of gravity produced a maximum change of 4.0 deg F in $t_s - t_{sat}$ at a heat flux of 200,000 Btu/hr-sq ft. That is, the increased acceleration lessened rather than improved the heat-transfer coefficient. The writer believes that with accelerations slightly less than the local acceleration of gravity the heat transfer would improve, but so minutely as to be unobserved in the tests reported here.

When acceleration is reduced, bubbles adhere to the heater and remain near the heater longer. In itself, this would add resistance to heat transfer. However, the fact that the bubble can attain larger size and promote more turbulence near the heater apparently more than compensates for this. Thus there should be some optimum acceleration from the standpoint of heat-transfer behavior at which the net improvement of heat-transfer coefficient is maximized. The data of Merte and Clark[10] and Costello and Tuthill seem to indicate that this acceleration will be somewhat less than the local acceleration of gravity although this is a surmise at present.

Analytic predictions of burnout heat flux are based on cases where the acceleration always has the same orientation with respect to the heater surface over the entire surface. In the case of an accelerating cylindrical surface this is not the case; this would seem especially important since varying the orientation of the acceleration would alter its effect on the stability of the boiling system. Stability criterion have been used extensively in deriving burnout heat-flux correlations.

In view of this, it is interesting to note that the burnout data still agree quite well with the analytic predictions. At the University of Washington, burnout data have been obtained for accelerating cylinders with accelerations from 20 to 40 times the local acceleration of gravity. Considerable work remains to reduce these data, but a preliminary reduction indicates that agreement with the analytic prediction that burnout flux is proportional to acceleration to the one-fourth power will be very good. Thus the authors' data and that obtained at Washington for accelerations above the local acceleration of gravity seem to agree with the analytic prediction of the effect of acceleration despite the fact that the analyses have been carried out on much simpler systems.

The writer congratulates the authors on their efforts and feels that this paper will aid materially in the understanding of the burnout phenomenon and the appraisal of various burnout heat flux correlations.

Authors' Closure

The authors would like to thank Dr. Adelberg and Professors Forster and Costello for their interesting discussions which are a valuable supplement to the paper.

With reference to the correlation constant C, we did not detect any shift in the boiling curve of heat dissipation versus temperature difference for the range of conditions that were studied. These conditions were limited to saturated pool boiling with moderate and high heat fluxes. As mentioned by Professor Costello, the change in $t_s - t_{sat}$ was also found to be small when the gravity field was increased to as much as $40g$. Further in-

[6] Max E. Ellion, "A Study of the Mechanism of Boiling Heat Transfer," Jet Propulsion Laboratory Memorandum No. 20-88, California Institute of Technology, March 1, 1954.

[7] Assistant Professor, Mechanical Engineering, University of Washington, Seattle, Wash. Assoc. Mem. ASME.

[8] L. Bernath, "A Theory of Local Boiling Burnout and Its Application to Existing Data," AIChE paper 110, presented at ASME-AIChE Heat Transfer Conference, Storrs, Conn., August, 1959.

[9] C. P. Costello and W. E. Tuthill, "Effects of Acceleration on Nucleate Pool Boiling," Presented at AIChE-IMIQ Meeting, Mexico City, June, 1960. To appear in AIChE Symposium.

[10] H. Merte, Jr., and J. A. Clark, "Pool Boiling in Accelerating Systems," published in this issue, pp. 233–242.

vestigation with more sensitive instrumentation would be desirable in the low gravity range.

From the present study, some rough computations can be made for the dimensionless group $\Pi = 3R_{max}/gt^2_{max}$, which is the ratio of the dynamic force to the buoyancy force on a bubble. For R_{max} the information in Fig. 6 can be used as an approximation. This gives the bubble diameters, for various gravity fields, at the time of detachment from the surface. Since these are the maximum sizes that the bubbles attain at the surface, we shall use one half of these diameters for R_{max}. Fig. 4 shows the rise of typical bubbles in two gravity fields, and the points of detachment from the surface are given. The authors have additional bubble histories for these gravity fields and for the other gravity fields which were studied in the experiment. We shall define t_{max} as the time from the origination of a bubble to the instant of detachment. The instant at which a bubble was formed could not be determined due to lack of resolution in the high-speed motion pictures, but a rough approximation can be obtained by trying to extrapolate the curves to zero height. This is very crude but still should give values for t_{max} which are not in error by more than a factor of about 2, and hence the Π values should be within an order of magnitude. The comparisons between different gravity fields should be better than this since the sets of data were each treated in the same fashion. Average data for various gravity fields are given in the table:

Fractional gravity g/g_n	R_{max}, in.	t_{max}, sec	Π $3R_{max}/gt^2_{max}$
0.055	0.29	0.32	0.40
0.126	0.22	0.17	0.47
0.282	0.20	0.14	0.28
0.475	0.15	0.067	0.55
1.0	0.12	0.045	0.46

The Π term does not exhibit any definite trend with gravity and remains essentially constant. This results from the large increase in the time scale as g is reduced which offsets the increase in R_{max}/g. It should be mentioned that the approximation of hemispherical bubbles growing radially may be poor for the boiling regime we investigated. Most of the bubbles that were observed were quite irregular during the period while they were attached to the surface.

The experiment proposed by Adelberg and Forster appears to be a good way to compare the shear forces due to forced flow with the buoyancy force. The results would probably be most meaningful for subcooled boiling since the two-phase flow that would result in saturated boiling for negative gravities might be quite different than for zero and positive gravities. For subcooled boiling, the experiment should yield criteria such as the degree of subcooling necessary for boiling to be independent of gravity. For subcooled pool boiling, the removal of heated liquid from the general neighborhood of the surface may be dependent on a free convection circulation since the stirring action of the bubbles is confined to a region close to the heated surface. The free convection will cease for zero gravity, so a small forced circulation may be necessary to keep the liquid subcooled near the surface. We recently saw some motion pictures taken at Wright Field of slightly subcooled boiling in zero gravity. The immersion heater had a large surface area compared with the size of the bubbles formed on it. The bubbles were propelled off the surface a short distance before condensing, so that the dynamic forces must have been large in this instance. The use of subcooled boiling is, of course, limited to applications where cooling is desired, but a net vapor generation is not required.

Professor Costello mentions the errors brought about by using small-diameter heating wires to determine the burnout heat flux. This situation could be aggravated in low gravity fields since in this instance the bubbles are much larger and hence the comparative scale of the wire size is reduced. Also for a heated wire in reduced gravity the bubbles can easily grow completely around the circumference of the wire, which is in contrast to bubbles spreading sidewise over a large surface. It would be very desirable to have experimental data for bubbles growing on large surfaces in low gravity fields.

It is interesting that the experimental results for burnout in high gravity fields also appear to substantiate the analytical predictions for the gravity dependence. The analytical predictions were made before any data were available for gravity fields other than one g. It is satisfying when the predictions of a simplified analysis are later verified by experimental evidence.

Measured Variations in Local Surface Temperatures in Pool Boiling of Water

S. T. HSU
Associate Professor of Mechanical Engineering, University of Wisconsin, Madison, Wis. Mem. ASME

F. W. SCHMIDT
Assistant Professor of Mechanical Engineering, University of Wisconsin, Madison, Wis. Assoc. Mem. ASME

An investigation of the surface-temperature variation during nucleate pool boiling at atmospheric pressure was conducted. The effect of surface temperature, heat flux, and heating-surface material was investigated. The temperature variation of the surface was found by a specially fabricated thermocouple placed in contact with it. The average maximum temperature variation may be found from the following equation:

$$\Delta T_{\text{avg max}} = c[q(f/\alpha)^{1/2}]^{-a} \frac{q\Delta T_{\text{sur-sat}}}{k}$$

The exponent a is a function of surface roughness. The rate of heat flow was denoted by q in Btu/sq ft-hr, α the thermal diffusivity in sq ft/hr, f the frequency of variations in cphr, k the thermal conductivity in Btu/ft-hr-deg F, and $\Delta T_{\text{sur-sat}}$ the temperature difference between the heating surface and the saturation temperature of water. The coefficient c and exponent a were determined experimentally for various heating-surface materials and surface finishes.

In recent years the importance of boiling heat transfer has increased. There are several different types of boiling which occur in boiling heat transfer. However, nucleate boiling, in which bubbles form on the heating surface, is by far the most desirable type for high heat-transfer rates. In order to understand further the phenomena occurring in nucleate boiling, numerous investigations have been made and the results have appeared in recent publications.

A study of the surface-temperature variation caused by bubble formation in nucleate boiling has been made at the University of Wisconsin. In order to accomplish this, experiments were carried out by varying the heating-surface material, the roughness of the surface, and the heat flux, so that their effect on the magnitude of the temperature variation of the heating surface in pool boiling of water at atmospheric pressure could be investigated.

A thermocouple probe consisting of a constantan wire enclosed in a stainless-steel hypodermic needle silver-soldered together at its tip was used to measure the temperature variations of the surface as the heat flux and the surface finish were varied. The signal from the thermocouple was recorded with a Sanborn recorder. The charts from the recorder were analyzed and the magnitude of surface-temperature variations was found.

Although considerable literature is available on the mechanism of bubble formation, the exact history of temperature fluctuation at the surface and its correlation with the heat flux are not yet known. This paper does not give the complete answer to the problem but serves as one phase of the information leading to ultimate solution.

Theoretical Considerations

To obtain an idea of the temperature variation present during the boiling process and to determine the factors which affect these variations, an analysis of the phenomena occurring on the surface was made. In discussing the test-specimen surface, it is necessary to differentiate between the surface directly in contact with the steam and that directly in contact with the liquid. When the bubble was initiated on the surface of the test specimen, the resistance to heat transfer on this heating surface covered by the bubble was caused by the low thermal conductivity of the steam in contact with it. As the bubble grew in size, a temperature difference developed between the bulk of the steam in the bubble and the molecules of the steam in contact with the heating surface. This temperature differential caused a density differential to exist and resulted in the natural convection of the vapor inside the bubble. The size and shape of the bubble formed, as well as the temperature difference present, affected the pattern and magnitude of these convection currents. The film coefficient between the steam and the heating surface and the film coefficient between the heated liquid and the heating surface had to be considered separately when looking at the heat transferred from the test-specimen surface where bubbles were present.

As the bubble continued to grow, not only did the film coefficient between the steam and specimen surface become significant, but the areas affected by this coefficient increased also. Thus a certain temperature pattern, on and below the specimen surface, resulted. This pattern continued to change while the bubble was growing in size. The bubble grew in size on the surface until the conditions were such that it escaped from the surface and rose. As the bubble departed, liquid rushed into contact with the heating surface. The temperature of the liquid directly in contact with the heating surface increased while the temperature of the heating surface decreased at this location. The resistance to heat flow again varied with time as the new thermal boundary layer was being formed. The variation was periodic but the events in each period did not remain the same. The frequency of the bubbles was affected by the liquid convection currents present.

The variation of the temperature on the surface because of the formation of bubbles presented a very complex problem. Essentially, a heat-transfer problem of three-dimensional unsteady-state conduction combined with variable film coefficients was present. The film coefficients were a function of time, frequency, shape, and other factors affecting the bubble growth.

After careful consideration it was decided that the best ap-

Contributed by the Heat Transfer Division of The American Society of Mechanical Engineers and presented at the ASME-AIChE Heat Transfer Conference, Buffalo, N. Y., August 15–17, 1960. Manuscript received at ASME Headquarters, February 15, 1960. Paper No. 60—HT-32.

proach would be to analyze the problem in various steps. Each step would represent a certain bubble size, and the temperature distribution would be determined by using numerical analysis. In this analysis, steady-state conditions were considered to exist in each step. If the steps were taken at small enough intervals the solution would approach the unsteady-state solution. Various assumptions had to be made. The heat flux was assumed to be 50,000 Btu/sq ft-hr and the diameter of the bubble at escape was assumed to be 0.045 in. The bubble was assumed to be hemispherical in shape. It was also assumed that the bubbles formed at a rate of 36 per sec. The period was 0.0278 sec and each bubble remained on the surface 54 per cent of the period. Therefore the bubble was on the surface for 0.015 sec of each period. The radius of the bubble varied with the square root of time. The heating-surface material was stainless steel with a thermal conductivity of $k = 14.4$ Btu/ft-hr-deg F, and a thermal diffusivity of $\alpha = 0.271$ sq ft/hr. The bulk temperature of the water was 210 F and the mean temperature of the heating surface was 220 F. The average film coefficient for the heat transfer between the water and the heating surface was assumed to be 5000 Btu/sq ft-hr-deg F. The average film coefficient between the steam and the heating surface was considered to be 50 Btu/sq ft-hr-deg F. From the boiling curves the film coefficient for steam was estimated at approximately one-one hundredth that of the liquid. Table 1 shows time and bubble diameter for each step.

Table 1 Bubble growth

Step	Time, sec	Bubble diam, in.
1	0.0000	No bubble
2	0.0001	0.003
3	0.0006	0.009
4	0.0017	0.015
5	0.0033	0.021
6	0.0054	0.027
7	0.0081	0.033
8	0.0113	0.039
9	0.0150	0.045

At 0.015 sec the bubble became detached from the heating surface. A square grid of 0.003 in. was selected for the relaxation pattern.

The temperature of the surface after the bubble departed was difficult to determine. As stated previously, the surface was cooled because of its contact with the liquid. An estimate of the surface temperature under the center of the bubble is shown in Fig. 1. Area A above the mean temperature must equal area B which is below the mean.

It can be seen readily that a certain bubble speed and rate of growth were assumed. These assumptions gave physical significance to the calculation even though it was apparent that the only factor changed in the various step analyses was the area covered by the bubble. The frequency of the bubbles was not considered here because steady-state heat flow was assumed for each step. The effect of the frequency of the bubbles on the surface temperature will be presented later.

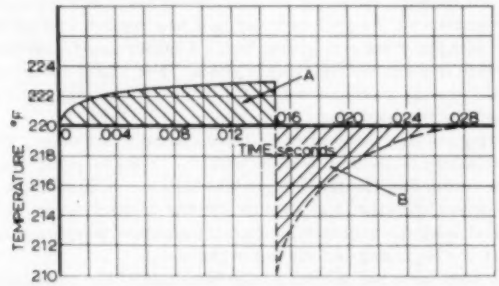

Fig. 1 Surface temperature variation at center of bubble for a complete cycle

In the analysis, only one bubble was considered. It was apparent that other bubbles adjacent to the bubble under consideration had some influence on the surface-temperature variation. As the bubble density increased and the bubbles grew closer together, the temperature of the surface was expected to increase because of the increased resistance to heat flow. This increase in the mean surface temperature did not necessarily mean an increase in the magnitude of the variations present. As the frequency increased, the number of variation cycles per unit time increased, but the amplitude usually became smaller.

Description of Apparatus

Heating Unit. A view of the assembly is shown in Fig. 2. The unit consisted of several pieces of 3-in-diam bar stock of various materials and thicknesses as stated in the following text.

The lower two pieces, composed of stainless steel on the bottom and copper on the top had two holes drilled into them. The center lines of the holes were located at the interface of the copper and the stainless steel. Installed in these holes were two 300-W cartridge heating elements. The heaters were connected in parallel so that the maximum total heat supplied was 600 W. A rheostat was located in the d-c power-supply line making it possible to vary the power supplied and the resulting heat flux. Since the thermal conductivity of the copper is approximately 20 times that of the stainless steel, the largest proportion of the heat from the heaters flows upward. Located directly above the copper was a piece of aluminum. From Fig. 2 it may be seen that three grooves were made on the top and bottom surfaces of the aluminum. These grooves were approximately 0.018 in. square and the two exterior grooves were placed approximately $^3/_8$ in. from the center groove which was located on a diameter of the bar.

Copper-constantan thermocouples were installed in these grooves. The copper and constantan wires, 0.010 in. diam, with their cotton insulation intact, were placed in the grooves from opposite sides and their junctions were silver-soldered. To insure good contact between the thermocouples and the aluminum piece, the sides of the grooves were center-punched to hold the thermocouple firmly. The junctions of the three thermocouples were staggered so that the junction of the center one was located directly at the center of the aluminum bar; the other two junctions were located $^3/_8$ in. on either side of a diameter drawn perpendicular to the grooves. The grooves on the bottom were the same as

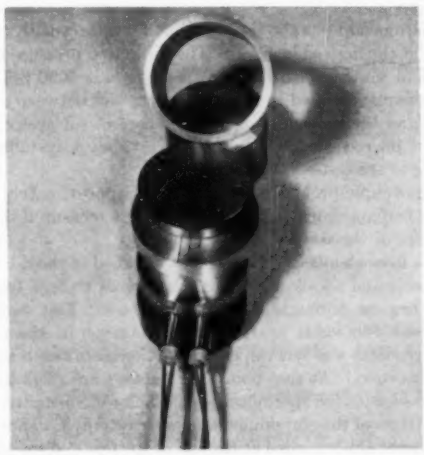

Fig. 2

those on the top but in a direction perpendicular to the top grooves.

By having the temperature drop across the aluminum, the thickness of the aluminum, and the thermal conductivity of the aluminum, the heat flux through the piece may be calculated. The assumption made in this calculation was that at the center section of the aluminum the heat flow in a radial direction is negligible, and the heat may be considered to flow only in an axial direction. Thus the one-dimensional steady-flow heat-transfer equation could be used without appreciable error.

Test Specimen. The test specimen was bolted directly to the aluminum and an aluminum tube was placed around the test specimen. An O-ring was used to seal the space between the aluminum tubing and the test specimen. In this manner a container for the water heated at the bottom with a known heat flux was constructed. The whole unit, excluding the aluminum tubing, was insulated with 2 in. of asbestos to minimize the heat loss in a radial direction, as well as in a downward direction from the stainless steel in which the heaters were partially imbedded.

Thermocouple Probe. A view of the probe is shown in Fig. 3. The probe was constructed by placing a piece of number 30-gage constantan wire, wrapped in cotton insulation, inside a piece of drawn glass. The glass was then inserted into a No. 17 stainless-steel hypodermic needle. The constantan wire and the tip of the hypodermic needle were then silver-soldered together. Care was taken to make this junction as small as possible. However, there was a physical limitation on the size of the junction because the smaller the junction the more easily it may be broken or damaged during use.

Experimental Procedure

Test Specimen. The material to be tested with the appropriate surface finish was installed in the heater assembly, as described previously. Table 2 lists several materials tested, with a description of the surface. The surface of the test material which came in contact with the aluminum plate was finely ground for all the specimens. When the unit was fully assembled, distilled water was added.

Table 2 Test-specimens finishes

Run	Description	RMS, microin.
101-102-103-104	Ground stainless steel	19
108-110-111	Ground stainless steel	104
112-113-114	Polished stainless steel	5.2
115-117-118	Polished aluminum	13
119-120	Ground stainless steel	21

The thermocouple probe was brought in contact with the test specimen at the desired location. The estimated pressure holding the probe in contact with the test specimen was 5000 psi. Such a high pressure was used to insure good contact between the test specimen and thermocouple so that the correct surface temperature could be recorded. The probe was always installed perpendicular to the test-specimen surface.

A thermocouple probe was also installed approximately $^3/_8$ in. above the test specimen. This thermocouple measured the bulk temperature of the water.

Heat-Flux Determination. The rheostat installed in the d-c heater line was adjusted to allow various heat fluxes to flow from the installed heaters through the test specimen. The controlled variable was the value of the current flowing in the circuit. Once the rheostat was set, the unit was allowed to reach an equilibrium condition. At that point, the temperatures indicated by the copper-constantan thermocouples, which were installed at the top and bottom of the aluminum plate, were recorded. These temperatures were also recorded at the end of the test and the average temperature difference across the aluminum was found.

Fig. 3

The heat flow at the center of the aluminum was treated as one-dimensional steady-state flow. The equation for the heat transferred in this case was

$$q = k \frac{\Delta T}{\Delta x} \text{ Btu/sq ft-hr} \qquad (1)$$

Procedure. The distance between the thermocouples ΔX and ΔT is the average temperature difference.

The thermal conductivity of the aluminum was 89.2 Btu/ft-hr-deg F and the distance between the thermocouples was 0.0625 ft. Equation (1) thus reduced to the following form:

$$q = 1428\Delta T \text{ Btu/sq ft-hr} \qquad (2)$$

Recording of Data. Once the system was brought into equilibrium, the temperatures indicated by the probes which were positioned on the test-specimen surface and above the test specimen were found by using a potentiometer. The galvanometer of the potentiometer was not able to dampen completely the variable signal from the surface probe. As a result, some difficulty was incurred in determining the average surface temperature.

The signal from the surface probe was connected to a Kin Tel d-c amplifier and then to the Sanborn recorder. The recorder ran for a 25-sec interval at a paper speed of 5 mm/sec. A zero compensator was used to center the recording wire of the recorder. These charts secured with the Kin Tel amplifier were analyzed for the maximum and minimum surface temperatures.

After the temperature variation during a 25-sec interval was recorded by using a Kin Tel d-c amplifier, a Tektronix preamplifier was connected to the recorder and was run for a 40-sec interval at a paper speed of 25 mm/sec. A higher paper speed was used here to facilitate the chart analysis. For a final check, the recorder was again connected to the Kin Tel amplifier and the charts were recorded again.

During the test, water often had to be added to the unit. The unit was always allowed to come back to a state of equilibrium before continuing the recording. The barometric pressure and the reference-junction temperature for the thermocouples were recorded, with the reference-junction temperature being recorded at both the beginning and the end of the test.

The tests were begun with a high heat flux of the magnitude determined by the maximum current which the heater could withstand (5 amp). In the succeeding tests, the heat flux was

decreased. Tests which were found to be questionable were repeated.

Analysis of Data. From the photographs of the charts, Fig. 4, it may be seen that the variations recorded do not appear to be periodic in nature. These charts were analyzed in two ways: By analyzing a 25-sec interval using the maximum variation method; by analyzing selected 1-sec intervals using the average variation method.

The analysis of the charts by the maximum variation method can be easily seen in Fig. 5. A 25-sec interval of the curve was divided into five periods of 5 sec each. The data recorded for a 5-sec period were:

(a) The frequency of the variation in cycles per second.
(b) The largest uninterrupted temperature variation.
(c) The average of the five largest uninterrupted temperature variations.
(d) The total deflection of the curve.

Averages for the 25-sec interval were determined for (a) frequency, (b) maximum uninterrupted variations, and (c) average five uninterrupted variations. For the 25-sec interval, the largest of the total deflections was recorded.

Because the analysis of the data by the average variation method was very lengthy, only five tests were analyzed. The first second of each 5-sec period was analyzed. Variations less than 0.5 mm corresponding to 0.0923 deg F, were not considered. The frequency and the average variations were found for each second. The average values for the 25-sec interval were found.

In both analyses just described the purpose was twofold: (a) To obtain a method of comparing data for different heat fluxes, surface finishes, and materials; (b) to give some indication of the maximum temperature variation and the frequency at which the variations occurred.

Discussion of Results

Boiling Curve. Upon analyzing the charts in the described manner, the effect of the heating-surface material, the finish of the heating surface, and the heat flux on the surface temperature and its variations were determined. For each surface finish several different runs were made. Each run represented a different location on the heating surface. The roughness of the surface was indicated by the RMS values given in microinches. These values were indicative of the surface finish. On the same surface finish the particular shapes of protrusion and cavities at various locations were not identical. When the probe was held in one location on the surface, the variation recorded was not the variation from one bubble-forming location but the resultant of all the variations induced by the bubble-forming spots surrounding the probe. The number and location of these other bubble-forming spots influenced the magnitude and frequency of the variations indicated by the probe.

Fig. 6 shows the relationship between the heat flux and the temperature of the heating surface minus the saturation temperature of the liquid for the heating surfaces tested. For a constant heat flux the temperature difference required, regardless of surface finish, was less for the stainless-steel heating surface than for the aluminum. The tendency of the aluminum to form an oxide may explain the reason for the higher temperature difference required. The formation of the oxide, called aging, resulted in either a shrinkage of the cavities in the material, or the filling of the cavities with oxide. A higher temperature difference was required in order to reduce the critical radius to a value equal to,

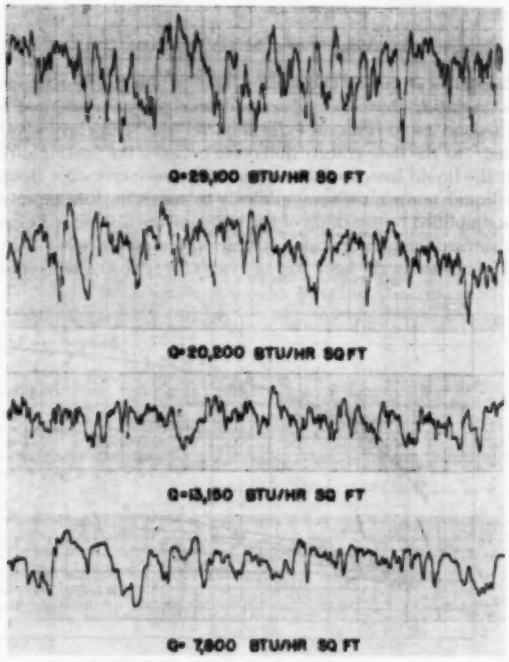

Fig. 4 Recorder charts for run No. 101; ground stainless steel; paper speed 25 mm/sec; RMS 19

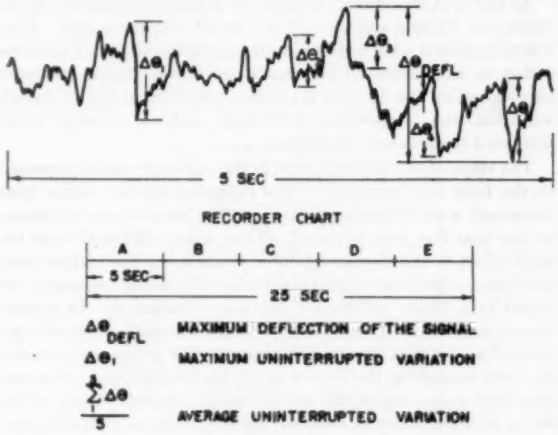

Fig. 5 Maximum variation analysis of recorder chart

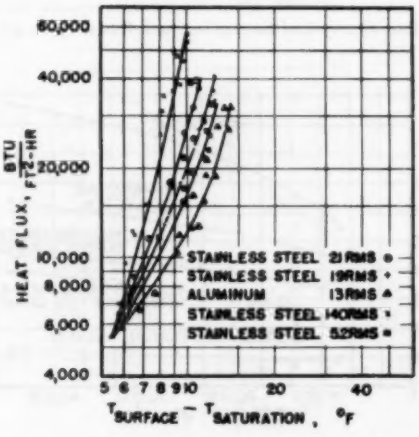

Fig 6 Boiling curves

or less than, the vapor in the cavities, thus enabling the bubbles to form and grow.

For the stainless steel an increase in the surface roughness effectively increased the size of the surface cavities, thereby reducing the surface temperature needed for the formation of bubbles. Any change in the surface of the heating material which altered the size of the cavities and the vapor trapped in them affected the surface temperature required for the formation of bubbles.

Temperature-Variation Data. For each run, the frequency, maximum uninterrupted temperature variation, average maximum uninterrupted temperature variation, and temperature deflection were plotted as a function of heat flux. A representative run is shown in Fig. 7. The general trends of these curves for various surfaces and locations were similar while the magnitude varied greatly. At high heat fluxes the number of bubble-forming locations was so great that a slight variation in the heat flux and a change in the number of locations did not greatly affect the frequency of the temperature variation as indicated by the probe. Consequently, the frequency remained nearly constant at high heat fluxes. As the heat flux was reduced further, a condition was reached wherein the frequency decreased very rapidly. The last of the bubble-forming locations near the probe were disappearing and the only variation present was caused by natural convection currents in the liquid. The frequency of the convection variations was very low. The heat flux at which this transition occurred was easily determined from the curves.

As the heat flux was decreased the temperature difference between the heating surface and the liquid also decreased. This, when combined with a decrease in bubble-forming locations, resulted in a decrease of the maximum uninterrupted temperature variation, the average maximum uninterrupted temperature variation, the temperature deflection, and the average uninterrupted temperature variations.

The slope of the boiling curve in the nucleate region increased as the heat flux increased. This indicated that at higher heat fluxes only a small increase occurred in the temperature difference as the heat flux was increased. This, when combined with the small effect of the increased bubble locations on the surface temperature, as previously mentioned when discussing frequency, resulted in a nearly constant temperature variation. In several runs it was observed that the temperature variation actually decreased as the heat flux was increased. The temperature variation was caused by the departure of the bubbles and the corresponding quenching of the surface by the liquid. With an increase in the number of bubbles, the frequency of variation may increase but the amplitude decreases.

In discussing the influence of surface roughness it was previously pointed out that, as the roughness increased, the temperature difference required for a given heat flux decreased. The increase in roughness also resulted in an increase in the number of bubble-forming nuclei present on the surface. However, the dominant factor influencing the surface-temperature variations was the decrease in temperature difference which resulted in smaller variations for rough surfaces. As the surface became smoother the temperature difference between the heating surface and liquid saturation temperature increased, while the number of bubble-forming locations and the frequency were slightly less. The curves shown in Fig. 8 may be explained in this way. The smallest variation was recorded with the 140-RMS surface. The variation appeared to be independent of the heating-surface material.

The maximum uninterrupted temperature variation, the average maximum uninterrupted temperature variation, the average uninterrupted temperature variation, and the temperature deflection were all influenced by the factors previously discussed. The temperature deflection indicated the difference between the maximum and minimum surface temperature during the runs. The maximum uninterrupted temperature variation indicated the largest uninterrupted temperature variation present while the average maximum uninterrupted temperature variation gave a more accurate indication of the temperature variations present since a large number of uninterrupted temperature variations were considered in determining its value. Because the maximum uninterrupted temperature variation indicated the temperature variation only at one instant it could be quite misleading, for variations of this magnitude might occur only once during the interval investigated while the other variations present were comparatively smaller.

The average uninterrupted temperature variation considered all the variations present but gave no indication of the magnitude of the largest variations occurring. It will be noted that the trend of the average temperature variation and average maximum temperature variation are similar as the heat flux is varied.

A relationship between the average maximum temperature variations and the temperature deflection for all surfaces is shown in Fig. 9. This relationship was expressed in an equation of the form

$$\Delta T_{avg}{}^{var} = 0.515(\Delta T_{defl})^{1.042} \tag{3}$$

Correlation of Data. The various factors affecting the temperature variations have been discussed previously and are now correlated, so as to form an expression for the temperature variations. As the temperature difference between the heating surface and the liquid increased, the variations also increased. Because the liquid temperature was difficult to measure, this expression was simplified by speaking of the temperature difference between the surface temperature and saturation temperature.

An increase in the heat flux had two effects on the temperature

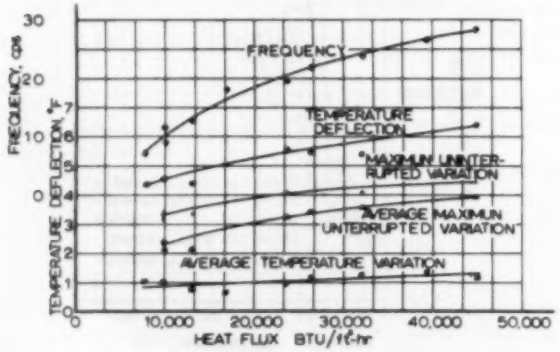

Fig. 7 Chart analysis for stainless steel 19 rms

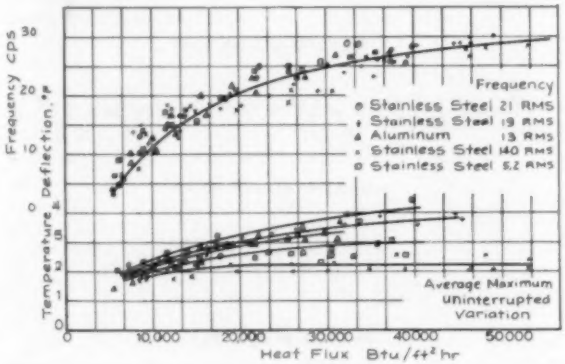

Fig. 8 Composite chart analysis

variations. One was that the temperature gradient in the material increased and caused a higher maximum surface temperature. The second effect was an increase in the film coefficient, resulting in an easier dissipation of heat from the surface to the liquid at the liquid-surface interface and tended to decrease the maximum temperature present. The first effect was the dominating one.

An increase in the thermal conductivity of the material allowed the material to transfer the heat more readily from the high-temperature region. This reduced the maximum surface temperature and thereby decreased the variation.

Since the probe was not located at the exact spot where bubbles were formed, the temperature variation at the probe depended upon the temperature changes at the bubble-forming locations surrounding the probe as discussed previously. The temperature variation was considered to be a function of the distance from the bubble and the temperature-transmitting properties of the material. From a study of periodic temperature change, an increase in the frequency of a signal at the surface decreased the maximum amplitude of the signal transmitted to some internal location. An increase in the thermal diffusivity of the material increased the maximum amplitude transmitted. As the distance was increased the maximum amplitude decreased. The ratio of the frequency and the thermal diffusivity was usually expressed to the one-half power when considering their effect on the temperature variation transmitted. An increase in the heat flux decreased the distance between these bubble-forming locations and the probe and thereby increased the amplitude transmitted. The variation recorded was the summation of all bubble locations. An increase in the heat flux might have resulted in an actual decrease in magnitude of the temperature variations because of the phase relationship of the various signals transmitted to the probe.

By taking these factors into consideration, the following relationship was formed:

$$\Delta T_{\text{avg max}} = c[\gamma(f/\alpha)^{1/2}]^{-a}(q\Delta T_{\text{sur-sat}}/k) \qquad (4)$$

A plot of

$$\frac{\Delta T_{\text{avg-max}}/k}{q\Delta T_{\text{sur-sat}}} \text{ versus } q(f/\alpha)^{1/2}$$

was made on logarithmic paper to determine the various constants. The curves for the various surfaces are shown in Fig. 10. A list of the appropriate coefficients and exponents is given in Table 3.

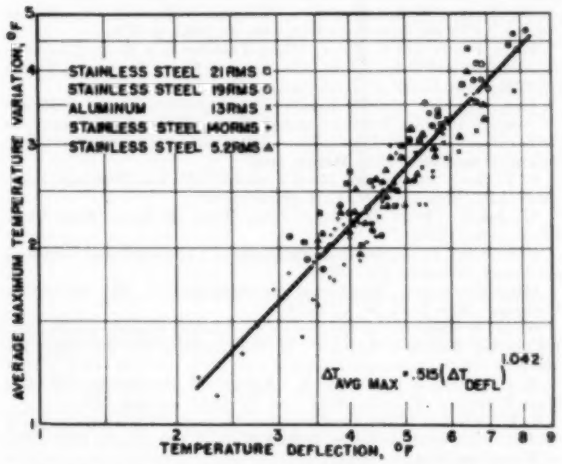
AVERAGE MAXIMUM TEMPERATURE VARIATION, °F
STAINLESS STEEL 21 RMS
STAINLESS STEEL 19 RMS
ALUMINUM 13 RMS
STAINLESS STEEL 140 RMS
STAINLESS STEEL 5.2 RMS
$\Delta T_{AVG\ MAX} = .515(\Delta T_{DEFL})^{1.042}$
TEMPERATURE DEFLECTION, °F

Fig. 9 Composite relationship between temperature deflection and average maximum temperature variation

Table 3 Coefficients and exponents for equation (4)

Surface description	a	c
Aluminum 13 RMS	0.706	41.2
Stainless steel 5.2 RMS	1.030	297.6
Stainless steel 19 RMS	0.630	5.865
Stainless steel 21 RMS	0.688	16.44
Stainless steel 140 RMS	0.920	484.6

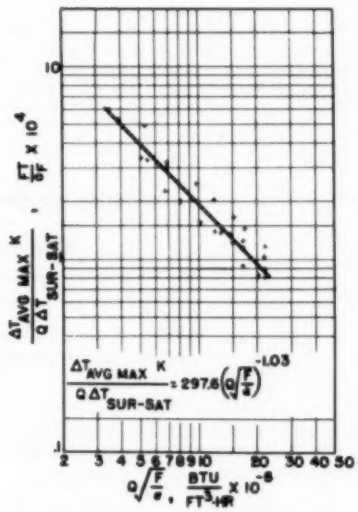

Fig. 10 Correlation of data for stainless steel 5.2 rms

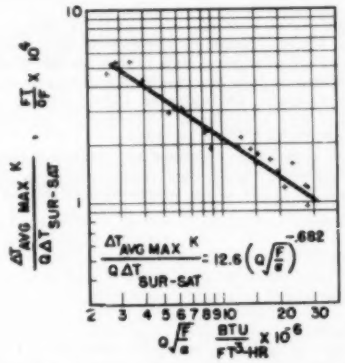

Fig. 11 Correlation of data for stainless steel 19 rms

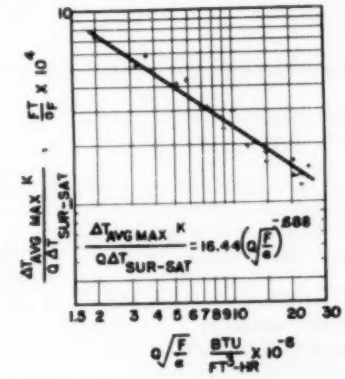

Fig. 12 Correlation of data for stainless steel 21 rms

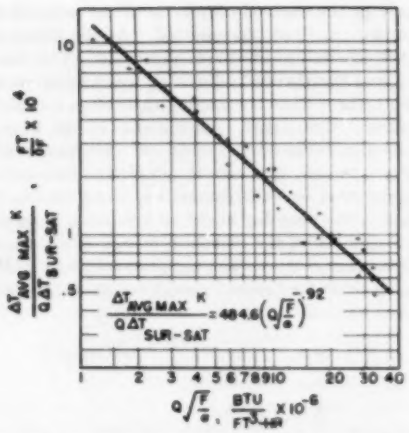
10
1
.5
1 2 3 4 5 6 7 8 9 10 20 30 40
$\frac{\Delta T_{AVG\ MAX}}{Q\Delta T_{SUR-SAT}}$, $\frac{FT}{Qf}$ x 10^4
$\frac{\Delta T_{AVG\ MAX}}{Q\Delta T_{SUR-SAT}} = 484.6\left(Q\sqrt{\frac{F}{\sigma}}\right)^{-.92}$
$Q\sqrt{\frac{F}{\sigma}}$, $\frac{BTU}{FT^3\text{-}HR}$ x 10^{-6}

Fig. 13 Correlation of data for stainless steel 140 rms

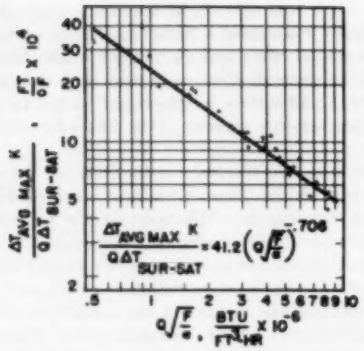

Fig. 14 Correlation of data for aluminum 13 rms

Conclusions

The foregoing findings have been observed from the experimentations: The surface temperature of the heating surface varied during nucleate boiling. The amplitude and frequency of variations were principally functions of the heat flux and the surface finish.

Bibliography

S. G. Bankoff, "Ebullition From Solid Surfaces in the Absence of a Pre-Existing Gaseous Phase," TRANS. ASME, vol. 73, 1957, pp. 735–740.

S. G. Bankoff, W. J. Colahan, Jr., and D. R. Bartz, "Summary of Conference on Bubble Dynamics and Boiling Heat Transfer Held at the Jet Propulsion Laboratory, June 14 and 15, 1956," Jet Propulsion Laboratory, Memorandum No. 20-137, California Institute of Technology, Pasadena, Calif., December 10, 1956.

H. S. Carslaw and J. C. Jaeger, "Conduction of Heat in Solids," Clarendon Press, Oxford, England, 1959.

C. Corty and A. S. Faust, "Surface Variables in Nucleate Boiling," *Chemical Engineering Progress Symposium*, series 51, 1955, pp. 1–12.

M. E. Ellion, "A Study of the Mechanism of Boiling Heat Transfer," Jet Propulsion Laboratory, Memorandum No. 20-88, California Institute of Technology, Pasadena, Calif., March 1, 1954.

E. A. Farber and R. L. Scorah, "Heat Transfer to Water Boiling Under Pressure," TRANS. ASME, vol. 79, 1948, pp. 369–384.

W. Firts, "Berechnung Des Maximal Volumens von Dampfblasen," *Physikalische Zeitschrift*, vol. 36, 1935, p. 379.

K. E. Foster and R. Greif, "Heat Transfer to a Boiling Liquid—Mechanism and Correlations," JOURNAL OF HEAT TRANSFER, TRANS. ASME, Series C, vol. 81, 1959, pp. 43–53.

F. C. Gunther and F. Kreith, "Photographic Study of Bubble Formation in Heat Transfer to Sub-Cooled Water," Jet Propulsion Laboratory, Progress Report No. 4-120, California Institute of Technology, Pasadena, Calif., March, 1950.

S. T. Hsu, "Engineering Heat Transfer," D. Van Nostrand Company, Inc., New York, N. Y., in publication.

M. Jakob, "Heat Transfer," John Wiley & Sons, New York, N. Y., vol. 1, 1949.

F. Kreith, "Principles of Heat Transfer," International Textbook Company, Scranton, Pa., 1959.

Milne-Thomson, "Theoretical Hydrodynamics," The Macmillan Company, New York, N. Y., 1955.

W. M. Rohsenow, "A Method of Correlating Heat-Transfer Data for Surface Boiling of Liquids," TRANS. ASME, vol. 74, 1952, pp. 969–976.

W. Rohsenow and J. A. Clark, "A Study of Mechanism of Boiling Heat Transfer," TRANS. ASME, vol. 73, 1951, pp. 604–620.

F. W. Schmidt, "The Predicted and Measured Variations in Local Surface Temperatures Under Boiling Water," PhD thesis, University of Wisconsin, August, 1959.

Natural-Circulation Tests With Water at 800 to 2000 Psia Under Nonboiling, Local Boiling, and Bulk Boiling Conditions[1]

O. J. MENDLER

A. S. RATHBUN
Assoc. Mem. ASME

N. E. VAN HUFF

A. WEISS
Assoc. Mem. ASME

Bettis Atomic Power Laboratory,
Westinghouse Electric Corporation,
Pittsburgh, Pa.

Natural and forced-circulation test data for a closed-loop system are presented and analyzed. The data were obtained at pressures of 800, 1200, 1600, and 2000 psia from the natural-circulation loop at the Bettis Laboratory, using single rectangular channel test sections (0.100 in. × 1.0 in. × 27.0 in. long, 0.200 in. × 1.0 in. × 27.0 in. long, and 0.250 in. × 1.0 in. × 27.0 in. long). Heat fluxes ranged from 50,000 Btu/hr-sq ft to burnout with inlet subcoolings of 20, 70, and 100 deg F. The results showed that single and two-phase pressure drop, burnout heat flux, and riser density measured under natural-circulation operation are no different from those measured with forced circulation at the same thermal and fluid flow conditions. For the loop studied, it was shown that natural-circulation-loop flow rates can be predicted to within 10 per cent for both single and two-phase flow. Some data for slip ratios at liquid velocities less than ½ fps and for two-phase exit losses were obtained. Flow fluctuations were noted during some of the natural-circulation runs; these occurred before burnout heat flux was reached. In some instances these fluctuations were severe enough to cause a premature burnout.

Introduction

In the design of a water-cooled and moderated, natural-circulation reactor plant, one of the most important problems is the accurate prediction of the circulation rate of the main coolant stream. If boiling occurs in some parts of the reactor core, the problem is complicated further because of the uncertainty in predicting pressure drop in two-phase flow, and the possibility of the occurrence of flow oscillations under certain operating conditions. Since a considerable amount of pressure drop and heat-transfer burnout information obtained under forced-circulation conditions already was available, it was considered desirable to demonstrate that these data were applicable to natural-circulation conditions.

Thus tests were run at the Bettis Atomic Power Laboratory on a natural-circulation closed loop operating with water at high pressures. It is the purpose of this paper to report the results of this study performed with the following specific objectives:

1 To compare experimental natural-circulation-loop flow rates with predicted flow rates.

[1] LEGAL NOTICE: This report was prepared as an account of Government sponsored work. Neither the United States (nor the United States Navy, nor the Commission), as dictated by governing contracts, nor any person acting on behalf of these agencies:

(*a*) Makes any warranty or representation, expressed or implied, with respect to the accuracy, completeness, or usefulness of the information contained in this report, or that the use of any information, apparatus, method, or process disclosed in this report may not infringe privately owned rights; or

(*b*) Assumes any liabilities with respect to the use of, or for damages resulting from the use of any information, apparatus, method, or process disclosed in this report.

As used in the above, "person acting on behalf of these agencies" includes any employee or contractor of these agencies to the extent that such employee or contractor prepares, handles or distributes, or provides access to, any information pursuant to his employment or contract with the (United States Navy or the Commission).

Contributed by the Heat Transfer Division of The American Society of Mechanical Engineers and presented at the ASME-AIChE Heat Transfer Conference, Buffalo, N. Y., August 15–17, 1960. Manuscript received at ASME Headquarters, June 2, 1960. Paper No. 60—HT-36.

Nomenclature

A = area, sq ft

D_e = hydraulic equivalent diam, ft

f = friction factor

G = mass velocity, lb/hr-sq ft

g = acceleration due to gravity, ft/hr²

h = heat-transfer coefficient, Btu/hr-sq ft-deg F, calculated from Dittus-Boelter correlation, $h = 0.023 \frac{k_B}{D_e} (\mathrm{Re})_B^{0.8} (\mathrm{Pr})_B^{0.4}$

k = thermal conductivity of fluid, Btu/hr-ft-deg F

ΔP = pressure drop, psf

P = system pressure, psi

R_v = void fraction, cu ft steam/cu ft mixture

T = temperature, deg F

ΔT_f = film temperature difference, deg F, $T_w - T_B = \Delta T_f = \phi/h$

ΔT_{in} = inlet subcooling, deg F, $T_{sat} - T_{in}$

V = velocity, fph

v = specific volume, cu ft/lb

$\bar{v}$ = mean specific volume of two-phase fluid mixture assuming homogeneous flow, cu ft/lb, $\bar{v} = v_f + x v_{fg}$

W = flow rate, lb/hr

x = quality, lb flowing steam/lb flowing mixture

z = distance in direction of flow, ft

ρ = density, pcf

ϕ_{Lo}^2 = Martinelli-Nelson two-phase friction parameter

ϕ = heat flux, Btu/hr-sq ft

μ = viscosity, lb/hr-ft

(Continued on next page)

2 To compare natural-circulation pressure drop, riser density, and heat-transfer burnout data with corresponding forced-circulation data.

3 To obtain information about two-phase exit losses and steam-water slip ratios at low water velocities.

Circulation rates in natural-circulation loops operating at high pressure have been studied previously with particular application to the boiler industry. Simply stated, for a given heat input and heat extraction, the loop flow will be that value where the frictional and accelerational losses around the loop are equal to the difference in the elevation head between the hot and cold portions (legs) of the loop

$$\sum_{\text{loop}} (\Delta P_{\text{elev}}) + \sum_{\text{loop}} (\Delta P_{\text{acc}}) + \sum_{\text{loop}} (\Delta P_{fr}) = 0 \qquad (1)$$

Lewis and Robertson [1],[1] Markson, Ravese, and Humphreys [2], Davis [3], and Kutateladze [4] have presented solutions to equation (1). However, each of these solutions was based on a number of simplifying assumptions, principally in the methods of estimating the various pressure drops in two-phase flow. The transient behavior of a closed natural-circulation loop operating near atmospheric pressure has been studied at the University of Minnesota [5, 6]. Here again, assumptions concerning the pressure drop components were necessary.

Actual comparisons between measured and predicted circulation rates have been very limited. Rowand [7] in a discussion of reference [2] presented such a comparison of flow rates based on a circulation test conducted on an open-pass type boiler, operating at 1350 psia. Lottes, et al. [8] also presented comparisons for an open loop natural-circulation boiling water reactor.

Description of Apparatus

Fig. 1 shows the heated test section and natural circulation loop. The main loop piping was fabricated from schedule 80 type 304 stainless steel, and was in the shape of a vertical rectangle 14.5 ft high and 15 ft long. Heat was added uniformly to the lower part of the left vertical leg through an electrically heated rectangular channel test section. Details of the test-section inlet and exit geometry are also shown in Fig. 1. The test section was connected to a riser made from 2-in. pipe; the other vertical leg is the downcomer and was made from $1^1/_2$-in. pipe. The top horizontal leg consisted of a double pipe heat exchanger and by-pass line in parallel; the bottom horizontal leg contained a 0.340-in-diam-orifice and a preheater. The flanged connections were sealed with Flexitallic gaskets. The loop auxiliaries consisted of a resin-bed ion exchanger and a pressurizer which were the same as those described in references [9, 10, 11]. A Westinghouse model 30A canned-rotor centrifugal pump was connected across a gate valve on the bottom horizontal leg. This pump was used during degassing and deionizing of the water and during forced-circulation tests.

The rectangular test sections were 27 in. long and 1 in. wide and were fabricated of type 304 stainless steel. The nominal spacings were 0.100 in., 0.200 in., and 0.250 in. The actual channel spacings deviated slightly from these nominal values and are listed in Table 5. Each test section had two pressure taps, spaced at 20 in. or 22 in., for measuring over-all pressure drop. A detailed description of the d-c power supply and the details of the test sections are found in references [9, 10, 11]. The test-section channels had surface finishes of 20 microin. (rms) or less and were considered hydraulically smooth. Pressure taps were located at various points around the loop; see Fig. 1.

Test Procedure

The test procedures, instrumentation control, experimental errors, and method of determining the burnout heat flux are discussed in detail in references [12 and 13] and were essentially the same as those discussed in references [10 and 11].

The loop was filled with demineralized water, degassed and deionized until a resistivity of a 1 megohm-cm and an O_2 content of 0.2 cc/kg were reached. The accuracy of the test section and loop instrumentation was confirmed by performing a series of runs during which the inlet and exit thermocouples of the test section were calibrated, and isothermal pressure-drop measurements across the test-section pressure taps were obtained. The average channel spacing was then determined from the isothermal pressure-drop data by selecting a channel spacing that made the measured friction factor coincide with the smooth Moody curve. (The measured channel spacing agreed with these values to within 1 to 2 mils.)

To determine flow instabilities, transducers were mounted across the orifice plate (see Fig. 1, taps 4 and 5) and the pressure taps of the test section (taps 1 and 2), and their output was recorded on a Sanborn recorder. The pressure differences were also read on U-tube manometers filled with CCl_4. These manometers were used as a measure of flow and test-section pressure drop.

[1] Numbers in brackets designate References at end of paper.

Table 1 Natural-circulation runs

Nominal test-section size	Values of inlet subcooling, ΔT_{in}, deg F 800 psia	1200 psia	1600 psia	2000 psia
0.100 in. × 1 in. × 27 in.	...	109	...	...
0.200 in. × 1 in. × 27 in.	20[a], 70[a]	20[a], 70[a], 109	20, 70[a], 109	70, 109
0.250 in. × 1 in. × 27 in.	20, 70, 109	20, 70, 109	20, 70	...

[a] Duplicated with forced circulation.

Nomenclature

Subscripts

acc = acceleration
B = evaluated at bulk-fluid temperature
BB = bulk boiling
BO = burnout
calc = calculated
cl = cold leg
elev = elevation
ent = entrance
ex = exit
exp = experimental
fr = friction
f = saturated liquid; film
fg = difference between saturated-liquid and saturated-vapor properties
g = saturated vapor
hl = hot leg
hx = heat exchanger
in = inlet
iso = isothermal
LB = local boiling
M-N = Martinelli and Nelson
p = pipe
r = riser
sat = at saturation conditions
T = total
TP = two-phase flow
ts = test section
w = wall

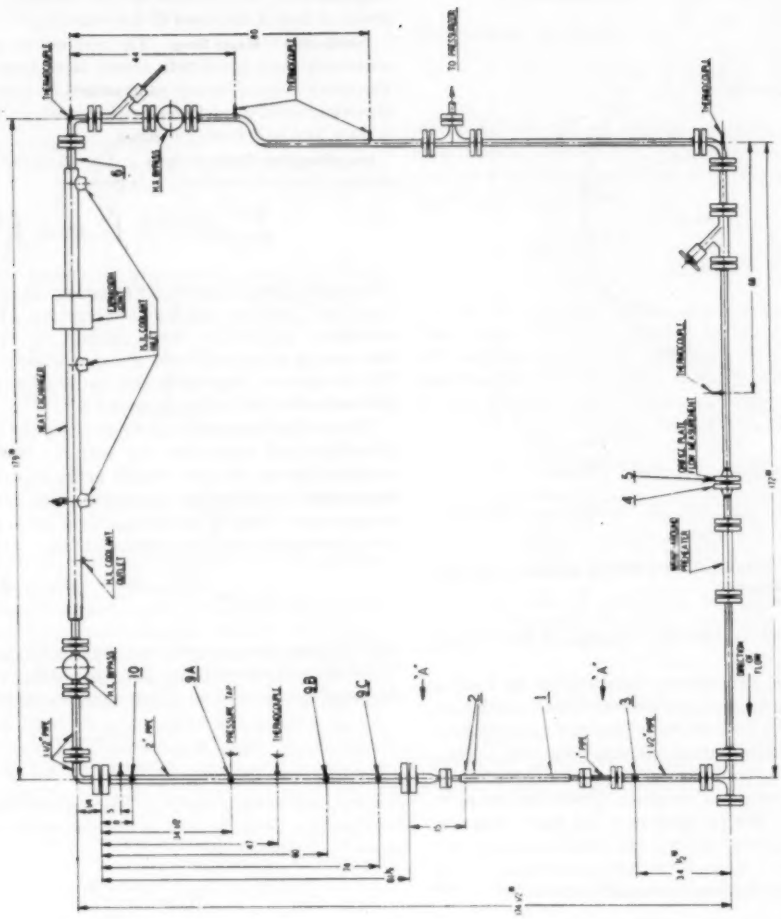

Fig. 1 Battis natural circulation loop

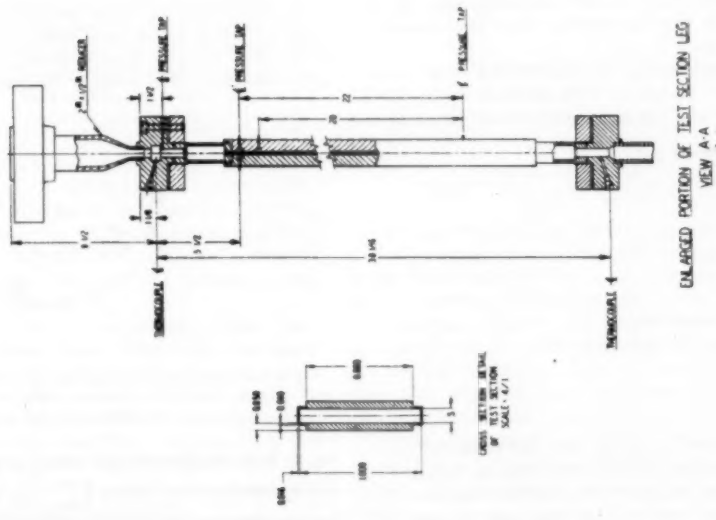

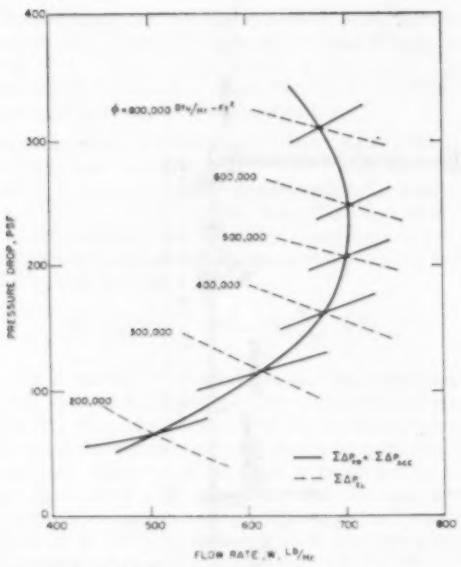

Fig. 2 Prediction of flow circulation for 0.210 in. channel, 1200 psia pressure, 109 deg F inlet subcooling

The transducers were used only for the indication of flow fluctuations.

The natural-circulation experiments were started by heating the loop to the required inlet temperature with forced circulation, using the test section as a heat source. After the required inlet temperature had been reached, the pump was turned off. Then, natural-circulation, steady-state conditions were established at test section heat-flux increments of about 50,000 Btu/hr-sq ft until burnout occurred. During these runs the water temperature was essentially constant between the heat-exchanger exit and the test-section inlet. Some of the natural-circulation runs were duplicated under forced-circulation conditions.

Calculation of Loop-Circulation Rates

For given conditions of static pressure, test-section inlet temperature and heat flux, equation (1) is solved for the loop flow at which the elevation head balances the loop resistance. It was found convenient to do this by plotting these two quantities against flow rate, Fig. 2.

Preliminary calculations indicated that pressure drops across only certain of the loop components were significant; the others were considered negligible. The significant pressure drops were:

(a) Elevation Pressure Drops

1 Test section.
2 Riser.
3 Downcomer.

(b) Frictional Pressure Drop

1 Test section.

(c) Acceleration and Form Losses

1 Inlet and exit plenum of the test section.
2 Orifice.
3 Loop acceleration.
4 Test section.

All of the foregoing losses except the elevation pressure drop in the riser and the inlet and exit plenum form losses in the test section were calculated from available data and correlations. Experimental pressure drops were used for these cases because correlations were not available for their prediction. Each significant pressure drop is discussed in the following.

Test-Section Pressure Drop. The test-section pressure drops were measured (and predicted) across taps 1 and 2, Fig. 1. The methods of prediction are summarized in Appendix 2 and include elevation, friction, and acceleration losses in the nonboiling, local boiling, and bulk boiling regimes.

Loop-Elevation Pressure Drop. The elevation term, or thermal driving head, of equation (1) is given by

$$\sum_{\text{loop}} (\Delta P_{\text{elev}}) = \int_{0}^{L}_{cl} \rho dz - \int_{0}^{L}_{hl} \rho dz \tag{2}$$

The single-phase densities for equation (2) are determined from the system pressure and fluid temperature. The densities in the two-phase regions are more difficult to evaluate because of the varying slip ratios (ratio of vapor velocity to fluid velocity). The two-phase densities in the test section were calculated by the methods described in Appendix 2.

Most of the elevation head difference in the loop was due to the 2-in-diam riser above the test section. Since few data were available for the effective density in the region where low velocities existed (0.1 to 0.5 fps) the experimental values of the effective density were used in predicting loop flow rates. The effective riser density could be calculated from

$$\bar{\rho}_{\text{riser}} = \frac{\Delta P_{\text{measured}} - \Delta P_{fr} - \Delta P_{\text{acc}}}{L} \tag{3}$$

where L is the distance corresponding to $\Delta P_{\text{measured}}$.

Calculations showed that ΔP_{fr} and ΔP_{acc} were negligible for the conditions of the test. Thus equation (3) reduced to

$$\bar{\rho}_{\text{riser}} = \frac{\Delta P_{\text{measured}}}{L} \tag{4}$$

and was used in equation (2). This value of $\bar{\rho}_{\text{riser}}$, together with the quality x, could be used to calculate void fractions R_g or slip ratios V_g/V_f as follows:

$$R_g = \frac{\rho_f - \bar{\rho}_{\text{riser}}}{\rho_{fg}} \tag{5}$$

$$\frac{V_g}{V_f} = \frac{\rho_f}{\rho_g}\left(\frac{x}{1-x}\right)\left(\frac{1-R_g}{R_g}\right) \tag{6}$$

Typical values of slip ratios are shown in Fig. 3 for runs with a 0.100-in. and 0.200-in. test section at 1200 psia. This figure shows that the slip ratio increases markedly with decreasing water velocity. This trend is confirmed by reference [16].

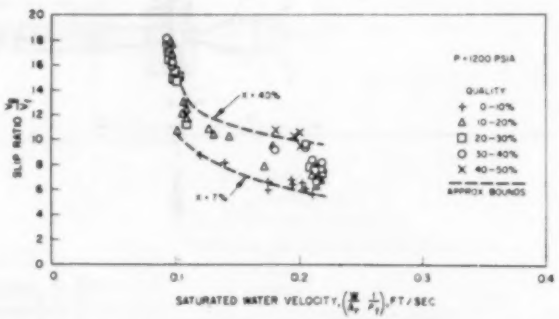

Fig. 3 Ratio of steam-to-water velocity in a 2-in-diam riser as a function of saturated water velocity $\left(\frac{WT}{A_T}\frac{1}{\rho_f}\right)$; channel spacings of test section preceding riser are: 0.101 in. and 0.210 in.

Loop-Acceleration Pressure Drop. A summation of the acceleration pressure drops due to area and density changes around the loop results in

$$\sum_{\text{loop}} \Delta P_{\text{acc}} = \frac{W^2}{2gA_{\text{ts}}^2}\left[\chi_{\text{ts-ex}} - \chi_{\text{sl}}\right]\left[1 - \left(\frac{A_{\text{ts}}}{A_{\text{hx}}}\right)\right]^2 \quad (7)$$

This equation is derived in Appendix 1.

Orifice Loss. The pressure drop for the loop orifice is given by

$$\Delta P = \frac{K}{2gA_p^2}\frac{W^2}{\rho_{cl}} = 0.008\,\frac{W^2}{\rho_{cl}} \quad (8)$$

(There was negligible pressure-drop recovery downstream from the orifice since the ratio of orifice to pipe diameter was small.)

Test-Section-Entrance Flange Loss. The loss from taps 1–3 across the entrance flange (Fig. 1) is given by

$$\Delta P_{\text{ent}} = \frac{K_{\text{ent}}\,W^2}{2g\,\rho_{cl}A_{\text{ts}}^2} \quad (9)$$

where K_{ent} is defined as

$$K_{\text{ent}} = A_{\text{ts}}^2\sum_{i}^{m}\frac{K_i}{A_i^2} + A_{\text{ts}}^2\sum_{i}^{n}\frac{f\,L_i}{D_{ei}\,A_i^2} \quad (10)$$

where K_i values, the single-phase expansion, and contraction losses, are taken from reference [14].

Table 2 lists the calculated and measured values of K_{ent} for two test sections. The measured value for the 0.200-in. test section was determined from isothermal runs. The large discrepancy between the calculated and measured value for the 0.200-in. channel was due to an inlet-temperature thermocouple which partially blocked the channel inlet. The measured values were used in calculating loop-circulation rates for this channel. No measured value was available for the 0.100-in. channel and the calculated value was used.

Table 2 Values of K_{ent}

Test-section spacing, in.	K_{ent} Calculated	Measured
0.100	0.8	...
0.200	2.1	3.8

Test-Section-Exit Flange Loss. The pressure drop across the test-section-exit flange (taps 2–9C) was measured during single and two-phase flow for all tests except those with the 0.100-in. test section. The measured value was used in predicting the loop-circulation rates. For predicting circulation rates with the 0.100 in. channel, a procedure was developed for estimating the pressure drop across the exit flange. This procedure may also be used for predicting two-phase exit losses in the absence of specific experimental data.

Two reports [15, 16] described the results of studies conducted at Argonne National Laboratory on the flow of air-water mixtures through contractions and expansions at pressures near atmospheric. The results in reference [15] were for horizontal flow, and include data on pressure drops as well as upstream and downstream densities. The results in reference [16] were for vertical flow, but include no pressure drop data.

The pressure drop across the test-section-exit flange (taps 2–9C) is made up of elevation losses, acceleration losses caused by changes in density and velocity, and a residual unrecoverable form or friction loss. The elevation and acceleration loss could be estimated but no method for predicting the unrecoverable two-phase form or friction loss was available. Thus an empirical correlation for these two-phase exit losses was developed from the measured total pressure drop across tap 2–9C and from the formulas for the elevation and acceleration losses:

$$\Delta P_{\text{form-exit}} = [\Delta P_{\text{meas}} - \Delta P_{\text{elev}} - \Delta P_{\text{acc}}]_{2\text{-}9C} \quad (11)$$

The elevation loss is given by

$$\Delta P_{\text{elev}} = \rho_{\text{ts}}\,\Delta z_2 + \rho_r\,\Delta z_3 + \int_{\text{tap 2}}^{\text{ts exit}}\rho_{\text{ts}}\,dz \quad (12)$$

where Δz_2 and Δz_3 are lengths associated with test section and riser density, respectively. The acceleration loss for a simultaneous change in density and velocity is given by equation (13) (see Appendix 1 for derivation).

$$\Delta P_{\text{acc}} = \frac{W^2}{2g}\left[\frac{1}{A_r} + \frac{1}{A_{\text{ts}}}\right]\left[\frac{\chi_r}{A_r} - \frac{\chi_{\text{ts}}}{A_{\text{ts}}}\right] \quad (13)$$

The form loss data, $\Delta P_{\text{form-exit}}$, was expressed in terms of a single-phase coefficient similar to the form of equation (9). The single-phase exit loss coefficient, K_{exit}, was calculated from equation (10) for the 0.100-in. channel. This was considered valid because there was good agreement between the measured and calculated K_{exit} values for the 0.200 in. channel, Table 3.

Table 3 Values of K_{exit} (single phase)

Test-section spacing, in.	K_{exit} Calculated	Measured
0.100	1.2	...
0.200	2.9	3.2

Four methods of correlating two-phase exit losses were examined. The first, equation (14), used the Martinelli-Nelson density:

$$\Delta P_{\text{form-exit}} = \frac{\rho_f}{\rho_{\text{M-N}}}\left(\frac{K_{\text{exit}}}{\rho_f A_{\text{ts}}^2}\,\frac{W^2}{2g}\right) \quad (14)$$

The second, equation (15), was based on the Martinelli-Nelson two-phase friction multiplier:

$$\Delta P_{\text{form-exit}} = \phi_{Lo}^2\left(\frac{K_{\text{exit}}}{\rho_f A_{\text{ts}}^2}\,\frac{W^2}{2g}\right) \quad (15)$$

The third, equation (16), used the fog-flow model density:

$$\Delta P_{\text{form-exit}} = \left(1 + \frac{x v_{fg}}{v_f}\right)\left(\frac{K_{\text{exit}}}{\rho_f A_{\text{ts}}^2}\,\frac{W^2}{2g}\right) \quad (16)$$

The fourth, equation (17), defined an experimental two-phase exit-loss coefficient:

$$\Delta P_{\text{form-exit}} = \frac{K_{\text{TPexit}}}{K_{\text{exit}}}\left(\frac{K_{\text{exit}}}{\rho_f A_{\text{ts}}^2}\,\frac{W^2}{2g}\right) \quad (17)$$

Equations (14, (15), (16), and (17) may be expressed as

$$\Delta P_{\text{form-exit}} = \beta\left(\frac{K_{\text{exit}}}{\rho_f A_{\text{ts}}^2}\,\frac{W^2}{2g}\right) \quad (18)$$

where K_{exit} is the single-phase exit-loss coefficient and β is a function of quality and pressure. The four methods are compared in Fig. 4 as a plot of β versus quality at 1200 psia. Equation (14) predicts values of exit pressure loss which are too low, equation (15) predicts values of exit pressure loss which are too high, and equation (16) predicts values which are reasonably close to, but slightly higher than the experimental values given by equation (17). Fig. 4(*a*) shows the agreement between the experimental and predicted β-values (fog-flow model) at 800, 1200, and 1600 psia. Equation (17), with K_{exit} of 1.2 and 3.2 for the 0.100-in. and 0.200-in. channels, respectively, was used in the flow prediction. In the absence of any data, equation (16) could be used.

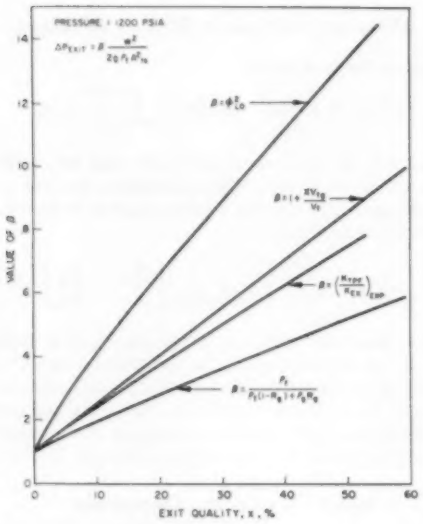

Fig. 4 Comparison of four methods for calculating two-phase pressure losses (not including acceleration)

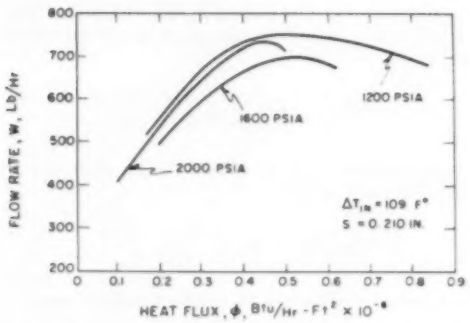

Fig. 5 Natural circulation flow rate as a function of heat flux (different pressures, same inlet subcooling)

Experimental Results

Loop-Circulation Rates. The effects of heat flux, inlet subcooling, channel spacing, and pressure on natural-circulation flow rates are shown in Figs. 5, 6, and 7. These trends are a result of the relative magnitudes of the component pressure drops.

The comparison between measured and predicted flow rates is shown in Fig. 7. Three calculated flow rates are shown; these three flow rates are based on calculating the test-section exit loss by the use of equations (14), (15), and (17). The results of this comparison are consistent with the discussion of the various methods for predicting test-section-exit flange losses. The predicted flow is within 5 per cent of the experimental flow under nonboiling conditions, but diverges as boiling begins. All three methods predict the trend of the flow-flux curve but vary markedly in accuracy of prediction. The use of equation (14) predicts flows up to 20 per cent too high and the use of equation (15) predicts flows up to 15 per cent too low in the boiling region. The use of equation (17) gives excellent agreement for both channel sizes with errors less than 5 per cent for all qualities. This agreement is expected for the 0.200-in. channel; the 0.100-in. results, however, show that the experimental β-values give good results for other channel sizes.

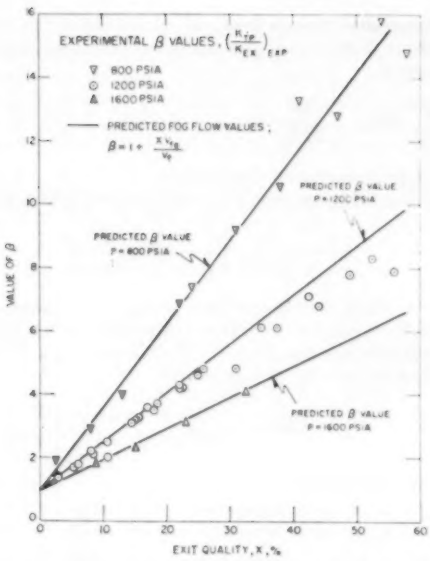
EXPERIMENTAL β VALUES, (H_TP/H_EX)_EXP
800 PSIA
1200 PSIA
1600 PSIA
PREDICTED FOG FLOW VALUES;
PREDICTED β VALUE P = 1200 PSIA
PREDICTED β VALUE P = 800 PSIA
PREDICTED β VALUE P = 1600 PSIA
VALUE OF β
EXIT QUALITY, x, %

Fig. 4(a) Comparison of experimental and predicted (fog flow) β-values; $S = 0.210$ in.

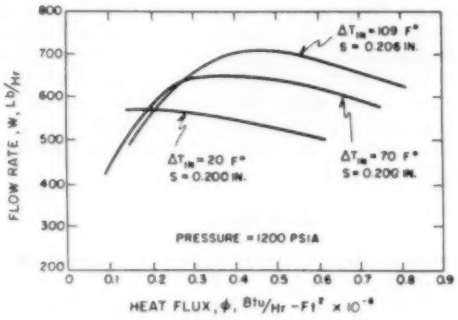

Fig. 6 Natural circulation flow rate as a function of heat flux (different inlet subcooling, same pressure)

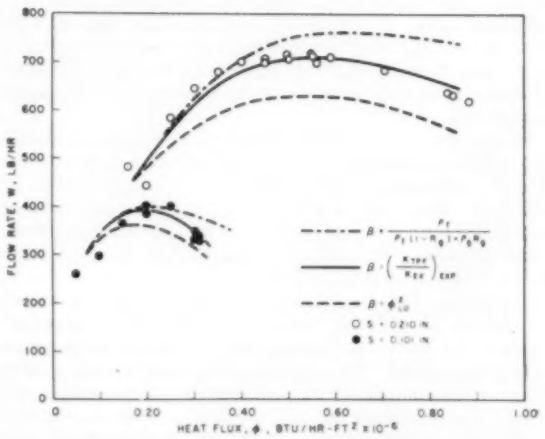

Fig. 7 Comparison of three methods for predicting flow circulation; $P = 1200$ psia

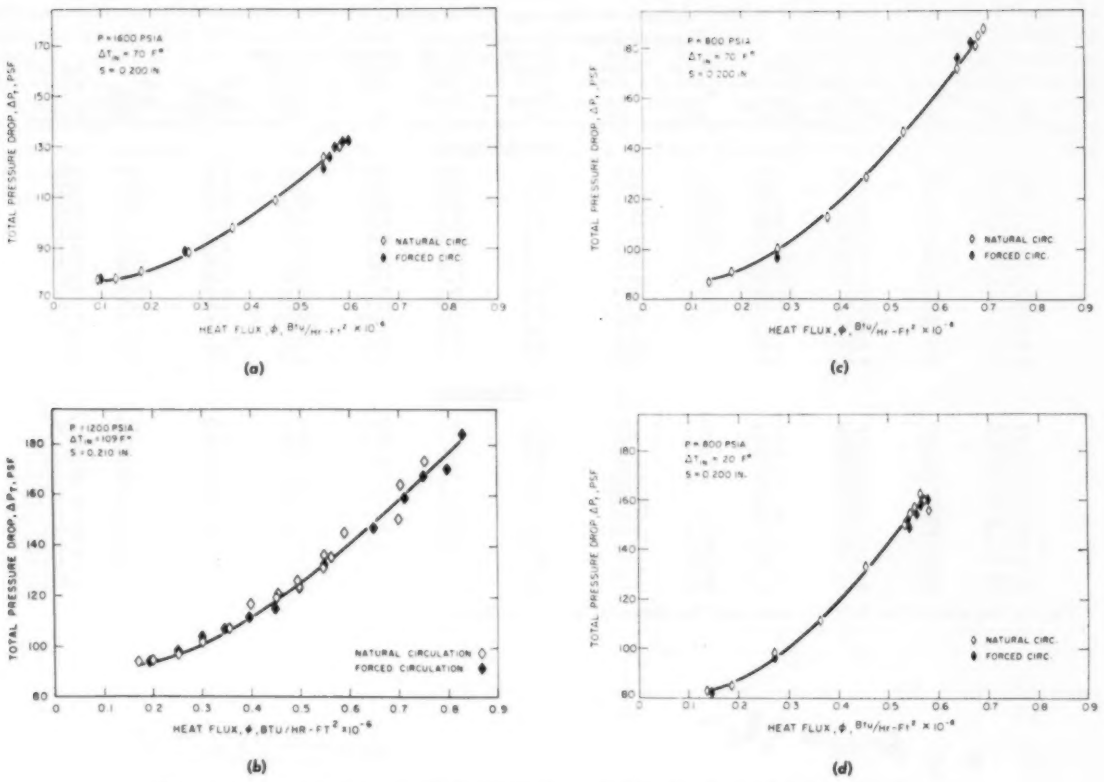

Fig. 8 Comparison of total test section pressure drop under forced and natural circulation conditions

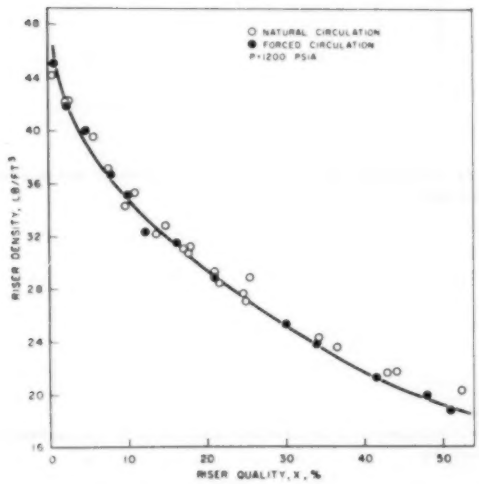

Fig. 9 Comparison of riser density under forced and natural circulation conditions (riser preceded by a 0.210-in. channel)

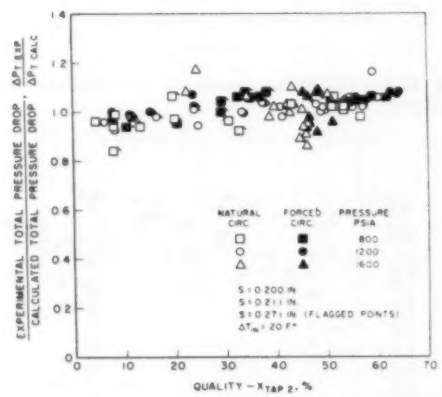

Fig. 10 Comparison of experimental and calculated test section total pressure drop

Table 4 Test-section pressure drop*

Pressure = 1200 psia S = 0.200 in.

Run No.	Inlet Temperature T_{in}, °F	Heat Flux $q/10^6$ Btu/hr-ft²	Mass Velocity $G/10^6$ lb/hr-ft²	Experimental Total Pressure Drop $\Delta P_{T\text{-exp}}$ psf	Calculated Total Pressure Drop $\Delta P_{T\text{-calc}}$ psf	Experimental Friction Pressure Drop $\Delta P_{f\text{-exp}}$ psf	Calculated Friction Pressure Drop $\Delta P_{f\text{-calc}}$ psf	Elevation Pressure Drop ΔP_{el} psf	Acceleration Pressure Drop ΔP_{acc} psf	$\frac{\Delta P_{f\text{-exp}}}{\Delta P_{f\text{-calc}}}$	$\frac{\Delta P_{T\text{-exp}}}{\Delta P_{T\text{-calc}}}$	Quality at 2nd Tap x = %
Natural Circulation												
188-1-1	545	0.136	0.406	79.5	85.2	14.0	19.9	56.0	9.3	0.70	0.93	8.2
188-1-3	550	0.281	0.385	85.2	91.2	30.1	40.0	38.4	16.7	0.85	0.94	24.6
188-1-4	551	0.367	0.387	103.4	103.4	52.0	52.0	29.2	22.2	1.00	1.00	33.2
188-1-5	548	0.461	0.393	116.4	129.2	66.0	84.9	24.4	29.8	0.95	0.98	43.2
188-2-1	550	0.586	0.368	135.5	130.3	76.6	71.4	27.2	36.7	1.07	1.04	53.7
188-2-3	551	0.908	0.379	120.0	126.6	71.4	68.0	23.8	33.0	1.05	1.03	47.8
188-2-4	550	0.510	0.376	127.0	128.8	70.1	68.1	23.5	33.4	1.03	1.02	49.1
188-2-5	551	0.521	0.389	130.6	130.9	72.0	72.4	23.2	35.4	0.99	1.00	48.9
188-2-6	550	0.532	0.385	133.5	130.9	74.2	71.4	23.2	36.1	1.04	1.01	49.7
188-2-7	552	0.542	0.359	130.0	127.9	72.3	70.1	21.7	36.0	1.03	1.02	55.1
188-2-8	552	0.552	0.358	131.9	129.0	73.9	71.0	21.2	36.9	1.04	1.02	57.1
188-3-1	550	0.563	0.374	143.2	134.9	82.5	74.2	21.9	38.7	1.11	1.06	58.6
188-3-2	549	0.574	0.379	145.4	137.2	83.4	75.0	22.0	40.0	1.11	1.06	58.6
188-3-3	547	0.585	0.378	147.2	138.5	84.1	75.5	21.9	41.2	1.11	1.06	59.6
188-3-5	550	0.604	0.365	148.9	140.4	85.5	77.0	20.6	42.8	1.11	1.06	60.2
Forced Circulation												
188-1-7	546	0.136	0.408	85.7	85.7	19.6	19.7	56.9	91.6	0.99	1.00	7.9
188-1-8	543	0.280	0.410	85.7	87.1	23.6	25.1	50.0	120.3	0.94	0.98	11.8
188-4-1	546	0.283	0.395	97.5	91.2	44.5	38.3	35.9	17.0	1.16	1.07	23.7
188-4-2	552	0.367	0.397	106.0	103.7	52.8	52.6	28.9	22.0	1.01	1.00	33.5
188-4-8	548	0.552	0.356	134.8	127.6	76.3	69.1	21.7	36.6	1.10	1.06	55.8
188-4-3	549	0.563	0.355	134.4	130.0	75.3	70.8	21.3	37.9	1.06	1.03	57.5
188-4-4	546	0.579	0.356	139.2	132.3	78.6	71.7	21.2	39.3	1.10	1.05	58.5
188-4-5	550	0.595	0.358	142.0	134.5	81.2	73.7	20.6	40.3	1.10	1.06	60.4
188-4-6	549	0.598	0.358	144.9	136.4	82.9	74.4	20.4	41.6	1.11	1.06	61.4
188-4-7	547	0.610	0.356	147.3	138.7	84.1	75.5	20.3	42.9	1.11	1.06	62.0
188-4-8	546	0.618	0.356	150.5	139.7	86.5	75.7	20.3	43.6	1.14	1.08	62.6
188-4-1	548	0.626	0.356	152.2	142.3	87.6	77.5	19.9	44.8	1.13	1.07	64.0
188-4-2	544	0.637	0.356	154.2	143.0	88.4	77.3	20.0	45.8	1.14	1.08	64.4

* The first tap was 4½ in. from the inlet, and the second 20 in. further downstream.

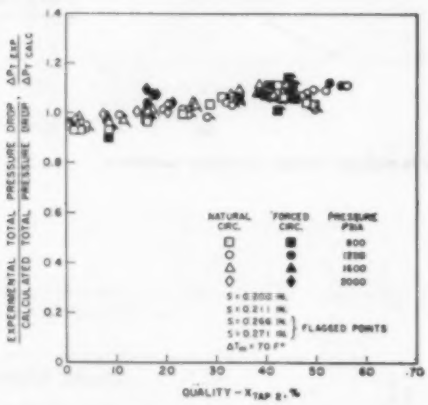

Fig. 11 Comparison of experimental and calculated test section total pressure drop

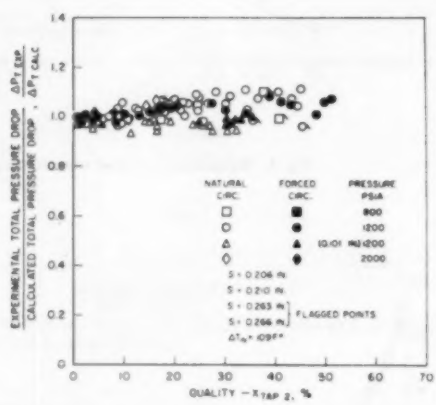

Fig. 12 Comparison of experimental and calculated test section total pressure drop

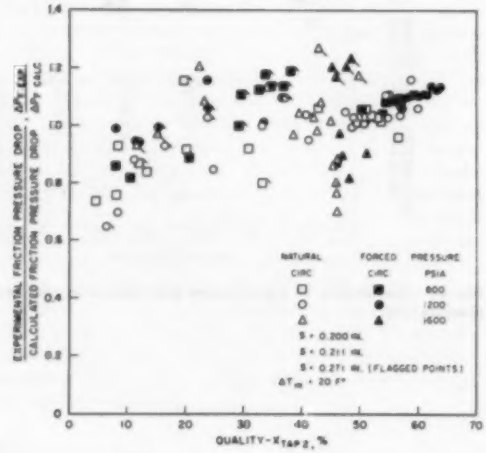

Fig. 13 Comparison of experimental and calculated test-section-friction pressure drop

Comparison of Forced and Natural-Circulation, Test-Section Pressure Drop, and Riser Density. Fig. 8 shows plots of measured total pressure drops across the test section under both natural and forced-circulation conditions at 800, 1200, and 1600 psia. Fig. 9 similarly shows a plot of riser density measured under forced and natural-circulation conditions. The forced-circulation runs duplicated the conditions existing during the corresponding natural-circulation runs. No significant difference between forced and natural-circulation pressure drop and riser density was noted.

Comparison of Test-Section Experimental and Calculated Test-Section Pressure Drop. Figs. 10 to 12 show a comparison between the measured and calculated values of the total pressure drop across the taps of the test section, ΔP_{1-2}. Data for some of the runs are shown in Table 4. Complete tabulations are included in references [12 and 13]. The elevation, acceleration, and friction pressure drop were calculated as described in Appendix 2. The

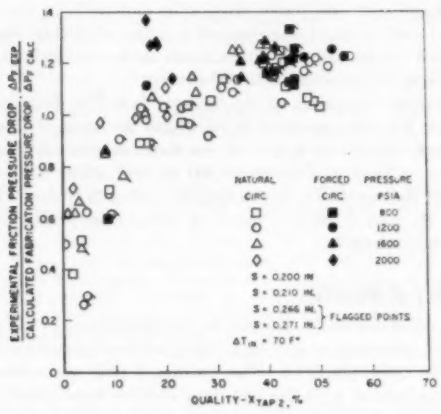

Fig. 14 Comparison of experimental and calculated test-section-friction pressure drop

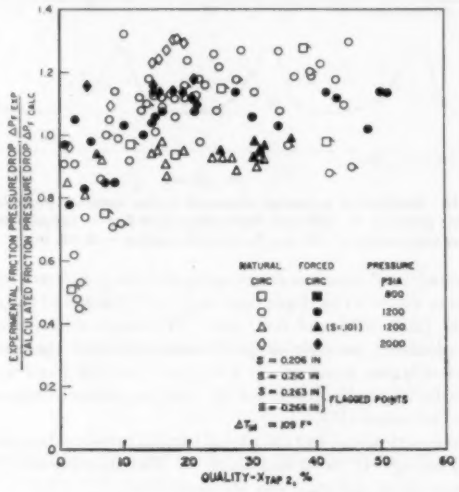

Fig. 15 Comparison of experimental and calculated test-section-friction pressure drop

Table 5 Burnout data

Run No.	Pressure Psia	Inlet Temperature T_{in}, °F	Burnout Heat Flux $\phi_{BO} \times 10^{-6}$ Btu/hr-ft^2	Mass Velocity $G \times 10^{-6}$ lb/hr-ft^2	Enthalpy at Burnout H_{BO} Btu/lb	Exit Quality x %	Actual Channel Spacing S, in.
184-31-5 **	800	499	0.585	0.326	954	64.4	0.200
184-34-1*	800	496	0.640	0.325	997	70.7	0.200
203-6-3**	800	500	0.378	0.291	744	34.0	0.271
203-17-5*	800	502	0.532	0.290	851	49.5	0.271
184-14-5	800	450	0.709	0.382	915	58.8	0.200
184-15-2*	800	444	0.667	0.393	867	51.8	0.200
203-10-4	800	448	0.699	0.363	807	43.1	0.271
203-11-5*	800	450	0.751	0.362	839	47.8	0.271
195-21-2	800	410	0.829	0.379	822	45.3	0.266
188-3-6	1200	547	0.615	0.356	996	69.3	0.200
188-6-2*	1200	544	0.637	0.356	1010	71.6	0.200
203-3-3*	1200	550	0.451	0.283	863	47.5	0.271
203-4-5*	1200	545	0.556	0.282	930	58.5	0.271
184-19-7	1200	498	0.747	0.411	960	63.4	0.200
184-20-6*	1200	497	0.753	0.413	960	63.4	0.200
195-16-4	1200	498	0.825	0.390	909	55.1	0.266
203-8-2	1200	496	0.805	0.374	906	54.6	0.271
203-8-5*	1200	498	0.802	0.382	897	53.1	0.271
182-5-6	1200	461	0.821	0.443	913	55.7	0.206
192-8-1*	1200	459	0.830	0.449	909	55.1	0.206
188-20-1	1200	460	0.830	0.463	885	51.1	0.211
195-5-4A	1200	456	0.807	0.372	876	49.7	0.263
195-12-3*	1200	456	0.832	0.334	936	59.5	0.266
167-18-6 **	1200	458	0.320	0.476	771	32.7	0.101
167-25-2*	1200	458	0.604	0.471	1077	82.5	0.101
188-12-3	1600	585	0.510	0.412	900	51.3	0.211
188-13-6*	1600	581	0.485	0.369	915	54.1	0.211
203-13-2	1600	580	0.562	0.359	897	50.7	0.271
203-13-8*	1600	588	0.559	0.359	904	52.0	0.271
184-17-2	1600	539	0.601	0.462	873	46.3	0.200
184-18-2*	1600	540	0.607	0.466	874	46.5	0.200
203-15-3	1600	535	0.670	0.399	860	43.9	0.271
203-15-8*	1600	537	0.664	0.398	860	43.9	0.271
184-4-5	1600	498	0.615	0.466	814	35.3	0.210
188-17-4	2000	561	0.485	0.523	790	25.5	0.211
188-17-8*	2000	564	0.447	0.528	776	22.5	0.211
184-3-5	2000	524	0.496	0.495	765	20.1	0.210
184-7-2*	2000	529	0.527	0.519	772	21.6	0.210

* Forced Circulation ** Fluctuating Flow

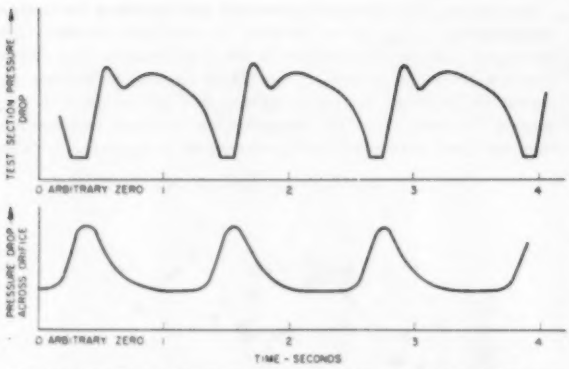

Fig. 16 Oscillatory behavior observed under natural circulation conditions; pressure = 1200 psia, test section heat flux = 320,000 Btu/hr-sq ft, inlet subcooling = 109 deg F, channel spacing = 0.101 in.

measured total pressure drops agree with the predicted pressure drops to within 10 to 15 per cent up to exit qualities of 65 per cent at 800, 1200, 1600, and 2000 psia. These curves also show that the calculated pressure drops become less than the measured values at higher qualities. It is believed that this trend is caused primarily by the limitations of the existing pressure-drop correlations; reference [17].

The experimental and calculated friction pressure drop are compared in Figs. 13 to 15 and Table 4. The experimental friction pressure drop $(\Delta P_{fr})_{exp}$ was obtained from:

$$(\Delta P_{fr})_{exp} = (\Delta P_T)_{exp} - (\Delta P_{elev} + \Delta P_{acc})_{calc} \qquad (19)$$

The calculated pressure drop components, ΔP_{fr}, ΔP_{elev}, and ΔP_{acc} are computed in accordance with the procedures of Appendix B.

The frictional pressure drop can be predicted to within 30 per cent at exit qualities above 10 per cent. At low exit qualities, the predicted friction drop can be as much as 70 per cent higher than the measured friction pressure drop. It is believed that this discrepancy is caused primarily by the inadequate relationship for calculating ΔP_{fr} in the local boiling region.

Loop-Flow Fluctuations. In nearly all natural-circulation runs, some fluctuations of a random nature were noted on the transducer that measured the pressure drop across the orifice flow meter. These fluctuations increased at higher exit qualities and lower pressures; they were not observed during corresponding forced-circulation runs.

During the run with the 0.100-in. channel, flow fluctuations of a cyclic nature began as the heat flux reached a value of 320,000 Btu/hr-sq ft, Fig. 16. Similar fluctuations have been reported in reference [6]. No satisfactory method of predicting their occurrence exists.

Burnout Heat Flux Under Natural and Forced Circulation. Burnout data obtained under forced circulation and natural circulation are presented in Table 5. The natural-circulation burnout data points were obtained by maintaining the inlet and cold-leg temperature and pressure constant and gradually increasing the test-section heat flux until burnout was reached. The forced-circulation burnout points were obtained by duplicating the loop flow (indicated by the manometer across the loop orifice) and inlet temperature of the corresponding natural-circulation burnout points.

In some natural-circulation runs, large flow fluctuations were noted before burnout was reached. These runs are also listed in Table 5. It is seen that for those runs where burnout occurred before large flow fluctuations began, no significant difference exists between forced-circulation and natural-circulation burnout. In most runs where flow fluctuations occurred, it was possible to increase the heat flux considerably before burnout was reached. When these runs were duplicated under forced circulation, burnout occurred at a heat flux 20–30 per cent higher than that under natural circulation. The forced-circulation flow rate, however, was set by using the manometer readings of the corresponding natural-circulation runs. These natural-circulation flow readings did not represent the true flow because of the flow fluctuations and consequently the duplication of these natural-circulation runs is questionable. During natural-circulation runs with the 0.100-in. channel, burnout occurred at a heat flux of 320,000 Btu/hr-sq ft immediately after the fluctuations began. The natural-circulation flow existing just prior to the fluctuations was then duplicated with forced circulation and the heat flux was increased until burnout was reached at a flux of 615,000 Btu/hr-sq ft. This shows that flow fluctuations under natural circulation conditions can cause premature burnout.

A detailed discussion of the burnout heat-flux data presented in Table 5 is not considered to be within the scope of this paper. However, it may be said that the data, in general, show that burnout in thicker channels (0.200 in. and 0.250 in.) seems to occur at the same heat flux as that occurring in thinner channels (0.050 in. and 0.100 in.) based on comparable fluid conditions and channel lengths.

Accuracy of Results

A detailed discussion of errors in instrumentation and control in similar high-pressure and high-temperature experiments can be found in reference [11]. The estimated over-all experimental errors associated with the test data may be summarized as follows:

Power Measurements (EI). Less than ±2 per cent (at point of measurement).

Local Heat Flux (ϕ). ±2 per cent in addition to error in power (assuming uniform resistivity).

Flow Rate (w). Less than ±1 per cent (provided large fluctuations do not exist).

Inlet Temperature (T_{in}). ±2 deg F.

Total Pressure Drop (ΔP_T). ±0.01 psi for both boiling and nonboiling conditions.

Conclusions

1 Pressure drop, burnout heat flux, and riser density measured under natural-circulation conditions are no different from those measured with forced circulation at the same fluid conditions provided that no large flow fluctuations are present.

2 Flow fluctuations can occur in two-phase natural-circulation flow which are not present during forced-circulation flow at the same conditions. These flow fluctuations increase at lower inlet subcooling and system pressures. Burnout can occur prematurely as a result of flow fluctuations.

3 For the loop studied, natural-circulation flow rates can be predicted within 10 per cent.

4 The total pressure drop across 0.200-in. × 1-in. × 27-in-long and 0.250-in. × 1-in. × 27-in-long test sections can be predicted to within 15 per cent up to qualities of 65 per cent using the pressure-drop correlations derived from tests on thinner channels.

Acknowledgments

The authors wish to express their appreciation to the Westinghouse Electric Corporation and the U. S. Atomic Energy Commission for permission to publish this work. The assistance of J. C. Pippert and J. W. Hunter in the design of the facility, the contribution of K. Katz, who initiated the experiments, the efforts of R. M. Weiss who performed the computations for the data reduction, and the guidance and interest of S. J. Green and K. M. Treadwell in all phases of the work are gratefully acknowledged.

References

1 W. Y. Lewis and S. A. Robertson, "The Circulation of Water and Steam in Water-Tube Boilers, and the Rational Simplification of Boiler Design," *The Institution of Mechanical Engineers*, vol. 143, 1940, p. 147.

2 A. A. Markson, T. Ravese, and C. G. R. Humphreys, "A Method of Estimating the Circulation in Steam-Boiler-Furnace Circuits," TRANS. ASME, vol. 64, 1942, p. 275.

3 R. F. Davis, "Expansion Theory of Circulation in Water Tube Boilers," *Engineering*, vol. 166, 1947, p. 145.

4 S. S. Kutateladze, "Heat Transfer in Condensation and Boiling," 2nd edition, State Scientific and Technical Publishers of Literature on Machinery (Moscow), 1952, (AEC Translation TR-3770).

5 C. D. Alstad, H. S. Isbin, N. R. Amundson, and J. P. Silvers, "The Transient Behavior of Single-Phase Natural Circulation Loop Systems," *AIChE Journal*, vol. 1, 1956, p. 417.

6 E. H. Wissler, H. S. Isbin, and N. R. Amundson, "The Oscillatory Behavior of a Two-Phase Natural Circulation Loop," *AIChE Journal*, vol. 3, 1956, p. 157.

7 W. H. Rowand, TRANS. ASME, vol. 64, 1942 p. 285.

8 P. A. Lottes, M. Petrick, and J. F. Marchaterre, "Lecture Notes on Heat Extraction From Boiling Water Power Reactors," ANL-6063, Argonne National Laboratory, October, 1959.

9 H. S. Jacket, J. D. Roarty, and J. E. Zerbe, "Investigation of Burnout Heat Flux in Rectangular Channels at 2000 Psia," TRANS. ASME, vol. 80, 1958, p. 391.

10 R. A. DeBortoli, S. J. Green, B. W. LeTourneau, M. Troy, and A. Weiss, "Forced-Convection Heat Transfer Burnout Studies for Water in Rectangular Channels and Round Tubes at Pressures Above 500 Psia," AEC Research and Development Report, WAPD-188, October, 1958 (available from Office of Technical Services, U. S. Dept. of Commerce, Washington 25, D. C.).

11 S. J. Green, B. W. LeTourneau, and M. Troy, "Forced Circulation Uniform Flux Burnout Studies for High-Pressure Water," ASME Paper No. 59—HT-25.

12 A. S. Rathbun, N. E. VanHuff, and A. Weiss, "Natural Circulation of Water at 1200 Psia Under Heated, Local Boiling and Bulk Boiling Conditions: Test Data and Analysis," WAPD-AD-TH-470, Bettis Atomic Power Laboratory, December, 1958.

13 O. J. Mendler and A. Weiss, "Natural Circulation Tests With Water in Rectangular Channels at 800 to 2000 Psia" WAPD-AD-TH-502, Bettis Atomic Power Laboratory, August, 1959.

14 W. M. Kays and A. L. London, "Compact Heat Exchangers," National Press, 1955.

15 B. L. Richardson, "Some Problems in Horizontal Two-Phase Two-Component Flow," ANL-5949, Argonne National Laboratory, December, 1958.

16 M. Petrick, "Two-Phase Air-Water Flow Phenomena," ANL-5787, Argonne National Laboratory, March, 1958.

17 B. W. LeTourneau and M. Troy, "Heating, Local Boiling, and Two-Phase Pressure Drop for Vertical Upflow of Water at Pressures Below 1850 Psia: Test Data and Correlations," WAPD-TH-410, Bettis Atomic Power Laboratory, October, 1958.

18 N. C. Sher and S. J. Green, "Boiling Pressure Drop in Thin Rectangular Channels," Chemical Engineering Progress Symposium, Series No. 23, Nuclear Engineering, Part VI, vol. 55, 1959.

19 W. H. Esselman, et al., "Thermal and Hydraulic Experiments for Pressurized Water Reactors," A-Conf. 15-P-453, presented at ICPUAE Geneva, September, 1958.

20 N. C. Sher, "Review of Martinelli and Nelson Pressure Drop Correlations," WAPD-TH-219, Bettis Atomic Power Laboratory, July, 1956.

21 R. C. Martinelli and D. B. Nelson, "Prediction of Pressure Drop During Forced Circulation Boiling of Water," TRANS. ASME, vol. 70, 1948, p. 695.

APPENDIX A

Acceleration Pressure Drop. In general, the acceleration force for a steady-state, one-dimensional continuum is:

$$dF_{acc} = \frac{dz}{g}\left[\frac{d(WV)}{dz}\right] = \frac{d(WV)}{g} \tag{20}$$

Now if the steam and water are assumed to travel at different velocities, the acceleration pressure drop (reversible) between any two points 1 and 2 becomes:

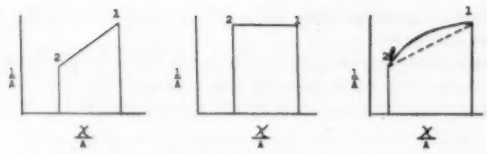

(a) Constant density (b) Constant area (c) Variable density and area

Fig. 17 Acceleration pressure drop

$$\Delta P_{acc} = \int_1^2 \left[\frac{d(W_g V_g) + d(W_f V_f)}{gA}\right] \tag{21}$$

but

$$V_g = \frac{W_g}{A_g \rho_g} = \frac{xW}{R_g A \rho_g} \tag{22}$$

and

$$V_f = \frac{W_f}{A_f \rho_f} = \frac{(1-x)W}{(1-R_g)A\rho_f} \tag{23}$$

Substituting (22) and (23) into (21) results in:

$$\Delta P_{acc} = \frac{W^2}{g}\int_1^2 \frac{1}{A}\, d\left(\frac{\chi}{A}\right) \tag{24}$$

Equation (24) can be used for both the nonboiling regions and the boiling regions where:

$$\chi = \frac{1}{\rho} \text{ for no bulk boiling, and}$$

$$\chi = \left[\frac{(1-x)^2}{1-R_g} + \frac{x^2}{R_g}\frac{\rho_f}{\rho_g}\right]\frac{1}{\rho_f} \text{ for bulk boiling}$$

Equation (24) will be used to calculate the acceleration pressure drop for the following three cases:

Case 1: The density of the fluid is constant and the flow area is variable from 1 to 2.

Case 2: The density of the fluid is variable and the flow area is constant from 1 to 2.

Case 3: The density and the flow area are both variable and the density is a function of the velocity.

For Case 1, (24) integrates to:

$$\Delta P_{acc_{1\text{-}2}} = \frac{W^2}{2g}\chi\left[\frac{1}{A_2^2} - \frac{1}{A_1^2}\right] \tag{25}$$

For Case 2, (24) becomes:

$$\Delta P_{acc_{1\text{-}2}} = \frac{W^2}{gA^2}(\chi_2 - \chi_1) \tag{26}$$

Case 3 is the condition that exists in the test section exit regions because of the dependence of the slip ratio on the velocity. This condition will be approximated by recognizing that (24) represents an area in the $(1/A, \chi/A)$ plane. In Fig. 17(*a*, *b*, and *c*) the area under the curve represents $\Delta P_{acc_{1\text{-}2}}$ for Cases 1, 2, and 3, respectively.

An approximation of the area in Fig. 17(*c*) is made by drawing a straight line between points 1 and 2. Then:

$$\Delta P_{acc_{1\text{-}2}} = \frac{W^2}{2g}\left[\frac{1}{A_2} + \frac{1}{A_1}\right]\left[\frac{\chi^2}{A_2} - \frac{\chi_1}{A_1}\right] \tag{27}$$

Equations (25), (26), and (27) were used to determine the

acceleration pressure drop ΔP_{acc} in the calculation of the test section exit losses.

The loop acceleration pressure drop was found by summing the individual acceleration pressure drops around the loop. With the omission of the negligible terms, this expression becomes:

$$\sum_{loop} \Delta P_{acc} = \frac{W^2}{2g A_{te}^2} [\chi_{te\text{-}ex} - \chi_{ei}] \left[1 - \left(\frac{A_{te}}{A_{hx}}\right)^2\right] \quad (28)$$

APPENDIX B

Test-Section Pressure Drop. The total test section pressure drop ΔP_T was measured from taps 1 to 2, Fig. 1. The equations used to predict this pressure drop are presented in references [17 to 19] for both single and two-phase vertical up-flow of water. In brief, these equations are:

Elevation Pressure Drop. The elevation pressure drop is calculated by equation (29).

$$\Delta P_{elev} = \int_{Z_1}^{Z_2} \rho dz \quad (29)$$

In the nonboiling and local boiling regions ρ is given by $\rho = 1/v_B$. In the bulk boiling region ρ is given by equation (30) for pressures from 800 to 1600 psia:

$$\rho_{BB} = \rho_f - R_g \rho_{fg} \quad (30)$$

where R_g is the modified Martinelli-Nelson void fraction, reference [20]. For pressures of 2000 psia ρ is given by equation (31).

$$\rho_{BB} = \frac{1}{\bar{v}} = \frac{1}{v_f + x v_{fg}} \quad (31)$$

Acceleration Pressure Drop. In the nonboiling and local boiling region

$$\Delta P_{acc} = \frac{G^2}{g} [v_{B2} - v_{B1}] \quad (32)$$

In the bulk boiling region for pressures from 800 to 1600 psia

$$\Delta P_{acc} = \frac{G^2}{g} \left[\left(\frac{(1-x)^2 v_f}{1-R_g} + \frac{x^2 v_g}{R_g}\right)_2 - \left(\frac{(1-x)^2 v_f}{1-R_g} + \frac{x^2 v_g}{R_g}\right)_1\right] \quad (33)$$

while for 2000 psia, equation (34) is applicable,

$$\Delta P_{acc} = \frac{G^2}{g} (\bar{v}_2 - \bar{v}_1) \quad (34)$$

where $\bar{v}$ is calculated from (31).

Friction Pressure Drop. In the nonlocal boiling (heated) and local boiling regions the friction pressure drop is given by

$$\Delta P_f = \frac{G^2}{2g D_e} \int_{Z_1}^{Z_2} f_{iso} \left(\frac{f}{f_{iso}}\right) v_B \, dz \quad (35)$$

For pressures from 800 to 1600 psia

$$\frac{f}{f_{iso}} = 1 - 0.001 \, \Delta T_f \quad (36)$$

for the no-local boiling (heated) region; ΔT_f is calculated from $\Delta T_f = \phi/h$ where h is given by $h = 0.023(k_B/D_e)(\mathrm{Re})_B^{0.8}(\mathrm{Pr})_B^{0.4}$. For the local boiling region the relationship for f/f_{iso} is

$$\frac{f}{f_{iso}} = 1 + \frac{T_B - T_{LB}^*}{T_{sat} - T_{LB}^*} \left[\left(\frac{f}{f_{iso}}\right)_{sat} - 1\right] \quad (37)$$

where $(f/f_{iso})_{sat}$ is equal to the value of ϕ_{LO}^2 at 4.2 per cent quality and T_{LB}^* is calculated from

$$T_{LB}^* = T_{sat} + \frac{60\left(\frac{\phi}{10^6}\right)^{1/4}}{e^{P/900}} - \frac{0.766\,\phi}{h} \quad (38)$$

When $T_B \geq T_{LB}^*$ and $H_B < H_{sat}$ use equation (37) to calculate f/f_{iso}. When $T_B < T_{LB}^*$ use equation (36).

For pressures of 2000 psia for the no-local boiling (heated) region

$$f/f_{iso} = 1 - 0.001915 \Delta T_f \quad (39)$$

where f/f_{iso} has a minimum values of 0.85.

For the local boiling region

$$\frac{f}{f_{iso}} = (1 - 0.0025\Delta T_{J-L}) \left[1 + 0.76\left(\frac{G}{10^6}\right)^{-5/4} \left(1 - \frac{\Delta T_{J-L}}{0.766 \Delta T_f}\right)\right] \quad (40)$$

where ΔT_{J-L}, considered as the effective temperature difference in the local boiling region, is equal to

$$\Delta T_{J-L} = T_{sat} + \frac{60\left(\frac{\phi}{10^6}\right)^{1/4}}{e^{P/900}} - T_B$$

Equation (39) should be used when $0.766\Delta T_f \leq \Delta T_{J-L}$, while equation (40) should be used when $0.766\ \Delta T_f > \Delta T_{J-L}$. Note that equation (40) reduces to (39) when $0.766\Delta T_f = \Delta T_{J-L}$.

The minimum value for $(1 - 0.0025\Delta T_{J-L})$ is 0.85. The value of f_{iso} is obtained from the local Reynolds number ($\mathrm{Re} = D_e G/\mu_B$) and the appropriate surface roughness.

In the bulk boiling region at 2000 psia the frictional pressure drop is calculated from

$$\Delta P_{f_{BB}} = \frac{G^2 f_{iso\text{-}sat} v_f}{2g D_e} \int_{Z_1}^{Z_2} \phi_{L_0}^2 \, dz \quad (41)$$

where $\phi_{L_0}^2$ is obtained from references [18 or 19] as a function of mass velocity and quality.

In the bulk boiling region at pressures from 800 to 1600 psia the frictional pressure drop is given by

$$\Delta P_{f_{BB}} = \frac{G^2 f_{iso\text{-}sat} v_f}{2g D_e} \int_{Z_1}^{Z_2} (\phi_{L_0}^2)_{M-N} \left(\frac{\phi_{L_0}^2}{\phi_{L_0}^2{}_{M-N}}\right) dz \quad (42)$$

where $\phi_{L_{0M-N}}^2$ is the Martinelli-Nelson ratio (reference [21]) and $\phi_{L_0}^2/\phi_{L_{0M-N}}^2$ is a correction factor given by equations (43) and (44). For $G \leq 0.7 \times 10^6$ lb/hr-ft^2, use

$$\left(\frac{\phi_{L_0}^2}{\phi_{L_0}^2{}_{M-N}}\right) = 1.36 + 0.005P + 0.1(G/10^6) - 0.000714P(G/10^6) \quad (43)$$

and for $G \geq 0.7 \times 10^6$ lb/hr-ft^2, use

$$\left(\frac{\phi_{L0}^2}{(\phi_{L0}^2)_{M-N}}\right) = 1.26 - 0.0004P + 0.119(10^6/G) + 0.00028P(10^6/G) \quad (44)$$

where $(f_{iso\text{-}sat})$ is obtained considering $\mathrm{Re} = D_e G/\mu_{sat}$ and the appropriate surface roughness.

Equations (41) to (44) show that the two-phase friction-factor multiplier also depends on mass velocity as well as quality at pressures below 2000 psia (reference [18] indicates this effect at 2000 psia). They were obtained from over-all pressure-drop data taken at pressures from 400 to 1600 psia across a 22-in. length of a

0.097-in. × 1-in. × 27-in-long channel and across a 60-in. length of a 0.070-in. × 2.25-in. × 72-in-long channel at a wide range of heat fluxes, mass velocities, and inlet temperatures [17]. The frictional pressure drop was determined by subtracting from the total pressure drop the acceleration and elevation pressure drop as determined from the modified Martinelli and Nelson void fractions [21]. The actual two-phase friction-factor ratio $\phi_{L_0}^2$ was found and the best estimate of these data was deduced in the form of a multiplier, equations (43) and (44), for the Martinelli and Nelson local two-phase friction factor.

DISCUSSION

H. S. Isbin[3]

A wealth of empirical correlations on two-phase, steam-water flow phenomena has been presented by the authors. Design equations and experimental data have been successfully incorporated into a system for predicting the over-all performance of a natural circulation loop. The authors have wisely eliminated those terms in their pressure drop analyses which were not important. Consequently, the significant factors and the effects of changes in these factors on the predictions become more apparent.

Even with this simplification, considerable detail is required for predicting pressure drops, for example, in the test sections. The special design equations used for nonboiling, local boiling, and bulk boiling reflect the extensive studies carried out by the Westinghouse Bettis Atomic Power Laboratory. The local boiling and boiling studies were made without the use of void measurements, and consequently the data reduction methods for determining the frictional pressure drop losses used combinations of models, depending upon the system pressure. Perhaps additional measurements are available now to improve the correlations.

Data for two-phase, steam-water, pressure losses in fittings and connectors are needed, and, as shown for the natural circulation loop, the test-section-exit flange loss is very significant. The authors' equation (16) appears to be in good agreement with the data at 800 and 1600 psia, and one would like to question what limits would be placed upon extended use of the relationships.

A dominant term in the analysis is the experimental pressure drop in the riser. Do the authors have any means of predicting the void fractions for pipe sizes larger than the 2-in. diameter riser used in the loop described?

We have been working on transient flows in natural circulation loops and we appreciate the difficulties in trying to account for the loop-flow fluctuations. With two-phase flow, oscillations can be predicted at low system pressures[7]. At high pressures, thus far we have found with a loop of different geometry that disturbances introduced still lead to very strongly damped oscillations. The models we have used provide for a continuous change in flow properties, and perhaps if one provides step changes in flow regimes corresponding to specified conditions that the sustained oscillations might be predicted.

[3] Professor, Department of Chemical Engineering, University of Minnesota, Minneapolis, Minn.

Authors' Closure

The authors are grateful for the comments and suggestions of Professor Isbin. They agree with him that there is a need for improving two-phase pressure drop correlations and note that a test program has been completed at the Bettis Atomic Power Laboratory to simultaneously measure incremental pressure drop and vapor fraction in thin rectangular channels over a wide range of pressures, flow rates, and qualities. Correlations derived from these data are expected to be an improvement over the presently used relationships.

Concerning the use of equation (16) at pressures other than those mentioned in the paper, the authors feel that additional experimental information is needed using different geometries before equation (16) could be extrapolated with confidence.

No data have been obtained in risers other than the 2-in diameter pipe used and, therefore, no correlation was developed that could be used for other pipe sizes.

Heat Transfer to Laminar Flow Across a Flat Plate With a Nonsteady Surface Temperature

R. D. CESS

Heat Transfer and Flow Section, Mechanics Department, Westinghouse Research Laboratories, Pittsburgh, Pa. Now, Associate Professor of Mechanical Engineering, North Carolina State College, Raleigh, N. C. *Assoc. Mem. ASME

Forced convection heat transfer is considered for laminar flow across a flat plate whose surface temperature varies with time. The case analyzed first is that of a step change in surface temperature, and series solutions are obtained which apply for both small and large time. These series results are used to construct an approximate solution which describes the entire time-history of the nonsteady heat-transfer process, and it is found that the results agree closely with an envelope composed of pure transient conduction and steady-state convection solutions. The analysis is then generalized to include any prescribed variation of surface temperature with time.

Introduction

FORCED-CONVECTION heat transfer from a surface whose temperature or heat flux is a prescribed function of time is becoming increasingly important, and a knowledge of this type of process is often necessary in the design of control systems, in determining time-temperature information, or in the evaluation of thermal stresses. Accordingly, several investigations have recently appeared [1, 2, 3, 4, 5][1] concerning the solution of the nonsteady energy equation for laminar and turbulent flows in the thermal entrance region of circular tubes and parallel flat plates.

On the other hand, very little work has been done with respect to external flows; i.e., boundary layer flow over a surface. The problem of laminar flow across a flat plate for which the surface temperature is a prescribed function of time has been considered by Sparrow and Gregg [6, 7]. However, this analysis applies only for small deviations from quasi-steady conditions.[2] Nonsteady laminar heat transfer at a two-dimensional stagnation point has also been considered by Sparrow [8]. In this case a solution applicable for all values of time was obtained through use of integral methods.

The purpose of the present investigation is to determine the entire time-history of the heat-transfer process for laminar flow across a flat plate with a nonsteady surface temperature. This situation is illustrated in Fig. 1. The free-stream velocity and temperature are constant. Initially the plate is at the free-stream temperature T_∞, while for $t > 0$ the surface temperature is a prescribed function of time, $T_w(t)$. The results for this case may readily be extended to include that for which steady-state heat transfer exists for $t < 0$.

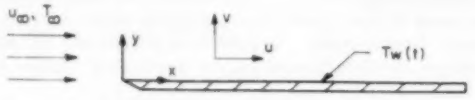

Fig. 1 Physical model and co-ordinate system

Step Change in Surface Temperature

Consider first the problem of a step change in surface temperature. Initially the plate and fluid are at temperature T_∞, whereupon the plate surface is suddenly changed to and maintained at a constant temperature T_w. Assuming incompressible flow with negligible viscous dissipation and constant fluid properties, and letting

$$\Theta = \frac{T - T_\infty}{T_w - T_\infty}$$

the equation expressing the conservation of energy within the fluid becomes

$$\frac{\partial \Theta}{\partial t} + u\frac{\partial \Theta}{\partial x} + v\frac{\partial \Theta}{\partial y} = \alpha\frac{\partial^2 \Theta}{\partial y^2} \qquad (1)$$

with the boundary conditions

$$\Theta = 0;\ x = 0 \qquad \Theta = 0;\ t = 0$$
$$\Theta = 0;\ y = \infty \qquad \Theta = 1;\ y = 0, \qquad x > 0, \quad t > 0$$

[1] Numbers in brackets designate References at end of paper.

[2] The term "quasi-steady" refers to the instantaneous application of steady-state results to a nonsteady process.

Contributed by the Heat Transfer Division of THE AMERICAN SOCIETY OF MECHANICAL ENGINEERS and presented at the ASME-AIChE Heat Transfer Conference, Buffalo, N. Y., August 15–17, 1960.

Manuscript received at ASME Headquarters, April 14, 1960. Paper No. 60—HT-7.

Nomenclature

$f(\eta)$ = Blasius stream function
k = thermal conductivity
Pr = Prandtl number, ν/α
q = local surface heat flux
Re = Reynolds number, $u_\infty x/\nu$
s = Laplace transform variable
t = time
T = temperature
u = velocity component in x-direction
v = velocity component in y-direction
x = distance co-ordinate measured along plate from leading edge
y = distance co-ordinate measured normal to plate
α = thermal diffusivity
β = constant = 0.3321
Γ = gamma function
$\eta = y\sqrt{u_\infty/\nu x}$
Θ = dimensionless temperature, $(T - T_\infty)/(T_w - T_\infty)$
Θ_n = functions of ξ $(n = 0, 1, 2, \ldots)$
λ = dummy variable of integration
ν = kinematic viscosity
$\xi = y/\sqrt{\nu t}$
$\tau = u_\infty t/x$
φ = function defined by Equation (11)
φ_n = functions of η $(n = 0, 1, 2, \ldots)$

Subscripts:

qs = quasi-steady heat transfer
w = conditions at plate surface
∞ = free-station conditions

The velocity components u and v are given by the well-known Blasius relations

$$u = u_\infty f' \tag{2}$$

$$v = \frac{1}{2}\sqrt{\frac{\nu u_\infty}{x}}\,(\eta f' - f) \tag{3}$$

where $f(\eta)$ is the dimensionless Blasius stream function [9], and

$$\eta = y\sqrt{\frac{u_\infty}{\nu x}}$$

The complete solution of Equation (1) represents a formidable task. Consequently, solutions of this equation will be obtained for the limiting cases of small and large time. These limiting solutions will in turn be used to construct an approximate result applicable for all values of time.

Solution for Small Time. To obtain a solution of Equation (1) for small values of time, it will be convenient to introduce two new independent variables defined by[2]

$$\tau = \frac{u_\infty t}{x} \qquad \xi = \frac{y}{\sqrt{\nu t}}$$

and a solution for small τ is sought. Noting that $\eta = \xi\sqrt{\tau}$, then from Equations (2) and (3), Equation (1) transforms to

$$(\tau - f'\tau^2)\frac{\partial\Theta}{\partial\tau} + \frac{1}{2}(f'\xi\tau - f\tau^{1/2} - \xi)\frac{\partial\Theta}{\partial\xi} = \frac{1}{\mathrm{Pr}}\frac{\partial^2\Theta}{\partial\xi^2} \tag{4}$$

Furthermore, the function $f(\eta)$ may be expressed as [9]

$$f = \frac{\beta}{2}(\xi\tau^{1/2})^2 - \frac{1}{2}\frac{\beta^2}{5!}(\xi\tau^{1/2})^5 + \ldots \tag{5}$$

where $\beta = 0.3321$.

A series solution will now be assumed of the form

$$\Theta = \Theta_0(\xi) + \Theta_1(\xi)\tau^{1/2} + \Theta_2(\xi)\tau + \Theta_3(\xi)\tau^{3/2} + \ldots \tag{6}$$

Upon substitution of Equations (5) and (6) into Equation (4) and collecting like powers of τ, ordinary differential equations describing the functions Θ_0, Θ_1, Θ_2, . . . are obtained. Considering the evaluation of these functions up to Θ_3, it is found that

$$\Theta_1 = \Theta_2 = \Theta_4 = \Theta_5 = 0$$

while Θ_0 and Θ_3 are the solutions of

$$\frac{1}{\mathrm{Pr}}\Theta_0'' + \frac{1}{2}\xi\Theta_0' = 0 \tag{7a}$$

$$\frac{1}{\mathrm{Pr}}\Theta_3'' + \frac{1}{2}\xi\Theta_3' - \frac{3}{2}\Theta_3 = \frac{\beta}{4}\xi^2\Theta_0' \tag{7b}$$

satisfying the boundary conditions

$$\Theta_0 = 1, \quad \Theta_3 = 0; \quad \xi = 0$$
$$\Theta_0 = 0, \quad \Theta_3 = 0; \quad \xi = \infty$$

It may readily be verified that the solutions of Equations (7) are

$$\Theta_0 = \mathrm{erfc}\left(\frac{\sqrt{\mathrm{Pr}}}{2}\xi\right) \tag{8a}$$

$$\Theta_3 = \frac{\beta}{2\sqrt{\mathrm{Pr}}}\left[\frac{1}{6\sqrt{\pi}}(1 + \mathrm{Pr}\,\xi^2)\exp\left(-\frac{\mathrm{Pr}}{4}\xi^2\right) - i^3\,\mathrm{erfc}\left(\frac{\sqrt{\mathrm{Pr}}}{2}\xi\right)\right] \tag{8b}$$

where $i^3\,\mathrm{erfc}(x)$ denotes the third repeated integral of the complementary error function [10].

For very small values of τ, only the first term in Equation (6) is significant, and

$$\Theta = \mathrm{erfc}\left(\frac{\sqrt{\mathrm{Pr}}}{2}\xi\right)$$

which represents one-dimensional transient conduction within the fluid. This result should be expected, since for very small values of time temperature gradients occur only very near the surface of the plate where u and v approach zero, and, consequently, convection effects are negligible.

Since one is mainly interested in evaluating the heat flux at the surface of the plate, the quantity of practical importance is the derivative

$$\left(\frac{\partial\Theta}{\partial y}\right)_{y=0}$$

In the following analysis, it will be convenient to have this derivative with respect to η. Since $\eta = \xi\sqrt{\tau}$

$$\frac{\partial\Theta}{\partial\eta} = \frac{1}{\tau^{1/2}}\frac{\partial\Theta}{\partial\xi}$$

and from Equation (6)

$$\left(\frac{\partial\Theta}{\partial\eta}\right)_{\eta=0} = \Theta_0'(0)\tau^{-1/2} + \Theta_2'(0)\tau + \ldots$$

Correspondingly, Equations (8) give

$$\Theta_0'(0) = -\sqrt{\frac{\mathrm{Pr}}{\pi}}$$

$$\Theta_3'(0) = \frac{\beta}{16}$$

so that

$$-\left(\frac{\partial\Theta}{\partial\eta}\right)_{\eta=0} = \left(\frac{\mathrm{Pr}}{\pi}\right)^{1/2}\tau^{-1/2} - \frac{\beta}{16}\tau + \ldots \tag{9}$$

and this represents the limiting solution for small values of time.

Solution for Large Time. For large values of time, the independent variables τ and η will be employed, and Equation (1) becomes

$$\frac{\partial\Theta}{\partial\tau} - f'\tau\frac{\partial\Theta}{\partial\tau} - \frac{1}{2}f\frac{\partial\Theta}{\partial\eta} = \frac{1}{\mathrm{Pr}}\frac{\partial^2\Theta}{\partial\eta^2} \tag{10}$$

A new function $\varphi(s, \eta)$ will further be defined as

$$\varphi(s, \eta) = s\int_0^\infty \Theta(\tau, \eta)e^{-s\tau}d\tau \tag{11}$$

such that φ/s represents the Laplace transform of Θ. Equation (10) transforms to

$$s\varphi + sf'\frac{\partial\varphi}{\partial s} - \frac{1}{2}f\frac{\partial\varphi}{\partial\eta} = \frac{1}{\mathrm{Pr}}\frac{\partial^2\varphi}{\partial\eta^2} \tag{12}$$

At first sight it might appear that little advantage has been gained in going from Equation (10) to Equation (12), since both equations are partial differential equations. However, a solution of Equation (10) does not exist in the form of a series in

[2] One may note that ξ is the similarity variable for one-dimensional transient conduction in a semi-infinite solid.

powers of τ or $1/\tau$. On the other hand, since large τ corresponds to small s, the solution of Equation (12) is appropriately represented by a power series of the form

$$\varphi = \varphi_0(\eta) + \varphi_1(\eta)s + \varphi_2(\eta)s^2 + \dots \tag{13}$$

Upon substituting Equation (13) into Equation (12) and collecting like powers of s, there is obtained

$$\frac{1}{\mathrm{Pr}}\varphi_0'' + \frac{1}{2}f\varphi_0' = 0 \tag{14a}$$

$$\frac{1}{\mathrm{Pr}}\varphi_1'' + \frac{1}{2}f\varphi_1' - f'\varphi_1 = \varphi_0 \tag{14b}$$

$$\frac{1}{\mathrm{Pr}}\varphi_2'' + \frac{1}{2}f\varphi_2' - 2f'\varphi_2 = \varphi_1 \tag{14c}$$

with the boundary conditions

$$\varphi_0 = 1, \qquad \varphi_1 = \varphi_2 = 0; \qquad \eta = 0$$
$$\varphi_0 = \varphi_1 = \varphi_2 = 0; \qquad \eta = \infty$$

For very small s ($\tau \to \infty$), only the first term in Equation (13) is significant, and taking the inverse transform

$$\Theta = \varphi_0(\eta)$$

This result represents steady-state heat transfer and is readily verified by noting that Equation (14a) corresponds to the steady-state Pohlhausen equation [9].

An interesting result of the foregoing solution is that Equations (14) are the same as the equations obtained by Sparrow and Gregg [6, 7] in analyzing small deviations from quasi-steady conditions. These equations have been solved numerically for Prandtl numbers of 0.01, 0.72, 1.0, and 10 by Sparrow and Gregg, and their results are listed in Table 1. Correspondingly, from Equation (13)

$$-\left(\frac{\partial\varphi}{\partial\eta}\right)_{\eta=0} = -\varphi_0'(0) - \varphi_1'(0)s - \varphi_2'(0)s^2 - \dots \tag{15}$$

and this represents the limiting solution for large time (small s) in terms of the Laplace transform variable s.

Table 1

Values of $\varphi_n'(0)$ from Sparrow and Gregg [7]

Pr	$\varphi_0'(0)$	$\varphi_1'(0)$	$\varphi_2'(0)$
0.01	−0.05160	−0.05845	0.01017
0.72	−0.2957	−0.7080	0.2370
1.0	−0.3321	−0.8775	0.3227
10	−0.7280	−3.997	3.070

Approximate Solution for All Time. It is now desired to obtain an approximate solution which may be employed for all values of time, and a method recently developed by Rosenzweig [11] appears to be directly applicable. Rosenzweig considered the nonsteady velocity problem of stagnation-point flow against a wall which moves impulsively in its own plane. Series solutions were obtained in terms of the Laplace transform variable s for both large and small values of s. These series results were in turn used to construct an approximate solution which could be employed for all s. The inverse transform then yielded the complete time-history for the nonsteady velocity problem.

In the present analysis an approximate solution is to be obtained for the derivative

$$\left(\frac{\partial\varphi}{\partial\eta}\right)_{\eta=0}$$

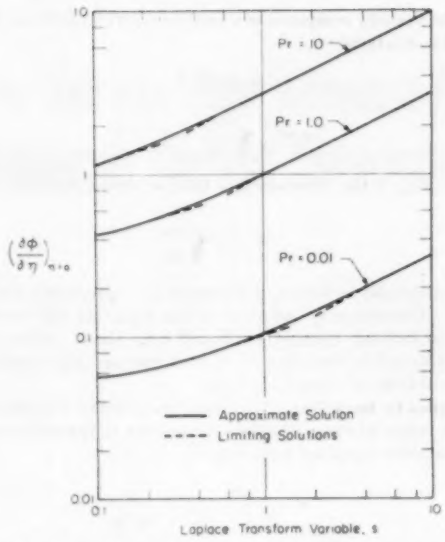

Fig. 2 Comparison of solutions for the transformed temperature derivative at the surface

The solution for small s is given by Equation (15), while for large s the transform of Equation (9) yields

$$-\left(\frac{\partial\varphi}{\partial\eta}\right)_{\eta=0} = (\mathrm{Pr})^{1/2}s^{1/2} - \frac{\beta}{16}s^{-1} + \dots \tag{16}$$

Following Rosenzweig, an approximate expression will be assumed of the form

$$-\left(\frac{\partial\varphi}{\partial\eta}\right)_{\eta=0} = a_1\frac{(s+a_2)}{(s+a_3)^{1/2}} + \frac{a_4 s}{(s+a_5)^2} \tag{17}$$

For small s this reduces to

$$-\left(\frac{\partial\varphi}{\partial\eta}\right)_{\eta=0} = \frac{a_1a_2}{a_3^{1/2}} + \left(\frac{a_1}{a_3^{1/2}} - \frac{a_1a_3}{2a_3^{3/2}} + \frac{a_4}{a_5^2}\right)s + \dots \tag{18}$$

while for large s

$$-\left(\frac{\partial\varphi}{\partial\eta}\right)_{\eta=0} = a_1s^{1/2} + a_1\left(a_2 - \frac{a_3}{2}\right)s^{-1/2} + a_4s^{-1} + \dots \tag{19}$$

The five constants appearing in Equation (17) will now be evaluated such that the first two terms in Equation (18) agree with Equation (15), and the first three terms in Equation (19) agree with Equation (16). This gives

$$a_1 = (\mathrm{Pr})^{1/2} \qquad a_2 = \frac{2}{\mathrm{Pr}}[\varphi_0'(0)]^2$$

$$a_3 = \frac{4}{\mathrm{Pr}}[\varphi_0'(0)]^2 \qquad a_4 = -\frac{\beta}{16}$$

$$a_5 = \sqrt{\frac{\beta\varphi_0'(0)}{16\varphi_0'(0)\varphi_1'(0) - 6\mathrm{Pr}}}$$

Equation (17) is compared in Fig. 2 with the limiting solutions given by Equations (15) and (16). It is seen that the approximate solution represents a logical joining of the two series results.

Heat-Transfer Results. Since the heat flux at the surface of the plate is given by the Fourier-Biot law as

$$\frac{q}{k\sqrt{\mathrm{Re}}(T_w - T_\infty)/x} = -\left(\frac{\partial\theta}{\partial\eta}\right)_{\eta=0}$$

then in terms of the function $\varphi(s, \eta)$

$$\frac{q}{k\sqrt{\mathrm{Re}}(T_w - T_\infty)/x} = -\mathfrak{L}^{-1}\left[\frac{1}{s}\left(\frac{\partial\varphi}{\partial\eta}\right)_{\eta=0}\right]$$

Combining this result with the approximate formulation given by Equation (17), the heat flux at the plate surface becomes

$$\frac{q}{k\sqrt{\mathrm{Re}}(T_w - T_\infty)/x} = 0.5642\sqrt{\frac{\mathrm{Pr}}{\tau}}\,e^{-a_3\tau} - 0.02076\tau e^{-a_4\tau} - \varphi_0'(0)\,\mathrm{erf}\left(\sqrt{a_4\tau}\right) \quad (20)$$

For convenience, the constants a_3 and a_4 have been listed in Table 2.

Table 2

Values of a_3 and a_4

Pr	a_3	a_4
0.01	1.065	1.208
0.72	0.4858	0.3182
1.0	0.4412	0.2861
10	0.2120	0.1341

For very small values of τ, Equation (20) reduces to

$$\frac{q}{k\sqrt{\mathrm{Re}}(T_w - T_\infty)/x} = 0.5642\sqrt{\frac{\mathrm{Pr}}{\tau}} \quad (21)$$

which, as should be expected, corresponds to one-dimensional transient conduction. For large τ, the steady-state result

$$\frac{q}{k\sqrt{\mathrm{Re}}(T_w - T_\infty)/x} = -\varphi_0'(0) \quad (22)$$

is obtained.

The surface heat flux as given by Equation (20) is shown in Fig. 3 together with the results of Equations (21) and (22). As τ increases the heat flux for Pr = 0.01 drops below the asymptotic one-dimensional conduction solution. Actually, the same effect occurs for the Pr = 1 and Pr = 10 cases, since the second term in Equation (9) is negative, but the result is too small to be observed in Fig. 3. Exactly the opposite effect has been found by Sparrow [8] for stagnation-point heat transfer; i.e., the initial deviation from the one-dimensional conduction solution was found to be positive rather than negative.

The physical explanation for this difference in behavior may be formulated in the following manner, and consider first the flat plate problem. For small time only the term $\partial\Theta/\partial\tau$ is significant on the left side of Equation (1). As time progresses the temperature field moves out into the velocity field and the convective terms $u\partial\Theta/\partial x$ and $v\partial\Theta/\partial y$ begin to affect the heat-transfer process. Now, during the time when convection effects are negligible the derivative $\partial\Theta/\partial x$ is zero while $\partial\Theta/\partial y$ is large. The first influence of convection is therefore solely through the term $v\partial\Theta/\partial y$. Since the quantity $\partial\Theta/\partial t$ is positive while $v\partial\Theta/\partial y$ is negative ($\partial\Theta/\partial y$ is negative and v is positive), the substantial derivative

$$\frac{D\Theta}{Dt} = \frac{\partial\Theta}{\partial t} + u\frac{\partial\Theta}{\partial x} + v\frac{\partial\Theta}{\partial y}$$

is reduced through the initial influence of convection. This means that a fluid particle observes a reduction in its time rate of change in temperature with reference to that for pure conduction, and this may be thought of as a stretching of the time scale. So, at a particular instant of time, the actual surface heat flux will be less than the value for pure conduction.

For stagnation-point flow, the term $v\partial\Theta/\partial y$ is positive since v is now negative. Consequently, convection increases the value of the substantial derivative, and the initial deviation from the pure conduction solution will be opposite to that for flow across a flat plate.

A rather surprising result shown in Fig. 3 is that the instantaneous heat flux goes slightly below the steady-state value and approaches steady state from below. Admittedly, this might be a consequence of the approximate nature of the solution, particularly since the effect first occurs in the mid-range of times when the solution is least accurate. A physical reason as to why this type of behavior might occur is not readily apparent. However, the same effect appears for nonsteady free convection from a vertical flat plate. This has been predicted analytically by Siegel [12] and observed experimentally.[4]

Arbitrary Surface Temperature

The preceding results may be extended to include the case for which the surface temperature is an arbitrary function of time, $T_w(t)$, for $t > 0$. Since the energy equation is linear, this generalization may be made through the use of Duhamel's theorem.[5] Expressing the time variation of surface temperature as $T_w(\tau)$, then by Duhamel's theorem [13] with reference to Equation (20), the surface heat flux is given by the Stieltjes integral

$$\frac{q}{k\sqrt{\mathrm{Re}/x}} = \int_0^\tau \left[0.5642\sqrt{\frac{\mathrm{Pr}}{\lambda}}\,e^{-a_3\lambda} - 0.02076\lambda e^{-a_4\lambda} - \varphi_0'(0)\,\mathrm{erf}\left(\sqrt{a_4\lambda}\right)\right]\frac{dT_w(\tau-\lambda)}{d(\tau-\lambda)}\,d\lambda \quad (23)$$

As an example of the use of this equation, consider a linear increase in surface temperature with time such that

$$T_w(t) - T_\infty = Mt$$

or

$$T_w(\tau - \lambda) - T_\infty = \frac{Mx}{u_\infty}(\tau - \lambda)$$

[4] See published discussion following reference [12].

[5] This is identical with the superposition techniques employed in previous nonsteady convection solutions [1, 2, 3, 4, 5, 7].

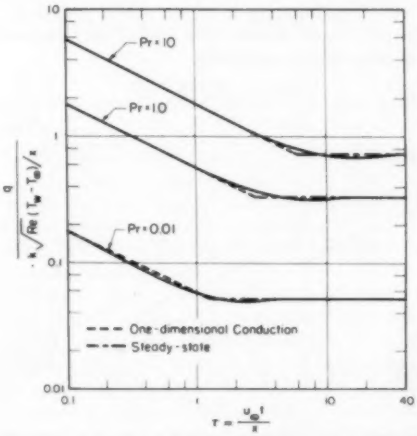

Fig. 3 Heat-transfer results for a step change in surface temperature

Upon substituting

$$\frac{dT_w(\tau - \lambda)}{d(\tau - \lambda)} = \frac{Mx}{u_\infty}$$

into Equation (23) and performing the integration, there is obtained

$$\frac{q}{q_{qs}} = 1 - \frac{1}{a_3\tau}\left[\operatorname{erf}\left(\sqrt{a_3\tau}\right) - \frac{1}{2} + 2i^2\operatorname{erfc}\left(\sqrt{a_3\tau}\right)\right] - \frac{1}{\varphi_0'(0)\tau}\left[\sqrt{\frac{\Pr}{a_3}}\operatorname{erf}\left(\sqrt{a_3\tau}\right) - 0.02076\left\{\frac{1}{a_3^2} - \left(\frac{\tau}{a_3} + \frac{1}{a_3^2}\right)e^{-a_3\tau}\right\}\right] \quad (24)$$

where q_{qs} is the quasi-steady heat flux given by Equation (22) as

$$\frac{q_{qs}}{k\sqrt{\mathrm{Re}/x}} = -\varphi_0'(0)(T_w - T_\infty)$$

For the linear increase in surface temperature

$$q_{qs} = -\varphi_0'(0)k\sqrt{\mathrm{Re}}\,\frac{M}{u_\infty}\,\tau$$

The ratio of instantaneous to quasi-steady heat transfer as given by Equation (24) is shown in Fig. 4. Also shown are Sparrow and Gregg's results [7] which apply for small deviations from quasi-steady conditions. For an arbitrary wall temperature, Sparrow and Gregg's solution may be written as

$$\frac{q}{q_{qs}} = 1 + \frac{1}{(T_w - T_\infty)}\sum_{n=1}^{\infty}\frac{\varphi_n'(0)}{\varphi_0'(0)}\frac{d^nT_w}{d\tau^n} \quad (25)$$

With a linear increase in surface temperature, this reduces to

$$\frac{q}{q_{qs}} = 1 + \frac{\varphi_1'(0)}{\varphi_0'(0)}\frac{1}{\tau} \quad (26)$$

and it is this expression that is represented by the broken curves in Fig. 4.

For large values of τ, the present analysis predicts values of q/q_{qs} which are slightly higher than those predicted by Equation (26). However, this difference is small, and as τ continues to increase the two solutions approach precise agreement. In fact, for very large τ the asymptotic form of Equation (24) is identical with Equation (26). For decreasing values of τ, the results of Sparrow and Gregg diverge from the present solution. This is to be expected, since Equation (26) applies only for small deviations from quasi-steady conditions.

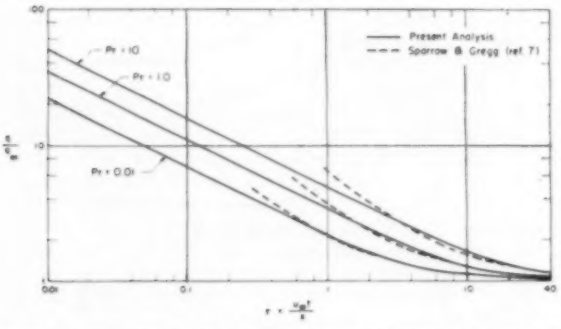

Fig. 4 Heat-transfer results for a linear increase in surface temperature with time

Actually, the relationship between the present analysis and the results of Sparrow and Gregg may be illustrated in a more general sense. Considering the large time solution for a step change in surface temperature given by Equation (15), then

$$-\frac{1}{s}\left(\frac{\partial\varphi}{\partial\eta}\right)_{\eta=0} = -\varphi_0'(0)s^{-1} - \varphi_1'(0) - \varphi_2'(0)s - \ldots$$

Taking the inverse transform term by term [14]

$$\frac{q}{k\sqrt{\mathrm{Re}}\,(T_w - T_\infty)/x} = -\varphi_0'(0) - \varphi_1'(0)\,\delta(\tau) - \varphi_2'(0)\frac{d\delta(\tau)}{d\tau} - \ldots$$

where $\delta(\tau)$ is the delta function. Extending this result to an arbitrary surface temperature variation, $T_w(\tau)$, Duhamel's theorem [13] gives

$$\frac{q}{k\sqrt{\mathrm{Re}/x}} = -\sum_{n=0}^{\infty}\varphi_n'(0)\int_0^\tau [T_w(\tau - \lambda) - T_\infty]\frac{d^n\delta(\lambda)}{d\lambda^n}\,d\lambda$$

Following Watson [15] successive integration by parts yields

$$\frac{q}{k\sqrt{\mathrm{Re}/x}} = -\varphi_0'(0)(T_w - T_\infty) - \sum_{n=1}^{\infty}\varphi_n'(0)\frac{d^nT_w}{d\tau^n}$$

which is the same as Sparrow and Gregg's solution given by Equation (25).

Simplified Method

Although Equation (23) describes the instantaneous heat flux for any prescribed variation of surface temperature with time, the evaluation of the integral is generally difficult. An alternate procedure will thus be presented which has been applied by Sparrow [8] to the stagnation-point problem with good success.

From Fig. 3, the instantaneous heat flux does not deviate appreciably from the broken curves representing the asymptotic one-dimensional conduction and steady-state convection solutions. Consequently, for a step change in surface temperature it may be assumed that the heat flux is essentially represented by the one-dimensional conduction solution for a finite time interval, after which the steady-state value applies. From Equations (21) and (22), this gives

$$\frac{q}{k\sqrt{\mathrm{Re}}(T_w - T_\infty)/x} = 0.5642\sqrt{\frac{\Pr}{\tau}};\quad \tau \le \tau_a \quad (27a)$$

$$\frac{q}{k\sqrt{\mathrm{Re}}(T_w - T_\infty)/x} = -\varphi_0'(0);\quad \tau \ge \tau_a \quad (27b)$$

where τ_a denotes the value of τ at the intersection of the two asymptotic solutions. By equating Equations (27)

$$\tau_a = \frac{\Pr}{3.142[\varphi_0'(0)]^2} = \frac{1.273}{a_3} \quad (28)$$

A physical significance may also be attached to τ_a. For all practical purposes, τ_a is a measure of the duration of the transient for a step change in surface temperature.

Consider now an arbitrary variation of surface temperature with time. Applying Duhamel's theorem to Equation (27), the surface heat flux is given by

$$\frac{q}{k\sqrt{\mathrm{Re}/x}} = 0.5642\sqrt{\Pr}\int_0^\tau \frac{1}{\lambda^{1/2}}\frac{dT_w(\tau - \lambda)}{d(\tau - \lambda)}\,d\lambda;\quad \tau \le \tau_a \quad (29a)$$

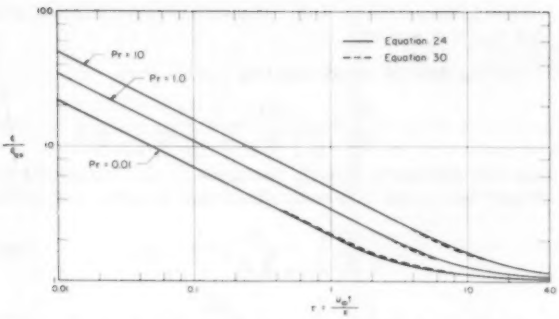

Fig. 5 Comparison of results for a linear increase in surface temperature with time

$$\frac{q}{k\sqrt{\mathrm{Re}/x}} = 0.5642\sqrt{\mathrm{Pr}}\int_0^{\tau_a}\frac{1}{\lambda^{1/2}}\frac{dT_w(\tau-\lambda)}{d(\tau-\lambda)}\,d\lambda;\quad \tau \geq \tau_a$$

$$-\varphi_0'(0)[T_w(\tau-\tau_a) - T_\infty] \quad (29b)$$

For a case of a linear increase in surface temperature with time, there is obtained

$$\frac{q}{q_{qs}} = 2\left(\frac{\tau_a}{\tau}\right)^{1/2};\quad \tau \leq \tau_a \qquad (30a)$$

$$\frac{q}{q_{qs}} = 1 + \frac{\tau_a}{\tau};\quad \tau \geq \tau_a \qquad (30b)$$

Comparison of this result with Equation (24) is shown in Fig. 5, and it may be seen that the agreement is excellent.

Discussion of Results

Asymptotic expressions may easily be obtained for a_3 and a_5 which are applicable for large Prandtl numbers. It is well known that $\varphi_0'(0)$ approaches an asymptotic behavior for high values of Prandtl number. This occurs since the velocity function $f'(\eta)$ is linear for small η, as may be seen from Equation (5) with $\eta = \xi/\sqrt{\tau}$, and for large Pr temperature gradients will be restricted within this linear range. Making use of this linear relationship, the asymptotic solution for $\varphi_0'(0)$ is found to be [16]

$$-\varphi_0'(0) = \frac{1}{\Gamma(4/3)}\left(\frac{\beta\mathrm{Pr}}{12}\right)^{1/3} = 0.3388(\mathrm{Pr})^{1/3} \qquad (31)$$

One would also expect that $\varphi_1'(0)$ should possess an asymptotic behavior, and with this in mind consider the quantity

$$\frac{\varphi_0'(0)\varphi_1'(0)}{\mathrm{Pr}}$$

This has the value 0.2908 for Pr = 1 and 0.2910 for Pr = 10, indicating that the asymptotic value is effectively 0.2910. Combination with Equation (31) gives

$$-\varphi_1'(0) = 0.859(\mathrm{Pr})^{2/3}$$

and

$$a_2 = 0.459(\mathrm{Pr})^{-1/3}$$

$$a_5 = 0.579(\mathrm{Pr})^{-1/3}$$

so that these expressions may be employed for high Prandtl number fluids.

Consider now the extension of the present results to situations for which a constant surface temperature different from T_∞ exists for $t < 0$. If this temperature difference is denoted by $(T_w - T_\infty)_i$, then steady-state heat transfer occurs for $t < 0$ given by Equation (22) as

$$\frac{q}{k\sqrt{\mathrm{Re}/x}} = -\varphi_0'(0)(T_w - T_\infty)_i$$

Equations (23) and (29) may then be applied to this case through addition of the foregoing term.

References

1 E. M. Sparrow and R. Siegel, "Thermal Entrance Region of a Tube Under Transient Heating Conditions," Proceedings of the Third U. S. National Congress of Applied Mechanics, 1958, pp. 817–826.

2 R. Siegel and E. M. Sparrow, "Transient Heat Transfer for Laminar Forced Convection in the Thermal Entrance Region of Flat Ducts," JOURNAL OF HEAT TRANSFER, TRANS. ASME, Series C, vol. 81, 1959, pp. 29–36.

3 R. Siegel, "Heat Transfer for Laminar Flow in Ducts With Arbitrary Time Variations in Wall Temperature," *Journal of Applied Mechanics*, vol. 27, TRANS. ASME, vol. 82, Series E, 1960, pp. 241–249.

4 E. M. Sparrow and R. Siegel, "Unsteady Turbulent Heat Transfer in Tubes," JOURNAL OF HEAT TRANSFER, TRANS. ASME, Series C, vol. 82, 1960, pp. 170–180.

5 R. D. Cess, "Laminar and Turbulent Convective Heat Transfer Under Nonsteady Thermal Conditions," PhD dissertation in Mechanical Engineering, University of Pittsburgh, 1959.

6 E. M. Sparrow and J. L. Gregg, "Nonsteady Surface Temperature Effects on Forced Convection Heat Transfer," *Journal of the Aeronautical Sciences*, vol. 24, 1957, pp. 776–777.

7 E. M. Sparrow and J. L. Gregg, "Prandtl Number Effects on Unsteady Forced-Convection Heat Transfer," NACA TN 4311, 1958.

8 E. M. Sparrow, "Unsteady Stagnation-Point Heat Transfer," NASA TN D-77, 1959.

9 H. Schlichting, "Boundary Layer Theory," McGraw-Hill Book Company, Inc., New York, N. Y., 1955.

10 H. S. Carslaw and J. C. Jaeger, "Conduction of Heat in Solids," Oxford University Press, London, England, 1948, pp. 370–373.

11 M. L. Rosenzweig, "The Response of the Laminar Boundary Layer to Impulsive Motions," PhD dissertation in Aeronautical Engineering, Cornell University, 1959. (Available also as TN-59-92, ASTIA No. 210-182.)

12 R. Siegel, "Transient Free Convection From a Vertical Flat Plate," TRANS. ASME, vol. 80, 1958, pp. 347–359.

13 R. V. Churchill, "Modern Operational Mathematics in Engineering," McGraw-Hill Book Company, Inc., New York, N. Y., 1944, pp. 214–216.

14 H. S. Carslaw and J. C. Jaeger, "Operational Methods in Applied Mathematics," Oxford University Press, London, England, second edition, 1948, p. 243.

15 J. Watson, "The Two-Dimensional Laminar Flow Near the Stagnation Point of Cylinder Which Has an Arbitrary Transverse Motion," *The Quarterly Journal of Mechanics and Applied Mathematics*, vol. XII, 1959, pp. 175–190.

16 R. D. Cess, "Magnetohydrodynamic Effects Upon Heat Transfer for Laminar Flow Across a Flat Plate," JOURNAL OF HEAT TRANSFER, TRANS. ASME, Series C, vol. 82, 1960, pp. 87–93.

DISCUSSION

C. L. Tien[6]

The author has certainly presented a stimulating analysis for joining the two known solutions in transient heat-convection problems, the Rayleigh type solution and the steady-state solution. One mathematical question, however, occurs to this writer concerning part of the analysis, on which the author's comment would be greatly appreciated.

In obtaining the solution for small time, the author has used Blasius' method of successive perturbations over the Rayleigh type solution. From the physical reasoning as stated in [9] it is quite clear that the Rayleigh type solution (8*a*) is a legitimate choice as the first approximation to this problem. The question arises in determining successive corrections to the Rayleigh type solution. In dealing with problems of unsteady

[6] Assistant Professor of Mechanical Engineering, University of California, Berkeley, Calif.

boundary layers it has been realized[7] that this method of successive perturbations could not take the effect of the leading edge into account because of its failure in obtaining successive corrections. This is not so in the present problem, in which the leading-edge effect has been considered through the velocity boundary layer. Nevertheless, this writer still questions whether this method of successive perturbations has included all the effects due to the leading edge.

In order to have a better understanding of this, let us devise a system which does not have the leading-edge effect on the velocity field but does on the temperature field. The simplest case seems to be the formation of thermal boundary layer in the thermal entrance region of flat ducts [1]. With the same physical reasoning as used in [9], the Rayleigh type solution is readily seen to be the first approximation. The use of method of successive perturbations fails to give any corrections to this Rayleigh type solution. This may be interpreted as an indication that the effect of the leading edge on the temperature field has not been taken into account by use of this method. While the evidence above is not conclusive, this writer feels that the method of successive perturbations is not a mathematically rigorous method for obtaining corrections to the first approximation, Rayleigh type solution.

Author's Closure

Dr. Tien raises an interesting point concerning the appearance of the leading edge effect in the present solution. To obtain a more complete understanding of this, consider the physical process for small times. As previously discussed, the first influence of convection upon the initial one-dimensional conduction process will result through the velocity component v, and this influence is represented by the higher-order terms in Equation (9). Now, as time increases a second convection influence will occur, and this will be the leading edge effect. In other words, there will be an additional influence of convection upon the heat-transfer process when a portion of the fluid initially located at $x = 0$ reaches a particular location x. Furthermore, in line with Dr. Tien's comments, it would appear that this leading edge effect is not accounted for in Equation (9), such that Equation (9) applies only for a finite initial time interval. Nevertheless, Equation (9) still serves the purpose for which it was intended; i.e., an applicable *small time* solution.

Now, if the leading edge effect is not present in the small time solution, Equation (9), then the only alternative would be its inclusion in the large time solution, Equation (15). To see whether or not this is reasonable, it is interesting to follow Dr. Tien's suggestion and devise a situation for which there is no initial convection influence (i.e., $v = 0$). One such situation is that of slug flow ($u_\infty = 0, v = 0$).

For slug flow the energy equation is of the form

$$\frac{\partial \Theta}{\partial t} + u_\infty \frac{\partial \Theta}{\partial x} = \alpha \frac{\partial^2 \Theta}{\partial x^2} \tag{32}$$

and this problem is directly analogous to that considered by Siegel,[8] from which it is easily shown that Equation (32) yields

$$-\left(\frac{\partial \Theta}{\partial \eta}\right)_{\eta=0} \sqrt{\frac{\mathrm{Pr}}{\pi}}\, \tau^{-1/2};\ \tau \leq 1 \tag{33a}$$

$$-\left(\frac{\partial \Theta}{\partial \eta}\right)_{\eta=0} = \sqrt{\frac{\mathrm{Pr}}{\pi}};\ \tau \geq 1 \tag{33b}$$

Equation (33*a*) represents pure one-dimensional conduction, while Equation (33*b*) is the steady-state solution. As discussed by Siegel,[8] the instantaneous transition from pure conduction to steady-state convection at $\tau = 1$ is due to all the fluid initially located at $x = 0$ reaching a particular axial location at the same time. In other words, this instantaneous transition is due solely to the leading edge effect.

Now, for slug flow $\beta = 0$ and this requires all but the first term in Equation (9) to be zero. Consequently, Equation (9) reduces directly to Equation (33*a*), although the condition $\tau \leq 1$ is not obtained. This is compatible, however, with the premise that Equation (9) does not include the leading edge effect.

Consider next Equation (12), which is applicable for large time. Since $f' = \eta$ for slug flow, this equation becomes

$$s\varphi + s\frac{\partial \varphi}{\partial s} - \frac{\eta}{2}\frac{\partial \varphi}{\partial \eta} = \frac{1}{\mathrm{Pr}}\frac{\partial^2 \varphi}{\partial \eta^2} \tag{34}$$

and has the solution

$$\varphi = e^{-s}\,\mathrm{erfc}\left(\frac{\sqrt{\mathrm{Pr}}}{2}\eta\right)$$

Upon taking the inverse transform, it is found that

$$-\left(\frac{\partial \Theta}{\partial \eta}\right)_{\eta=0} = \sqrt{\frac{\mathrm{Pr}}{\pi}};\ \tau \geq 1 \tag{35}$$

and this corresponds directly with Equation (33*b*). Consequently, since the condition $\tau \geq 1$ is due solely to the leading edge effect, this would in turn suggest that in the laminar flow analysis the leading edge effect is included, at least in an approximate sense, within Equation (15).

[7] Sin-I Cheng, "Some Aspects of Unsteady Laminar Boundary Layer Flows," *Quarterly of Applied Mathematics*, vol. 14, 1957, pp. 337–352.

[8] R. Siegel, "Transient Heat Transfer for Laminar Slug Flow in Ducts," *Journal of Applied Mechanics*, vol. 26, TRANS. ASME, vol. 81, 1959, pp. 140–142.

IN TWO PARTS

Film Cooling With Multiple Slots and Louvers

Experimental results are presented for film cooling of an adiabatic plate downstream of one to ten slots (Part 1) and two to twenty rows of discrete punched louvers (Part 2) in a subsonic turbulent flow under zero pressure gradient. The adiabatic wall temperatures downstreams of the last equivalent slot were measured and correlated in terms of the flow parameters, equivalent slot number and slot spacing, and distances downstreams of the last equivalent slot.

Part 1 Multiple Continuous Slots

J. H. CHIN S. C. SKIRVIN[1] L. E. HAYES F. BURGGRAF

Flight Propulsion Division, General Electric Company, Cincinnati, Ohio.

Introduction

FILM COOLING is used in many fields to protect structural surfaces from a high-temperature stream. Some applications are in furnaces of the steel industry [1][2] and in turbojet combustor and afterburner liners. Similarly, film heating has uses in wind shield and wing deicing. These applications have promoted a number of experimental and theoretical investigations. Wieghardt [2], Seban, Chan, and Scesa [3], and Seban [4] injected warm air through ports to heat a downstream surface exposed to a cold main stream. Tribus and Klein [5] used a heat-sink model to obtain a solution for the two-dimensional turbulent boundary-layer energy equation. Papell and Trout [6] obtained data for a wide range of main-stream velocity, main-stream temperature, and slot height. Hatch and Papell [7] used a simplified theoretical flow model to correlate data of film cooling or heating by tangential gas injection. Chin, Skirvin, Hayes, and Silver [8] presented data and correlation for adiabatic wall temperatures downstream of a single, tangential injection slot with cold and hot injections and varied hydrodynamic starting lengths.

Part 1 of this paper extends the previous results [8] and presents dimensionless experimental adiabatic wall temperatures downstream of one, two, three, four, five, and ten nearly tangential slots. Analysis of the data yields an empirical correlation generalized for n slots. Part 2 presents dimensionless adiabatic wall temperatures downstream of multiple rows of discrete punched louvers.

Apparatus and Experiments

The experiments were carried out in the same low-speed (up to 180 fps), low-temperature (up to 160 F) wind tunnel described in the previous paper on single-slot film cooling [8]. The wind tunnel consisted of an inlet duct, a hot-water-to-air heat exchanger, a centrifugal blower, a diffuser, a $7^1/_2$-ft by $7^1/_2$-ft plenum, a screen section, an acceleration section, a 20-ft-long 18-in. by 18-in. test section, and an exhaust duct. The test panel replaced a 90-in. segment of the wind-tunnel test-section floor, beginning 30 in. from the accelerating section.

A schematic side view of the ten-slot test panel is shown in Fig. 1. The active width of the panel was 12 in. Table 1 summarizes the pertinent facts about the materials and dimensions of the test panel. Modeling clay was used to fill joints between the test panel and the wind-tunnel floor and to block some of the slots in order to vary the number of slots upstream of the "adiabatic" instrumented panel. Figs. 2 and 3 show the ten-slot test panel in the wind tunnel and the clay blockage of the slots, respectively.

[1] Assoc. Mem. ASME.

[2] Numbers in brackets designate References at end of paper.

Contributed by the Heat Transfer Division of THE AMERICAN SOCIETY OF MECHANICAL ENGINEERS and presented at the ASME-AIChE Heat Transfer Conference, Buffalo, N. Y., August 15–17, 1960. Manuscript received at ASME Headquarters, June 2, 1960. Paper No. 60—HT-35.

Nomenclature

A = single-slot parameter $(\rho_S/\rho_g)^{-1.5}(V_S/V_g)^{-1.0}\mathrm{Re}_s^{-0.2}\mathrm{Re}_L^{0.19}(X/S)$

d = distance between successive slots, ft

$f(\phi)$ = single-slot function represented by equations (10) to (12)

F = flow parameter $(\rho_S/\rho_g)^{-1.5}(V_S/V_g)^{-1.0}\mathrm{Re}_S^{-0.2}\mathrm{Re}_L^{0.19}$

h_c = heat-transfer coefficient on bottom side of instrumented panel, Btu/hr-sq ft-deg F

h_g = heat-transfer coefficient on top side of instrumented panel, Btu/hr-sq ft-deg F

k = thermal conductivity of instrumented panel material, Btu/hr-ft-deg F

l = thickness of instrumented panel, ft

L = hydrodynamic starting length upstream of first open slot, ft

n = number of open slots

Re_L = main-stream Reynolds number $V_g\rho_g L/\mu_g$

Re_S = injection Reynolds number $V_S\rho_S S/\mu_S$

S = slot height, ft

t_a = true adiabatic surface temperature of instrumented panel, deg F

t_g = main-stream temperature, deg F

t_S = injected air temperature, deg F

t_w = measured surface temperature of instrumented panel, deg F

V_g = main-stream velocity, fps

V_S = mean injection velocity through open slots, fps

X = distance downstream of last open slot, ft

α = exponent on F in trial correlation

η = measured adiabatic film cooling effectiveness $(t_g - t_w)/(t_g - t_s)$

η_a = true adiabatic film cooling effectiveness $(t_g - t_a)/(t_g - t_s)$

μ_g = main-stream air viscosity, lb/sec ft

μ_S = injected air viscosity, lb/sec ft

ρ_g = main-stream air density, pcf

ρ_S = injected air density, pcf

ϕ = parameter in over-all correlation

$$\sum_{n} -\left[\frac{1.3}{1+0.02\left(\frac{d}{S}\right)}\right]_F \frac{X}{S}$$

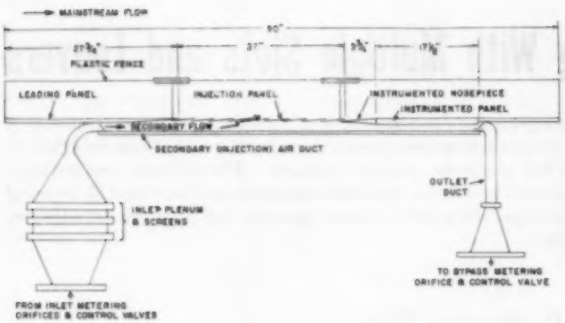

Fig. 1 Schematic side view of ten-slot film-cooling test panel

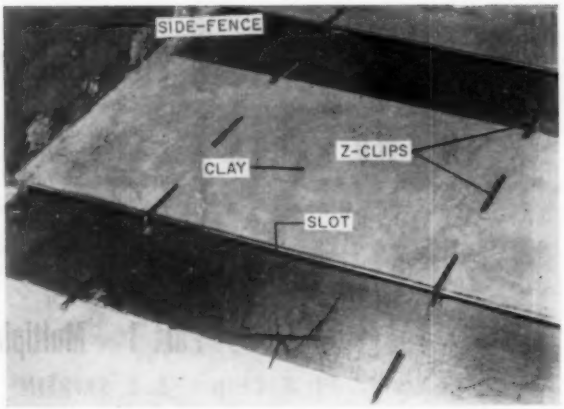

Fig. 3 Clay blockage of slots

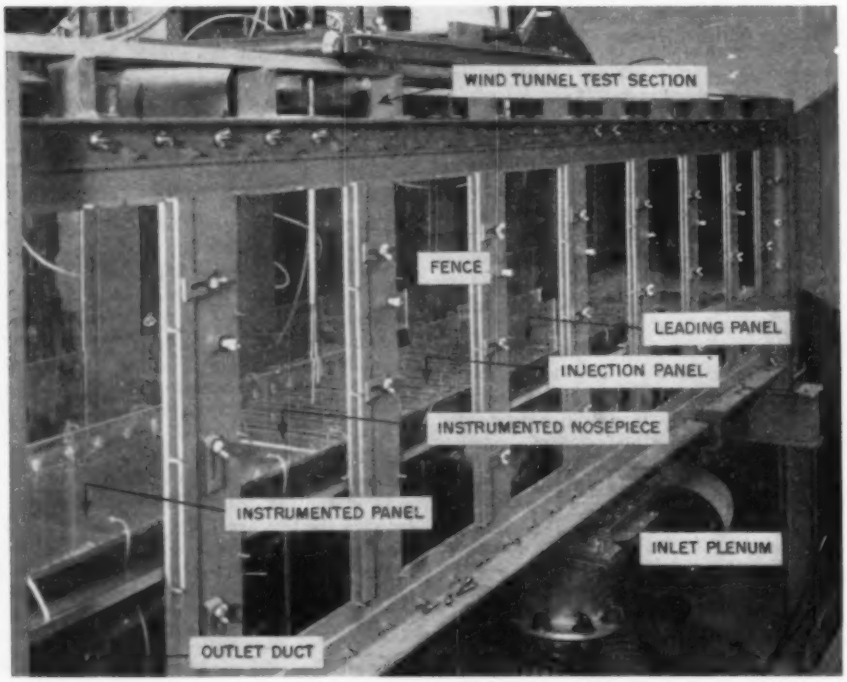

Fig. 2 Ten-slot test panel installed in heat-transfer wind tunnel

The injection panel slots (Table 1) were formed by 9 stainless-steel plates $^1/_{16}$ in. thick at a 3-deg inclination to the mainstream direction. The longitudinal spacing between slots was 3 in. with $^3/_4$ in. overlap to form a flow channel for the injected air. The average slot height was 0.115 in. Zee-shaped brass clips were placed in each slot 3 in. on each side of the panel center line to preserve the slot height and to minimize upward bowing of the injection panel under pressure loads.

The secondary-air duct which passed beneath the injection panel was $1^3/_4$ in. deep. The bypass flow which passed through the secondary-air duct without being ejected through the slots was metered by a downstream orifice run in order to determine, in combination with an upstream orifice run, the mass flow through the slots. Back pressure could be varied in the downstream bypass duct to aid in controlling the mass flow through the slots. However, the effect of bypass flow variation was found negligible[3] and, hence, all data in the present paper are for zero bypass flow.

Test-panel instrumentation consisted of static pressure taps in the plastic side fences and in the floor of the secondary-air duct, or flush surface thermocouples in the leading panel, instrumented nosepiece, and instrumented panel, and of fixed probe thermocouples which sensed the secondary-air temperature. All thermocouples used in the experiments were copper-constantan except for the 40-gage chromel-alumel thermocouple which was used for boundary-layer traverses. Surface thermocouples were 28 gage and were placed in transverse grooves filled with epoxy resin, similar to the technique described in reference [8].

Flush surface thermocouples were located every $^9/_{16}$ in. along

[3] If the slots peeled off the secondary-air boundary layers completely and injected into the main stream, the net heat transfer from the hotter main stream to the secondary stream would be zero.

Table 1 Structural components of multiple-stage film cooling test panel

Component	Material	Basic Dimensions	Remarks
Leading Panel	1/2 in. thick SS[7]	12 in. wide x 27 3/4 in. long	Tapered to knife edge downstream; has thermocouples.
Injection Panel	(9) 1/16 in. thick SS Plates	12 in. wide x 3 3/4 in. long (3/4 in. overlap)	3° inclination to mainstream; symmetrical bevel leading and trailing edges.
Instrumented Nosepiece	1 in. SS stock	12 in. wide x 4 1/2 in. long; wedge-shaped, 0-1 in. thick	3° inclination on upper surface; forms bottom of tenth slot.
Instrumented Panel	1 in. canvas-phenolic resin laminate	12 in. wide x 17 1/2 in. long	Intended to simulate an adiabatic test panel.
Aft Filler Panel	1/2 in. canvas-phenolic resin laminate	12 in. wide x 1/4 in. long	Filler panel downstream of instrumented panel.
Plastic Fences	1/4 in. thick acryllic resin	6 in. high x 90 in. long (in 3 pieces)	Used to minimize tunnel sidewall effects; have static pressure taps.
Sidewalls of Secondary Duct	1 in. SS stock	Approximately 1 3/4 in. high x 72 in. long	Chief structural members.
Floor of Secondary Duct	1/2 in. canvas-phenolic resin laminate	1/4 in. wide x 72 in. long	Has static pressure taps and ports for probe insertion.
Inlet and Outlet Ducts	1/4 in. Aluminum plate		

[7] SS designates type 304 Stainless Steel

the center line of the instrumented nosepiece and instrumented panel. At every tenth station four additional thermocouples were installed transversely to monitor transverse temperature gradients in the plate. In addition to the thermocouples on the upper surface, there were 4 thermocouples on the bottom surfaces of the instrumented nosepiece and the instrumented panel. Temperatures indicated by these latter thermocouples were used as a guide in making conduction corrections in the measured upper surface temperatures for low film-cooling effectiveness values.

Additional surface thermocouples were located on the top and bottom of the leading panel at 3 stations along the center line, including one set of transverse thermocouples. Leading panel thermocouples were used chiefly to aid in determining when thermal equilibrium had been attained by the test panel.

All thermocouple outputs were recorded directly as temperatures by a 120-point recording pyrometer except for the boundary-layer traversing thermocouple whose output was fed directly to an X-Y recorder (typical profiles, Fig. 4).

Experiments were run with a hot main stream (150 or 160 F) and a cool secondary stream (70 to 90 F) and appreciable time (1 to 2 hr) was required to heat up the structure of the wind tunnel and to bring the test panel into thermal equilibrium.

Flow-condition data and dimensionless surface-temperature data at 15 locations along the center line of the instrumented nosepiece and instrumented panels are given in Table 2.

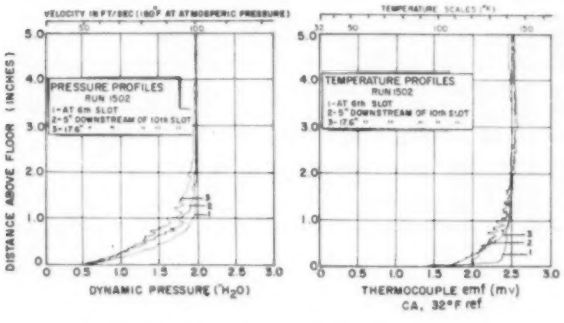

Fig. 4 Typical boundary-layer profiles, run 1502

Boundary-layer traverses upstream of the injection section were made. The results indicated that the boundary layer was turbulent and that the hydrodynamic starting length was comparable to the physical distance from the acceleration section to the first injection slot [8].

Analysis of Data

The experimental data in Table 2 consist of the adiabatic effectivenesses downstream of the last slot, main stream and secondary stream temperatures, average injection and main stream velocities and their ratios, and a flow parameter F. The adiabatic effectiveness η is defined as the ratio of the temperature difference between the local main stream and the local adiabatic wall to that between the local main stream and the injection stream. Typical η versus X/S variations for $V_g = 150$ fps are given in Figs. 5(a and b) for $n = 1$ and $n = 5$ with $d/S = 26.1$, respectively.

Observation of Fig. 5 and similar plots for other runs indicates that there is generally a leveling of η at large X/S, particularly for small values of η. This leveling of η may be attributed to conduction leakage through the test plate to the cooler back-

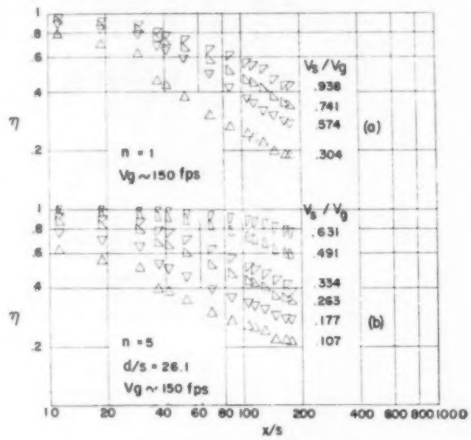

Fig. 5 Typical η versus X/S

Table 2 Data, multiple slot

Run	Symbol	Fig.	T_0	V_0 ft/sec	T_0/T_s	i_0 (°)	i_2 (°)	r	η_2 at X/D^2 = 7.91	11.39	18.61	29.22	36.52	40.35	50.70	68.35	86.17	107.2	114.3	128.3	145.9	167.4	177.8
Re. 10 Slot Open, n = 1, L = 64.75 in.																							
1102	+		99	46.0	.163	144.4	89.2	3.08	.851	.812	.761	.714	.583	.542	.478	.388	.333	.301	.284	.279	.250	.243	.243
1104	×	4a	99	85.1	.058	146.0	90.0	1.38	.966	.929	.886	.857	.768	.732	.696	.600	.538	.500	.481	.464	.421	.389	.389
1106	□		99	112.0	1.113	144.2	86.0	.95	.966	.943	.908	.871	.796	.768	.725	.648	.605	.560	.550	.528	.484	.459	.459
1101	△		153	46.6	.304	146.5	87.5	5.01	.808	.784	.695	.632	.457	.431	.371	.302	.267	.241	.233	.222	.198	.190	.190
1103	▽	4a	152	87.2	.574	146.5	89.0	2.21	.922	.896	.844	.795	.681	.652	.591	.492	.426	.374	.358	.342	.304	.287	.278
1105	◇		152	112.3	.761	146.0	85.6	1.57	.944	.919	.876	.838	.753	.720	.670	.576	.513	.455	.440	.414	.372	.348	.339
1107	▽		151	141.8	.938	147.0	86.7	1.16	.972	.955	.919	.879	.813	.779	.746	.660	.614	.564	.547	.522	.466	.438	.438
Slots 9, 10 Open, n = 2, 4/3 = 26.1, L = 81.75 in.																							
1204	+		100	23.3	.233	144.5	89.9	7.48	.868	.810	.742	.685	.537	.493	.448	.368	.337	.306	.297	.282	.257	.251	.250
1206	×	4b	101	42.7	.424	144.1	83.8	3.36	.935	.914	.875	.844	.758	.718	.650	.550	.496	.444	.429	.401	.366	.343	.343
1208	□		99	63.0	.635	143.9	81.9	1.98	.960	.948	.919	.895	.849	.853	.817	.748	.696	.632	.609	.573	.525	.491	.483
1201	△		152	24.4	.161	146.9	87.2	11.36	.784	.688	.642	.552	.410	.396	.384	.296	.267	.240	.240	.223	.203	.199	.199
1205	▽	4b	151	42.8	.284	146.1	83.0	5.38	.872	.841	.776	.714	.578	.553	.480	.415	.364	.331	.318	.303	.284	.268	.257
1207	◇		151	63.1	.419	145.7	83.0	3.23	.958	.933	.893	.856	.758	.743	.662	.571	.509	.443	.424	.399	.372	.346	.332
1209	▽		148	98.4	.653	145.8	79.3	1.74	1.00	.989	.971	.954	.883	.881	.879	.787	.767	.705	.680	.646	.601	.564	.541
Slots 8, 10 Open, n = 2, 4/3 = 52.7, L = 78.75 in.																							
1402	+		99	23.2	.235	145.1	84.8	7.39	.770	.735	.662	.612	.461	.433	.380	.315	.289	.267	.264	.249	.230	.229	.221
1404	×		99	41.7	.423	143.0	83.5	3.65	.878	.844	.800	.756	.617	.593	.539	.435	.387	.350	.338	.319	.287	.281	.272
1406	□	4a	99	72.2	.722	142.3	81.1	1.69	.967	.953	.922	.899	.837	.828	.776	.707	.647	.590	.575	.542	.505	.475	.459
1408	○		99	108.8	1.098	143.7	78.0	.98	.986	.979	.956	.938	.896	.889	.869	.817	.781	.743	.734	.709	.682	.662	.639
1401	△		151	23.5	.156	145.0	85.1	12.00	.678	.620	.534	.480	.350	.338	.296	.252	.230	.214	.209	.202	.192	.183	.181
1403	▽	4b	151	42.5	.278	147.8	83.1	5.64	.830	.785	.709	.649	.490	.476	.414	.348	.317	.289	.280	.269	.247	.241	.233
1405	◇		150	72.2	.483	145.6	81.0	2.73	.937	.915	.875	.832	.733	.708	.639	.549	.477	.428	.412	.386	.353	.336	.333
1407	▽		152	100.7	.668	144.5	79.1	1.80	.972	.960	.937	.910	.852	.838	.789	.723	.658	.599	.580	.546	.508	.468	.456
Slots 7, 10 Open, n = 2, 4/3 = 78.3, L = 75.75 in.																							
1702	+		99	24.8	.252	143.2	89.0	6.36	.760	.714	.646	.598	.456	.419	.373	.299	.270	.252	.255	.244	.225	.216	.216
1704	×	4a	99	46.7	.463	145.0	90.0	3.04	.891	.864	.818	.774	.673	.627	.573	.473	.433	.391	.382	.356	.320	.302	.298
1706	□		99	84.4	.692	144.8	88.2	1.95	.963	.939	.898	.862	.782	.756	.717	.615	.571	.509	.495	.465	.421	.396	.389
1707	○		100	113.3	1.04	145.5	84.0	1.04	.986	.979	.951	.935	.902	.886	.862	.813	.778	.748	.740	.707	.678	.658	.642
1701	△		153	23.5	.153	146.0	89.2	12.20	.643	.590	.511	.454	.338	.299	.285	.229	.220	.211	.202	.194	.176	.176	.176
1703	▽	4b	153	39.3	.257	146.5	82.0	6.06	.783	.744	.659	.597	.446	.433	.392	.296	.302	.279	.271	.259	.234	.225	.225
1705	◇		150	68.9	.458	146.0	81.0	2.85	.908	.885	.838	.791	.669	.646	.585	.485	.463	.407	.388	.367	.325	.308	.298
1708	▽		152	100.6	.660	146.2	83.2	1.70	.984	.968	.944	.895	.836	.816	.765	.668	.638	.570	.545	.536	.484	.452	.448
Slots 6, 8, 10 Open, n = 3, 4/3 = 52.2, L = 72.75 in.																							
1506	+		100	17.0	.149	144.0	87.1	11.35	.681	.638	.575	.531	.404	.383	.366	.295	.278	.262	.253	.244	.228	.225	.223
1504	×	4a	100	29.4	.296	144.0	87.7	5.46	.838	.803	.745	.696	.574	.546	.495	.414	.359	.332	.320	.308	.282	.270	.267
1502	□		100	47.8	.481	146.2	81.2	2.82	.926	.908	.872	.840	.758	.731	.687	.560	.502	.455	.443	.418	.358	.372	.366
1508	○		99	66.3	.672	144.0	77.8	1.82	.968	.956	.937	.917	.864	.844	.818	.725	.666	.606	.592	.559	.526	.496	.490
1510	◇		100	85.7	.857	145.2	78.2	1.32	.985	.975	.963	.948	.908	.893	.897	.789	.810	.766	.752	.722	.684	.668	.636
1505	△		150	17.2	.115	146.0	85.9	17.73	.596	.547	.478	.436	.329	.314	.293	.235	.216	.231	.225	.218	.211	.200	.198
1503	▽	4b	150	29.8	.200	147.0	86.1	8.56	.796	.758	.696	.635	.483	.425	.381	.327	.296	.273	.264	.258	.232	.227	.225
1501	◇		151	47.6	.315	146.8	82.0	4.67	.899	.867	.788	.735	.596	.574	.506	.432	.387	.353	.340	.332	.306	.292	.287
1507	▽		150	66.1	.441	145.2	77.2	2.98	.959	.932	.896	.853	.722	.684	.626	.544	.492	.443	.429	.409	.377	.360	.356
1509	▽		150	85.6	.571	145.8	78.0	2.19	.973	.966	.940	.913	.848	.823	.776	.706	.718	.569	.566	.545	.487	.459	.444
Slots 1, 4, 7, 10 Open, n = 4, 4/3 = 78.3, L = 57.75 in.																							
1812	+		99	12.4	.118	144.4	89.0	16.00	.603	.558	.502	.464	.357	.339	.305	.240	.247	.238	.235	.224	.206	.215	.215
1810	×	4c	100	19.4	.182	145.5	84.0	8.82	.753	.707	.642	.590	.472	.449	.387	.325	.309	.275	.274	.268	.249	.249	.239
1808	□		99	33.2	.316	145.2	81.0	4.88	.868	.836	.789	.742	.609	.586	.526	.424	.393	.373	.352	.373	.314	.309	.296
1806	◇		99	51.0	.484	144.4	76.5	2.34	.936	.909	.868	.859	.768	.734	.682	.609	.550	.505	.492	.470	.438	.419	.412
1804	○		99	68.8	.599	144.2	81.6	1.87	.970	.955	.936	.914	.830	.796	.783	.703	.655	.602	.578	.562	.514	.492	.490
1816	○		99	86.1	.818	145.0	78.4	1.33	.991	.988	.976	.961	.918	.938	.913	.895	.868	.800	.811	.796	.745	.729	.713
1811	△		149	12.5	.079	146.0	89.0	27.30	.705	.663	.608	.538	.386	.386	.368	.293	.286	.277	.299	.297	.199	.174	.174
1809	▽	4c	149	19.3	.122	147.0	86.0	14.28	.839	.800	.751	.675	.503	.459	.399	.333	.313	.290	.295	.233	.219	.217	.217
1807	◇		153	33.4	.205	145.8	80.5	7.70	.773	.747	.668	.610	.464	.441	.395	.362	.379	.328	.310	.273	.257	.218	.262
1805	▽		151	51.1	.321	146.8	84.2	3.95	.940	.914	.864	.806	.655	.713	.578	.532	.662	.535	.507	.470	.363	.366	.323
1803	▽		152	68.6	.390	145.3	80.2	3.09	.925	.900	.857	.816	.696	.665	.586	.527	.641	.462	.433	.373	.371	.333	.304
1801	▽		154	86.3	.527	145.5	77.5	2.06	.963	.948	.926	.898	.799	.798	.770	.669	.748	.566	.552	.529	.498	.471	.463
Slots 2, 7, 8, 9, 10 Open, n = 5, 4/3 = 26.1, L = 72.75 in.																							
1306	+		99	17.5	.177	144.5	81.1	10.30	.784	.752	.708	.656	.532	.510	.460	.398	.368	.339	.334	.319	.290	.219	.216
1308	×	4c	100	26.2	.262	144.1	79.0	6.14	.878	.851	.813	.771	.644	.636	.578	.495	.452	.411	.406	.387	.355	.344	.342
1306	□		101	39.9	.395	144.1	78.5	3.60	.944	.933	.913	.889	.838	.822	.787	.686	.589	.559	.559	.530	.498	.479	.470
1309	○		98	51.1	.520	143.0	77.3	2.52	.979	.971	.949	.941	.927	.915	.888	.833	.788	.732	.717	.686	.636	.579	.595
1311	○		100	73.7	.739	143.0	73.9	1.57	.991	.987	.981	.971	.970	.965	.957	.936	.925	.910	.902	.886	.858	.838	.836
1303	△		151	14.2	.107	145.0	82.0	19.00	.667	.619	.554	.510	.377	.382	.366	.278	.273	.257	.272	.240	.219	.214	.213
1301	▽	4b	152	28.1	.177	147.0	73.8	10.10	.905	.871	.808	.758	.631	.608	.543	.399	.342	.339	.329	.317	.276	.283	.281
1305	◇		152	40.0	.253	144.5	78.9	5.84	.956	.928	.882	.830	.690	.662	.601	.523	.471	.433	.427	.401	.346	.352	.345
1308	▽	4c	150	54.1	.334	144.8	77.3	4.17	.962	.937	.898	.857	.787	.759	.708	.631	.572	.517	.505	.474	.440	.422	.382
1310	▽		150	73.8	.451	144.9	76.8	2.54	.983	.971	.942	.918	.929	.919	.888	.830	.778	.721	.717	.675	.625	.596	.588
1312	▽		152	87.7	.631	145.1	72.9	1.83	.993	.986	.981	.971	.970	.968	.957	.931	.913	.886	.877	.837	.809	.781	.770
Slots 2, 4, 6, 8, 10 Open, n = 5, 4/3 = 52.2, L = 60.75 in.																							
1606	+		99	9.54	.096	144.3	87.0	22.8	.833	.822	.773	.662	.337	.319	.293	.258	.266	.232	.232	.223	.211	.208	.206
1604	×	4b	100	17.5	.178	145.0	84.2	10.1	.731	.691	.628	.582	.454	.420	.387	.327	.306	.284	.281	.271	.253	.248	.246
1602	□		100	25.8	.290	144.0	77.5	6.88	.840	.814	.775	.736	.598	.566	.519	.430	.389	.371	.360	.338	.306	.298	.298
1608	○		100	42.8	.438	144.2	79.0	3.33	.908	.893	.862	.837	.747	.715	.683	.572	.528	.500	.471	.469	.426	.410	.410
1610	○		99	52.6	.537	144.5	80.5	2.62	.941	.927	.902	.895	.836	.819	.777	.670	.630	.581	.573	.562	.508	.477	.477
1612	○		100	71.9	.753	145.4	80.0	1.53	.988	.982	.969	.957	.962	.930	.913	.870	.839	.801	.786	.793	.766	.752	.739
1603	△		151	9.57	.064	145.4	87.0	37.9	.661	.623	.575	.569	.264	.260	.263	.221	.214	.195	.192	.187	.178	.177	.178
1605	▽	4b	151	17.5	.116	147.2	84.2	19.7	.896	.881	.813	.671	.358	.362	.316	.277	.258	.239	.235	.229	.213	.210	.209
1601	▽		152	28.1	.185	145.2	79.9	9.96	.786	.751	.668	.616	.481	.429	.381	.338	.314	.295	.291	.275	.225	.203	.262
1607	◇		150	42.4	.284	144.8	78.6	5.14	.871	.841	.785	.732	.584	.575	.527	.457	.403	.377	.361	.332	.278	.267	.267
1609	▽		150	52.5	.350	144.0	80.0	3.44	.906	.885	.839	.803	.695	.659	.606	.523	.471	.431	.413	.378	.347	.332	.327
1611	▽		151	71.9	.496	147.2	80.6	2.49	.961	.949	.928	.896	.823	.811	.795	.692	.732	.602	.572	.549	.521	.497	.482
All 10 Slots Open, n = 10, 4/3 = 26.1, L = 57.75 in.																							
2035	+		110	10.1	.099	150.6	84.0	23.3	.700	.6 1	.610	.598	.481	.442	.437	.372	.371	.332	.321	.333	.279	.294	.296
2027	×	4d	116	16.3	.140	154.8	92.1	13.3	.815	.783	.734	.710	.603	.581	.541	.469	.439	.408	.410	.368	.340	.343	.340
2026	□		114	29.9	.262	153.2	83.1	5.75	.907	.899	.873	.856	.802	.789	.746	.660	.598	.546	.553	.502	.454	.477	.486
2033	○		113	39.3	.348	155.2	87.3	4.02	.943	.962	.943	.929	.901	.898	.866	.795	.754	.770	.795	.740	.696	.607	.607
2031	△		148	9.6	.057	157.3	95.8	41.3	.558	.511	.459	.431	.350	.327	.309	.255	.237	.236	.214	.231	.220	.198	.208
2029	▽	4d	145	16.2	.098	157.3	92.9	20.1	.739	.699	.686	.534	.483	.466	.430	.340	.334	.317	.307	.298	.248	.256	.255
2007	▽		163	28.6	.175	156.5	86.3	9.34	.933	.836	.798	.758	.647	.606	.588	.517	.453	.446	.435	.417	.353	.364	.358
2005	▽		146	40.8	.296	157.1	81.9	4.63	.973	.955	.930	.903	.828	.836	.790	.760	.669	.636	.621	.591	.525	.536	.526
2008	▽		159	89.0	.526	157.5	83.9	2.21	.998	.997	.991	.988	.981	.978	.968	.928	.915	.887	.883	.876	.833	.807	.800
2030	□	4d	184	33.7	.183	157.0	84.8	8.66	.872	.845	.798	.753	.650	.636	.584	.508	.474	0.444	.439	.414	.374	.3 1	.3 0
2028	□		182	42.3	.238	158.5	83.9	6.75	.921	.898	.867	.827	.744	.717	.681	.607	.560	0.529	.517	.479	.462	.447	.436
2027	□		185	70.4	.381	158.7	82.2	3.29	.982	.979	.962	.940	.912	.903	.872	.805	0.721	0.714	.696	.652	.621	.621	.621
2036	□		195	89.3	.483	158.6	83.8	2.44	1.005	.999	.992	.995	.980	.972	.955	.914	.880	0.858	.838	.816	.773	.757	.746

[a] First 4 positions are located on aerial instrumented nacelles.

side environment. On the assumption that back-side temperature equals injection temperature and that conduction is two-dimensional, the following equation is obtained from the proportionality between the temperature drops and the thermal resistances:

$$\frac{t_a - t_w}{t_w - t_g} = \frac{1/h_g}{\frac{1}{h_c} + \frac{l}{k}} = \frac{h_c/h_g}{1 + (h_c l/k)} \tag{1}$$

Rewriting (1):

$$\frac{t_g - t_w}{t_g - t_g} - \frac{t_g - t_a}{t_g - t_g} = \left(\frac{t_g - t_g}{t_g - t_g} - \frac{t_g - t_w}{t_g - t_g}\right) \frac{h_c/h_g}{1 + (h_c l/k)}$$

yields

$$\eta - \eta_a = (1 - \eta) \frac{h_c/h_g}{1 + (h_c l/k)} \tag{2}$$

Equation (2) indicates that the difference between the experimentally measured value and the true adiabatic effectiveness increases as η decreases and may become significant in log η plots for small values of η. Substituting estimated values of the parameters typical for runs in Fig. 5:

$h_c = 1$ Btu/hr sq ft F, $h_g = 15$ Btu/hr sq ft F, $k = 0.175$ Btu/hr ft F, and

$l = {}^1/_{12}$ ft into equation (2) yields:

$$\eta - \eta_a = 0.045\,(1 - \eta)$$

Therefore, at $\eta = 0.2$, the conduction error in effectiveness amounts to 0.036 as compared to 0.014 at $\eta = 0.7$. Bottom temperature information confirms qualitatively that conduction error is generally small for the front half of the instrumented panel but becomes more and more significant for the rear half as η decreases. Furthermore, at small values of η, the accuracy of temperature recording, the slight timewise variation of t_g, and the small deviation from two dimensionality may become significant. Consequently, an arbitrary criterion for correlation purpose was to de-emphasize data points in Table 2 with low effectiveness generally occurring near the panel downstream end (X/S greater than 107.2, the region of the last six effectiveness points). The approximate criterion was:

$\eta(X/S = 107.2) > 0.5$, no point was de-emphasized
$0.5 > \eta(X/S = 107.2) > 0.45$, last point was de-emphasized
$0.45 > \eta(X/S = 107.2) > 0.40$, last 2 points were de-emphasized, etc.,

until $\eta(X/S = 107.2) < 0.2$, all last 6 points were deemphasized.

Observation of Fig. 5 and similar plots for other runs indicates also a "discontinuity" between the instrumented nosepiece and instrumented panel effectivenesses. This discontinuity was apparently also due to conduction through the metal instrumented nosepiece. However, for the first three positions at $X/S < 20$, the temperature difference across the instrumented nosepiece was generally small; consequently, the conduction error was relatively small.

In reference [8] the parameter

$$A = (\rho_S/\rho_g)^{-1.5}\,(V_S/V_g)^{-1.0}\,\mathrm{Re}_S^{-0.2}\,\mathrm{Re}_L^{0.19}\,(X/S) \tag{3}$$

was used to correlate the single-slot effectiveness for $V_S/V_g < 1$ according to the following empirical equations:

$$\eta = 1, \quad A \leq 15 \tag{4}$$

$$\eta = 1.5A^{-0.15}, \quad 15 \leq A \leq 72 \tag{5}$$

$$\eta = 12.7A^{-0.65}, \quad 72 \leq A \tag{6}$$

In the experiments, the variation of V_g over the length of the test panel was small. The flow parameter F is then defined for convenience to consider the effect of the variables other than downstream distance in the parameter A

$$F = (\rho_S/\rho_g)^{-1.5}(V_S/V_g)^{-1.0}\mathrm{Re}_S^{-0.2}\mathrm{Re}_L^{0.19} = A(S/X) \tag{7}$$

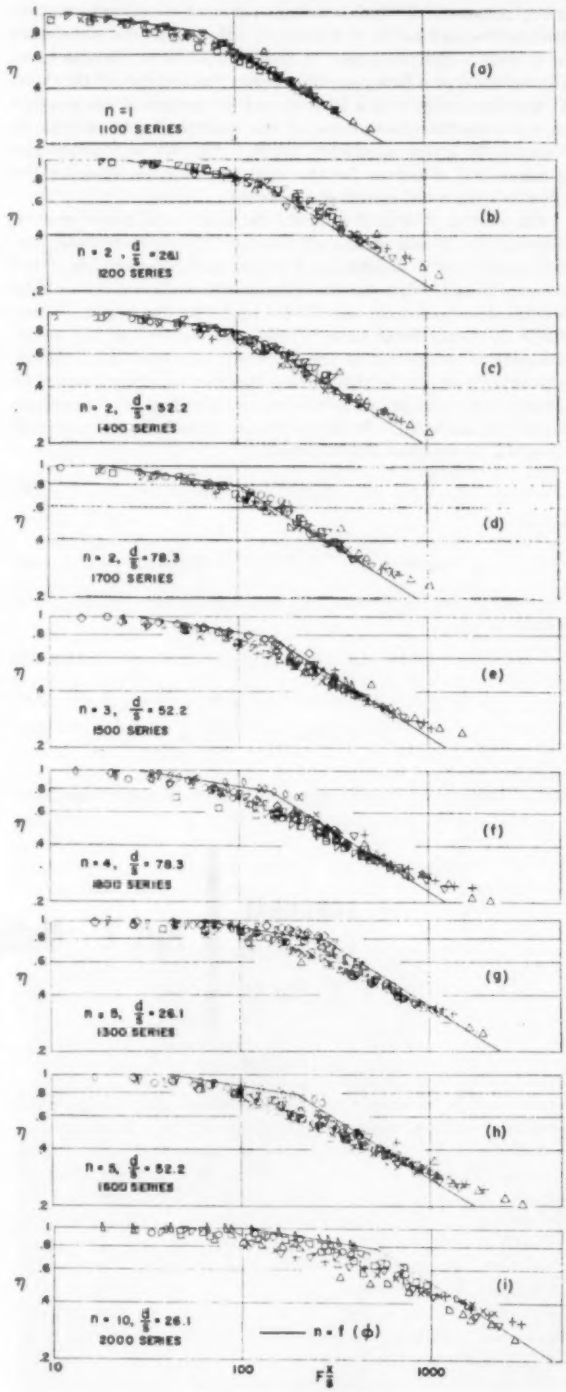

Fig. 6 η versus $F\,X/S$

As was the case for the data in reference [8], curves of log η versus log X/S show similarity in the present data. Within a set of runs; i.e., the 1300 series, it is possible to select a "standard" curve and to match other curves with the standard by translating the abscissa. Preliminary curve matching indicated that η could be empirically correlated in terms of the group parameter $F^{\alpha}X/S$, α being a constant dependent on other parameters such as the slot number. However, trial correlation of α with n indicated that α was insensitive to changes in n, the variation of α being possibly within the accuracy of the data. It was found that with a little spread of the data it was possible to correlate the effectiveness of the individual sets of runs in terms of the group parameter FX/S. Fig. 6(a to i) shows the η versus FX/S curves for the nine sets of runs, showing the effect of slot number and slot spacing.

The curves in Fig. 6 indicate similarity and hence can be matched by a translation of abscissa. Two asymptotic extremes are useful as additional points in the correlation. One extreme is that, when the slot spacing is zero, the n-slot assembly is equivalent to a single slot with n times the slot height. Since FX/S is proportional to $S^{-1.3}$, the effectiveness of the n-slot assembly is a function of the modified parameter $n^{-1.3}\,FX/S$. The other extreme is that, when the slot spacing approaches infinity, only the last slot is effective and the single-slot equations (4) to (6) are valid. With the above considerations, the final empirical correlation was obtained:

$$\eta = f(\phi) \tag{8}$$

where

$$\phi = n^{-\{1.3/[1+0.02(d/S)]\}}F(X/S) \tag{9}$$

and $f(\phi)$ is the single-slot function represented by the three equations:

$$f(\phi) = 1,\ \phi \leq 15 \tag{10}$$

$$f(\phi) = 1.5\phi^{-0.18},\ 15 \leq \phi \leq 72 \tag{11}$$

$$f(\phi) = 12.7\phi^{-0.65},\ 72 \leq \phi \tag{12}$$

Valid for $V_s/V_g \leq 1$.

Fig. 7 shows the data for the nine sets of runs and illustrates the simplicity of the over-all correlation. The solid line represents equations (10) to (12).

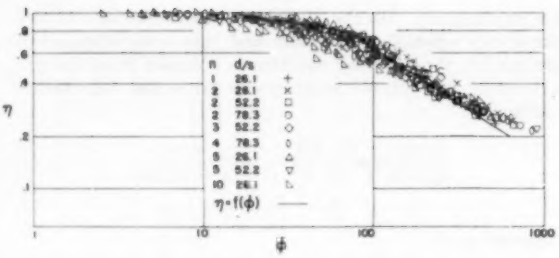

Fig. 7 η versus ϕ

For comparison, the predicted η versus FX/S curves according to the over-all correlation are also given in Fig. 6(a to i). It is seen that, as the slot number increases, the over-all correlation becomes less satisfactory, indicating that more complicated expressions are needed if a better correlation is desired.

Observation of the η versus X/S curves for large values of V_s/V_g and for large values of n indicates the possibility of another "region" of correlation analogous to the region for $1 \leq V_s/V_g \leq 2$ in reference [8]. However, the "transition" point from one region to another is not very well defined for different slot numbers.

In favor of the simplicity of the over-all correlation for the present paper, the possibility of improved correlation and analyses will be left for future work.

Summary

Experimental adiabatic wall temperatures downstream of 1, 2, 3, 4, 5, and 10 identical, nearly tangential slots were measured, with variations of injection to main-stream velocity ratio, main-stream velocity level, and slot spacing. Analysis of the data yielded an empirical correlation generalized for n slots, the film-cooling effectiveness being expressible in terms of the single-slot function of reference [8] with the single-slot parameter A modified by a factor for variation of slot number and ratio of slot spacing to slot height.

F. BURGGRAF
J. H. CHIN
L. E. HAYES

Part 2 Multiple Rows of Discrete Louvers

Introduction

In contrast to the interest in film cooling with continuous two-dimensional slots, only a relatively small amount of work in film cooling with rows of discrete ports has been reported. Wieghardt [2] presented some data for the effect of discharge from one and two rows of oblong holes. His results showed that the discrete holes were less effective than continuous slots with the same quantity of injection air and that an arrangement of two staggered rows of holes was not quite as unfavorable as a single row of holes.

This report extends the results of Part 1 and presents dimensionless adiabatic wall temperatures downstream of two, four, six, eight, ten, and twenty rows of punched crescent louvers as are often used in turbojet combustor and afterburner liners. The results were correlated on the basis that each pair of adjacent louver rows could be simulated by a continuous slot located midway between them and with an effective slot height to give the same total flow area. Satisfactory correlation was obtained in terms of the multiple-slot parameters developed in Part 1.

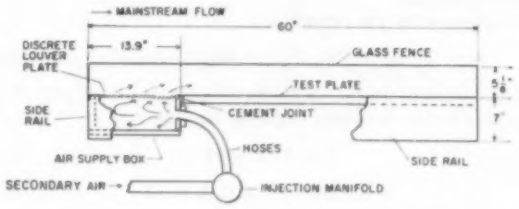

Fig. 8 Schematic side view of discrete louver test apparatus

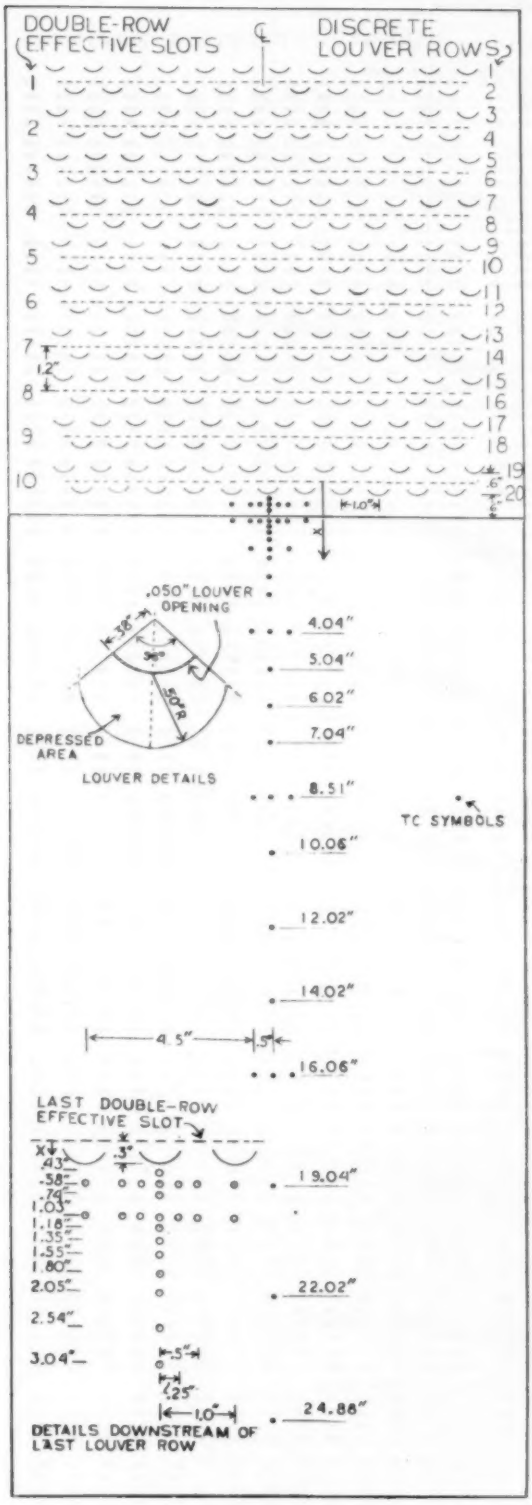

Fig. 9 Louver and adiabatic plate details

Apparatus and Experiments

The multiple-slot test panel in Part 1 was replaced by a multiple-louver test panel 60 in. in length and with its leading edge 30 in. from the accelerating section.

A schematic side view of the discrete louver test apparatus is shown in Fig. 8. Secondary air entered a manifold where the flow was distributed to the air supply box through four hoses. The air-supply box in turn served to distribute air through louvers in the discrete louver panel. Injection into the air-supply box was introduced in the opposite direction to the main-stream air flow to promote flow uniformity through the discrete louvers.

The discrete louver plate was made of nominal 0.063-in. stainless-steel plate die-punched to form staggered slots of a form used in many jet-engine combustor and afterburner liners. Details of the panel are given in Fig. 9. Each slot was adjusted to 0.050 in. with feeler gages within a tolerance of 0.001 in. by bending the upper slot lips. Neoprene gasketing and screws sealed the panel to form a lid for the air-supply box. The louvered panel was observed to have an inward bow of 0.2 in. from the punching operation. Pressure testing at the highest supply box pressure and flows of test conditions showed that the panel was rigid enough to prevent any observable change. A photograph of the discrete louver panel installed in the wind tunnel is shown in Fig. 10. The gaps existing around the panel as shown were filled and made smooth with epoxy resin prior to testing.

The test plate in Fig. 8 was made of 1-in-thick phenolic canvas-based laminate. It was the same plate used in previous single-slot experiments [8] but with its position in the side rails changed, its length shortened, and extra thermocouples added.

Temperatures were measured by means of 28-gage copper-constantan wall thermocouples and 24-gage copper-constantan loop-type probes. All surface thermocouples were exposed flush with the surface and their leads were lain in a transverse direction as close to the surface as possible. In the discrete louver plate, thermocouple leads lay along the underside of the plate and connected to the beads through $^1/_{16}$-in-diam holes filled with epoxy resin. On the test plate, thermocouple leads and beads lay in epoxy-resin-filled transverse grooves in the surface. Between the test plate and louvered plate, thermocouples were cemented in place with epoxy resin. Loop-type probes were used to measure the main-stream temperature,

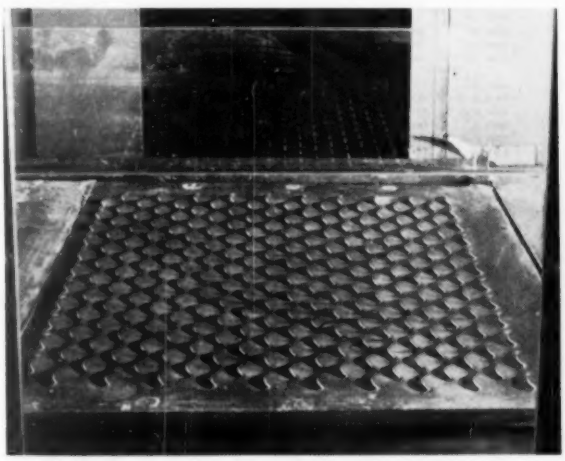

Fig. 10 Louver panel installed in heat-transfer wind tunnel

Table 3 Data, multiple louver

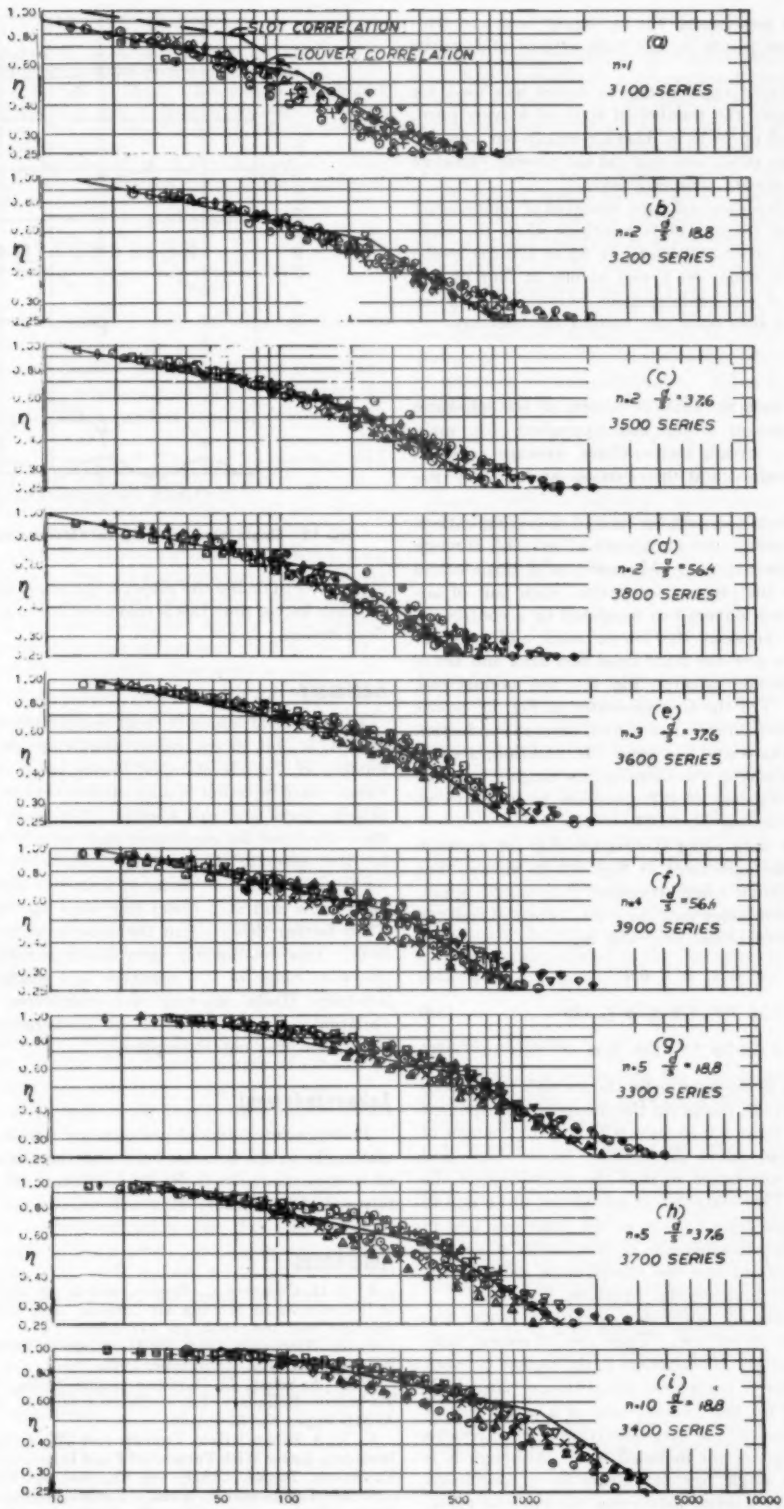

Fig. 11 η versus FX/S

temperatures at four positions in the air-supply box, and temperatures at upstream points in the main stream and in the injection stream.

Fiber-reinforced plastic tape in double layers was used for louver blockage to vary the number of rows of louvers open. The tape stood up well up to 15 in. H_2O air-supply-box pressure under hot main-stream conditions and did not present excessive altering of the main-stream boundary layer.

The main body of experimental data consisted of temperature readings for the fixed thermocouple locations when the main stream air was set at about 160 F and at 85 or 170 fps levels; the injection flow was about 80 F and at one of four or five levels, and for one of ten configurations representing various numbers of equivalent slots open and various slot spacings.

Analysis of Data

The experimental data in Table 3 consist of the adiabatic effectivenesses downstream of the last equivalent slot, main stream and secondary stream temperatures, average injection and main-stream velocities and their ratios, and a flow parameter F.

Fig. 11(*a* to *i*) presents the data for each of the configurations tested from one equivalent slot (two rows of louvers) through ten equivalent slots (twenty rows of louvers), with three values of slot spacing. For the present correlation, each pair of adjacent rows of staggered louvers was simulated by a continuous slot located midway between the louver rows and with an effective slot height to give the same total flow area and hence the same average injection velocity, Fig. 9. The average slot height was 0.0637 in. For the data presented in Fig. 11, points with effectiveness below 0.25 were not plotted because conduction leakage through the plate was too large. In addition, a small correction might be made on the other points ranging approximately from at effectiveness of 0.3—decrease by 0.03, to at effectiveness of 0.7—decrease by 0.014.

Examination of the data using the relationship for multiple slots showed reasonable agreement at high FX/S values; but at the intermediate range where equation (11) would apply, the measured values were lower than for slots. For the multiple discrete louvers the correlation proposed is:

$$\eta = 1, \ \phi \leq 6.9 \tag{13}$$

$$\eta = 1.5\phi^{-0.21}, \ 6.9 \leq \phi \leq 128 \tag{14}$$

$$\eta = 12.7\phi^{-0.65}, \ 128 \leq \phi \tag{15}$$

This set of equations is the same as for the multiple continuous slots, equations (10) to (12), except for the change of the exponent of ϕ in equation (11) from -0.15 to -0.21 and for changes of the ϕ limits. Fig. 11(*a*) shows the modified louver curve and also the original slot correlation so that the magnitude of the change can be seen. This reduction is considered to be due to mixing of the discharges from louvers in the same row and in adjacent rows. Further downstream of the louver panel the flow becomes more uniform and the effectiveness data can be correlated again by the multiple-slot equation.

The correlation is directly applicable along the center line downstream of the last louver row. There are, of course, sidewise variations to reduce the effectiveness in the regions between louvers. Fig. 12 shows a transverse temperature pattern at various values of X/S for the "worst" case of a single row of louvers. A limited amount of single-louver-row effectiveness data was also taken, but is not included here. Although it is possible to simulate a single row of louvers by a continuous slot, it was felt that with a single louver row the sidewise variation was comparable to the axial variation so that giving only center-line data could be misleading. No correlation has been attempted to define the sidewise variation since with the normal multiple louver rows this is smoothed out in a reasonable distance downstream.

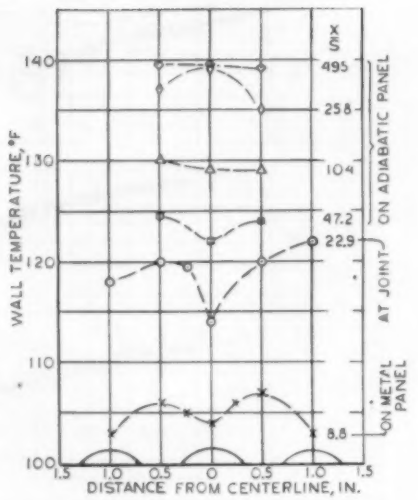

Fig. 12 Single louver row typical sidewise temperature profiles

Summary

Experimental adiabatic wall temperatures downstream of 1, 2, 3, 4, 5, and 10 equivalent slots, corresponding to twice this number of discrete stamped louver rows, were measured with variations of injection to main-stream velocity ratio, main-stream velocity level, and slot spacing. The same correlating parameters developed for continuous slots were found to be applicable to the discrete louver case. However, the effectiveness for louvers started to decay at a shorter distance from the last louver row and at a faster rate than for the continuous slots. Then farther downstream the louvers were as effective as the slots. This relationship provides reasonable correlation over the wide range of slot numbers and spacings covered experimentally. Data showing the transverse wall temperature variation are also presented for a single row of louvers but correlation was not attempted.

Acknowledgment

The experience and advice of many persons have contributed materially to the present work and the authors are grateful to all and particularly to E. R. G. Eckert, R. H. Norris, A. H. Silver, and M. Tribus.

References

1 J. H. Chesters, C. Holden, and A. D. Robertson, "Protection of Refractories by Moving Air Curtain," *Journal of the Iron and Steel Institute*, vol. 185, 1957, pp. 177–200.

2 K. Wieghardt, "Hot-Air Discharge of De-Icing," AAF Trans. No. F-TS-919-RE, December, 1946.

3 R. A. Seban, H. W. Chan, and S. Scesa, "Heat Transfer to a Turbulent Boundary Layer Downstream of an Injection Slot," ASME Paper No. 57—A-36.

4 R. A. Seban, "Heat Transfer and Effectiveness for a Turbulent Boundary Layer With Tangential Fluid Injection," JOURNAL OF HEAT TRANSFER, TRANS. ASME, vol. 82, 1960, pp. 303–312.

5 M. Tribus and J. Klein, "Forced Convection From Non-Isothermal Surfaces," Heat Transfer Symposium, Engineering Research Institute, University of Michigan Press, 1953, pp. 211–233.

6 S. S. Papell and A. M. Trout, "Experimental Investigation of

Air Film Cooling Applied to an Adiabatic Wall by Means of an Axially Discharging Slot," NASA TN D-9, August, 1959.

7 J. E. Hatch and S. S. Papell, "Use of a Theoretical Flow Model to Correlate Data for Film Cooling or Heating an Adiabatic Wall by Tangential Injection of Gases of Different Fluid Properties," NASA TN D-130, November, 1959.

8 J. H. Chin, S. C. Skirvin, L. E. Hayes, and A. H. Silver, "Adiabatic Wall Temperature Downstream of a Single, Tangential Injection Slot," ASME Paper No. 58—A-107.

DISCUSSION

S. Stephen Papell[4]

The authors are to be commended for obtaining multiple slot film-cooling data which is certainly a definite contribution. The data correlation presented is quite effective but because its scope and application were not clearly defined in the paper, the discusser should like to add a word of caution concerning its use.

There are two points to consider! The first is concerned with the type of data obtained in order to develop a general correlation and the second with the possibility of extrapolating the correlation to flow conditions more akin to actual cooling problems.

The injection air multiple slot test panel used to obtain these data cannot be considered a typical configuration for film cooling application. There is no doubt that uses may be found for this particular type but a more general type of test rig would have to be used in order to obtain maximum cooling effectiveness for a minimum cost in coolant weight flow. This point is quite significant since I am sure that when a cooling problem presents itself it is only natural for us to try to use as little coolant flow as possible. For gaseous film cooling, maximum cooling effectiveness on a weight flow basis can only be obtained by proper control of coolant flow through each slot because the free stream flow conditions change downstream of each successive slot. In addition to controlling the coolant flow through each slot, it would also be necessary to obtain temperature measurements between the slots if a correlation were to be obtained which would enable us to properly design a configuration that could be cooled with a minimum cost in coolant weight flow. Unfortunately, this type of data was not obtained, thereby restricting the usefulness of the correlation presented in this paper.

I make this point in defense of *gaseous* film cooling because if a comparison between various types of cooling were to be made, for a specific application, it would not be right to use this correlation. This equation would definitely underestimate the effectiveness of multiple slot film cooling on a weight flow basis.

My second point is to question the possibility of extrapolating this correlation based on low temperature and low velocity data to use at high temperatures and velocities. The method of obtaining the correlation is strictly empirical and there appears to be no theoretical basis to allow this extrapolation. On the contrary, there appears some justification that this should not be done. There is available some single slot higher temperature data at approximately 2000 deg R (reference [6]) which has been found to deviate significantly from the curve predicted by this correlation.

Let me reiterate now that this paper is a definite contribution to the film cooling field because it contains the only multiple slot data correlation of any significance. My only suggestion is that its limitations be understood.

R. A. Seban[5]

It is remarkable that the authors have succeeded in correlating the multiple-slot results at all, even though the correlation shows substantial scatter and, as they point out, must be regarded as a prelude to further analysis. In view of the complexity of the flow in these systems in consequence of which superposition of the experimental solution for the single slot is probably untenable, it may be that the correlation of the paper will turn out to be more permanent than a first appraisal might indicate it to be.

The present results for a single slot confirm the authors' earlier presentation [8] and are unique in comparison with other results for systems of this type in the -0.65 power dependence of the effectiveness in the final power law regime. Certainly there exists some different feature in the authors' experimental arrangement, compared to other systems from which the final power law dependence has been to the 0.80 power of the distance downstream of the slot. One question that arises is the possible effect of radiation in this connection. When heat conduction effects are neglected, the wall temperature is specified by the relation

$$h\,(t_{aw} - t_w) = h_r\,(t_w - t_\infty)$$

where t_∞ is the temperature of the surroundings with which radiant energy interchange takes place, through an effective radiation conductance h_r which will be of the order of unity if the emittance of the test surface is unity. In these terms the true effectiveness η_a and the measured effectiveness η are related as:

$$\eta_a = \left(1 + \frac{h_r}{h}\right)\eta - \frac{h_r}{h}\left(\frac{t_\infty - t_g}{t_s - t_g}\right)$$

If the temperature t_∞ is the same as the gas temperature then the last term is zero; there is an error in the effectiveness but the slope of the observed value remains the same in a logarithmic representation as it is for the true value. If $t_\infty < t_g$, as is possible with a heated gas stream, then the slope changes. For instance, with $h_r/h = 1/10$ and $t_\infty - t_g/t_s - t_g = 0.40$, the slope of the true effectiveness would need to be about -0.73 to obtain a value of -0.65 for the observed coefficient, though this is approximate because in this case both η_a and η cannot have a power law dependence on the downstream distance. It would consequently be of interest to have the authors' appraisal of the temperature of the wind tunnel wall and of the emittance of the test surface as they existed in the experiments which produced these effectiveness values.

Authors' Closure

The authors appreciate the discussions by Mr. Papell and Professor Seban, who have contributed to the understanding of gaseous film cooling.

In regard to Mr. Papell's first point, the authors agree that the multiple-slot test panel used may not represent the optimum case with a maximum cooling effectiveness for a minimum cost in coolant weight flow. This optimum case depends specifically upon the main-stream axial condition distribution and can only be obtained by proper slot flow control to suit each special application. Inasmuch as there are unlimited main-stream variations, such as pressure and temperature gradient, and in view of the very limited existing multiple-slot data, it is only logical in a research program to obtain first data for the simplest case—the case with essentially constant free stream velocity and coolant flow from slot to slot. The fact that wall temperature measurements were not made between the slots was partly due to instrumentation difficulty and partly due to the understanding that the injection panel could be considered as an upstream film-cooling section or a "generator" of initial velocity and temperature profiles for the adiabatic wall downstream of the last slot. Furthermore, one will realize upon closer consideration that measurements made downstream of the last slot effectively yield information between slots. For instance, the adiabatic

[4] Aeronautical Research Scientist, NASA, Cleveland, Ohio.

[5] Professor, Mechanical Engineering Department, University of California, Berkeley, Calif. Mem. ASME.

wall temperatures after the second slot for a three-slot panel are equivalent to that after the last slot for a two-slot panel, with the corresponding main-stream and injection conditions. The effect of heat transfer is studied in further multiple-slot experiments.

The authors certainly agree with Mr. Papell in that one should be careful in extrapolation. It may be possible that other unaccounted variables, such as the turbulence level, contribute to the difference among different data.

In regard to Professor Seban's remark on the correction of radiation effect, the authors estimated that h_r/h might be in the order of 0.07 and $t_\infty - t_s/t_s - t_g$ in the order of 0.14 so that $(h_r/h)\ (t_\infty - t_g)/(t_s - t_s)$ was in the order of 0.01. Radiation then had a relatively small effect on the slope of the effectiveness.

Velocity Distributions, Temperature Distributions, Effectiveness and Heat Transfer for Air Injected Through a Tangential Slot Into a Turbulent Boundary Layer

J. P. HARTNETT[1]
R. C. BIRKEBAK[2]
E. R. G. ECKERT[3]

A detailed study of the heat transfer for tangential air injection through a single slot into a turbulent boundary layer on a flat plate is presented; the results apply to a specific slot size, one injection rate, and a fixed free-stream velocity. Boundary-layer velocity and temperature profiles for a number of positions downstream from the point of injection are presented as well as plate-temperature distribution and heat-transfer data for adiabatic and constant heat input-wall boundary conditions.

Introduction

A PROMISING method for protecting a surface exposed to a high-temperature environment involves the introduction of a coolant liquid or gas through discrete slots appropriately positioned along the surface as shown in Fig. 1. This cooling scheme, commonly called film-cooling, has already found application in gas turbines and rocket nozzles and in the future may be of value in cooling leading edges of hypersonic aircraft.

The initial study of the effects of hot-air injection from a discrete slot into a turbulent boundary layer was made by Wieghardt [1].[4] This study consisted of the measurement of the adiabatic wall-temperature distribution downstream from the point of injection, and the subsequent development of the velocity and temperature boundary-layer profiles. In Wieghardt's investigation, the secondary or injected air was introduced in a direction almost parallel to the main stream. Next to study film-cooling

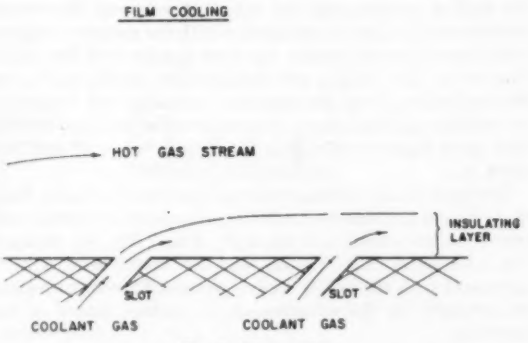

Fig. 1 Film-cooling

was Scesa [2], who injected the secondary air flow in a direction normal to the main flow. This study included measurements of the adiabatic wall-temperature distribution and the heat transfer with film-cooling for the case of constant wall temperature. It was found by Scesa that the standard solid-wall turbulent heat-transfer relations can be used for film-cooling if the heat-transfer coefficient is based on the difference between the wall temperature and the adiabatic wall temperature. Seban, et al. [3, 4], performed experiments for tangentially injected air with a slightly different slot configuration than Wieghardt [1], Fig. 26. Their reported dimensionless adiabatic wall-temperature distribution, the so-

[1] Professor of Mechanical Engineering, University of Minnesota, Minneapolis, Minn. Mem. ASME.
[2] Instructor, Department of Mechanical Engineering, University of Minnesota, Minneapolis, Minn.
[3] Professor of Mechanical Engineering, University of Minnesota, Minneapolis, Minn. Mem. ASME.
[4] Numbers in brackets designate References at end of paper.

Contributed by the Heat Transfer Division of THE AMERICAN SOCIETY OF MECHANICAL ENGINEERS and presented at the ASME-AIChE Heat Transfer Conference, Buffalo, N. Y., August 15–17, 1960. Manuscript received at ASME Headquarters, May 23, 1960. Paper No. 60—HT-31.

Nomenclature

B = constant of proportionality
C, C^1 = constants of proportionality
C_p = specific heat at constant pressure, Btu/lb$_M$, deg F
E = energy of injected air per sec, Btu/sec
h = heat-transfer coefficient, Btu/hr-sq ft-deg F
I = momentum flow per sec
K = defined in equation (26)
L = width of plate, in.
M = blowing rate parameter, defined in equation (1)
$\dot{m}$ = flow rate of secondary air, lb$_M$/sec
q = heat flux at surface, Btu/hr-sq ft
Re_x = Reynolds number, (UX/ν)
s = slot height, in.
St = Stanton number, $(h/\rho UC_p)$
T = temperature, deg F
T^* = average film temperature or reference temperature, deg F
U = velocity, fps
X' = distance downstream from slot leading edge, in.
X = distance downstream from effective leading edge of hydrodynamic boundary layer, in.
y = distance normal to wall, in.

(Continued on next page)

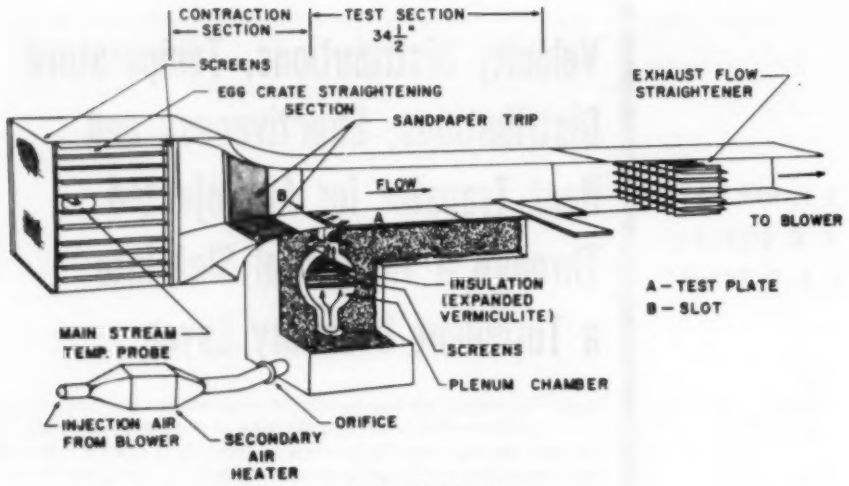

Fig. 2 Wind tunnel

called effectiveness, is somewhat at variance with that of Wieghardt. Included in these studies of Seban are heat-transfer-results far downstream from the point of injection which confirm the findings of Scesa that the standard solid-wall heat-transfer relations may be used in conjunction with the measured adiabatic wall temperatures to predict the heat transfer with film cooling. Chin, et al. [5] using a slot configuration similar to [3] have obtained values of the dimensionless adiabatic wall temperature for various injection rates. The correlation achieved for these data gives higher results than the data of Seban [3] and Wieghardt [1].

The latest results for tangential injection are reported by Papell, et al. [6] and are concerned with large temperature differences between the free stream and the injected air. The slot configuration is similar to that of Seban, and the effectiveness is in fair agreement with the earlier study. Several different correlations are proposed for the effectiveness for various ranges of mass injection.

This paper describes a complete study of the effects of tangential air injection into the free stream on the boundary-layer velocity and temperature profiles with adiabatic and constant wall-heat input boundary conditions. In this study a free-stream velocity of 165 fps was used throughout the program. The injection studies were restricted to a single slot size and a single blowing rate.

Experimental Apparatus

Wind Tunnel. The wind tunnel used for this investigation is shown in Fig. 2. The main flow of air is drawn through a straightening section, a diffuser section, into the test section, followed by a straightening section, and from here into the exhaust chambers. A blower removes the air from the chamber. The secondary or film-cooling air is introduced through an air heater, a standard thin-plate orifice, into a plenum chamber, and through the slot into the main flow as shown in Fig. 2.

The straightening section consists of a screen, an egg-crate section, and three additional damping screens. The egg crate, made of 1-in. square openings 15 in. long, was used to remove any rotation in the flow.

The diffuser-section inlet dimensions of 28 × 22 in. contract to 10 × 6 in. at the test-section inlet. The change in area is a smooth transition, and flow-visualization studies verified that no flow separation occurred. In this region, 6.5 in. ahead of the test section, a 6/0-grid emery-cloth strip 10 in. wide × 4 in. long is installed to "trip" the boundary layer and insure completely turbulent flow.

The test section of the tunnel is 6 in. high and 10 in. wide, and is capable of a velocity of approximately 165 fps with the available blower. The side and top walls of the tunnel are fabricated of plexiglas to allow visualization studies to be accomplished. Following the test section is an egg-crate straightening section, 9 in. long with $^3/_4 \times {}^3/_4$ grid. The floor of the tunnel is a specially constructed machined-steel plate $^3/_8$ in. thick, 10 in. wide, and 17 in. long and serves as the test surface. Provisions are made for either one or two injection slots in the base plate.

The slot configuration, Fig. 3, is a duplication of the geometry utilized by Wieghardt [1]. In the installation of this section, the slot height is kept uniform by inserting gages of the correct height at several positions across the tunnel. When in adjustment, the gages were removed.

The flow rate of the secondary air is measured by thin plate-orifice meters, constructed according to the ASME Code Stand-

Nomenclature

y_E = energy thickness, defined in equation (12)

y_I = a momentum thickness defined in equation (8)

y_m = a mass thickness defined in equation (6)

δ^* = displacement thickness, in., defined by equation (3)

δ_i = momentum thickness, in., defined by equation (5)

δ_T = "thermal" thickness, in., defined by equation (9)

θ_T = boundary-layer temperature thickness, in., defined by equation (16)

ν = kinematic viscosity, sq ft/sec

ρ = density, lb_M/cu ft

η = "effectiveness" for film cooling, defined in equation (14)

Subscripts

avg = average measurement

BL = boundary layer

s = slot

St = starting length

w = wall

∞ = free stream

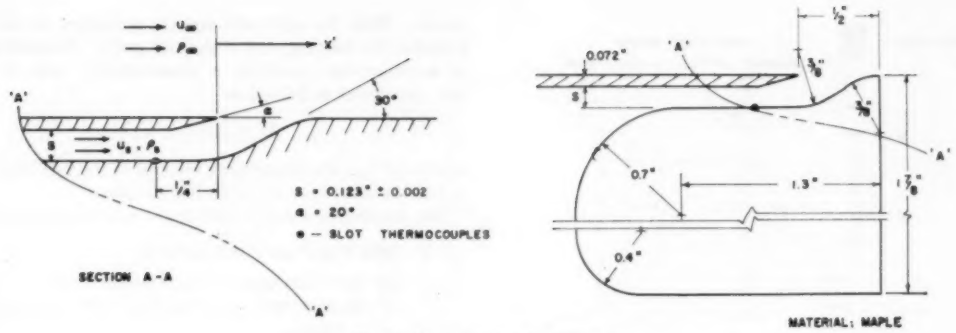

Fig. 3 Shape of air-injection slot

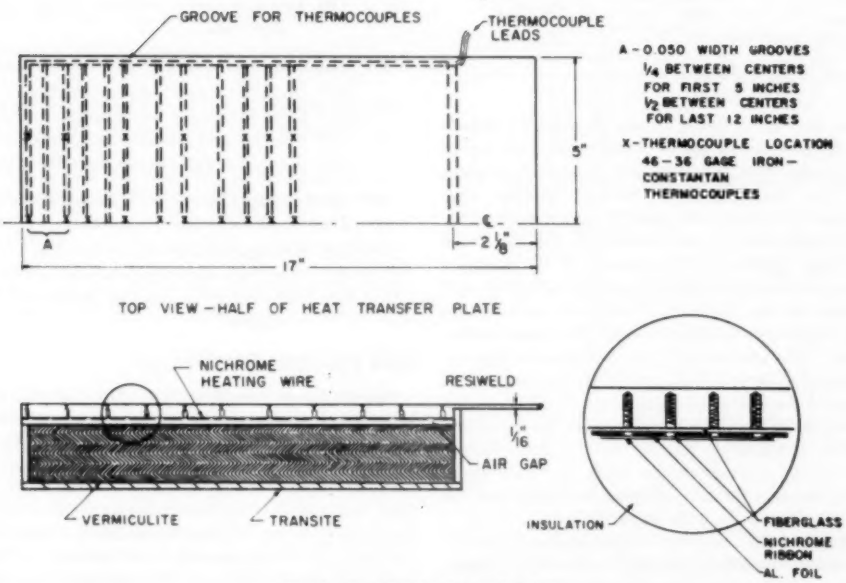

Fig. 4 Sketch of heat-transfer plate

ards [7]. Several orifices were made to cover the desired flow-rate ranges. The secondary-air heater, shown in Fig. 2, consists of Nichrome ribbons stretched back and forth across the duct and arranged in such a way as to insure adequate mixing of the air flow, thereby smoothing out any temperature inequalities.

Heat-Transfer Plate. The heat-transfer test section, shown in Figs. 4 and 5, is constructed to minimize longitudinal heat transfer, thereby allowing its use for the adiabatic wall measurements as well as for the heat-transfer studies. This is accomplished by grooving the mild-steel plate, leaving 0.016 in. of metal and filling in the grooves with a low-conductivity material—epoxy resin. The underside of the plate in Fig. 5 clearly shows that the grooves are more closely spaced at the leading edge of the plate where rapid temperature variations are anticipated. With this construction the effective thermal conductivity in the longitudinal direction (in the flow direction) is only 7 per cent of the effective thermal conductivity in the transverse direction. Thermocouples are embedded in the grooves between the epoxy and the steel allowing accurate measurements of the surface-temperature distribution. The plate is heated from below by individual Nichrome ribbons bonded by epoxy resin to the back of each segment of the plate, with an intervening layer of fiberglas electrically insulating the heater from the plate (see insert in Fig. 4). Aluminum foil is placed beneath the heater units to minimize the radiation losses. The large number of separate heaters with independent control of each unit permits the study of various thermal boundary conditions along the test length including the constant heat-input boundary condition and the constant wall-temperature case. The test section was mounted

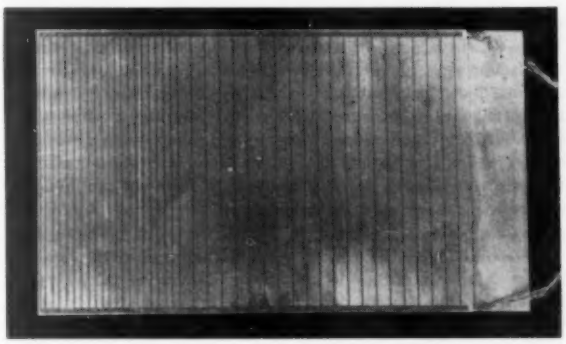

Fig. 5 Underside of heat-transfer plate

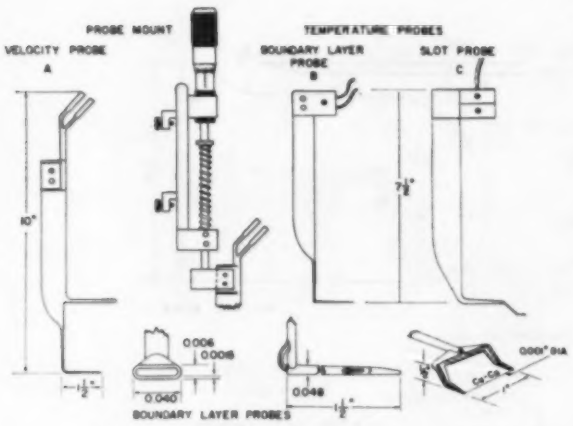

Fig. 6

in place as shown in Fig. 2, being separated from the plastic walls of the wind tunnel by an air gap of $^1/_{32}$ in. Below the heater section was 8 in. of vermiculite to minimize undesired heat losses.

Instrumentation. The boundary-layer velocity profiles were measured with a small flattened total-pressure probe with an attached free-stream static-pressure probe shown in Fig. 6. Probe tips were made from 0.036-in-OD stainless-steel hypodermic-needle tubing, the end of which was thinned to 0.0015-in. wall thickness, then flattened to a 0.003-in. × 0.037-in. opening and honed smooth. A probe tip was accepted only after examination under a microscope. The probes were mounted on a sliding carriage with a micrometer head which provided both axial and vertical positioning of the probe for measurements. The probes could be inserted in one of the three grooves cut in the top of the tunnel test section at positions of $^1/_4$, $^1/_2$, and $^3/_4$ of the tunnel width, allowing velocity surveys to be made at these three positions across the tunnel. Contact between the probe and the model was indicated electrically with an ohmmeter.

In the measurement of the temperature profiles the two completely different probes, shown in Fig. 6, were constructed. These two probes were designed to minimize conduction and radiation errors. Probe B is similar to the velocity probe but with an exit area hole at the end of the boundary-layer tube. A 36-gage iron-constantan thermocouple junction was located within this tube. Probe C was a claw-type probe with a 0.001-in-diam thermocouple wire stretched across the claw portion. These probes were calibrated and for a number of the early runs complete temperature profiles were measured with each of the two probes. The individual profiles measured with probe B were in good agreement with those found with probe C. In no case did the local measured temperature differ by more than 0.3 deg F from one probe to the other. Because of the ruggedness of probe B, it was used for the remaining tests.

Experimental Procedure. The object of the investigation was to obtain detailed information on the boundary-layer velocity profiles downstream from a slot with both unheated and heated air injections for adiabatic and constant wall-heat input boundary conditions. For the nonisothermal runs, temperature profiles were also sought, along with a specification of the adiabatic wall-temperature distribution and the local heat-transfer performance.

Before the initiation of the film-cooling studies, extensive velocity and heat-transfer measurements were accomplished with the inlet slot covered, thereby providing a solid flat plate in a turbulent boundary layer. This solid-plate investigation revealed the flow conditions in the wind tunnel and also demonstrated the reliability of the temperature and heat-flux measurements. With the inlet slot opened, secondary air could be injected at the leading edge of the test plate. To specify this rate of secondary-air injection, a mass-velocity ratio or blowing-rate parameter is defined as

$$M = (\rho U)_{slot}/\rho_\infty U_\infty \quad (1)$$

where $(\rho U)_{slot}$ is average mass velocity at the exit of the slot and $\rho_\infty U_\infty$ the mass velocity in the free stream.

The research was carried out in the following sequence:

I *Solid Flat-Plate Measurements:*
- (*a*) Boundary-layer velocity profiles.
- (*b*) Heat transfer to a flat plate with unheated starting length.

II *Isothermal Flow Study:*
- (*a*) Boundary-layer velocity profiles with secondary-air injection.

III *Adiabatic Wall Study With Heated Injection Air:*
- (*a*) Boundary-layer velocity profiles.
- (*b*) Boundary-layer temperature profiles.
- (*c*) Velocity and temperature profiles at slot exit.
- (*d*) Adiabatic wall-temperature distribution.

IV *Heat-Transfer Study With Heated Air Injection—Constant Heat-Input Boundary Condition:*
- (*a*) Boundary-layer velocity profiles.
- (*b*) Boundary-layer temperature profiles.
- (*c*) Constant heat input to plate with film-cooling heat transfer.

Solid Flat-Plate Measurement

Boundary-Layer Velocity Profiles. Using a solid plate with no air injection, boundary-layer velocity measurements were made at various stations in the tunnel test section. The initial velocity profiles were compared to establish laminar and turbulent boundary-layer velocity profiles and the comparison indicated that the velocity distribution was neither laminar nor fully turbulent. In an attempt to establish a fully turbulent boundary layer, a sandpaper trip was installed in the front of the tunnel as shown in Fig. 2. Fully established turbulent velocity profiles were then found in the test section; in addition, at any one axial position in the tunnel, the velocity profiles at the center line and the one-quarter and three-quarter width positions were in agreement. The measured center-line profiles are presented in a dimensionless manner in Fig. 7. These profiles, at several

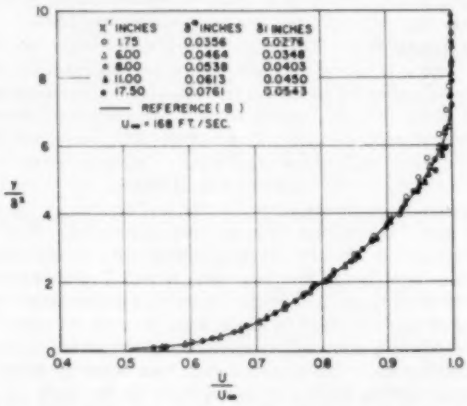

Fig. 7 Comparison of boundary-layer velocity profiles at center line of tunnel

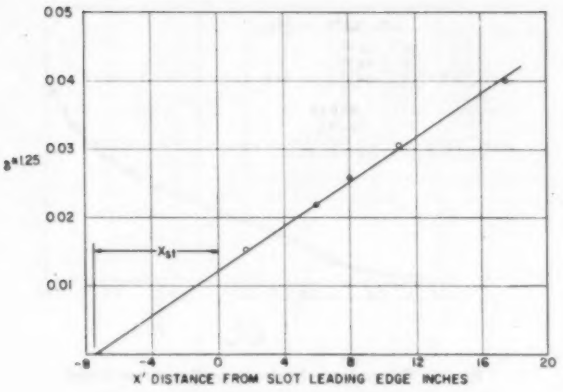

Fig. 8 Starting length determination U_∞ = 168 fps

positions along the tunnel, are seen to be in good agreement with one another and with the profile reported by Klebanoff and Diehl [8].

Under the assumption that the boundary layer originated as a turbulent one, it is possible with the aid of the velocity measurements to determine the effective starting location of the boundary layer. This information is of obvious value to the film-cooling studies as well as in making comparisons with other experimental data. The boundary-layer growth for turbulent flow along a flat plate can be expressed in terms of the displacement thickness:

$$\delta^* = C(\nu/U_\infty)^{1/5}X^{4/5} \tag{2}$$

where the displacement thickness δ^* is given by

$$\delta^* = \int_0^\infty \left(1 - \frac{\rho U}{\rho_\infty U_\infty}\right) dy \tag{3}$$

The value δ^* can be determined by integration of the measured velocity profiles. A plot of the resulting $(\delta^*)^{1.25}$ versus the distance from the actual leading edge of the closed slot X' can be extrapolated to the position when δ^* is zero, thereby determining the effective location of the start of the turbulent boundary layer. As shown in Fig. 8, the effective starting length to the slot leading edge is 7.5 in. Starting lengths of previous film-cooling investigations varied over a large range of lengths; Seban [4] of 2.5 in., Chin, et al. [5] of 41 and 239 in., and Wieghardt [1] of 28.5 in.

Heat Transfer to a Flat Plate With Unheated Starting Length. On completion of the flat-plate velocity-distribution studies, the heat transfer to the solid plate with an unheated starting length of 8 in. was investigated. A check on the reliability of the wall-temperature and heat-flux measurements was made with the grooved heat-transfer plate. Two distinct heat-transfer boundary conditions were imposed: (*a*) A heat-pulse input to the wall, and (*b*) a constant wall-heat input boundary condition. These two boundary conditions are shown schematically in Fig. 9.

The heat-pulse-input-measured wall-temperature distribution is compared with the wall-temperature distribution calculated with the procedure outlined in [9] when the heat-input distribution is given. This comparison is shown in Fig. 10. For such an extreme condition there is only fair agreement between measured and calculated wall temperatures. The spreading out of the experimental distribution is apparently due to the remaining thin metal strip on the plate surface. Conversely, the measured wall temperatures indicated in that figure were used, in conjunction with the calculation procedure outlined in [9], to calculate the total heat input from the wall temperatures. This procedure

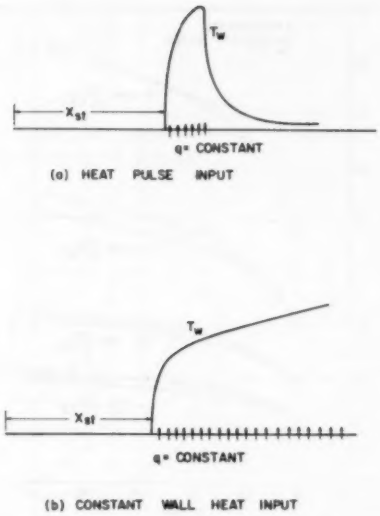

Fig. 9 Heat-input and wall-temperature distributions—solid wall

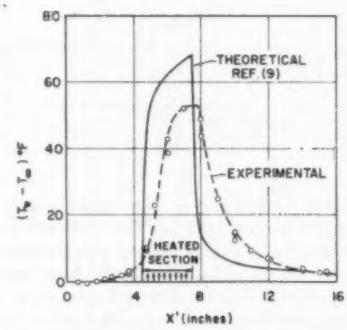

Fig. 10 Heat-pulse temperature distribution

yielded a value of the heat input equal to 397 Btu/hr as compared to the actual measured heat input of 399 Btu/hr.

As an additional check on the measurement technique, a constant heat input was applied to the entire length of the heat-transfer plate. Wall-temperature measurements were made and the heat-transfer coefficients were calculated from these measured results. The measured wall-temperature variations for four heat inputs are shown in Fig. 11, where they are compared with the predicted temperature distribution calculated by the procedure described in [9]. The property values required for the determination of the wall temperature were based on T^*, where T^* is defined as:

$$T^* = \frac{(T_w)_{avg} + T_\infty}{2} \tag{4}$$

The calculations were repeated using properties based on the free-stream temperature and on the average wall temperature; the resulting temperature distributions were within ±2 per cent of the results obtained using the reference temperature T^*. (In each case, the use of the free-stream property values gave the lowest predicted wall-temperature value.)

The difference between the experimental and calculated wall temperature, evident in Fig. 11, is apparently the result of an uncertainty in the heated width of the plate used in the calculations. The uncertainty arises because of the construction of the outer

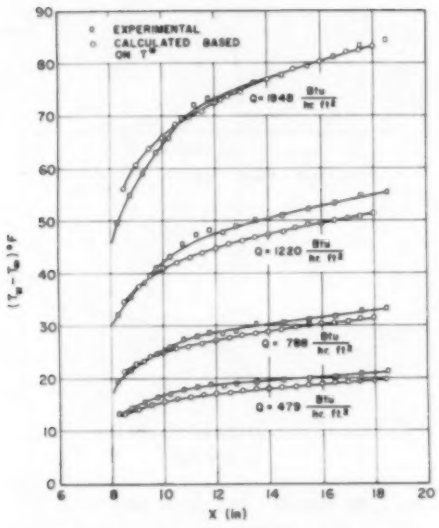

Fig. 11 Temperature distribution—solid wall

Table 1

Q(meas), Btu/hr	Q(calc T^*), Btu/hr	Error, per cent
348	371	+6.7
574	588	+2.4
890	946	+6.3
1420	1400	−1.4

edge of the plate, Figs. 4 and 5. Two choices as to the heated width of the plate are possible: (*a*) The total width of the plate, and (*b*) the width inside the two epoxy ribs that run lengthwise down the plate. In the calculation of the heat rate (Btu/hr-sq ft), the maximum width of the plate was used (L = 10 in.). An estimate of the possible error in using the width as 10 in. is 4 per cent.

Conversely, the total heat input was calculated from the measured wall temperatures. The calculated measured total heat inputs are shown in Table 1, where it is seen that the agreement was always better than 6.7 per cent. These results indicate that the plate is satisfactory for the heat-transfer measurements.

Isothermal Flow Study With Secondary-Air Injection

Boundary-Layer Velocity Profiles. In the preceding section the main flow conditions were established; i.e., a turbulent boundary layer having its effective starting point 7.5 in. before the slot leading edge. The injection slot shown in Fig. 3 was next installed and a check on the uniformity of the air flow from the slot at various positions across the channel was made. These velocity-profile measurements taken at 1/4, 1/2, and 3/4 of the channel width L, at a position 3/4 in. from the slot leading edge, are shown in Fig. 12 in dimensionless form, and convincingly demonstrate that the flow is uniform across the channel. These profiles were reproducible from one day to another.

A further condition to be specified is the velocity profile in the slot itself. These measurements were performed and the resulting slot-velocity profile is shown in Fig. 13, as a solid line. A mass-flow balance was calculated using this measured velocity profile. It agreed within 7 per cent with the mass flow measured by the orifices, thereby establishing confidence in the measured profile.

The positions for the measurements of the velocity profiles were selected to obtain a detailed idea of the flow development

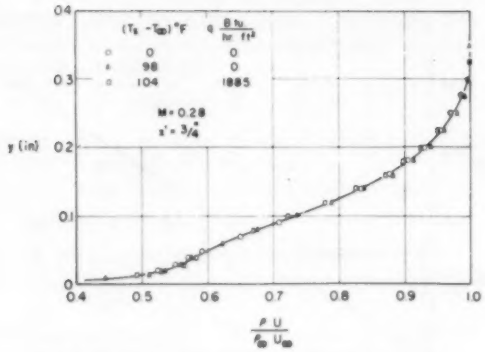

Fig. 12 Comparison of velocity profiles across tunnel

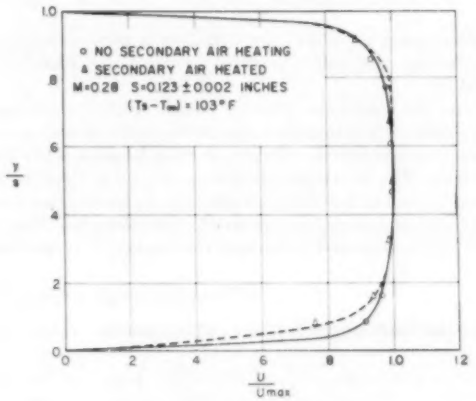

Fig. 13 Slot velocity profiles

near the slot. The first measurements were made just after the trailing edge of the slot. Far downstream from the slot the measurements were used to study the transition to fully developed flow. Fig. 14 shows the resulting profiles obtained at six stations downstream from the point of injection for a mass-velocity-ratio parameter of 0.28. If the velocity profiles at positions E and F are plotted in a dimensionless manner and compared to the fully developed turbulent-velocity profiles of Klebanoff and Diehl [8], their shapes coincide with the fully developed profile 90 slot heights downstream from the slot leading edge. At position D, Fig. 14, the dimensionless velocity is still changing and has not yet attained a fully developed profile.

From the measured velocity profiles, the displacement and momentum thickness δ^* and δ_i, respectively, were calculated. The displacement thickness was defined previously in equation (3) and the definition of the momentum thickness is expressed as

$$\delta_i = \int_0^\infty \left(1 - \frac{U}{U_\infty}\right) \frac{\rho U}{\rho_\infty U_\infty}\, dy \qquad (5)$$

The results of these calculations are shown in Figs. 15 and 16. Far downstream from the points of injection where the velocity profiles are fully developed, a new effective starting length could be defined to describe the resulting boundary-layer growth.

The efficiency of the injected-air layer can be evaluated by determining how rapidly the injected mass and momentum introduced through the slot are transported toward the free stream. The mass of air injected into the boundary layer per sec from

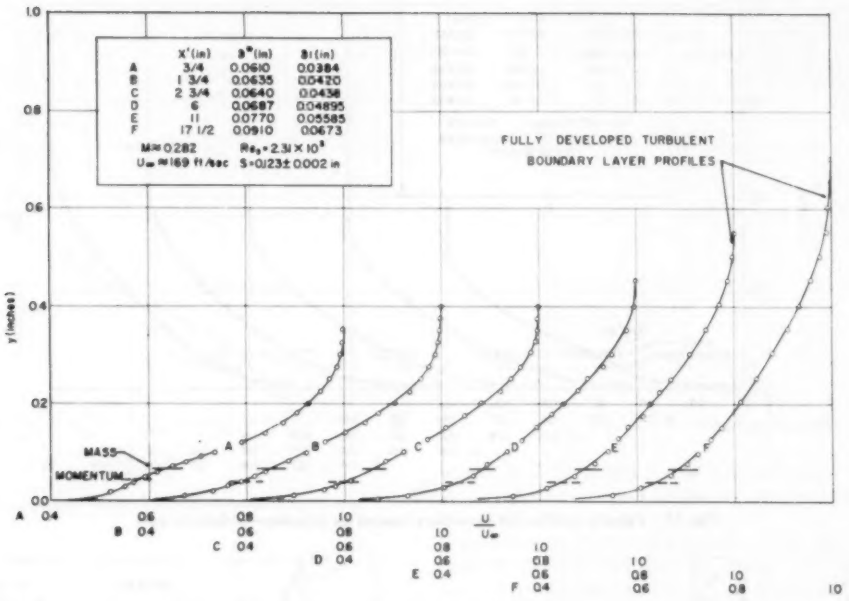

Fig. 14 Velocity profile for secondary air injection (isothermal) $(T_s - T_\infty) = 0$

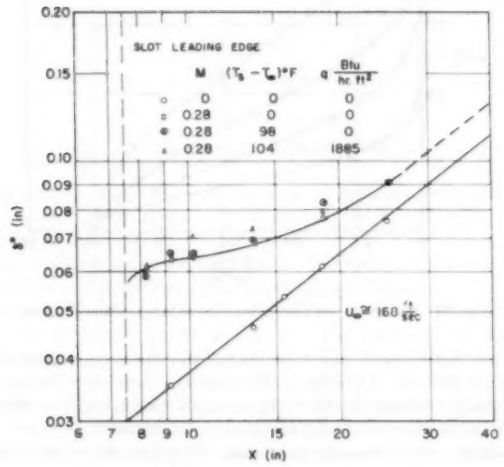

Fig. 15 Displacement thickness with air injection

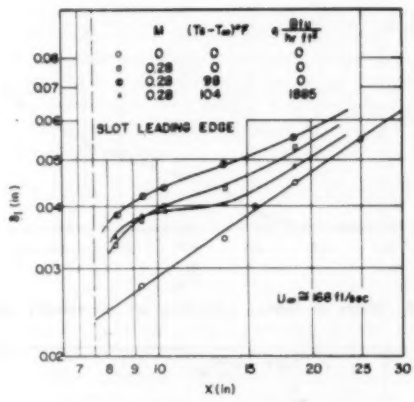

Fig. 16 Momentum thickness δ_i

the slot is calculated from the orifice-meter measurements. This measured mass is then equated to a mass in the boundary layer by the following equation:

$$\dot{m}_S = \dot{m}_{BL} = L\rho_\infty U_\infty \int_0^{y_m} \frac{\rho U}{\rho_\infty U_\infty}\, dy \text{ lb}_M/\text{sec} \qquad (6)$$

where y_m equals the height in the boundary layer under which the same quantity of mass per sec is contained as injected by the slot.

In a similar way, the X-momentum per sec associated with the injected air from the slot was calculated from the following equation:[6]

$$I_S = \dot{m}_S M U_\infty \text{ lb}_M\text{-ft/sec}^2 \qquad (7)$$

[6] Assuming the secondary air enters tangentially to the test surface.

This momentum per sec is then equated to the momentum in the boundary layer with the following equation:

$$I_S = I_{BL} = L\rho_\infty U_\infty \int_0^{y_I} \frac{\rho}{\rho_\infty}\left(\frac{U}{U_\infty}\right)^2 dy \qquad (8)$$

Here, y_I equals the height in the boundary layer under which the same quantity of momentum per sec is contained as injected from the slot. Performing the indicated operations gives the results shown in Fig. 14 (solid line—mass transport, dashed line—momentum transport), where it may be seen that there is little effective transport toward the free stream of the mass and momentum introduced through the slot.

Adiabatic Wall Boundary Conditions

Boundary-Layer Velocity Profiles. For heated injection air the velocity profiles are shown in Fig. 17, where they appear similar in shape to the isothermal profiles. A comparison of mass-veloc-

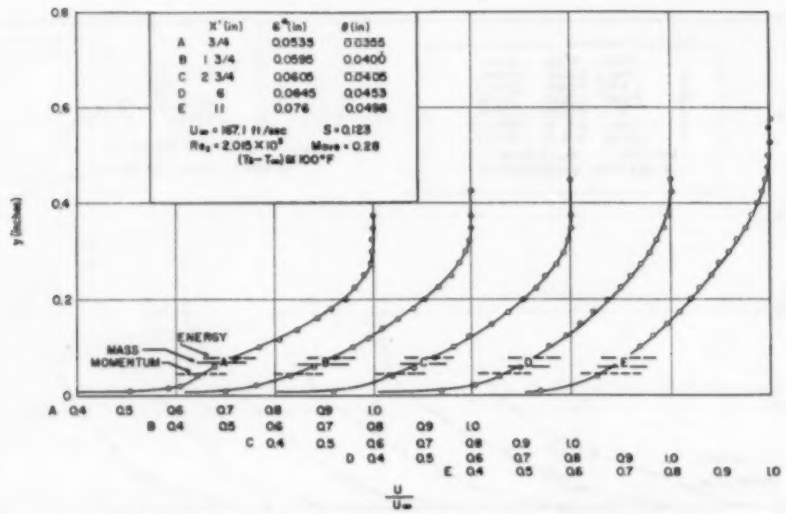

Fig. 17 Velocity profiles for secondary heated air injection—adiabatic wall

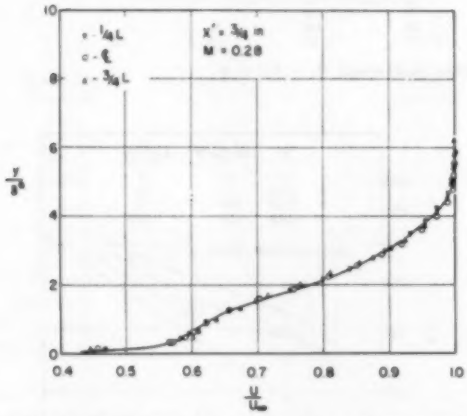

Fig. 18 Effects of heated secondary air on velocity profile

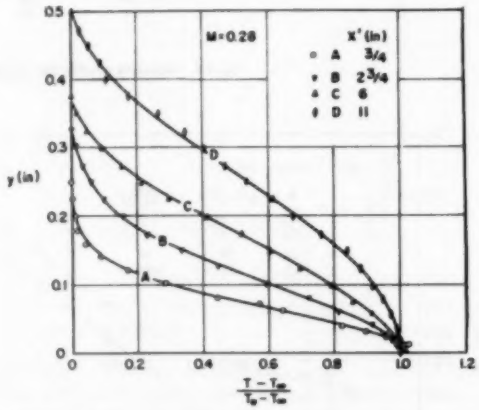

Fig. 20 Adiabatic-wall boundary-layer temperature profiles

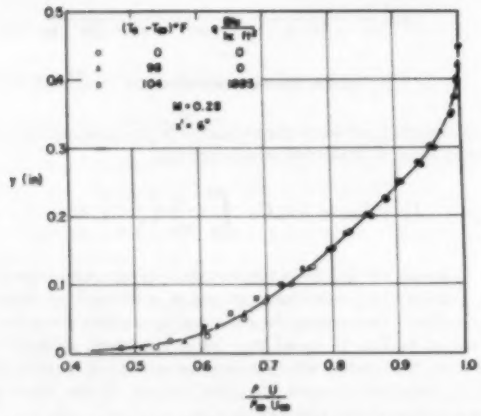

Fig. 19 Effects of heated secondary air on velocity profile

ity profiles for this case and the isothermal case is made for positions A and D in Figs. 18 and 19. The profiles compared on this basis have the same shape, since ρ decreases with temperature, U increases, and the product ρU remains constant.

The displacement and momentum thicknesses are shown in Figs. 15 and 16. The effects of heated injection air indicates no noticeable change in the displacement thickness, but shows a noticeable decrease in the momentum thickness.

Boundary-Layer Temperature Profiles. The boundary-layer temperature profiles measured at four locations downstream from the slot are shown in Fig. 20. These results may be presented on a single curve if the boundary-layer temperature thickness δ_T, as first used by Wieghardt, is introduced:

$$\delta_T = \int_0^\infty \frac{T - T_\infty}{T_{aw} - T_\infty}\, dy \tag{9}$$

This definition of δ_T normalizes the temperature profiles, as δ^* does for the velocity profiles. Fig. 21 shows the results in a dimensionless manner from which we see that the adiabatic boundary-layer temperature profiles are similar. Using a semiempirical approach, Wieghardt was able to show that the boundary-layer temperature profiles for the adiabatic wall condition could be correlated by an exponential function. In Fig. 21, the solid line represents the correlation of the temperature distribution by

$$\frac{T - T_\infty}{T_{aw} - T_\infty} = \exp\left[-0.768(y/\delta_T)^{12/7}\right] \tag{10}$$

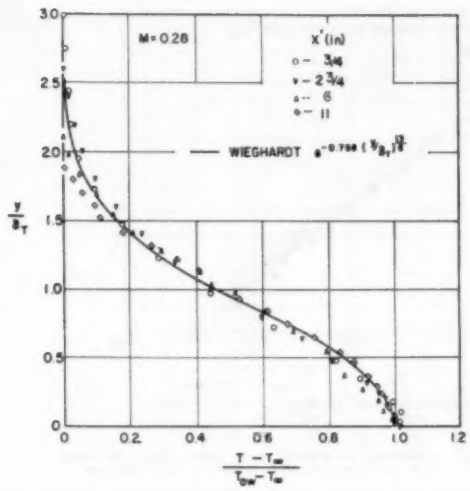

Fig. 21 Dimensionless temperature profile—adiabatic wall

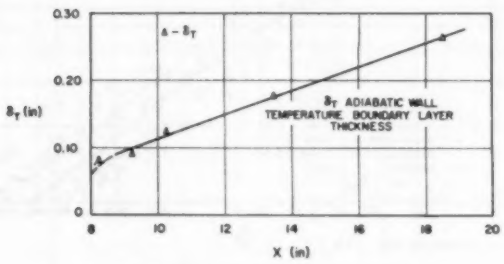

Fig. 22 Temperature boundary-layer growth

This same equation is seen to be in good agreement with the results of the present study. The manner in which δ_T changes with x is shown in Fig. 22.

Slot Temperature and Velocity Profiles. Temperature and velocity profiles were determined at the slot exit to establish the secondary-air state. The slot-temperature profile was measured using probe C with the results shown in Fig. 23. The temperature profile, with respect to the center line of the slot, is not symmetrical because of the heat conduction to the upper lip. An estimate of the maximum possible heat addition from the lip to the free stream is 4 per cent of that added by the injected air. Fig. 13 (dotted curve) shows the measured velocity profile in the slot for heated secondary air.

The rate may now be determined at which the mass, momentum, and energy, introduced through the slot, are transported toward the free stream. The momentum equation (7) is modified to take into account temperature effects. The energy flow per sec from the slot is

$$\dot{E}_s = C_p S L \rho_m T_m U_m \int_0^1 \frac{U}{U_m}\, d\left(\frac{y}{S}\right) \text{ Btu/sec} \qquad (11)$$

where ρ_m, T_m, and U_m are the maximum values of each of these parameters in the slot. This equation is then equated to an energy equation for the boundary layer:

$$\dot{E}_s = \dot{E}_{BL} = \int_0^{y_E} C_p \rho U T L \, dy$$

$$= C_p L \rho_\infty U_\infty T_\infty \int_0^{y_E} \frac{U}{U_\infty}\, dy \text{ Btu/sec} \qquad (12)$$

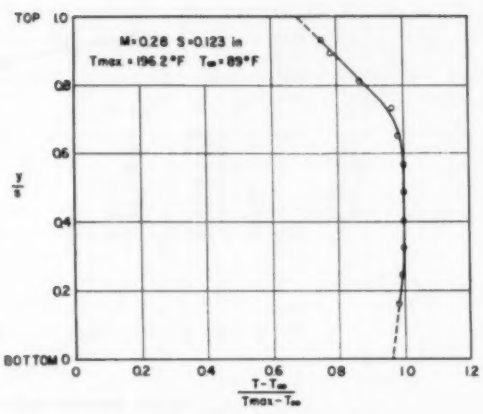

Fig. 23 Slot temperature profile

where y_E is the height in the boundary layer under which the same quantity of energy per sec is contained as introduced through the slot.

As shown in Fig. 17, the results at this blowing rate indicate that the mass, momentum, and energy introduced through the slot are not transported toward the outer edge of the boundary layer, but remain close to the surface.

Adiabatic Wall-Temperature Distribution. With confidence established in the heat-transfer test measurements, heated secondary air was injected from the slot and the resulting adiabatic temperature distribution was determined. The usual choice of parameters was made to represent the data. These same parameters are suggested in a semiempirical analysis presented in the Appendix. If the results are confined to air with constant fluid properties, the adiabatic wall-temperature ratio η is a function of the following parameters:

$$\eta = f(\text{Re}_s, X/MS, X_{ST}/S, \text{ and slot geometry}) \qquad (13)$$

where the dimensionless adiabatic wall temperature (effectiveness) is defined by

$$\eta = (T_{aw_x} - T_\infty)/(T_{slot} - T_\infty) \qquad (14)$$

and T_{slot} is the temperature of the air leaving the slot and T_{aw_x} is the adiabatic wall temperature. The results of the adiabatic wall-temperature distribution are shown in Fig. 24, in terms of the dimensionless distance from the slot leading edge, X'/MS, where X' is the actual distance from the slot leading edge, M is the injection parameter, and S is the slot height. The temperature of the injected air T_{slot} is measured in the position shown in Fig. 3, and was varied from 10 to 150 deg F above the temperature of the free stream ($T_\infty \cong 70$ F). At large values of the parameter X'/MS, the difference between the adiabatic wall temperature and the free-stream temperature ($T_{aw} - T_\infty$) is so small that a small fluctuation in either the free-stream temperature or the mass-injection rate will make a considerable variation in ($T_{aw} - T_\infty$) which gives rise to the scatter in the data. The data are correlated for $X'/MS \geq 60$ by the relation:

$$\eta = 16.9(X'/MS)^{-3/10} \qquad (15)$$

A calculation based on the theoretical analysis by Klein and Tribus [10] for a line heat source at the leading edge of a flat plate (i.e., a zero hydrodynamic starting length) gives a constant of 21.2 for a slot Reynolds number of 2100. One of the possible causes of the discrepancy between the constant of Klein and Tribus, 21.2, and the present one, 16.9, may be a hydrodynamic starting-length effect. The lower value of the present constant

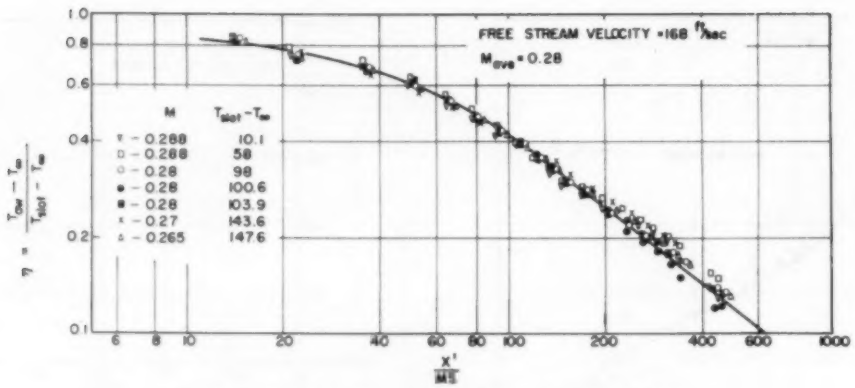

Fig. 24 Adiabatic wall temperatures for secondary-air injection

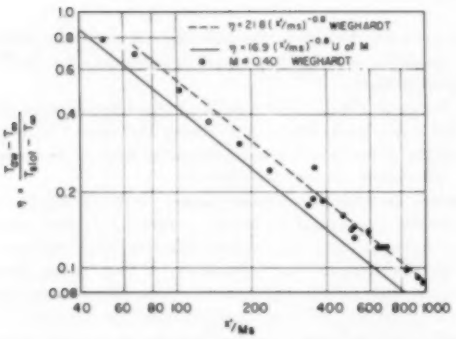

Fig. 25 Comparison of results with previous measurement of Wieghardt

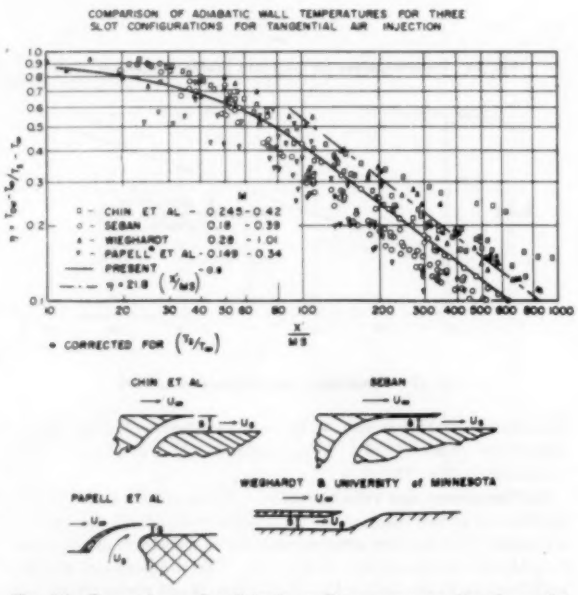
COMPARISON OF ADIABATIC WALL TEMPERATURES FOR THREE SLOT CONFIGURATIONS FOR TANGENTIAL AIR INJECTION
M
□ - CHIN ET AL - 0.245 - 0.42
○ - SEBAN 0.18 - 0.38
△ - WIEGHARDT 0.28 - 1.01
▽ - PAPELL ET AL - 0.149 - 0.34
PRESENT - 0.6
$\eta = 21.8 \left(\frac{X'}{MS}\right)^{-0.8}$
* CORRECTED FOR $\left(\frac{T_S}{T_\infty}\right)$
$\frac{X}{MS}$
CHIN ET AL
SEBAN
PAPELL ET AL
WIEGHARDT & UNIVERSITY of MINNESOTA

Fig. 26 Comparison of adiabatic wall temperatures for three slot configurations for tangential air injection

for a finite starting length as compared to the value for a zero starting length is also borne out in recent measurements of Seban [12] and Chin, et al. [5]. These latter investigators found that the effectiveness η decreases with an increasing starting length at least in the region far downstream from the point of air injection (i.e., at $X'/MS \geq 100$).

A comparison with the measurements of Wieghardt for a similar slot configuration is given in Fig. 25. The comparison is made for $X'/MS \geq 60$ with the dashed line representing the correlation of Wieghardt for all values of the dimensionless blowing rate less than or equal to unit (i.e., $M \leq 1.0$) and for slot Reynolds numbers between 3700 and 12,600. If Wieghardt's correlation is modified to represent only his lower blowing rates, $M \leq 0.40$ (the solid points in Fig. 25), the constant is changed from 21.8 for the dashed line to 19.5.

Based on the foregoing discussion, we would expect that the value of Wieghardt's constant would be less than 16.9 as found in the present investigation since the hydrodynamic starting length in Wieghardt's experiments was 28.5 in. as compared with 7.5 in. for the present program. This inconsistency may possibly be the result of an inaccurate measurement by Wieghardt of the entering injectant air temperature T_{slot} as it is not clearly stated in his report how this measurement was accomplished. Notwithstanding the discrepancy in the value of the constant in equation (15), the agreement of the present measurements with those of Wieghardt is fair, and both investigations are in agreement with the conclusion of the Appendix; namely, that the effectiveness is proportional to $(X'/MS)^{-0.8}$ at distances far downstream from the slot.

Experimental film-cooling results obtained with several different tangential-slot configurations are available for comparison—Wieghardt [1], Seban [4], Chin, et al. [5], Papell, et al. [6][6]—and the present results. The effectiveness values reported by these investigators is shown in Fig. 26 as a function of the important parameter X'/MS. In view of the different slot configurations and the different hydrodynamic conditions present in these several studies, it is surprising that there is not more variation in the effectiveness—in fact, a single curve can be drawn which will represent the reported values with a deviation of ±40 per cent. It is clearly not possible at the present time to state the specific causes of this variation but this must await more carefully controlled experiments in which the governing parameters are varied in a well-defined and systematic fashion. In the meantime, a reasonable estimate of the effectiveness for practical applications can be obtained from Fig. 26.

Constant Wall-Heat Input Boundary Conditions

Velocity Profiles With Secondary Air Heating. Velocity profiles

[6] Papell's data are for a large temperature difference between the free stream and injected air and have been corrected by $(T_S/T_\infty)^{1/2}$ as suggested by Papell to agree with present results.

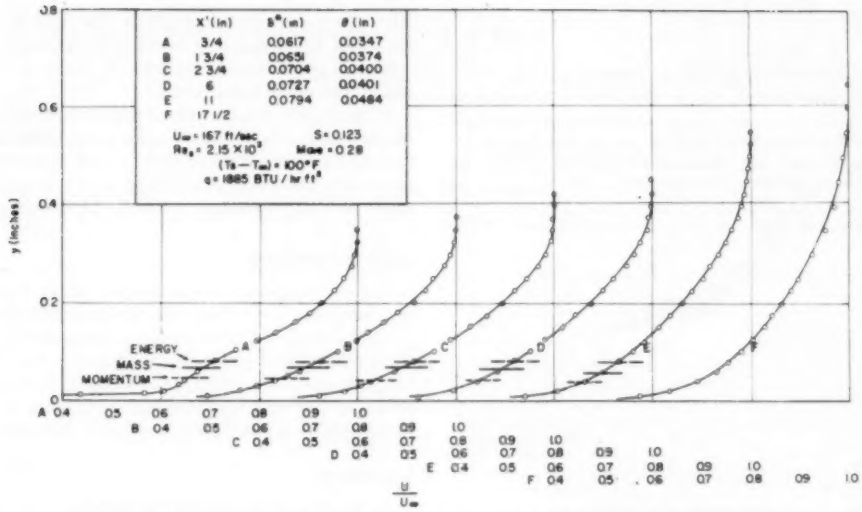

Fig. 27 Velocity profiles for secondary heated-air injection with constant wall heat input

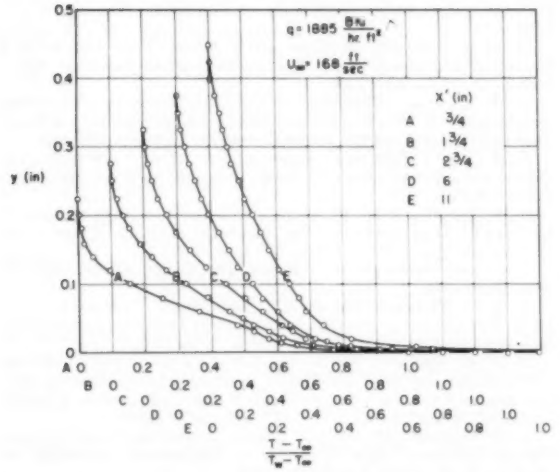

Fig. 28 Boundary-layer temperature profiles with film-cooling, constant wall heat input

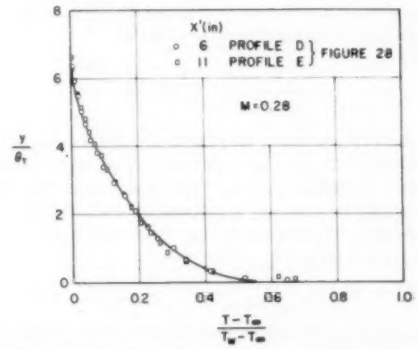

Fig. 29 Dimensionless temperature profiles with film-cooling, constant wall heat input

were measured at the same locations as for the isothermal and adiabatic wall cases. These profiles are shown in Fig. 27 and have shapes similar to the earlier measurements. The mass-velocity profiles at positions A and D are compared with the isothermal and adiabatic wall profiles in Figs. 18 and 19. This method of comparison not only reduces the mass-velocity profiles to the same general shape but actually results in complete coincidence of the profiles. It should be emphasized that this agreement of the mass-velocity profiles is valid only when the dimensionless mass injection is constant for all three cases; i.e., the value of M is constant.

The displacement and momentum thicknesses are shown in Figs. 15 and 16. From the definition of δ^*, equation (3), and δ_i, equation (5), property variations resulting from temperature differences should not affect the displacement thickness, since $\rho U/\rho_\infty U_\infty$ is used. The momentum thickness will decrease with an increase of temperature difference between the wall and free stream, since U/U_∞ appears in the equation. This effect is shown in Figs. 15 and 16.

Boundary-Layer Temperature Profiles. The measured temperature profiles for heated injection air with constant heat input to the wall are given in Fig. 28. As would be expected, no similarity is evident except far downstream from the injection point. The thermal boundary layers are made dimensionless by defining a thermal thickness θ_T:

$$\theta_T = \int_0^\infty \frac{T - T_\infty}{T_w - T_\infty}\, dy \tag{16}$$

The temperature profiles at positions D and E in Fig. 28 were made dimensionless by using this defined thermal thickness θ_T, and the results are plotted in Fig. 29, where it is seen that the curves for the two positions coincide, indicating a fully developed thermal boundary layer.

The rate at which the mass momentum and energy brought in by the injected air is transported toward the free stream is indicated in the figure; again, as in the isothermal and adiabatic measurements, it is clear that the injected mass momentum and energy remain close to the solid surface and are not transported toward the free stream.

Heat Transfer With Film-Cooling. The heat-transfer measurements covered a range of heat inputs from 485 to 1920 Btu/hr-sq ft, while the secondary or injected air was varied from 0 to 100 deg F above the free-stream temperature. The boundary condition imposed on the heated plate was that of constant heat flux. The

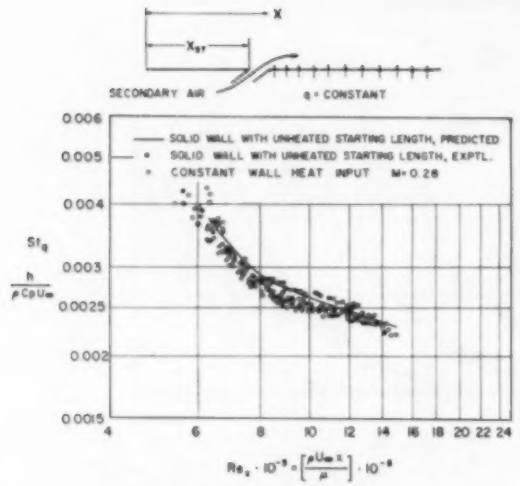

Fig. 30 Local heat transfer with air injection

results are shown in Fig. 30 in terms of the Stanton number $h/\rho C_p U_\infty$ versus the Reynolds number $U_\infty X/\nu$, with the heat-transfer coefficient being defined as follows:

$$h_x = \left(\frac{q}{T_w - T_{aw_x}}\right) \tag{17}$$

In equation (17) the adiabatic wall temperature T_{aw} is the local value corresponding to the particular free-stream injected air conditions; its value may be determined from Fig. 24. The properties used to calculate the Reynolds and Stanton numbers for film-cooling were based on the following equation for the reference temperature [11]:

$$T^* = 1/2(T_w - T_\infty) + T_\infty + 0.22(T_{aw} - T_\infty) \tag{18}$$

where T_w and T_{aw} are local values of the temperature. It should be noted that this expression reduces to equation (4) for the solid-wall measurements since in that case the adiabatic wall temperature is equal to free-stream temperature. The selection of this reference temperature for evaluation of the physical properties (ρ, U, and C_p) represents an attempt to account for the variation in these property values. It has been demonstrated previously that the foregoing reference temperature is valid for both laminar and turbulent flow over isothermal solid surfaces [11] in that it allows the use of constant-property prediction equations (with properties evaluated at T^*) even in those cases where large property variations occur.

Separate representation is given in Fig. 30 to data obtained with air injection (open circles) and data obtained with the slot closed designated as "solid wall with unheated starting length" (solid circles). For this particular mass-injection rate $M = 0.28$, there is no difference in the dimensionless heat-transfer performance with or without film-cooling. Also shown in the figure as a solid line is the predicted value of the Stanton number for the solid wall with an unheated starting length corresponding to the conditions of the investigation. This analytical prediction is in excellent agreement with the experimental measurements. The significant conclusion to be drawn from Fig. 30 is that standard solid-wall heat-transfer relations may be used for predicting the heat-transfer coefficient in the presence of film-cooling; the actual heat transfer is then calculated from equation (17) and requires the knowledge of the adiabatic wall temperature, which, for the present geometry, may be obtained from Fig. 24.

The earlier experimental results of Scesa [2] for air injected normally (i.e., perpendicularly to the main flow direction) and Seban [4] for tangentially injected air also support the use of the solid-wall predictions for calculating the heat-transfer coefficient in the presence of film-cooling.

In conclusion, it is possible at the present time to make reasonable estimates of the heat-transfer performance with film-cooling in a zero-pressure gradient flow in that Fig. 26 yields a good approximate value of the adiabatic wall-temperature distribution while [9] may be used to determine the heat-transfer coefficient.

Acknowledgments

The study reported herein is a part of the film-cooling research program being carried out with the financial support of the Office of Naval Research Power Branch on Contract Nonr 710 (14) and the authors acknowledge this assistance. The authors also wish to express their appreciation to Thomas F. McCarthy for his aid in obtaining and reducing the experimental data, and to Eileen Lego for her patience and skillful typing of the manuscript.

References

1 K. Wieghardt, "Ueber das Ausblasen von Warmluft für Enteisen," ZBW Research Report No. 1900 (ARF translation Rest. No. F-TS-919-Re, Wright Field, August, 1946).

2 S. Scesa, "Effect of Local Normal Injection on Flat-Plate Heat Transfer," PhD thesis, University of California, Berkeley, Calif., 1954.

3 R. A. Seban, H. W. Chan, and S. Scesa, "Heat Transfer to a Turbulent Boundary Layer Downstream of an Injection Slot," ASME Paper No. 57—A-36.

4 R. A. Seban, "Heat Transfer and Effectiveness for a Turbulent Boundary Layer With Tangential Fluid Injection," JOURNAL OF HEAT TRANSFER, TRANS. ASME, Series C, vol. 82, 1960, pp. 303–312.

5 J. Chin, S. Skirvin, L. Hayes, and A. Silver, "Adiabatic Wall Temperature Downstream of a Single Injection Slot," ASME Paper No. 58—A-104.

6 S. Papell and A. M. Trout, "Experimental Investigation of Air Film-Cooling Applied to an Adiabatic Wall by Means of an Axially Discharging Slot," NASA TN D-9, 1959.

7 "Flow Measurements," Power Test Codes, ASME 19.5: 4-1959, chapter 4.

8 P. S. Klebanoff and Z. W. Diehl, "Some Features of Artificially Thickened Fully Developed Turbulent Boundary Layers With Zero Pressure Gradient," NACA Report 110, 1952.

9 J. P. Hartnett, E. R. G. Eckert, and Roland Birkebak, "Calculations of Convection Heat Transfer to Non-Isothermal Surfaces Exposed to a Fluid Stream With Wedge Type Surface Pressure Gradient," WADC TR 57-753, ASTIA No. AD 142236.

10 J. Klein and M. Tribus, "Forced Convection From Non-Isothermal Surfaces," Heat Transfer, a Symposium, University of Michigan Press, Ann Arbor, Mich., 1953.

11 E. R. G. Eckert, "Survey on Heat Transfer at High Speeds," WADC TR 54-70, Wright Air Development Center, Wright-Patterson Air Force Base, Ohio, April, 1954.

12 R. A. Seban, private communication.

APPENDIX

Extending the analysis of Wieghardt [1], a relationship can be established between the effectiveness η, the blowing-rate parameter M, and the slot Reynolds number Re_s, from the velocity and temperature profiles far downstream of the injection point. The excess energy contained at any cross section downstream from the slot must be equal to the energy added at the point of injection.

$$\dot{E}_{slot}\,\frac{\text{Btu}}{\text{sec}} = \int \rho U C_p L(T - T_\infty)\,dy \tag{19}$$

rearranging the right-hand side one gets the following:

$$\dot{E}_{slot} = [\rho_\infty U_\infty C_p L(T_{aw} - T_\infty)] \int_0^\delta \left(\frac{\rho U}{\rho_\infty U_\infty}\right)\left(\frac{T - T_\infty}{T_{aw} - T_\infty}\right) dy \tag{20}$$

Using the experimental data as a guide, the mass velocity profile far downstream from the point of injection is represented by

$$\frac{\rho U}{\rho_\infty U_\infty} = \left(\frac{y}{\delta}\right)^{1/7} \tag{21}$$

The adiabatic boundary-layer temperature profile can be represented by Fig. 20,

$$\frac{T - T_\infty}{T_{aw} - T_\infty} = \exp\left[-C\left(\frac{y}{\delta}\right)^{10/9}\right] \cong \exp\left[-C\left(\frac{y}{\delta}\right)^2\right] \tag{22}$$

Substituting equations (21) and (22) into equation (20) gives

$$\dot{E}_{slot} = [\rho_\infty U_\infty C_p L(T_{aw} - T_\infty)] \cdot \int_0^\delta \left(\frac{y}{\delta}\right)^{1/7} \exp\left[-C\left(\frac{y}{\delta}\right)^2 dy\right] \tag{23}$$

Expanding the term $\exp\left[-C\left(\frac{y}{\delta}\right)^2\right]$ and keeping only the first three terms, one gets

$$\dot{E}_s = [\rho_\infty U_\infty C_p L(T_{aw} - T_\infty)] \cdot \int_0^\delta \left(\frac{y}{\delta}\right)^{1/7} \left[1 - C\left(\frac{y}{\delta}\right)^2 + C^2\left(\frac{y}{\delta}\right)^4\right] dy \tag{24}$$

Integrating equation (24) results in

$$\dot{E}_s = \rho_\infty U_\infty C_p L(T_{aw} - T_\infty)[7\delta(1/8 - C/22 + C^2/36)] \tag{25}$$

Let

$$K = 7(1/8 - C/22 + C^2/36)$$

and noting that δ grows as

$$\delta = BX/\mathrm{Re}_x^{1/5} \tag{26}$$

therefore

$$\dot{E}_s = C'\rho_\infty U_\infty C_p LX\mathrm{Re}_x^{-1/5}(T_{aw} - T_\infty) \tag{27}$$

E_s can be put into the form

$$\dot{E}_s = \dot{m}_s C_p(T_s - T_\infty) = C_p MSL\rho_\infty U_\infty(T_s - T_\infty) \tag{28}$$

therefore

$$C_p MSL\rho_\infty U_\infty(T_s - T_\infty) = C'C_p\rho_\infty U_\infty LX\mathrm{Re}_x^{-1/5}(T_{aw} - T_\infty)$$

defining

$$\eta = \frac{T_{aw} - T_\infty}{T_s - T_\infty}$$

results in

$$\eta = K'M\left(\frac{S}{X}\right)\mathrm{Re}_x^{1/4} \tag{29}$$

where $K' = 1/C'$.

This equation can be rearranged in terms of the slot Reynolds number to give

$$\eta = K'\left(\frac{X}{MS}\right)^{-4/10}\mathrm{Re}_s^{1/10} \tag{30}$$

This equation represents the data quite well far downstream from the point of injections and also agrees with the theoretical results of Klein and Tribus [10]:

$$\eta = 5.77(\mathrm{Pr})^{2/5}(\mathrm{Re}_s)^{1/10}\left(\frac{X}{MS}\right)^{-4/10} \tag{31}$$

DISCUSSION

J. H. Chin[7]

First of all, I would like to congratulate the authors for their fine and careful experiments. Further data of different blowing rates would be of interest.

Second, I would like to discuss certain "differences" between "Film Heating" and "Film Cooling" in some practical situations. For adiabatic wall, the boundary-layer temperature profiles with temperatures expressed as $\frac{t - t_\infty}{t_w - t_\infty}$ have the same characteristic

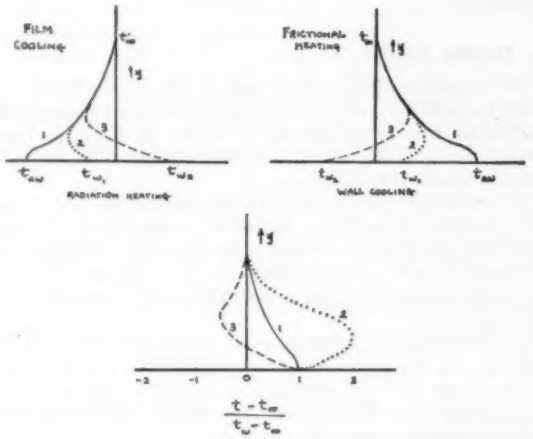

Fig. 31

shape for both film heating and film cooling. However, in film cooling when radiation sources, such as luminous particles, are present in the free stream, wall temperature may be higher than the "film" temperature near the wall, as shown in the slide. With film heating, the wall has to be cooled to generate the same shape of dimensionless temperature profile. It is of interest to note that the dimensionless temperature profile for film cooling with radiation heating has some similarity to the temperature profile for frictional heating with wall cooling.

R. A. Seban[8]

These welcome results on a film-cooling system reveal the details of performance of a situation in which the flow is disturbed less by the injection air than it is in the tangential injection systems for which results have been reported previously. Velocity profiles, as close to the slot as $x/s = 6$, show, as in Fig. 14, remarkably little influence of the low velocity of the injection air. This rather implies a strong turbulent transport initially, possibly due to the slight angle of the injection. Studies on systems of the type associated with this writer in Fig. 26 show, in contrast, some remainder of the slot velocity at distances as close as this. This increased transport may account for the slightly lower initial values of the effectiveness compared to those found in reference [4] for a similar velocity ratio.

Downstream, in the power law regime, the performance is almost identical. The correlation proposed in reference [4]

[7] Flight Propulsion Division, General Electric Company, Cincinnati, Ohio. Now at Lockheed Missiles and Space Division, Sunnyvale, Calif.

[8] Professor of Mechanical Engineering, University of California, Berkeley, Calif. Mem. ASME.

$$\eta = 25(m)^{0.4}\left(\frac{ms}{x}\right)^{0.8}$$

predicts values of the effectiveness 10 per cent below those of equation (15) at $m = 0.28$. At different values of m, greater differences occur, and this produces some of the scatter shown in Fig. 26.

The heat-transfer results shown in Fig. 30 also demonstrate the effect of the initial flow in this instance. In the system of reference [4] the coefficient in the initial region was low and was influenced by the slot flow, while in the present situation the results of Fig. 30 reveal that the free stream flow is the predominant influence on the flow conditions near the wall which determine the local heat transfer.

S. Stephen Papell[9]

My comments are concerned mainly with attempting to explain the ±40 per cent scatter of data taken from the many film-cooling investigators as presented in Fig. 26. In doing this, I also hope to point out the limitation of the usefulness of the data correlation presented in this paper.

An examination of Fig. 26 shows that most of the data follow the same slope of the present correlation although the level varies ±40 per cent. Consistent slopes suggest good data; therefore the difference in level can be attributed to the fact that the x/ms parameter does not have the necessary terms in it to generalize all the data.

I have two specific points to make. One is concerned with the difference of the slot configurations as related to the actual secondary air injection angle and the second is concerned with the attempt to correlate high temperature and high velocity data with Wieghardt's parameter, $x/(ms)$.

First, I would like to state that part of the spread of the data in Fig. 26 can be attributed directly to the differences of the slot configurations. Even though these slots were designed so that the guiding walls near the exit were nearly tangential to the test plate, I would expect that flow measurements would show that the secondary air discharges at various angles other than tangential. This angle also varies depending on the mass velocity of the free stream. NASA TN D-299 was published in order to show the effect on gaseous film cooling of coolant injection through slots whose actual injection angles (not slot angle) were varied from 0 to 90 deg relative to the test plate. It is shown that this effect can be quite significant. I suggest that this angle effect be evaluated before attempting to correlate data from various configurations.

My second point is to explain why it is not surprising that the reference [6] data do not correlate with Wieghardt's parameter. Fig. 26 shows that while some reference [6] data points fall close to the present correlation, others seem to fall off by 40 per cent. Prior to publication of reference [6], the authors attempted to correlate film cooling using Wieghardt's parameter with limited success. It was found that low temperature, low velocity data similar to that obtained by Wieghardt correlated fairly well but the higher temperature and velocity data fell off considerably. These results are demonstrated quite effectively in Fig. 26 of the present paper. It is obvious that the temperature ratio correction to the correlation presented in reference [6], when applied to the present correlation, was not sufficient to overcome the basic difference in both correlations.

I would like to add a word of caution concerning application of the correlation presented in this paper. The correlation obtained using low temperature and low velocity data is strictly empirical and, as such, its use cannot be extrapolated to higher temperatures and velocities.

[9] Aeronautical Research Scientist, NASA, Cleveland, Ohio.

Authors' Closure

The authors wish to thank Messrs. Chin, Seban, and Papell for their significant discussions.

They are, in the main, concerned with the presentation of the film effectiveness as obtained by various investigators and presented in Fig. 26 of this paper. The differences among the values obtained in the various investigations are significant and the authors feel that a determination of the parameters which cause these differences is one of the most urgent tasks in film-cooling research. Some of the possible reasons have been pointed out by the discussers; however, it is felt that other parameters may be involved as well, and an investigation into this situation is actually the aim of a study presently under way in the Heat Transfer Laboratory.

The experimental research on film cooling carried out at this laboratory is intentionally confined to temperature differences which are sufficiently small so that the influence of property variations can be neglected. This is done because the number of remaining parameters is still considerable. They include: 1 Slot geometry; 2 free stream Reynolds number; 3 definition of slot temperature; 4 slot Reynolds number; 5 blowing rate parameter; and 6 pressure gradient along film-cooled surfaces. The remark of one discusser that this should be kept in mind in the use of correlations presented in our paper is certainly appropriate. The restriction to small temperature differences brings also the advantage that film cooling and film heating become similar processes which are described by the same relation for film effectiveness and heat-transfer coefficient with proper selection of the boundary conditions.

PETER GRIFFITH[1]
GRAHAM B. WALLIS[2]

Two-Phase Slug Flow

Introduction

When two phases flow concurrently in a pipe, they can distribute themselves in a number of different configurations. The gas can be uniformly dispersed throughout the liquid in the form of small bubbles. There can be large gas bubbles almost filling the tube. There can be an annulus of liquid and core of vapor with or without drops of liquid in it. The interface can be smooth or wavy. When one describes how the phases are distributed, one is specifying the flow regime. Such a description is necessary before any mathematical model can be constructed which will predict a quantity such as pressure drop.

It is naïve to expect that a single mathematical model would adequately encompass all possible two-phase flow regimes, even for a single geometric configuration. Therefore we shall begin by saying that for this work the results that have been obtained and the conclusions that have been drawn apply only to fully developed slug flow in a round vertical pipe.

Slug flow is characterized by large bubbles, almost filling the tube, which are separated by slugs of liquid. The nose of the bubble is rounded and the tail generally flat. One may or may not find small bubbles in the slug following the large bubble. (Typical slug-flow bubbles are pictured in Fig. 4.)

Bubbles very similar to these have been studied by Dumitrescu [1],[3] and Davis and Taylor [2]. Both these references consider the same problem. How rapidly will a closed tube full of liquid empty when the bottom is suddenly opened to the atmosphere? The approach used by both authors is to assume that the asymptotic rise velocity (for large times) can be calculated from potential-flow theory. The boundary condition at the pipe wall is that the velocity is axial. At the bubble boundary it is assumed that the pressure is constant. The problem is then to find the shape of the bubble that would satisfy the constant-pressure boundary condition. This was done approximately, and in both cases the comparison with experiment was satisfactory, though the deviations became large for small tubes.

The work of Davis and Taylor, and Dumitrescu served as the starting point for this investigation. The boundary condition at the bubble wall for large bubbles, constant pressure, was still valid to an excellent approximation, and the finiteness of the slug-flow bubbles did not appear to make much difference in their rise velocity.

In the next section an expression for the mean density will be developed which will be expressed in terms of the pipe area, the bubble rise velocity, and the flow rates of the two phases. In subsequent sections the observations made of bubble shape, length, and velocity will be described and then a comparison of computed and measured densities given. Finally, a method for predicting the pressure drop will be presented and the prediction compared with experiment.

Average Density of Mixture in Slug Flow

Assume as a control volume a section of vertical pipe which goes from the entrance of the pipe to the middle of one slug. Fix the control volume in space, Fig. 1, line "a." Continuity will yield the result that, when both phases are incompressible, the velocity in the slug well ahead of the tip of the bubble is simply the total volume flow rate divided by the pipe area.[4] If the velocity of the bubble is V_b with respect to the liquid ahead of it, then the velocity of the bubble with respect to the ground will be

$$\frac{Q_f + Q_g}{A_p} + V_b$$

The time it takes for a representative sample, that is one average bubble and one average slug, to pass a given section of the pipe will be

[1] Associate Professor of Mechanical Engineering, M.I.T., Cambridge, Mass. Assoc. Mem. ASME.

[2] Research Assistant, Department of Mechanical Engineering, M.I.T., Cambridge, Mass. At present, Research Fellow, Atomic Energy Establishment, Winfrith Heath, Dorset, England.

[3] Numbers in brackets designate References at end of paper.

Contributed by the Heat Transfer Division of The American Society of Mechanical Engineers and presented at the ASME-AIChE Heat Transfer Conference, Buffalo, N. Y., August 15–17, 1960. Manuscript received at ASME Headquarters, May 31, 1960. Paper No. 60—HT-28.

[4] It can be shown by a more complete analysis that the present formulation also holds for a compressible gas.

Nomenclature

A_p = pipe cross section area = $\pi D_p^2/4$
A_w = pipe area equal to $\pi D_p(L_s + L_b)$ in equation (10)
C_1, C_2 = dimensionless constants used to calculate bubble rise velocities from equation (8). To be evaluated from Figs. 8 and 9
D_p = pipe diameter
g = acceleration of gravity
L = length
L_s = slug length
L_b = bubble length
m = dimensionless constant relating bubble volume to length in equation (6) equal to 0.913 for potential flow
n = dimensionless constant relating bubble volume to length in equation (6) equal to 0.526 for potential flow
N_{Re_b} = $V_b\rho_f D_p/\mu_f$, bubble Reynolds number
N_{Re_f} = $[(Q_f + Q_g)/A_p](D_p\rho_f)/\mu_f$, liquid Reynolds number
P = pressure
Q_f = liquid flow rate
Q_g = gas flow rate
V_b = bubble rise velocity with respect to liquid ahead of bubble
V_w = mean water velocity
v_b, v_f, v_g, v = bubble volume, liquid volume, vapor volume, and total volume
ρ_a = average density
ρ_g = gas density
ρ_f = liquid density
τ_w = wall shear stress
τ_w' = wall shear stress for fully developed flow for liquid at mixture velocity
Δt = period for one slug and one bubble to pass a section of the pipe

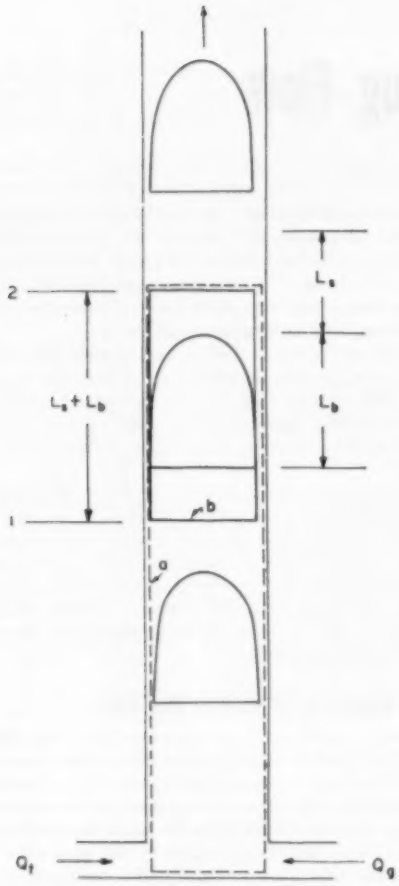

Fig. 1 Control volumes mentioned in text

$$\Delta t = \frac{(L_s + L_b)A_p}{Q_f + Q_g + V_b A_p} \tag{1}$$

Δt is then the period for the bubbles.

Let us continue by considering the time average flow rate of the gas phase past a section. During one period one bubble of volume v_b will pass; therefore the average flow rate for the gas will be

$$Q_g = v_b/\Delta t \tag{2}$$

The average density in a volume containing two phases is

$$\rho_a = \rho_f \left[1 - \frac{v_b}{v}\right] + \rho_g \frac{v_b}{v} \tag{3}$$

In terms of the phase densities, the average density of a typical pipe section containing one bubble and one slug will be

$$\rho_a = \rho_f \left[1 - \frac{v_b}{(L_s + L_b)A_p}\right] + \rho_g \left[\frac{v_b}{(L_s + L_b)A_p}\right] \tag{4}$$

When equation (1) is substituted into (2) and the result substituted into (4), one obtains:

$$\rho_a = \rho_f \left[\frac{Q_f + V_b A_p}{Q_f + Q_g + V_b A_p}\right] + \left[\frac{\rho_g Q_g}{Q_f + Q_g + V_b A_p}\right] \tag{5}$$

This is the desired expression. Therefore, if one has the value for the bubble-rise velocity, it is possible to calculate what the mean density in the pipe is.

Bubble Length and Slug Length

Let us assume that an approximate empirical formula relating bubble length to volume exists in the following form

$$v_b = A_p(mL_b - nD_p) \tag{6}$$

Such a formula has been fitted to the calculated shape of Dumitrescu, which is valid only for the potential flow case. However, such a formula could as well be fitted to any bubble whether the conditions of potential flow are satisfied or not. The constants m and n would simply be somewhat different.

If one fixes the slug length, the bubble length is fixed by continuity considerations on the gas phase and the ratio of gas to liquid flow. Let us suppose that the slug length is specified and the relation between bubble length and volume is that of equation (6). Substituting (1) and (6) into (2) results in this expression for bubble length

$$L_b = \frac{Q_g L_s + n D_p(Q_g + Q_f + V_b A_p)}{m(Q_g + Q_f + V_b A_p) - Q_g} \tag{7}$$

This equation relates to bubble length, to the slug length, and various other known quantities.

As long as the bubble volume versus length relationship is adequately represented by a formula of the type of equation (6), equation (7) is valid. For the particular case of *potential* flow around the bubble, the constants in equation (6) can be evaluated and are

$$\begin{aligned} m &= 0.913 \\ n &= 0.526 \end{aligned} \quad \text{for} \quad L/D < 20$$

These constants are dimensionless. Though the shape must be altered if the flow around the bubble is not irrotational, it appears as though the foregoing values for m and n work quite well whether the flow is irrotational or not; that is, the bubble shape is relatively insensitive to velocity profile of the liquid as it approaches the bubble.

The analysis for pressure drop will be presented in a later section.

Experimental Apparatus

A diagram of the apparatus is shown in Fig. 2.

The central feature is the 18-ft vertical tube in which flow studies are made. This tube is made of three 6-ft sections of plexiglas tubing which are finished flat at the ends and are joined together to form the continuous length by gluing them firmly into plexiglas blocks which have been drilled out to fit the outside diameter of the tube.

The uppermost 6-ft section carries six pressure taps at 1-ft intervals and these are connected to vertical water manometers. Hose clamps are used in the connecting lines so that the manometers may either be isolated or the flow to them suitably throttled to damp out pressure fluctuations. The tubes leading from each pressure tap to the corresponding manometer slant downward. This prevents air bubbles from entering the manometer and making accurate readings impossible.

Near its upper end the main tube passes through a block which is used to anchor it to the wooden board supports. A flexible hose connects the top end of the tube to the discharge tank in which air and water are separated. This tank is drained by a further length of hose which feeds weigh buckets as required. By inserting a small-diameter flexible hose into the top of the tube, it is also possible to produce downflow in the test section.

At its lower end, the tube carries a plastic block suitably drilled to provide inlet ports for the air and water supply. Air is fed through a $^1/_8$-in-diam hole inclined downward toward the tube inlet and water is supplied through a $^3/_8$-in-diam horizontal hole. Needle valves in hot and cold-water supply lines control the flow rate and water temperature. Air supply is also controlled by a needle valve in the line. Before entering the apparatus, the air passes through a filter and metering orifice plate. Three sizes of tube were used in these experiments: 1, $^3/_4$, and $^1/_2$-in. ID.

Photographs of the flow patterns were taken in the upper half of the top tube section. Behind the tube there is a white sheet of paper which has horizontal lines drawn on it at $^1/_2$-in. intervals. A 2 microsec flash[5] is employed and photographs are obtained on 35mm Kodak Panatomic X film. The negatives were then analyzed on a microfilm reader. Illumination is from the front, to the side, and below the center line. In this way, bubbles and scale are illuminated as uniformly as possible using only one flash source.

Experimental Methods and Results

Measurements of bubble-rise velocities were made in both still and moving water. First, the water velocity was set by means of the needle valves. Next, a single bubble was introduced by rapid opening and closing of the air supply valve. Bubble length was between 2 and 10 diameters. Bubbles were timed with a stop watch over a standard length of 9 ft, the first mark being 3 ft from the inlet. An experimental limitation is the accuracy of the stop watch ($^1/_{10}$ sec) so that rise times of less than 5 sec were not found to be sufficiently accurate. Water flow rates are measured to suitable accuracy by use of a weigh bucket. Both upward and downward flow of the water were investigated and cold and hot water were used to investigate the effects of Reynolds number.

[5] "Microflash" type 1530-A manufactured by General Radio, Cambridge, Mass.

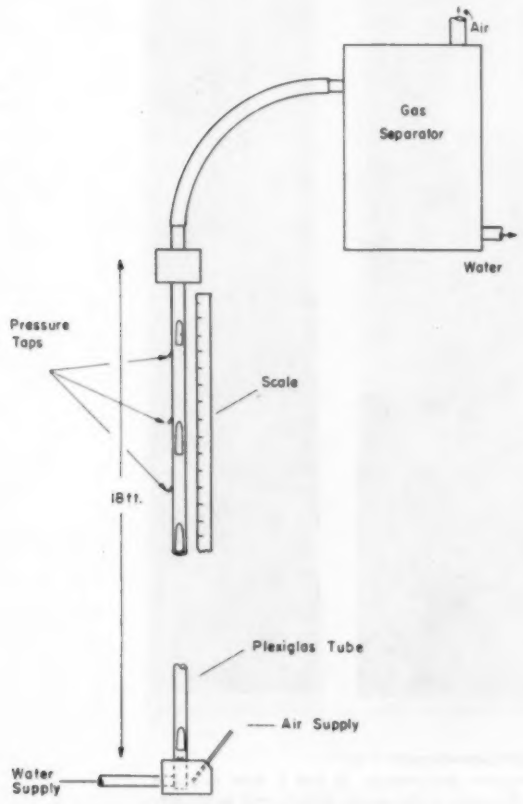

Fig. 2 Main features of the apparatus

At a given water flow rate the bubble-rise velocity was found to be independent of the length once the bubble was large enough so that its shape approximated that of the potential-flow theory. Consistency of results in this respect was remarkable, involving, in general, only changes of the order of stop-watch accuracy between the two extremes. Apparently, the hydrodynamics at the nose of the bubble is the sole determining factor.

At first it was expected that the velocity of the air bubble relative to the mean water velocity would be independent of the stream velocity. However, a few experiments soon showed that this was not the case. The bubble velocity is appreciably altered as the stream-velocity profile changes. Results for the three pipes at various water temperatures are shown in Fig. 3.

As the downflow water velocity was increased, a point was reached at which the stable character of the bubble suddenly changes. Instead of assuming the smooth steady shape of previous experiments, the nose of the bubble began to distort, to become alternately eccentric on one side or another, and to lean over to one side of the tube. As a general rule, the rise velocity would change quite randomly as the shape changed, being higher the greater the distortion of the nose. The bubble appeared quite "uncertain" which shape to assume so that readings of its velocity showed considerable variation from one experiment to the next. Finally, as downflow water velocity was further increased, the unsymmetrical shape became dominant and the motion became steady again. The transition point is marked with a cross in Fig. 3.

With the present apparatus it is possible to cover a range of slug flows varying from the first development of this regime at the transition from bubbly flow up to conditions where the slugs are either several feet long (high-quality flow) or so severely distorted by shear stress and turbulent forces that new phenomena begin to appear. Because of air-supply limitations, it was impossible to obtain the transition to annular flow with this apparatus.

The largest pipe provides the best illustration of normal slug flow since in its case the effects of viscosity and surface tension are least.

Under "normal slug-flow conditions" the flow appears as shown

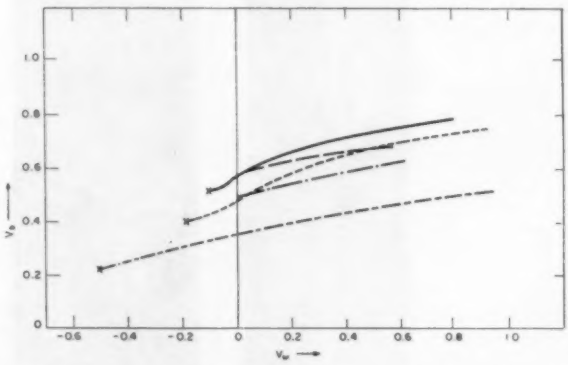

Fig. 3 Bubble velocity V_b against average water velocity V_w in ft/sec

———	1-in. pipe with cold water	10 deg C
— — —	1-in. pipe with hot water	34 to 49 deg C
- - - - - - -	3/4-in. pipe with cold water	10 deg C
—·—·—	3/4-in. pipe with hot water	23 to 50 deg C
—··—··—	1/2-in. pipe with cold water	10 deg C

x denotes onset of bubble instability as described in the text

in Fig. 4. A series of bubbles, just like those observed by G. I. Taylor or Dumitrescu, flow up the pipe, separated by "plugs" of water which are relatively free of bubbles. The wake of the previous bubble is smoothed out by turbulent mixing and by eddies so that its effect on the next bubble is negligible. Some small bubbles are formed in the wake by being torn off the back of the main bubble, but these soon reach an equilibrium concentration with as many being formed as are reabsorbed. The smallest bubbles formed in this way are unable to keep pace with the parent and are swept downstream, either to be absorbed by some later bubble or to coalesce among themselves until they reach sufficient size to rise with the same velocity as the large bubbles.

It should be stressed that this kind of ideal flow is only to be found over a limited range of flow rates and regions. Theoretically, slug flow is possible at almost any flowing quality, the bubble length simply adjusts accordingly. In fact, in investigating the development of slug flow from the "bubbly" flow regime, it was found that it was quite possible to have bubbly flow at the tube entrance whereas a few feet higher up chance encounters would create a bubble sufficiently large to fill the tube and to start to grow into a typical slug-flow bubble by absorbing its neighbors. By varying flow rates, it was possible to extend this "entrance region" to the full 18 ft of pipe whereas it was suspected that in a longer pipe, slug flow would be the ultimate stable regime. Of course, the bubbles are also growing as they rise due to the drop in hydrostatic pressure, but undoubtedly the entrance region effects predominate. Fig. 5 shows these effects 16 ft from pipe entrance. This effect is probably a major cause of deviations among the data of various experiments on transition from bubble to slug flow. When this "transition" occurs, and how it

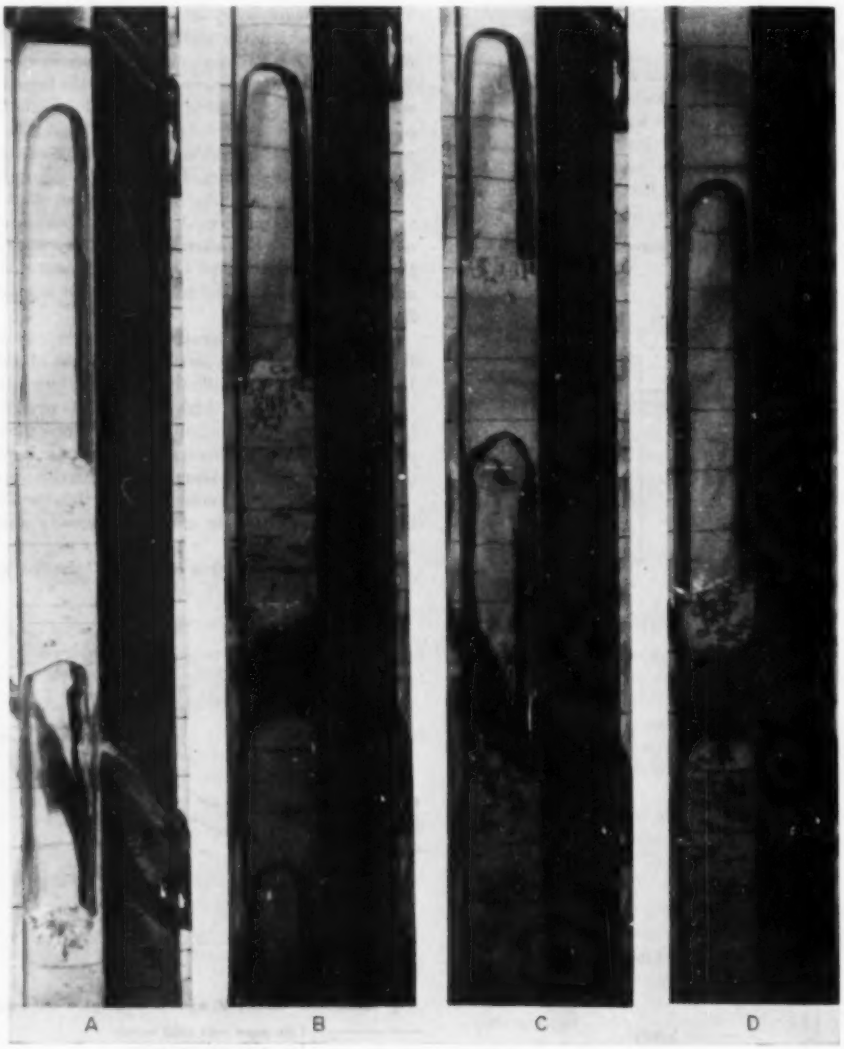

Fig. 4 $Q_g = 0.073$ $Q_f = 0$ in CFM pipe diameter 1 in.

Typical low-speed flow. Bubbles are short and smooth and have short wakes. A and C show stages in the agglomeration process. The lower bubble is caught in the wake of the upper, distorts, and accelerates rapidly.

is defined, is a function of the particular apparatus used, the method of gas injection, length (or perhaps better time) from injection to point of observation, and perhaps some other variables.

It is interesting to note that there is an attraction between rising bubbles which decreases rapidly with separation distance. As slug flow develops, there is a continual "sucking up" of the lower of a pair of bubbles into the upper one. Once the bubbles get closer than a few diameters, this process proceeds rapidly, in times of the order of a second. The explanation for this phenomenon is that the wake of the first bubble gives rise to a water-velocity profile which causes the second bubble to rise faster. A more detailed discussion of this will be presented later.

In the 1-in. pipe it was possible to observe bubbles of approximately the ideal form which were 6 ft and more in length. The only noticeable way in which these bubbles differ from the shorter ones is in the increase in surface waves at the air-water interface. The skin of the bubble presents an increasingly rough appearance, presumably due to turbulence in the liquid film, and consequent capillary waves on the surface.

At higher flow rates the bubble wakes become more agitated, a larger number of small bubbles are torn off at the tail and, consequently, the whole wake becomes richer in bubbles. This results in several small bubbles being swept down as far as the following bubble. These may remain intact for some distance as they are drawn into the flow around the large bubbles. The bubble interface becomes distorted in the neighborhood of these small bubbles.

The phenomena observed in this $^3/_4$-in. pipe are, in general, exactly parallel to those observed in the 1-in. pipe. Photographs were only taken in this case to obtain a certain amount of data about bubble and slug lengths.

Fig. 5 $Q_g = 0.208$ $Q_f = 0.288$ in CFM pipe diameter 1 in.
Photographs of entrance effects some 200 diameters from inlet. The small bubbles are in the process of agglomeration to form small G. I. Taylor bubbles.

It is in the 1/2-in. pipe that the effects of surface tension begin to become pronounced. In fact, the study of slug flow has to be confined to qualities and flow rates well above the bubble-flow regime because of the appearance of "bowler-hat" bubbles in profusion at intermediate qualities. These hat-shaped bubbles are formed in a stream at the air inlet and flow upward in a row. Their mutual attraction now results in the formation of several pseudo-G. I. Taylor bubbles which have the over-all dimensions of normal slug-flow bubbles, but which consist of a series of hat-shaped bubbles stacked closely one on top of the other. At low flow rates these bubbles do not agglomerate easily and no final smooth bubble is formed in the length of the apparatus. Even at high air flows, the very long G. I. Taylor bubbles still may have unabsorbed caps attached since the agglomeration rate at the nose is small.

Pressure-drop data for all three tubes were read directly from the water manometers on the last 6 ft of pipe. It was checked that the pressure drop was linear and steady over the six pressure taps, and then the pressure difference between first and last was recorded. Results are shown in Table 1. The effect of pressure fluctuations on the manometer readings was kept to a minimum by adjusting the hose clamps.

Lengths of bubbles and slugs were read directly off the 35-mm negatives using a microfilm viewer. For each experiment a full 36-exposure roll of film was used, each exposure covering 3 ft of pipe. The most valuable results of these experiments were obtained with the 1/2-in. pipe. This is due to the greater completeness of the data in view of the fact that one camera frame often covered a range of several bubble lengths. In the case of the 1-in. pipe, often only part of the pattern was visible.

Results for the 1/2-in. pipe are shown in histogram form in Fig. 6. The spread in bubble lengths is considerable. Slug lengths are more regular, both over one experiment and from one experiment to the next. This result is to be expected in view of the fact that the limiting process in determining bubble lengths is an agglomeration process determined by the velocity profiles in the bubble wake. After slugs reach a certain length the attraction between bubbles becomes very small and a fairly regular slug length is obtained. For higher flow rates where shear stresses and turbulence are considerable, both bubble and slug lengths become steadily less regular.

Slug and bubble lengths are related to each other via flow rates and bubble rise velocity as in equation (7). Slug length is a useful parameter to quote because of its relative invariance. Maximum and minimum mean slug lengths for various flow rates in a given pipe are shown against pipe diameter in Fig. 7. Further and more detailed data are needed to make possible an analysis in terms of wake dynamics.

Note that actual bubble length may be less than the theoretical calculated from continuity considerations because of the air volume associated with the small bubbles in the wake.

Analysis of Experimental Results and Comparisons With Theory

A constant rise velocity independent of length is to be expected from the experimental results and theory of both G. I. Taylor and Dumitrescu for cases where wall shear stresses are negligible. The pressure-boundary condition on the bubble surface in the same in all cases and eddies behind the bubble have

Table 1 Pressure drop data

1/2-in. pipe Q_g, CFM	Q_f, CFM	Superficial velocity $\left(\frac{Q_g+Q_f}{A_p}\right)$, fps	$\Delta P/\Delta L$ Observed in H_2O/in.	$\Delta P/\Delta L$ Theoretical in H_2O/in.	Observed L_b, in.	L_s, in.
0.136	0.118	3.1	0.695	0.623	3.67	3.02
0.165	0.119	3.5	0.630	0.577	4.48	3.14
0.192	0.117	3.8	0.615	0.536	4.95	3.12
0.252	0.118	4.5	0.561	0.482	6.40	3.38
0.304	0.124	5.2	0.53	0.493	8.21	3.90
0.296	0.262	6.8	0.900	0.856	5.47	4.68
0.294	0.272	6.9	0.917	0.878	5.31	4.74
3/4-in. pipe						
0.046	...	0.25	0.638	0.707		
0.080	...	0.43	0.517	0.604		
0.125	...	0.68	0.420	0.511		
0.201	...	1.09	0.302	0.411		
0.321	...	1.74	0.145	0.313		
0.053	0.050	0.56	0.730	0.778		
0.084	0.049	0.72	0.642	0.692		
0.134	0.048	0.99	0.542	0.594		
0.116	0.119	1.27	0.700	0.727		
0.192	0.124	1.71	0.580	0.609		
0.341	0.128	2.54	0.430	0.475		
0.265	0.264	2.87	0.67	0.673		
0.387	0.261	3.51	0.56	0.623		
0	0.261	1.48	0.015	0.045		
1-in. pipe						
0.073	...	0.22	0.750	0.745	5.65	10
0.094	...	0.29	0.712	0.704	6.3	13
0.124	...	0.37	0.658	0.652	8.1	13
0.160	...	0.49	0.607	0.602	10.7	15
0.078	0.124	0.62	0.835	0.823	2.9	10.5
0.098	0.122	0.67	0.803	0.799	3.6	13
0.127	0.124	0.77	0.758	0.756	4.8	13
0.166	0.126	0.89	0.702	0.706	6.5	10.5
0.209	0.127	1.03	0.653	0.659	8.2	15
0.208	0.288	1.51	0.765	0.750	1	...
0.322	0.288	1.87	0.663	0.659	6.5	10
0.463	0.293	2.31	0.577	0.573	9.8	13

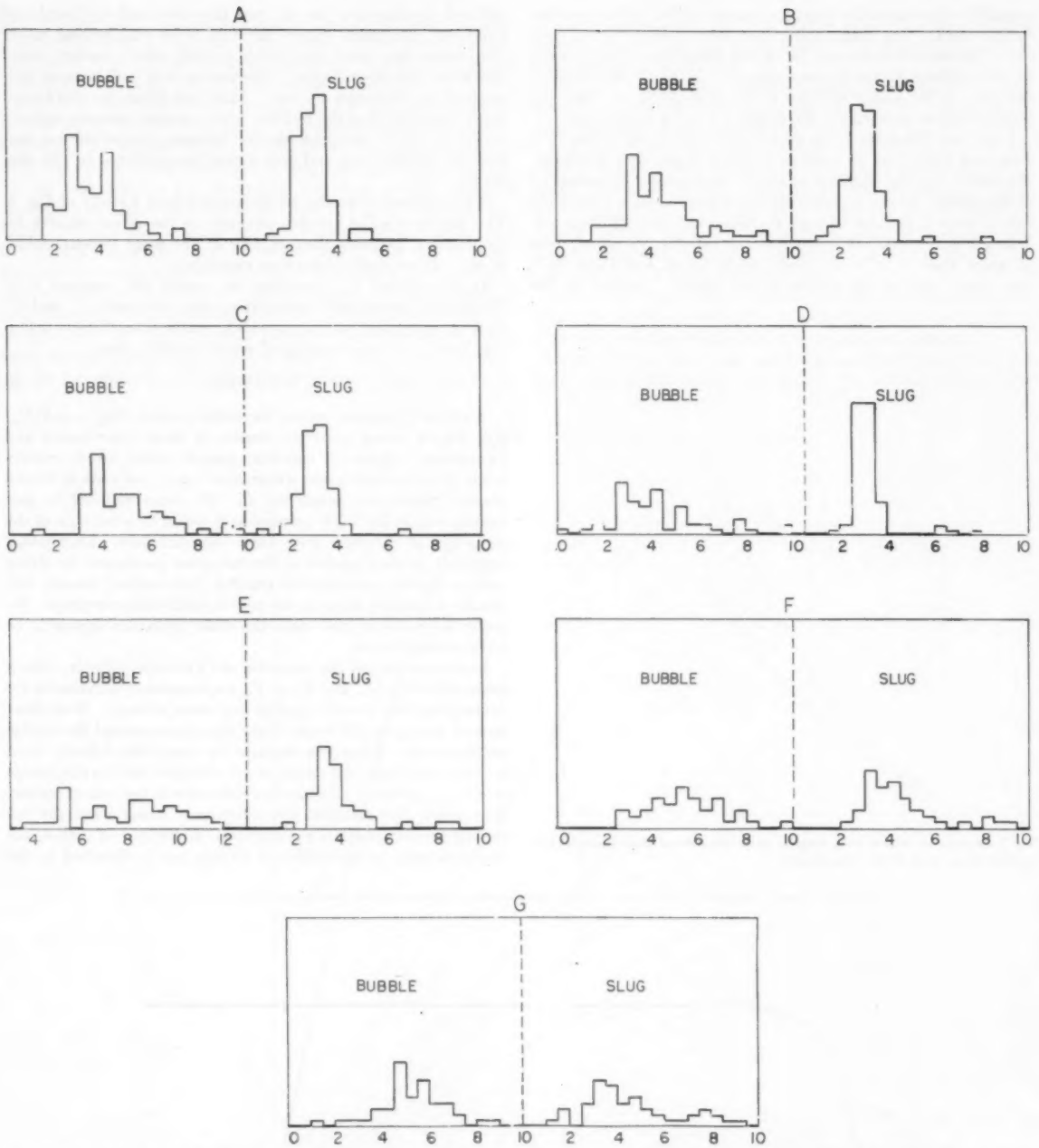

Fig. 6 Histogram results for bubble and slug lengths in 1/2-in-diam pipe. The co-ordinates are number of slugs or bubbles (from arbitrary constant) versus length over pipe diameter.

A $Q_g = 0.136$ $Q_f = 0.118$ Mean $L_b = 3.67$ in. Mean $L_s = 3.02$ in.
B $Q_g = 0.165$ $Q_f = 0.119$ Mean $L_b = 4.48$ in. Mean $L_s = 3.14$ in.
C $Q_g = 0.192$ $Q_f = 0.117$ Mean $L_b = 4.95$ in. Mean $L_s = 3.12$ in.
D $Q_g = 0.252$ $Q_f = 0.118$ Mean $L_b = 6.40$ in. Mean $L_s = 3.38$ in.
E $Q_g = 0.304$ $Q_f = 0.124$ Mean $L_b = 8.21$ in. Mean $L_s = 3.90$ in.
F $Q_g = 0.294$ $Q_f = 0.272$ Mean $L_b = 5.47$ in. Mean $L_s = 4.68$ in.
G $Q_g = 0.289$ $Q_f = 0.262$ Mean $L_b = 5.31$ in. Mean $L_s = 4.74$ in.

negligible effect upon the smooth character of the flow around the bubble itself. One might think that shear stresses would slow down the water flow around the bubble which would be expected to rise slightly slower in consequence. In fact, the observed tendency is for longer bubbles to rise slightly faster than the shorter ones so presumably the problem is not a simple one.

Laird and Chisholm [3] in an experimental investigation in a 2-in-diam tube claim an increase of about 10 per cent in bubble-rise velocity as the length is increased from some 2 diameters to 25 diameters. In our experiments, no changes of such magnitude were observed, perhaps because no bubbles of over 12 diameters in length were timed. Variations in rise velocity, we found, were no more than 2 or 3 per cent, while Laird and Chisholm's data show considerable spread in this region. Because of the method of admitting the air into the tube used by Laird and Chisholm, one might expect the fluid to be still moving rather than stationary when the bubble arrived, which motion would also affect the rise velocity. This motion may well be more pronounced for the longer bubbles. Laird and Chisholm also found, experimentally, that the bubbles were constant-pressure surfaces and that most of the pressure drop between two points was contributed by the slug and was almost proportional to the slug length.

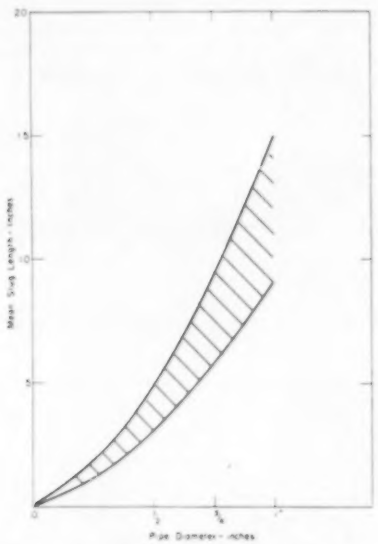

Fig. 7 Range of mean slug lengths as a function of pipe diameter for various flow rates of the two phases

Two qualitative results are immediate from a study of Fig. 3. The bubble relative velocity increases as the water velocity increases and increases more rapidly in the more viscous, colder liquid. The second result seems surprising.

In an attempt to rationalize the results the constant C of Taylor and Dumitrescu was split up into two parts, C_1 and C_2. C_1 is the governing coefficient in static water when C_2 is by definition unity. C_2 is a function of water velocity, thus:

$$V_b = C_1 C_2 (g D_p)^{1/2} \tag{8}$$

A plot of C_1 against bubble Reynolds number ($\mathrm{Re}_b = \rho_f V_b D_p / \mu_f$), Fig. 8, using both the results of these experiments and Dumitrescu's gives an excellent smooth curve which rapidly tends to a constant value within less than 1 per cent of Dumitrescu's theoretical results for C_1. It seems rational to plot against bubble Reynolds number as it would be a measure of the departure of the field from ideal potential flow. Dumitrescu originally plotted against a dimensionless parameter involving surface tension, presumably arguing that surface tension will change the bubble shape at the nose in small-diameter pipes. We prefer Reynolds number since the water dynamics appear to be the governing factor.

Rationalization of the variation of C_2 is more difficult. Obviously, both V_b, V_w, and $V_b + V_w$ are important parameters for determining the velocity profiles and shear stresses. Wall shear stresses acting on the water which runs down around the bubble are less in the upflow case because the mean flow velocity must be subtracted from the velocities calculated relative to the bubble in order to calculate absolute flow velocities in the case of upflow. Presumably the potential flow solution is wrong when the oncoming velocity profile is not uniform. In the case of upflow, the profile as seen by the bubble is already partly distorted in the

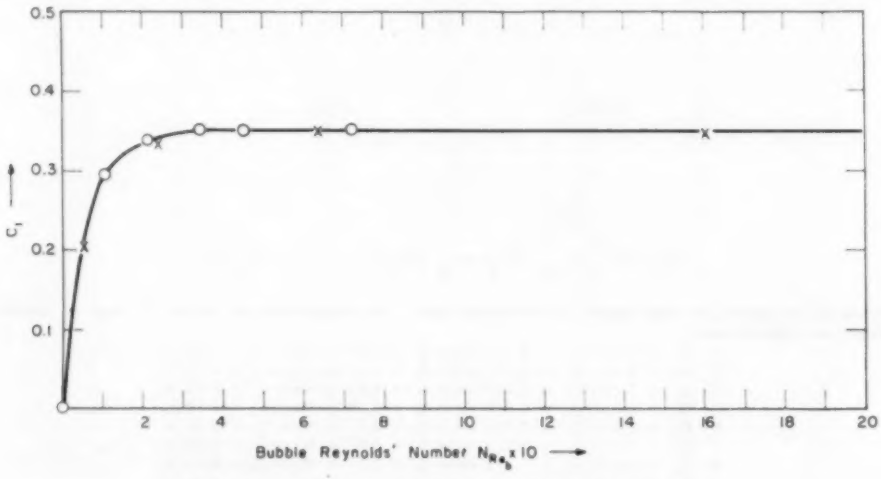

Fig. 8 Dimensionless constant C_1 against bubble Reynolds number
x = results of Dumitrescu
0 = results of Griffith and Wallis
Dumitrescu's theory gives $C_1 = 0.350$ for potential flow.
G. I. Taylor in a more approximate analysis obtains $C_1 = 0.328$.

direction necessary to pass the bubble; hence we might expect greater flow rates around the bubble and a higher rise velocity. Analysis of such a problem would be complex, but perhaps could be attempted by a variation of Dumitrescu's method.

Since the oncoming velocity profile and the nature of the flow around the bubble are determined by Reynolds number, it seems logical to try a correlation plot on this basis. There are only two independent Reynolds numbers for long bubbles. These could be taken as the one for the stream and that for the bubble. The plot which gave best results is shown in Fig. 9. Points were found to fall in the "laminar line" to a good degree of accuracy for bubble Reynolds numbers below 3000. For the bubble Reynolds numbers between 3000 and 5000 results do not co-ordinate well and are scattered around in a general area of the graph, presumably a transition region where turbulent flow is starting to be initiated. At higher bubble Reynolds numbers, results are again more consistent but with the present apparatus it was impossible to explore the fully developed turbulent region properly. It seems logical, though, that, as the velocity profile becomes flatter at large pipe Reynolds number, C_2 should approach 1. This appears to be the case.

There is a suggestion of transition phenomena in the main water flow, i.e., dependent on Re_w, and this obscures the results of the other transition determined by Re_b.

It is unfortunate that most of these experiments cover the regions of transition-flow phenomena, since this makes a correlation of the data more difficult. The results for totally laminar flow are consistent and reliable. The results for $Re_b > 3000$ are average curves which may be used for practical purposes with some approximation, certainly giving better result than the assumption that C_2 is constant and unity.

In the case of practical interest when a string of bubbles follow one another, other effects such as slug-length Reynolds number and wake-velocity profiles, may also become important.

In general, the shape was very stable and the bubble proceeded up the pipe as if it were a solid object. No satisfactory explana-

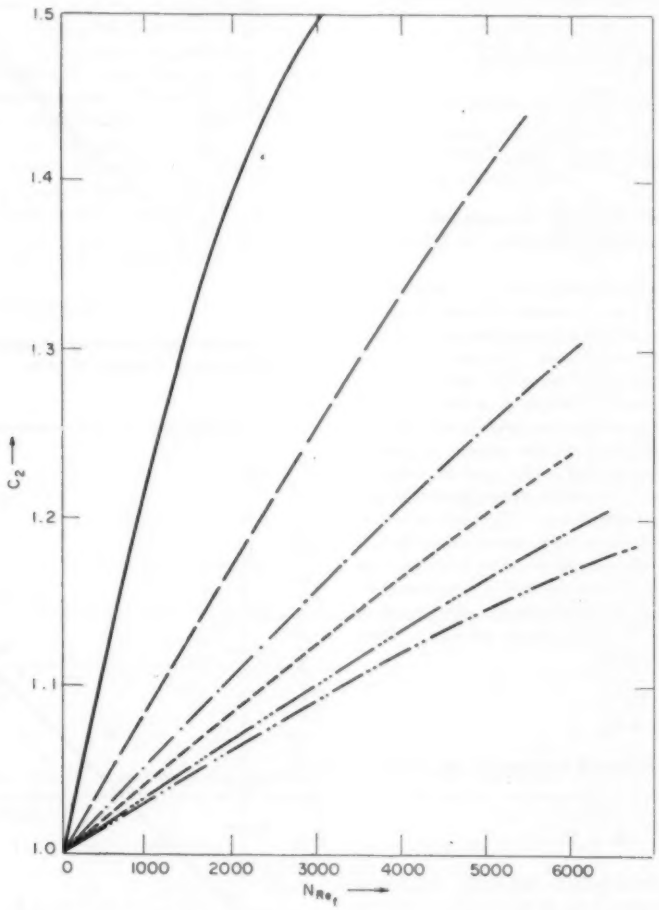

Fig. 9 Coefficient C_2 against liquid Reynolds number for various values of bubble Reynolds number

———	"Laminar"	$N_{Re_b} = 0 \rightarrow 3000$
— — —	"Transition"	$N_{Re_b} = 4000$
—·—·—	"Transition"	$N_{Re_b} = 5000$
- - - - - - -	"Transition"	$N_{Re_b} = 6000$
-·-·-·-·-	"Turbulent"	$N_{Re} = 7000$
—·—·—·—	"Turbulent"	$N_{Re_b} = 8000$

tion or theory was formed for the bubble instability which was observed for downflow. It is also unknown as yet whether such instability could occur for upflow in very large pipes or if a reversed water flow is essential.

No direct measurements of density were attempted on this apparatus. However, it was found that measurements had been made elsewhere [4], by means of a radioactive technique and these have been used for a comparison. These results are unique in that a 4-m calming section was used before the measurements were made. The comparison of the calculated density and the measured density is shown in Fig. 10. In calculating the rise velocity of the bubbles C_2 was assumed to be one because the bubble Reynolds numbers were so high and well above the region in which the data reported here was taken.

If one considers a typical section of pipe which contains one slug and one bubble, and takes a control volume moving with the bubbles at bubble velocity, it is obvious from symmetry considerations that the momentum fluxes in and out are identical. Such a control volume as illustrated in Fig. 1, control volume b. Therefore the momentum equation applied between sections 1 and 2 is

$$(P_1 - P_2)A_p - \rho_a g(L_s + L_b)A_p - \tau_w A_w = 0 \qquad (9)$$

When one solves for the pressure drop, the result is

$$(P_1 - P_2) = \rho_a g(L_s + L_b) + \tau_w \frac{A_w}{A_p} \qquad (10)$$

ρ_a is evaluated from the preceding theory. The accurate evaluation of τ_w is not, at this time, possible. However, the following is the recommended procedure:

If the flow around the bubble is examined closely, it is observed that the flow may be up and it may be down with respect to the pipe wall. This is because the bubble is a constant-pressure surface for which the tip is a stagnation point. To an observer on the bubble the velocity of the liquid around the bubble is then approximately $(2gz)^{1/2}$ where z is the distance from the tip of the bubble. For a sufficiently long bubble, the throughput velocity may be sufficiently small so that the downflow velocity is greater and the wall shear stress acts up instead of down on the material in the pipe. The average shear stress over a representative length of bubble and slug can then go either way. The answer to the question of the mean wall shear stress lies in knowing the details of the velocity distribution in the core of liquid in the pipe. As yet this is unknown so this approximate method is recommended. Evaluate the wall shear stress as if the pipe were full of liquid in fully developed flow moving at the mixture velocity. Then multiply this shear stress by the ratio

$$\frac{Q_f}{Q_f + Q_g}$$

The wall shear stress to be substituted in equation (10) is then

$$\tau_w = \tau_w' \frac{Q_f}{Q_f + Q_g} \qquad (11)$$

When the average wall shear stress is large and down, this helps, while when the average shear stress is up, it adds almost nothing as the velocities are so low.

When the pressure drop data, reported in Table 1 and references [4 and 8], are treated in the manner indicated and compared with the experiments, the result is shown in Fig. 11. For these experiments the shear-stress term of equation (9) was only about 1 per cent for the 1 and $^3/_4$-in. pipes, while it was as high as 50 per cent of the total pressure drop for the $^1/_2$-in. pipe. This was due primarily to the larger velocities. The reason for the apparent success of such a simple correlating scheme lies in the fact that the friction contribution on the wall tends to cancel out as part of the flow is up and part is down. The only contribution then is due to the slugs and at high velocity, where friction is important, the friction of pipe wall occupied by slugs is approximately $\frac{Q_f}{(Q_f + Q_g)}$. It is interesting to note in Fig. 11 that the deviations for the lowest velocities in the 1 and $^3/_4$-in. pipes are opposite in sign from those at the higher velocities. This is to be expected.

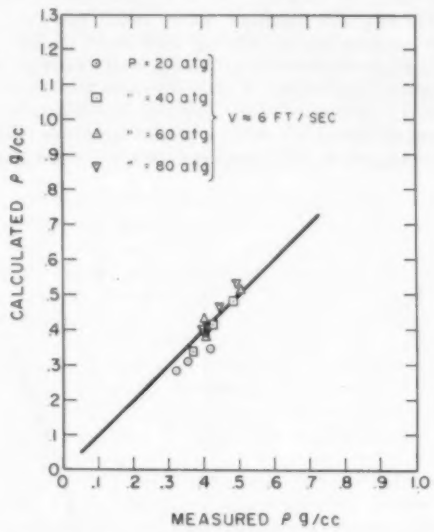

Fig. 10 Density data of reference [4] compared to the calculated results. The pressures are in atmospheres gage.

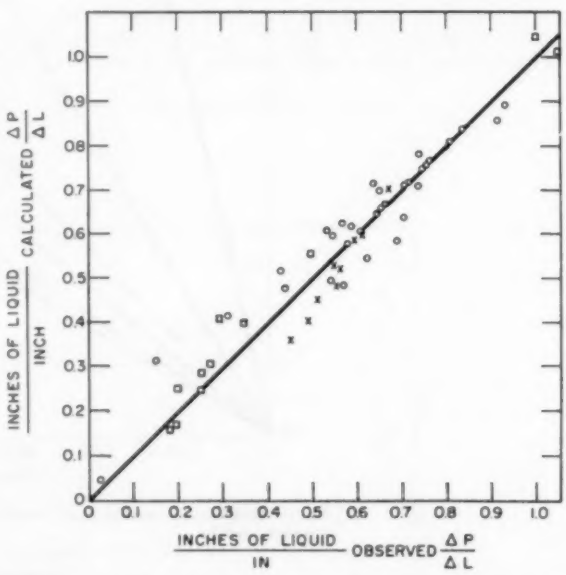

Fig. 11 Calculated versus observed pressure drop using data of Table 1 and references [4 and 8] and the methods outlined in this paper

x = reference [4]
○ = Table 1
□ = reference [8]

Range of Application of These Results

In so far as these results apply to only a particular flow regime, it is necessary, to apply them, that one know, in the absence of any visual observations, what the flow regime is. For this purpose a flow-regime map is presented in Fig. 11.

The co-ordinates for this map were originally suggested in reference [5]. Justification for them can be seen in equation (7) if one examines the character of the denominator. For certain values of the volume-flow rates and bubble-rise velocity this denominator goes to 0. This means the bubble length becomes infinite; i.e., a transition to annular flow occurs. As the values for the constants m and n are only approximate, the exact transition criteria obtained directly from this formula would probably not be too good but the transition criteria it suggests might be quite serviceable. The criteria one obtains from this formula directly are in a particular relation between Q_g/Q_f and V_bA_p/Q_g. If one recalls V_b is approximately a constant times $(gD_p)^{1/2}$ an equivalent set of criteria could be the ones used in Fig. 12. This set is superior due to better behavior at the limits.

The annular slug-flow transition has been placed to include all the known slug-flow points. The justification for this lies in the observation that entrance effects can persist for very great lengths but that once slug flow is achieved it is exceedingly stable in that no apparent tendency to change exists. Therefore if slug flow can exist at all it is the regime characteristic of the fully developed condition and should appear on this map.

There is also a region of bubbly flow shown. It is not certain that it belongs on this map at all. However, it has been found [6], that when the void fraction is less than 0.18, there is almost no tendency for slugs to develop spontaneously. Therefore a single line for a 1-in. pipe has been drawn to delineate the bubbly flow regime. It has been assumed in placing this line that the rise velocity of the bubbles with respect to the liquid is 0.8 fps and that they are uniformly distributed across the channel. Some slug-flow points fall into the bubbly region. This is not surprising if one recalls that slug flows are quite stable and if they can exist at all they exhibit no tendency to change. Apparently the entrance conditions in these experiments were such that slug flow was forced.

The basic cause for the instability of bubbly flow lies in the fact that the rise velocities of the different size bubbles are different. Therefore there is a tendency for them to overtake each other and agglomerate. No such tendency exists for the slug-flow bubbles as they all rise with the same velocity.

Summary

For convenience, the method of calculating slug flows is summarized here. The time average pressure gradient neglecting wall shear stress is

$$\rho_a\theta = g\rho_f\left[\frac{Q_f + V_bA_p}{Q_f + Q_g + V_bA_p}\right] + \left[\frac{g\rho_gQ_g}{Q_f + Q_g + V_bA_p}\right] \quad (5)$$

$$V_b = C_1C_2(gD_p)^{1/2} \quad (8)$$

in which C_1 and C_2 are evaluated from Figs. 8 and 9.

The slug length can be obtained from Fig. 7. The bubble length can then be obtained from

$$L_b = \frac{Q_aL_a + n(D_p)(Q_g + Q_f + V_bA_p)}{m(Q_g + Q_f + V_bA_p) - Q_g} \quad (7)$$

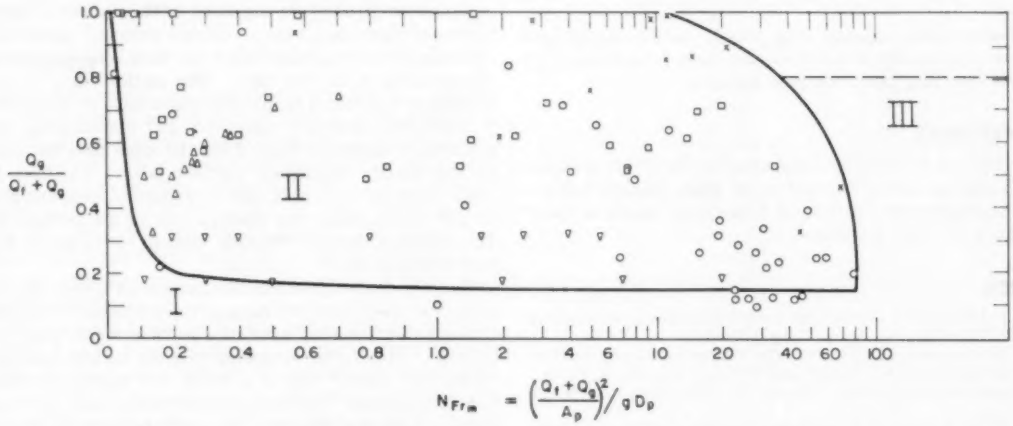

Fig. 12 Flow regime map for a vertical pipe in fully developed slug flow. Each point shown is one at which slug flow existed. Other flow regimes can exist for these values of the co-ordinates but they do not appear to be the flow regimes characteristic of fully developed flow.

Point	Reference	D	L/D	Combination	Pressure
○	[7]	0.722 in.	63	Air water	1 ata
△	[4]	2.34 in.	67	Steam water	21, 41, 61, 81
□	[5]				1 ata
▽	This work	0.5 in.	430	Air water	1 ata
		0.75 in.	288	Air water	1 ata
		1.00 in.	215	Air water	1 ata
x	8	1.00 in.	260	Air water	36 psia

Region I Bubble

II Slug (including semiannular)

III Annular and mist

The dividing line between the bubble and the slug region is given for a 1-in. pipe using the criterion mentioned in the text.

As long as the shape can be approximated by the shape that would exist in a potential flow

$$\begin{aligned} m &= 0.913 \\ n &= 0.526 \end{aligned} \quad \text{for} \quad 2 < L_b D_p < 20$$

The period of the pressure fluctuations is approximately

$$\Delta t = \frac{(L_s + L_b)A_p}{Q_f + Q_g + V_b A_p} \tag{1}$$

The magnitude of the pressure fluctuations is approximately

$$\Delta(\Delta P) = L_s g \rho_f \tag{12}$$

for taps which are more than one slug length apart. The pressure gradient is, from equation (9)

$$\frac{\Delta P}{\Delta L} = \rho_s g + \frac{4\tau_w}{D_p} \tag{13}$$

τ_w is obtained from equation (10) as

$$\tau_w = \left[\frac{Q_f}{Q_f + Q_g}\right] \tau_w' \tag{11}$$

Conclusions

1 Entrance effects can persist for great lengths, $L/D = 300$, and long times, in developing two phase flows.

2 Wall shear stresses at moderate and low velocities contribute only slightly to the pressure drop in slug flows.

3 Bubble-rise velocities in slug flow are quite sensitive to the velocity profile in the water ahead of the bubbles. The effect of wall shear stress manifests itself primarily through the velocity profiles.

4 Pressure drop, density, slug length, bubble length and fluctuation pressure drops, and frequencies can be calculated for fully developed slug flow with good accuracy.

Acknowledgments

This work has been entirely supported by the Office of Naval Research and has been performed in the Heat Transfer Laboratory of Massachusetts Institute of Technology, which is under the direction of W. M. Rohsenow.

References

1 D. T. Dumitrescu, "Strömung an einer Luftblase in senkrechten Rohr," ZAMM, 1943, vol. 23, no. 3, pp. 139–149.

2 R. M. Davis and G. I. Taylor, "The Mechanics of Large Bubbles Rising Through Extended Liquids and Through Liquids in Tubes," *Proceedings of the Royal Society*, London, vol. 200, series A, 1950, pp 375–390.

3 A. D. K. Laird and A. Chisholm, "Pressure and Forces Along Cylindrical Bubbles in a Vertical Tube," *Industrial and Engineering Chemistry*, vol. 48, August, 1956, pp. 1316–1318.

4 K. Schwartz, VDI—Forschungsheft, issue B, 20, no. 445, 1954, pp. 1–44.

5 B. K. Koslov, "Types of Gas-Liquid Mixtures and Stability Boundaries in Vertical Tubes," *Zuhr. Tech. Fiz.*, vol. 24, no. 4, 1952, p. 656.

6 R. V. Bailey, P. C. Zmola, F. M. Taylor, and R. J. Planchet, "Transport of Gases Through Liquid-Gas Mixtures," Tulane University and Oak Ridge National Lab. Available from P. C. Zmola, Combustion Engineering, Windsor, Conn.

7 C. Brancart, "An Experimental Study of Two-Phase Flow Regimes," SB thesis, Department of Mechanical Engineering, M.I.T., Cambridge, Mass., June, 1958.

8 G. W. Govier, B. A. Radford, and J. S. C. Dunn, "The Upward Flow of Air-Water Mixtures, I. Effect of Air and Water Rates on Flow Pattern, Holdup, and Pressure Drop," *Canadian Journal of Chemical Engineering*, August, 1957, p. 58.

DISCUSSION

R. A. S. Brown[6] and G. W. Govier[7]

The authors have presented an interesting analysis of the geometrical relationships for the case of two-phase slug flow. Equation (5) relating average density to the volumetric flow rates of the phases and the linear velocity of the bubble is quite general and should be as reliable as the value of the bubble velocity used. The authors propose that the bubble velocity be determined by a modification of the Taylor and Dumitrescu equation incorporating two constants, C_1 and C_2. While the constant C_1 appears reasonably well established on both theoretical and experimental grounds, the same can hardly be said for the constant C_2. Fig. 9 presenting values of C_2 for various liquid Reynolds numbers and bubble Reynolds numbers is apparently based upon actual data although these are not presented. The use of the same symbol (N_{Re_f}) to denote the mixture Reynolds number (in the Nomenclature) and the liquid Reynolds number (in Fig. 9) is unfortunate.

Workers at the University of Alberta [9, 10, 11][8] have obtained data on the flow pattern, holdup ratio, and pressure drop for the upward vertical flow of air-water mixtures. (The authors have referred to some of these data in connection with their Fig. 11.) While some 100 data points in the slug flow region are available from these studies, about half of them are beyond the liquid Reynolds number range of Fig. 9. The data include measurements of the "in situ" air-water volume ratios which are readily convertible to average density values. This permits the values calculated with equations (5) and (7) and Figs. 8 and 9 to be checked.

A representative sample of these comparisons is given in Table 2. The agreement is generally poor and especially so at high air velocities. Presumably this is due to inadequacies in the method of predicting the bubble velocity.

Equations (9) and (12), suggested by the authors as expressions for the pressure drop over a "control volume," cannot be criticized except, as the authors point out, there is no satisfactory way of evaluating τ_w at this time. The method they propose for estimating τ_w appears to involve considerable oversimplification. A comparison between calculated and experimental pressure gradients is shown in Table 2 for the same tests for which the average density comparison has been made. The discrepancies noted between calculated and experimental pressure gradients do not correspond to the discrepancies in the average density. This indicates that the "friction" term in equations (9) and (12) may well be in error.

The co-ordinates chosen by the authors for correlating the flow pattern are essentially the same as those proposed by Kozlov [4] although their resulting correlation or "flow regime map" is quite different. It is rather surprising that the authors have omitted "froth" or "churn" flow as a stable flow pattern between slug and annular flows. This has been observed by most other workers certainly including [9 to 12]. The authors appear to believe that this is a transition or entrance flow. Froth flow, however, should be rather quickly stabilized due to the high rates of energy transfer in turbulent mixing. It should, therefore, have a relatively short entrance section and the stable flow should develop rapidly. The correlations of the conditions under which froth flow prevails would seem to confirm this.

In conclusion, it is believed that the method of calculation of average density proposed by the authors may prove valuable. The proposed correlation of bubble velocity, however, does not seem adequate in view of the poor agreement of most of the

[6] PhD candidate in Chemical Engineering, University of Alberta, Edmonton, Alberta, Canada.

[7] Dean, Faculty of Engineering, University of Alberta, Edmonton, Alberta, Canada.

[8] Numbers [9 to 12] designate References at end of discussion.

Table 2 Comparison of calculated and experimental data

Tube diam, in.	Mid-point pressure, psia	Mid-point temp, deg F	Water rate, ft³/sec	Air rate[a], ft³/sec	Average density Calculated[b], lb/ft³	Average density Experimental, lb/ft³	Pressure gradient Calculated[c], ft water/ft	Pressure gradient Experimental, ft water/ft
0.630	18	68	0.000149	0.00372	15.58	16.86	0.251	0.203
0.630	18	68	0.000149	0.0146	4.99	11.77	0.083	0.150
0.630	18	64	0.000290	0.00374	17.32	19.06	0.280	0.218
0.630	18	64	0.00063	0.00358	21.91	21.47	0.357	0.286
0.630	18	75	0.00183	0.00627	21.59	22.59	0.371	0.342
0.630	18	75	0.00183	0.0152	11.13	16.53	0.222	0.284
0.630	36	66	0.000149	0.00391	15.09	19.26	0.243	0.187
0.630	36	67	0.000290	0.00387	16.99	17.88	0.275	0.203
1.025	36	70	0.00040	0.0066	22.97	22.94	0.369	0.293
1.025	36	72	0.00040	0.0331	6.63	14.27	0.108	0.180
1.025	36	72	0.00359	0.0598	7.22	13.57	0.138	0.318
1.025	36	76	0.00359	0.0209	2.38	8.87	0.099	0.254

[a] At mid-point pressure and temperature.
[b] Calculated from equations (5) and (7) and Figs. 8 and 9 of Griffith and Wallis.
[c] Calculated from equations (5), (7), (10), and (12) and Figs. 8 and 9 of Griffith and Wallis.

average density values. The proposed method of estimating the pressure gradient appears to be unreliable.

References

9 G. W. Govier, B. A. Radford, and J. S. C. Dunn, "The Upward Vertical Flow of Air-Water Mixtures I. Effect of Air and Water Rates on Flow Pattern, Holdup, and Pressure Drop," *Canadian Journal of Chemical Engineering*, vol. 35, 1957, pp. 58–70.

10 G. W. Govier and W. L. Short, "The Upward Vertical Flow of Air-Water Mixtures II. Effect of Tubing Diameter on Flow Pattern, Holdup, and Pressure Drop," *Canadian Journal of Chemical Engineering*, vol. 36, 1958, pp. 195–202.

11 R. A. S. Brown, G. A. Sullivan, and G. W. Govier, "The Upward Vertical Flow of Air-Water Mixtures III. Effect of Gas Phase Density on Flow Pattern, Holdup, and Pressure Drop," *Canadian Journal of Chemical Engineering*, vol. 38, 1960, pp. 62–66.

12 B. K. Kozlov, "Forms of Flow of Gas-Liquid Mixtures and Their Stability Limits in Vertical Tubes," *Zhurnal Tekhnicheskoi Fiziki*, vol. 24, 1954, pp. 2285–2288.

Authors' Closure

We are glad to receive the discussion of Dean Govier and Mr. Brown as their work is almost the only work in which sufficiently complete measurements were made to make a comparison with this work possible. The various points raised by the discussions will be considered in turn but before that is done it is worth while to restate the objectives of this work. We have shown that by choosing the correct kinematic description of a two-phase flow configuration it is possible to rationally predict quantities such as density and pressure drop, without a minimum of the correct experimental information.

The central point raised by Brown and Govier concerns the correctness of C_2 as given by Fig. 9. C_2 is correct but the data of Govier, Radford, and Dunn are in part taken in an entrance region. The flow is therefore not fully developed slug flow and this theory does not and should not be expected to apply. In our experiments we found entrance effects were significant up to 12 ft from the entrance so measurements were recorded on only the last 6 ft of the 18-ft test section. The densities can be as much as a factor of three higher in such an entrance region. Since the writing of this paper a systematic study of these entrance effects has been made and the results are presented in a thesis.[9]

It is perhaps unfortunate that we attempted a comparison of these data with this theory but we felt some comparison should be made with other existing data. The entrance effects are small for the larger density runs but where the slug flow bubbles approach the length of the tube (as the last three runs of Table 1) the comparison should be poor as the entire tube is in an entrance region.

[9] Raphael Moissis, "Entrance Effects in a Developing Slug Flow," ScD thesis, M.I.T., June, 1960.

Table 3 Bubble-rise velocity data

D_p	V_b, ft/sec	V_w, ft/sec	Temp, deg C
3/4"	0.481	0	10
	0.506	0.043	10
	0.546	0.121	10
	0.550	0.128	10
	0.579	0.214	10
	0.609	0.273	10
	0.637	0.346	10
	0.666	0.431	10
	0.666	0.487	10
	0.657	0.593	10
	0.749	0.918	10
	0.461	−0.023	10
	0.439	−0.072	10
	0.420	−0.115	10
	0.405	−0.197	10
	0.392	−0.197	10
	0.389 / 0.394	−0.232	10
	0.412	−0.294	10
	0.443	−0.443	10
	0.676	+0.435	11
	0.578	0.204	16
	0.585	0.487	23.5
	0.578	0.219	24.5
	0.576	0.508	34
	0.542	0.178	37
	0.533	0.129	38
	0.528 / 0.513	0.079	38
	0.551 / 0.537	0.206	39
	0.556 / 0.504	0.262	42
	0.588 / 0.572	0.370	44
	0.606 / 0.620	0.579	48
	0.997	0	47
	0.447 / 0.450	−0.230	47
	0.406	−0.406	50
1"	0.577	0	10
	0.685	0.224	10
	0.707	0.385	10
	0.708	0.500	10
	0.785	0.793	10
	0.81	0.99	10
	0.529	−0.052	10
	0.520	−0.098	10
	0.546 / 0.526	−0.143	10
	0.615	0.144	34
	0.634	0.232	37
	0.640	0.307	39
	0.615	0.135	39
	0.669	0.442	45
	0.577	0	49
	0.676	0.556	49

The data taken on bubble-rise velocities from which C_2 was determined are presented in Table 3.

The meaning of the symbol N_{Re_f}, as used in the Nomenclature and in the text in the list of symbols, is the same so it should have the same symbol. It is the Reynolds number of the liquid in the slug.

The co-ordinates of the flow-regime map of Fig. 12 are not sufficient to completely determine the flow regime. The bubbly-slug transition is sensitive to liquid purity and the slug-annular transition apparently depends on other fluid properties as well. Nevertheless, this pair of co-ordinates appears to be the best single pair that could be chosen for a map. Because of the inadequacies of this map, the conditions at which the experimental data have been taken have also been tabulated. In the light of these simplifications and keeping in mind the objective of showing where slug flow was rather than where the other flow regimes are, the omission of froth flow between annular and slug does not seem too serious. It does belong there, however.

In conclusion, we would like to say that two-phase flow is a very complicated field and if order is to be made of it each flow regime will have to be analyzed in turn. We have presented an analysis for slug flow, which is one of these regimes, and have shown the central role of gravity and the bubble-rise velocity in determining density of a slug flow system.

Dynamic Response of Heat Exchangers Having Internal Heat Sources—Part IV[1]

W. J. YANG[2]
J. A. CLARK[3]
V. S. ARPACI[4]

This paper investigates the dynamic response of a heat exchanger having a sinusoidally time-dependent rate of internal heat generation. Results for both the transient-periodic and the steady-periodic, or frequency response, are given. These results include the response of the wall and fluid temperatures and the wall-fluid temperature difference. A phenomena of resonance in the amplitude ratio and phase shift is disclosed. Analytical results are obtained through the use of the Laplace transform technique. Experimental results are presented which compare favorably with the theoretical analysis. Heat exchangers to which these results apply include the heterogeneous nuclear reactor.

Introduction

This is the last in a series of four papers prepared by the authors and their associates on the dynamics of heat exchangers having internal heat sources. Throughout this work, which has encompassed a period of approximately six years, analysis has been focused on the heat exchanger in which a transient process is introduced by a time-dependent but spacially uniform rate of internal heat generation. In the previous three papers [1, 2, 3][5] this time-dependent rate of heat generation has included the following three cases: (i) step-change, (ii) linear change, and (iii) arbitrary time rate of change. In all cases the inlet temperature and fluid (coolant) flow rate were constant and analytical solutions were obtained for the fluid bulk temperature, the temperature of the duct wall, and the fluid-wall temperature difference, all as continuous functions of both time and space. In most cases experimental data were reported showing favorable comparison with the analytical results.

The present paper investigates the case in which the heat-generation rate varies sinusoidally with time. Analytical and experimental results for the response of the fluid temperature, wall temperature, and fluid-wall temperature difference for both the transient-periodic and steady-periodic states are given. This latter state provides the results which determine the frequency response of the heat exchanger. The frequency-response analysis constitutes a significant part of the results presented and a condition of "resonance" is discussed. A more detailed description of this research than is possible to include here may be found in reference [4]. Heat exchangers to which these and the previous results may be applied include the electrical heater, a chemical reactor in which a chemical reaction occurs within the solid walls and a heterogeneous nuclear reactor.

Summary of the Present Problem

The analytical results obtained here were found by formal mathematical integration of the governing differential equations using the Laplace transformation technique, as was done in

[1] A publication of the Heat Transfer and Thermodynamics Laboratory, Department of Mechanical Engineering, University of Michigan, Ann Arbor, Mich.

[2] Research Engineer, Mitsui Engineering and Shipbuilding Co., Tamano Okayama, Japan. Formerly, Graduate student, Department of Mechanical Engineering, University of Michigan, Ann Arbor, Mich.

[3] Professor of Mechanical Engineering and Professor-in-charge, Heat Transfer and Thermodynamics Laboratory, University of Michigan, Ann Arbor, Mich. Assoc. Mem. ASME.

[4] Assistant Professor of Mechanical Engineering, Heat Transfer and Thermodynamics Laboratory, University of Michigan, Ann Arbor, Mich.

[5] Numbers in brackets designate References at end of paper.

Contributed by the Heat Transfer and Instruments & Regulators Divisions and presented at the Winter Annual Meeting, New York, N. Y., November 27–December 2, 1960, of THE AMERICAN SOCIETY OF MECHANICAL ENGINEERS. Manuscript received at ASME Headquarters, July 28, 1960. Paper No. 60—WA-127.

Nomenclature

A = cross-sectional area of fluid, ft²
A_ω = cross-sectional area of wall, ft²
A_θ = defined by equation (10), dimensionless
A_t = defined by equation (13), dimensionless
a_1 = defined by equation (3a), ft³ deg F hr/Btu
a_2 = defined by equation (3b), hr
a_3 = defined by equation (3a), hr
a_4 = defined by equation (3b), ft
B_θ = defined by equation (11), dimensionless
B_t = defined by equation (14), dimensionless
b_1 = $a_2 + a_3 = (M + 1)/K$, hr
b_2 = $a_2a_3 = M/K^2$, (hr)²
c_p = specific heat of fluid, Btu/lb$_M$ deg F
$c_{p\omega}$ = specific heat of wall, Btu/lb$_M$ deg F
f_1 = defined by equation (34)
f_2 = defined by equation (35)
$F_{12}, \ldots, F_{16}$ = functions defined in table of Appendix
$G_{12}, \ldots, G_{16}$ = functions defined in table of Appendix
h = coefficient of heat transfer between wall and fluid, Btu/ft² hr deg F
I_ϕ = Bessel function of first kind of zero order
K = $hA/\rho c_pV$ for fluid, 1/hr
K_ω = $hA_\omega/(\rho c_pV)_\omega$ for wall, 1/hr
k = (k)th term of series
M = $a_2/a_3 = (\rho c_pV)_\omega/\rho c_pV$, wall-fluid heat capacity ratio, dimensionless
p = Laplace variable, 1/hr
p_{xc}'' = initial power input, Btu/ft² hr
q^* = $\tau^*/a_3 = K\tau^*/M$, dimensionless time
r_o = outer radius of tube, ft
r_i = inner radius of tube, ft
r = $a_3x/a_2a_4 = Kx/Mu$, dimensionless axial distance

(Continued on next page)

references [1, 2, and 3]. Such a method has the disadvantage of complexity but the advantage of exactness and that it provides a solution continuous in both time and space. It also is subject to parameterization. In reference [4] the frequency response of this system also was obtained by the technique of substituting $i\omega$ for s, the Laplace variable, in the system (Laplace) transfer function. Such a method was shown [4] to be valid on this type of system. The frequency response so obtained and that determined from the analytical results for the steady-periodic states were found to be identical.

Although this work is analytical in approach it is important to emphasize that often it is convenient and practical to program this kind of problem on digital or analog computing machines starting from an approximate numerical analysis of the system. In such a case the solution as presented here could be used as a check solution. Even in this present analytical solution it was necessary to employ an IBM 704 to tabulate two new functions, ψ_7 and ψ_8, found as a result of the formal integration.

Literature Survey

In the interest of brevity only new literature or other pertinent papers that have come to the authors' attention will be discussed here. References [1, 2, and 3] include a large number of papers and books having important bearing on this subject, all of which have been previously reviewed.

Stein [6] in an important paper presents theoretical results for the response of a nuclear-reactor coolant channel to several types of transients, including that of a sinusoidal time variation in heat generation. His results for this case are for the periodic-steady state or frequency response and are not evaluated. Experimental data are not reported. Storrer [14, 20] has presented a generalized analysis of the frequency response of nuclear reactor to power oscillations. Specific results without an effect of axial variation are given for the reactor having a cylindrical fuel element.

The response of a heat exchanger having a constant rate of internal heat generation but a sinusoidally time-varying inlet temperature is analyzed and results plotted and evaluated in reference [4]. The dynamic characteristics of this system are shown to be identical with those of a two-fluid heat exchanger which has been analyzed by Profos [5] and Takahashi [11, 12]. Stein [6] also presents an analysis of this system but without evaluation. Owing to the linearity of the governing differential equations the dynamic response of this type of heat exchanger subjected to a simultaneous timewise variation in both the rate of internal heat generation and the inlet fluid temperature may be obtained by superposition of the individual responses.

Cohen and Johnson [7] in a study of the frequency response of a two-fluid heat exchanger disclosed theoretically the characteristic of resonance in the amplitude ratio of the temperature of one of the fluids. This is similar to a result found in this present study and is discussed later. In an investigation of the dynamics of multipass heat exchangers, Masubuchi [8] also showed the existence of a peak or point of resonance in the fluid temperature amplitude ratio at a certain frequency. A resonance characteristic under the influence of an oscillating flow transient in a steam-heated 2-pass heat exchanger is suggested by the results of Lees and Hougen [9]. These authors demonstrated the applicability of pulse testing methods to the investigation of the dynamics of heat exchangers. Zoss, et al. [10] have examined the dynamics of a heat-exchange system experimentally and compared the results with those predicted from the response characteristics of the elements of its control system.

Studies currently are under way by the authors continuing this general investigation of the dynamic response of these types of heat exchangers by considering the case of hydromechanic or flow transients. This case presents problems somewhat different from those encountered in the case of transients imposed by a time-dependent rate of heat generation.

Analysis

The physical system analyzed is shown in Fig. 1. This consists of a circular duct through which a coolant flows steadily, and in the solid walls of which energy is generated. In the steady state, all of this energy appears as a flow of heat at the interface between coolant and solid causing the coolant to increase in enthalpy (and temperature) as it flows through the duct. The outside surface of the duct is adiabatic. During the transient, however, both the duct-wall material and the coolant experience local temperature excursions, the magnitudes of which and their difference being evaluated here as a function of space and time. A circular duct has been selected for convenience in comparison of theory and experiment. Where a nonsymmetrical geometry is involved in the analysis, such as a triangular flow cross section,

Nomenclature

$s = x/a_3 = Kx/u$, dimensionless axial distance
$T(x)$ = fluid temperature amplitude for oscillation at frequency ω, see equation (16), deg F
$T_0(x)$ = fluid temperature amplitude for zero frequency oscillation, see equation (22), deg F
t_0 = inlet fluid temperature, deg F
$t(x, \tau) = t_1(x) + t_2(x, \tau)$, temperature of fluid, deg
$t_1(x)$ = initial fluid temperature, deg F
$t_2(x, \tau)$ = transient fluid temperature, deg F
u = velocity of fluid, ft/hr
V = volume of fluid, ft³
V_ω = volume of wall, ft³
x = axial distance, ft
α_θ = phase lag of wall, defined by equation (18), radians
α_t = phase lag of fluid, defined by equation (12), radians
γ = defined by equation (24)
$\gamma^* = \tau^*/a_3 = K\tau^*$, dimensionless time
δ = defined by equation (23)
$\theta(x, \tau) = \theta_1(x) + \theta_2(x, \tau)$, temperature of wall, deg F
$\theta(x)$ = wall temperature amplitude for oscillation at frequency, see equation (15), deg F
$\theta_0(x)$ = wall temperature amplitude for zero frequency oscillation, see equation (21), deg F
$\theta_1(x)$ = initial wall temperature, deg F
$\theta_2(x, \tau)$ = transient wall temperature deg F
ρ = density of fluid, lb_M/ft^3
ρ_ω = density of wall, lb_M/ft^3
τ = time, hr
$\tau^* = \tau - x/u$, hr
$\varphi(\tau)$ = transient heat generation rate, Btu/ft³ hr
Φ = amplitude of sinusoidal heat-generation rate, Btu/ft³ hr
$\psi_2^{**}(s, q^*)$ = function defined by equation (50)
$\psi_4(r, \gamma^*)$ = function defined by equation (51)
$\psi_7(s, q^*, \Omega)$ = function defined by equation (52)
$\psi_8(s, q^*, \Omega)$ = function defined by equation (53)
ω = angular velocity, rad/hr
$\Omega = a_3\omega = M\omega/K$, dimensionless angular velocity

the results given may be reduced to an area-to-volume ratio and, to a degree of approximation, can be used for other geometry for which the restraints on the solution apply.[6] The solution will be valid as presented for flow inside circular ducts and between parallel plates.

The following assumptions are imposed on the solution:

(*a*) The fluid temperature and velocity are represented by a single value (lumped) at the flow cross section.

(*b*) The duct wall temperature does not depend on radius. Valid for thin-walled metal systems.

(*c*) Axial heat conduction is negligible in both fluid and duct walls and heat flows only to the coolant. This is a reasonable assumption when the Peclet number exceeds 100 [13]. The outer surface is adiabatic.

(*d*) The heat-transfer coefficient is constant with length and time.

(*e*) The fluid is incompressible and all fluid properties are constant. The flow channel has constant area.

(*f*) Energy (heat) generation within the walls is constant with length but is time-dependent.

(*g*) The temperature of the fluid entering the duct is constant and equal to t_0.

With these assumptions the application of the First Law of Thermodynamics and the law of conservation of mass for an incompressible fluid to the system shown in Fig. 1(*b*) produces the following two differential equations, one for the duct wall, the other for the fluid. Details of this derivation are outlined in reference [3], Appendix 1

Wall

$$-(\theta - t) + a_1 p_x''(\tau) = a_3 \frac{\partial \theta}{\partial \tau} \tag{1}$$

[6] The nature of the approximation is discussed in reference [3].

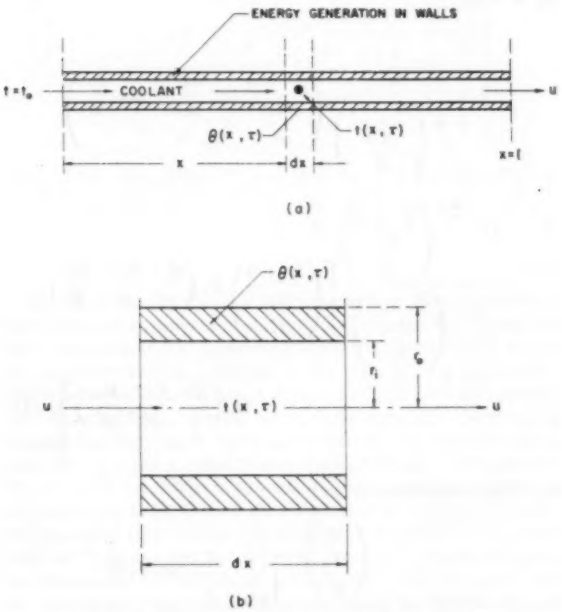

Fig. 1 Simulated coolant channel

Fluid

$$(\theta - t) = a_2 \frac{\partial t}{\partial \tau} + a_4 \frac{\partial t}{\partial x} \tag{2}$$

For a circular duct and in generalized terms, the constants are written:

$$a_1 = \frac{r_o^2 - r_i^2}{2r_i h} = \frac{1}{(\rho c_p)_\omega K_\omega}, \quad a_3 = \frac{\rho c_p r_i}{2h} = \frac{1}{K} \tag{3a}$$

$$a_2 = \frac{(\rho c_p)_\omega (r_o^2 - r_i^2)}{2r_i h} = \frac{1}{K_\omega}, \quad a_4 = \frac{\rho c_p r_i}{2h} u = \frac{u}{K} \tag{3b}$$

and

$$p_x''(\tau) = p_{x_0}'' + \Phi \sin \omega\tau \tag{3c}$$

where p_{x0}'' is the initial uniform heat-generation rate and $\Phi \sin \omega t$ is the time-variant heat-generation-rate function, having a zero value at zero time, which introduces the transient into the system. As shown in reference [3], Appendix 1, both functions $\theta(x, \tau)$ and $t(x, \tau)$ of equations (1) and (2) are split into two components, one being a steady-state part $t_1(x)$ and $\theta_1(x)$ the other of the transient contribution $t_2(x, \tau)$ and $\theta_2(x, \tau)$. For purposes of transient analysis, it is necessary only to carry out detailed mathematical analysis of the latter functions. It will be noted that $t_1(x) = t(x, 0)$ and $\theta_1(x) = \theta(x, 0)$. Hence the governing differential equations become

Wall

$$-(\theta_2 - t_2) + \frac{1}{(\rho c_p)_\omega K_\omega} \phi(\tau) = \frac{1}{K_\omega} \left(\frac{\partial \theta_2}{\partial \tau} \right) \tag{4}$$

Fluid

$$\theta_2 - t_2 = \frac{1}{K} \left(\frac{\partial t_2}{\partial \tau} \right) + \frac{u}{K} \left(\frac{\partial t_2}{\partial x} \right) \tag{5}$$

where

$$\phi(\tau) = \Phi \sin \omega\tau = \Delta(q/A)(A/V)_\omega \sin \omega\tau \tag{6}$$

Equations (4) and (5) are operated on by the Laplace-transform technique. The transformed equations in transient fluid temperature t_2, transient wall temperature θ_2, and transient fluid-wall-temperature difference $\Delta t_2 = \theta_2 - t_2$ are integrated with the appropriate initial and boundary conditions, the inverse transformation performed, and then recombined with the steady-state functions $t_1(x)$ and $\theta_1(x)$ as outlined in detail in Appendix. The nature of the mathematical attack on this problem produces solutions for $t(x, \tau)$, $\theta(x, \tau)$, and $\Delta t(x, \tau)$ in two domains of physical time: Case 1, a physical time following the introduction of the transient which is greater than zero but equal to or less than x/u; and Case 2, a physical time equal to or greater than x/u. It will be noted that the physical time x/u is that required for fluid particles flowing at a velocity u to traverse the distance x. The results for Cases 1 and 2 for a sinusoidal timewise-variant internal heat generation are as follows for $t(x, \tau)$ and $\theta(x, \tau)$. The results for $\Delta t(x, \tau)$ may be formed from $\theta(x, \tau) - t(x, \tau)$ and are not given here but may be found in Appendix.

Case 1 $0 \leq \dfrac{\tau u}{x} \leq 1$

(*a*) wall temperature $\theta(x, \tau)$

$$\frac{\theta(x,\tau)-\theta(x,0)}{\frac{\Delta(q/A)}{h}\left(1+\frac{Kx}{u}\right)} = \frac{M}{(M+1)\frac{M\omega}{K}\left(1+\frac{Kx}{u}\right)}\left\{1+\frac{\frac{1}{M}e^{-(M+1)\frac{K\tau}{M}}}{1+\left(\frac{M+1}{\frac{M\omega}{K}}\right)^2} + \frac{\sqrt{\left[\frac{1}{M}\left(\frac{M+1}{\frac{M\omega}{K}}\right)^2\right]+\left[1+\frac{1}{M}+\left(\frac{M+1}{\frac{M\omega}{K}}\right)^2\right]^2}}{1+\left(\frac{M+1}{\frac{M\omega}{K}}\right)^2}\times \sin\left[\omega\tau-\tan^{-1}\left[\frac{1+\frac{1}{M}+\left(\frac{M+1}{\frac{M\omega}{K}}\right)^2}{\frac{1}{M}\left(\frac{M+1}{\frac{M\omega}{K}}\right)}\right]\right]\right\} \quad (7)$$

(b) Fluid temperature $t(x,\tau)$

$$\frac{t(x,\tau)-t(x,0)}{\frac{\Delta(q/A)}{h}\cdot\frac{Kx}{u}} = \frac{\frac{M}{M\omega/K}}{\frac{Kx}{u}(M+1)}\left\{1-\frac{e^{-(M+1)\frac{K\tau}{M}}}{1+\left(\frac{M+1}{\frac{M\omega}{K}}\right)^2} + \frac{\frac{M+1}{\frac{M\omega}{K}}\sqrt{1+\left(\frac{M+1}{\frac{M\omega}{K}}\right)^2}}{1+\left(\frac{M+1}{\frac{M\omega}{K}}\right)^2}\times \sin\left[\omega\tau-\tan^{-1}\left(-\frac{M+1}{\frac{M\omega}{K}}\right)\right]\right\} \quad (8)$$

Case $2\ \frac{\tau u}{x} \geq 1$

(c) Wall temperature $\theta(x,\tau)$

$$\frac{\theta(x,\tau)-\theta(x,0)}{\frac{\Delta(q/A)}{h}\left(1+\frac{Kx}{u}\right)} = \frac{M}{(M+1)\frac{M\omega}{K}\left(1+\frac{Kx}{u}\right)}\times \left\{1+\frac{\frac{1}{M}e^{-(M+1)\frac{K\tau}{M}}}{1+\left(\frac{M+1}{\frac{M\omega}{K}}\right)^2} - e^{-\frac{Kx}{u}}\left[\psi_2^{**}\left(\frac{Kx}{u},\frac{K\tau^*}{M}\right) - \frac{\frac{1}{M}e^{-(M+1)\frac{K\tau^*}{M}}}{1+\left(\frac{M+1}{\frac{M\omega}{K}}\right)^2}\psi_4\left[\frac{1}{M}\left(\frac{Kx}{u}\right),\ M\left(\frac{K\tau^*}{M}\right)\right]\right] + \sqrt{A_\theta^2+B_\theta^2}\sin\left[\omega\tau^*-\tan^{-1}\left(-\frac{B_\theta}{A_\theta}\right)\right]\right\} \quad (9)$$

where

$$A_\theta = \sin\frac{\omega x}{u} + \frac{\frac{1}{M}}{1+\left(\frac{M+1}{\frac{M\omega}{K}}\right)^2}\left(\frac{M+1}{\frac{M\omega}{K}}\cos\frac{\omega x}{u}+\sin\frac{\omega x}{u}\right) + \frac{e^{-\frac{Kx}{u}\left(\frac{M+1}{\frac{M\omega}{K}}\right)}}{1+\left(\frac{M+1}{\frac{M\omega}{K}}\right)^2}\left[\left(\frac{M+1}{\frac{M\omega}{K}}\right)\psi_6\left(\frac{Kx}{u},\frac{K\tau^*}{M},\frac{M\omega}{K}\right) + \psi_7\left(\frac{Kx}{u},\frac{K\tau^*}{M},\frac{M\omega}{K}\right)\right] \quad (10)$$

$$B_\theta = -\cos\frac{\omega x}{u} + \frac{\frac{1}{M}}{1+\left(\frac{M+1}{\frac{M\omega}{K}}\right)^2}\left(\frac{M+1}{\frac{M\omega}{K}}\sin\frac{\omega x}{u}-\cos\frac{\omega x}{u}\right) + \frac{e^{-\frac{Kx}{u}\left(\frac{M+1}{\frac{M\omega}{K}}\right)}}{1+\left(\frac{M+1}{\frac{M\omega}{K}}\right)^2}\left[\left(\frac{M+1}{\frac{M\omega}{K}}\right)\psi_7\left(\frac{Kx}{u},\frac{K\tau^*}{M},\frac{M\omega}{K}\right) - \psi_{6_1}\left(\frac{Kx}{u},\frac{K\tau^*}{M},\frac{M\omega}{K}\right)\right] \quad (11)$$

(d) Fluid temperature $t(x,\tau)$

$$\frac{t(x,\tau)-t(x,0)}{\frac{\Delta(q/A)}{h}\frac{Kx}{u}} = \frac{\left(\frac{M}{\frac{M\omega}{K}}\right)}{\frac{Kx}{u}(M+1)}\left\{1-\frac{e^{-(M+1)\frac{K\tau}{M}}}{1+\left(\frac{M+1}{\frac{M\omega}{K}}\right)^2} + e^{-\frac{Kx}{u}}\left[-\psi_2^{**}\left(\frac{Kx}{u},\frac{K\tau^*}{M}\right)\right.\right.$$

$$- \frac{e^{-(M+1)\frac{K\tau^*}{M}}}{1 + \left(\frac{M+1}{\frac{M\omega}{K}}\right)^2} \psi_4\left[\frac{1}{M}\left(\frac{Kx}{u}\right), M\left(\frac{K\tau^*}{M}\right)\right]$$

$$+ \sqrt{A_t^2 + B_t^2} \sin\left[\omega\tau^* - \tan^{-1}\left(-\frac{B_t}{A_t}\right)\right]\Bigg\} \quad (12)$$

where

$$A_t = \sin\frac{\omega x}{u} - \frac{1}{1 + \left(\frac{M+1}{\frac{M\omega}{K}}\right)^2}\left(\frac{M+1}{\frac{M\omega}{K}}\cos\frac{\omega x}{u} + \sin\frac{\omega x}{u}\right)$$

$$+ \frac{e^{-\frac{Kx}{u}}}{1 + \left(\frac{M+1}{\frac{M\omega}{K}}\right)^2}\left\{\left[(1+M) + \left(\frac{M+1}{\frac{M\omega}{K}}\right)^2\right] \times \right.$$

$$\left. \psi_8\left(\frac{Kx}{u}, \frac{K\tau^*}{M}, \frac{M\omega}{K}\right) - \frac{1}{M}\left(\frac{M+1}{\frac{M\omega}{K}}\right)\psi_7\left(\frac{Kx}{u}, \frac{K\tau^*}{M}, \frac{M\omega}{K}\right)\right\} \quad (13)$$

$$B_t = -\cos\frac{\omega x}{u} - \frac{1}{1 + \left(\frac{M+1}{\frac{M\omega}{K}}\right)^2}\left(\frac{M+1}{\frac{M\omega}{K}}\sin\frac{\omega x}{u} - \cos\frac{\omega x}{u}\right)$$

$$+ \frac{e^{-\frac{Kx}{u}}}{1 + \left(\frac{M+1}{\frac{M\omega}{K}}\right)^2}\left\{\left[(1+M) + \left(\frac{M+1}{\frac{M\omega}{K}}\right)^2\right] \times \right.$$

$$\left. \psi_7\left(\frac{Kx}{u}, \frac{K\tau^*}{M}, \frac{M\omega}{K}\right) + \frac{1}{M}\left(\frac{M+1}{\frac{M\omega}{K}}\right)\psi_8\left(\frac{Kx}{u}, \frac{K\tau^*}{M}, \frac{M\omega}{K}\right)\right\} \quad (14)$$

Equations (7), (8), (9), and (12) represent the general solutions for the dynamic response of the wall temperature $\theta(x, \tau)$ and the fluid temperature $t(x, \tau)$ above their initial steady-state values for a sinusoidal time variation in the rate of heat generation. These solutions include the transient-periodic and the steady-periodic conditions. Owing to its definition, the difference in temperature between the wall and fluid $\Delta t(x, \tau)$ may be formed from $\theta(x, \tau) - t(x, \tau)$ using the results mentioned. The quantity $\Delta(q/A)$ is the amplitude of the zero frequency heat flux oscillation corresponding to Φ, that of the volumetric heat-generation rate. In the second time domain the response is described by the functions ψ_3^{**}, ψ_4, ψ_7, and ψ_8. The functions ψ_3^{**} and ψ_4 are given in reference [3]. ψ_7 and ψ_8 are new functions with this paper and are discussed in Appendix. These functions were evaluated using an IBM 704 digital computer and are presented in detail in references [4 and 16] where their numerical reduction was obtained for values of s, q, and Ω from 0.10 to 10. Two representative figures for ψ_7 and ψ_8 are included here as Figs. 2 and 3.

The dynamic behavior of the wall and fluid temperatures as described by equations (7) to (14) are functions of the six dimen-

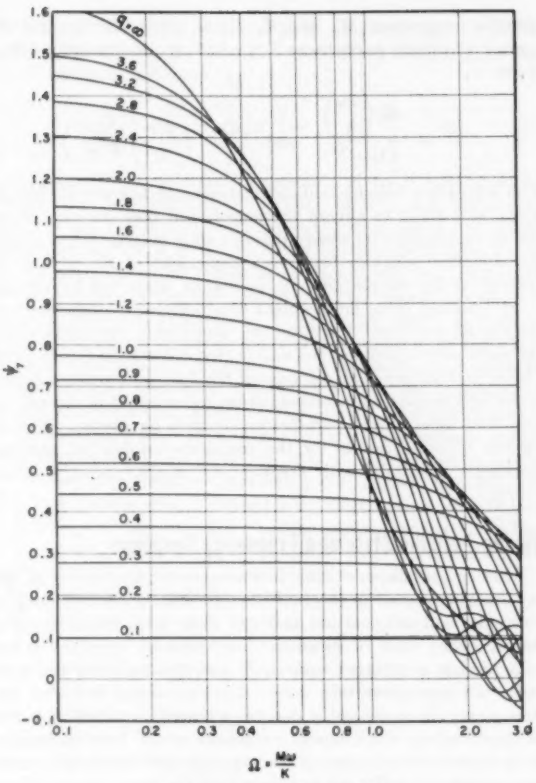

Fig. 2 ψ_7 versus Ω, $s = 0.5$

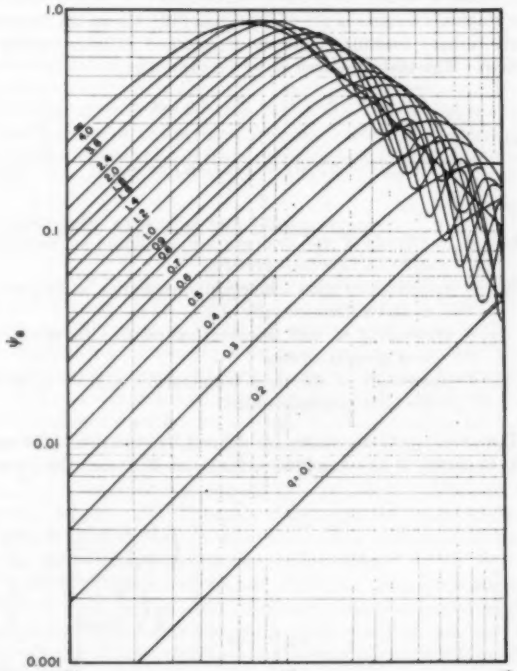

Fig. 3 ψ_8 versus Ω, $s = 0.5$

sionless parameters M, $M\omega/K$, Kx/u, $\omega x/u$, $K\tau/u$, and $\omega\tau$, among which the parameters Kx/u and $\omega\tau$ are not independent since

$$\frac{Kx}{u} = \frac{M\left(\frac{\omega u}{x}\right)}{(M\omega/K)} \quad \text{and} \quad \omega\tau = \left(\frac{K\tau}{M}\right)\left(\frac{M\omega}{K}\right)$$

This leaves four independent dimensionless parameters M, $M\omega/K$, $\omega x/u$, and $K\tau/u$ to govern the response of this system. When the system reaches its steady-periodic state at large values of time the dynamic behavior becomes independent of $K\tau/M$ and $\omega\tau$ (except as the simple periodic oscillation described by sin $(\omega\tau - \alpha)$) leaving three independent dimensionless parameters controlling its response. Furthermore, for physical system in which the ratio heat capacity of the wall to that of the fluid is very small ($M = 0$), the frequency response of the fluid temperature is governed by a single dimensionless parameter and that of the wall by only two independent parameters, as may be shown. A comparison of these results for the transient-periodic (or, starting transient) condition with experimental measurement is given below.

Steady-Periodic State and Frequency Response

After a considerable time following the introduction of the sinusoidal transient in internal heat generation of frequency ω, both the wall temperature and the fluid temperature reach a corresponding state of sinusoidal oscillation of frequency ω but each having a different amplitude and phase-shift relative to $\phi(\tau)$, the heat-generation rate. This condition is called the steady-periodic state and it denotes a condition which may also be described by the frequency response of the heat exchanger. Prior to the establishment of this state the heat exchanger passes through what is called the transient-periodic state. Both of these conditions or states are given as continuous functions of time by the results in equations (7), (8), (9), and (12), the steady-periodic state being a limiting condition approached at large values of time τ. This state is described by the expressions

$$\theta(x, \tau) - \theta(x, 0) = \theta(x) \sin(\omega\tau - \alpha_\theta) \tag{15}$$

and

$$t(x, \tau) - t(x, 0) = T(x) \sin(\omega\tau - \alpha_t) \tag{16}$$

where

$\theta(x)$ = amplitude of wall temperature oscillation at frequency ω, and a function only of x

$T(x)$ = amplitude of fluid temperature oscillation at frequency ω, and a function only of x

α_θ = phase-shift of wall temperature relative to $\phi(\tau)$, the heat-generation rate

α_t = phase-shift of the fluid temperature relative to $\phi(\tau)$, the heat-generation rate

The steady-periodic states are defined by equations (15) and (16) in terms of the amplitudes $\theta(x)$ and $T(x)$ and the phase-shifts α_θ and α_t of the wall and fluid temperatures. These quantities have been determined in two ways, both producing identical results. One method [4] consisted of substituting $i\omega$ for s in the system (Laplace) transfer function $\bar{F}(s)$ and determining the absolute value of the result $\bar{F}(i\omega)$ to obtain the amplitude. The phase-shift is found from the ratio of the real and imaginary parts of $\bar{F}(i\omega)$. The second method [4] was to evaluate equations (9) and (12) at large (infinite) values of time at which $e^{-K\tau}$ and $e^{-K\tau^*}$ become essentially zero. The results are similar in form to equations (15) and (16). From these the following expressions are obtained for the phase-shifts and the ratio of the amplitudes $\theta(x)$ and $T(x)$ at frequency ω to the same amplitudes $\theta_0(x)$ and $T_0(x)$ which would result should the oscillation in heat generation of amplitude Φ be imposed on the system at zero frequency.

(e) Wall temperature amplitude $\theta(x)$ and phase shift α_θ

$$\frac{\theta(x)}{\theta_0(x)} = \frac{e^{-\delta}\sqrt{\left(\frac{M+1}{\frac{M\omega}{K}} - \frac{M\omega}{K}\right)^2 + (M+2)^2}}{\left[1 + \left(\frac{M+1}{\frac{M\omega}{K}}\right)^2\right]\frac{1}{M}\left(\frac{M\omega}{K}\right)^2\left(1 + \frac{Kx}{u}\right)\left[1 + \left(\frac{M\omega}{K}\right)^2\right]}$$

$$\left\{\left[\frac{\frac{1}{M}\left[1 + \left(\frac{M\omega}{K}\right)^2\right]e^{\delta}}{\sqrt{\left[\left(\frac{M+1}{\frac{M\omega}{K}}\right) - \frac{M\omega}{K}\right]^2 + (M+2)^2}} \times \sin\left(\gamma + \tan^{-1}\frac{\frac{M+2}{M+1}}{\frac{M\omega}{K}} - \frac{M\omega}{K}\right)\right]^2 + \left[-\frac{\left(\frac{M+1}{\frac{M\omega}{K}} + \frac{1}{M}\frac{M\omega}{K}\right)\left[1 + \left(\frac{M\omega}{K}\right)^2\right]e^{\delta}}{\sqrt{\left[\left(\frac{M+1}{\frac{M\omega}{K}}\right) - \frac{M\omega}{K}\right]^2 + (M+2)^2}} + \cos\left(\gamma + \tan^{-1}\frac{\frac{M+2}{M+1}}{\frac{M\omega}{K}} - \frac{M\omega}{K}\right)\right]^2\right\}^{1/2} \tag{17}$$

and

$$\alpha_\theta = \tan^{-1}\left\{\frac{\frac{\left(\frac{M+1}{M\omega/K} + \frac{1}{M}\frac{M\omega}{K}\right)e^{\delta}\left[1 + \left(\frac{M\omega}{K}\right)^2\right]}{\sqrt{\left(\frac{M+1}{M\omega/K} - \frac{M\omega}{K}\right)^2 + (M+2)^2}} - \cos\left(\gamma + \tan^{-1}\frac{\frac{M+2}{M+1}}{\frac{M\omega}{K}} - \frac{M\omega}{K}\right)}{\frac{\frac{1}{M}e^{\delta}\left[1 + \left(\frac{M\omega}{K}\right)^2\right]}{\sqrt{\left(\frac{M+1}{M\omega/K} - \frac{M\omega}{K}\right)^2 + (M+2)^2}} + \sin\left(\gamma + \tan^{-1}\frac{\frac{M+2}{M+1}}{\frac{M\omega}{K}} - \frac{M\omega}{K}\right)}\right\} \tag{18}$$

(*f*) Fluid temperature amplitude $T(x)$ and phase shift α_t

$$\frac{T(x)}{T_0(x)} = \frac{\sqrt{1+\left(\frac{M+1}{M\omega/K}\right)^2}\, e^{-\delta}}{\frac{Kx}{u}\left[1+\left(\frac{M\omega/K}{M+1}\right)^2\right]\frac{(M+1)^2}{M}} \times \left\{\left[-\frac{e^{\delta}}{\sqrt{1+\left(\frac{M+1}{M\omega/K}\right)^2}} + \sin\left(\gamma + \tan^{-1}\frac{\frac{M\omega}{K}}{M+1}\right)\right]^2 + \left[-\frac{e^{\delta}}{\sqrt{1+\left(\frac{M\omega/K}{M+1}\right)^2}} + \cos\left(\gamma + \tan^{-1}\frac{M\omega/K}{M+1}\right)\right]^2\right\}^{1/2} \tag{19}$$

and

$$\alpha_t = \tan^{-1}\left\{\frac{\frac{e^{\delta}}{\sqrt{1+\left(\frac{M\omega/K}{M+1}\right)^2}} - \cos\left[\gamma + \tan^{-1}\left(\frac{M\omega/K}{M+1}\right)\right]}{-\frac{e^{\delta}}{\sqrt{1+\left(\frac{M+1}{M\omega/K}\right)^2}} + \sin\left[\gamma + \tan^{-1}\left(\frac{M\omega/K}{M+1}\right)\right]}\right\} \tag{20}$$

In equations (17), (18), (19), and (20) the functions $\theta_0(x)$, $T_0(x)$, δ, and γ are defined as follows,

$$\theta_0(x) = \frac{\Delta(q/A)}{h}\left(1 + \frac{Kx}{u}\right) \tag{21}$$

$$T_0(x) = \frac{\Delta(q/A)}{h}\left(\frac{Kx}{u}\right) \tag{22}$$

$$\delta = \frac{\left(\frac{Kx}{u}\right)\left(\frac{M\omega}{K}\right)^2}{1+\left(\frac{M\omega}{K}\right)^2} \tag{23}$$

$$\gamma = \frac{Kx}{u}\left[\frac{M\omega/K}{1+\left(\frac{M\omega}{K}\right)^2} + \frac{1}{M}\left(\frac{M\omega}{K}\right)\right] \tag{24}$$

While equations (17) to (20) are relatively complex there is no way of reducing them further and still retain their generality. In the interest of saving space the results for $\alpha_{\Delta t}$ and $\Delta t = \theta - t$ are not discussed here although they are extensively analyzed in reference [4] and are found in Appendix in analytical form. These functions may be obtained from equations (15) and (16), however, remembering they bear a vector relationship to θ and t, α_t and α_θ.

The foregoing results for the amplitude ratios and phase shifts while algebraically complex are governed by only three independent dimensionless parameters M, $M\omega/K$, and Kx/u. The actual steady-periodic response of $\theta(x,\tau)$ and $t(x,\tau)$ also are functions of the dimensionless quantity $\omega\tau$ through the simple periodic function sin $(\omega\tau - \alpha)$, but this is trivial. Also, the magnitude of responses are governed by the dimensional quantity $\Delta(q/A)/h$ which is established independently by the nature of the imposed transient and the properties of the physical system. Another dimensionless parameter $\omega x/u$ may be derived from the three just mentioned. Hence it is possible to describe the amplitude ratio $\theta(x)/\theta_0(x)$, $T(x)/T_0(x)$, and the phase-shifts α_θ and α_t in the steady-periodic state by the independent dimensionless quantities, M, Kx/u, and $\omega x/u$ only, as

$$\left(\frac{\theta(x)}{\theta_0(x)}, \frac{T(x)}{T_0(x)}, \alpha_\theta, \alpha_t\right) = f\left(M, \frac{Kx}{u}, \frac{\omega x}{u}\right) \tag{25}$$

The amplitude ratio and phase-shifts given in equations (17) to (20) have been computed for values of $M = 0.5$, 1.0, and 10, $Kx/u = 0.1$, 1.0, and 10, and $\omega x/u$ in the range 0.1 to 100. These are shown in Figs. 4, 5, 6, and 7. Of significance in these results is the phenomena of resonance in amplitude and phase-shift of the response of the wall and fluid. This appears contrary to that characteristic reported by Paynter [15] where it was suggested that the frequency response of a system such as this would have a nonincreasing amplitude and nondecreasing phase-lag with increasing frequency. Other than this, the frequency-response characteristics shown in Figs. 4 to 7 have the properties of an amplitude ratio of 1 at zero frequency and zero at infinite frequency. The phase-shifts are zero at zero frequency and at large frequencies approaching 90 deg for the wall and oscillating about 180 deg for the fluid. In the case of both the wall and fluid the response lags the oscillation in heat generation, as would be expected. An interesting result is obtained in the case of the phase-shift of the fluid-wall temperature difference. While this case is not analyzed here, for the reasons stated in the foregoing, the result for its phase relationship is included in Fig. 8. Of interest here is the phase-*lead* that can exist for certain values of M and Kx/u. At large values of the frequency the phase-shift approaches a lag of 90 deg.

The influence of the parameters M and Kx/u on the amplitude ratio $T(x)/T_0(x)$ and phase-shift α_t for the fluid at the first point of resonance is shown in Figs. 9 and 10. The amplitude ratio decreases rapidly with an increase in M, the wall-fluid heat-capacity ratio, for all values of Kx/u while the phase-shift approaches a fairly constant value for M greater than about 1 following a very rapid decrease in the range of M from 0 to 1. The continuous decrease in the amplitude ratio with increase in M results from the relative increase in the heat capacity of the wall which introduces an inertness into the system and reduces the temperature oscillation of the wall itself and hence also that of the fluid.

Experimental Apparatus and Measurement

The experimental apparatus used to check the theory is shown schematically in Fig. 11. It consisted of an insulated, electrically heated standard $^5/_8$ OD-BWG 16, 304 stainless-steel tube (ID = 0.495 in.) 36 inches in length preceded by an equal length of jacketed tubing maintained at the inlet water temperature. This served the double purpose of establishing a fully developed hydromechanic condition as well as eliminating an influence on the inlet flow of coolant resulting from an axial conduction along the tube. The fluid pumped through the test section was Ann Arbor Municipal water, treated locally for softening, and sent to the drain after use in the experimental apparatus. The inside surface of the heated section was inspected frequently for contamination but none was detected. A steady-state flow was established and measured using a calibrated sharp-edged orifice.

Sinusoidal variation in the rate of internal heat generation was obtained by a mechanically programmed and controlled oscillation of the auto transformer core feeding a-c voltage into a 50 kw Hansen-Van Winkle and Munning Germanium rectifier (25v, d-c, 2000 amp) which is part of the permanent facilities of the Laboratory. The internal heat-generation rate was determined from instantaneous measurement and recording of test section (d-c) voltage and current.

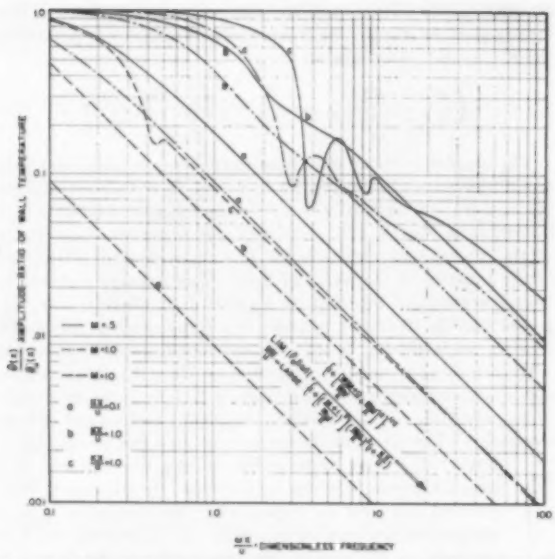

Fig. 4 Effect of the parameters M, Kx/u, and $\omega x/u$ on the amplitude-ratio response of the wall temperature

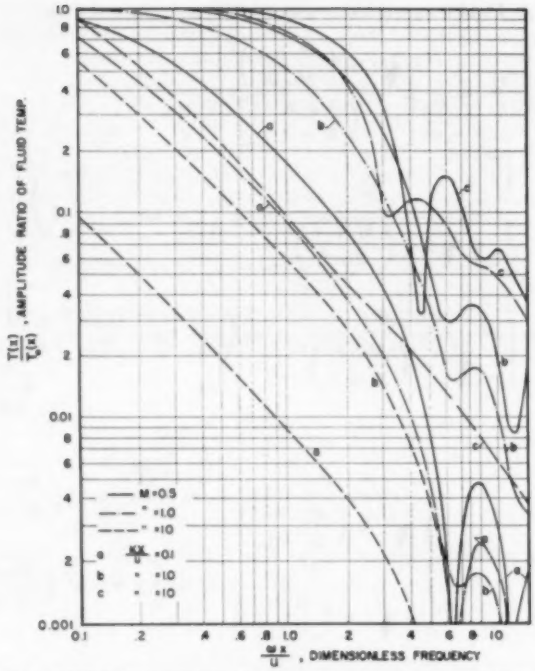

Fig. 5 Effect of the parameters M, Kx/u, and $\omega x/u$ on the amplitude-ratio response of fluid temperature

Test-section fluid and wall temperatures were measured using calibrated iron-constantan (30 gage) thermocouples. The outlet fluid (water) temperature was determined by a thermocouple downstream from a mixing baffle made of very thin aluminum having negligible heat capacity. The wall thermocouple wires were welded directly and separately to the outer wall of the test section by a capacitor-discharge technique. Attempts were made to attach each of the wires of such a thermocouple in a plane of constant (test-section) voltage. However, it was found that the influence of any small misalignment could be very accurately determined by calibration and, hence, the effect of d-c pickup on the thermal emf of the thermocouple was subject to correction.

All transient measurements of thermal emf and other voltage for test-section current and voltage were obtained simultaneously using a Minneapolis-Honeywell model 1012 Visicorder. This unit is a direct recording oscillographic recorder having 36 channels and a range of chart speeds from 0.1 to 160 in. per second. Heiland M40-120 mirrored galvanometers were employed in the unit. Each thermocouple and/or voltage circuit was calibrated to obtain the relationship between indicated voltage from the galvanometer deflection and open circuit voltage. A typical transient record is shown in Fig. 12. Some a-c pickup is evident but this was greatly reduced by inductively winding the detection circuits external from the instrument. A slight flat portion exists at the maximum amplitudes of E and I, the test-section voltage and current which resulted from a small amount of backlash in a flexible coupling in the auto-transformer mechanical-drive mechanism. This caused a negligible departure from a sinusoidal timewise variation in internal-heat-generation rate.

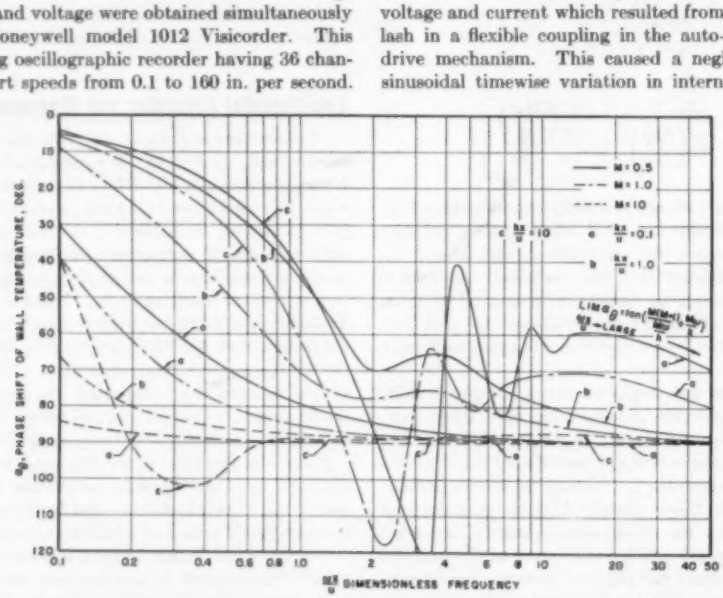

Fig. 6 Effect of the parameters M, Kx/u, and $\omega x/u$ on the phase-shift response of the wall temperature

Steady-state voltage measurements were made using a model 8662 Leeds and Northrup precision potentiometer for the purpose of determining the general operation of the apparatus. Heat-transfer data were taken in the steady-state for Reynolds numbers ranging from 10,000 to 35,000. Heat balance checks indicated agreement within 2 to 4 per cent between the water enthalpy rise, the mean electric-power dissipation from E and I measurements, and the integrated local heat flux from current and local electrical resistivity measurements. Determination of the local values of heat-transfer coefficient disclosed an expected thermal-entry length effect with fairly constant coefficients for L/d_i greater than about 24. This is midway between results of Aladyev [17] and Hartnett [18]. The length-mean heat-transfer data correlated within ±5 per cent of $St\ Pr_f^{2/3} = 0.021\ Re_f^{-0.20}$, which is about 9 per cent below that of McAdams [19]. This steady-state correlation was used to compute the heat-transfer coefficients for comparison of the theory with the experimental data.

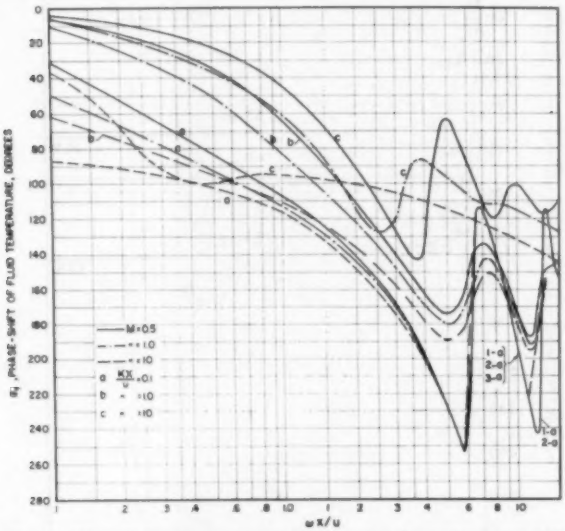

Fig. 7 Effect of the parameters M, Kx/u, and $\omega x/u$ on the phase-shift response of fluid temperature

Comparison of Theory With Experimental Data

Typical transient-periodic state response of fluid and wall temperatures are shown in Figs. 13 and 14. Fig. 13 shows the experimental data of the fluid bulk temperature response to agree very well with the theoretical curve in this state. The experimental results of wall-temperature response shown in Fig. 14 fall fairly well on the theoretical curve, except that the phase-shift is larger, a result probably due to a heat capacity lag in the wall thermocouples. The physical time intervals in the first time domain for the both responses are very short but the recordings show they agree well with the theoretical calculations. Also shown in these figures are the envelopes for the maximum amplitude of the fluid and wall response in both time domains.

The comparison of the measured and theoretical response in the steady-periodic state are shown in Figs. 15, 16, and 17 for both the wall and the fluid. These results are presented as amplitude ratio $\theta(x)/\theta_0(x)$ and $T(x)/T_0(x)$ versus frequency ω and are called the frequency-response characteristics of the system for the specified conditions.

The response recordings of the wall thermocouples at stations No. 6 and 9 (θ_6 and θ_9), which are free of the d-c pickup, are almost purely sinusoidal (Fig. 12) although the other wall thermocouples having a d-c pickup are less sinusoidal in their response. This is due to the fact that the magnitude of the d-c pickup by each wall thermocouple is different with different voltage applied to the test section. For this reason, the frequency response of the wall temperature was investigated at stations No. 6 and 9 only. Fig. 17 shows the frequency-response characteristics of the wall temperature at Kx/u equal to 0.302, Station 9. This result indicates that the experimental results of the wall temperature amplitude-ratio falls below the theoretical results particularly at high frequency. The phase-shift response on the contrary is higher than but almost parallel to the theoretical one and agrees fairly well at the high frequency.

This discrepancy is probably due to the heat capacity lag of the wall thermocouples. The wall thermocouple of station No. 9 is close to the bus bar on one side and the pressure tap on the other. The uncertainty estimations for confidence limits on the mean of 95 per cent are evaluated for the amplitude-ratio and phase-shift of the wall and fluid temperature by the method of reference [21]. The uncertainty intervals increase with increase in frequency, since at high frequency the galvanometer deflections

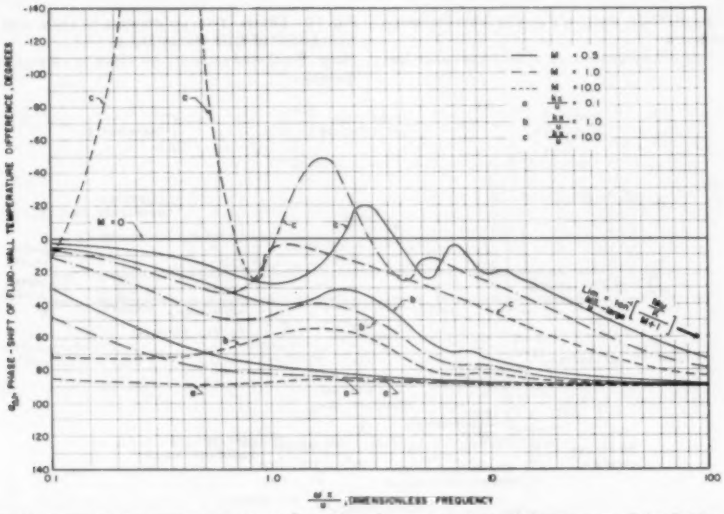

Fig. 8 Effect of the parameters M, Kx/u, and $\omega x/u$ on the phase-shift response of the fluid-wall temperature difference

corresponding to the temperature amplitude about the mean temperature become very small.

For the wall temperatures at $Kx/u = 0.302$ and $\omega = 50$ cycles per minute, the uncertainty intervals of the amplitude-ratio response is ±24.4 per cent, and for the phase-shift response it is ±34.3 per cent of their corresponding mean values for 95 per cent confidence in the mean.

The frequency response of the fluid bulk temperature, shown in Figs. 15 and 16, is measured at station 11, located after the mixing baffle and corresponds to that at test section exit. The experimental results of both amplitude-ratio and phase-shift responses agree well with their theoretical curves. The uncertainty intervals are also shown for 95 per cent of confidence in the mean. The heat-transfer coefficient used in the theoretical computation is the integrated mean value where fluid properties are based on the film temperature.

Resonance phenomena both in the amplitude-ratio and phase-shift response of the water temperature occur at the frequencies of 95 cycles per minute for the former and 80 cycles per minute for the latter. Also shown are the multiple points of resonance in both amplitude and phase shift at higher frequencies. Within the range of variables shown the phase shift oscillates about 180 degrees at higher frequencies.

Owing to the increasing percentage in uncertainty interval at high frequency and the difficulties in making a physical measurement these data have not been extended to sufficiently high frequencies in this research to demonstrate the resonance indicated by the theoretical computations. This is occasioned by the physical limitations of the present experimental apparatus. The thermal emf of the temperature amplitude at the first point of

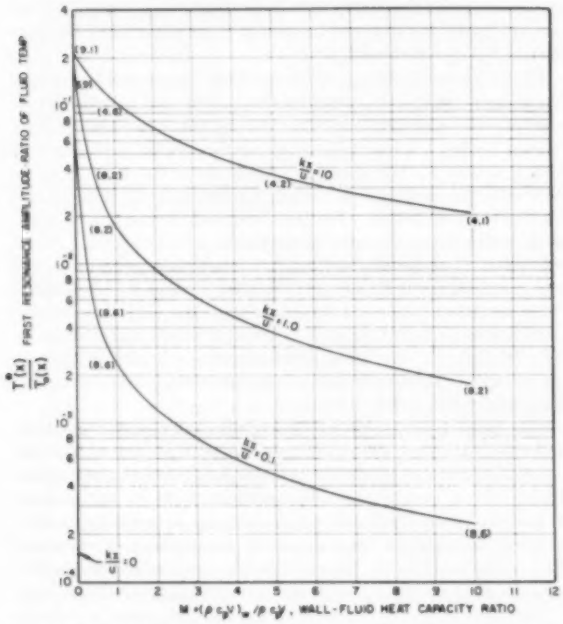

Fig. 9 Effects of the parameters M, $K\omega/u$, and $\omega x/u$ on the first resonance amplitude-ratio of fluid temperature
Note: Bracketed quantity on curve is value of $\omega x/u$ at first resonance frequency ω^*

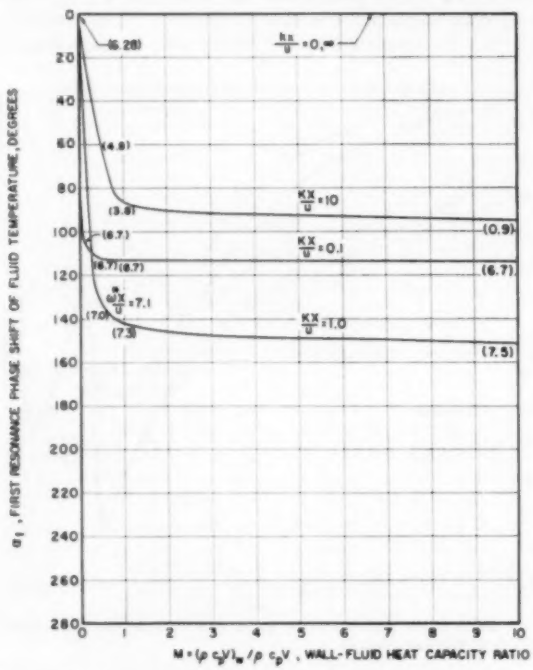

Fig. 10 Effects of the parameters M, $\omega x/u$, and Kx/u on the first resonance phase-shift of fluid temperature
Note: Bracketed quantity on curve is value of $\omega x/u$ at first resonance frequency ω^*

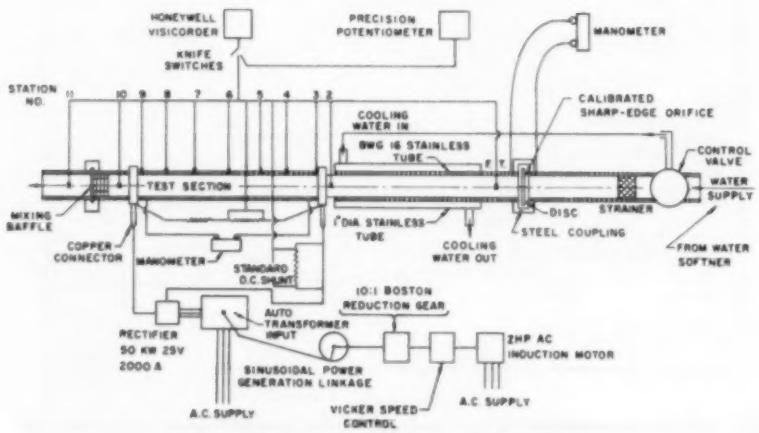

Fig. 11 Schematic diagram of experimental apparatus

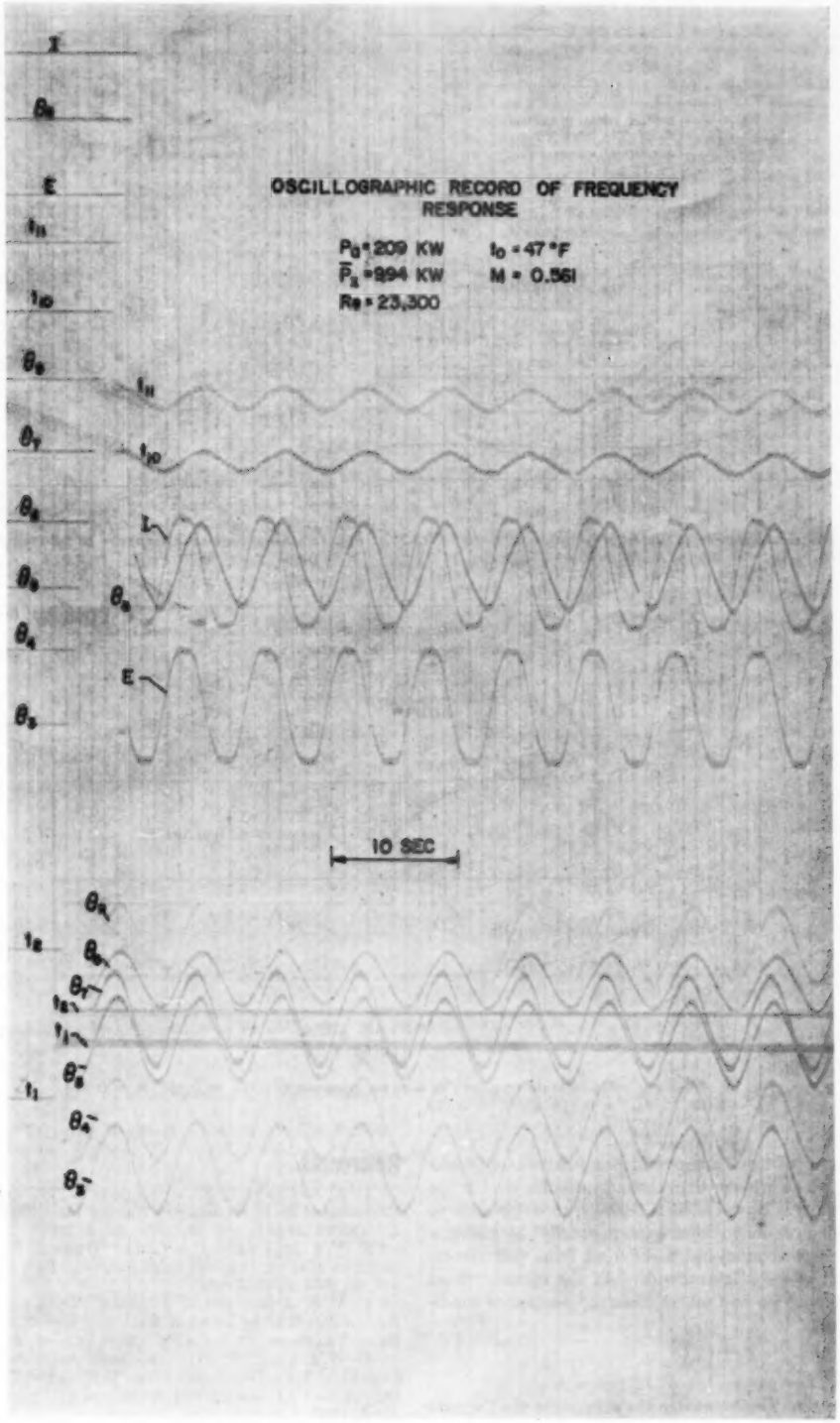

Fig. 12 Oscillographic record of frequency response

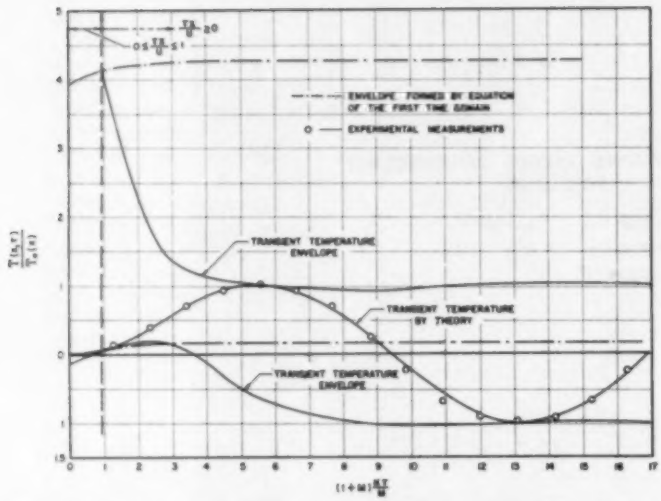
ENVELOPE FORMED BY EQUATION OF THE FIRST TIME DOMAIN
EXPERIMENTAL MEASUREMENTS
TRANSIENT TEMPERATURE ENVELOPE
TRANSIENT TEMPERATURE BY THEORY
TRANSIENT TEMPERATURE ENVELOPE

Fig. 13 Transient periodic-state response of water temperature at $Kx/u = 0.321$, $M = 0.561$, $K_w = 2470$, $P_a/P_{Da}'' = 0.218$, $M\omega/K = 0.653$

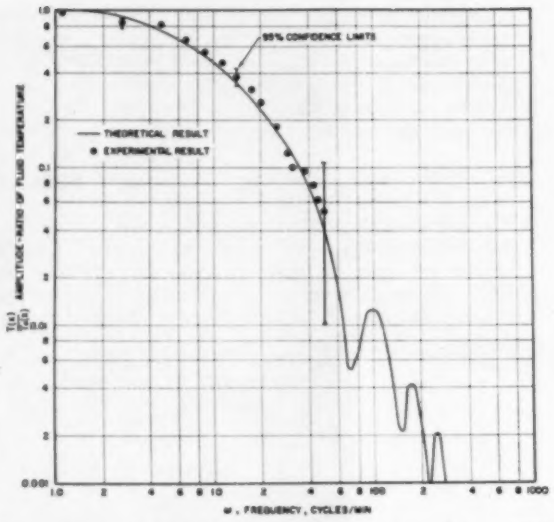

Fig. 15 Amplitude-ratio response of fluid temperature at $Kx/u = 0.321$, $M = 0.561$, $K_w = 2470$, $P_a/P_{Da}'' = 0.218$

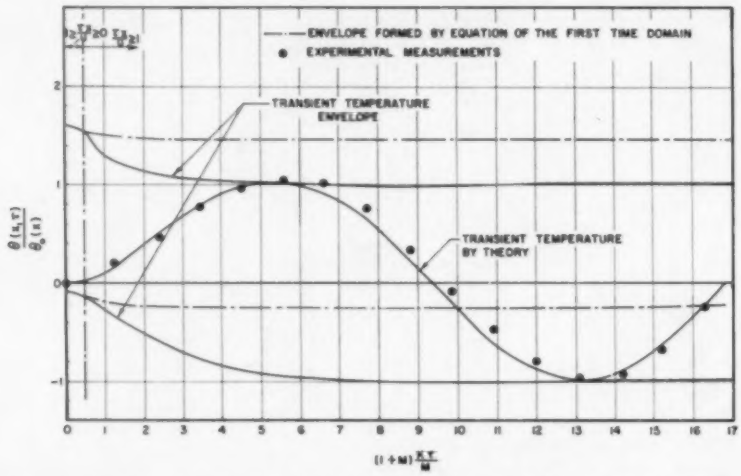
ENVELOPE FORMED BY EQUATION OF THE FIRST TIME DOMAIN
EXPERIMENTAL MEASUREMENTS
TRANSIENT TEMPERATURE ENVELOPE
TRANSIENT TEMPERATURE BY THEORY

Fig. 14 Transient periodic-state response of wall temperature at $Kx/u = 0.161$, $M = 0.561$, $K_w = 2470$, $P_a/P_{Da}'' = 0.218$, $M\omega/K = 0.653$

resonance is the order of 1 to 3 microvolts for operating conditions shown in Fig. 15, which is lower than the output noise level of the ordinary d-c amplifier. However, it is believed to be possible to observe the resonance phenomena experimentally by using a somewhat longer test section and a different fluid-wall system having a smaller heat-capacity ratio M. At the moment these alterations are in progress so that an observed resonance condition can be reported.

Acknowledgment

The authors gratefully acknowledge the support of the Department of Mechanical Engineering, University of Michigan, in providing funds for the experimental apparatus and services for its construction and operation. The IBM 704 computing program was conducted under a grant from the Horace H. Rackham School of Graduate Studies and was carried out at the computer center at the University. This assistance is greatly appreciated.

References

1 J. A. Clark, V. S. Arpaci, and K. M. Treadwell, "Dynamic Response of Heat Exchangers Having Internal Heat Sources—Part I," TRANS. ASME, vol. 80, 1958, pp. 612–624.

2 V. S. Arpaci and J. A. Clark, "Dynamic Response of Heat Exchangers Having Internal Heat Sources—Part II," TRANS. ASME, vol. 80, 1958, pp. 625–634.

3 V. S. Arpaci and J. A. Clark, "Dynamic Response of Heat Exchangers Having Internal Heat Sources—Part III," JOURNAL OF HEAT TRANSFER, TRANS. ASME, Series C, vol. 81, 1959, pp. 253–266.

4 W. J. Yang, "The Dynamic Response of Heat Exchangers With Sinusoidal Time Dependent Internal Heat Generation," PhD thesis, Department of Mechanical Engineering, University of Michigan, April, 1960.

5 P. Profos, "Die Behandlung von Regelproblemen Vermittels des Frequenzganges des Regelkreises und irhe Anwendung auf die Temperaturregelund Durchstromter Roheysteme," Leemann and Co., Zurich, Switzerland, 1943.

6 R. P. Stein, "Transient Heat Transfer in Reactor Coolant Channels," NSAEC, AECLU 3600, October, 1957.

7 W. C. Cohen and E. F. Johnson "Dynamic Characteristics of

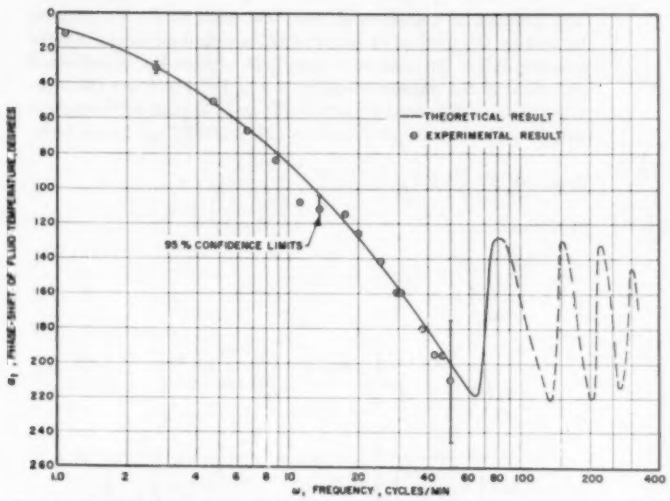

Fig. 16 Phase-shift response of fluid temperature at $Kx/v = 0.321$, $M = 0.561$, $K_\omega = 2470$, $P_a/P_{0x}{}^r = 0.218$

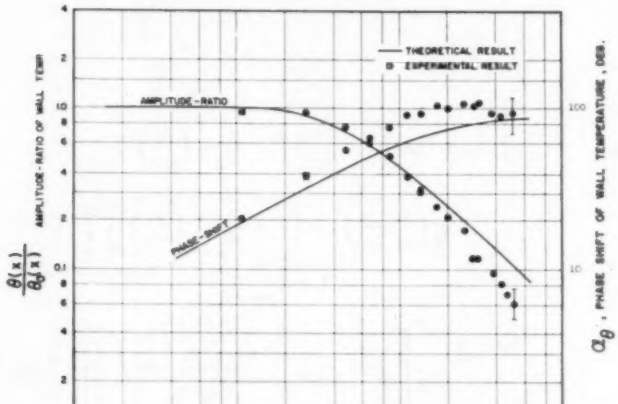

Fig. 17 Frequency response of wall temperature at $Kx/v = 0.302$, $M = 0.561$, $K_\omega = 2470$, $P_a/P_{0x}{}^r = 0.218$

Double-Pipe Heat Exchangers," *Industrial and Engineering Chemistry*, vol. 48, June, 1956, p. 1031.

8 M. Masubuchi, "Dynamic Response and Control of Multipass Heat Exchangers," *Journal of Basic Engineering*, TRANS. ASME, Series D, 1960, pp. 51–65.

9 S. Lees and J. O. Hougen, "Pulse Testing a Model Heat Exchange Process," *Industrial and Engineering Chemistry*, vol. 48, 1956, pp. 1064–68.

10 L. M. Zoss, N. W. Gollin, and R. I. Edelman, "Dynamic Response Analysis of Air Heater Temperature Control System," *Industrial and Engineering Chemistry*, vol. 48, 1956, pp. 1069–1073.

11 Y. Takahashi, "You Need No Computers to Graphically Determine the Dynamics of Heat Percolation," *Control Engineering*, vol. 2, May, 1955, pp. 46–50.

12 Y. Takahashi, "Transfer Function Analysis of Heat Exchangers," "Automatic and Manual Control," edited by A. Tustin, Buttersworth Science Publishing Co., London, England, 1952, p. 235.

13 P. U. Schneider, "Effect of Axial Fluid Conduction on Heat Transfer in Entrance Regions of Parallel Plates and Tubes," TRANS. ASME, vol. 79, 1957, p. 765.

14 Fred Storrer, "Temperature Response to Power Oscillations in a Solid Fuel Reactor," Paper 12–7, *Trans. American Nuclear Society*, 1959 Annual Meeting, Gatlinburg, Tennessee, June, 1959.

15 H. M. Paynter, "On an Analogy Between Stochastic Processes and Monotone Dynamic Systems," Regelungstechnik, Moderne Theorien und ihre Vermendbaskeit, Kapitel VII, Statistische Methoden, Verlag R. Oldenbourg, Munchen, Germany, pp. 243–250.

16 W. J. Yang, J. A. Clark, and V. S. Arpaci, "Evaluation of the Functions ψ_7 and ψ_8," manuscript in preparation, May, 1960.

17 I. T. Aladyev, "Experimental Determination of Local and Mean Coefficients of Heat Transfer for Turbulent Flow in Pipes," NACA TM 1356, February, 1954.

18 J. P. Hartnett, "Experimental Determination of the Thermal Entrance Length for the Flow of Water and of Oil in Circular Pipes," *Mechanical Engineering*, vol. 72, 1955, p. 263.

19 W. H. McAdams, "Heat Transmission," third edition, McGraw-Hill Book Company, Inc., New York, N. Y., 1954.

20 Fred Storrer, "Amplitude and Phase of Fuel and Coolant Temperatures Throughout a Reactor During Power Oscillations," Paper 12–9, *Trans. American Nuclear Society*, Supplement to Nuclear Science and Engineering, vol. 1, no. 1, June, 1958.

21 S. J. Kline and F. A. McClintock, "Describing Uncertainties in Single-Sample Experiments," *Mechanical Engineering*, vol. 75, 1953, pp. 3–8.

APPENDIX

The Integration of Equations (4) and (5)

Equations (4) and (5) may be operated on by the Laplace operator with respect to time τ to produce the following transformed equations,

$$-(\bar{\theta}_1 - \bar{t}_1) + a_1\Phi\frac{\omega}{p^2+\omega^2} = a_2[p\bar{t}_2 - \theta_2(x,0)] \quad (26)$$

and

$$(\bar{\theta}_2 - \bar{t}_2) = a_3[p\bar{t}_2 - t_2(x,0)] + a_4\frac{d\bar{t}_2}{dx} \quad (27)$$

The boundary and initial conditions to be imposed according to the results of reference [3], Appendix 1, are:

$$t_2(x,0) = 0 \quad (28)$$

$$\theta_2(x,0) = 0 \quad (29)$$

Hence equations (26) and (27) become

$$-(\bar{\theta}_2 - \bar{t}_2) + a_1\Phi\frac{\omega}{p^2+\omega^2} = a_2p\bar{t}_2 \quad (30)$$

$$(\bar{\theta}_2 - \bar{t}_2) = a_3p\bar{t}_2 + a_4\frac{d\bar{t}_2}{dx} \quad (31)$$

Solving equations (30) and (31) for $\bar{t}_2(x,p)$ gives

$$\frac{d\bar{t}_2}{dx} + f_1\bar{t}_2 = f_2 \quad (32)$$

The solution of this linear first-order differential equation, with the boundary condition $\bar{t}_2(0,p) = 0$, is

$$\bar{t}_2 = \frac{f_2}{f_1}(1 - e^{-f_1x}) \quad (33)$$

where

$$f_1 = \frac{1}{a_4}\left(1 + a_3p - \frac{1}{1+a_2p}\right) \quad (34)$$

$$f_2 = \frac{a_1}{a_4}\frac{\Phi\omega}{p^2+\omega^2}\frac{1}{1+a_2p} \quad (35)$$

Substituting equation (33) into equations (30) and (31) and solving for θ_2, gives

$$\frac{\bar{\theta}_2}{\Phi a_1\left(1+\frac{x}{a_4}\right)} = \frac{a_2}{b_2\left(1+\frac{x}{a_4}\right)} \frac{\frac{1}{a_2}+p}{p\left(\frac{b_1}{b_2}+p\right)} \frac{\omega}{p^2+\omega^2}$$

$$- \frac{1}{a_2 b_2\left(1+\frac{x}{a_4}\right)} e^{-\frac{x}{a_4}} e^{-\frac{x}{u}p} \frac{\omega}{p^2+\omega^2} \frac{e^{\frac{1}{\frac{a_2 a_4}{x}\left(p+\frac{1}{a_2}\right)}}}{p\left(\frac{b_1}{b_2}+p\right)\left(\frac{1}{a_2}+p\right)}$$

$$= \frac{1}{b_1\left(1+\frac{x}{a_4}\right)} F_{13}(p) \frac{\omega}{p^2+\omega^2}$$

$$- \frac{1}{a_2 b_1\left(1+\frac{x}{a_4}\right)} e^{-\frac{x}{a_4}} e^{-\frac{x}{u}p} F_{14}(p) F_{15}(p) \frac{\omega}{p^2+\omega^2} \quad (36)$$

In like manner, the fluid-wall-temperature difference

$$\Delta\bar{t}_2 = \bar{\theta}_2 - \bar{t}_2$$

is found to be

$$\frac{\Delta\bar{t}_2}{\Phi a_1} = \frac{a_2}{b_2} \frac{1}{\left(\frac{b_1}{b_2}+p\right)} \frac{\omega}{(p^2+\omega^2)}$$

$$+ \frac{1}{b_2} e^{-\frac{x}{a_4}} e^{-\frac{x}{u}p} \frac{\omega}{p^2+\omega^2} \frac{1}{\left(\frac{b_1}{b_2}+p\right)} \frac{e^{\frac{1}{\frac{a_2 a_4}{x}\left(p+\frac{1}{a_2}\right)}}}{\left(\frac{1}{a_2}+p\right)}$$

$$= \frac{a_2}{b_2} F_{15}(p) \frac{\omega}{p^2+\omega^2} + \frac{1}{b_2} e^{-\frac{x}{a_4}} e^{-\frac{x}{u}p} F_{15}(p) F_{16}(p) \frac{\omega}{p^2+\omega^2} \quad (37)$$

where $b_1 = a_1 + a_2$ and $b_2 = a_2 a_3$.

In equations (36) and (37) the functions F_{13}, F_{14}, F_{15}, and F_{16} are Laplace-transformed functions in the variable p which have corresponding original functions G_{13}, G_{14}, G_{15}, and G_{16} in the variable τ obtained by performing an inverse transformation on the function F. The Laplace-transformed function F and the inverse-transformed functions G appropriate to equations (36) and (37) are listed in the following table:

The product of transformed functions, such as $F_{14}\,F_{16}$, may be treated by the method of convolution, a technique of the inverse transformation for product of functions. Hence the transformed equations in the physical domain of x and τ, which are the solutions to the differential equations (4) and (5), and for boundary and initial conditions of equations (28) and (29) are found to be

Case 1, $0 \leq \frac{\tau u}{x} \leq 1$

Wall temperature

$$\frac{\theta_2(\tau)}{a_1\left(1+\frac{x}{a_4}\right)\Phi}$$

$$= \frac{1}{b_1\left(1+\frac{x}{a_4}\right)} \int_0^\tau \sin\omega\xi \left[1 + \frac{a_2}{a_2} e^{-\frac{b_1}{b_2}(\tau-\xi)}\right] d\xi$$

$$= \frac{1}{b_2\omega\left(1+\frac{x}{a_4}\right)} \left\{1 - \cos\omega\tau + \frac{a_2}{a_2} \frac{1}{1+\left(\frac{b_1}{b_2\omega}\right)^2} \times \left[\frac{b_1}{b_2\omega}\sin\omega\tau - \cos\omega\tau + e^{-\frac{b_1}{b_2}\tau}\right]\right\}$$

$$= \frac{1}{b_2\omega\left(1+\frac{x}{a_4}\right)} \left\{1 + \frac{\frac{a_2}{a_2} e^{-\frac{b_1}{b_2}\tau}}{1+\left(\frac{b_1}{b_2\omega}\right)^2} + \frac{\sqrt{\left(\frac{a_2}{a_2}\frac{b_1}{b_2\omega}\right)^2 + \left[1+\frac{a_2}{a_2}+\left(\frac{b_1}{b_2\omega}\right)^2\right]^2}}{1+\left(\frac{b_1}{b_2\omega}\right)^2} \times \sin\left[\omega\tau - \tan^{-1}\left[\frac{1+\frac{a_2}{a_2}+\left(\frac{b_1}{b_2\omega}\right)^2}{\frac{a_2}{a_2}\frac{b_1}{b_2\omega}}\right]\right]\right\} \quad (38)$$

Fluid-wall temperature difference

$$\frac{\Delta t_2(\tau)}{a_1\Phi} = \frac{a_2}{b_2} e^{-\frac{b_1}{b_2}\tau} \int_0^\tau e^{\frac{b_1}{b_2}\xi} \sin\omega\xi d\xi$$

	$F(p)$		$G(\tau)$	Restriction
F_{13}	$a_2\left(\frac{b_1}{b_2}\right)\frac{\frac{1}{a_2}+p}{p\left(\frac{b_1}{b_2}+p\right)}$	G_{13}	$1+\frac{a_2}{a_2}e^{-\frac{b_1}{b_2}\tau}$	$\tau > 0$
F_{14}	$\frac{b_1}{b_2}\frac{1}{p\left(\frac{b_1}{b_2}+p\right)}$	G_{14}	$1-e^{-\frac{b_1}{b_2}\tau}$	$\tau > 0$
F_{15}	$\frac{1}{\frac{b_1}{b_2}+p}$	G_{15}	$e^{-\frac{b_1}{b_2}\tau}$	$\tau > 0$
F_{16}	$e^{\frac{1}{\frac{a_2 a_4}{x}\left(\frac{1}{a_2}+p\right)}} \Big/ \left(\frac{1}{a_2}+p\right)$	G_{16}	$e^{-\frac{\tau}{a_2}} I_0\left[2\left(\frac{x\tau}{a_2 a_4}\right)^{1/2}\right]$	$\tau > 0$

$$= \frac{1}{b_1\omega}\frac{1+\frac{a_3}{a_2}}{1+\left(\frac{b_1}{b_2\omega}\right)^2}\left[\frac{b_1}{b_2\omega}\sin\omega\tau - \cos\omega\tau + e^{-\frac{b_1}{b_2}\tau}\right]$$

$$= \frac{1}{a_2\omega\left[1+\left(\frac{b_1}{b_2\omega}\right)^2\right]}\left\{e^{-\frac{b_1}{b_2}\tau} + \sqrt{1+\left(\frac{b_1}{b_2\omega}\right)^2}\times \sin\left[\omega\tau - \tan^{-1}\left(\frac{b_2\omega}{b_1}\right)\right]\right\} \quad (39)$$

Fluid temperature

$$\frac{t_2(\tau)}{\frac{a_1 x}{a_4}\Phi} = \frac{a_4}{b_1\omega x}\left\{1 - \cos\omega\tau - \frac{1}{1+\left(\frac{b_1}{b_2\omega}\right)^2}\times \left[\frac{b_1}{b_2\omega}\sin\omega\tau - \cos\omega\tau + e^{-\frac{b_1}{b_2}\tau}\right]\right\}$$

$$= \frac{a_4}{b_1\omega x}\left\{1 - \frac{e^{-\frac{b_1}{b_2}\tau}}{1+\left(\frac{b_1}{b_2\omega}\right)^2} + \frac{1}{\sqrt{1+\left(\frac{b_1}{b_2\omega}\right)^2}}\times \sin\left[\omega\tau - \tan^{-1}\left(-\frac{b_1}{b_2\omega}\right)\right]\right\} \quad (40)$$

Case 2 $\frac{\tau\omega}{x} \geq 1$

Wall temperature

$$\frac{\theta_2(x,\tau)}{a_1\Phi\left(1+\frac{x}{a_4}\right)} = \frac{\theta_2(\tau)}{a_1\Phi\left(1+\frac{x}{a_4}\right)} - \frac{e^{-\frac{x}{a_4}}}{b_1\omega\left(1+\frac{x}{a_4}\right)}\times \left\{\psi_2^{**}(s,q^*) - \frac{a_3}{a_2}\frac{e^{-\frac{b_1}{b_2}\tau^*}}{1+\left(\frac{b_1}{b_2\omega}\right)^2}\psi_4(r,\gamma^*) - \frac{\frac{b_1}{b_2\omega}}{1+\left(\frac{b_1}{b_2\omega}\right)^2}\left[\left(\frac{b_1}{b_2\omega}\cos\omega\tau^* + \sin\omega\tau^*\right)\psi_7(s,q^*,\Omega) + \left(\frac{b_1}{b_2\omega}\sin\omega\tau^* - \cos\omega\tau^*\right)\psi_8(s,q^*,\Omega)\right]\right\}$$

$$= \frac{1}{b_1\omega\left(1+\frac{x}{a_4}\right)}\left\{1 + \frac{\frac{a_3}{a_2}e^{-\frac{b_1}{b_2}\tau}}{1+\left(\frac{b_1}{b_2\omega}\right)^2} - e^{-\frac{x}{a_4}}\left[\psi_2^{**}(s,q^*) + \frac{\frac{a_3}{a_2}e^{-\frac{b_1}{b_2}\tau^*}}{1+\left(\frac{b_1}{b_2\omega}\right)^2}\psi_4(r,\gamma^*)\right] + \sqrt{A_\theta^2 + B_\theta^2}\sin\left[\omega\tau - \tan^{-1}\left(-\frac{B_\theta}{A_\theta}\right)\right]\right\} \quad (41)$$

Fluid-wall temperature difference

$$\frac{\Delta t_2(x,\tau)}{a_1\Phi} = \frac{\Delta t_2(\tau)}{a_1\Phi} + \frac{1}{b_1\omega}\frac{1+\frac{a_2}{a_3}}{1+\left(\frac{b_1}{b_2\omega}\right)^2}e^{-\frac{x}{a_4}}\left\{\frac{a_3}{a_2}e^{-\frac{b_1}{b_2}\tau^*}\psi_4(r,\gamma^*) + \left(\frac{b_1}{b_2\omega}\sin\omega\tau^* - \cos\omega\tau^*\right)\psi_7(s,q^*,\Omega) - \left(\frac{b_1}{b_2\omega}\cos\omega\tau^* + \sin\omega\tau^*\right)\psi_8(s,q^*,\Omega)\right\}$$

$$= \frac{1}{a_2\omega\left[1+\left(\frac{b_1}{b_2\omega}\right)^2\right]}\left\{e^{-\frac{b_1}{b_2}\tau} + \frac{a_3}{a_2}e^{-\frac{x}{a_4}}e^{-\frac{b_1}{b_2}\tau^*}\psi_4(r,\gamma^*) + \sqrt{A_{\Delta t}^2 + B_{\Delta t}^2}\sin\left[\omega\tau^* - \tan^{-1}\left(-\frac{B_{\Delta t}}{A_{\Delta t}}\right)\right]\right\} \quad (42)$$

Fluid temperature

$$\frac{t_2(x,\tau)}{\frac{a_1 x}{a_4}\Phi} = \frac{t_2(\tau)}{\frac{a_1 x}{a_4}\Phi} + \frac{a_4}{b_1\omega x}e^{-\frac{x}{a_4}}\left\{-\psi_2^{**}(s,q^*) - \frac{e^{-\frac{b_1}{b_2}\tau^*}}{1+\left(\frac{b_1}{b_2\omega}\right)^2}\psi_4(r,\gamma^*) + \frac{1}{1+\left(\frac{b_1}{b_2\omega}\right)^2}\left[\left[\left(\frac{b_1}{b_2\omega}\right)^2 + 1 + \frac{a_2}{a_3}\right]\cos\omega\tau - \frac{a_2}{a_3}\frac{b_1}{b_2\omega}\sin\omega\tau\right]\psi_7(s,q^*,\Omega) + \left[\left[\left(\frac{b_1}{b_2\omega}\right)^2 + 1 + \frac{a_2}{a_3}\right]\sin\omega\tau + \frac{a_2}{a_3}\frac{b_1}{b_2\omega}\cos\omega\tau\right]\psi_8(s,q^*,\Omega)\right]\right\} = \frac{a_4}{b_1\omega x}\left\{1 - \frac{e^{-\frac{b_1}{b_2}\tau}}{1+\left(\frac{b_1}{b_2\omega}\right)^2} + e^{-\frac{x}{a_4}}\left[-\psi_2^{**}(s,q^*) - \frac{e^{-\frac{b_1}{b_2}\tau^*}}{1+\left(\frac{b_1}{b_2\omega}\right)^2}\psi_4(r,\gamma^*)\right] + \sqrt{A_t^2 + B_t^2}\sin\left[\omega\tau - \tan^{-1}\left(-\frac{B_t}{A_t}\right)\right]\right\} \quad (43)$$

where

$$A_\theta = \sin\frac{\omega x}{u} + \frac{a_3/a_2}{1+\left(\frac{b_1}{b_2\omega}\right)^2}\left(\frac{b_1}{b_2\omega}\cos\frac{\omega x}{u} + \sin\frac{\omega x}{u}\right) + \frac{e^{-\frac{x}{a_4}}\left(\frac{b_1}{b_2\omega}\right)}{1+\left(\frac{b_1}{b_2\omega}\right)^2}\left[\left(\frac{b_1}{b_2\omega}\right)\psi_8(s,q^*,\Omega) + \psi_7(s,q^*,\Omega)\right] \quad (44)$$

$$B_s = -\cos\frac{\omega x}{u} + \frac{a_3/a_2}{1+\left(\frac{b_1}{b_2\omega}\right)^2}\left(\frac{b_1}{b_2\omega}\sin\frac{\omega x}{u} - \cos\frac{\omega x}{u}\right) + \frac{e^{-\frac{x}{a_4}}\left(\frac{b_1}{b_2\omega}\right)}{1+\left(\frac{b_1}{b_2\omega}\right)^2}\left[\left(\frac{b_1}{b_2\omega}\right)\psi_7(s, q^*, \Omega) - \psi_8(s, q^*, \Omega)\right] \quad (45)$$

$$A_{\Delta t} = \left(\frac{b_1}{b_2\omega}\right)\cos\frac{\omega x}{u} + \sin\frac{\omega x}{u} + e^{-\frac{x}{a_4}}\left[\left(\frac{b_1}{b_2\omega}\right)\psi_7(s, q^*, \Omega) - \psi_8(s, q^*, \Omega)\right] \quad (46)$$

$$B_{\Delta t} = \left(\frac{b_1}{b_2\omega}\right)\sin\frac{\omega x}{u} - \cos\frac{\omega x}{u} + e^{-\frac{x}{a_4}}\left[-\psi_7(s, q^*, \Omega) + \left(\frac{b_1}{b_2\omega}\right)\psi_8(s, q^*, \Omega)\right] \quad (47)$$

$$A_t = \sin\frac{\omega x}{u} - \frac{1}{1+\left(\frac{b_1}{b_2\omega}\right)^2}\left[\left(\frac{b_1}{b_2\omega}\right)\cos\frac{\omega x}{u} + \sin\frac{\omega x}{u}\right] + \frac{e^{-\frac{x}{a_4}}}{1+\left(\frac{b_1}{b_2\omega}\right)^2}\left\{\left[\left(\frac{b_1}{b_2\omega}\right)^2 + \frac{a_2}{a_3}\right]\psi_8(s, q^*, \Omega) - \frac{a_2}{a_3}\left(\frac{b_1}{b_2\omega}\right)\psi_7(s, q^*, \Omega)\right\} \quad (48)$$

$$B_t = -\cos\frac{\omega x}{u} - \frac{1}{1+\left(\frac{1}{b_2\omega}\right)^2}\left[\left(\frac{b_1}{\omega b_2}\right)\sin\frac{\omega x}{u} - \cos\frac{\omega x}{u}\right] + \frac{e^{-\frac{x}{a_4}}}{1+\left(\frac{b_1}{b_2\omega}\right)^2}\left\{\left[\left(\frac{b_1}{b_2\omega}\right)^2 + \frac{a_2}{a_3}\right]\psi_7(s, q^*, \Omega) + \frac{a_2}{a_3}\left(\frac{b_1}{b_2\omega}\right)\psi_8(s, q^*, \Omega)\right\} \quad (49)$$

$$\psi_2^{**}(s, q^*) = \frac{1}{a_2}\int_0^{\tau^*} e^{-\frac{\xi}{a_3}} I_0\left[2\left(\frac{x\xi}{a_2 a_4}\right)^{1/2}\right] d\xi = \sum_{k=0}^{\infty}\frac{s^k}{(k!)^2}\int_0^{q^*} e^{-z}z^k dz \quad (50)$$

$$\psi_4(r, \gamma^*) = \frac{1}{a_2}\int_0^{\tau^*} e^{\frac{\xi}{a_3}} I_0\left[2\left(\frac{x\xi}{a_2 a_4}\right)^{1/2}\right] d\xi = \frac{a_2}{a_3}\sum_{k=0}^{\infty}\frac{r^k}{(k!)^2}\int_0^{\gamma^*} e^z z^k dz \quad (51)$$

$$\psi_7(s, q^*, \Omega) = \frac{1}{a_2}\int_0^{\tau^*} e^{-\frac{\xi}{a_3}} I_0\left[2\left(\frac{x\xi}{a_2 a_4}\right)^{1/2}\right]\cos\omega\xi d\xi = \sum_{k=0}^{\infty}\frac{s^k}{(k!)^2}\int_0^{q^*} e^{-z}z^k\cos\Omega z dz \quad (52)$$

$$\psi_8(s, q^*, \Omega) = \frac{1}{a_2}\int_0^{\tau^*} e^{-\frac{\xi}{a_3}} I_0\left[2\left(\frac{x\xi}{a_2 a_4}\right)^{1/2}\right]\sin\omega\xi d\xi = \sum_{k=0}^{\infty}\frac{s^k}{(k!)^2}\int_0^{q^*} e^{-z}z^k\sin\Omega z dz \quad (53)$$

The function $\psi_2^{**}(s, q^*)$ has been computed and presented by J. W. Rizika and this function along with $\psi_4(r, \gamma^*)$ is given in reference [2]. $\psi_7(s, q^*, \Omega)$ and $\psi_8(s, q^*, \Omega)$ are new functions introduced in this paper whose numerical reduction was obtained using an IBM 704 digital computer.

DISCUSSION

Joel O. Hougen[7]

This paper describes a large amount of ingenious experimental work and a considerable amount of mathematical theory and labor, and the authors are to be commended on these aspects.

I am, however, somewhat distressed concerning the following points:

No account has been taken of the fact that the fluid within the tube undergoes mixing. Experimental evidence is conclusive that a rather large amount of mixing occurs, and that this partly determines transient behavior.

The authors would have benefited by consulting with people familiar with dynamic analysis work in devising experimental techniques and presenting data. Considerations of the "transient periodic-state response" as a separate phenomenon appears to me to be overspecialized since an adequate transfer function can be used to predict responses to any type of input provided system parameters remain unchanged.

The apparent simplicity of the over-all performance functions also suggest that the mathematical models could likewise be simplified and that empirical determination of significant parameters might be the most practical approach.

I cannot but agree with Stuart W. Churchill when he remarks in *Chemical Engineering Progress*, November, 1960, page 26: "The solution of boundary-value problems, regardless of whether they bear any useful or apparent relationship to the world, is currently in vogue in most engineering meetings and publications; certain types of routine, if difficult, experimental investigations, such as the measurement of eddy diffusivities, are also O.K. On the other hand, papers presenting the results of exploratory experimentation, or new ideas, or new interpretations of old work, are out of fashion, and seem to inspire great irritation among the majority of reviewers."

D. C. Union and P. E. A. Cowley[8]

The authors are to be congratulated upon their continuing excellent investigations into the dynamics of heat exchangers. In the interest of furthering this work, it is suggested that the method of real-time data reduction outlined in the following be used to obtain frequency response measurements in the region of resonance.

The method consists of a cross-correlation (without time shift) of the process response with the process excitation using a simple analog computer.[9] Measurements of frequency response may be made in spite of extremely adverse signal to noise ratios.

The equipment required consists of a 10-amplifier analog computer (such as a Donner Model 3400) and two sine-cosine potentiometers. The analog computer circuit is given in Fig. 18. The sine-cosine pots serve as function generators and multipliers. The input filters shown in the figure are for the purpose of removing drifts from the process response signals.[10]

[7] Systems Engineering Consultant for the Monsanto Chemical Company, St. Louis, Mo.

[8] Engineers, Shell Development Company, Emeryville, Calif.

[9] P. E. A. Cowley, "The Application of an Analog Computer to the Measurement of Process Dynamics," TRANS. ASME, vol. 79, 1957, pp. 823–832.

[10] N. Wiener, "Exploration, Interpolation, and Smoothing of Stationary Time Series," John Wiley & Sons, Inc., New York, N. Y., 1950, p. 11.

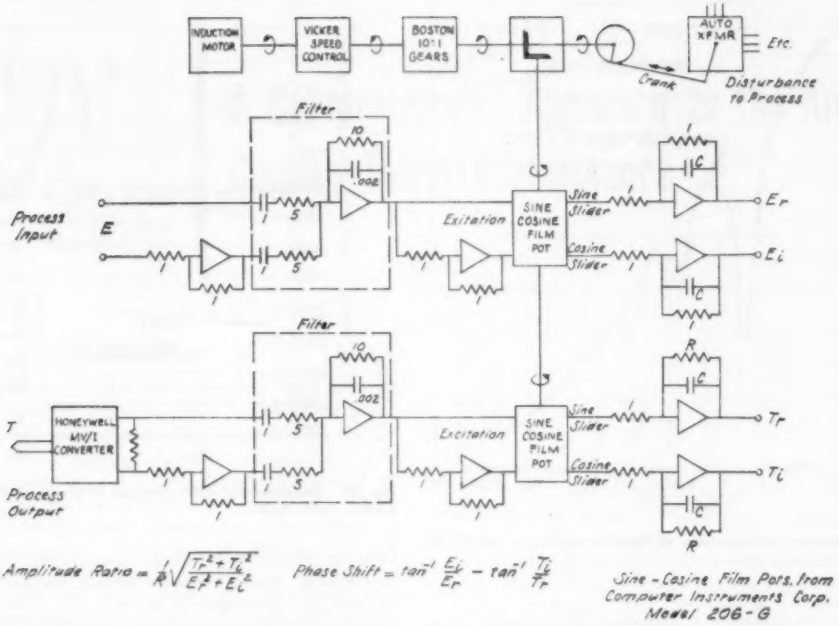

Fig. 18 Analog computer circuit for data reduction

The theoretical resonance phenomenon given by equations (19) and (20) and illustrated in Figs. 15 and 16 has been reported in the literature.[11,12] Partial experimental verification has been given by DeBolt.[13] Further verification by extension of the range of frequency response measurement would be desirable.

Authors' Closure

We wish to express our appreciation for the thoughtful and relevant comments and contributions of Messers Hougen, Union, and Cowley.

In the light of Mr. Hougen's discussion we should restate the objectives of each of the papers in this series of four papers: Namely, to obtain an "exact" analytical solution, continuous in space (x) and time (τ), to a theoretical model closely resembling a physical system and to conduct suitable experimental measurements for verification of this solution and to check its inherent assumptions. Our experimental program never has suffered from lack of emphasis. In fact, it would be fair to say that our theoretical model was derived from an appreciation for and experience with physical systems and not the other way around. We have as little regard for "designing the world" as Mr. Hougen implies he has.

Mr. Hougen's comment in regard to mixing is not clear but we assume he means axial, turbulent mixing. It is true we did ignore this effect as we did not wish to further complicate our results and because we assumed its influence to be small. While for this type of transient process this would be difficult to prove, the axial turbulent mixing may be supposed to be proportional to the root mean square value of the axial turbulent velocity fluctuation, u'_x. With this view the ratio of axial turbulent transport to convective transport may be considered as proportional to u'_x/u. Although this is an imperfect view of the process since simultaneous enthalpy fluctuations ought to be considered in such an evaluation of mixing (for which no data could be found) the magnitude of this ratio reported in the literature does suggest the reasonableness of the model adopted. Laufer's data[14] for the turbulent flow of air at a Reynolds number of 500,000 indicate an average value of u'_x/u to be about 0.05. Our maximum Reynolds number was only 35,000 with much of the data taken at Reynolds numbers in the range of 25,000, or $^1/_{20}$th of that of Laufer, with the (probable) corresponding reduction in u'_x/u. In the final analysis this question of mixing also should be examined with regard to the comparison of our experimental results with the response predicted by the theory. As is evident from Figs. 13 through 17 (and those given in this Closure) this comparison is favorable thus lending justification to the theoretical model. Simultaneous turbulent exchange (mixing) and molecular diffusion in the radial direction are included in the use of the heat-transfer coefficient taken from correlations for turbulent flow. Axial molecular diffusion could be ignored since the Peclet number exceeded 100.[13] Our assumptions in regard to mixing are not unusual in the area of convection analysis, especially that treating steady-state systems. The data available on this question for transient, turbulent flows are meager and we would welcome specific information which could be used to fully evaluate this effect.

The method we have adopted for presenting the frequency response results of our experimental system, Figs. 15, 16, and 17, is not significantly different from that generally employed. Figs. 4, 5, 6, 7, and 8 are simply generalized frequency response presentations which allow a broader interpretation of the system dynamics. The "transient periodic-state" is not presented as a separate phenomenon but as that part of the transient in which

[11] W. C. Cohen and E. F. Johnson, "Dynamic Characteristics of Double-Pipe Heat Exchangers," *Industrial and Engineering Chemistry*, vol. 48, 1956, pp. 1031–1034.

[12] H. Thal-Larsen, "Dynamics of Heat Exchangers and Their Models," *Journal of Basic Engineering*, TRANS. ASME, Series D, vol. 82, 1960, pp. 489–504.

[13] R. R. DeBolt, "Dynamic Characteristics of a Steam-Water Heat Exchanger," MS thesis, University of California, Berkeley, Calif., 1954.

[14] J. Laufer, "The Structure of Turbulence in Fully Developed Pipe Flow," NACA Tech. Report 1174, 1954.

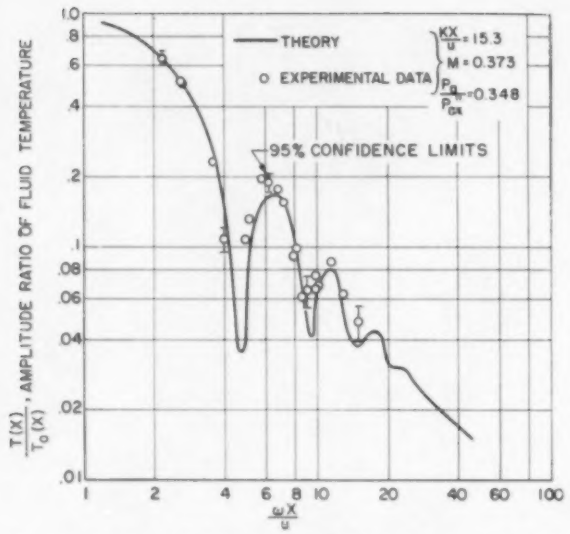

Fig. 19 Experimental determination of fluid temperature amplitude ratio and comparison with theory

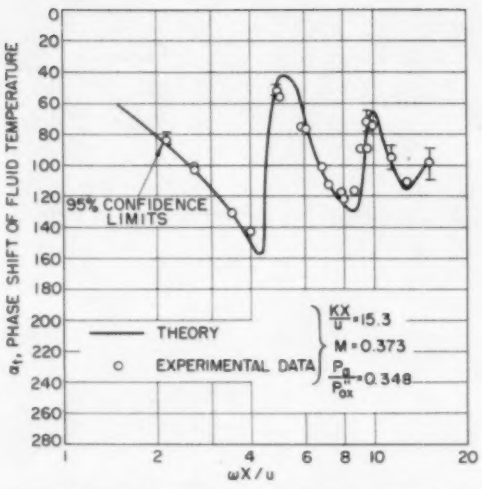

Fig. 20 Experimental determination of phase-shift response and comparison with theory

the initial state of the system still influences the response. This representation is very common in these types of analyses, e.g., Carslaw and Jaeger.[15] Furthermore, there are situations such as start-up operations and the behavior of rocket components, for example, which can only be described by "starting-transient" type of formulations. In such transients as these the response is directly related to the initial state of the system.

An empirical determination of the governing parameters seems fruitless to us if the mathematical model bears a reasonable resemblance to the physical system. Since in the case presented here agreement between theory and experiment is demonstrated and a procedure given for the estimation, a priori, of the system variables (ρ, c_p, Λ, u, h, and so forth) there seems little purpose in abandoning the results of the parameterization presented in the paragraph following equation (14) and in equation (25).

The quotation from Professor Churchill leaves little room for argument and we heartily endorse it. In view of our results, however, we fail to see its relevance in the present discussion. Certainly the use of applied mathematics for the solution of engineering problems pre-dates the present era. An arbitrary code for censorship based on an individual or group concept of "usefulness" hardly seems desirable, workable, or in the best interests of technological progress.

The contribution presented by Messers Union and Cowley is most welcome and we wish to acknowledge their efforts with appreciation. Since the writing of the original paper we have extended the experimental measurements using a different heat exchanger in order to investigate further into the condition of resonance. In other respects the system employed for this was similar to that shown in Fig. 11. This work, which was conducted by Mr. Victor D. Blankenship as a graduate student project in the Department of Mechanical Engineering, involved the construction of a heat exchanger designed to operate near the first point of resonance in Fig. 5 for the case of $M = 0.5$ and $Kx/u = 10$. The final design resulted in a single tube heat exchanger consisting of 50 ft of $^5/_{16}$ BWG-20 aluminum tubing cooled by an internal flow of water ($M = 0.373$ and $Kx/u = 15.3$) and heated by direct passage of d-c current. Outlet fluid temperatures were measured downstream from a mixing baffle using a copper-constantan 30-gage thermocouple connected to a model 1012 Minneapolis-Honeywell "Visicorder" oscillographic recorder. The results for the frequency response in terms of fluid temperature amplitude ratio and phase shift are shown in Figs. 19 and 20. These constitute experimental verification of the condition of resonance and at least two resonance peaks may be observed.

[15] H. S. Carslaw and J. C. Jaeger, "Conduction of Heat in Solids," Oxford University Press, London, England, 1959, pp. 64, 399.

DONALD R. BAKER
The Marley Company,
Kansas City, Mo.
Mem. ASME

HOWARD A. SHRYOCK
The Marley Company,
Kansas City, Mo.

A Comprehensive Approach to the Analysis of Cooling Tower Performance

Introduction

THE GENERALLY accepted concept of cooling tower performance was developed by Merkel [1, 2][1] in 1925. A number of assumptions and approximations were used to simplify the development of the final equation. Accuracy is sacrificed as a result, but modifications may be made in the application to minimize the extent of the resulting errors.

The development of the final equation has been covered in many texts and references. The procedure, therefore, is well known, but it is probably not so well understood. One reason for this is that the authors have taken short cuts and omitted steps to arrive at the final equation. A detailed explanation of the procedure is given in Appendix A.

Merkel Equation

The analysis combines the sensible and latent heat transfer into an over-all process based on enthalpy potential as the driving force. The process is shown schematically in Fig. 1 where each particle of the bulk water in the tower is assumed to be surrounded by an interface to which heat is transferred from the water. This heat is then transferred from the interface to the main air mass by (*a*) a transfer of sensible heat, and (*b*) by the latent heat equivalent of the mass transfer resulting from the evaporation of a portion of the bulk water. The two processes are combined, ingeniously, into a single equation:

$$Ldt = KadV(h' - h) = Gdh \qquad (1)$$

which gives, by integration

$$\frac{KaV}{L} = \int_{t_1}^{t_2} \frac{dt}{h' - h} \qquad (2)$$

$$\frac{KaV}{G} = \int_{h_1}^{h_2} \frac{dh}{h' - h} \qquad (3)$$

This is accomplished, in part, by ignoring any resistance to mass transfer from bulk water to interface; by ignoring the temperature differential between the bulk water and interface; and by ignoring the effect of evaporation. The analysis considers an increment of a cooling tower having one sq ft of plan area, and a cooling volume V containing a sq ft of exposed water surface per cubic foot of volume. The flow rates are L lb of water and G lb of dry air per hour. Two errors are introduced when the evaporation loss is ignored. The water rate varies from L at the water inlet to $(L - L_E)$ at the outlet. The heat balance, (equation (16*a*) and (16*b*) in Appendix A) is not

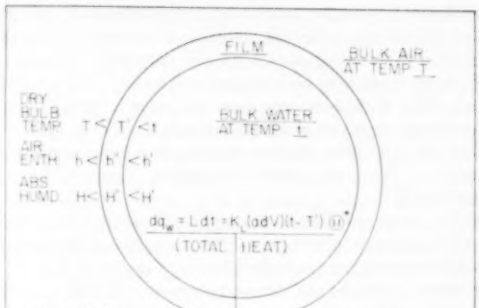
FILM
BULK AIR AT TEMP T
BULK WATER AT TEMP t
DRY BULK TEMP T < T' < t
AIR ENTH h < h' < h'
ABS HUMD H < H' < H'
dq = L dt = K (adV)(t - T') (ii)
(TOTAL HEAT)
(SENSIBLE)
(MASS)
dq = K (adV)(T' - T) (i)
dm = K' (adV)(H' - H) (iii)
r dm = dq = r K' (adV)(H' - H) (iv)

Fig. 1 Heat and mass-transfer relationships between water, interfacial film, and air. Numbers refer to equations in Appendix A.

[1] Numbers in brackets designate References at end of paper.

Contributed by the Heat Transfer Division and presented at the Winter Annual Meeting, New York, N. Y., November 27–December 2, 1960, of THE AMERICAN SOCIETY OF MECHANICAL ENGINEERS. Manuscript received at ASME Headquarters, July 26, 1960. Paper No. 60—WA-85.

Nomenclature

a = area of water interface, sq ft/cu ft
c_{pa} = specific heat of dry air at constant pressure, Btu/lb deg F
c_{pv} = specific heat of water vapor at constant pressure, Btu/lb deg F
G = air flow rate, lb dry air/hr
h = enthalpy of moist air, Btu/lb dry air
h_1 = enthalpy of moist air, entering tower
h_2 = enthalpy of moist air, leaving tower
h' = enthalpy of moist air, at bulk water temperature
h'' = enthalpy of moist air, at interface temperature
H = absolute humidity (humidity ratio) of main air mass, lb vapor/lb dry air
H_1 = absolute humidity of main air mass entering tower
H_2 = absolute humidity of main air mass leaving tower
H'' = absolute humidity at interface
H' = absolute humidity, saturated at water temperature
K = over-all unit conductance, mass transfer between saturated air at mass water temperature and main air stream, lb/hr (sq ft) (lb/lb)
K' = unit conductance, mass transfer, interface to main air stream, lb/hr (sq ft) (lb/lb)
K_g = over-all unit conductance, sensible heat transfer between main water body and main air stream, Btu/(hr)(sq ft) (deg F)

(*Continued on next page*)

$$Gdh = Ldt, \tag{4}$$

but

$$Gdh = Ldt + GdH(t_1 - 32) \tag{5}$$

The assumptions simplify both the development of the final equation and its application in the solution of cooling tower problems. Accuracy is reduced, but the importance of this is a matter of individual needs.

Application of Basic Equation

Equation (2), or (3), conforms to the transfer-unit concept in which a transfer-unit represents the size or extent of the equipment that allows the transfer to come to equilibrium. The integrated value corresponding to a given set of conditions is called the Number of Transfer Units (NTU) which is a measure of the degree-of-difficulty of the problem.

The equation is not self-sufficient so does not lend itself to direct mathematical solution. The usual procedure is to integrate it in connection with the heat balance expressed by equation (4). The basic equation reflects mass and energy balances at any point within a tower, but without regard to the relative motion of the two streams. It is solved by some means of mechanical integration that considers the relative motion involved in counterflow or crossflow cooling, as the case may be.

The counterflow cooling diagram is represented graphically in Fig. 2. Water entering the top of the tower at t_1 is surrounded by an interfacial film that is assumed to be saturated with water vapor at the bulk water temperature. This corresponds to point A on the saturation curve. As the water is cooled to t_2, the film enthalpy follows the saturation curve to point B. Air entering the base of the tower at wet-bulb temperature T_{WB} has an enthalpy corresponding to C' on the saturation curve. The driving force at the base of the tower is represented by the vertical distance BC. Heat removed from the water is added to the air so its enthalpy increases along the straight line CD, having a slope equaling the L/G ratio and terminating at a point vertically below point A. The counterflow integration is explained in detail in Appendix B.

Air and water conditions are constant across any horizontal section of a counterflow tower. Both conditions vary horizontally and vertically in a crossflow tower as shown in Fig. 3. Hot water enters across the OX axis and is cooled as it falls downward. The solid lines show constant water temperatures. Air entering from the left across the OY axis is heated as it moves to the right, and the dotted lines represent constant enthalpies.

Because of the horizontal and vertical variation, the cross section must be divided into unit-volumes having a width dx and a height dy, so that dV in equation (1) is replaced with $dxdy$ and it becomes

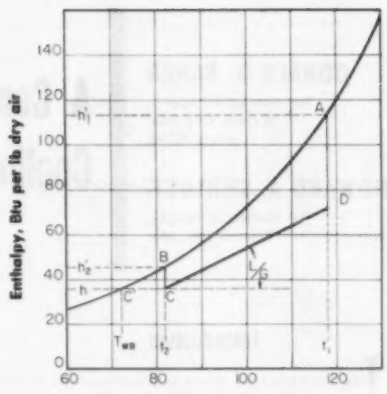

Fig. 2 Counterflow cooling diagram

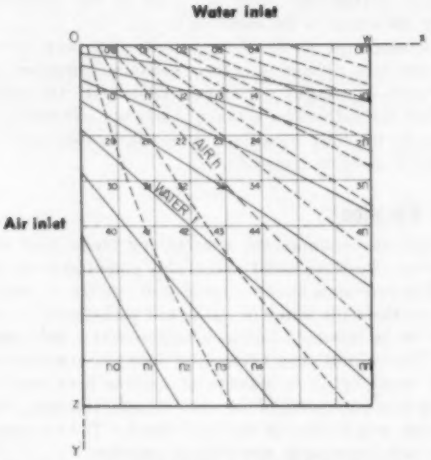

Fig. 3 Water temperature and air enthalpy variation through a crossflow cooling tower

$$Ldtdx = Gdhdy = Kadxdy(h' - h) \tag{6}$$

Cross-sectional shape is taken into account by considering $dx/dy = w/z$ so that $dL/dG = L/G$. The ratio of the over-all flow rates thus apply to the incremental volumes and the integration considers an equal number of horizontal and vertical increments.

Nomenclature

K_G = over-all unit conductance, sensible heat transfer between interface and main air stream, Btu/(hr)(sq ft)(deg F)

K_L = unit conductance, heat transfer, bulk water to interface, Btu/(hr)(sq ft) (deg F)

L = mass water rate, lb/hr

L_E = mass evaporation loss, lb/hr

m = mass-transfer rate, interface to air stream, lb/hr

q_L = rate of latent heat transfer, interface to air stream, Btu/hr

q_S = rate of sensible heat transfer, interface to air stream, Btu/hr

q_W = rate of heat transfer, bulk water to interface, Btu/hr

r = latent heat of evaporation, assumed constant in system

s = unit heat capacity (humid heat) of moist air, Btu/(deg F) (lb dry air)

t = bulk water temperature, deg F

t_1 = bulk water temperature at inlet (hot-water), deg F

t_2 = bulk water temperature at outlet (cold-water), deg F

T = dry-bulb temperature of air stream, deg F

T_0 = datum temperature for water vapor enthalpy, deg F

T' = dry-bulb temperature of air at interface, deg F

T_{WB} = wet-bulb temperature, air stream, deg F

V = active tower volume, cu ft/sq ft plan area

w = width of crossflow filled volume, ft

z = height of filled volume, ft

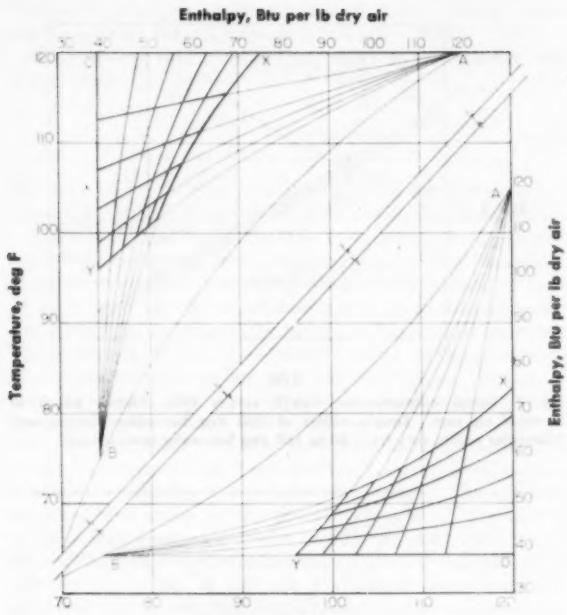

Fig. 4 Crossflow cooling diagram

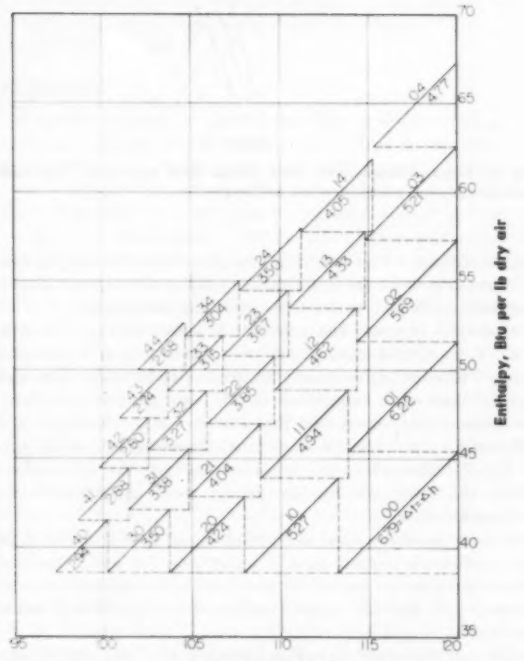

Fig. 5 Plot of crossflow calculations from Table 1(c)

The mechanical integration, explained in detail in the Appendix C, starts with the unit-volume at the top of the air inlet, and successively considers each unit-volume down and across the section. A crossflow cooling diagram, based on 5 increments down and across, is shown in Fig. 4. Fig. 5 shows the same data plotted to a larger scale, with each unit-volume considered as a counterflow tower. The co-ordinates in the lower corner of Fig. 4 correspond to those commonly used in the counterflow diagram, Fig. 2, but the reverse image, in the upper corner, has the water and air inlets positioned to correspond to the cross section in Fig. 3. The inlet water temperature corresponds to OX which intersects the saturation curve at A. The enthalpy of the entering air corresponds to OY which intersects the saturation curve at B.

Logical reasoning will show that water falling through any vertical section will always be moving toward colder air. For a tower of infinite height, the water will be approaching air at the entering wet-bulb temperature as a limit. The water temperature, therefore, approaches B as a limit at infinite height, and follows one of the curves of the family radiating from B. The family of curves has OY as one limit at the air inlet and the saturation curve AB as the other limit for a vertical section at infinite width.

Air moving through any horizontal section is always moving toward hotter water. For a tower of infinite width, air will be approaching water at the hot-water temperature as a limit. The air moving through any horizontal section, therefore, approaches A as a limit, following one of the curves of the family radiating from A. This family of curves varies from OX as one limit at the water inlet to AB for a tower of infinite height.

The counterflow tower diagram considers the area between the saturation curve and the air-operating line CD in Fig. 2. The crossflow diagram considers the saturation curve and the area of overlap of the two families of curves radiating from A and B.

Tower Coefficients

The theoretical calculations reduce a set of performance conditions to a numerical value that serves as a measure of the degree-of-difficulty. The NTU corresponding to a set of hypothetical conditions is called the *required* coefficient and is an evaluation of the problem. The same calculations applied to a set of test conditions is called the *available* coefficient of the tower involved.

Required Coefficient. Cooling towers are specified in terms of hot-water, cold-water, and wet-bulb temperature, and the water rate that will be cooled at these temperatures. The same temperature conditions are considered as variables in the basic equations, but the remaining variable is L/G ratio instead of water rate. The L/G ratio is convertible into water rate when the air rate is known.

A given set of temperature conditions may be achieved by a wide range of L/G ratios. This is shown diagrammatically for the counterflow tower in Fig. 6. The imaginary situation corresponding to an infinite air rate results in $L/G = 0$ which is represented by the horizontal operating line CD_0. This results in the maximum driving force and the minimum *required* coefficient. As the air rate decreases progressively, the L/G ratio increases and the slope of the operating line increases. This decreases the driving force and the *required* coefficient increases. The maximum L/G ratio for a given set of conditions is represented by the operating line that terminates on, or becomes tangent to, the saturation curve as shown by CD_3 in Fig. 6.

Crossflow cooling is more complex and the relationships may be visualized by examining the large-scale plot of the example in Fig. 5. Each incremental volume is plotted as a counterflow tower with the operating lines having a slope corresponding to $L/G = 1$ as used in the example. An increase in air rate, representing a decrease in L/G ratio, will decrease the height of each incremental volume. The over-all effect is more accurately reflected by the families of curves in Fig. 4. Considering the diagram at the bottom, the reduction in the height of the incremental volumes has the effect of reducing the length of OX so the length of OY must be increased to obtain the desired cold-water tem-

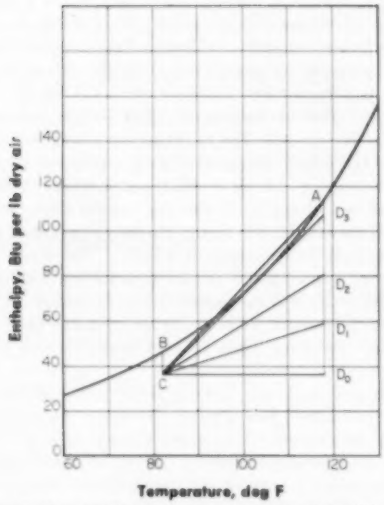

Fig. 6 Counterflow cooling diagrams for constant conditions, variable L/G ratios

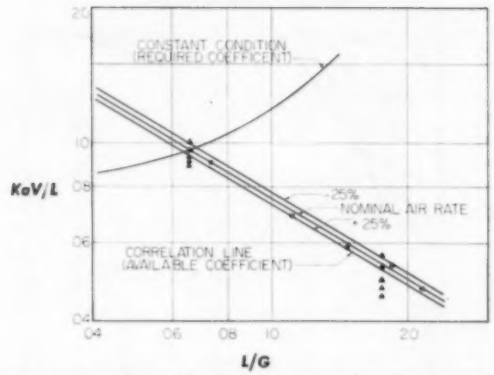

Fig. 7 Tower characteristic, KaV/L versus L/G. Plotted points at nominal air rate. Square points at 100 deg hot-water temperature. Triangular points vary from 80 to 160 deg hot-water temperature.

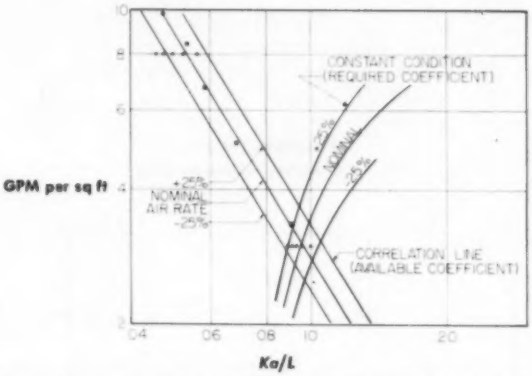

Fig. 8 Tower characteristic, Ka/L versus GPM per sq ft. Correlation lines and plotted points identical to those in Fig. 7.

perature. The area of overlap decreases in height and increases in width until it becomes the straight line OB at an infinite air rate, corresponding to $L/G = 0$. This is identical to the counterflow tower and the two *required* coefficients are the same.

An increase in L/G ratio, corresponding to a decrease in air rate, causes the area of overlap to increase in height and decrease in width. It becomes a tall, narrow wedge extending into the apex at A. The curves never become tangent to AB at an intermediate point so the minimum air rate and maximum L/G ratio occur when the average wet-bulb temperature of the outgoing air equals the hot-water temperature. This corresponds to CA for the counterflow tower in Fig. 6. The minimum air rates will be the same for the two types of tower if the counterflow operating line terminates on the saturation curve. The minimum air rate will be less for the crossflow tower if the operating line of the counterflow tower becomes tangent to the saturation curve at an intermediate point.

A series of calculations may be used to establish a curve relating the *required* coefficient to L/G ratio at various temperature conditions for each type of tower. Both types of tower have the same minimum value and both will increase to infinity at the minimum air rates. The two coefficients increase at different rates so the intermediate values are not the same unless the curves intersect, as sometimes happens.

The intermediate values are different because different methods are used in the calculation. It is misleading to infer, however, that a difference in *required* coefficient indicates that one type of tower faces a greater degree-of-difficulty or needs greater capacity to meet the conditions. If the conditions represent test points for both towers, the same calculations represent the *available* coefficients, and the two values represent identical capacities.

Available Coefficients. The *required* coefficient is the theoretical analysis of a hypothetical situation. The variations with L/G ratio are usually expressed as a series of curves for various temperature conditions. It is possible to design a tower that will operate at any point on any one of these curves. It is also possible within practical limits to find an air rate and water loading at which any cooling tower will operate at any set of temperature conditions.

The point on a *required* coefficient curve at which a tower will operate is called its *available* coefficient for the conditions involved. The *available* coefficient is not a constant but varies with operating conditions. The operating characteristic of a cooling tower is developed from an empirical correlation that shows how the *available* coefficient varies with operating conditions.

One type of tower characteristic is shown in Fig. 7 in which KaV/L is plotted against L/G for parameters of constant air rate. The correlation usually approximates a family of straight, parallel lines when logarithmic co-ordinates are used, but there is no fundamental reason why this should occur. The *required* coefficient for a given set of conditions is superimposed as the curve in Fig. 7. The points of intersection indicate the L/G ratios at which the tower will operate at the given conditions for the various air rates.

A more sensitive type of correlation, as shown in Fig. 8, has the coefficients plotted against water rate (or water loading).[2] The correlation curves are farther apart when this type of correlation is used, and the *required* coefficient must be plotted for each air rate.

The correlation shown in Fig. 7 tends to confine the parameters to a rather narrow band. The characteristic is frequently represented as a single curve that ignores the effect of variations in air velocity. The average curve corresponds approximately to

$$\frac{KaV}{L} \sim \left(\frac{L}{G}\right)^n \qquad (7)$$

[2] The coefficient used is Ka/L which is KaV/L divided by height. The change does not alter the correlation.

The exponent n varies within a range of about -0.35 to -1.1, and the average value is between -0.55 and -0.65.

A correlation that considers variations in air velocity will approximate

$$\frac{KaV}{L} \sim (L)^n(G)^m \tag{8}$$

The value of n is the same as in the foregoing, but m falls within a range of 0.60 and 1.1 and is usually somewhat less than unity.

The *available* coefficient should be independent of temperature levels because these are evaluated in the calculations. Experience shows, however, that fluctuations occur that are related to temperature, the hot-water temperature having the greatest influence. The coefficients decrease as the hot-water temperature increases. The problem is frequently avoided by basing the correlation on tests conducted at a constant hot-water temperature. Errors are then introduced when the correlation is used to predict performance at other temperatures. The extent of the error is reduced by applying an empirical hot-water correction factor [7].

The correlation curves shown in Figs. 7 and 8 represent tests conducted at 100 deg F hot-water temperature. The effect of temperature is shown by the plotted points which represent a series of tests conducted at the nominal air rate (1800 lb per hour per sq ft) but at hot-water temperatures varying from 80 to 160 deg F. Tests at 100 deg F hot-water temperature are plotted as squares and the triangles represent other temperatures. Tests at the other air rates show a similar scatter but are omitted from the plot to avoid confusion.

These fluctuations may be traced to the effect of assumptions made in developing the basic equation. Modifications may be made in the calculations to minimize the effects.

Modifications

The use of equation (4) ignores the effect of evaporation so results in an enthalpy rise that is too low. This is overcome by using equation (5). Evaporation is usually ignored but it causes the water rate to vary from L at the water inlet to $L - L_E$ at the outlet. The ratio of water-to-air varies from L/G at the top to $(L - L_E)/G$ at the bottom. The crossflow calculations start at the top of the tower when the water rate is L and this is reduced as evaporation occurs. The counterflow calculations start at the bottom where the actual water rate is $(L - L_E)$ and this must be gradually increased until it becomes L at the top. A trial-and-error calculation is needed to determine the value of L_E.

Heat Balance Corrections. The effect of these two corrections is shown in Table 1 for counterflow calculations. Example I relates NTU to range when calculated in the usual manner without modification. Example II shows the effect of calculating the enthalpy rise with equation (5), but considers a constant L/G ratio. Example III uses equation (5) and also varies the water rate so that $(L - L_E)/G = 1.1633$ at the bottom and this gradually increases to the design condition of $L/G = 1.20$ at the water inlet.

The use of equation (5) in Example II results in a 4.4 per cent increase in NTU at a 40-degree range. Example III is more accurate because it also varies the water rate, and this increases the NTU by only 1.34 per cent at the 40-degree range. These changes tend to counteract the effect of temperature level on the coefficients.

True Versus Apparent Potential. The theoretical analysis is developed around coefficients that refer to the interface as shown in Fig. 1. The total heat is transferred as sensible heat from the bulk water to the interface

$$Ldt = K_L adV(t - T') \tag{11}$$

Merkel combined the equations covering mass and energy transfer from the film to the bulk air into the single equations based on enthalpy potential

$$Ldt = K'adV(h'' - h) \tag{27}$$

The integrated form of equation (27) provides a means of evaluating the NTU on the basis of the *true* driving force. Simplification results from ignoring the temperature gradient between the bulk water and interface, and considering an apparent potential based on the bulk water temperature. These two potential differences are compared graphically in Fig. 9.

If water at temperature t is assumed to be surrounded by a saturated film at the same temperature, it corresponds to point B and enthalpy h'. The film will actually be at the lower temperature T' represented by B' and having an enthalpy h''. The main air stream at enthalpy h corresponds to point C. The apparent potential difference is $(h' - h)$ while the true difference is $(h'' - h)$.

Equating equations (11) and (27), we get

$$\frac{h'' - h}{T' - t} = -\frac{K_L}{K'} \tag{9}$$

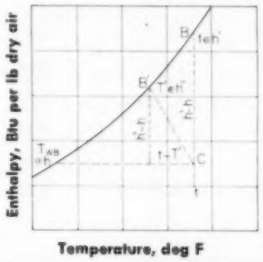

Fig. 9 True versus apparent potential difference

The slope of $B'C$, Fig. 9, is $(h'' - h)/(T' - t)$ which, by equation (9), equals the ratio of the two coefficients. If the coefficients are constant, the slope will be constant. The *true* driving force is always lower than the *apparent*, but the extent of the reduction depends on the position of C with respect to the saturation curve.

It is almost an insurmountable task to determine the slope from a measurement of the temperature gradient. The objective, from the standpoint of cooling tower design, is not to find the slope but to minimize the effects of temperature variations on the coefficient. This objective is attained by finding the slope that minimizes the fluctuations.

Offset Ratio for Crossflow Cooling. This has been investigated in connection with crossflow towers and the counterflow study is in progress. The crossflow integration had been programmed for an electronic digital computer. A supplemental modifying program was prepared which uses equation (5) to calculate enthalpy rise, and varies the L/G ratio as a result of evaporation loss. A second modifying program was prepared which uses an offset ratio to calculate the true driving force.

The fluctuations being considered are relatively small so are easily masked by experimental error. The first step in the investigation was to obtain extremely accurate test data for analysis.

Tests were run on a 12-ft high crossflow cell containing a standard type of industrial filling. A second series of tests were run on a 3-ft high cell containing a close-packed type of filling. Special care was taken to obtain maximum accuracy and crossplots were made of all data. A few points that did not fall on smooth curves were rejected and not used in the calculations.

Range	Example I No Modification N.T.U.	Example II Eq.(16a), Constant L/G N.T.U.	Example III Eq.(16a), Variable L/G N.T.U.	L/G
1	0.1048	0.1051	0.1046	1.1633
2	0.2106	0.2115	0.2105	1.1641
3	0.3171	0.3192	0.3170	1.1649
4	0.4246	0.4279	0.4245	1.1658
5	0.5317	0.5372	0.5317	1.1666
10	1.0531	1.0762	1.0564	1.1710
15	1.5294	1.5770	1.5387	1.1755
20	1.9350	2.0080	1.9523	1.1802
25	2.2631	2.3577	2.2886	1.1850
30	2.5203	2.6315	2.5533	1.1899
35	2.7244	2.8422	2.7581	1.1949
40	2.8775	3.0037	2.9159	1.2000

Table 1(a) Effect of modifications on counterflow coefficients. Using equation (16a) for heat balance, and varying L/G ratio.

1 water Temp. t	2 Enthalpy at t h'	3 Enthalpy of air h	4 Enthalpy difference (h'-h)	5 $\frac{1}{(h'-h)}$	6 $\frac{1}{(h'-h)_{mean}}$	7 $\frac{dt}{(h'-h)}$	8 $\int \frac{dt}{(h'-h)}$	9 Range °F
80	43.69	34.09	9.60	.1043	.1049	.1049	.1049	1
81	44.78	35.29	9.49	.1055	.1059	.1059	.2108	2
82	45.90	36.49	9.41	.1067	.1067	.1067	.3175	3
83	47.04	37.69	9.35	.1070	.1071	.1071	.4246	4
84	48.20	38.89	9.33	.1072	.1072	.1072	.5318	5
85	49.43	40.09	9.34	.1071	.1043	.5215	1.0533	10
90	55.93	46.09	9.84	.1016	.0996	.4980	1.5513	15
95	63.32	52.09	10.23	.0977	.0856	.4280	1.9793	20
100	71.73	58.09	13.64	.0734	.0657	.3285	2.3078	25
105	81.34	64.09	17.25	.0580				

Table 1(b) Example of counterflow calculation of NTU for 80 deg F cold-water temperature, 70 deg F entering wet-bulb temperature, and L/G 1.20

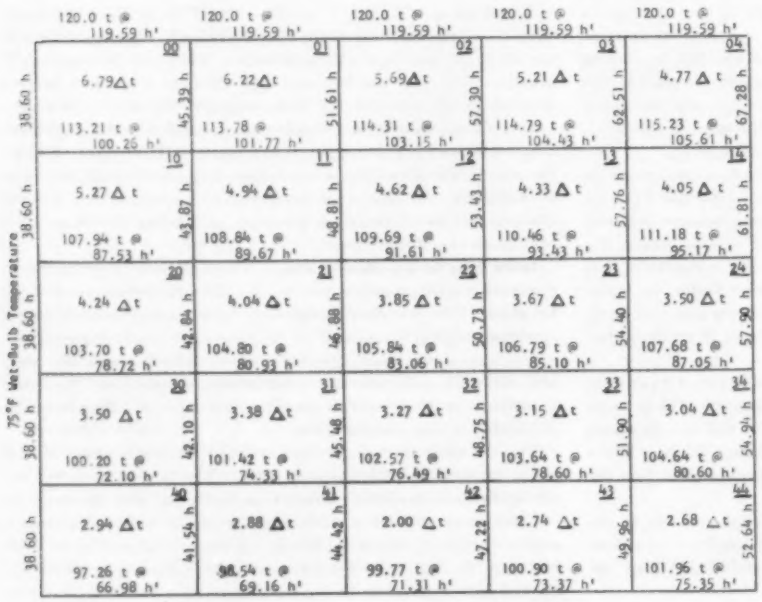

Table 1(c) Example of crossflow calculations for 120 deg F hot-water temperature, 75 deg F entering wet-bulb temperature and L/G = 1.0

The various modifications were applied to the calculation on a trial-and-error basis. The general procedure was to apply modifications to a group of points and use the results as a guide when calculating the next set. This eliminated the need of applying all combinations to all points. The results are shown in Tables 2 and 3.

The offset ratio is handled in the program by assuming a temperature offset, calculating the resulting potential difference, and then checking the accuracy of the assumption. This logic makes it easier to consider the reciprocal of equation (9) so the offset ratios shown in Table 2 and 3 refer to

$$\frac{T' - t}{h'' - h} = -\frac{K'}{K_L} \tag{10}$$

The fluctuations were reduced to a minimum for both test towers by basing the heat balance on equation (5), varying the L/G ratio to account for evaporation, and by using an offset slope of -0.09 as defined by equation (10). It will be noted that, in each case, a greater offset is needed for the lower L/G ratios, and a smaller offset for the higher ratios. The three modifications will not completely overcome the trends although the final fluctuations are insignificant within the normal range of operating conditions.

The first calculations were based on the properties of air at the standard barometric pressure of 29.92 in. Hg which is common practice. The tests were conducted at a slightly lower atmospheric pressure so the psychrometric subroutines were altered to reflect conditions at the existing pressure. The last two columns in Table 3 show that nothing was gained by this change.

Conclusions

The difficulties encountered in predicting cooling tower performance are directly related to the precision that is required. There is no general agreement on what constitutes an acceptable degree of accuracy. The users are reluctant to allow a tolerance of $^1/_2$ deg in approach when acceptance tests are involved. Tower capacity is more accurately expressed in terms of water rate for a given set of conditions. This capacity is approximately propor-

Table 2 Effect of modifications on crossflow coefficients, large cell. Considering offset ratio, barometric pressure, and evaporation which includes equation (16a) and variable L/G ratio.

Conditions				No Modification		.15 Offset		.10 Offset		.0725 Offset		.09 Offset With Evap. Loss		
H.W.	C.W.	W.B.	L/G	N.T.U.	% Dev. From Aver.	N.T.U.	% Dev. From Aver.	N.T.U.	% Dev.	N.T.U.	% Dev.	N.T.U.	N.T.U. @ Aver. L/G	% Dev.
69.2	62.3	47.7	1.088	.9533	+ 2.64	1.0630	- 2.75	1.0268	- 1.18	1.0063	- .18	1.049	1.033	- 1.1
85.1	71.7	47.7	1.09	.9292	+ 0.04	1.0702	- 2.10	1.0238	- 1.47	.9974	- 1.06	1.032	1.029	- 1.5
99.6	78.5	46.6	1.09	.9398	+ 1.12	1.1163	+ 2.12	1.0584	+ 1.85	1.0251	+ 1.69	1.0614	1.058	+ 1.3
119.1	86.8	46.8	1.12	.8919	- 4.04	1.1228	+ 2.72	1.0476	+ 0.82	1.0037	- 0.44	1.049	1.059	+ 1.3
				Max.	6.70	Max. %	5.5	Max. %	3.3	Max. %	2.75	Max. %		2.8
78.9	71.4	47.5	1.96									0.763	0.756	- 0.4
90.1	79.1	48.9	1.99									0.766	0.764	+ 0.6
102.0	86.8	51.2	2.04									0.761	0.768	+ 1.2
108.5	89.8	46.1	2.04									0.742	0.749	- 1.3
												Max. %		2.5
88.0	71.6	44.3	0.954									1.073	1.075	- 0.4
99.1	77.3	47.4	0.928									1.099	1.087	+ 0.6
111.6	84.6	54.6	0.964									1.071	1.078	- 0.2
												Max. %		1.0

Table 3 Effect of modifications on crossflow coefficients, small cell. Considering offset ratio and evaporation which includes equation (16a) and variable L/G ratio.

CONDITIONS				.07 OFFSET		.07 OFFSET WITH EVAP.		.15 OFFSET WITH EVAP.		.10 OFFSET WITH EVAP.		.09 OFFSET WITH EVAP.		.09 OFFSET WITH EVAP. @ 29.14" Hg.	
H.W.	C.W.	W.B.	L/G	N.T.U.	% Dev.	N.T.U.	% Dev.	N.T.U.	% Dev.	N.T.U.	% Dev.	N.T.U.	% Dev.	N.T.U.	% Dev.
70.4	66.9	55.2	1.74	.6053	+3.10	.6143	+2.64	.6533	-4.14	.6293	+.016	.6243	+ .99	.6241	+ .68
100.7	87.5	55.7	1.70	.5851	- .34										
119.5	97.8	56.0	1.765							.6258	-.54	.6146	-.58		
150.3	111.1	56.0 62.1	1.76	.5709	-2.76	.5826	-2.64	.7097	+4.14	.6326	+.54	.6157	-.41	.6156	-.68
				Max.%	5.86		5.28		8.28		1.08		1.57		1.36
79.7	69.8	57.2	.654	1.0697	+ .86					1.1062	-.87	1.0968	-.24	1.0965	-.35
120.4	86.1	58.1	.656							1.1138	-.20	1.0908	-.21		
150.5	93.1	58.9	.659	1.0515	-.86					1.1279	+1.07	1.1044	+.45	1.1042	+.35
				Max.%	1.72						1.94		.69		.70

tional to variations in approach when other conditions are constant, so $^1/_2$ deg corresponds to a difference of 10 per cent in capacity for a 5-deg approach. This provides an indication of what constitutes a reasonable maximum limit of acceptable tolerance.

The existence of the need for a means of predicting performance may be taken as an indication that the usual procedures are not giving satisfactory results. The problem may be due to inexperience or to inadequate test procedures that do not provide reliable test results, or to errors introduced by the method of calculation. All of these items are involved and an improvement in one will provide a means of improving the others.

The needs of the user and manufacturer are not the same, and the difficulties encountered will vary with the type of problem involved. These include comparing test results to guarantee, using test results to predict performance at other conditions, comparing capacities when bids are analyzed, and developing the rating table for a new cooling tower.

This paper deals with the errors in the mathematical analysis and describes the means of minimizing them. Each improvement makes the analysis more difficult. No attempt has been made to evaluate this or to consider the effect of each source of error on the over-all accuracy.

We are faced with the unfortunate fact that it is difficult to attain an accuracy that is within our maximum limits of acceptability although this does not represent a high degree of precision. Care is needed to obtain test data having an accuracy of $^1/_2$ degree or 10 per cent in capacity. The method of analysis may have inherent errors that exceed these limits. The general failure to obtain satisfactory results may be due, to a large extent, to the failure to exert sufficient effort to solve a problem that is inherently difficult. It may be that a justifiable effort will not yield an answer of acceptable accuracy.

The object of this paper is to describe methods that will give a satisfactory answer, without regard to the effort needed. A method that does not provide an acceptable degree of accuracy is all but worthless, regardless of how easy it may be. The limits of acceptability and the effort to be expended will be up to the individual, and each will obviously seek the easiest means of attaining the desired end.

APPENDIX A

Development of Basic Equations

Heat is removed from the water by a transfer of sensible heat due to a difference in temperature levels, and by the latent heat equivalent of the mass transfer resulting from the evaporation of a portion of the circulating water. Merkel combined these into a single process based on enthalpy potential differences as the driving force.

The analysis [3] considers an increment of a cooling tower having one sq ft of plan area, and a cooling volume V, containing a sq ft of exposed water surface per cubic foot of volume. Flowing through the tower are L lb of water and G lb of dry air per hour.

Transfer Rate Equations. The air at any point has a dry bulb temperature T, an absolute humidity (lb water vapor per lb dry air) H, and a corresponding enthalpy h. The water, having a bulk temperature t, Fig. 1, is surrounded by an interfacial film having a temperature T'. The temperature gradients are such that $T < T' < t$.

The specific heat of water is assumed to be unity and a constant, so the symbol will be omitted from the equations for simplicity. The rate of heat transfer from the bulk water to the interface is:

$$dq_W = Ldt = K_L a dV(t - T') \tag{11}$$

A portion of this heat is transferred as sensible heat from the interface of the main air stream. This rate is:

$$dq_S = K_G a dV(T' - T) \tag{12}$$

The interfacial air film is assumed to be saturated with water vapor at temperature T', having a corresponding absolute humidity H'. The procedure is to ignore any resistance to mass transfer from the water to the interface, but to consider the mass transfer of vapor from the film to the air, as

$$dm = K' a dV(H' - H) \tag{13}$$

Considering the latent heat of evaporation as a constant, r, the mass rate in equation (13) is converted to heat rate by multiplying by r,

$$r dm = dq_L = rK' a dV(H' - H) \tag{14}$$

Mass and Energy Balances. Under steady state, the rate of mass leaving the water by evaporation equals the rate of humidity increase of the air, so

$$dm = GdH \tag{15}$$

The heat lost by the water equals the heat gained by the air. The usual practice is to ignore the slight reduction in L due to evaporation, in which case

$$Gdh = Ldt \tag{16a}$$[1]

The enthalpy of moist air is defined as

$$h = c_{pa}(T - T_0) + H[r + c_{p_v}(T - T_0)]$$

Both H and T are variables, so the differential is

$$dh = c_{pa} dT + Hc_{p_v} dT + [r + c_{p_v}(T - T_0)]dH$$

or

$$dh = (c_{pa} + Hc_{p_v})dT + [r + c_{p_v}(T - T_0)]dH$$

Humid heat is defined as

$$s = c_{pa} + Hc_{p_v}$$

so

$$dh = sdT + [r + c_{p_v}(T - T_0)]dH \tag{17}$$

in which the first term on the right represents *sensible* and the second *latent* heat.

Equating dh in equation (16a) and (17)

$$Ldt = GsdT + [r + c_{p_v}(T - T_0)]GdH \tag{18}$$

Fundamental Equations. The sensible heat relationship $dq_S = GsdT$ is used to convert equation (12) to

$$dq_S = K_G a dV(T' - T) = GsdT \tag{19}$$

---

[1] A more rigorous analysis considers evaporation loss, so L lb enters but $(L - L_E)$ lb of water leaves the tower, and the heat balance is

$$G(h_2 - h_1) = L(t_1 - 32) - (L - L_E)(t_3 - 32) \tag{a}$$

$$G(h_2 - h_1) = L(t_1 - t_2) + L_E(t_2 - 32) \tag{b}$$

since

$$L_E = G(H_2 - H_1)$$

$$G(h_2 - h_1) = L(t_1 - t_2) + G(H_2 - H_1)(t_2 - 32) \tag{c}$$

Expressed as a differential equation,

$$Gdh = Ldt + GdH(t_2 - 32) \tag{16b}$$

The last term in equation (16b) represents the heat required to raise the liquid water evaporated from the base (32 deg F) to the cold-water temperature. An enthalpy rise calculated by equation (16a) is low by an amount corresponding to this heat of the liquid.

The mass-transfer relationship $dm = GdH$ is used to convert equation (13) to

$$dm = K'adV(H'' - H) = GdH \tag{20}$$

Lewis [4] found that, for a mixture of air and water vapor

$$\frac{K_G}{K's} \cong 1 \tag{21}$$

The ratio differs for other gases and vapors, but it fortuitously approaches unity for moist air. The relationship expressed in equation (21), incidentally, explains why the wet-bulb approximates the temperature of adiabatic saturation for an *air-water* mixture.

Substituting $K_G = K's$ in equation (19)

$$dq_s = K'sadV(T' - T) = GsdT \tag{22}$$

Substituting equation (22) for $GsdT$ and equation (20) for GdH in equation (18)

$$Ldt = K'sadV(T' - T) + [r + c_{p_v}(T - T_0)]K'adV(H'' - H)$$

collecting

$$Ldt = K'adV\{s(T' - T) + [r + c_{p_v}(T - T_0)](H'' - H)\} \tag{23}$$

From the enthalpy equation, we get for the air stream

$$h = c_{p_a}(T - T_0) + H[r + c_{p_v}(T - T_0)]$$

$$h = c_{p_a}T - c_{p_a}T_0 + Hr + Hc_{p_v}T - Hc_{p_v}T_0$$

$$h = c_{p_a}T + Hc_{p_v}T - c_{p_a}T_0 + H(r - c_{p_v}T_0)$$

since

$$s = c_{p_a} + Hc_{p_v}$$

$$h = sT - c_{p_a}T_0 + H(r - c_{p_v}T_0) \tag{24}$$

Similarly, the enthalpy of the interface is

$$h'' = sT' - c_{p_a}T_0 + H''(r - c_{p_v}T_0) \tag{25}$$

Solving equations (24) and (25) for T and T', substituting the results in equation (23) and collecting

$$Ldt = K'adV(h'' - h) + c_{p_v}T(H'' - H) \tag{26}$$

The second term on the right is relatively small so, following the example of Merkel, it is customarily dropped. Doing this and equating to equation (16*a*)

$$Ldt = K'adV(h'' - h) = Gdh \tag{27}$$

This final equation relates the air stream to the interfacial film, the conditions of which are indeterminate for all practical purposes. This difficulty is overcome by a final approximation in which T' is assumed to equal T. The coefficients K_G and K' are then replaced by *over-all* coefficients K_g and K, respectively. Assuming the Lewis relationship still applies

$$\frac{K_g}{Ks} \cong 1 \tag{28}$$

There is no fundamental reason why this should be so, and Koch [5] reports the ratio is more nearly equal to 0.9 but common practice assumes it to apply. Using equation (28) instead of equation (21), the development from equation (22) on yields

$$Ldt = KadV(h' - h) = Gdh \tag{29}$$

Integrating

$$\frac{KaV}{L} = \int_{t_1}^{t_2} \frac{dt}{h' - h} \tag{30a}$$[4]

or

$$\frac{KaV}{G} = \int_{h_1}^{h_2} \frac{dh}{h' - h} \tag{30b}$$

Equations (30*a*) and (30*b*) are convertible into one another and are two forms of the basic equation.

APPENDIX B

Counterflow Integration [4, 6]

All vertical sections through a counterflow tower are the same, so the counterflow integration considers such a section having 1 sq ft of plan area in which the water is cooled from t_1 to t_2. This converts L and G to lb per hr per sq ft and V to volume per sq ft of plan area. The cooling diagram may be represented graphically as shown in Fig. 2. The diagram is built around the saturation curve relating temperature to the enthalpy of moist air.

Water entering the top of the tower at a temperature t_1, is surrounded by an interfacial film which equation (30*a*) assumes to be saturated at the bulk water temperature. This film corresponds to point A at the hot-water condition having an enthalpy h_1'. As the water is cooled, the film follows the saturation curve to point B, corresponding to the cold-water temperature t_2 and having an enthalpy h_2'.

Air entering at wet-bulb temperature T_{WB} has an enthalpy h, corresponding to C' on the saturation curve. The potential difference at the base of the tower is $h_2' - h_1$, represented by the vertical distance BC. Heat removed from the water is added to the air, and from equation (16*a*), $dh = L/G\ dt$. Thus, the air enthalpy follows a straight line from C, at a slope corresponding to the L/G ratio, and terminates at a point D which is vertically below A.

The driving force at any point in the tower is represented by the vertical distance between AB and CD. The mechanical integration is accomplished by a method of quadrature in which the area $ABCD$ is divided into a series of incremental areas corresponding to successive increments of temperature change.

Counterflow calculations start at the bottom of the tower since that is the only point where both air and water conditions are stipulated. Considering an example in which the cold-water temperature is 80 deg F, air enters at 70 deg F wet-bulb, and the L/G ratio is 1.2, the successive steps are shown in Table 1(*b*).

The cold-water temperature is entered at the top of column 1, and successive temperatures are entered below. The example arbitrarily uses 1 deg F increments to 85 and 5 deg F increments, thereafter. The enthalpy of saturated air for each temperature in column 1 is obtained from the psychrometric tables and entered in column 2.

Entering air at 70 deg F wet-bulb has an enthalpy of 34.09 Btu/lb which is entered at the top of column 3. The relationship $dh = L/G\ dt$ is used to calculate successive enthalpies in column 3. The potential difference for each increment is column 2 minus column 3 which is entered in column 4. The driving force appears in the denominator of equation (30*a*) so the reciprocal of column 4 is entered in column 5. The entering and leaving values from column 5 are averaged for each temperature increment and entered in column 6. Multiplying this average by the cor-

[4] If the last term in equation (26) had not been dropped, the basic equation would be

$$\frac{KaV}{L} = \int_{t_1}^{t_2} \left[\frac{dt}{h' - h} - \frac{c_{p_v}T(H' - H)}{L(h' - h)} \right]$$

The last term is exceedingly small, being the quotient of a relatively small numerator and a much larger denominator.

responding temperature change gives the NTU for the increment which is entered in column 7. The summation of column 7, shown in column 8, is the integrated NTU for the cooling range shown in column 9.

The variations of NTU in column 7 serve as a measure of the relative size of the increments of temperature change. This relationship may be used to determine temperature distribution with respect to tower height. The procedure used to calculate Table 1 considers arbitrary increments of temperature change and calculates volume per sq ft of plan area, so V is numerically equal to height. An alternate procedure is to select arbitrary increments of NTU for column 7 (representing increments of height) and calculate the corresponding temperature changes. That is the basis of the crossflow calculation where the double integration must consider horizontal and vertical increments of space.

APPENDIX C

Crossflow Integration [7]

Fig. 3 is a cross section of a crossflow tower having w width and z height. Hot water enters across the OX axis and is cooled as it falls downward. The solid lines show constant water temperature conditions across the section. Air entering from the left across the OY axis is heated as it moves to the right. The dotted lines show constant air enthalpies across the section.

Because of the horizontal and vertical variations, the cross section must be divided into unit-volumes having a width dx and a height dy so that dV in equation (29) is replaced with $dxdy$ and the equation becomes

$$Ldtdx = Gdhdy = Kadxdy(h' - h) \tag{31}$$

The double integration may consider a series of horizontal sections between 0 and the height z giving

$$\int_0^z \frac{Kady}{L}\Bigg]_{x=\text{const}} = \int_{t_1}^{t_2} \frac{dt}{h' - h}\Bigg]_{x=\text{const}} \tag{32a}$$

Alternately, a series of vertical sections between 0 and width w is

$$\int_0^w \frac{Kadx}{G}\Bigg]_{y=\text{const}} = \int_{h_1}^{h_2} \frac{dh}{h' - h}\Bigg]_{y=\text{const}} \tag{32b}$$

The L/G ratio refers to over-all flow rates so does not apply to the ratio at a point within a tower unless the $w = z$. The ratio of the number of vertical-to-horizontal steps will equal the ratio of height-to-width if $dx = dy$. The calculations are simplified by considering incremental volumes that are geometrically similar in shape to the tower cross section. Then, $dx/dy = w/z$ and $dL/dG = L/G$, so the over-all L/G ratio applies to each incremental volume, and the steps down and across are equal in number regardless of shape.

The mean driving force in counterflow cooling is calculated by averaging the reciprocals of the entering and leaving potential differences. That is mathematically correct except for the small error introduced by assuming a straight-line relationship exists between the two conditions. A comparable means of calculating the mean driving force for crossflow cooling is not so easily achieved because each unit-volume is as complex as the tower as a whole.

The simplest procedure is to assume that the entering potential difference exists throughout the unit-volume, but this driving force is always greater than the true average. An alternate is to average the reciprocals of the entering and leaving conditions. This corresponds to parallel flow so the average will be too low. The true mean value is between these two methods. Averaging the potential differences instead of their reciprocals gives a value smaller than the former, but greater than the latter and more closely approximates the true value. That is the recommended method which is used in the following example.

Table 1c shows the results of the crossflow calculations when water enters from the top at a uniform temperature of 120 deg F and air enters from the left at a uniform wet-bulb temperature of 75 deg F. The over-all L/G ratio is 1.0 and each incremental volume represents 0.1 Transfer-Units.

The crossflow calculations must start at the top of the air inlet since this is the only unit-volume for which both entering air and water conditions are known. The calculations for this first unit-volume are:

1 Inlet conditions

Water at 120 deg F	$119.59\ h_1'$
Air at 75 deg F wet-bulb	$38.60\ h_1$
	$80.99\ (h_1' - h_1)$ in

2 Mean driving force will be less. Assume $67.90\ (h' - h)_{avg}$ corresponding to $dt = 6.79$ deg F for 0.1 NTU. Since $L/G = 1$, $dt = dh$.

3 Outlet conditions

120.0 deg − 6.79 deg = 113.21 deg F	$100.26\ h_2'$
$38.60 + 6.79 =$	$45.39\ h_2$
	$54.87\ (h_2' - h_2)$ out

4 Checking, $\dfrac{80.99 + 54.87}{2} \times 0.1 = 6.79\ dt$

This calculation gives the temperature of the water entering the next lower unit-volume and the enthalpy of the air entering the unit-volume to the right. The calculations proceed down and across as shown in Table 1(c). Averaging 2 steps down and across corresponds to 0.2 NTU, averaging 3 down and across corresponds to 0.3 NTU, and so on.

These relationships are shown in the crossflow diagram in Fig. 4, and Fig. 5 shows the same data from Table 1(c) plotted to a larger scale. The crossflow diagram is also built around the saturation curve AB and consists of two families of curves representing equations (32a) and (32b). The co-ordinates in the lower corner of Fig. 4 correspond to those used in the counterflow diagram, Fig. 2, but the reverse image, in the upper corner, has the water and air inlets positioned to correspond to the cross section in Fig. 3. Equation (32a) is the partial integral through successive vertical sections that relates water temperature to height. The inlet water temperature corresponds to OX which intersects the saturation curve at A. The enthalpy of the entering air corresponds to OY which intersects the saturation curve at B.

The water is cooled as it falls through any vertical section, its temperature following one of the family of curves representing equation (32a) that radiate from B. Inspection of the data in Table 1(c) will show the falling water is always moving toward cooler air that approaches the entering wet-bulb temperature as a limit. The curves tend to coincide with OY as one limit at the air inlet and with the saturation curve AB as the other limit for a tower of infinite height.

The air enthalpy increases as it moves across any horizontal section, the enthalpy following one of the family of curves representing equation (32b) that radiate from A. As shown in Table 1(c), the air is always moving toward warmer water that tends to approach the entering water temperature as a limit. These curves tend to coincide with OX as one limit at the water inlet, and with the saturation curve AB as the other limit for a tower of infinite width.

The water in all parts of a tower tends to approach the entering wet-bulb temperature as a limit at point B. The wet-bulb temperature of the air in all parts of the tower tends to approach the hot-water temperature at point A. The single operating line CD of the counterflow diagram in Fig. 2 is replaced in the crossflow diagram by a zone represented by the area intersected by the two families of curves.

References

1 F. Merkel, "Verdunstungskuehlung," VDI Forschungsarbeiten No. 275, Berlin, 1925.

2 H. B. Nottage, "Merkel's Cooling Diagram as a Performance Correlation for Air-Water Evaporative Cooling Systems," *ASHVE Transactions*, vol. 47, 1941, p. 429.

3 ASRE Data Book, Basic vol., 6th edition, 1949, p. 361.

4 W. H. Walker, W. K. Lewis, W. H. Adams, and E. R. Gilliland, "Principles of Chemical Engineering," 3rd edition, McGraw-Hill Book Company, Inc., New York, N. Y., 1937.

5 J. Koch, "Unterschung and Berechnung von Kuehlwerken," VDI Forschungsheft No. 404, Berlin, 1940.

6 J. Lichtenstein, "Performance and Selection of Mechanical-Draft Cooling Towers," TRANS. ASME, vol. 65, 1943, p. 779.

7 D. R. Baker and L. T. Mart, "Cooling Tower Characteristics as Determined by the Unit-Volume Coefficient," *Refrigerating Engineering*, 1952.

8 H. S. Mickley, "Design of Forced Draft Air Conditioning Equipment," *Chemical Engineering Progress*, vol. 45, 1949, p. 739.

DISCUSSION

J. Lichtenstein[5]

This paper reviews the theory and resulting equations currently employed in the calculation and analysis of cooling towers. It points out that the theory neglects certain physical factors, particularly the quantity of water evaporated during the cooling process and the resistance to heat flow from the water to the surrounding saturated air film.

Taking these two factors into account results in equations and methods which become cumbersome and which mask the simple relationships previously established.

It is, of course, legitimate for a theory which attempts to describe a physical phenomena to suppress those factors whose effect on the over-all results is small enough as to be within the degree of accuracy of the available testing procedures. Absolute exactitude is sacrificed for the sake of the clarity with which the effects of the essential factors on the phenomena are described.

May I ask the authors, therefore, whether the corrections introduced in their paper would really show up in the results obtained in testing a cooling tower? Their sample calculations do not seem to indicate that. If I remember correctly, the best accuracy obtainable between heat balances on the air and water side in the testing of cooling towers is between 5 and 6 per cent.

Since the main effort of the authors is to obtain a better correlation between theoretical prediction and actual performance of cooling towers, I wonder whether other factors not considered in this paper may not play a more important role. The cooling tower theory, as the authors point out, is based on the performance of a unit tower with air and water quantities well defined. Its application to an actual tower assumes that all unit towers are working alike and in parallel. This of course, is not the case. It depends on the design how closely the real tower approaches the idealized tower of equal units. In the actual tower each unit tower works with a different inlet and exit water temperature and with a different (L/G) ratio.

If over-all average water inlet and exit temperature obtained in a test are used, then the theory describes the performance of some average unit tower whose location and L/G ratio are unknown.

I wonder whether the introduction of a factor to correct for this situation might not be more effective in aligning theory and practice. In other words, a factor which would measure the degree of approach to the idealized tower on which the theory is based.

The difficulty of obtaining consistent results in the testing of cooling towers is, of course, well known. One of the main factors that governs test results, the atmospheric wet-bulb temperature, entering the tower pulsates during the test, is affected by changing wind conditions, and even is affected by the character of the environment in which the tower is installed. A reasonable tolerance in the guarantees for a type of equipment as cooling towers represent, is therefore, unavoidable.

[5] Burns & Roe, Inc., New York, N. Y.

R. W. Norris[6]

The authors are to be congratulated on an excellent technical review of Merkel's original work. Also, they have pointed out where deviations exist from the basic equation which affect cooling tower performance. It is generally agreed that consideration must be given to account for the liquid evaporation loss, as per equation (16*b*). This becomes more important at the higher L/G ratios whereby the lb vapor/lb dry air is greatly increased. Also, as noted in the article, increasingly hotter inlet water temperatures result in a lowering of the KaV/L values for a given fill design, once again becoming more pronounced at the higher L/G ratios. These two factors are perhaps the most important deviations from Merkel's equation, especially for a counterflow type tower.

It is hoped that the authors in the future will extend their work into developing and publishing theoretical and actual performance graphs for crossflow cooling towers. Information available on counterflow towers enables the user to more easily evaluate soundness of bids, predict performance at other than design conditions, and compare test results with guarantees. Lichtenstein developed a series of KaV/L versus L/G curves in 1943 for counterflow type towers. More recent work has improved upon these curves, whereby they are sufficiently accurate for setting forth the theoretical requirements to be met by a particular tower design. It is then necessary for the manufacturer to establish experimentally KaV/L versus L/G values for a particular fill spacing, number of grid decks, cooling duty, and so on. Due to the sparse information available, it is somewhat difficult for a user to readily approximate tower dimensions and fan horsepower requirements for crossflow towers for a given cooling duty.

Over the past three years we have noted, as an industrial user, a decided and much needed improvement in the number of towers meeting their performance guarantee. At one time, practically every tower we tested failed to meet the guarantee. It is not uncommon now for us to obtain towers producing cold water inlet temperatures slightly exceeding design although we occasionally still find some towers deficient. It appears to us that the methods now available to manufacturers for predicting tower performance are sufficiently accurate from the critical users' standpoint, and at the same time do not cause a tower manufacturer to bid an oversize tower that penalizes his competitive position. We feel that the next step should be correlation of crossflow data in a form that can readily be used by the industrial tower purchaser.

Authors' Closure

We are especially pleased by the fact that the two discussions are presented by personal friends with whom we have been acquainted for many years. The questions raised are quite important because they reflect views that are widely held within the industry.

Figs. 7 and 8 of the text show two methods of plotting test points to establish a tower characteristic. These plotted points represent a series of extremely accurate tests run in the laboratory. The test conditions were varied to cover the range needed to construct a rating table. The problem is to correlate these test results, and the basic point of contention is concerned with the method of doing this. It seems to be the custom for everyone but us to draw a single curve through the band of scattered points. The fluctuations we show have been reported by others, and no

[6] Engineering Department, E. I. du Pont de Nemours & Co., Inc., Wilmington, Del.

one denies that they occur. The fluctuations are measurable and predictable, and we have considered them in our correlation for 15 years. The process is not cumbersome or time-consuming, but the inconvenience should not govern the choice of a procedure. The question must be resolved by running tests to determine the accuracy of each method and choosing the one that gives acceptable results.

We are asked in the discussions if the modifications suggested will really show up in a test, if they represent a degree of precision that exceeds the accuracy of a test, and if other factors may not be of greater importance. All of these questions are also related to accuracy, and the questions must be answered by conducting tests. Anyone who does this will be immediately confronted with the difficulties involved. It is not easy to establish a correlation because all of the errors are reflected as an erratic scattering of the plotted points. The sources of error must be traced, and the accuracy of the methods used to trace the errors must be evaluated. We have done this, and our paper describes the methods we have developed to overcome the difficulties.

We are concerned with the procedure that must be used to answer all of these questions. It provides the means of determining the accuracy of a test. This enables us to evaluate the various factors involved, and that is necessary before we can decide which factors are more important.

We recognize the fact that the required degree of accuracy will vary with individual needs. It is not our intention to establish these limits or to advocate a high degree of precision. Our prime objective is to point out the need of defining the desired limits of accuracy, and then conducting tests to determine what accuracy is attained.

Mr. Norris expresses the desire for more published coefficients that may be used to predict performance, and others have made the same request. The problems involved in this connection were partially answered when Dr. Lichtenstein asked for factors to relate the performance of the small test cell with the performance of the full-size tower in the field.

It is generally assumed that a given type of filling has a fixed characteristic that applies to all towers containing that filling. The characteristic of a cooling tower is determined by the entire assembly, and it varies with changes in the tower containing the filling.

We are aware of the demand for coefficients, but feel there is a greater need for more accurate means of developing them *for the tower in question*. The use of published coefficients provides a sense of false security that may lead to gross errors. It should be pointed out, in this connection, that it is quite difficult for a user to check the accuracy of these coefficients by field tests.

The request for coefficients has been encouraged by statements we frequently hear to the effect that information is available that will enable anyone to predict cooling tower performance. This is another example of a generalized statement that ignores the need of specifying the desired limits of accuracy. We have found it extremely difficult to get anyone to make a commitment on what is to be considered an acceptable degree of accuracy. This reluctance may be due, in part, to the fact that it is extremely difficult to determine what accuracy is being obtained.

A review of the discussion will show that the questions are all concerned with selecting an acceptable means of analyzing cooling tower performance. An acceptable method must have an acceptable degree of accuracy. The questions must be resolved, not by discussion, but by testing to determine the accuracy of the various methods. Each individual will then be able to choose a method having an acceptable degree of accuracy. We feel that the divergent views exist because this has not been done.

Film-Boiling Heat Transfer From a Horizontal Surface

P. J. BERENSON
Assistant Professor of Mechanical Engineering, M.I.T., Cambridge, Mass. Presently, with A. D. Little, Inc., Santa Monica, Calif.

Taylor-Helmholtz Hydrodynamic Instability and its significance with regard to film boiling heat transfer from a horizontal surface is discussed. It is shown that near the minimum film-boiling heat flux, the bubble spacing and growth rate is determined by Taylor Instability neglecting the effect of fluid depth and viscosity. Utilizing a simplified geometrical model, an analytical expression for the heat-transfer coefficient near the minimum in film pool boiling from a horizontal surface was derived. Combining this equation with the available correlation for the minimum heat flux yields an analytical equation for the temperature difference at the minimum, which defines the location of the minimum point. The above equations agree with the available experimental measurements made on n-pentane and carbon tetrachloride within ±10 per cent.

I Introduction

THE OBJECT of this work was to analyze film-boiling heat transfer from a horizontal surface. The difficulty which arose when attempting to analyze this problem was the fact that the vapor flow geometry was not clear. In particular, the bubble spacing and orientation with respect to one another had not been defined.

In analyzing film boiling from a horizontal tube one knows that the vapor flows up around the tube, departing as bubbles from the top of the tube. The vapor flow pattern on a horizontal plate was not so obvious. Visual observations by the author of the bubble pattern which exists on a horizontal surface gave the impression that the bubbles are located in some type of regular lattice, perhaps hexagonal or square. The photograph shown by Borishansky [1][1] also exhibits an approximately regular bubble pattern.

Presumably the vapor generated in the vicinity of a given growing bubble flows in toward the bubble location, combines, and departs. This process repeats itself continuously, leading to a steady stream of individual bubbles departing from the liquid-vapor interface. If one knew the bubble spacing; i.e., the effective length of the vapor flow path, it would be possible to analyze this process utilizing the conventional approach of Bromley [2]. It is demonstrated in the following section that the bubble spacing and the rate of growth of the bubble are determined, independent of heat-transfer effects, by hydrodynamic considerations.

[1] Numbers in brackets designate References at end of paper.

Contributed by the Heat Transfer Division and presented at the Winter Annual Meeting, New York, N. Y., November 27–December 2, 1960, of THE AMERICAN SOCIETY OF MECHANICAL ENGINEERS. Manuscript received at ASME Headquarters, August 1, 1960. Paper No. 60—WA-147.

II Taylor-Helmholtz Hydrodynamic Instability

A Introduction. The behavior of an interface separating two fluids of different density when subjected to disturbances, such as the liquid-vapor interface in film boiling, has received considerable attention in the past decade. At the present time it is possible to determine the effect of acceleration, surface tension, viscosity, relative velocity, and finite fluid depth on the interface dynamics.

Taylor [3] first clearly formulated the problem, considering only the effect of acceleration and fluid depth. He showed that the interface is unstable; that is, a disturbance will grow with time, if the acceleration is directed from the lighter to the heavier fluid. An example of this is vapor beneath liquid in a gravitational field.

Taylor's analysis of the problem assumes potential flow. The form of the interface disturbance introduced into the first-order perturbation analysis is given by the following equation.

$$\eta = \eta_o e^{-int} \cos mx = \eta_o e^{bt} \cos mx \tag{1}$$

The meaning of the various terms in the above equation are defined in the Nomenclature. The wave number m is related to

Nomenclature

A = area, ft²
D = diameter, ft
R = radius of curvature, ft
T = temperature, deg F
V = velocity, ft/sec
a = vapor film thickness, ft
b = $-in$ growth coefficient, 1/sec
c = wave speed, ft/sec
g = acceleration of gravity, ft/sec²
g_c = conversion factor 32.2, lb_M ft/lb sec²
h = heat-transfer coefficient, Btu/hr ft² deg F
Δh = average enthalpy difference between vapor and liquid, Btu/lb_M
k = thermal conductivity, Btu/hr ft deg F
m = wave number, 1/ft
n = wave frequency, 1/sec
p = pressure, lb/ft²
q = heat-transfer rate, Btu/hr
r = radius, ft
t = time, sec
w = flow rate, lb_M/sec
x = length co-ordinate, ft
β = constant, equation (18)
δ = average bubble height, ft
Δ = change or difference
η = distance perpendicular to liquid-vapor interface, ft
λ = wavelength, ft
μ = vapor viscosity lb/hr ft
ρ = density, lb_M/ft³
σ = surface tension, lb/ft

Subscripts

b = bubble
f = film
l = liquid
m = mass
min = minimum
o = initial or reference value
v = vapor

Superscript

* = maximum or maximizing

the wavelength by the following relation,

$$m = \frac{2\pi}{\lambda} \tag{2}$$

The result of the above analysis was an expression for n as a function of the fluid properties, the acceleration, and the wavelength. From equation (1) it is seen that if n is real, the disturbance is periodic in time, and therefore stable. However, if n is imaginary, the disturbance grows exponentially with time. Taylor's results, applied to the case of a liquid resting above a vapor in a gravitational field, state that the interface is unstable for disturbances of all wavelengths.

The first-order approximations used in the analysis presumably limit the applicability of the results to the extent that the amplitude of the wave must be much less than the wavelength. However, Lewis [4] experimentally showed that Taylor's theory satisfactorily predicted the growth of the instability as long as the amplitude was less than 0.4 λ. The two-dimensional analysis was also found to adequately describe the three-dimensional physical situation.

The analytical approach used by Taylor has been utilized to solve the problem including the effects of relative velocity parallel to the interface and surface tension. The analysis and results are summarized by Lamb [5] and Milne-Thompson [6]. Section 14.53 of Milne-Thompson presents the general result, from which the expression for n for any particular case can be derived. In particular, it was found that surface tension tends to stabilize the interface, making disturbances of short wavelength stable, and decreasing the growth rate for long wavelength disturbances.

It has become conventional to refer to those instabilities of the above type which occur in the absence of relative velocity effects as Taylor Instability. When relative velocity is important, the phenomenon is called a Helmholtz Instability.

Bellman and Pennington [7] analytically included the effect of viscosity on Taylor Instability for the case of infinite fluid depth. They found that viscosity does not remove an instability which would otherwise exist; it merely slows the interface growth rate.

The experiments of Allred and Blount [8] serve to confirm the validity of the above analysis. The two-dimensional theory adequately describes three-dimensional effects and may be used provided the amplitude is less than 0.4 λ.

B Application of Taylor-Helmholtz Instability to Film Boiling From a Horizontal Surface

1 Stability Equations. The general solution of the irrotational flow kinematic equation yields the following relation between wave speed, gravity, surface tension, fluid velocity parallel to the interface, and fluid depth, for the case of a liquid over a vapor [6].

$$m\rho_v(V_v - c)^2 \coth ma + m\rho_l(V_l - c)^2 \coth ma_l = g_c\sigma m^3 - g(\rho_l - \rho_v) \tag{3}$$

The wave speed c is defined by the following relation.

$$c = \frac{n}{m} \tag{4}$$

The simplifying assumptions which are valid for film boiling from a horizontal surface in the absence of forced convection are,

$$V_l = 0 \qquad \coth ma_l = 1 \tag{5}$$

Combining equations (3) and (5) yields the result

$$m\rho_v(V_v - c)^2 \coth ma + m\rho_l c^2 = g_c\sigma m^3 - g(\rho_l - \rho_v) \tag{6}$$

The parameter of interest in predicting the growth of the two-phase boundary is the coefficient of t in equation (1); that is $-in$. This growth coefficient is abbreviated with the letter b in the following sections.

A number of simplifying assumptions can be introduced into equation (6) which make it possible to obtain explicit expressions for c and therefore b. The equations for the growth coefficient b, which result from specific assumptions, are presented below.

(a) Assume the effect of vapor velocity and depth are negligible, i.e.,

$$V_v = 0 \qquad \coth ma = 1 \tag{7}$$

Combining equations (7), (6), and (4) results in the following expression for b.

$$b = \left[\frac{g(\rho_l - \rho_v)m}{\rho_l + \rho_v} - \frac{g_c\sigma m^3}{\rho_l + \rho_v}\right]^{1/2} \tag{8}$$

(b) Assume the effect of vapor velocity is negligible, and that the vapor thickness is very small, i.e.,

$$V_v = 0 \qquad \coth ma = \frac{1}{ma} \tag{9}$$

Combining equations (9), (6), and (4) yields

$$b = \left[\frac{g(\rho_l - \rho_v)m}{\rho_l + \rho_v/ma} - \frac{g_c\sigma m^3}{\rho_l + \rho_v/ma}\right]^{1/2} \tag{10}$$

(c) Assume the effect of vapor thickness is negligible, i.e.,

$$\coth ma = 1 \tag{11}$$

Combine equations (11), (6), and (4) to obtain

$$b = \left[\frac{\rho_l\rho_v V_v^2 m^2}{(\rho_l + \rho_v)^2} + \frac{g(\rho_l - \rho_v)m}{\rho_l + \rho_v} - \frac{g_c\sigma m^3}{\rho_l + \rho_v}\right]^{1/2} \tag{12}$$

(d) Assume the vapor film is very thin, i.e.,

$$\coth ma = \frac{1}{ma} \tag{13}$$

Combining equations (13), (6), and (4) yields

$$b = \left[\frac{\rho_l\rho_v V_v^2 m^2}{(\rho_l + \rho_v/ma)^2 ma} + \frac{g(\rho_l - \rho_v)m}{\rho_l + \rho_v/ma} - \frac{g_c\sigma m^3}{\rho_l + \rho_v/ma}\right]^{1/2} \tag{14}$$

2 Application to Film Boiling. Examining the above expressions for b, it is observed that once the fluid properties are fixed, the value of b only depends on the wave number, i.e., the wavelength of the disturbance. Due to the form of the equations, b is real, imaginary, or zero depending on the particular value of the wave number. If a disturbance occurs whose wavelength corresponds to a real value of b, the interface is unstable, growing at a rate given by equation (1). The larger the value of b, the greater the growth rate of the boundary. Therefore the particular wavelength which is most likely to become visible is that possible wavelength which yields the maximum value of b.

In general, in any mechanical system small disturbances of all wavelengths are present. Therefore the wavelength which is most likely to become visible is that wavelength which maximizes b in the applicable equation. The growth rate of the boundary is then given by equation (1), with the maximum value of b inserted for $-in$. The boundary continues to grow until it ruptures when a bubble departs from the node. The bubble period is therefore established by equation (1) and the maximum value of b, and the bubble spacing is given by the dominant wavelength, i.e., that wavelength which maximizes b.

Applying one of the above results for b to a particular case serves to illustrate the use and physical interpretation of the stability analysis. Fig. 1 is a plot of b versus m for n-pen ane when the effects of finite depth and velocity are neglected, equation (8). This shows that disturbances of wave number less than 196, or wavelength greater than 5.1×10^{-3} ft, are unstable for the system considered. The dominant wavelength, that which maximizes b, is equal to 8.85×10^{-3} ft. Since the curve in Fig. 1 is relatively flat near the maximum, one would expect to observe a spread of wavelengths lying on each side of the maximizing value. Other things being equal, the average wavelength observed should be approximately equal to the maximizing value.

While equation (8) serves to qualitatively illustrate the application of the stability analysis results to film boiling, it has not yet been established which expression for b provides the correct quantitative results; that is, what simplifications are valid. Utilizing the results of Bellman and Pennington [7] one can show that viscosity has a completely negligible effect on the interface growth for n-pentane in particular, and all fluids of practical interest to film boiling, in general.

The effect of vapor film thickness and velocity were not obviously negligible. Calculations based on the experimental results indicated that the film thickness is of the order of 10^{-4} ft, and the vapor velocity is of the order of 1 ft/sec.

To determine the importance of vapor film thickness and vapor velocity on the interface behavior in film boiling, b was plotted versus m using equations (12) and (14). The value of the vapor film thickness was assumed constant at the average value computed from the experimental results. The vapor velocity varies considerably within the film as shown by equation (44) in the Appendix. To evaluate the importance of vapor velocity a characteristic value of the velocity evaluated at a radius from the bubble equal to $\lambda/3$, was used, which resulted in the following equation for the vapor velocity.

$$V_v = 0.0717 \frac{k_{vf}\Delta T\lambda}{\rho_{vf}\Delta h a^2} = 0.45 \frac{k_{vf}\Delta T}{\rho_{vf}\Delta h a^2 m} \tag{15}$$

The choice of the radius at which the velocity was evaluated is somewhat arbitrary, therefore the results should not be strictly interpreted quantitatively. However, the resulting effect of vapor velocity on the instability was accurate enough to indicate qualitative effects and to suggest what assumptions are reasonable.

It is interesting to note that the vapor velocity is directly proportional to the temperature difference. Referring to equation (14) it is seen that as the vapor velocity increases, b increases. Therefore the growth rate of the boundary tends to increase as the temperature difference is increased. Combining equation (15) with equations (12) and (14) yields the following expressions.

Neglecting the effect of vapor film thickness:

$$b = \left[\frac{0.203\rho_l\rho_v}{(\rho_l+\rho_v)^2}\left(\frac{k_{vf}\Delta T}{\rho_{vf}\Delta h a^2}\right)^2 + \frac{g(\rho_l-\rho_v)m}{\rho_l+\rho_v} - \frac{g_c\sigma m^3}{\rho_l+\rho_v}\right]^{1/2} \tag{16}$$

Including the effect of vapor film thickness:

$$b = \left[\frac{0.203\rho_l\rho_v}{(\rho_l+\rho_v/ma)^2}\left(\frac{k_{vf}\Delta T}{\rho_{vf}\Delta h a^2}\right)^2 \frac{1}{ma} + \frac{g(\rho_l-\rho_v)m}{\rho_l+\rho_v/ma} - \frac{g_c\sigma m^3}{\rho_l+\rho_v/ma}\right]^{1/2} \tag{17}$$

The values of the vapor film properties used were those collected by Bromley [9]. The results of plotting b versus m for various temperature differences characteristic of film boiling are as follows. When neglecting vapor film thickness by using equation (16), velocity has a negligible effect on the value of b for temperature differences less than 500 deg F. However, calculating b from equation (17), which includes the effect of film thickness, yields values of b which show a significant effect of vapor velocity, and therefore film thickness, at values of temperature difference nearer the value at the minimum. The results of the latter calculation, for n-pentane, are presented in Fig. 2.

Referring to Fig. 2, it is seen that, while vapor velocity affects the bubble spacing and growth rate at moderate values of the temperature difference in film boiling, as the minimum temperature is approached the effect of vapor velocity becomes negligible. The effect of film thickness, when velocity is neglected, is also shown in Fig. 2. Under these conditions, it is reasonable to neglect the effect of vapor film thickness on the bubble spacing and growth rate. In particular, the value of m, at maximum b, which establishes the bubble spacing is not noticeably changed. Therefore in the neighborhood of the minimum heat flux it is reasonable to assume that equation (8) specifies the bubble spacing and growth rate. Zuber [10] first proposed these assumptions in his analysis of the minimum heat flux, which is presented with minor modification in reference [11].

3 Discussion. The bubble spacing in film boiling from a horizontal surface is fixed by the value of the wavelength which maximizes b in the appropriate equation. Near the minimum heat flux it is reasonable to neglect the effect of vapor velocity and vapor film thickness, therefore equation (8) describes the behavior of the two-phase interface.

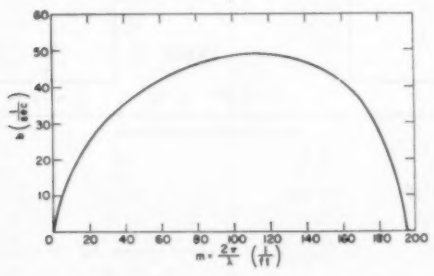

Fig. 1 Plot of b as a function of m for n-pentane neglecting the effect of velocity and fluid depth

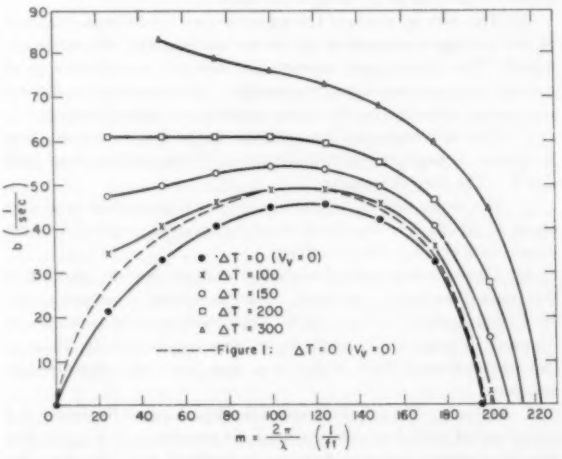

Fig. 2 Plot of b as a function of m from equation (17) for n-pentane

Once the two-phase boundary begins to grow, the growth continues until a bubble departs from the node. Bubble departure has been observed by the author, and is shown in the photographs of Santangelo [12], to occur when the amplitude is approximately equal to the bubble diameter. After the bubble departs, the interface snaps back toward the solid surface, providing the disturbance necessary to start the growth of the neighboring antinode. For neighboring locations on the interface to alternately grow and collapse, the bubble pattern must be visualized as a square lattice. At any time two bubbles are growing in any λ^2 area.

III Analysis of Film Boiling From a Horizontal Surface

A Introduction and Assumptions. As a result of the preceding section and the experimental results, it is apparent that the bubble spacing in film boiling from a horizontal surface is fixed by hydrodynamic considerations. A list of the assumptions utilized in the analysis and a short discussion of their validity follows:

(*a*) Near the minimum heat flux, the bubble spacing is unaffected by the vapor velocity and the vapor film thickness. Referring to Fig. 2, it is seen that there is a negligible change in the value of m which maximizes b at values of the temperature difference near the minimum. This same assumption is utilized in the analysis of the minimum heat flux and leads to a correct result.

(*b*) The vapor flows radially into the bubble. In the vicinity of the bubble this is probably an excellent approximation and this is where the vapor velocity and therefore the viscous shear stress is greatest.

(*c*) The momentum forces are negligible in comparison with the viscous forces. Calculation of the Reynolds number shows this to be an excellent assumption.

(*d*) The flow is laminar. The Reynolds number calculation also verifies this statement.

(*e*) The change in height of the vapor-liquid boundary between the bubbles is negligible compared to the average height of the bubble above interface. Since the bubble dimensions are two orders of magnitude greater than the film thickness, this must be valid.

(*f*) The viscous drag of the liquid-vapor interface on the vapor flow lies between zero and the value corresponding to a stationary boundary. These are the two extremes possible without forced convection.

(*g*) The kinetic energy of the vapor is negligible in comparison with the enthalpy change. This assumption can be shown to be accurate to much better than 1 per cent.

(*h*) The average value of the vapor properties are equal to those at the average temperature of the hot surface and the saturated liquid. This is not quite correct, but will not introduce a great enough error to invalidate the results. Also, evaluating the experimental constant on this basis eliminates most of the error.

(*i*) Heat is transferred through the vapor film by conduction. Radiation is negligible at temperature differences less than 1000 deg F. The flow is laminar.

(*j*) The vapor flowing to any one bubble is generated in an area equal to $\lambda^2/2$. The results of stability analysis applied to three dimensions require this condition.

(*k*) The two-dimensional stability analysis may be applied to the three-dimensional problem. The experimental investigations of Taylor Instability [4 and 8] have verified this assumption. The only change which might have been required is the value of the constant and this change was less than the experimental accuracy.

B Analysis. The actual shape of the liquid-vapor interface, and the physical model used in the analysis are shown in Fig. 3. For one-dimensional viscous flow in cylindrical co-ordinates, the momentum equation reduces to the following:

$$\frac{dp}{dr} = \frac{\beta \mu_f V_v}{g_c a^2} \tag{18}$$

The constant β is equal to 12 if the vapor-liquid boundary has the same effect as a stationary wall, and 3 if there is no shear stress at the boundary (9).

The vapor velocity varies with radius according to the following equation, derived in the Appendix.

$$V_v = \frac{k_{vf}\Delta T}{\rho_{vf}\Delta h a^2} \frac{\lambda^2/2 - \pi r^2}{2\pi r} \tag{19}$$

Combining equations (19) with (18) yields

$$dp = \frac{\beta \mu_f k_{vf}\Delta T}{g_c a^4 \rho_{vf}\Delta h} \frac{\lambda^2/2 - \pi r^2}{2\pi r}\, dr \tag{20}$$

The pressure difference required to sustain the flow is obtained by integrating equation (20) from r_1, where $p = p_1$, to r_2, where $p = p_2$. Referring to Fig. 3, it is seen that r_1 equals the bubble radius which is obtained from the equation resulting from the experimental measurements, presented in Table 1.

$$r_1 = \frac{D_b}{2} = 2.35\sqrt{\frac{g_c \sigma}{g(\rho_l - \rho_v)}} \tag{21}$$

The radius r_2, as a result of assumption j is obtained from the following expression.

$$\pi r_2^2 = \frac{\lambda^2}{2} \tag{22}$$

The appropriate wavelength is obtained from equation (8) as a result of assumption a. The wavelength which grows the fastest, and therefore dominates, is that which maximizes b, where for this case b is given by

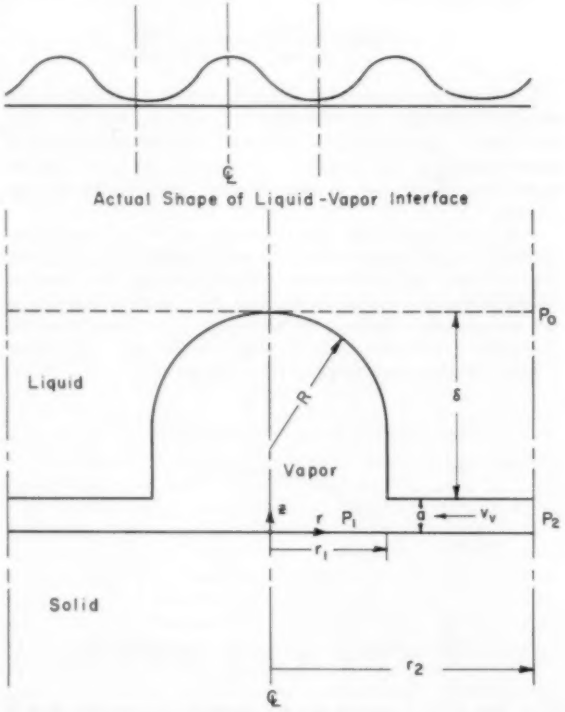

Fig. 3 Physical model of film boiling from a horizontal surface

$$b = -in = \left[\frac{g(\rho_l - \rho_v)m}{\rho_l + \rho_v} - \frac{g_o\sigma m^3}{\rho_l + \rho_v}\right]^{1/2} \tag{23}$$

Differentiating equation (23) with respect to m and solving for the value which maximizes b, yields the following result.

$$m^* = \left[\frac{g(\rho_l - \rho_v)}{3g_o\sigma}\right]^{1/2} = \frac{2\pi}{\lambda^*} \tag{24}$$

Equation (20) is now integrated and combined with equations (21), (22), and (24) to yield the required pressure difference.

$$p_2 - p_1 = \frac{8\beta}{\pi}\,\frac{\mu_f k_{vf}\Delta T}{g_o a^4 \rho_{vf}\Delta h}\,\frac{g_o\sigma}{g(\rho_l - \rho_v)} \tag{25}$$

This pressure difference is supplied by the difference in gravity head. Referring to Fig. 3, at a height δ above the film, the pressure is independent of radius and equal to p_0. The following relations exist between p_0, p_1, and p_2.

$$p_2 - p_v = \delta\rho_l\,\frac{g}{g_o} \tag{26}$$

$$p_1 - p_o = \delta\rho_v\,\frac{g}{g_o} + \frac{2\sigma}{R} \tag{27}$$

Where the second term on the right in the latter equation takes into account the pressure difference due to the curvature of the bubble and the surface tension. Solving the above two equations for the pressure difference gives,

$$p_2 - p_1 = \delta(\rho_l - \rho_v)\,\frac{g}{g_o} - \frac{2\sigma}{R} \tag{28}$$

The radius of curvature R is equal to the bubble radius given by equation (21). It is reasonable to assume that δ the average height of the bubble above the vapor film is proportional to the bubble diameter where the proportionality constant must be less than one. Borishansky [1] has measured the proportionality constant, with the following results.

$$\delta = 0.68D_b = 3.2\sqrt{\frac{g_o\sigma}{g(\rho_l - \rho_v)}} \tag{29}$$

Table 1 Results of bubble diameter measurements

n-Pentane

q/A, Btu/hr ft²	D_b, in. ±10%	q/A, Btu/hr ft²	D_b, in. ±10%
6800	0.29	10500	0.28
6800	0.29	10500	0.26
6800	0.26	11500	0.28
6800	0.25	11500	0.24
6800	0.29	11500	0.26
10500	0.28	6600	0.29
10500	0.23	6600	0.28
10500	0.28	11500	0.33
10500	0.30		

$D_{b\ v} = 0.28$ in.

Carbon tetrachloride

q/A, Btu/hr ft²	D_b, in. ±10%	q/A, Btu/hr ft²	D_b, in. ±10%
8000	0.26	8000	0.26
8000	0.28	8000	0.24
8000	0.26	8000	0.25
8000	0.26		

$D_{b\,avg} = 0.26$ in.

Combining equations (28), (29), and (21) gives for the available pressure difference

$$p_2 - p_1 = 2.34\,\frac{g}{g_o}\,(\rho_l - \rho_v)\sqrt{\frac{g_o\sigma}{g(\rho_l - \rho_v)}} \tag{30}$$

Equating equation (20) to equation (30), and solving for the vapor film thickness between the bubbles yields,

$$a = \left[\frac{1.09\beta\mu_f k_{vf}\Delta T}{\Delta h\rho_{vf}g(\rho_l - \rho_v)}\sqrt{\frac{g_o\sigma}{g(\rho_l - \rho_v)}}\right]^{1/4} \tag{31}$$

The average vapor film thickness for the entire surface which gives the same heat-transfer rate as the above is equal to equation (31) multiplied by the ratio of the total surface area to the area between the bubbles, yielding the result below.

$$a = 1.4\left[\frac{1.09\beta\mu_f k_{vf}\Delta T}{\Delta h\rho_{vf}g(\rho_l - \rho_v)}\sqrt{\frac{g_o\sigma}{g(\rho_l - \rho_v)}}\right]^{1/4} \tag{32}$$

Incorporating the two extreme values of β in the result and solving for the vapor film thickness yields

$$a = \begin{matrix}2.6\\ \text{or}\\ 1.9\end{matrix}\left[\frac{\mu_f k_{vf}\Delta T}{\Delta h\rho_{vf}g(\rho_l - \rho_v)}\sqrt{\frac{g_o\sigma}{g(\rho_l - \rho_v)}}\right]^{1/4} \tag{33}$$

Evaluating the constant from the experimental results at the minimum (11) gives the final correlation equation.

$$a = 2.35\left[\frac{\mu_f k_{vf}\Delta T}{\Delta h\rho_{vf}g(\rho_l - \rho_v)}\sqrt{\frac{g_o\sigma}{g(\rho_l - \rho_v)}}\right]^{1/4} \tag{34}$$

A heat-transfer coefficient may be defined by applying the following equation.

$$q = \frac{k_{vf}}{a}\,A\Delta T = hA\Delta T \tag{35}$$

Combining equation (35) with (34) and solving for h yields

$$h = 0.425\left[\frac{k_{vf}{}^3\Delta h\rho_{vf}g(\rho_l - \rho_v)}{\mu_f\Delta T}\sqrt{\frac{g_o\sigma}{g(\rho_l - \rho_v)}}\right]^{1/4} \tag{36}$$

C Discussion. It is interesting to compare the above result with that of Bromley [9] for horizontal tubes which is given below.

$$h = 0.62\left[\frac{k_{vf}{}^3\Delta h\rho_{vf}g(\rho_l - \rho_v)}{\mu_f\Delta TD}\right]^{1/4} \tag{37}$$

The major difference is the substitution of $\sqrt{\dfrac{g_o\sigma}{g(\rho_l - \rho_v)}}$ for the tube diameter D. These are the geometrical scale factors for horizontal plates and tubes, respectively. From dimensional analysis this change might have been predicted. In both equations the experimental value of the constant was the average of the values obtained utilizing the extreme values of β. The similarity between equations (36) and (37) provides added confidence in the validity of equation (36) since Bromley's equation has been thoroughly verified.

Presumably equation (36) is only valid in the neighborhood of the minimum since the assumed bubble spacing only applies there. It is suspected that the range of practical application is larger than implied due to the small influence of the characteristic length on the heat-transfer coefficient. Equation (36) probably applies to temperature differences as high as 1000 deg for some fluids. This remains to be verified. The heat-transfer coefficient predicted by equation (36) represents the lower limit for those cases in which velocity affects the interface stability.

IV Analysis of the Temperature Difference at the Minimum Heat Flux

The results of the preceding section, combined with the analysis of Zuber [10] make it possible to predict the temperature difference at the minimum for fluid-surface combinations with finite values of contact angle [11].

The equation for the minimum temperature difference may be written as follows from the heat conduction equation

$$(\Delta T)_{min} = \frac{(q/A)_{min}}{(h)_{min}} \tag{38}$$

The heat flux at the minimum is given by equation (A-83) in reference [11].

$$(q/A)_{min} = 0.09\rho_{vf}\Delta h\left[\frac{g(\rho_l - \rho_v)}{\rho_l + \rho_v}\right]^{1/4}\left[\frac{g_c\sigma}{g(\rho_l - \rho_v)}\right]^{1/4} \tag{39}$$

The above equation deviates from the available data [11] for *n*-pentane and CCl_4 by only ± 1 per cent.

Combining equations (39), (38), and (36) yields the following expression for the minimum temperature difference in film pool boiling from a horizontal surface.

$$(\Delta T)_{min} = 0.127\frac{\rho_{vf}\Delta h}{k_{vf}}\left[\frac{g(\rho_l - \rho_v)}{\rho_l + \rho_v}\right]^{2/3}\left[\frac{g_c\sigma}{g(\rho_l - \rho_v)}\right]^{1/2}\left[\frac{\mu_f}{g_c(\rho_l - \rho_v)}\right]^{1/3} \tag{40}$$

The agreement between the experimental results obtained by the author [11] and the temperature difference predicted by equation (40) is given below. The pressure is one atmosphere.

Fluid	ΔT_{min} measured (deg F)	ΔT_{min} predicted (equation 40) (deg F)
n-pentane	105 ± 10%	98
carbon tetrachloride	145 ± 10%	153

The ±10 per cent agreement between equation (40) and the experimental values also defines the limits of equation (36).

V Summary of Results and Conclusions

(*a*) It is quantitatively reasonable to neglect the effect of vapor velocity and film thickness on the liquid-vapor boundary behavior in film boiling near the minimum temperature difference.

(*b*) An analytical expression, equation (36), is derived which predicts the heat-transfer coefficient for film pool boiling from a horizontal surface within ±10 per cent.

(*c*) Combining the analytical expression for the minimum heat flux with the above expression for the heat-transfer coefficient, yields an expression for the temperature difference at the minimum-minimum which agrees with the experimental results within ±10 per cent.

APPENDIX

Vapor Velocity Parallel to Surface in Film Boiling

1 Assumptions

(*a*) Vapor film thickness *a* is constant between bubbles.

(*b*) The vapor flows radially inward.

(*c*) The vapor generated in an area equal to $\lambda^2/2$ flows to one bubble.

(*d*) The geometry is given by Fig. 3.

2 Analysis

Continuity:

$$w = \rho_{vf}V_v A = \rho_{vf}V_v 2\pi r a \tag{41}$$

First law:

$$q = w\Delta h \tag{42}$$

Heat transfer:

$$q = \frac{k_{vf}}{a}(\pi r_2^2 - \pi r^2)\Delta T \tag{43}$$

From assumption *c*, $\lambda^2/2 = \pi r_2^2$. Eliminating q and w from equations (41), (42), and (43), and solving for the vapor velocity V_v yields the following relation.

$$V_v = \frac{k_{vf}\Delta T}{\rho_{vf}\Delta h a^2}\frac{\frac{\lambda^2}{2} - \pi r^2}{2\pi r} \tag{44}$$

Acknowledgments

The author is indebted to Prof. Peter Griffith for many helpful, encouraging, and stimulating discussions which led to an understanding of the problem and the analytical tools available. The research was supported by the National Science Foundation under NSF Grant No. G-6305.

References

1 V. M. Borishansky, "Heat Transfer to a Liquid Freely Flowing Over a Surface Heated to a Temperature Above the Boiling Point," in "Problems of Heat Transfer During a Change of State," by S. S. Kutateladze, 1959, AEC-tr-3405.

2 L. A. Bromley, "Heat Transfer in Stable Film Boiling," *Chemical Engineering Progress*, vol. 46, May, 1950, pp. 221–227.

3 G. I. Taylor, "The Instability of Liquid Surfaces When Accelerated in a Direction Perpendicular to Their Plane, I," *Proceedings, Royal Society of London*, vol. 201, series A, 1950, p. 192.

4 D. J. Lewis, "The Instability of Liquid Surfaces When Accelerated in a Direction Perpendicular to Their Plane, II," *Proceedings, Royal Society of London*, vol. 202, series A, 1950, p. 81.

5 H. Lamb, "Hydrodynamics," Dover Publications, New York, N. Y., 1945, p. 455.

6 L. M. Milne-Thompson, "Theoretical Hydrodynamics," The Macmillan Company, New York, N. Y., 1950, p. 371.

7 R. Bellman and R. H. Pennington, "Effects of Surface Tension and Viscosity on Taylor Instability," *Quarterly of Applied Mathematics*, vol. 12, 1954, p. 151.

8 J. C. Allred and G. H. Blount, "Experimental Studies of Taylor Instability," Univ. of California, Los Alamos Laboratory, Report LA-1600, February 1, 1954.

9 L. A. Bromley, "Heat Transfer in Stable Film Boiling," PhD thesis, Dept. of Chem., Univ. of California, Berkeley, Calif., June, 1948.

10 N. Zuber, "Hydrodynamic Aspects of Boiling Heat Transfer," PhD thesis, Department of Engineering, UCLA, June, 1959.

11 Paul J. Berenson, "Transition Boiling Heat Transfer From a Horizontal Surface," M.I.T. Heat Transfer Laboratory Technical Report No. 17, Cambridge, Mass., March 1, 1960.

12 J. W. Westwater and J. G. Santangelo, "Photographic Study of Boiling," *Industrial and Engineering Chemistry*, vol. 47, August, 1955, p. 1605

DISCUSSION

Yih-yun Hsu[2]

The author is congratulated for his contribution to the knowledge of boiling heat transfer and his excellent presentation. It is very interesting to see that film boiling from a horizontal plate

[2] Aeronautical Research Scientist, NASA, Lewis Research Center, Cleveland, Ohio.

can be expressed in the same form as Bromley's equation for a vertical surface. However, due to this very similarity, the limitation of Bromley's equation has to be imposed on the present case too. It was observed by Professor Westwater and the writer[3] that Bromley's equation, which was based on the assumption of a laminar flow, did not apply to a tall vertical surface due to the onset of turbulence. Thus, unless the wavelength here is small so that the Re of the vapor film is less than 100 or so, the existence of turbulence should be considered also. The quantity $\sqrt{\frac{g_0\sigma}{g(\rho_L - \rho_V)}}$ is usually small for ordinary conditions. However, in some special situation such as when g is much less than g_{earth}, it could very well be a quantity large enough to warrant careful consideration.

Novak Zuber[4]

The writer takes this opportunity to congratulate Dr. Berenson for his contribution toward the understanding of boiling heat transfer.

There are two kinds of experiments that are conducted in investigation of the two-phase flow and of the boiling process. In the first group are experiments that are conducted with full-scale apparatus. These experiments are costly and time-consuming but they yield results that can be applied directly to a design of a nuclear reactor or of a power plant for space application. However, these experiments, because of the complexity of the phenomenon, because of incomplete instrumentation, and other experimental difficulties, very seldom provide detailed information which is needed for integrating the results and the understanding of the boiling process. The experiments of the second group can be performed on a laboratory bench. These experiments are relatively cheap and require a short time to provide the desired information. Although the results cannot be applied directly to a system design, these experiments yield basic information and data which are needed for the understanding and for a general, quantitative formulation of the problem. Therefore, although for immediate design problems, experiments of the first group are more important, over a long period the second group will prove not only more valuable but essential. There are probably too many experiments of the first kind and, unfortunately, too few of the second.

The work of Dr. Berenson reported in this paper and in references [11 and 13][5] belongs to the second group. The experimental data are valuable because they clearly indicate the basic characteristic of film boiling as well as of the maximum, i.e., critical heat flux in nucleate boiling from a horizontal surface.

In references [14, 15, and 16] it was proposed that transitional boiling and, therefore, the critical heat flux and the minimum heat flux in film boiling are characterized by the effect of hydrodynamic instabilities. It was postulated that the critical heat flux is limited by the combined effect of Taylor and Helmholtz instabilities, whereas the minimum heat flux in film boiling is limited by the effect of Taylor instability only. It was postulated also that, because of Taylor instability, the interface tends to break into "unit cells" of area λ^2 where

$$2\pi\sqrt{\frac{g_0\sigma}{g(\rho_L - \alpha_V)}} \leq \lambda \leq 2\pi\sqrt{\frac{3g_0\sigma}{g(\rho_L - \rho_V)}} \qquad (45)$$

To formulate the problem the assumption was made that from each cell two bubbles originate per period where the bubble diameter was given by

$$3.14 = \frac{2\pi}{2} \leq \frac{D}{\sqrt{\frac{g_0\sigma}{g(\rho_L - \rho_V)}}} \leq \frac{2\pi}{2}\sqrt{3} = 5.44 \qquad (46)$$

From these postulates and assumption it was possible to derive the following expression for the maximum (i.e., critical) heat flux in nucleate pool boiling from a horizontal surface.

$$0.120 = \frac{\pi}{24}\frac{3}{\sqrt{2\pi}}\frac{1}{(3)^{1/4}} \leq \frac{(q/A)_{max}}{\rho_V \Delta h\left[\frac{g_0\sigma g(\rho_L - \rho_V)}{\rho_V^2}\right]^{1/4}} \leq \frac{\pi}{24}\frac{3}{\sqrt{2\pi}} = 0.157 \qquad (47)$$

and the following expression for the minimum heat flux in film boiling from a horizontal surface

$$0.110 = \frac{\pi}{24}\frac{\sqrt{2\pi}}{3} \leq \frac{(q/A)_{min}}{\rho_V \Delta h\left[\frac{g_0\sigma g(\rho_L - \rho_V)}{(\rho_L + \rho_V)^2}\right]^{1/4}} \leq \frac{\pi}{24}\frac{\sqrt{2\pi}}{3}(3)^{1/4} = 0.142 \qquad (48)$$

The inequalities in equations (46), (47), and (48) result from the spectrum of unstable disturbances given in equation (45).

Although it was shown in references [14, 15, and 16] that the results predicted by equations (46), (47), and (48) were in good agreement with available experimental data, a detailed experimental verification of the basic mechanism was not available. Consequently, at the time (in 1958) the validity of the postulates, of the assumptions as well as of the basic mechanism (hydrodynamic instability) was questioned by a number of investigators. Their doubt was motivated especially by the fact that if the basic mechanism which brings about the changes in the boiling process is a hydrodynamic instability, then the inevitable conclusions to be drawn from the analysis [cf., equations (47) and (48)] were: 1 That the maximum (critical) heat flux in nucleate boiling from a horizontal surface was *independent* of the temperature; and 2 that both the critical heat flux and the minimum heat flux in film boiling from a horizontal surface are independent of the transport properties of the fluid.

The experiments of Dr. Berenson reported in this paper and in references [11 and 13] have confirmed the basic premise that the changes in the boiling process are indeed caused by hydrodynamic instabilities. These experiments have shown that the critical heat flux from a horizontal surface is indeed independent of the temperature. This fact was also demonstrated in the experiments recently reported by Stock in reference [17].

The conclusion which can be drawn from these results and which can be applied to the important problem of determining the critical heat flux in forced convection is that any analysis of this problem should focus the attention on the stability problem. We note here that there are *several* modes in which the instabilities can cause the system to reach the critical flux.

Professor Tribus and the writer are happy to see that the model proposed in references [14, 15, and 16] was useful in extending the analysis to the entire film-boiling region. They are also happy to see that the results predicted by equations (46) and (48) are in agreement with the experimental data tabulated in this paper.

In closing, the writer would like again to congratulate Dr. Berenson for obtaining the experimental data and for extending the analysis to the entire film-boiling region.

[3] Y. Y. Hsu and J. W. Westwater, "Approximate Theory for Film Boiling on Vertical Surfaces," *Chemical Engineering Progress* (Symposium Series), AIChE, Heat Transfer Conference, Storrs, Conn., August, 1959, vol. 56, pp. 15–24.

[4] General Engineering Laboratory, General Electric Company, Schenectady, N. Y.

[5] Numbers in brackets from [13 to 17] designate References at end of discussion.

References

13 P. J. Berenson, "Transitional Boiling Heat Flux," AIChE Preprint No. 18, Fourth National Heat Transfer Conference, Buffalo, N. Y., 1960.

14 N. Zuber, "On the Stability of Boiling Heat Transfer," ASME TRANS, vol. 80, 1958, p. 711.

15 N. Zuber and M. Tribus, "Further Remarks on the Stability of Boiling Heat Transfer," AEC Report AECU 3631, U. S. AEC Technical Information Service, Oak Ridge, 1958.

16 N. Zuber, "Hydrodynamic Aspects of Boiling Heat Transfer," AEC Report AECU 4439, U.S. AEC Technical Information Service, Oak Ridge, 1959.

17 B. Stock, "Observation on Transitional Boiling Heat Transfer Phenomena," Argonne National Laboratory Report ANL 6175, 1960.

Author's Closure

The author wishes to thank both Drs. Yih-yun Hsu and Novak Zuber for their comments. As Dr. Hsu points out, the analysis only applies for laminar flow. Due to the small wavelengths i.e., flow path length, laminar flow probably exists in most practical cases. However, this should always be verified if there is any doubt.

The author wishes to take this opportunity to thank Dr. Zuber for his work on the stability of boiling heat transfer, which originally suggested the importance and application of Taylor-Helmholtz instability to boiling heat transfer. The one difference in interpretation of the application of the foregoing instability to boiling heat transfer lies in the selection of the wavelength. The author feels that while there is a range of visible wavelengths, the average value will always be close to the most unstable wavelength given by equation (24). The growth rate of the first critical wavelength given on the left-hand side of equation (45) is zero; therefore, it should never appear. The author once again thanks Dr. Zuber for his comments and contributions.

An Integral Treatment of Two-Phase Boundary Layer in Film Condensation

J. C. Y. KOH
Aero-Space Division,
Boeing Airplane Company,
Seattle, Wash.

By using the integral method, the task of solving the complicated two-phase boundary-layer differential equations in laminar-film condensation has been reduced to the simple work of solving an algebraic equation. It was shown analytically that the parameter $[(\rho\mu)_L/(\rho\mu)_v]^{1/3}$ can be removed from the film-condensation problem and hence only two parameters, $c_p\Delta T/h_{fg}$ and Pr, are involved. The calculated results in heat transfer and condensate flow rates agree very well with the results from the exact solution of the boundary-layer equations. With $[(\rho\mu)_v/(\rho\mu)_L]^{1/3}$ remaining as a parameter, it is believed that the present method can be used to solve the analogous two-phase boundary-layer problem in laminar film boiling.

Introduction

LAMINAR film condensation on a vertical plate was first analyzed by Nusselt [1][1] in 1916 by neglecting the acceleration terms and the nonlinear temperature distribution in the liquid film. Rohsenow [2] considered the nonlinear temperature distribution but continued to neglect the acceleration terms from the equation of motion. Sparrow and Gregg [3] treated the similar problem through the framework of boundary-layer theory. However, they neglected the drag force at the liquid vapor interface. Recently, Koh, Sparrow, and Hartnett [4] analyzed the film condensation problem by solving the complete liquid and vapor boundary-layer equations simultaneously. They found that for a liquid with large Prandtl number, or liquid with small Prandtl number but also small $c_p\Delta T/h_{fg}$, the interface drag exerted on the liquid by the vapor is negligibly small. However, for a low Prandtl number liquid and large $c_p\Delta T/h_{fg}$, the calculated heat transfer based on the assumption of negligibly small shear stress at the interface is too high by as much as 25 per cent. Surprisingly, they also found that the parameter $(\rho\mu)_L/(\rho\mu)_v$ does not have a significant effect on film condensation heat transfer. The purposes of this note are twofold:

1 To present some simplified equations through the integral method for the solution of the two-phase film-condensation problem.

2 To explain analytically that the parameter $(\rho\mu)_L/(\rho\mu)_v$ can be removed from the film-condensation heat-transfer calculation.

[1] Numbers in brackets designate References at end of paper.

Contributed by the Heat Transfer Division of THE AMERICAN SOCIETY OF MECHANICAL ENGINEERS., and presented at the Winter Annual Meeting, New York, N. Y., November 27–December 2, 1960, Manuscript received at ASME Headquarters, August 26, 1960. Paper No 60—WA-253.

Analysis

Fig. 1 is a sketch of the physical model and co-ordinate system. A vertical plate at a constant surface temperature T_w is suspended in a large volume of pure vapor at the saturation temperature T_s. We shall assume that at steady state there exists continuous laminar liquid and vapor layers, simultaneously. The integrated momentum equation for the liquid layer is as follows:

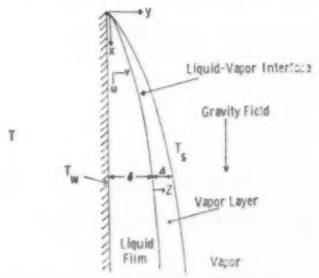

Fig. 1 Physical model and co-ordinate system

Nomenclature

a = coefficient for the liquid layer velocity profile
$c_L = \left[\frac{g}{4\nu_L^2}\frac{\rho_L - \rho_v}{\rho_L}\right]^{1/4}$
c_p = specific heat at constant pressure
$c_v = \left[\frac{g}{4\nu_v^2}\frac{\rho_L - \rho_v}{\rho_L}\right]^{1/4}$
g = acceleration due to gravity
h = local heat-transfer coefficient, $q/T_s - T_w$
h_{fg} = latent heat of condensation
K = coefficient for the temperature profile
k_L = thermal conductivity of liquid
M = local condensate flow rate
Nu_x = local Nusselt number, $\mathrm{Nu}_x = hx/k_L$
Pr = Prandtl number, $\mu_L C_p/k_L$
q = local heat-transfer rate per unit area
T = temperature
u = velocity component in x-direction
v = velocity component in y-direction
X_1, X_2 = defined in equations (6) and (7), respectively
x = co-ordinate measuring distance along plate from leading edge
y = co-ordinate measuring distance normal to plate
z = $y - \delta$
α = constant of proportionality, equations (3) and (12)
β = constant of proportionality equations (4) and (13)
δ = thickness of condensate layer
Δ = thickness of vapor boundary layer
μ = absolute viscosity
ν = kinematic viscosity
ρ = density

Subscripts

L = liquid
0 = at y or z equal to 0
s = saturated
v = vapor
w = wall
δ = at the liquid-vapor interface

$$\frac{d}{dx}\int_0^\delta u^2 dy - u_\delta \frac{d}{dx}\int_0^\delta u dy = \nu_L \left(\frac{\partial u}{\partial y}\right)_\delta - \nu_L \left(\frac{\partial u}{\partial y}\right)_0 + g\frac{\rho_L - \rho_v}{\rho_L}\delta \quad (1)$$

We shall assume the velocity profile to have the following form

$$\frac{u}{u_\delta} = a\left(\frac{y}{\delta}\right) - \frac{1}{2}\frac{g}{\nu_L}\frac{\rho_L - \rho_v}{\rho_L}\frac{\delta^2}{u_\delta}\left(\frac{y}{\delta}\right)^2 + \left(1 - a + \frac{1}{2}\frac{g}{\nu_L}\frac{\rho_L - \rho_v}{\rho_L}\frac{\delta^2}{u_\delta}\right)\left(\frac{y}{\delta}\right)^3 \quad (2)$$

Notice the foregoing equation satisfies the following conditions: at $y = 0$, $u = 0$, and $\nu_L\left(\frac{\partial^2 y}{\partial y^2}\right)_0 = -g\frac{\rho_L - \rho_v}{\rho_L}$; at $y = \delta$, $u = u_\delta$. We shall assume that u_δ and δ take the following forms:

$$u_\delta = 4\alpha_L \nu_L c_L^2 x^{1/2} \quad (3)$$

$$\delta = \beta_L \frac{1}{c_L} x^{1/4} \quad (4)$$

If equation (2) is substituted into equation (1) and the integration and differentiation are carried out, we get

$$a = \frac{1}{2}\left(X_1 + \sqrt{X_1^2 - X_2^2}\right) \quad (5)$$

where

$$X_1 = \frac{15}{32} + \frac{11}{32}\frac{\beta_L^2}{\alpha_L} - \frac{63}{8}\frac{1}{\alpha_L \beta_L^2} \quad (6)$$

$$X_2^2 = \frac{3}{8} + \frac{63}{4}\frac{1}{\alpha_L^2} + \frac{63}{2}\frac{1}{\alpha_L \beta_L^2} - \frac{1}{16}\frac{\beta_L}{\alpha_L}\left(1 + 2\frac{\beta_L^2}{\alpha_L}\right) \quad (7)$$

The integral momentum equation for the vapor layer can be written as follows:

$$\frac{d}{dx}\int_\delta^{\delta+\Delta} u^2 dy + u_\delta^2 \frac{d\delta}{dx} - u_\delta v_\delta = -\nu_v \left(\frac{\partial u}{\partial y}\right)_\delta \quad (8)$$

Using the boundary condition $\left(\rho v_\delta - \rho u_\delta \frac{d\delta}{dx}\right)_L = \left(\rho v_\delta - \rho u_\delta \frac{d\delta}{dx}\right)_v$ and the liquid layer velocity profile, equation (2), it is easy to find that

$$\left(\rho u_\delta \frac{d\delta}{dx} - \rho v\right)_v = \left(\rho \frac{d}{dx}\int_0^\delta u dy\right)_L = \frac{3}{4}\alpha_L \beta_L c_L \rho_L \nu_L x^{-1/4}\left(a + 1 - \frac{1}{6}\frac{\beta_L^2}{\alpha_L}\right) \quad (9)$$

Hence the integral equation (8) becomes:

$$\frac{d}{dx}\int_0^\Delta u^2 dz + u_\delta \frac{1}{\rho_v}\left[\frac{3}{4}\alpha_L \beta_L c_L \rho_L \nu_L x^{-1/4}\left(a + 1 - \frac{\beta_L^2}{6\alpha_L}\right)\right] + \nu_v\left(\frac{\partial u}{\partial z}\right)_0 = 0 \quad (10)$$

We shall assume that the velocity profile, interface velocity, and vapor layer thickness take the following forms:

$$\frac{u}{u_\delta} = 1 - 2\frac{z}{\Delta} + \left(\frac{z}{\Delta}\right)^2 \quad (11)$$

$$u_\delta = 4\alpha_v \nu_v c_v^2 x^{1/2} \quad (12)$$

$$\Delta = \beta_v \frac{1}{c_v} x^{1/4} \quad (13)$$

If the relations of equations (11) to (13) are substituted into equation (10), one gets

$$\frac{3}{4}\left(\frac{\alpha_L}{\alpha_v}\right)^2 \frac{\beta_L}{\beta_v}\left(\frac{c_L}{c_v}\right)^3 \left(\frac{\nu_L}{\nu_v}\right)^2 \frac{\rho_L}{\rho_v}\left(a + 1 - \frac{1}{6}\frac{\beta_L^2}{\alpha_v}\right) - \frac{2}{\alpha_v \beta_v^2} + 1 = 0 \quad (14)$$

Using the definitions of c_L and c_v, and the boundary condition $(u_\delta)_L = (u_\delta)_v$, it is found that

$$\left(\frac{c_L}{c_v}\right)^3 \left(\frac{\nu_L}{\nu_v}\right)^2 \left(\frac{\rho_L}{\rho_v}\right) = \sqrt{\frac{(\rho\mu)_L}{(\rho\mu)_v}} \quad (15)$$

$$\alpha_L = \alpha_v \quad (16)$$

Hence equation (14) can be solved for β_v to get

$$\beta_v = \frac{3}{8}\beta_L \sqrt{\frac{(\rho\mu)_L}{(\rho\mu)_v}}\left(a + 1 - \frac{1}{6}\frac{\beta^2_L}{\alpha_L}\right)\left[-1 + \sqrt{1 + \frac{8/\alpha_v}{\left\{\frac{3}{4}\beta_L \sqrt{\frac{(\rho\mu)_L}{(\rho\mu)_v}}\left(a + 1 - \frac{1}{6}\frac{\beta_L}{\alpha_v}\right)\right\}^2}}\right] \quad (17)$$

In condensation problems, the last term under the square root of equation (17) is much less than one. Thus, by binomial expansion, β_v can be correctly expressed by the following equation:

$$\beta_v = \frac{8}{3}\frac{1}{\alpha_L \beta_L}\frac{1}{\sqrt{\frac{(\rho\mu)_L}{(\rho\mu)_v}}\left(a + 1 - \frac{1}{6}\frac{\beta_L^2}{\alpha_L}\right)} \quad (18)$$

By substituting the velocity profiles for both liquid and vapor into the boundary condition $\left(\mu\frac{\partial u}{\partial y}\right)_L = \left(\mu\frac{\partial u}{\partial y}\right)_v$ at interface, one gets another expression for β_v:

$$\beta_v = \frac{\beta_L}{\sqrt{\frac{(\rho\mu)_L}{(\rho\mu)_v}}\left(2a - 3 - \frac{1}{2}\frac{\beta_L^2}{\alpha_L}\right)} \quad (19)$$

Equating equations (18) and (19), one gets

$$a = \frac{24 + 4\frac{\beta_L^2}{\alpha_L} + 3\alpha_L \beta_L^2 - \frac{1}{2}\beta_L^4}{16 - 3\alpha_L \beta_L^2}$$

Hence the parameter $\sqrt{\frac{(\rho\mu)_L}{(\rho\mu)_v}}$ cancels each other [see equations (18) and (19)] and does not appear in the condensation problem. This explains the numerical results of reference [4] that this parameter does not have a significant effect on condensation heat transfer. The combination of equations (5) and (19) gives

$$\frac{1}{2}\left(X_1 + \sqrt{X_1^2 + X_2^2}\right) = \frac{24 + 4\frac{\beta_L^2}{\alpha_L} + 3\alpha_L \beta_L^2 - \frac{1}{2}\beta_L^4}{16 - 3\alpha_L \beta_L^2} \quad (20)$$

Where X_1 and X_2 are functions of α_L and β_L as defined in equations (6) and (7).

As shown in reference [3], the liquid layer thickness δ (and hence β_L) is related to the physical quantity $c_p \Delta T / h_{fg}$ and can be considered as a parameter and, consequently, equation (20) allows us to determine α_L (and hence u_δ) for any given β_L (and hence $c_p \Delta T / h_{fg}$). Once α_L is found, the heat transfer can be found by solving the energy equation. The integrated energy equation can be written as follows:

$$\frac{d}{dx}\int_0^\delta u(T - T_s)dy = \frac{k_L}{\rho_L c_p}\left[\left(\frac{\partial T}{\partial y}\right)_\delta - \left(\frac{\partial T}{\partial y}\right)_s\right] \quad (21)$$

Assume that the temperature profile has the following form:

$$\theta = \frac{T - T_s}{T_w - T_s} = 1 + \left(K - \frac{3}{2}\right)\left(\frac{y}{\delta}\right) + \left(\frac{1}{2} - K\right)\left(\frac{y}{\delta}\right)^3 \quad (22)$$

Notice that the foregoing temperature profile satisfies the boundary conditions $\theta = 1$ and $\frac{\partial^2\theta}{\partial y^2} = 0$ at $y = 0$; and $\theta = 0$ at $y = \delta$.

We can now substitute equations (2) and (22) into equation (21) to get the following equation for the computation of K

$$K = \frac{\frac{1}{2}\frac{1}{\mathrm{Pr}}\frac{1}{\alpha_L\beta_L^2} - \frac{17}{140} + \frac{3a}{140} + \frac{17}{1680}\frac{\beta_L^2}{\alpha_L}}{\frac{2}{35} + \frac{8}{105}a - \frac{11}{840}\frac{\beta_L^2}{\alpha_L} + \frac{1}{\mathrm{Pr}}\frac{1}{\alpha_L\beta_L^2}} \quad (23)$$

The energy balance at the interface, $k_L\left(\frac{\partial T}{\partial y}\right)_\delta = \rho_L h_{fg}\frac{d}{dx}\int_0^\delta udy$ provides the following expression for $\frac{c_p\Delta T}{h_{fg}}$:

$$\frac{c_p\Delta T}{h_{fg}} = \frac{3}{8}\mathrm{Pr}\frac{\alpha_L\beta_L^2}{K}\left(a + 1 - \frac{1}{6}\frac{\beta_L^2}{\alpha_L}\right) \quad (24)$$

The heat transfer from the liquid film to the wall can be calculated by the following equation

$$\mathrm{Nu}_x\left[\frac{4\rho_L\nu_L^2}{g(\rho_L - \rho_v)x^3}\right]^{1/4} = \frac{1}{\beta_L}\left(\frac{3}{2} - K\right) \quad (25)$$

The condensate flow rate, $M = \int_0^\delta \rho_L\, udy$, can be calculated from

$$\frac{M}{\rho_L\nu_L c_L x^{3/4}} = \alpha_L\beta_L\left(a + 1 - \frac{1}{6}\frac{\beta_L^2}{\alpha_L}\right) \quad (26)$$

Hence, for any prescribed β_L, one can determine α_L from equation (20). For any given Prandtl number, one can then calculate K, $c_p\Delta T/h_{fg}$, heat transfer, and condensate flow rate from equations (23), (24), (25), and (26), respectively. This will enable us to construct graphs of heat transfer and condensate flow rates as a function of $c_p\Delta T/h_{fg}$ with the Prandtl number of the liquid as a parameter.

Results

The results of heat-transfer and condensate flow rates at various $c_p\Delta T/h_{fg}$ with Prandtl number as a parameter are shown in Figs. 2(*a*), 2(*b*), and 3(*a*), 3(*b*), respectively. The corresponding values from the exact solution of the boundary-layer equations as reported in reference [4] are also shown in the figures for comparison. It is seen from these figures that the results of the simplified calculation agree with the exact solution very well. The maximum deviation between the present results and that of reference [4] is about 5 per cent. Since the governing equations for film boiling heat-transfer calculation are identical to those reported in this note except that $(\rho\mu)_L/(\rho\mu)_v$ is replaced by $(\rho\mu)_v/(\rho\mu)_L$ for the boiling case, it is believed that the present method can be used for the film boiling heat-transfer calculation. Since $(\rho\mu)^*/(\rho\mu)_L$ is much less than one, it is expected that this parameter would play an important role in the film-boiling heat transfer.

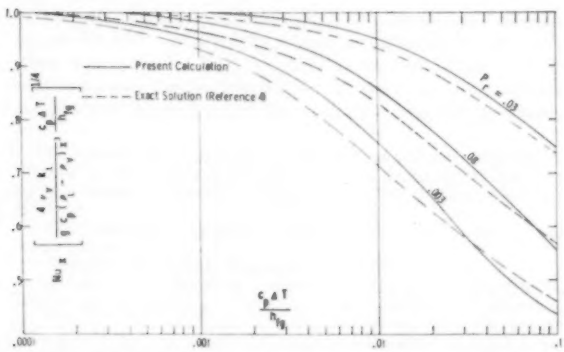

Fig. 2(*a*) Local heat-transfer results (low Prandtl number)

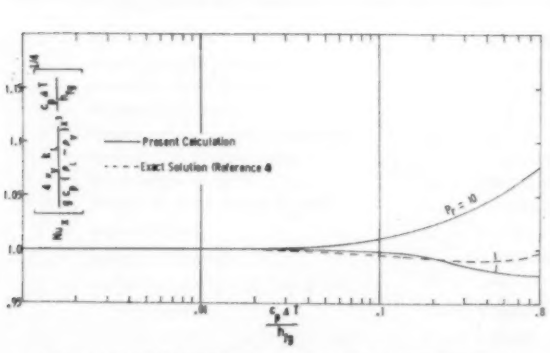

Fig. 2(*b*) Local heat-transfer results (high Prandtl number)

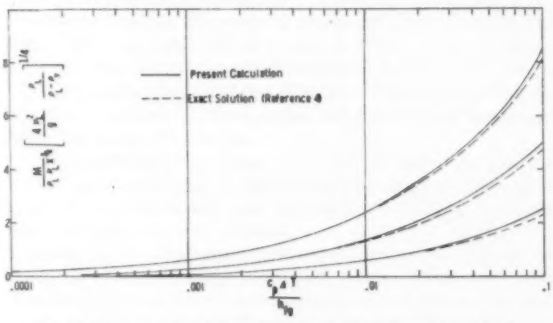

Fig. 3(*a*) Local condensate flow results (low Prandtl number)

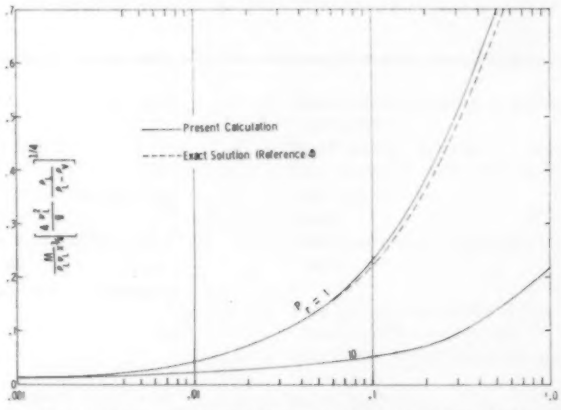

Fig. 3(*b*) Local condensate flow results (high Prandtl number)

Acknowledgment

The author wishes to acknowledge his appreciation to Mrs. Donna Firth and Mr. John Hughes for their help in the numerical calculation.

References

1 W. Nusselt, "Die Oberflachen Kondensation des Wasserdampfes," *Zeitschrift des Vereins deutscher Ingenieure*, vol. 60, 1916, pp. 541 and 569.

2 W. M. Rohsenow, "Heat Transfer and Temperature Distribution in Laminar-Film Condensation," TRANS. ASME, vol. 78, 1956, pp. 1645–1648.

3 E. M. Sparrow and J. L. Gregg, "A Boundary-Layer Treatment of Laminar-Film Condensation," JOURNAL OF HEAT TRANSFER, TRANS. ASME, Series C, vol. 81, 1959, pp. 13–18.

4 C. Y. Koh, E. M. Sparrow, and J. P. Hartnett, "The Two-Phase Boundary Layer in Laminar-Film Condensation," to be published in the *International Journal of Heat and Mass Transfer*.

G. B. WALLIS[2]
Research Fellow, Atomic Energy Establishment, Dorchester, England

J. H. HEASLEY[3]
Senior Engineer, Dynatech Corporation, Cambridge, Mass.

Oscillations in Two-Phase Flow Systems[1]

This paper contains a mathematical analysis of three modes of oscillation of a simple two-phase flow, natural-circulation system, together with qualitative results of experiments with a small-scale loop model.

Introduction

In recent years the problem of oscillations in boiler tubes, natural-circulation loops, and two-phase flow chemical systems has become of great interest to engineers. Experiments have been performed and results are available in the literature, but there is still a shortage of adequate theoretical understanding of the phenomena.

Often, the onset of oscillations represents the limit of operating conditions for a given system. Several rules of thumb are available for precautions which should be taken in the design of such systems and for the kinds of modification to a given setup which will tend to cure the instability. What is now needed is a logical theoretical basis for the prediction of system performance in advance and for systematic optimization of the various parameters.

The problem is not a simple one. Even steady-state theoretical predictions of two-phase flows are still inadequate for many design purposes.

What we attempt to do in this paper is to present mathematical models for a few of the common types of oscillation found in two-phase flow systems. The analysis was originally derived in the course of consulting work to explain the behavior of a particular experimental apparatus and has no claim to complete generality, although it is felt that similar procedures could be applied to different systems.

The basic approach is to consider the loop as a dynamic system of nonlinear time delays, storage elements, and resistances. Standard methods of control-theory analysis can then be applied to predict the onset of instabilities.

Previously, the greatest difficulty has been the analysis of the dynamic response of the heated section. The usual approach has been to write the partial differential flow equations in Eulerian form, specify the boundary conditions, and use a method of small perturbations to linearize the problem. Engineering approximations or "lumping" procedures are often employed and can give good results in some cases.

If the same problem is formulated in Lagrangian terms, it is found that the usual trouble experienced with mixed partial differential equations in space and time co-ordinates can be overcome by expressing the position of a fluid particle in terms of a "residence time" in the parts of the system and integrals over time. This approach was first used in 1728 by John Bernoulli [1],[4] who was led to a study of difference-differential equations [2]. The integral formulation has the virtue of including the boundary conditions in the equation and showing the "cause-and-effect" nature of the problem.

The equations are nonlinear. A small perturbation technique is used to obtain tractable operational expressions and a Nyquist locus [3, 4] technique is used to investigate stability whenever simple criteria cannot be derived.

Apart from the mathematics, attempts are made to explain the mechanism for oscillations in physical terms. These qualitative descriptions are borne out by experience with a simple glass loop which was constructed at Microtech Research. The design and operation of the loop is described in a later section.

[1] This work was performed for Bettis Atomic Power Laboratory, Pittsburgh, Pa., operated for the U. S. Atomic Energy Commission by Westinghouse Electric Corporation under Contract AT-11-1-GEN-14.

[2] Formerly, Senior Engineer, Microtech Research Company, Cambridge, Mass.

[3] Formerly, Microtech Research Company.

Contributed by the Heat Transfer Division and presented at the Winter Annual Meeting, New York, N. Y., November 27–December 2, 1960, of The American Society of Mechanical Engineers. Manuscript received at ASME Headquarters, August 22, 1960. Paper No. 60—WA-209.

[4] Numbers in brackets designate References at end of paper.

Nomenclature

A = flow area
A_h = pipe-flow area of heater
A_r = pipe-flow area of riser
H = heater-tube length
h = heater axial spatial co-ordinate
h_{fg} = enthalpy of vaporization
L = total length of riser
l = height at some point in riser
M = loop inertia
P_h = heater perimeter
Q_f = volume rate of liquid flow to riser from heater
Q_g = volume rate of gas flow to riser from heater
s = perturbation exponent
T = residence time in riser for fluid just leaving
T_0 = value of t_0 at $h = H$
t = time
t_b = time to remove subcooling from entering liquid
t_0 = time a given fluid particle starts evaporating
t_{tr} = $t - t_0$, transit time of evaporating fluid
V = velocity
$\mathcal{V}$ = volume
V_b = bubble rise velocity relative to water velocity in slug
V_g = bubble absolute velocity
$V_0(t)$ = liquid velocity at entry to heater at time t
v_f = liquid specific volume
v_{fg} = vaporization specific volume
W = mass-flow rate
x = quality
y = length to end of subcooled region
z = $h - y$
α = $P_h \phi v_{fg} / A_h h_{fg}$, parameter characteristic of heated section
Δ = symbol for perturbations or increment
ϕ = heater heat flux
ρ = density
ρ_f = density of liquid

It is hoped that this work will provide food for thought and progress in the study of two-phase flow oscillations.

No attempt has been made to explain oscillatory behavior which is a result of flow-regime transitions. The mechanism in this latter case is probably the interchange of energy between the two flowing phases.

It should be stressed that any analysis of this kind must be based on the dynamic response of system components. This implies the introduction of control-theory concepts, such as transfer functions, which are frequency dependent. Steady-state results only predict stability criteria for zero frequency disturbances and may be quite misleading if applied to general stability analysis.

Pentane Natural-Circulation Loop

The model which was used for the qualitative study of oscillations is shown in Fig. 1. The construction materials were glass and Tygon tubing throughout. Pentane was chosen as a working fluid because of its low boiling point at atmospheric pressure, 97 deg F. Glass stopcocks were used to control the flow rate and provide flow restrictions at several points in the loop.

Heat is supplied to the boiling section by forced convection using hot water; the vapor is condensed with cold water. The arrangement of heater, riser, condenser, pressurizer, and control valve is typical of similar research devices elsewhere.

The model does not represent fully the behavior of a typical high-pressure boiler loop for several reasons. Heat flux is not constant in the model, being a function of pentane velocity. In addition, there is the possibility of flashing occurring in the riser as the liquid head drops. Nevertheless, it was remarkable how well the loop demonstrated the types of oscillations analyzed for a constant heat flux and constant-pressure system.

Oscillations Due to Changes in Riser Buoyancy

Description. The first mode of oscillation which we shall consider is that in which cyclic variations of vapor content in a long riser cause periodic fluctuations in the loop flow rate. The riser acts essentially as a buoyancy capacitance with time delay while the rest of the loop contributes frictional and inertia terms.

This kind of oscillation is likely to predominate when a long, large-diameter riser is used with a short, small-diameter heated section. In this case the response of the heater to a disturbance in flow rate is rapid compared with the period of loop oscillations. Steady-state results may be used to describe the conditions in the single-phase part of the loop and in the heated section while the dynamic transients in the riser have to be considered in detail. There is no buoyancy term associated with the condenser or vapor separator. It is assumed that pressure drops in the elements of the loop are so low compared with the absolute pressure that compressibility effects and changes in fluid properties can be ignored.

A sketch of the heater and riser is shown in Fig. 2.

Analysis. Let boiling start at a distance y up the heated section. The flow rates of vapor and liquid leaving the heated section are then given by the equations

$$Q_g = \frac{P_h \phi v_g}{h_{fg}} (H - y) = \frac{v_g \alpha}{v_{fg}} (H - y) A_h \tag{1}$$

$$Q_f = \left[W - \frac{A_h \alpha}{v_{fg}} (H - y) \right] v_f \tag{2}$$

For constant subcooling at entry to the heated section and constant heat flux, any given fluid particle will take some constant time t_h to start evaporation (i.e., to lose subcooling):

$$\therefore y = V_b t_h \tag{3}$$

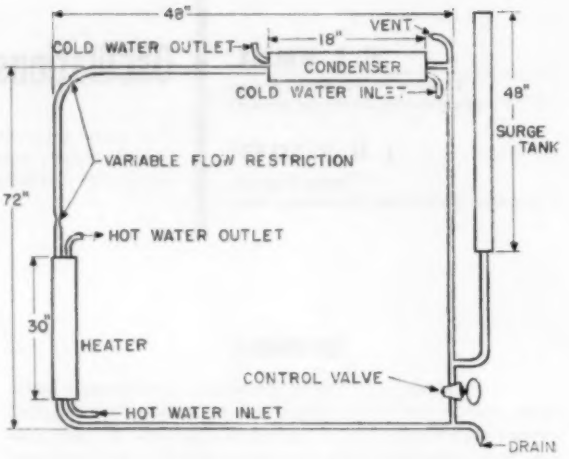

Fig. 1 Pentane natural-circulation loop

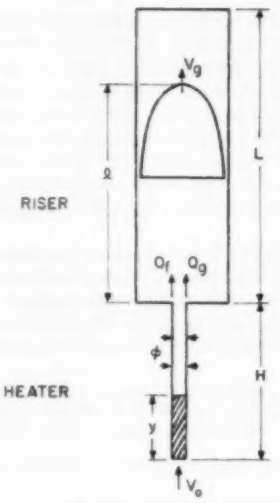

Fig. 2 Heater and riser

The time spent by the gas in the riser is given implicitly by the equation

$$L = \int_{t-T}^{t} V_g(t) dt \tag{4}$$

where T is the residence time in the riser for vapor which is just leaving at $l = L$ and V_g is the gas velocity in the riser. In general, V_g will be some function of Q_g and Q_f.

A long vertical tube in which a mixture of phases is flowing at low velocity provides ideal conditions for the development of "slug flow." For this example it is assumed that the equations derived by Griffith and Wallis [5] for slug flow apply to the riser, in which case

$$V_g = V_b + \frac{Q_f + Q_g}{A_r} \tag{5}$$

where V_b is the bubble velocity for slug flow.

The total vapor volume in the riser is given by the equation

$$G = \int_{t-T}^{t} Q_g(t) dt \tag{6}$$

From (1), (2), and (5) we can calculate V_g:

$$V_g = V_b + \frac{A_h v_g \alpha (H - y)/v_{fg} + v_f [W - A_h \alpha (H - y)/v_{fg}]}{A_r} \tag{7}$$

Using (3) and substituting for W in terms of V_0 this becomes

$$V_g = V_b + \alpha H \frac{A_h}{A_r} + V_0 \frac{A_h}{A_r} (1 - \alpha t_b) \tag{8}$$

We are now in a position to calculate loop dynamics:

Pressure drop
around whole loop = 0

= acceleration term + friction term
− buoyancy term

$$= M \frac{dV_0}{dt} + f(V_0) - \frac{G}{A_r} (\rho_f - \rho_g) \tag{9}$$

The quantity M represents the unit of change of loop pressure drop per unit rate of change of inlet velocity to the test section and is calculated as described in the Appendix.

The term $f(V_0)$ is the total steady-state pressure drop in the loop, apart from the riser, as a function of throughput velocity with the other parameters remaining constant. It is essentially a friction term, but also incorporates the effect of buoyancy variations in the heated section.

From (3), (6), and (1),

$$G = \int_{t-T}^{t} \frac{v_g \alpha}{v_{fg}} (H - V_0 t_b) A_h dt \tag{10}$$

In steady state $(dV_0/dt) = 0$, and V_0 and V_g are constant. Thus we have, from (4) and (8),

$$L = T \left[V_b + \alpha H \frac{A_h}{A_r} + V_0 \frac{A_h}{A_r} (1 - \alpha t_b) \right] \tag{11}$$

and hence the value of T.

Consider a small perturbation ΔV_0 in the inlet velocity to the heated section. Equation (9) becomes

$$M \frac{d\Delta V_0}{dt} + \frac{\partial f}{\partial V_0} \Delta V_0 - \Delta G \frac{(\rho_f - \rho_g)}{A_r} = 0 \tag{12}$$

For a given loop $(\partial f/\partial V_0)$ may be obtained from friction-factor data or experimental results at the particular operating point.

The perturbed form of (10) is

$$\Delta G = \Delta T \left[\frac{v_g \alpha}{v_{fg}} (H - V_0 t_b) A_h \right] - \int_{t-T}^{t} \frac{v_g \alpha}{v_{fg}} t_b A_h \Delta V_0 dt \tag{13}$$

and the perturbed form of (11) obtained from (4) and (8),

$$\Delta L = 0 = \Delta T V_g + \frac{A_h}{A_r} (1 - \alpha t_b) \int_{t-T}^{t} \Delta V_0 dt \tag{14}$$

Eliminating ΔG and ΔT from (12), (13), and (14), we eventually obtain an equation in ΔV_0 alone.

$$M \frac{d\Delta V_0}{dt} + \frac{\partial f}{\partial V_0} \Delta V_0 + \beta \int_{t-T}^{t} \Delta V_0 dt = 0 \tag{15}$$

with

$$\beta = \frac{(\rho_f - \rho_g)}{A_r} \left[\frac{\alpha v_g (H - V_0 t_b) A_h^2 (1 - \alpha t_b)}{v_{fg} A_r V_g} + \frac{v_g}{v_{fg}} \alpha t_b A_h \right] \tag{16}$$

Equation (15) may be investigated for stability by putting $\Delta V_0 = \epsilon e^{st}$; thus,

$$\left[Ms + \frac{\partial f}{\partial V_0} + \frac{\beta}{s} (1 - e^{-sT}) \right] \epsilon e^{st} = 0 \tag{17}$$

The system is unstable if the roots of equation (17) for s have positive real parts.

For the limiting case, s will be pure imaginary. In that case let $s = i\omega$ and equate real and imaginary parts of (17) to zero

$$-M\omega^2 + \beta(1 - \cos \omega T) = 0 \tag{18}$$

$$\frac{\partial f}{\partial V_0} \omega + \beta \sin \omega T = 0 \tag{19}$$

If now, equation (18) is solved for ω and the result substituted in (19), we have a criterion for $(\partial f/\partial V_0)$ which the loop must satisfy for marginal stability. Higher values of $(\partial f/\partial V_0)$ increase the system damping and hence, the stability.

This kind of oscillation was observed in the pentane loop when flow restrictions were reduced to a minimum and the main control valve was wide open. The cyclic variations of vapor build-up and flow rate were clearly seen, as well as the phase lag between them. Periods for this type of oscillation were in the neighborhood of 10 sec and are, in general, of the order of the transit time of the vapor in the riser.

Oscillations Excited by the Heated Section

Heated-Section Dynamics. The heated section has complex dynamic characteristics, including the effects of time delay, acceleration, friction, and buoyancy. The first step in considering oscillations which have their origin in the heated section is to write the equations describing the physical phenomena occurring there. In this chapter the behavior of the heated section is described mathematically. Application to the stability of a natural-circulation loop and the problem of "chugging" in boiler tubes are then considered.

Analysis. Consider the straight, vertical, constant-area heater tube shown in Fig. 3. It is assumed that the tube is operating with steady, uniform heat flux and that the slip velocity between the phases is negligible. In general, the inlet liquid will be subcooled and in this analysis we shall assume that subcooling is constant.

For a high-pressure system local changes in pressure will have a negligible effect on the fluid properties.

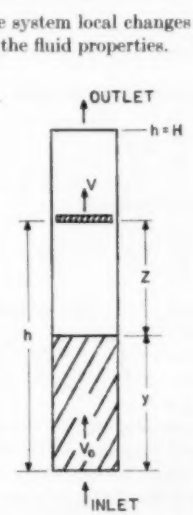

Fig. 3 Heated section

Let boiling start at a distance y up the tube. A fluid particle takes a given time t_b to lose subcooling. Thus, if V_0 varies with time,

$$y(t) = \int_{t-t_b}^{t} V_0(\tau)d\tau \tag{20}$$

Consider an element of fluid of mass m which is flowing up the heater and boiling:

$$\text{Volume of element} = m(v_f + xv_{fg}) = \mathcal{V} \text{ cu ft}$$

$$\text{Evaporation rate} = \phi \frac{\mathcal{V}}{A_h} \frac{P_h}{h_{fg}} \text{ lb/hr}$$

$$\therefore \frac{dx}{dt} = \frac{\text{evaporation rate}}{m}$$

$$= \frac{\phi P_h}{A_h h_{fg}} (v_f + xv_{fg})$$

$$= \alpha \left(\frac{v_f}{v_{fg}} + x \right) \tag{21}$$

where

$$\alpha = P_h \phi v_{fg} / A_h h_{fg}$$

Equation (21) can be integrated to give

$$x(t, t_0) = \frac{v_f}{v_{fg}} [e^{\alpha(t-t_0)} - 1] \tag{22}$$

where t_0 is defined as the time at which x is zero; i.e., at $z = 0$. In fact, t_0 is the time at which a given fluid element starts to evaporate and may be treated as a parameter identifying that fluid element.

Let z be the co-ordinate of a fluid particle at time t.

Consider a control volume of fixed length z' with its lower boundary moving with the interface at y and with z' chosen so that $z = z'$ at time t:

$$\text{Volume flow into control volume} = A_h \left(V_0 - \frac{dy}{dt} \right)$$

$$\text{Volume flow out} = A_h \frac{dz}{dt}$$

$$\text{Volume generated by boiling} = A_h \alpha z' = A_h \alpha z$$

From a volume balance for incompressible flow,

$$\frac{dz}{dt} = V_0 - \frac{dy}{dt} + \alpha z \tag{23}$$

Substituting equation (20) gives

$$\frac{dz}{dt} = \alpha z + V_0(t - t_b) \tag{24}$$

The solution to equation (24) in integral form is

$$z(t, t_0) = e^{\alpha t} \int_{t_0}^{t} e^{-\alpha \tau} V_0(\tau - t_b)d\tau \tag{25}$$

where again $z = 0$ at $t = t_0$.

At any time t, the position, quality, velocity, and acceleration of a given fluid element may now be calculated in terms of the parameter t_0 and functions of V_0. From these values the frictional, acceleration, and gravitational pressure drops can be computed. For example:

Fluid velocity at h

$$V = \frac{\partial y}{\partial t} + \frac{\partial z}{\partial t}$$

From (23)

$$V = \alpha z + V_0(t) \tag{26a}$$

$$\therefore V = \alpha h - \alpha y + V_0(t) \tag{26b}$$

From (20)

$$V = \alpha h - \alpha \int_{t-t_b}^{t} V_0(\tau)d\tau + V_0(t) \tag{26c}$$

Fluid acceleration at h

$$= \frac{\partial^2 y}{\partial t^2} + \frac{\partial^2 z}{\partial t^2}$$

From (26a) and (24)

$$= \alpha^2 z + \alpha V_0(t - t_b) + \frac{dV_0(t)}{dt} \tag{27a}$$

From (20)

$$= \alpha^2 h - \alpha^2 \int_{t-t_b}^{t} V_0(\tau)d\tau + \alpha V_0(t - t_b) + \frac{dV_0(t)}{dt} \tag{27b}$$

and from (22)

$$\rho(t, t_0) = \rho_f e^{-\alpha(t-t_0)} \tag{28}$$

For the fluid which is just leaving the tube $h = H$; from (20) and (25)

$$H = y + z = \int_{t-t_b}^{t} V_0(\tau)d\tau + e^{\alpha t} \int_{T_0}^{t} e^{-\alpha \tau} V_0(\tau - t_b)d\tau \tag{29}$$

where T_0 is the value of t_0 for $h = H$. This equation gives T_0 implicitly in terms of H.

The total pressure drop through the tube is given by the equation

$$\Delta P = \int_0^H \left\{ \frac{f\rho V^2}{2gD} + \frac{\rho}{g} \frac{dV}{dt} + \rho \right\} dh \tag{30}$$

where f is the appropriate friction factor.

At any given time t we can integrate over the variable t_0 by writing

$$dh = \left(\frac{\partial h}{\partial t_0} \right)_t dt_0 \tag{31}$$

Formulation of the equations for the heated-section dynamics is now essentially complete. The equations can be used to predict heated-section response to flow perturbations with the boundary conditions of the particular problem under consideration. One such problem is the pulsing of flow in boiler tubes; another the flow oscillations in a natural-circulation loop.

Loop-Flow Oscillations Caused by Heated-Section-Exit Pressure Drop. Equation (30) can be used as it stands, and in combination with equations describing the behavior of other elements in the loop, to derive criteria for the stability of a natural-circulation system. The resulting equations are rather complicated and the final stability criterion is not easy to interpret physically. There is also considerable doubt about what is actually meant by the "friction factor" which we have conveniently used up to now in the analysis. It is better in many cases to consider each particular system on its merits and to try to simplify the equations.

The following section describes a modified approach which was derived for a specific application in which most of the loop pres-

sure drop was associated with a constriction at the top of the heated section. The results also give an insight into a possible mechanism for oscillations, even without the presence of a constriction, since in many practical systems most of the pressure drop in the heated section occurs near the exit where velocities and shear stresses are high.

Under these circumstances the mechanism for oscillations is as follows: As the flow rate changes, vapor is accumulated in the heated section while the flow rate is low. This vapor "plug" gives rise to a decrease in pressure drop when it reaches the heater exit. An increase in flow rate results. The flow surge is stopped as new subcooled liquid flows up the heater and reduces the exit quality, while the exit velocity is still high.

The oscillation frequency is governed by the time taken by the heater to complete its thermal and hydrodynamic cycle.

Results of preliminary tests in the Microtech Research pentane loop also show that the effect of a constriction above the exit from the heated section is to induce instability. A piece of high-quality fluid passing through the constriction causes the pressure drop to decrease considerably. This increases the flow rate but there is a time lag before the quality at the constriction is affected. Instability can result.

The period of oscillations of this type is of the order of 1 to 2 sec and is, in general, approximately equal to the transit time in the heated section.

Mathematical Model and Assumptions. For a simplified model of the loop, we assume a flow constriction located at the end of the heated section. In deriving the dynamic equation for the loop, it is assumed that the change in friction drop in this constriction is the only driving force, and that this force acts on the inertia of the system.

Analysis. With the previous notation, consider a small perturbation in flow rate so that the inlet velocity to the heater may be written

$$V_0 + \epsilon e^{st} \tag{32}$$

From (20) and (25)

$$y = V_0 t_b + \epsilon e^{st} \cdot \frac{1}{s}(1 - e^{-st_b}) \tag{33}$$

$$z = \frac{V_0}{\alpha}\left[e^{\alpha t_{tr}} - 1\right] + \epsilon e^{st}\,\frac{e^{-st_b}}{(s-\alpha)}\left[1 - e^{(\alpha - s)t_{tr}}\right] \tag{34}$$

where $t_{tr} = t - t_0$ is the transit time from instant of evaporation to the point z for the fluid element now at z.

The velocity perturbation at a given h is calculated from (26c):

$$\Delta V = \left[-\frac{\alpha}{s}(1 - e^{-st_b}) + 1\right]\epsilon e^{st} \quad \text{for} \quad h > y \tag{35}$$

It is, in fact, constant along the tube.

The density perturbation is calculated from (28):

$$\Delta\rho = \rho_f e^{-\alpha t_{tr}}(-\alpha \Delta t_{tr}) = -\alpha\rho\Delta t_{tr} \tag{36}$$

The perturbed form of (29) at constant h is

$$\Delta h = 0 = \epsilon e^{st}\left[\frac{1 - e^{-st_b}}{s} + \frac{e^{-st_b}}{s-\alpha}\left(1 - e^{(\alpha - s)t_{tr}}\right)\right] + V_0 e^{\alpha t_{tr}}\Delta t_{tr} \tag{37}$$

Δt_{tr} may now be eliminated from (36) and (37) to give

$$\Delta\rho = \frac{\alpha\rho}{V_0 e^{\alpha t_{tr}}}\left[\frac{1 - e^{-st_b}}{s} + \frac{e^{-st_b}}{s-\alpha}\left(1 - e^{(\alpha - s)t_{tr}}\right)\right]\epsilon e^{st} \tag{38}$$

Let us now assume that the pressure drop at the exit varies as the product ρV^2 for small variations about the operating point. This is equivalent to assuming that the friction factor is a weak function of quality. At the exit $t_{tr} = T_{tr}$.

Denoting the steady-state two-phase exit pressure drop by F we have

$$\Delta F = F\left[\frac{\Delta\rho}{\rho} + \frac{2\Delta V}{V}\right] \tag{39}$$

$\Delta\rho$ and ΔV may now be eliminated with the use of (35) and (38) to yield

$$\Delta F = \frac{F}{V_0 e^{\alpha t_{tr}}}\left\{\alpha\left[\frac{1 - e^{-st_b}}{s} + \frac{e^{-st_b}}{s-\alpha}\left(1 - e^{(\alpha - s)T_{tr}}\right)\right] + 2\left[\frac{-\alpha}{s}(1 - e^{-st_b}) + 1\right]\right\}\epsilon e^{st} \tag{40}$$

$$= \frac{F}{V_0 e^{\alpha t_{tr}}}\left[\frac{\alpha e^{-st_b}}{s-\alpha}\left(1 - e^{(\alpha - s)T_{tr}}\right) - \frac{\alpha}{s}(1 - e^{-st_b}) + 2\right]\epsilon e^{st} \tag{41}$$

The dynamic equation for the loop is

$$Ms\epsilon e^{st} + \Delta F = 0 \tag{42}$$

where M is the equivalent loop inertia. Equation (42) may be written in the standard form

$$\left[1 + \frac{\Delta F}{Ms\epsilon e^{st}}\right]\epsilon e^{st} = 0 \tag{43}$$

The stability criterion is now derived from the study of the Nyquist locus of the transfer function [3, 4]:

$$Y(s) = \frac{\Delta F}{Ms\epsilon e^{st}} = \frac{F}{MV_0 e^{\alpha T_{tr}}}\left[\frac{\alpha e^{-st_b}}{s(s-\alpha)}\left(1 - e^{(\alpha - s)T_{tr}}\right) - \frac{\alpha}{s^2}(1 - e^{-st_b}) + \frac{2}{s}\right] \tag{44}$$

The Nyquist locus is a plot of $Y(i\omega)$ in the Argand diagram. In this diagram, a simple criterion of stability is that the locus should not enclose the point $(-1, 0)$ as ω takes on all real values. To plot the locus we have

$$Y(i\omega) = \frac{F}{MV_0 e^{\alpha T_{tr}}}\left[\frac{\alpha(i\alpha - \omega)}{\omega(\alpha^2 + \omega^2)}\,e^{-i\omega t_b}\left(1 - e^{\alpha T_{tr}}e^{-i\omega T_{tr}}\right) + \frac{\alpha}{\omega^2}(1 - e^{-i\omega t_b}) - \frac{2i}{\omega}\right] \tag{45}$$

If we write $Y = U + iV$, and separate real and imaginary parts, it is found after some algebra that

$$U = \frac{F}{MV_0 e^{\alpha T_{tr}}}\left\{\frac{\alpha}{\omega(\alpha^2 + \omega^2)}\left[(1 - e^{+\alpha T_{tr}}\cos\omega T_{tr})\right.\right.$$
$$\left.(-\omega\cos\omega t_b + \alpha\sin\omega t_b) - (\alpha\cos\omega t_b + \omega\sin\omega t_b)e^{\alpha T_{tr}}\sin\omega T_{tr}\right]$$
$$\left. + \frac{\alpha}{\omega^2}(1 - \cos\omega t_b)\right\} \tag{46}$$

$$V = \frac{F}{MV_0 e^{\alpha T_{tr}}}\left\{\frac{\alpha}{\omega(\alpha^2 + \omega^2)}\left[(1 - e^{\alpha T_{tr}}\cos\omega T_{tr})\right.\right.$$
$$\left.(\alpha\cos\omega t_b + \omega\sin\omega t_b) + e^{\alpha T_{tr}}\sin\omega T_{tr}(-\omega\cos\omega t_b + \alpha\sin\omega t_b)\right]$$
$$\left. + \frac{\alpha}{\omega^2}\sin\omega t_b - \frac{2}{\omega}\right\} \tag{47}$$

The equations look complicated but they may easily be solved by graphical means. Note that $V_0 e^{\alpha T_{tr}}$ is the exit velocity from the heated section. M is the loop inertia calculated as an equiva-

lent mass moving at the velocity V_0. The factor $F/(MV_0e^{\alpha T_{tr}})$ scales the size of the Nyquist locus. If F is increased, the locus increases in size and approaches instability. If the loop inertia is increased, the loop stability is increased. These results are intuitively reasonable since F represents an exciting force and M an inertia or inherent sluggishness of the loop.

The function

$$Y(i\omega)\,\frac{MV_0e^{\alpha T_{tr}}}{F}\ \text{sec}$$

is shown in Fig. 4 for the parameters of a typical natural-circulation loop. The predicted criterion for stability in this case, in which there was a large pressure difference associated with the exit end of the heated section, agreed well with experimental results.

In this particular case, instability is approached rapidly as the heat flux is increased. This is fortunate, since it enables a safe maximum operating heat flux to be designated within close tolerances.

Methods of Curing Oscillatory Behavior of This Kind. Since the Nyquist locus is scaled by the factor (F/MV_0), stability can be increased by the following three techniques:

1 Increase loop inertia.

2 Decrease the pressure drop associated with the heated section, and particularly the heated-section exit.

3 Increase the over-all throughput velocity by lowering the average friction factor. This means that the flow should be obstructed as little as possible.

Parallel Channel Oscillations

The equations developed in the preceding section may also be applied to the problem of chugging in boiler channels. A previous analysis of this system has been presented by Quandt [6], who was able to arrive at a solution by lumping techniques. The following analysis uses the Lagrangian method.

For this problem, the boundary condition is that the pressure drop across the heated section remain constant.

Equation (30) is written in perturbed form:

$$0 = \rho_f\left[\frac{gfV_0\Delta V_0}{gD} + \frac{y}{g}\frac{d\Delta V_0}{dt}\right] + \int_y^H \Delta\rho\left[1 + \frac{1}{g}\frac{dV}{dt} + \frac{fV^2}{2gD}\right]dh + \int_y^H \rho\left[\frac{fV\Delta V}{gD} + \frac{1}{g}\frac{\Delta dV}{dt}\right]dh \quad (48)$$

To evaluate the integrals we need the values of V, ρ, dV/dt, ΔV, $\Delta\rho$, $\Delta dV/dt$ at points along the tube:

V is given by (26c) or (26a)

$$V = \alpha h + V_0(1 - \alpha t_h) \quad (49)$$

$$= \alpha z + V_0 \quad (49a)$$

$$= V_0e^{\alpha t_{tr}} \text{ from (34)} \quad (49b)$$

ρ by (28) $\quad \rho = \rho_f e^{-\alpha t_{tr}}$ (50)

$$= \rho_f\left[1 + \frac{\alpha z}{V_0}\right]^{-1} \text{ from (34)} \quad (50a)$$

ΔV by (35) $\quad \Delta V = \left[-\frac{\alpha}{s}(1 - e^{-st_h}) + 1\right]\epsilon e^{st}$ (51)

$\Delta\rho$ by (28) and (38)

$$\Delta\rho = \frac{\alpha\rho_f}{V_0e^{2\alpha t_{tr}}}\left[\frac{1 - e^{-st_h}}{s} + \frac{e^{-st_h}}{s - \alpha}(1 - e^{(\alpha - s)t_{tr}})\right]\epsilon e^{st} \quad (52)$$

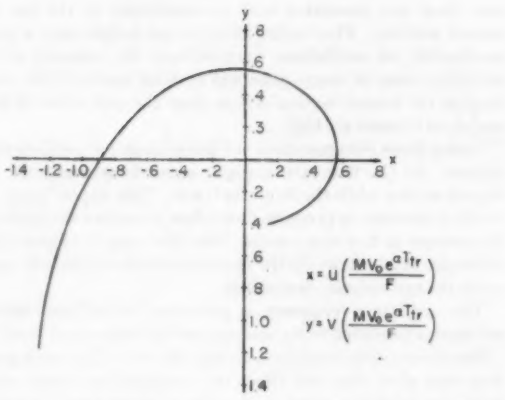

Fig. 4 Typical Nyquist locus for 1200-psia water loop $Y(i\omega)(MV_0e^{\alpha T_{tr}}/F)$ sec

$\frac{\Delta dV}{dt}$ by (27b)

$$\frac{\Delta dV}{dt} = \left[-\frac{\alpha^2}{s}(1 - e^{-st_h}) + \alpha e^{-st_h} + s\right]\epsilon e^{st} \quad (53)$$

$\frac{dV}{dt}$ by (27a)

$$\frac{dV}{dt} = \alpha V_0\,e^{\alpha t_{tr}} \quad (54)$$

Now, at any given time t, each particle may be described in terms of the variable t_{tr}. Hence integration over h may be transformed to integration over t_{tr} by means of the substitution

$$dh = \left(\frac{\partial h}{\partial t_{tr}}\right)_t dt_{tr} \quad (55)$$

which gives, from (33) and (34)

$$dh = (V_0e^{\alpha t_{tr}} + \text{small terms})dt_{tr}$$

$$= V_0e^{\alpha t_{tr}}dt_{tr} \quad (55a)$$

since the perturbation is assumed small.

The first integral appearing in (48) may now be evaluated

$$\int_y^H \Delta\rho\left(1 + \frac{1}{g}\frac{dV}{dt} + \frac{fV^2}{2gD}\right)dh = \epsilon e^{st}\alpha\rho_f\int_0^{T_{tr}}\left(1 + \frac{\alpha V_0}{g}e^{\alpha t_{tr}} + \frac{fV_0^2}{2gD}e^{2\alpha t_{tr}}\right)\left[\frac{1 - e^{-st_h}}{s} + \frac{e^{-st_h}}{(s - \alpha)}(1 - e^{(\alpha - s)t_{tr}})\right]e^{-\alpha t_{tr}}dt_{tr} \quad (56)$$

$$= \epsilon e^{st}\left[C_1\frac{(1 - e^{-st_h})}{s} + C_2\frac{e^{-st_h}}{(s - \alpha)} + C_3\frac{e^{-st_h}}{s(s - \alpha)}(e^{-sT_{tr}} - 1) + C_4\frac{e^{-st_h}(e^{(2\alpha - s)T_{tr}} - 1)}{(2\alpha - s)(s - \alpha)} + C_5\frac{e^{-st_h}}{(s - \alpha^2)}(e^{(\alpha - s)T_{tr}} - 1)\right] \quad (57)$$

For the second integral it is found easier to work in terms of z. Substitution from (49a), (50a), (51), and (53) yields

$$\int_y^H \rho \left(\frac{fV\Delta V}{gD} + \frac{1}{g} \frac{\Delta dV}{dt} \right) dh$$

$$= \epsilon e^{st} \int_0^{(H-y)} \frac{\rho_f}{\left(1 + \frac{\alpha z}{V_0}\right)} \left\{ \frac{f(\alpha z + V_0)}{gD} \left[1 - \frac{\alpha}{s} (1 - e^{-sl_h}) \right] \right.$$

$$\left. + \frac{1}{g} \left[\frac{-\alpha^2}{s} (1 - e^{-sl_h}) \right] + \alpha e^{-sl_h} + s \right\} dz \quad (58)$$

$$= \epsilon e^{st} \left[C_6 + C_7 e^{-sl_h} + C_8 s + \frac{C_9}{s} (1 - e^{-sl_h}) \right] \quad (59)$$

Equation (48) can now be put in the standard form

$$0 = [1 + Y(s)] \epsilon e^{st}$$

and the Nyquist locus drawn to investigate stability.

The form of the final transfer function is rather complex. In particular problems it may be possible to neglect some of the terms but in general there is no way of telling what kinds of approximation are justifiable. Once the calculation procedure is set up, the plotting of the Nyquist locus is a fairly simple matter.

Oscillations Caused by a Restriction at Top of Riser

Description. When a tight flow restriction is placed at the top of the riser so that the liquid in the upper horizontal leg cannot run back, a peculiar mode of oscillation is observed. The heater blows back strongly and circulation stops. The liquid in the riser runs back into the heater and evaporates.

The vapor, bubbling through the remaining liquid in the riser, escapes through the restriction to the condenser. The vapor volume in the system increases; the increase is taken up in the pressurizer. This continues until the riser is completely dry; then the liquid in the cold leg flows up through the heater; the boiling mixture enters the riser, and the cycle begins again. The period for this type of oscillation for the pentane loop averages about 2 min.

This type of oscillation graphically shows the effect of high pressure drop in the two-phase section of a natural-circulation system. During part of the cycle the driving head is at its maximum since the hot leg is all vapor, yet there is no circulation because the pressure drop at the restriction is so high.

APPENDIX

Consider a series of frictionless connected pipes of area A_i, length l_i, containing fluid of density ρ_i, moving with velocity V_i, across which the pressure drop is Δp_i.

For fluid acceleration in one pipe

$$\Delta p_i A_i = \frac{\rho_i A_i l_i}{g} \frac{dV_i}{dt} \quad (60)$$

For continuity of flow

$$\rho_i V_i A_i = \rho_h A_h V_h \quad (61)$$

where the h subscripts refer to heater inlet.

Elimination of V_i from (60) and (61) and summation over-all pipes yields

$$\sum \Delta p_i = \sum \frac{\rho_h A_h}{g} \frac{l_i}{A_i} \frac{dV_0}{dt} \quad (62)$$

$$\therefore M = \frac{\rho_h A_h}{g} \sum \frac{l_i}{A_i} \quad (63)$$

Acknowledgment

The authors are indebted to Westinghouse Electric Corporation for permission to publish results which were originally derived in the course of consulting work with them.

References

1 John Bernoulli, "Meditationes de Chordia Vibrantibis," *Academiae Scientiarum Imperialis Petropolitanae*, vol. 3, 1728.

2 Edmund Pinney, "Ordinary Difference-Differential Equations," University of California Press, Berkeley, Calif., 1958.

3 W. R. Evans, "Control-System Dynamics," McGraw-Hill Book Company, Inc., New York, N. Y., 1954.

4 R. H. Macmillan, "An Introduction to the Theory of Control in Mechanical Engineering," Cambridge University Press, Cambridge, England, 1951.

5 P. Griffith and G. B. Wallis, "Slug Flow," Technical Report No. 15, ONR 7-7673, Massachusetts Institute of Technology, Cambridge, Mass., May, 1959.

6 E. R. Quandt, Jr., "Analysis of Parallel Channel Transient Response and Flow Oscillations," WAPD-AD-TH-489, April, 1959.

Film Boiling in a Forced-Convection Boundary-Layer Flow

R. D. CESS[1]
Heat Transfer and Flow Section, Mechanics Department, Westinghouse Research Laboratories, Pittsburgh, Pa. Assoc. Mem. ASME

E. M. SPARROW
Professor of Mechanical Engineering, University of Minnesota, Minneapolis, Minn. Assoc. Mem. ASME

An analysis has been made to determine the heat transfer and friction characteristics in forced-convection film boiling on a flat plate. It is shown that the resulting two-phase flow problem can be formulated exactly within the framework of laminar boundary-layer theory. Solutions covering the parameter range of practical interest have been obtained by a combination analytical-numerical method. Heat-transfer and skin-friction results are presented both graphically and as simple, closed form analytical expressions. Relative to the case of pure liquid flow, the skin friction is substantially reduced due to film boiling. The heat transfer is found to increase as $(\Delta T)^{1/2}$, a much smaller dependence than in other convection phenomena.

Introduction

Previous analytical studies [1 to 5][2] of film boiling have been concerned with the situation where the fluid motion is generated by gravity forces and forced convection is absent. In the present analysis, consideration is given to film boiling in forced-convection boundary-layer flows where gravity forces are negligible. One example of where such a situation may arise is in the motion of a previously aerodynamically heated surface through water. In another application, film boiling is actually being considered as a means to reduce the drag experienced by bodies moving through liquids.

The physical situation which has been chosen for study here is the laminar boundary-layer flow over a flat plate as pictured in Fig. 1.[3] A stream of pure liquid approaches the plate. Under the influence of a sufficiently high surface temperature, film boiling occurs, and there thus coexist liquid and vapor boundary layers. The surface temperature will be taken to be uniform and the liquid is assumed to be saturated. Radiation heat transfer is neglected.

The two-phase flow problem just outlined can be formulated as an exact solution of the laminar boundary-layer equations. Accurate solutions covering the parameter range of potential interest have been obtained by a combined analytical-numerical method which circumvents the need for lengthy digital computer calculations.

The realities of film boiling may include such difficult-to-analyze factors as interfacial waviness and film instability. In common with prior boundary-layer studies of film boiling and condensation, it has been necessary to omit these factors in the present investigation.

Analysis

Conservation Equations and Boundary Conditions. The velocity and temperature distributions are governed by the basic principles of mass, momentum, and energy conservation. For the

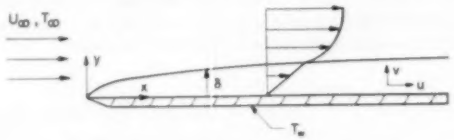

Fig. 1 Physical model and co-ordinate system

[1] Now, Associate Professor of Mechanical Engineering, North Carolina State College, Raleigh, N. C.

[2] Numbers in brackets designate References at end of paper.

[3] A contemporary but approximate analysis [11] of the present problem which deals with liquid water was discovered by the authors at the time of preprinting.

Contributed by the Heat Transfer Division and presented at the Winter Annual Meeting, New York, N. Y., November 27–December 2, 1960, of The American Society of Mechanical Engineers. Manuscript received at ASME Headquarters, August 1, 1960. Paper No. 60—WA-148.

Nomenclature

A = velocity derivative, $F'(0)$
c_p = specific heat at constant pressure
f = dimensionless vapor stream function, equation (6)
F = dimensionless liquid stream function, equation (7)
h = local heat-transfer coefficient, $q/(T_w - T_\infty)$
$\bar{h}$ = average heat-transfer coefficient, $Q/x(T_w - T_\infty)$
k = thermal conductivity of vapor
$\dot{m}$ = mass flow at interface
Nu = local Nusselt number, hx/k
Pr = Prandtl number, $c_p\mu/k$
Q = over-all heat-transfer rate
q = local heat-transfer rate per unit area
Re = Reynolds number, $U_\infty x/\nu_L$
T = static temperature; T_w, wall temperature; T_∞, free-stream temperature
U_∞ = free-stream velocity
u = velocity component in x-direction
v = velocity component in y-direction
x = co-ordinate measuring distance along plate from leading edge
y = co-ordinate measuring distance normal to plate
α = thermal diffusivity
β = integration constant
δ = thickness of vapor film
η = vapor similarity variable, equation (6)
η_δ = dimensionless vapor film thickness
θ = dimensionless temperature, $(T - T_\infty)/(T_w - T_\infty)$
μ = absolute viscosity
ν = kinematic viscosity
ξ = liquid similarity variable, equation (7)
ρ = density
τ = wall shear stress
ψ, Ψ = stream functions

Subscripts

L = liquid properties

vapor, which we will identify by *unsubscripted properties*, the boundary-layer form of the conservation laws is

$$\frac{\partial u}{\partial x} + \frac{\partial v}{\partial y} = 0 \tag{1}$$

$$u\frac{\partial u}{\partial x} + v\frac{\partial u}{\partial y} = \nu\frac{\partial^2 u}{\partial y^2} \tag{2}$$

$$u\frac{\partial T}{\partial x} + v\frac{\partial T}{\partial y} = \alpha\frac{\partial^2 T}{\partial y^2} \tag{3}$$

As written, these equations correspond to a constant property vapor. However, it is easy to show that for a variable property vapor characterized by: $\rho\mu$ = constant, ρk = constant, and Pr = constant, the final heat-transfer and skin-friction results are identical to those predicted by the constant property analysis. For simplicity, we will carry through the analysis for constant properties.

The liquid has been assumed to be at saturation. As a consequence, the liquid temperature is essentially constant and the energy equation need not be considered. The mass and momentum conservation equations as written in equations (1) and (2) also apply to the liquid, but now a subscript L is used to identify the properties of the liquid.

To complete the description of the problem, it is necessary to give the conditions of continuity at the liquid-vapor interface and the boundary conditions. At the interface between liquid and vapor, it is required that continuity be preserved for the following flow-connected quantities: (*a*) Tangential velocity; (*b*) tangential shear; (*c*) mass flow crossing interface.

In references [6 and 7], it has been shown that, within the limits of the boundary-layer assumptions, the continuity requirements on quantities (*a*), (*b*), and (*c*) are equivalent to imposing

$$u_{\text{liq}} = u_{\text{vap}} \tag{4a}$$

$$\mu_L\left(\frac{\partial u}{\partial y}\right)_{\text{liq}} = \mu\left(\frac{\partial u}{\partial y}\right)_{\text{vap}} \tag{4b}$$

$$\rho_L\left(u\frac{d\delta}{dx} - v\right)_{\text{liq}} = \rho\left(u\frac{d\delta}{dx} - v\right)_{\text{vap}} \tag{4c}$$

In addition, temperature continuity is also required at the interface, so

$$T = T_\infty \tag{4d}$$

Finally, the boundary conditions imposed at the plate surface and in the undisturbed flow are

$$y = 0\text{: } u = v = 0, \qquad T = T_w \tag{5a}$$

$$y \to \infty\text{: } u \to U_\infty \tag{5b}$$

These matching and boundary conditions, together with the conservation laws, provide a complete statement of the problem. Now, efforts can be directed toward rephrasing the governing equations into more tractable form and then finding solutions.

Similarity Transformation. To bring the problem into a more tractable form, we introduce a change of variables by means of a boundary-layer similarity transformation.

For the vapor film, the new variables are defined by

$$\eta = \frac{y}{2}\sqrt{\frac{U_\infty}{\nu x}}, \qquad f(\eta) = \frac{\psi}{\sqrt{\nu U_\infty x}}, \qquad \Theta(\eta) = \frac{T - T_\infty}{T_w - T_\infty} \tag{6}$$

From this, it follows that

$$u = \frac{\partial\psi}{\partial y} = \frac{U_\infty}{2}f', \qquad v = -\frac{\partial\psi}{\partial x} = \frac{1}{2}\sqrt{\frac{\nu U_\infty}{x}}\left[\eta f' - f\right] \tag{6a}$$

where the primes denote differentiation with respect to the independent variable η. Correspondingly, for the liquid there is introduced

$$\xi = \frac{y}{2}\sqrt{\frac{U_\infty}{\nu_L x}}, \qquad F(\xi) = \frac{\Psi}{\sqrt{\nu_L U_\infty x}} \tag{7}$$

with the velocities given by

$$u = \frac{\partial\Psi}{\partial y} = \frac{U_\infty}{2}F', \qquad v = -\frac{\partial\Psi}{\partial x} = \frac{1}{2}\sqrt{\frac{\nu_L U_\infty}{x}}\left[\xi F' - F\right] \tag{7a}$$

and in this instance the primes represent differentiation with respect to ξ.

When the transformations defined by equations (6) and (7) are introduced into the conservation equations (1) to (3), there results

$$f''' + ff'' = 0 \tag{8}$$

$$\theta'' + \text{Pr}\, f\theta' = 0 \tag{9}$$

$$F''' + FF'' = 0 \tag{10}$$

Equations (8) and (10) are Blasius-type equations, respectively, corresponding to the velocity problem in the vapor and liquid. Equation (9) is the transformed vapor energy equation.

The matching and boundary conditions may also be rephrased in terms of the new variables. First, it may be noted that, at the interface, $y = \delta$ (see Fig. 1), and correspondingly the value of η at the interface is denoted by η_δ. The interfacial value of ξ might also be denoted as ξ_δ. However, since the actual value of ξ does not enter the governing equations—neither in the differential equation (10) nor in the boundary conditions—we can, without any loss of generality, take $\xi = 0$ *at the liquid-vapor interface*. Then applying the transformations (6) and (7) to the matching and boundary conditions (4) and (5), there is obtained:

$$\text{plate surface:} \qquad f(0) = f'(0) = 0\,, \theta(0) = 1 \tag{11a}$$

$$\text{interface:} \begin{cases} F(0) = \left[\dfrac{\rho\mu}{(\rho\mu)_L}\right]^{1/2} f(\eta_\delta) \\ F'(0) = f'(\eta_\delta) \\ F''(0) = \left[\dfrac{\rho\mu}{(\rho\mu)_L}\right]^{1/2} f''(\eta_\delta) \\ \theta(\eta_\delta) = 0 \end{cases} \tag{11b}$$

$$\text{free stream:} \quad F' \to 2 \quad \text{as} \quad \xi \to \infty \tag{11c}$$

The ordinary differential equations (8) through (10) together with the boundary conditions (11) provide a complete set for determining the three unknowns, provided that three parameters are specified. Two of the parameters, the Prandtl number Pr and the matching ratio $(\rho\mu)_L/\rho\mu$ are tabulated properties of the fluid. The other parameter η_δ, which is the dimensionless thickness of the vapor film, would not be known a priori. It is therefore advantageous to replace it by another group which would presumably be known as a part of the specification of the problem. From an energy balance at the interface

$$-k\frac{\partial T}{\partial y} = \dot{m}h_{fg} \tag{12}$$

where $\dot{m}$ is the mass flow across the interface and h_{fg} is the latent heat. Taking $\dot{m}$ from the right side of equation (4*c*) and introducing the new variables, equation (12) becomes

$$\frac{c_p\Delta T}{h_{fg}} = \text{Pr}\,\frac{f(\eta_\delta)}{[-\theta'(\eta_\delta)]} \tag{13}$$

with $\Delta T = T_w - T_\infty$. Once solutions are available as a function of η_δ, corresponding values of $c_p\Delta T/h_{fg}$ can be calculated. Hence it is possible to replace η_δ with the more convenient parameter $c_p\Delta T/h_{fg}$.

Simplification and Solution. Solutions to the governing equations (8) to (11) could, of course, be obtained by use of electronic digital computers. However, with very little loss of accuracy, such a lengthy calculation procedure can be circumvented by the approach to be followed here. What with the uncertainty factors such as instability and wave motion which occur in film boiling, there would be little incentive to strive for the ultra-high precision which is afforded by use of a digital computer.

The first step in simplifying the problem is to set aside the effects of inertia forces and energy convection in the vapor film. Later, in the discussion, we will examine this simplification in greater detail and demonstrate that it is, in fact, permissible for the range of parameters which may be found in practice. With this, equations (8) and (9) are reduced to

$$f''' = 0, \qquad \theta'' = 0 \tag{14}$$

Solutions of these equations satisfying the boundary conditions (11*a*) and the last of (11*b*) are

$$f = \frac{\beta}{2}\eta^2, \qquad \theta = 1 - \frac{\eta}{\eta_\delta} \tag{15}$$

where the integration constant β still remains to be determined from the interface matching conditions (11*b*). Utilizing the third of these conditions, it is found that

$$\beta = \left[\frac{(\rho\mu)_L}{\rho\mu}\right]^{1/2} F''(0) \tag{16}$$

Additionally, from the second and third matching conditions

$$\eta_\delta = \frac{f'(\eta_\delta)}{f''(\eta_\delta)} = \left[\frac{\rho\mu}{(\rho\mu)_L}\right]^{1/2} \frac{F'(0)}{F''(0)} \tag{17}$$

With these, and with $f(\eta_\delta)$ and $\theta'(\eta_\delta)$ from equation (15), the interface energy balance (13) may be evaluated, giving

$$\left[\frac{c_p\Delta T}{\Pr\, h_{fg}}\right]\left[\frac{(\rho\mu)_L}{\rho\mu}\right] = \frac{1}{2}\,\frac{[F'(0)]^2}{[F''(0)]^3} \tag{18}$$

It is thus seen that β, η_δ, and $[c_p\Delta T/h_{fg}\Pr]$ are all determined as soon as the values of $F'(0)$ and $F''(0)$ from the liquid solution are known.

Next, turning to the liquid, it may be observed that the velocity problem is governed by a Blasius-type equation (10) plus boundary conditions of the form $F'(0) = A$, $F(0) = B$, and $F'(\infty) = 2$. We may look upon such a system as describing a flow with a vectored blowing at $\xi = 0$. A significant simplification in the problem is suggested by the first of the matching conditions (11*a*) which may be rewritten as

$$F(0) = \frac{f(\eta_\delta)}{[(\rho\mu)_L/\rho\mu]^{1/2}}$$

The $\rho\mu$ ratio which appears in the denominator is generally a large number. For instance, for water the value of $(\rho\mu)_L/\rho\mu$ is 40,000 at atmospheric pressure (212 deg F) and decreases to 850 at 250 psi ($\simeq$400 deg F) and then to 43 at the pressure of 1550 psi ($\simeq$600 deg F). For mercury and for ethanol at one atmosphere, the values of $(\rho\mu)_L/\rho\mu$ are 460,000 and 22,000, respectively. On the other hand, the values of $f(\eta_\delta)$ which occur in the present problem are of unit order. Consequently, the $F(0)$ values with which we will have to deal will generally be quite small. Further, from experience with unidirectional blowing (i.e., $F'(0) = 0$) it is known that when $F(0)$ is very small the surface shear stress is hardly different from the value corresponding to no blowing. From this line of reasoning, we are persuaded to proceed with the solution for the liquid under the condition that $F(0) = 0$. Later, a few comparisons will be made with solutions where nonzero $F(0)$ has been retained. From this, it will be seen that the simplification is indeed permissible.

With this, the velocity problem has been reduced to

$$F''' + FF'' = 0 \tag{19a}$$

$$F(0) = 0, \qquad F'(0) = A, \qquad F'(\infty) = 2 \tag{19b}$$

For each assigned value of A, this system can be solved; and in particular, the value of $F''(0)$ corresponding to the prescribed A value can be obtained. Then with the pair of numbers $F'(0)$, $F''(0)$, we can return to equations (16), (17), and (18) and calculate β, η_δ, and $[c_p\Delta T/h_{fg}\Pr][(\rho\mu)_L/\rho\mu]$. Additionally, it will be shown later that the pair $F'(0)$, $F''(0)$ is all that is needed to determine heat-transfer and wall shear stress.

A portion of the needed solutions of equation (19) can be obtained by adapting the Emmons-Leigh [8] table of solutions for the apparently different problem of blowing or suction *normal* to a flat plate. This can be accomplished by the use of a fictitious origin for ξ. It is only necessary to search the various blowing tables for the places where $F = 0$ ($F' \neq 0$), and it is here that ξ is taken to be zero. With this as an origin, the tabulations correspond to the solution of equation (19). In particular, the values of F' and F'' at this origin correspond to the $F'(0)$ and $F''(0)$ which we are seeking. In this way, values of $F'(0)$ and the corresponding $F''(0)$ have been obtained over the range $0 \leq F'(0) \leq 1.175$, and this information is listed in Table 1.

Since the results from the Emmons-Leigh tables terminate at $F'(0) = 1.175$, it is necessary to obtain additional solutions for equation (19) in the range $1.175 < F'(0) < 2.0$. This was accomplished by using a successive approximation procedure similar to that outlined by Piercy and Preston [9]. The details of this calculation are given in the Appendix, and the corresponding values of $F'(0)$ and $F''(0)$ are listed in the middle portion of Table 1.

Finally, as $F'(0)$ approaches 2, the function $F(\xi) \to 2\xi$. By replacing F by 2ξ in equation (19) and carrying out the solution, it is found that the asymptotic relation between $F'(0)$ and $F''(0)$ is

$$F''(0) = \frac{2}{\sqrt{\pi}}\,[2 - F'(0)] \tag{20}$$

Table 1 Values of $F'(0)$, $F''(0)$, and related functions

$F'(0)$	$F''(0)$	$[F'(0)]^3/[F''(0)]^2$	$F''(0)/F'(0)$
0.000	1.328	0.0000	∞
0.491	1.218	0.0795	2.48
0.668	1.135	0.179	1.70
0.787	1.067	0.428	1.36
0.877	1.011	0.659	1.15
1.005	0.926	1.18	0.921
1.117	0.842	1.97	0.754
1.175	0.799	2.54	0.680
1.20	0.787	2.79	0.656
1.30	0.700	4.48	0.539
1.40	0.612	7.32	0.437
1.50	0.519	12.5	0.346
1.60	0.423	22.9	0.264
1.70	0.322	47.2	0.189
1.80	0.218	122	0.121
1.90	0.111	558	0.0584
1.92	0.0904	866	0.0471
1.94	0.0678	1590	0.0349
1.96	0.0451	3700	0.0230
1.98	0.0226	15,200	0.0114
2.00	0.00	∞	0.00

The value of $F'(0)$ and the corresponding $F''(0)$ have been listed in Table 1 for the range $1.92 \leq F'(0) \leq 1.98$.

With the information listed in Table 1, the task of solving the governing equations can be regarded as completed. The constant β (related to the wall shear stress), the dimensionless film thickness η_δ, and the parameter $[c_p\Delta T/h_{fg}\mathrm{Pr}][(\rho\mu)_L/\rho\mu]$ can be evaluated from equations (16), (17), and (18). We are now in a position to proceed with the determination of the heat-transfer and skin-friction characteristics.

Results

Heat Transfer. The local heat transfer at the plate surface is given by Fourier's law as

$$q = -k\left(\frac{\partial T}{\partial y}\right)_{y=0}$$

Introducing the transformed variables of equation (6) and making use of the temperature solution (15), the expression for q becomes

$$q = \frac{k}{2}\sqrt{\frac{U_\infty}{\nu x}}\,(T_w - T_\infty)\,\frac{1}{\eta_\delta} \tag{21}$$

But, in turn, η_δ may be eliminated by equation (17), giving

$$q = \frac{k}{2}\sqrt{\frac{U_\infty}{\nu x}}\,(T_w - T_\infty)\left[\frac{(\rho\mu)_L}{\rho\mu}\right]^{1/2}\frac{F''(0)}{F'(0)} \tag{22}$$

To construct a dimensionless representation, a local heat-transfer coefficient and Nusselt and Reynolds numbers will be defined as follows:

$$h = \frac{q}{T_w - T_\infty}, \qquad \mathrm{Nu} = \frac{hx}{k}, \qquad \mathrm{Re} = \frac{U_\infty x}{\nu_L} \tag{23}$$

where it is noted that k is logically the vapor conductivity and ν_L is the viscosity of the liquid free stream. With these, the heat transfer takes the form

$$\frac{\mathrm{Nu}}{\sqrt{\mathrm{Re}}}\left(\frac{\mu}{\mu_L}\right) = \frac{1}{2}\,\frac{F''(0)}{F'(0)} \tag{24}$$

Using the tabulated values of $F'(0)$ and $F''(0)$, the Nusselt-Reynolds expression has been evaluated and is plotted in Fig. 2 as a function of the single group

$$\left[\frac{c_p\Delta T}{h_{fg}\mathrm{Pr}}\right]\left[\frac{(\rho\mu)_L}{\rho\mu}\right] \tag{25}$$

which was computed from equation (18). For large values of the abscissa variable (25), the asymptotic relation between $F'(0)$ and $F''(0)$ as given by equation (20) is valid. By introducing equation (20) into the Nusselt number expression (24) and rearranging, there results

$$\frac{\mathrm{Nu}}{\sqrt{\mathrm{Re}}}\left(\frac{\mu}{\mu_L}\right)\left[1 + \sqrt{\pi}\left(\frac{\mathrm{Nu}}{\sqrt{\mathrm{Re}}}\right)\left(\frac{\mu}{\mu_L}\right)\right]^{1/2} = 0.5\left[\frac{(\rho\mu)_L}{\rho\mu}\,\frac{c_p\Delta T}{h_{fg}\,\mathrm{Pr}}\right]^{-1/2} \tag{26}$$

It is remarkable that equation (26), which was derived for asymptotic conditions, is highly accurate far outside the asymptotic range. For example, for a value of the abscissa group (25) of 10, the Nusselt number given by equation (26) is only about 1 per cent higher than that from the more complete calculation. And so, equation (26) may for all practical purposes be regarded as defining almost the entire Nusselt number curve of Fig. 2. It can, of course, be used for all abscissa values higher than those of the figure. A somewhat simpler, but slightly less accurate computational formula may be obtained by setting aside the square root bracket on the left side of equation (26), giving

$$\frac{\mathrm{Nu}}{\sqrt{\mathrm{Re}}}\left(\frac{\mu}{\mu_L}\right) = 0.5\left[\frac{(\rho\mu)_L}{\rho\mu}\,\frac{c_p\Delta T}{h_{fg}\,\mathrm{Pr}}\right]^{-1/2} \tag{27}$$

At an abscissa value of 100, the prediction of equation (27) is in error by 3 per cent; and when the abscissa decreases to 10, the error increases to 6.5 per cent. For applications at moderate pressures, $(\rho\mu)_L/\rho\mu$ is quite large, and equation (27) may be used with little error.

It is interesting to consider the effect of the temperature difference ΔT on heat transfer. First of all, from equation (27) it is seen that

$$h \sim (\Delta T)^{-1/2}$$

The heat-transfer coefficient decreases with the temperature difference, and this is related to the increased thickness of the vapor film. The dependence of the heat transfer on ΔT then follows as

$$q \sim (\Delta T)^{1/2}$$

Thus compared to other convective transfer phenomena, the dependence of q upon ΔT is much smaller in forced-convection film boiling.

Results for the over-all heat transfer may be obtained by integration of the local results. Defining an average heat-transfer coefficient $\bar{h}$ as

$$\bar{h} = \frac{Q}{T_w - T_\infty} = \frac{\int_0^x q\,dx}{x(T_w - T_\infty)} \tag{28}$$

it follows that $\bar{h} = 2h$.

Skin Friction. The shear stress exerted on the wall by the flowing fluid may be evaluated from the Newtonian shear relation

$$\tau = \mu\left(\frac{\partial u}{\partial y}\right)_{y=0}$$

Introducing the transformed variables of equations (6) and (6a), this becomes

$$\tau = \frac{\rho U_\infty^2}{4}\sqrt{\frac{\nu}{U_\infty x}}\,f''(0) \tag{29}$$

But, from equation (15) $f''(0) = \beta$, and in turn β may be expressed in terms of $F''(0)$ by equation (16). Using this, and introducing a liquid Reynolds number as defined in equation (23), the shear stress expression becomes

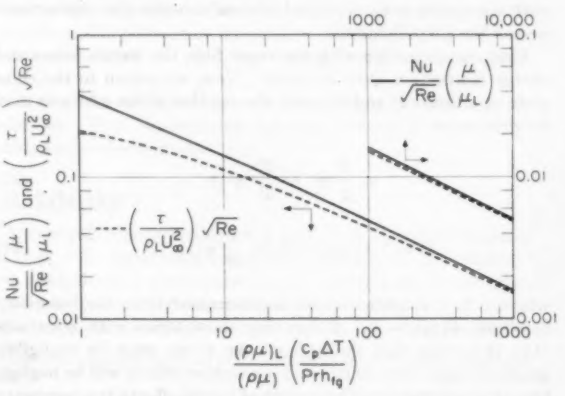

Fig. 2 Variation of local heat transfer and skin friction

$$\frac{\tau}{(\rho_L U_\infty^2)} \sqrt{\mathrm{Re}} = \frac{F''(0)}{4} \tag{30}$$

This relationship has been evaluated using the values of $F''(0)$ as listed in Table 1. The results thus obtained have been plotted in Fig. 2 with the abscissa evaluated from equation (18). A closed form expression for the wall shear can be obtained by combining the asymptotic $F'(0)$, $F''(0)$ relationship (20) with equation (30), giving

$$\frac{(\tau/\rho_L U_\infty^2)\sqrt{\mathrm{Re}}}{\left[1 - \sqrt{\pi}(\tau/\rho_L U_\infty^2)\sqrt{\mathrm{Re}}\right]^{3/2}} = 0.5\left[\frac{(\rho\mu)_L}{\rho\mu}\frac{c_p\Delta T}{h_{fg}\,\mathrm{Pr}}\right]^{-1/3} \tag{31}$$

It is found that this is a remarkably good representation of the results over the entire abscissa range. For instance, with an abscissa value of 10, equation (31) gives a shear stress value which is only 1.5 per cent higher than that from the more complete solution. For large values of the abscissa, the denominator on the left side of equation (31) can be set aside. However, the shear stress result thus obtained is somewhat less accurate than the simplified Nusselt number formula (27). For instance, at an abscissa value of 1000, setting aside the denominator factor in equation (31) leads to an error of 4 per cent.

For sufficiently large values of the abscissa (say > 1000), an interesting relationship between heat transfer and skin friction is found from equation (27) and equation (31) (with denominator deleted) to be

$$\mathrm{Nu}\left(\frac{\mu}{\mu_L}\right) = \frac{\tau}{\rho_L U_\infty^2}\mathrm{Re} \tag{32}$$

This may be regarded as a kind of Reynolds analogy.

With the wall shear stress results now at our disposal, it is interesting to inquire as to the potential capabilities of film boiling in reducing the skin friction relative to that for the flow of a pure liquid. For such a single phase flow, $F''(0) = 1.328$ and

$$\frac{\tau}{\rho_L U_\infty^2}\sqrt{\mathrm{Re}} = 0.332$$

Noting that practical values of $[c_p\Delta T/h_{fg}\mathrm{Pr}]$ will be of unit order and that $(\rho\mu)_L/\rho\mu$ may be very large ($\simeq$10,000 to 100,000 at atmospheric pressure), it is seen from Fig. 2 that very great drag reductions are potentially possible under film-boiling conditions.

Examination of Simplifying Assumptions

In deriving the solutions of the governing equations, certain simplifying assumptions were introduced. It is now desirable, with the results in hand, to go back and consider the appropriateness of the simplifications.

First, in connection with the vapor film, the inertia forces and energy convection were set aside. Now, we return to the complete equations (8) and (9), and observe that series solutions may be written as

$$f = \frac{\beta}{2}\eta^2 - \frac{\beta^2}{5!}\eta^5 + \cdots\cdots \tag{33}$$

$$\theta = 1 - \sigma\eta + \beta\,\mathrm{Pr}\,\frac{\sigma}{4!}\eta^4 + \cdots\cdots \tag{34}$$

where σ is a constant which is determined from the boundary condition $\theta(\eta_\delta) = 0$. Comparing these series with equations (15), it is clear that the higher-order terms must be negligibly small to insure that inertia and convection effects will be negligible. Considering first the neglect of inertia effects, it is necessary that

$$\frac{\beta^2}{5!}\eta_\delta^5 \ll \frac{\beta}{2}\eta_\delta^2$$

Evaluating β and η_δ, respectively, from equations (16) and (17) and using equation (18), this condition becomes

$$\frac{c_p\Delta T}{h_{fg}\,\mathrm{Pr}} \ll 30 \tag{35}$$

Since $\mathrm{Pr} \simeq 1$ for vapors and practical values of $c_p\Delta T/h_{fg}$ are of unit order, it is seen that the restriction imposed by equation (35) is easily met. Next, turning to the neglect of energy convection, it is necessary that

$$\beta\,\mathrm{Pr}\,\frac{\sigma}{4!}\eta_\delta^4 \ll \sigma\eta_\delta$$

Eliminating β and η_δ as before, it is found that

$$\frac{c_p\Delta T}{h_{fg}} \ll 12 \tag{36}$$

Once again, the restriction imposed by equation (36) is readily satisfied. Consequently, from these arguments we are led to believe that the neglect of inertia forces and energy convection has only a very small influence on the results.

The second simplifying assumption, made in connection with the liquid boundary layer, was to suppose that $F(0)$ could be taken as zero. This simplification was suggested by the fact that $(\rho\mu)_L/\rho\mu$ is exceedingly large. To check the effect of neglecting the $F(0)$, it would be desirable to have solutions where $F(0) \neq 0$ has been retained. A few such solutions can be obtained from the Emmons-Leigh tables, but unfortunately, only for very restricted values of the parameters. Except for high pressures, a fair test of the simplifying assumption would be to make a comparison at a value $(\rho\mu)_L/\rho\mu \simeq 1000$, and a test for very high pressures would correspond to $(\rho\mu)_L/\rho\mu > 10$. However, the $\rho\mu$ ratios available from the Emmons-Leigh tables lie outside the usual practical range. If we denote Nu^* and τ^* as the results evaluated from the Emmons-Leigh solution with $F(0) \neq 0$, then Table 2 shows a comparison with the Nu and τ values from the present analysis.

Table 2 Comparison of results with $F(0) \neq 0$ and $F(0) = 0$

$\frac{(\rho\mu)_L}{\rho\mu}$	$\frac{c_p\Delta T}{h_{fg}\,\mathrm{Pr}}$	$\frac{\mathrm{Nu}}{\mathrm{Nu}^*}$	$\frac{\tau}{\tau^*}$
2.40	1.90	0.86	0.95
4.53	0.430	0.93	0.97
8.18	0.179	0.98	0.99
9.36	0.142	0.98	0.99

These $\rho\mu$ ratios are well below the usual practical range. Nevertheless, even for these drastic conditions, the results from the simplified analysis are remarkably accurate. In this light, we are persuaded that for realistic values of the $\rho\mu$ ratio, the results based on the $F(0) = 0$ simplification will be practically indistinguishable from those with $F(0) \neq 0$.

References

1 L. A. Bromley, "Heat Transfer in Film Boiling," *Chemical Engineering Progress*, vol. 46, 1950, p. 221.

2 M. E. Elion, "A Study of the Mechanism of Boiling Heat Transfer," Memo No. 20-88, Jet Propulsion Laboratory, California Institute of Technology, 1954.

3 Y. P. Chang, "Wave Theory of Heat Transfer in Film Boiling," JOURNAL OF HEAT TRANSFER, TRANS ASME, Series C, vol. 81, 1959, p. 1.

4 Y. Y. Hsu and J. W. Westwater, "Approximate Theory for Film Boiling on Vertical Surfaces," Third ASME-AICHE National Heat Transfer Conference, Storrs, Conn., August, 1959.

5 P. W. McFadden and R. J. Grosh, "High-Flux Heat Transfer Studies: An Analytical Investigation of Laminar Film Boiling," AEC Research and Development Report ANL-6060, 1959.

6 J. C. Y. Koh, E. M. Sparrow, and J. P. Hartnett, "The Two Phase Boundary Layer in Laminar Film Condensation," to be published in the International Journal of Heat and Mass Transfer.

7 R. D. Cess, "Laminar-Film Condensation on a Flat Plate in the Absence of a Body Force," to be published in *Zeitschrift für Angewandte Mathematik und Physik*.

8 H. W. Emmons and D. C. Leigh, "Tabulation of the Blasius Function With Blowing and Suction," Ministry of Supply, Aeronautical Research Council Technical Report, C. P. No. 157, 1954.

9 N. A. V. Piercy and G. H. Preston, "A Simple Solution of the Flat Plate Problem of Skin Friction and Heat Transfer," *Philosophical Magazine*, vol. 21, 1936, p 995.

10 H. S. Carslaw and J. C. Jaeger, "Conduction of Heat in Solids," second edition, Clarendon Press, Oxford, England, 1959, pp. 483-485.

11 W. S. Bradfield, "Plane Laminar Forced Convection Film Boiling With Subcooling," Convair Scientific Research Laboratory, Research Note No. 35, July, 1960

APPENDIX

Successive Approximation Solution

We are seeking solutions of the system

$$F''' + FF'' = 0;\ F(0) = 0,\quad F'(0) = A,\quad F'(\infty) = 2 \tag{19}$$

Using a method similar to that of reference [9], a successive approximation solution of equation (19) may be written as

$$F_{n+1}' = (2 - A)\frac{\int_0^\xi \exp\left[-\int_0^\xi F_n d\xi\right] d\xi}{\int_0^\infty \exp\left[-\int_0^\xi F_n d\xi\right] d\xi} + A \tag{37}$$

As a first approximation, let $F_1 = 2\xi$. Introducing this into equation (37) there is obtained

$$F_2' = (2 - A)\,\mathrm{erf}\,(\xi) + A \tag{38}$$

where erf (ξ) is the error function (see ref. [10]). Two additional integrations yield

$$\int_0^\xi F_2 d\xi = 0.25(2 - A) - 0.564\,(2 - A)\xi + \xi^2 - (2 - A)i^2\,\mathrm{erfc}\,(\xi) \tag{39}$$

The quantity $i^2\,\mathrm{erfc}(\xi)$ is the second repeated integral of the complementary error function and is discussed and tabulated in reference [10].

Now, the result which is of interest is the $F''(0)$ corresponding to the prescribed value of $F'(0) = A$. By differentiating equation (37) and setting $\xi = 0$, we get

$$F_2''(0) = \frac{2 - A}{\int_0^\infty \exp\left[-\int_0^\xi F_2 d\xi\right] d\xi} \tag{40}$$

So, the third approximation $F_3''(0)$ is determined by numerically integrating equation (40) making use of equation (39).

Consideration was first given to the case where $A = 1.175$. It was found that the same result for $F''(0)$ was obtained with integration step sizes of 0.1 and 0.2. Hence the 0.2 integration step size is regarded as adequate. The numerical value of $F_3''(0)$ corresponding to $A = 1.175$ was calculated from equation (40) to be 0.806. On the other hand, the Emmons-Leigh tables give $F''(0) = 0.799$. Thus the third approximation is in error by only 0.9 per cent. For increasing values of A, the third approximation becomes increasingly more accurate.

DISCUSSION

Daniel Bershader[4]

Here is an example of two-phase flow which lends itself to a Blasius-type boundary-layer analysis. Application of the boundary-layer equations is made separately to each phase, with suitable continuity conditions imposed at the interface. The assumption is made that the products $\rho\mu$ and ρk are constant in order to simplify the analysis. Such assumptions are not bad for air in a range near room temperature. However, it would be worth while for the authors to indicate quantitatively what these variations are for liquid-vapor systems of engineering interest.

The basic features of the solution are that the local skin friction and heat transfer vary with the inverse square root of distance from the leading edge of the flat plate, in accord with the Blasius theory for a single-phase system. Further, the heat transfer is found to depend on the square root of the wall-stream temperature difference. This is of interest in that the dependence is weaker than in other cases of convective flow. Physically, this weaker dependence would appear reasonable in view of the role played by the latent heat.

The linear velocity distribution in the vapor phase coupled with the channeling of the vapor between two higher density "walls" reminds one to some extent of a Couette flow situation, with modifications which involve the phase changes. It would perhaps be of interest to compare the heat transfer and skin friction obtained here with the case of Couette flow where there is an appreciable temperature difference between the walls. It would also be helpful, perhaps, if the authors would take some concrete numerical examples to illustrate actual magnitudes of friction, heat transfer, and dimensions of the vapor layer.

The analysis of the simplifying assumptions gives further strength to the paper and to the assurance of the results. The work is a useful contribution to the two-phase boundary flow problem. Are there any experiments with which to compare the present results?

Warren M. Rohsenow[5]

It should be remembered that the analysis presented requires that all of the vapor generated remains in the film. Visual experiments currently being conducted in our laboratory on forced-convection film boiling inside of horizontal and vertical tubes indicates that much of the vapor formed actually appears in the core, which becomes a mixture of liquid and vapor. The film thickness may, in fact, be nearly uniform along the tube. Experimental heat-transfer results are of the order of four times those obtained by this type of analysis.

The results obtained in the present paper may be applicable to a vertical flat plate or to the outside of a horizontal tube with natural convection or very low velocity vertical forced convection.

It is necessary to know when the assumptions of this paper are applicable. This requires experimental results, preferably including visual observations.

R. H. Sabersky[6]

I thoroughly enjoyed studying this paper by Professors Sparrow and Cess. By ingeniously using the classical tools of boundary-layer analysis, they have succeeded in obtaining an almost exact solution to a physically very complicated problem.

The various assumptions which had to be made are stated

[4] Lockheed Missile Systems Div.; and Stanford University, Stanford, Calif.

[5] Professor of Mechanical Engineering, M.I.T., Cambridge, Mass. Mem. ASME.

[6] California Institute of Technology, Pasadena, Calif.

clearly and advantage has been taken of simplifications which can be made on the basis of engineering considerations. It is interesting to note that, having made the computations, it seems that an additional assumption of this sort can be made. For values of the parameters $\rho\mu/\rho_L\mu_L$ and $c_p\Delta T/h_{fg}$ which are generally expected, the results indicate that the tangential velocity at the interface deviates by only a few per cent from the free-stream value. For these cases it appears, therefore, that one may assume the liquid velocity to be constant and equal to the free-stream velocity everywhere. With this additional assumption the film-boiling model becomes very simple. It consists of a vapor film separating the solid wall from the liquid. The velocity and temperature profile in the vapor are linear and the velocity and temperature in the liquid are constant and equal to the free-stream values.

The authors discuss the justifications for their assumption in detail. Some additional comments on the validity of the assumption of constant pressure, however, might have been of interest. In many examples one must expect the liquid flow field to cause small pressure gradients in the direction of flow. Because of the low density of the vapor compared to that of the liquid, such gradients could very significantly influence the velocity profile in the vapor film. This in turn would affect the film thickness, the friction coefficient, as well as the heat-transfer coefficient.

To assess the importance of this factor as well as of the other assumptions, and to ascertain the area of applicability of the results of the theory, comparison with experimental data would be of great interest. Such a comparison may well form the subject of a future research project.

Authors' Closure

The authors extend their appreciation to the discussers for their interesting and illuminating comments.

In answer to Dr. Bershader's remark about variable properties, the assumptions that $\rho\mu$ and ρk are constant were made to keep the numerical aspects of the analysis within reasonable bounds. We feel that this simplification is consistent with our aim to determine the general level of the drag and heat transfer. The suggestion relating to a Couette flow model is interesting and merits further investigation.

The matter of experimental data is, of course, of first importance in establishing the utility of the analysis. In this connection, a recent experimental study by W. S. Bradfield[7] and associates demonstrated that there are situations where a stable vapor film exists and where large reductions in drag are realized.

[7] W. S. Bradfield, R. O. Barkdoll, and J. T. Byrne, "Film Boiling on Hydrodynamic Bodies," Convair Scientific Research Laboratory, Research Note 37, December, 1960.

Journal of HEAT TRANSFER — Technical Briefs

This section consists of contributions of 750 words or less (about 2½ double-spaced typewritten pages, including figures). Technical Briefs will be reviewed and approved by the specific division's reviewing committee prior to publication. After approval such contributions will be published as soon as possible, normally in the next issue of the Journal

Subcooled Forced-Convection Film Boiling on a Flat Plate

R. D. CESS[1] and E. M. SPARROW[2]

Introduction

FORCED-CONVECTION film boiling on a flat plate has recently been analyzed in reference [1][3] for the situation in which the liquid is at the saturation temperature. However, in many applications the liquid may be subcooled, and this may substantially alter the characteristics of the film-boiling process. It is thus the purpose of the present note to extend the analysis of [1] to include the effects of a subcooled liquid. The physical model and coordinate system are illustrated in Fig. 1. The liquid has a free-stream temperature T_∞ which is lower than the saturation temperature T_{sat}. It is evident that T_{sat} is the temperature which will prevail at the liquid-vapor interface ($y = \delta$).

During the course of the present work, a contemporary investigation has appeared [2] which also deals with subcooled film boiling on a flat plate. The analysis of reference [2] was carried out in an approximate manner by using integral methods within the liquid boundary layer, and the results were obtained only for water. The present study employs an exact boundary-layer formulation and provides results for liquids of all Prandtl numbers.

Analysis

To extend the results of [1] to include subcooling, it is necessary to consider conservation of energy within the liquid. For the sake of brevity, the nomenclature and results of [1] will be employed directly. Now, the boundary-layer form of the energy equation applicable to the liquid may be written as

$$u\frac{\partial T}{\partial x} + v\frac{\partial T}{\partial y} = \alpha_L\frac{\partial^2 T}{\partial y^2} \tag{1}$$

where the subscript L denotes the liquid properties, while no subscript refers to properties of the vapor. Defining a dimensionless temperature as $\varphi = (T - T_\infty)/(T_{sat} - T_\infty)$ and employing the similarity transformation [1]: $\xi \sim (y - \delta)x^{-1/2}$, $F(\xi) \sim x^{-1/2}\Psi$, equation (1) becomes

$$\frac{d^2\varphi}{d\xi^2} + \mathrm{Pr}_L F(\xi)\frac{d\varphi}{d\xi} = 0, \quad \xi \geq 0 \tag{2}$$

with the boundary conditions

$$\varphi(0) = 1, \quad \varphi(\infty) \to 0$$

The solution of equation (2)[4] will now be obtained for three Prandtl number categories: Pr_L of unity, low Pr_L, and high Pr_L. For $\mathrm{Pr}_L = 1$, it may be shown that similarity exists between the liquid velocity and temperature distributions, so that $\varphi(\xi)$ may be expressed in terms of the dimensionless stream function $F(\xi)$. The final result is found to be

$$\varphi'(0) = -\frac{F''(0)}{2 - F'(0)}; \quad \mathrm{Pr}_L = 1 \tag{3}$$

For very low Prandtl numbers, the methods of reference [3] show that the thermal boundary layer will extend well beyond the velocity boundary layer, such that the potential flow result $F(\xi) = 2\xi$ may be employed. Substituting this into equation (2) and integrating, there is obtained

$$\varphi'(0) = -2\sqrt{\frac{\mathrm{Pr}_L}{\pi}}; \quad \text{low } \mathrm{Pr}_L \tag{4}$$

Next, for very high Prandtl numbers, the thermal boundary layer will be restricted to a thin region near the interface, and we may thus employ an expression for $F(\xi)$ which applies only for small ξ. So, expanding $F(\xi)$ in a Maclaurin series and retaining only the first nonzero term, then $F(\xi) = F'(0)\xi$. Correspondingly, equation (2) yields

$$\varphi'(0) = -\sqrt{\frac{2\mathrm{Pr}_L F'(0)}{\pi}}; \quad \text{high } \mathrm{Pr}_L \tag{5}$$

The next step in the analysis is to apply an energy balance at the liquid-vapor interface ($y = \delta$), which gives

$$-k\left(\frac{\partial T}{\partial y}\right)_{vap} + k_L\left(\frac{\partial T}{\partial y}\right)_{liq} = \dot{m}h_{fg} \tag{6}$$

where $\dot{m}$ is the mass flow across the interface. Using the results of [1], this expression may be rewritten as

$$\frac{(\rho\mu)_L}{(\rho\mu)}\left(\frac{c_p\Delta T}{\mathrm{Pr}h_{fg}}\right)\left[1 + \Gamma\frac{F'(0)}{F''(0)}\varphi'(0)\right] = \frac{1}{2}\frac{[F'(0)]^2}{[F''(0)]^2} \tag{7}$$

where Γ is a parameter related to the degree of subcooling and is defined as

$$\Gamma = \left(\frac{\mathrm{Pr}}{\mathrm{Pr}_L}\right)\left(\frac{c_{pL}\Delta T_L}{c_p\Delta T}\right)$$

with $\Delta T = T_w - T_{sat}$ and $\Delta T_L = T_{sat} - T_\infty$. It is evident that $\Gamma = 0$ corresponds to the case of no subcooling ($T_\infty = T_{sat}$), for which equation (7) reduces to equation (18) of [1]. Equation (7) will be used in constructing the final presentation of results where both heat transfer and friction will be given as a function of $[(\rho\mu)_L/(\rho\mu)][c_p\Delta T/\mathrm{Pr}h_{fg}]$.

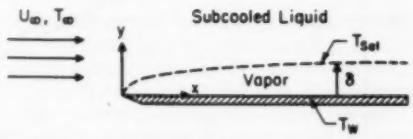

Fig. 1 Physical model and co-ordinate system

[1] Westinghouse Research Laboratories, Pittsburgh, Pa. Now, Associate Professor of Mechanical Engineering, North Carolina State College, Raleigh, N. C. Assoc. Mem. ASME.

[2] Professor of Mechanical Engineering, Heat Transfer Laboratory, University of Minnesota, Minneapolis, Minn. Assoc. Mem. ASME.

[3] Numbers in brackets designate References at end of paper.

[4] Since we are mainly interested in heat transfer at the interface, only results for $\varphi'(0)$ will be given.

Contributed by the Heat Transfer Division of THE AMERICAN SOCIETY OF MECHANICAL ENGINEERS. Manuscript received at ASME Headquarters, January 17, 1961.

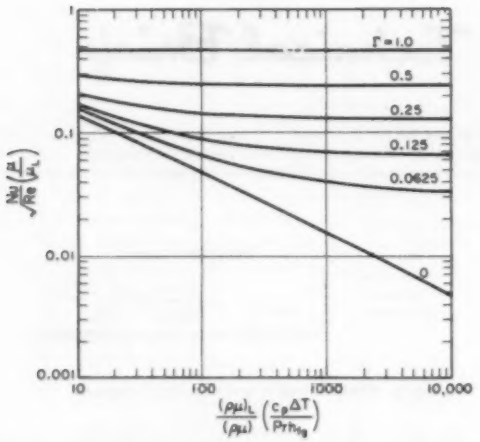

Fig. 2 Local heat-transfer results for liquids with Prandtl number of one

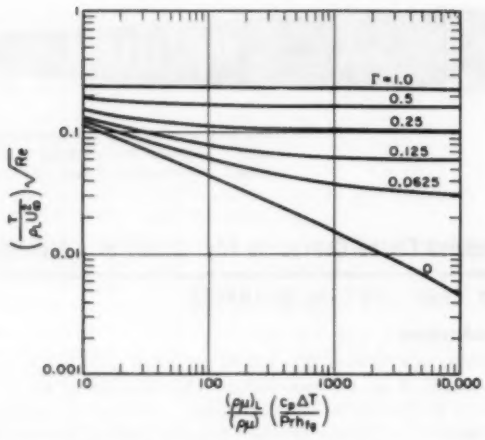

Fig. 3 Local shear-stress results for liquids with Prandtl number of one

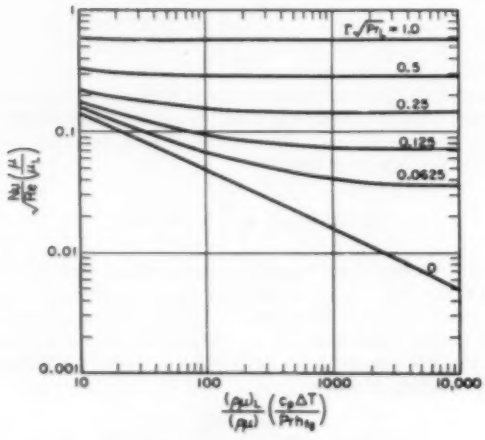

Fig. 4 Local heat-transfer results for liquids with low Prandtl numbers

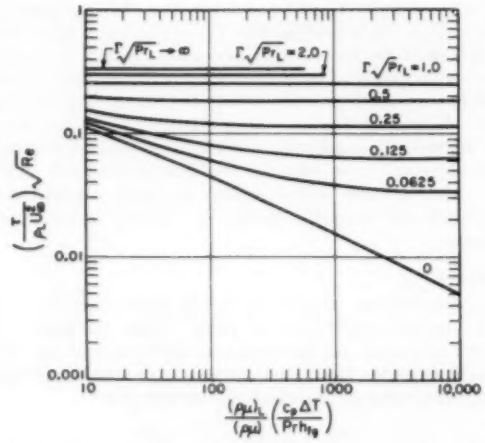

Fig. 5 Local shear-stress results for liquids with low Prandtl numbers

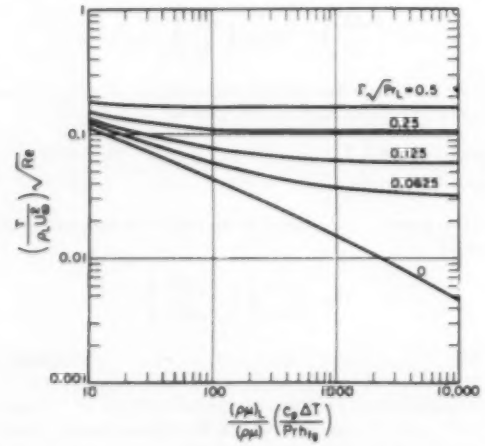

Fig. 6 Local heat-transfer results for liquids with high Prandtl numbers

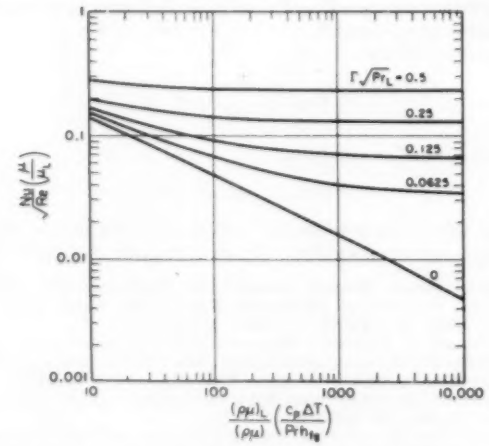

Fig. 7 Local shear-stress results for liquids with high Prandtl numbers

Results

Dimensionless parameters will now be defined as

$$\mathrm{Nu} = \frac{hx}{k}, \quad h = \frac{q}{\Delta T}; \quad \mathrm{Re} = \frac{U_\infty x}{\nu_L}$$

where it is noted that h is expressed in terms of the temperature difference across the vapor film only; i.e., $\Delta T = T_w - T_{sat}$. With these definitions, together with the procedure of [1], the heat transfer q and friction τ at the plate surface are expressed, respectively, by

$$\frac{\mathrm{Nu}}{\sqrt{\mathrm{Re}}}\left(\frac{\mu}{\mu_L}\right) = \frac{1}{2}\,\frac{F''(0)}{F'(0)} \tag{8}$$

$$\frac{\tau}{\rho_L U_\infty^2}\sqrt{\mathrm{Re}} = \frac{F''(0)}{4} \tag{9}$$

Using the tabulated values of $F'(0)$ and $F''(0)$ from Table 1[5] of [1], together with equations (3) and (7), the heat transfer and skin-friction groupings have been evaluated for $\mathrm{Pr}_L = 1.0$. These results are illustrated in Figs. 2 and 3. In the same manner, the low and high Pr_L cases have been evaluated using equations (4) and (5), respectively, in equation (7). Although Pr_L enters as a parameter in the $\varphi'(0)$ expressions, it is readily apparent in both cases that Γ and Pr_L combine to form the single group $\Gamma\sqrt{\mathrm{Pr}_L}$. The heat-transfer and shear-stress results are given in Figs. 4 and 5 for low Prandtl number liquids, and in Figs. 6 and 7 for high liquid Prandtl numbers.

It can be seen that subcooling appreciably affects the film-boiling results, causing an increase in both heat transfer and skin friction. The effect will be most severe for low Prandtl number liquids (liquid metals), for which $\Gamma\sqrt{\mathrm{Pr}_L}$ ($\sim 1/\sqrt{\mathrm{Pr}_L}$) can attain relatively high values. For very large $\Gamma\sqrt{\mathrm{Pr}_L}$, the skin-friction grouping approaches the single-phase value 0.332 as illustrated in Fig. 5. Finally, in connection with Fig. 4, the expression

$$\frac{\mathrm{Nu}}{\sqrt{\mathrm{Re}}}\left(\frac{\mu}{\mu_L}\right) = \Gamma\sqrt{\frac{\mathrm{Pr}_L}{\pi}} \tag{10}$$

represents an applicable high $\Gamma\sqrt{\mathrm{Pr}_L}$ asymptotic result for $\Gamma\sqrt{\mathrm{Pr}_L}$ values larger than those plotted.

References

1 R. D. Cess and E. M. Sparrow, "Film Boiling in a Forced-Convection Boundary-Layer Flow," published in this issue, pp. 357–362.

2 W. S. Bradfield, "Plane Laminar Forced Convection Film Boiling With Subcooling," Convair Scientific Research Laboratory, Research Note No. 35, July, 1960.

3 R. J. Grosh and R. D. Cess, "Heat Transfer to Fluids With Low Prandtl Numbers for Flow Across Plates and Cylinders of Various Cross Section," Trans. ASME, vol. 80, 1958, p. 667.

Flow Visualization and Velocity Measurement in Natural Convection With the Tellurium Dye Method[1]

R. EICHHORN[2]

The purpose of this technical brief is to re-emphasize a technique of flow visualization and velocity measurement proposed a few years ago by F. X. Wortman for use in forced convection water flow [1, 2].[3] This method, which electrically produces in water an intense black dye trace, is particularly suitable for qualitative and quantitative observation of natural convection flows, and, in the opinion of the author, is superior to the usual techniques employing chemical dyes in liquid flows or smoke or kerosene vapor in air flows. The balance of this brief is devoted to a description of the technique, the apparatus required, and a few examples of its use.

Exposition of the Method

The theory behind the production of tellurium dye traces has been carefully developed by Wortman and will not be presented here. If metallic tellurium is employed as cathode and another metal as anode, both being introduced in an electrolyte solution and an external d-c voltage is applied between the cathode and anode (see Fig. 2), a complex reaction takes place at the surface of the cathode producing as a net result a colloidal suspension of finely divided particles of elemental tellurium. The advantages of this suspension as a dye trace are: The intense blackness of the dye; the low settling rate of the small individual particles (about 0.1 mm/sec); the low rate of diffusion of the dye trace (less than 10^{-3} mm/sec); the possible minuteness and variety of the probes used for introduction of the dye; and the ease of control via the electrical power input to the probe. In addition, the required voltages and power inputs are low—an important factor in natural convection where disturbance to the flow must be minimized.[4]

Tellurium is a brittle metal which cannot be drawn or extruded.

[5] Graphical interpolation of the tabulated results was necessary in this computation.

[1] Publication from the Heat Transfer Laboratory, University of Minn.

[2] Assistant Professor, Princeton University, Princeton, N. J.

Contributed by the Heat Transfer Division of The American Society of Mechanical Engineers. Manuscript received at ASME Headquarters, April 4, 1961.

[3] Numbers in brackets designate References at end of paper.

[4] For example, free-convection flows in air cannot be studied readily with kerosene vapor where, because of the large droplets, the settling rate is high. On the other hand, smoke (which, in addition, diffuses rapidly) must be cooled to the temperature of the flow in order that extraneous buoyancy forces are not introduced.

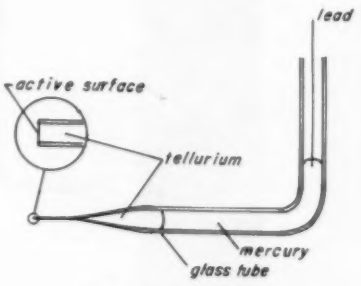

Fig. 1 Diagram of probe

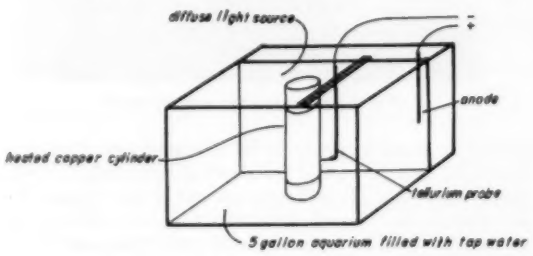

Fig. 2 Experimental apparatus

Fig. 3 Natural-convection streamline on a vertical surface as visualized with the tellurium dye trace method

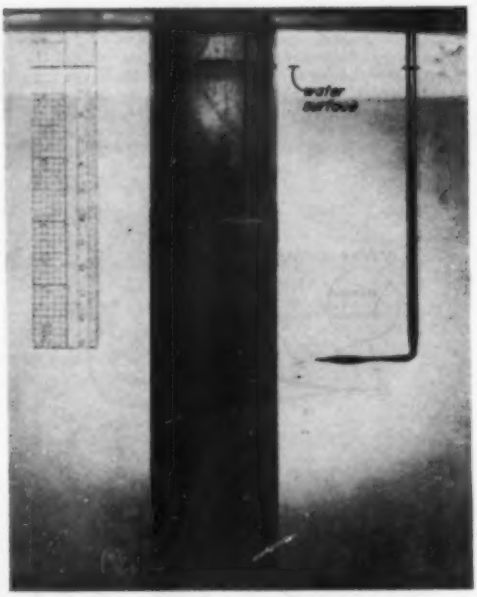

Fig. 4 Free-convection velocity profile

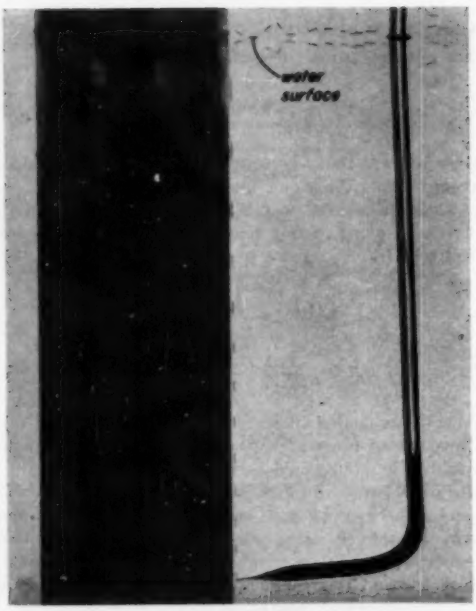

Fig. 5 Pulsed tellurium dye trace

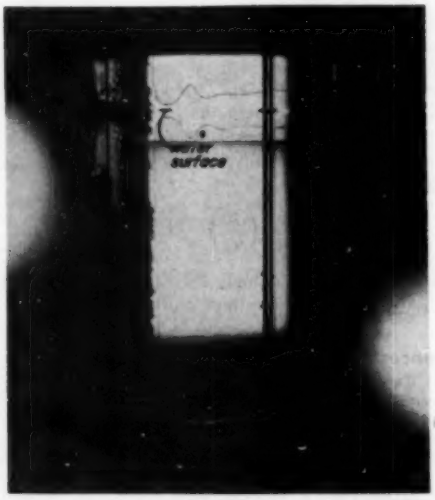

Fig. 6 Flow at top of cylinder at low heating rate

Wires are usually produced by the Taylor process in which a few bits of the metal are placed in a glass tube and heated in a bunsen burner flame until the tellurium has melted and the glass is soft. By drawing the tubing (taking care that the metal stays in the necked-down portion of the tube, not always an easy task), fine wires and sharply pointed probes can be produced. An example of the latter is sketched in Fig. 1. Probes made in this way were used in the exploratory studies described in the next section. Two such probes as those shown in Fig. 1 were made at the same time, the interconnecting necked-down portion being saved for use as tellurium wires after etching away the glass tube with hydrofluoric acid. Final preparation of the probes involved the introduction of mercury into the glass tube to facilitate electrical contact with the tellurium and sanding the end of the tube flush to expose an active surface of tellurium. Probes manufactured in this way could be used for about ten minutes before requiring rejuvenation which consisted simply of sanding the active end of the tube. Ordinary tap water was used for this experiment and the probes operated satisfactorily with applied voltages of the order of one volt. As discussed by Wortman, the tellurium can be vapor deposited on wires or surfaces of another metal.

Examples

Several simple experiments were conducted to demonstrate the feasibility of the method. Two models were used, the first, a 2-in. diameter electrically heated vertical cylinder 5 in. long,

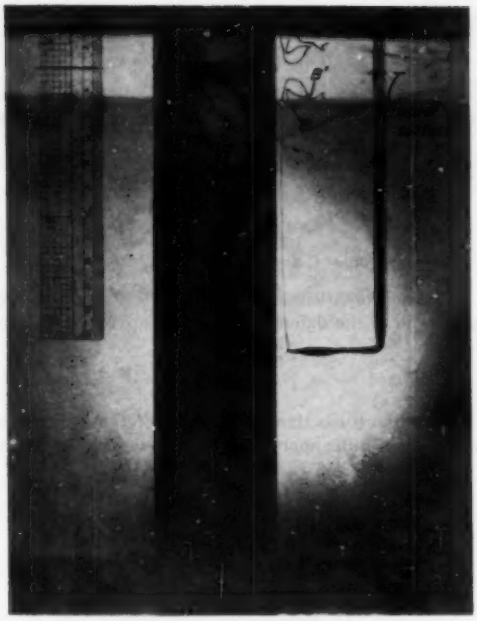

Fig. 7 Flow at top of cylinder at high heating rate

the second consisting of two parallel aluminium plates 8 in. by 10 in., one electrically heated, the other cooled with water. In the latter case studies were made on the volume of fluid confined between the plates. All experiments were performed in a 5-gal aquarium tank. Only photographs of the flow about the vertical cylinder are presented here.

Fig. 2 shows a schematic diagram of the experimental setup employed with the heated cylinder.

Sample photographs (retouched to replace contrast lost in reproduction) obtained with the apparatus shown in Fig. 2 are presented in Figs. 3 to 7. The first photograph, Fig. 3, shows a continuous dye trace introduced near the outer edge of the boundary layer. This picture shows the extent to which the settling rate of the dye trace is important since the fluid velocity close to the probe is very small compared to the velocity within the boundary layer. In the figures the double pattern observed at the top is due to a reflection from the lower surface of the water. The interesting flow pattern there observed will be discussed later. The bubbles on the surface of the cylinder are due to gases driven out of the water.

Fig. 4 shows a dye trace obtained by placing the probe tip close to the model surface and then withdrawing it rapidly while at the same time turning on the dye. The film was exposed a second or two later. The characteristic shape of the free-convection profile is clearly evident even though accurate measurements would hardly result from such an operation. The extraneous bits of dye are left over from previous attempts.

The result of applying a rectangular wave of voltage to the probe placed in the outer portion of the boundary layer is shown in Fig. 5. This method was found to operate best when the direction of the potential was reversed during the off portion of the cycle.

At the higher heating rates an interesting vortex phenomena was observed at the surface of the water. This is illustrated in Figs. 3, 6, and 7. Quantitatively, these phenomena can be explained as follows: The rising boundary layer on the surface can be likened to an annular jet. Upon reaching the free surface this jet is forced to turn a corner and is thus given a component of angular momentum which it tends to preserve. At low heating rates (Fig. 6) the streamlines assume a damped wave shape. At high heating rates, however, annular vortexes are repeatedly formed near the free surface. These roll up until a certain size is reached whereupon they move away from the cylinder and another vortex begins to form. The manner of breakup is clearly shown in Figs. 3 and 7. Although the photos were taken of different vortexes, the phenomenon was repeatedly observed. The dye stream labeled A in Fig. 3 has originally bridged the gap labeled A′. Similarly in Fig. 7, the point B′ represents the breaking point of the dye trace and will now move outward as has the gap A′ in Fig. 4. Simultaneously, all of the material marked B (originally ahead of B′) will coil up inside the vortex as represented by A in Fig. 3. The gap A′ will not be present in Fig. 7 since the dye was initiated soon enough.

It was not feasible to obtain a high enough Grashof number with the vertical cylinder to permit the observation of the onset of instability waves and the subsequent formation of a turbulent flow pattern. With the parallel plate apparatus, it was possible to observe on both the heated and cooled plates the formation of instability waves of the Tollmien-Schlichting type and their roll up into vortexes. These were very clear to the eye but could not be photographed successfully because of refractive index changes within the boundary layer.

Studies of free-convection flow using the tellurium dye method are being continued at Princeton University where it is planned to make quantitative measurements of the flow field about a uniform temperature horizontal plate and a vertical plate with a step change in wall temperature.

Conclusion

It has been demonstrated that the tellurium dye trace method of qualitatively and quantitatively studying flows of water as developed by Wortman for use in forced convection is equally suited for use in free-convection flows and is possibly superior to other means presently employed for that purpose. In addition, this technique is simple enough in application so that it can be developed as a teaching aid in undergraduate laboratory instruction.

Acknowledgment

The studies of the tellurium dye trace method in natural convection flows reported herein were initiated by the author and the experiments were conducted in the Heat Transfer Laboratory of the University of Minnesota. The encouragement and helpful suggestions of Dr. E. R. G. Eckert are gratefully appreciated.

References

1 F. X. Wortman, "Eine Methode zur Beobachtung und Messung von Wasserstömungen mit Tellur," *Zeit. f. angs. Physik*, vol. 5, 1953, p. 201

2 F. X. Wortman, "Untersuchung instabiler Grenzschichtschwingungen in einem Wasserkanal mit der Tellurmethode," in 50 Jahre Grenzschichtforschung, Vieweg, Braunschweig, 1955.

Truncation Error Estimates for Numerical and Analog Solutions of the Heat-Conduction Equation[1]

N. H. FREED[2] and C. J. RALLIS[3]

A practical method is presented for obtaining a meaningful estimate of the truncation error associated with fully finite difference forms of the heat-conduction equation. The analysis is applied in this instance to the Liebmann analog equations. It may also be used with other manual and analog methods of computation, where the error due to mesh size is relatively large. An example is given deriving error estimates for a case of one-dimensional heat flow.

Introduction

THE ERRORS associated with the use of finite-difference approximations in the solution of transient heat-transfer problems become significant in analog and numerical computation, where it is not feasible to have large numbers of finite space-and-time intervals. It appears, however, that no satisfactory method for evaluating these errors has been evolved. This note is intended to aid in the estimation of these errors.

The analysis presented in the following was developed originally for estimating the accuracy attainable in a particular application of the Liebmann analog method [1, 2].[4] It may be extended, however, to other finite-difference equations (for example, the explicit Binder-Schmidt method [3]) and also the partly finite-difference relationship as used in the RC analog [4] and analog computer techniques [5]. The approximate solution of steady-state problems by resistance networks or purely numerical procedures may also be treated by this approach.

The method is basically iterative, but one iteration is generally sufficient to provide a reliable estimate. When the method is applied to the Liebmann analog, the computation of error may be readily performed on the actual analog. Alternatively, it may be performed analytically as in the following example.

Analysis

The heat-conduction equation in one dimension is

$$\frac{\partial^2 T}{\partial x^2} = \frac{1}{\alpha}\frac{\partial T}{\partial t} \tag{1}$$

with the associated conditions $T(x, 0) = f(x);\ 0 \le x \le L$

$$\begin{aligned} T(0, t) &= g_1(t) \quad t > 0 \\ T(L, t) &= g_2(t) \quad t > 0 \end{aligned} \tag{1a}$$

The foregoing equation in an implicit finite-difference form is

$$\frac{\delta_m^2 T_{m,n}}{h^2} - \frac{h^2}{12}\left(\frac{\partial^4 T}{\partial x^4}\right)_{m,n} - \frac{h^4}{360}\left(\frac{\partial^6 T}{\partial x^6}\right)_{m,n} - \cdots\cdots$$

$$= \frac{\nabla_n T_{m,n}}{\alpha k} + \frac{k}{2\alpha}\left(\frac{\partial^2 T}{\partial t^2}\right)_{m,n} - \frac{k^3}{6\alpha}\left(\frac{\partial^3 T}{\partial t^3}\right)_{m,n} + \cdots \tag{2}$$

$$(m = 1, 2, \ldots M;\ n = 1, 2 \ldots)$$

This may be rewritten as

$$\delta_m^2 T_{m,n} = D\nabla_n T_{m,n} + u_{m,n} \tag{3}$$

where [6, 7] $T_{m,n}$ is the exact solution of the differential equation, and the high order derivative terms $u_{m,n}$ are known as the difference correction.[5]

The equations for which exact solutions are obtained by numerical or analog methods are the difference equations

$$\delta_m^2 w_{m,n} = D\nabla_n w_{m,n} \tag{4}$$

$$(m = 1, 2 \ldots M;\ n = 1, 2 \ldots)$$

with boundary conditions equivalent to (1*a*), where $w_{m,n}$ is the exact solution of the difference equations approximating to (1).

Defining

$$v_{m,n} = T_{m,n} - w_{m,n} \tag{5}$$

where $v_{m,n}$ is the truncation error of the solution and represents the actual error in the approximate solution, and subtracting (4) from (3) gives:

$$\delta_m^2 v_{m,n} = D\nabla_n v_{m,n} + u_{m,n} \tag{6}$$

$$(m = 1, 2 \ldots M;\ n = 1, 2 \ldots)$$

with the condition that $v_{m,0} = v_{0,t} = v_{L,t} = 0$ (6*a*)

Thus equation (6), representing error propagation, is almost identical with (3), there being M such equations for every n. By analog or manual computation, these equations are conveniently solved by an iterative method, solving first (4) over the region of interest. Making the approximation

$$w_{m,n} \simeq T_{m,n} \tag{7}$$

values for $u_{m,n}$ may be obtained by a well-known numerical method [8], which involves approximating derivatives in terms of function values. If required the first approximation ${}^1u_{m,n}$ may be used in (5) to obtain more accurate $u_{m,1}$ and hence ${}^2v_{m,1}$. (The convergence of this process has been established by Albasiny [9].) Alternatively ${}^1v_{m,1}$ may be used in (6) for calculating ${}^1v_{m,2}$. In practice we are not concerned with an exact solution but only require a reliable error estimate.

Example. Consider the case of one-dimensional conduction in an infinite plate:

$$\frac{\partial^2 T}{\partial x^2} = \frac{1}{\alpha}\frac{\partial T}{\partial t} \quad \text{for} \quad 0 \le x \le L \tag{8}$$

with the conditions

$$T(x, 0) = 1;\ T(0, t) = T(L, t) = 0 \text{ for } t > 0 \tag{8a}$$

The exact solution here is [10]

$$T = \frac{4}{\pi}\sum_{n=1}^{\infty}\frac{1}{n}\exp\left[-\left(\frac{n\pi}{2}\right)^2\frac{4\alpha t}{L^2}\right]\sin\frac{n\pi x}{L} \tag{9}$$

$$n = 1, 3, 5, \ldots$$

The solution of the difference equation (4) (with $\alpha = 0.2$ ft²/hr and $L = 0.2$ ft) was obtained in this case analytically [11], using $M = 10$, $D = 2.5$, and is shown in Table 1, to $m = 5$ (the problem is symmetrical).

Using these values and (7), ${}^1u_{m,1}$ is calculated as shown in Table 2.

---

[1] This work was performed with the aid of financial assistance from the South African Atomic Energy Board.

[2] South African Atomic Energy Board Bursar and Graduate Student, Department of Mechanical Engineering, University of the Witwatersrand, Johannesburg, South Africa.

[3] Senior Lecturer, Department of Mechanical Engineering, University of the Witwatersrand, Johannesburg, South Africa.

[4] Numbers in brackets designate References at end of paper.

Contributed by the Heat Transfer Division of THE AMERICAN SOCIETY OF MECHANICAL ENGINEERS. Manuscript received at ASME Headquarters, December 28, 1960.

[5] Previous attempts at error determination appear to have been confined to a numerical evaluation of these terms. However, experience showed that there is seldom correlation between the value of $u_{m,n}$ and error at the corresponding point (cf., Tables 2 and 3).

Table 1 Solution of the difference equations

n \ m	1	2	3	4	5
1	0.765	0.945	0.987	0.997	0.999
2	0.621	0.879	0.966	0.992	0.998
3	0.526	0.813	0.935	0.979	0.989
4	0.460	0.754	0.900	0.961	0.977
5	0.412	0.703	0.865	0.940	0.960
6	0.375	0.658	0.830	0.916	0.940
7	0.346	0.620	0.797	0.890	0.918
8	0.322	0.586	0.765	0.863	0.893

Using these values and (7), ${}^1u_{m1}$ is calculated as shown in Table 2.

Table 2 Evaluation of the difference correction[a]

m	1	2	3	4	5
u_{m1}	0.041	−0.063	−0.040	−0.018	−0.018

[a] Values include third-order time derivatives and fourth-order space derivatives.

Writing (6) (for $n = 1$) in the form

$$\mathbf{A}\,{}^1\mathbf{v}_1 = {}^1\mathbf{u}_1 - D\mathbf{v}_0 \tag{10}$$

where the nonzero elements of $\mathbf{A}$ are of the form

$$\begin{bmatrix} -(D+2) & 1 & & & \\ 1 & -(D+2) & 1 & & \\ & \cdots & \cdots & \cdots & \\ & & 1 & -(D+2) & 1 \\ & & & 1 & -(D+2) \end{bmatrix}$$

leads to the explicit equation

$${}^1\mathbf{v}_1 = \mathbf{A}^{-1}({}^1\mathbf{u}_1 - D\mathbf{v}_0) \tag{11}$$

Taking advantage of the large number of zero elements in the tridiagonal matrix $\mathbf{A}$, the inversion follows easily, the solution of (11) being shown in Table 3.

Table 3 Actual and predicted errors[a]

m	1	2	3	4	5
Solution of (9)	0.737	0.974	1.000	1.000	1.000
Solution of (4)	0.765	0.945	0.987	0.997	0.999
Actual error $v_{m,1}$	−0.028	0.029	0.013	0.003	0.0014
Predicted error $v_{m,1}$	−0.003	0.013	0.012	0.008	0.007

[a] All values for $n = 1$.

For $m = 1, 2$ near the boundary, the error in prediction caused by the discontinuity in the initial conditions [12] is noticeable. Although the discrepancy at $m = 4, 5$ is not significant, the magnitude of the difference correction is small and successive iterations will improve the solution at these points.

Equivalent Method When Using the Liebmann Analog.[6] This is considerably simpler than the process outlined in the foregoing and involves feeding in the $u_{m,n}$ as correction currents. This process can only be performed when a complete solution has been obtained and the correction currents calculated for each time interval. Error estimates and hence an improvement in the solution are thus obtained with negligible additional effort.

Discussion and Conclusions

The method presented in the foregoing enables an approximation to the truncation error $v_{m,n}$ to be calculated, the value of the estimate depending on the number of iterations performed. The numerical treatment of discontinuities is always difficult, but fortunately the error contribution to both the solution and the estimates from this source is rapidly attenuated in a stable scheme. Discrepancies in the estimates from numerical approximations to derivatives are found to be negligible. When $D < 8$ (approximately) there is seldom need to compute ${}^1v_{m1}$ and ${}^1v_{m2}$ in problems having discontinuities (although this is easily accomplished from (6) once $\mathbf{A}^{-1}$ has been found), as the error is invariably largest in the first time interval. Where a matrix method of solution of the difference equations (4) has been used [14], the matrix $\mathbf{A}^{-1}$ is already available and the additional labor in estimating the error and hence improving the solution, is again insignificant. The method may also be applied to two and three-dimensional problems, and to regions having specified time-variable boundary conditions.

[6] An early attempt at the reduction of truncation errors near boundaries in a resistance analog of the steady-state Poisson equation is described by Liebmann [13].

Nomenclature

δ_m^2 = central difference operator w.r.t. m: $\delta_m^2 T_{m,n} = T_{m+1,n} - 2T_{m,n} + T_{m-1,n}$

∇_n = backward difference operator w.r.t. n: $\nabla_n T_{m,n} = T_{m,n} - T_{m,n-1}$

m = integer locating point along x-axis, $m = x/\delta x$

n = integer locating point along t-axis, $n = t/\delta t$

D = mesh parameter $= \dfrac{\delta x^2}{\alpha \delta t} = \dfrac{h^2}{\alpha k}$

h = finite space interval $= \delta x$

k = finite time interval $= \delta t$

${}^jv_{m,n}$ and ${}^ju_{m,n}$ = jth approximation to $v_{m,n}$ and $u_{m,n}$, respectively

$\mathbf{A}$ = matrix defined by (6) and (10)

$\mathbf{v}_n$, $\mathbf{u}_n$ = column vectors having components v_m, u_m, respectively

References

1(*a*) G. Liebmann, "A New Electrical Analog Method for the Solution of Transient Heat-Conduction Problems," TRANS. ASME, vol. 78, 1956, pp. 655–665.

1(*b*) G. Liebmann, "Solution of Transient Heat-Transfer Problems by the Resistance-Network Analog Method," TRANS. ASME, vol. 78, 1956, pp. 1267–1272.

2 R. P. Benedict, "Liebmann Network Approximations to One-Dimensional Transient Heat Conduction Problems," ASME Paper No. 58—A-221, 1958.

3 G. M. Dusinberre, "Numerical Analysis of Heat Flow," McGraw-Hill Book Company, Inc., New York, N. Y., 1949.

4 D. I. Lawson and J. H. McGuire, "The Solution of Transient Heat-Flow Problems by Analogous Electrical Networks," *Proceedings of the Institution of Mechanical Engineers*, vol. 167, series A, 1953, pp. 275–287.

5 F. C. Harbert, "Analogue Computer Techniques (Part 2). An Approximate Method for the Solution of Partial Differential Equations," *Electronic Engineering*, vol. 32, no. 385, March, 1960.

6 G. Blanche, "On the Numerical Solution of Parabolic Partial Differential Equations," *Journal of Research NBS*, vol. 50, 1953, p. 343.

7 J. Douglas, Jr., "On the Numerical Integration of Quasi-Linear Parabolic Differential Equations," *Pacific Journal of Mathematics*, vol. 6, 1956, pp. 35–42.

8 W. E. Milne, "Numerical Solutions of Differential Equations," John Wiley & Sons, Inc, New York, N. Y., 1953.

9 E. L. Albasiny, "On the Numerical Solution of a Cylindrical Heat Conduction Problem," *Quart. J. Mech. and App. Maths*, vol. 13, part 3, 1960, pp. 374–384.

10 P. J. Schneider, "Conduction Heat Transfer," Addison-Wesley, Mass., 1955.

11 F. B. Hildebrand, "Methods of Applied Mathematics," Prentice-Hall, New York, N. Y., 1954.

12 S. H. Crandall, "Implicit Versus Explicit Recurrence Formulas for the Linear Diffusion Equation," *J. Assoc. Comp. Mach*, vol. 2–3, 1955, pp. 42–49.

13 G. Liebmann, "Resistance Network Analogues," Proc. Int. Analogy Computation Meeting, Brussels, Belgium, 1955, pp. 346–369. Presses Academiques Europeennes, Brussels.

14 W. G. Bickley and J. McNamee, "Matrix and Other Direct Methods for the Solution of Systems of Linear Difference Equations," *Phil. Trans. Roy. Soc.*, London, England, vol. 252, series A, no. 1005, 1960, pp. 69–131.

Frictional Pressure Drop in Noncircular Ducts

R. I. HODGE[1]

Introduction

THE FRICTIONAL pressure drop in fully developed turbulent flow within noncircular ducts generally can be calculated from the Fanning equation, by using one of the empiricisms for friction factor established for circular tubes modified by the substitution of a hydraulic diameter, Δ. For example, the Blasius empiricism for friction factor

$$f_B = 0.079\,(N_{Re})^{-0.25},$$

may be modified by writing the Reynolds number

$$N_{Re} = \frac{\rho \Delta V}{\mu} = \frac{4W}{\mu S}$$

where

ρ = density
V = velocity
μ = viscosity
W = mass flow rate
S = perimeter

This yields an expression for the friction factor

$$f_B = C_1 W^{-0.25} \mu^{0.25} S^{0.25}$$

where

C_1 is a constant.

The frictional pressure gradients may then be obtained from the Fanning equation, similarly modified:

$$\frac{dp}{dz} = \frac{4 f_B}{\Delta} \frac{\rho V^2}{2g} \tag{1}$$

which when expanded becomes

$$\frac{dp}{dz} = C_2 W^{1.75} \mu^{0.25} \rho^{-1.00} S^{1.25} A^{-3.00} \tag{1a}$$

where

A = cross-sectional area
C_2 = constant.

However, equation (1a) does not always yield an accurate estimate of the frictional gradient. It breaks down when the duct cross-sectional area contains wedge-shaped zones where two adjacent sides approach closely. This was demonstrated in a recent paper by Eckert and Irvine [1][2] in which pressure-drop data were reported for a duct having a cross section in the form of an isosceles triangle of apex angle 11.46 deg. From Fig. 5 of that paper it appears that the gradient was about 0.85 times the value given by equation (1a). In other words, the gradient would be described by an expression of the form of equation (1), on the substitution of an effective friction factor, f', such that

$$f'/f_B = 0.85$$

for this particular duct.

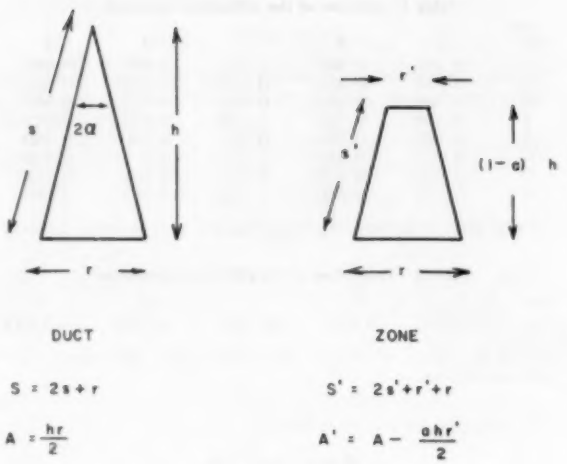

Fig. 1 Nomenclature

The following analysis suggests that the effective friction factor may be calculated for such noncircular ducts by using these modified bulk flow empiricisms; however, the modification involves the substitution of a hydraulic diameter other than the geometrical value $\Delta = 4A/S$.

Analysis

The geometry of the duct appears in the expression (1a) in the form $S^{1.25} A^{-3.00}$. This then is a measure of the hydraulic effectiveness of the channel. If a zone having a factor $(S')^{1.25}(A')^{-3.00}$ which is less than the geometrical value can be delineated entirely within the geometrical area, it will be hydraulically more effective than the full duct. Since less work would be developed by viscous dissipation in such a zone, it might be expected that there would be a concentration of the flow within the zone. That such zones exist in ducts of triangular cross section can be readily shown.

A zone shape which does not include a narrow wedge, and which is amenable to simple mathematical analysis, is shown in Fig. 1. This zone is formed by a boundary drawn parallel to the base at a proportion, a, of the elevation from the apex. The ratio of the zone perimeter to the geometrical perimeter is

$$\frac{S'}{S} = \left[\frac{(1-a)\sec\alpha + (1+a)\tan\alpha}{\sec\alpha + \tan\alpha}\right] \tag{2}$$

and the corresponding area ratio is

$$\frac{A'}{A} = (1 - a^2) \tag{3}$$

For the zone to be more effective than the full duct

$$\frac{(S')^{1.25}}{(A')^{3.00}} < \frac{S^{1.25}}{A^{3.00}}$$

or

$$\left(\frac{A'}{A}\right)^{2.4} - \left(\frac{S'}{S}\right) > 0 \tag{4}$$

The most effective zone will be that giving a maximum in equation (4); for a given triangular duct this occurs when

$$\frac{d}{da}\left[\left(\frac{A'}{A}\right)^{2.4} - \left(\frac{S'}{S}\right)\right] = 0 \tag{5}$$

---

[1] Nuclear Engineering Branch, Reactor Research & Development Division, Atomic Energy of Canada Limited, Chalk River, Ontario, Canada.

[2] Numbers in brackets designate References at end of paper.

Contributed by the Heat Transfer Division of THE AMERICAN SOCIETY OF MECHANICAL ENGINEERS. Manuscript received at ASME Headquarters, January 14, 1960.

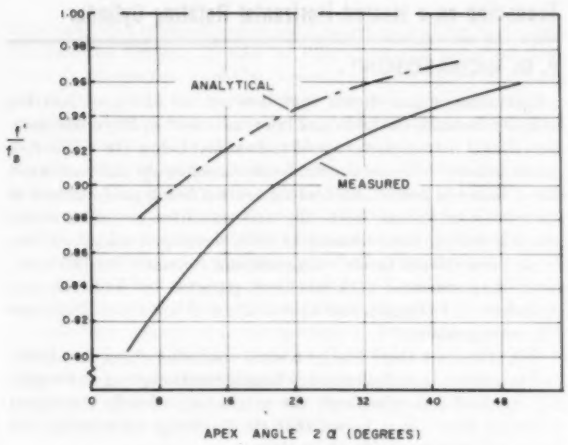

Fig. 2 Effective friction factor versus duct apex angle
(Measured values from reference [2] and analytical solution.)

Expanding (4) as a binomial, differentiating and substituting the first term in a in equation (5) gives

$$a = \frac{5}{24}\left[\frac{\sec\alpha - \tan\alpha}{\sec\alpha + \tan\alpha}\right] \tag{5a}$$

If it is now assumed that in fully developed flow in a triangular duct the flow is entirely concentrated within the zone given by equations (2), (3), and (5a), and that the boundary layer between flowing and stagnant fluid is similar to that adjacent to solid surfaces, then the Blasius empiricism may be applied to the zone to give the duct effective friction factor. Thus

$$\frac{f'}{f_B} = \left(\frac{S'}{S}\right)^{1.25}\left(\frac{A'}{A}\right)^{-3.00} \tag{6}$$

Comparison With Test Data

For the case $2\alpha = 11.46$ deg, the ratio calculated from equation (6) is 0.906. This is to be compared with the value 0.85 deduced from reference [1]. In a more recent paper by Carlson and Irvine, Jr. [2], data are reported for a wide range of triangular-shaped ducts. Effective friction factors deduced from Fig. 10 of that paper are presented in Fig. 2 with corresponding solutions of equation (6).

In all cases the analytical solution is a higher value than the test measurement. This may be explained by the fact that the most effective zone is not of the shape assumed in Fig. 1. If, for example, the corners of the isosceles trapezoid had been rounded, a higher maximum would be obtained in equation (4), with corresponding reduction in the ratio given by equation (6). However, such shapes are not amenable to mathematical solution, and a semi-intuitive graphical method would have to be used.

The analysis thus suggests that the Blasius empiricism, modified by the substitution of the hydraulic diameter of the most effective zone within the geometrical area of the duct, can be used in the Fanning equation, similarly modified, to give a good estimate of the frictional pressure drop in all noncircular ducts.

References

1 E. R. G. Eckert and T. F. Irvine, Jr., "Pressure Drop and Heat Transfer in a Duct With Triangular Cross Section," JOURNAL OF HEAT TRANSFER, TRANS. ASME, Series C, vol. 82, 1960, p. 125.

2 L. W. Carlson and T. F. Irvine, Jr., "Fully Developed Pressure Drop in Triangular Shaped Ducts," ASME Paper No. 60—WA-100.

A Musical Heat Exchanger

ROBERT LEMLICH[1]

AN INCREASING INTEREST in the effect of vibration on heat transfer has appeared in recent years. This is evidenced by the growing number of papers on the subject, two of which have been published in the JOURNAL OF HEAT TRANSFER during the past year alone [1, 3].[3] In light of this the present writer reports here the results of some simple experiments in which he investigated the effect on forced convective heat transfer produced by a vibrating musical reed.[3]

The apparatus employed involved a 0.745-in. ID, 27.5-in. long, copper, double pipe heat exchanger with condensing steam at substantially atmospheric pressure in the annulus and air forced through the core by a blower. A removable clarinet mouthpiece fitted with a bamboo reed was placed in a tygon tube and incorporated in the air stream upstream from the exchanger inlet, as shown in Fig. 1. Starting from rest, as the blower speed was gradually increased a certain point would be reached at which the silent reed would "break into song" and resonate down the exchanger. This occurred at a Reynolds number of 2200 based on core diameter. Further increase in the blower speed increased the audible intensity of the vibration and increased the air pressure upstream from the reed. However, it did not substantially alter the air flow rate. The principal frequency of vibration was about 600 cps which corresponds to the third harmonic for the entire 3 ft long vibrating column of air. With further increase in blower speed the reed ceased vibrating and closed against the mouthpiece aperture, virtually preventing any air flow through the core. Very similar results were obtained with a like exchanger 51 in. in length, the only difference being that here the nearly invariant Reynolds number was 2800 although the cutoff pressure was lower. The principal frequency was again roughly 600 cps, indicating resonance at a higher harmonic than for the shorter exchanger.

The average heat-transfer coefficient h on the air side was calculated from the usual equation $q = hA\Delta t$, with q evaluated from the over-all temperature change of the flowing air and Δt taken as the logarithmic mean. The very small thermal resistances of the wall and condensing steam film were neglected.

---

[1] Department of Chemical Engineering, University of Cincinnati, Cincinnati, Ohio.

[2] Numbers in brackets designate References at end of paper.

[3] NOTE: These hitherto unpublished experiments were conducted by the author in 1952 at the Polytechnic Institute of Brooklyn.

Contributed by the Heat Transfer Division of THE AMERICAN SOCIETY OF MECHANICAL ENGINEERS. Manuscript received at ASME Headquarters, February 20, 1961.

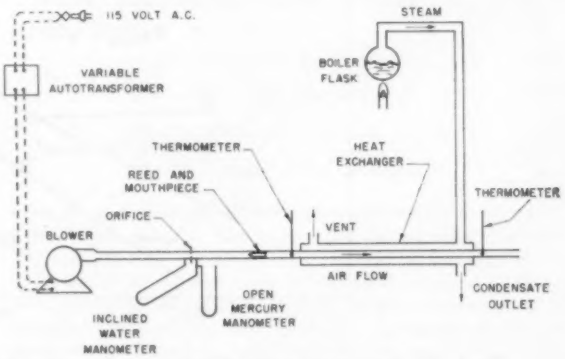

Fig. 1 Schematic diagram

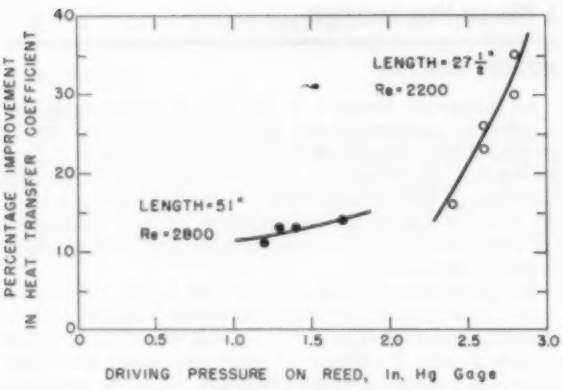
PERCENTAGE IMPROVEMENT IN HEAT TRANSFER COEFFICIENT
LENGTH = 27½"
Re = 2200
LENGTH = 5½"
Re = 2800
DRIVING PRESSURE ON REED, In. Hg Gage

Fig. 2 Results with vibrating reed

The vibration produced improvements in h up to 35 per cent, as shown in Fig. 2. These results were obtained with a number 2 reed moistened with a glycerol-water solution to minimize chipping. Reeds of other stiffness as well as reeds and mouthpieces of some other musical instruments were also employed, but with less satisfactory results.

The improvement in h increased with audible intensity, which in turn increased with the driving pressure on the reed. Thus at fixed frequency the resistance to heat transfer in these singing exchangers decreased as the amplitude of vibratory disturbance increased. This accords with similar observations reported for vibrations produced by other means [2].

References

1 J. P. Holman, "The Mechanism of Sound Field Effects on Heat Transfer," JOURNAL OF HEAT TRANSFER, TRANS. ASME, Series C, vol. 82, 1960, pp. 393–396.

2 R. Lemlich, "Vibration and Pulsation Boost Heat Transfer," a survey, *Chemical Engineering*, vol. 68, no. 10, 1961, pp. 171–176.

3 H. N. McManus and E. E. Soehngen, "Flow Separation and Acoustic Effects," JOURNAL OF HEAT TRANSFER, TRANS. ASME, Series C, vol. 82, 1960, pp. 166–169.

Transition on a Heated Horizontal Rotating Cylinder

P. D. RICHARDSON[1]

EXPERIMENT has shown that flow on an unheated rotating cylinder becomes unstable and later turbulent at Reynolds numbers (based on peripheral speed and radius) below 100. The flow on an isolated horizontal cylinder is considerably different when the cylinder is heated, natural convection being predominant at low rotational speeds, instability and transition occurring as the speed is raised, heat transfer in fully developed turbulent flow being proportional to $Re^{2/3}$ (considering constant Prandtl number). Experimental work has been reported by Anderson and Saunders [1],[2] Dropkin and Carmi [2], and Kays and Bjorklund [3], among others.

With this case there has been some confusion about instability and transition to turbulence due largely to attempting to identify the onset of transition with the attainment of fully developed turbulent flow. It is hoped that the following explanation and Fig. 1 will help to clarify the matter.

Anderson and Saunders [1] suggested that the critical Reynolds number is given by an expression of the form

$$Re_{crit} \sim \sqrt{\frac{Gr}{Pr}}$$

It is possible to plot such a function on a graph with Nusselt and Reynolds numbers as co-ordinates by utilizing the fact that in laminar flow, for free convection (considering Prandtl number constant)

$$Nu \sim Gr^{1/4}$$

so that

$$Re_{crit} \sim Nu^2.$$

[1] Division of Engineering, Brown University, Providence, R. I.

[2] Numbers in brackets designate References at end of paper.

Contributed by the Heat Transfer Division of THE AMERICAN SOCIETY OF MECHANICAL ENGINEERS. Manuscript received at ASME Headquarters, August 12, 1960.

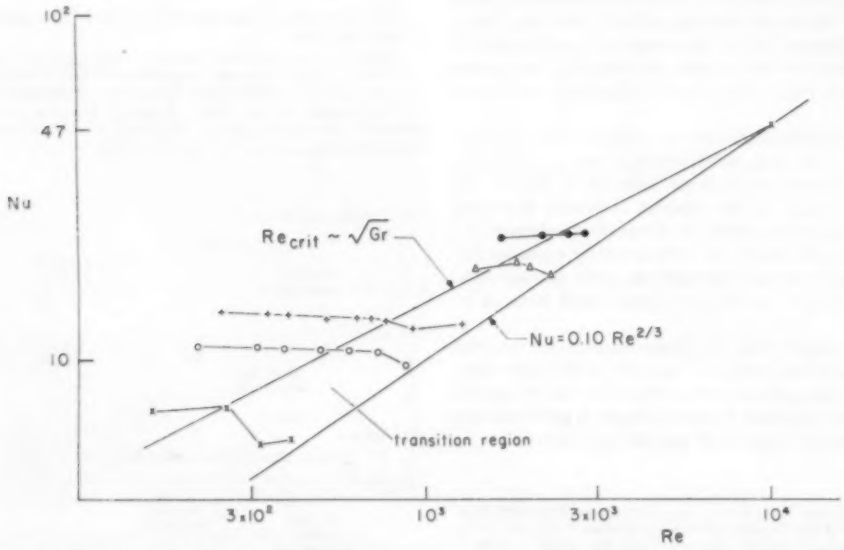

Fig. 1 The experimental results of Anderson and Saunders for fully developed turbulent flow, correlated by $Nu = 0.10\ Re^{2/3}$, have been omitted for clarity. The transition from laminar to turbulent natural convection occurs at about $Nu = 47$.

It is clear that such a function must intersect that for heat transfer from the rotating cylinder by fully developed turbulent flow. Such an intersection might be expected to occur under conditions where there is no transition region, flow there going almost immediately from laminar to fully developed turbulent flow. This would probably occur at the Grashof number which corresponds to transition in simple natural convection for the stationary cylinder: The corresponding Nusselt number is about 47. The line for the critical Reynolds number in Fig. 1 was made to intersect the line for developed turbulent flow at this Nusselt number, a wedge-shaped transition region being thereby defined. It may be noted how the experimental results of Anderson and Saunders (plotted in the figure) fit into the region, the fall in the heat transfer that occurs with the increase in Reynolds number just before attainment of developed turbulent flow now being seen to be associated with transition conditions.

In view of the asymmetry of the flow pattern, a more detailed analytical approach is not practicable.

References

1 J. T. Anderson and O. A. Saunders, "Convection From an Isolated Heated Horizontal Cylinder Rotating About Its Axis," *Proceedings of the Royal Society*, London, vol. 217, 1953, p. 555.

2 D. Dropkin and A. Carmi, "Natural Convection Heat Transfer From a Horizontal Cylinder Rotating in Air," TRANS. ASME, vol. 79, 1957, pp. 741–749.

3 W. M. Kays and I. S. Bjorklund, "Heat Transfer From a Rotating Cylinder With and Without Crossflow," TRANS. ASME, vol. 80, 1958, p. 70.

Free Convection With Blowing or Suction

E. M. SPARROW[1] and R. D. CESS[2]

Introduction

THE EFFECTS of blowing and suction on the free convection flow and heat transfer about a vertical plate have recently been considered by Eichhorn [1].[3] The analysis was carried out under the condition that the buoyancy forces are due only to temperature differences, with the mass transfer entering the problem only as a prescribed flow through the plate surface. As a logical first step, he investigated the particular distributions of surface temperature and blowing (or suction) rate which lead similar solutions of the laminar boundary-layer equations. Corresponding to a wall temperature variation $T_w - T_\infty = Bx^n$ (x = distance along plate measured from leading edge), it was found that similar solutions are possible only when the blowing velocity $v_w \sim x^{(n-1)/4}$. As discussed by Eichhorn, the distributions of T_w and v_w which are required by similarity are quite restrictive. The purpose of the present note is to extend the analysis to more general distributions of T_w and v_w by lifting the similarity condition. Specific consideration is given to the case of an isothermal wall with uniform blowing (or suction). But, it will be shown that the method employed here applies equally well to distributions of the form: $v_w = Ax^m$, $T_w - T_\infty = Bx^n$, where m and n may be chosen independently.

[1] Professor of Mechanical Engineering, Heat Transfer Laboratory, University of Minnesota, Minneapolis, Minn. Assoc. Mem. ASME.

[2] Westinghouse Research Laboratories, Pittsburgh, Pa. Now, Associate Professor of Mechanical Engineering, North Carolina State College, Raleigh, N. C. Assoc. Mem. ASME.

[3] Numbers in brackets designate References at end of paper.

Contributed by the Heat Transfer Division of THE AMERICAN SOCIETY OF MECHANICAL ENGINEERS. Manuscript received at ASME Headquarters, February 15, 1961.

Analysis

The starting point of the analysis is the boundary-layer equations appropriate to laminar flow over a vertical plate

$$\text{continuity:} \quad \frac{\partial u}{\partial x} + \frac{\partial v}{\partial y} = 0 \tag{1}$$

$$\text{momentum:} \quad u\frac{\partial u}{\partial x} + v\frac{\partial u}{\partial y} = g\beta(T - T_\infty) + \nu\frac{\partial^2 u}{\partial y^2} \tag{2}$$

$$\text{energy:} \quad u\frac{\partial T}{\partial x} + v\frac{\partial T}{\partial y} = \alpha\frac{\partial^2 T}{\partial y^2} \tag{3}$$

The co-ordinates x and y, respectively, measure distances along and normal to the plate, and u and v are the corresponding velocity components. The fluid properties α, β, and ν denote the thermal diffusivity, expansion coefficient, and kinematic viscosity.

The continuity equation may be satisfied by introducing a stream function by the customary definition

$$u = \partial\Psi/\partial y, \quad v = -\partial\Psi/\partial x \tag{4}$$

Then, to bring the momentum and energy equations into tractable form, we introduce the following transformation

$$\eta = \frac{cy}{x^{1/4}}, \quad \xi = \frac{v_w x^{1/4}}{4\nu c}, \quad c = \left[\frac{g\beta(T_w - T_\infty)}{4\nu^2}\right]^{1/4} \tag{5a}$$

$$\Psi/4\nu c x^{3/4} = f(\xi, \eta) = f_0(\eta) + \xi f_1(\eta) + \ldots . \tag{5b}$$

$$\frac{T - T_\infty}{T_w - T_\infty} = \theta(\xi, \eta) = \theta_0(\eta) + \xi\theta_1(\eta) + \ldots \tag{5c}$$

The new variable η may be immediately recognized as coinciding with the similarity variable for free convection over an isothermal, impermeable wall; while ξ is essentially a stretching of x which contains the blowing (or suction) velocity v_w. Utilizing the transformation equations (5a) and (5b), the velocity components may be evaluated from equation (4) as

$$u = 4\nu c^2 x^{1/2}\frac{\partial f}{\partial \eta}, \quad v = -\frac{4\nu c}{x^{1/4}}\left[\frac{3}{4}f - \frac{\eta}{4}\frac{\partial f}{\partial \eta} + \frac{\xi}{4}\frac{\partial f}{\partial \xi}\right] \tag{6}$$

The transformation as defined by equations (5) was constructed specifically for uniform T_w and uniform v_w. It may be generalized to other conditions, and this will be shown later.

With equations (5) and (6), the momentum and energy equations may be rewritten in terms of the new variables. Then, in each of the resulting equations, terms are grouped according to powers of ξ which multiply them. In this way, we are led to a set of ordinary differential equations for determining the functions $f_0, f_1, \ldots, \theta_0, \theta_1, \ldots$

$$f_0''' + 3f_0 f_0'' - 2(f_0')^2 = -\theta_0 \tag{7a}$$

$$\theta_0'' + 3\mathrm{Pr}\, f_0\theta_0' = 0 \tag{7b}$$

$$f_1''' + 3f_0 f_1'' - 5f_0' f_1' + 4f_0'' f_1 = -\theta_1 \tag{8a}$$

$$\theta_1''/\mathrm{Pr} + 3f_0\theta_1' - f_0'\theta_1 = -4f_1\theta_0' \tag{8b}$$

where the primes denote differentiation with respect to η, and Pr is the Prandtl number. It may be noted that equations (7a) and (7b) coincide with the governing equations for free convection on an isothermal, impermeable vertical plate, solutions of which are tabulated in references [2 and 3]. It thus remains to solve equations (8a) and (8b), and these will provide the first order effects of the blowing (or suction) on the free convection.

To complete the statement of the problem, it remains to specify the boundary conditions. Corresponding to the physical con-

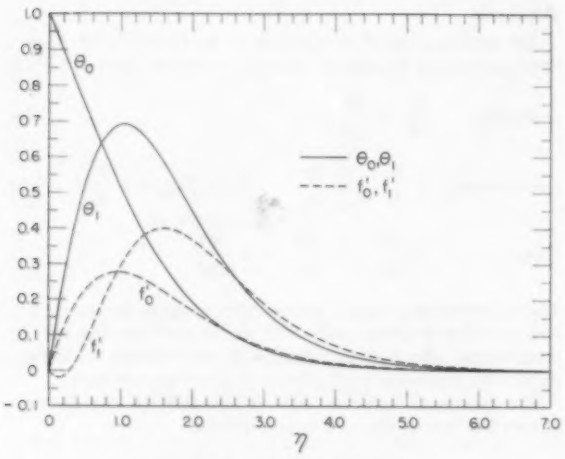

Fig. 1 The functions θ_0, θ_1, f_0', and f_1'

ditions that $u = 0$, $v = v_w$, and $T = T_w$ at $y = 0$ and that $u \to 0$ and $T \to T_\infty$ as $y \to \infty$, the functions f and θ take on the following boundary values

$$\left.\begin{aligned} f_0 = f_0' = 0, \quad \theta_0 = 1 \\ f_1 = -1, \quad f_1' = \theta_1 = 0 \end{aligned}\right\} \eta = 0 \qquad \left.\begin{aligned} f_0' \to 0, \quad \theta_0 \to 0 \\ f_1' \to 0, \quad \theta_1 \to 0 \end{aligned}\right\} \eta \to \infty \tag{9}$$

With the completion of the mathematical formulation of the problem, solutions may now be discussed. In common with Eichhorn, consideration was given to free convection in gases. The tabulated results for $f_0(\eta)$ and $\theta_0(\eta)$ corresponding to a Prandtl number of 0.72 as listed in reference [2] served as input data for equations (8a) and (8b). These were solved simultaneously by numerical means on an IBM 704 electronic computer. From this solution, the temperature and velocity derivatives at the surface may be obtained. These are listed in the following along with the corresponding results for θ_0' and f_0'' from reference [2].

Table 1 Temperature and velocity derivatives Pr = 0.72

$\theta_0'(0)$	$\theta_1'(0)$	$\theta_1'(0)/\theta_0'(0)$	$f_0''(0)$	$f_1''(0)$
−0.5046	1.40	−2.77	0.676	−0.318

The information contained in Table 1 will be utilized in the heat-transfer calculation which follows. Additionally, the functions f_0', f_1', and θ_0, θ_1, respectively, related to the velocity and temperature profiles, are plotted in Fig. 1.

Heat-Transfer Results

The local rate of heat transfer passing (per unit area) from the surface to the fluid may be calculated by Fourier's law $q = -k(\partial T/\partial y)_{y=0}$. Introducing the new variables of equations (5a) and (5c), the heat-transfer expression takes the form

$$q/q_0 = 1 + \xi[\theta_1'(0)/\theta_0'(0)] + \ldots . \tag{9a}$$

$$= 1 - 2.77\left[\frac{v_w x^{1/4}}{4\nu c}\right] + \ldots ., \quad \text{Pr} = 0.72 \tag{9b}$$

where q_0 represents the local heat-transfer rate for the case of an isothermal, impermeable wall and is given by

$$\frac{q_0 x}{k(T_w - T_\infty)} = [-\theta_0'(0)]\left[\frac{g\beta(T_w - T_\infty)x^3}{4\nu^2}\right]^{1/4} \tag{10}$$

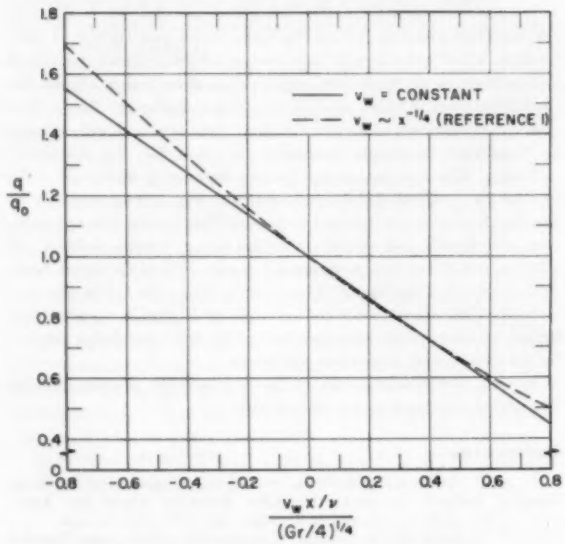

Fig. 2 Effect of blowing and suction on local heat transfer

This last expression corresponds to the standard Nusselt-Grashof relation for free convection. Since v_w is positive for blowing and negative for suction, equation (9b) provides the expected result that blowing decreases the heat transfer, while suction increases the heat transfer.

To facilitate interpretation of the results, equation (9b) has been plotted (solid line) in Fig. 2. For comparison purposes, Eichhorn's results are also shown (dashed line). The abscissa variable corresponds to 4ξ, while the Grashof number, Gr, equals $g\beta(T_w - T_\infty)x^3/\nu^2$. To gain perspective as to the magnitude of the blowing (or suction) velocities involved, we may use as a reference quantity the maximum velocity u_{max} corresponding to an isothermal, impermeable plate. From reference [2], u_{max} for Pr = 0.72 is given by

$$u_{max} = 0.552\,\frac{\nu}{x}\,\text{Gr}^{1/2}$$

Utilizing this, it is easily shown that the abscissa variable of Fig. 2 is equivalent to

$$0.78\,\text{Gr}^{1/4}\,\frac{v_w}{u_{max}}$$

Suppose we consider an abscissa value of ±0.4, which corresponds to a 28 per cent change in heat transfer. Then $v_w/u_{max} = 0.512/\text{Gr}^{1/4}$. For a Grashof number of 10^8, $v_w/u_{max} = 0.016$; while when $\text{Gr} = 10^8$, $v_w/u_{max} = 0.00512$. It is thus demonstrated that very small blowing or suction velocities can significantly effect the heat transfer.

Another interesting aspect of Fig. 2 is the close agreement between the present results and those of Eichhorn. This indicates that at a fixed x-position with a given v_w, the local heat flux is relatively independent of the details of the upstream blowing or suction distribution. In other words, the boundary layer has a "poor memory" with respect to the upstream mass transfer history. To provide further perspective for this result, it may be noted that for a given v_w at x, there is 1/3 more upstream mass transfer when $v_w \sim x^{-1/4}$ than when v_w = constant.

The series solution cannot, of course, be evaluated at too large values of ξ. The maximum and minimum abscissa values (±0.8) correspond to $\xi = \pm 0.2$. If, as expected, the ratio of

$\theta_2'(0)/\theta_0'(0)$ is comparable to $\theta_1'(0)/\theta_0'(0)$, then the error in $|q/q_0 - 1|$ due to series truncation may be on the order of 20 per cent at the maximum and minimum abscissa locations. At abscissa values of ± 0.4, the expected error in $|q/q_0 - 1|$ is on the order of 10 per cent. Additionally, experience suggests that $\theta_2'(0)/\theta_0'(0)$ will be positive; and correspondingly, an added term $\xi^2[\theta_2'(0)/\theta_0'(0)]$ in equation (9*a*) would be positive. This would bend the solid line of Fig. 2 upward about the fixed point $q/q_0 = 1$ at $\xi = 0$, thereby providing closer coincidence with the dashed curve at the extreme points of the abscissa. Finally, since the series is constructed for small v_w, it cannot predict the asymptotic solution for large suction (negligible free convection).

As discussed by Eichhorn, the blowing condition which would be experimentally most tractable is the uniform distribution. The resulting surface temperature would be determined by the wall thermal conductivity, the surface emissivity, and the blowing rate. For a moderately varying surface temperature, it would be expected that the local heat flux could be calculated by local application of the uniform wall temperature results.

Other Boundary Conditions

Variations of wall temperature and blowing (or suction) velocity of the form $T_w - T_\infty = Bx^n$, $v_w = Ax^m$ can be accommodated by the analysis without basic modification. It is only necessary to replace equation (5*a*) by the alternate transformation

$$\eta = c_1 y x^{\frac{n-1}{4}}, \quad \xi = \frac{Ax^{\frac{4m-n+1}{4}}}{4\nu c_1}, \quad c_1 = \left[\frac{g\beta B}{4\nu^2}\right]^{1/4} \tag{11a}$$

and to redefine f as

$$f(\xi, \eta) = \Psi/4\nu c_1 x^{\frac{n+3}{4}} \tag{11b}$$

With these, the analysis proceeds along the same lines as before.

References

1 R. Eichhorn, "The Effect of Mass Transfer on Free Convection," JOURNAL OF HEAT TRANSFER, TRANS. ASME, Series C, vol. 82, 1960, pp. 260–263.

2 Simon Ostrach, "An Analysis of Laminar Free Convection Flow and Heat Transfer About a Flat Plate Parallel to the Direction of the Generating Body Force," NACA TR 1111, 1953.

3 E. M. Sparrow and J. L. Gregg, "Details of Exact Low Prandtl Number Boundary-Layer Solutions for Forced and for Free Convection," NASA Memo 2-27-59E, 1953.

On Jenkins Model of Eddy Diffusivities for Momentum and Heat

C. L. TIEN[1]

A KNOWLEDGE of the relation between the eddy diffusivities for momentum and heat, ϵ_M and ϵ_H, is always required for the prediction of heat-transfer characteristics in turbulent flow. Under certain idealized conditions, Tien [1][2] has shown the exact equivalence of ϵ_M and ϵ_H. Experimental observations, however, have shown a dependence of the ratio (ϵ_H/ϵ_M) on the Prandtl number. By use of a modified mixing-length theory, Jenkins [2] proposed a physical model and obtained an expression of the ratio (ϵ_H/ϵ_M) which indicates a dependence on the Prandtl number and the dimensionless ratio (ϵ_M/ν), where ν is the kinematic viscosity. Though the predicted results deviate from experimental measurements [3], they do give a correct trend for the variation with the Prandtl number and the turbulence level. The present note is to discuss this physical model and its validity in actual physical systems.

The essence of Jenkins' model is that the moving particles (i.e., eddies) lose their energy and momentum through molecular conductivity and viscosity while in flight. The eddies were assumed to be complete spheres having a radius equal to the mixing length. From previous studies on the structure of atmospheric turbulence [4], it is known that the mixing-length concept is realistic if the mixing length represents the size or diameter of the largest eddies which are moving vertically with respect to the solid boundary. Quantitatively, this gives a maximum eddy size of 7 per cent of the pipe diameter at the center of the pipe [5]. Jenkins' assumption on eddy size should therefore be corrected by a factor of two.

This type of physical model is obviously a Lagrangian one, however, within the eddies the temperature field can be regarded as Eulerian as is implied in Jenkins' analysis. The Eulerian equation for the fluctuation-temperature field of a fluid is given as

$$\frac{\partial v}{\partial t} + u_i \frac{\partial v}{\partial x_i} = \alpha \nabla^2 v \tag{1}$$

where v is the fluctuation temperature, u_i is the velocity component along x_i-direction, α is the thermal diffusivity, and ∇^2 is the Laplacian. Jenkins neglected the second term on the left of (1) implicitly and obtained a result equivalent to that of heat conduction in a solid sphere. Since the fluid in the sphere is not still (in fact, the large eddies are regarded consisting of a number of small eddies [6]), this is legitimate only when the molecular transfer effects are expected to dominate the inertia transfer effects. Quantitative estimates of the relative importance of different terms can be obtained by order-of-magnitude considerations. If the heat-conduction terms $\alpha\nabla^2 v$ are considered to be among the dominate terms, the convective terms are of the relative order of magnitude of $[\mathrm{Pr}\ v'\lambda_v/\nu]$, where Pr is the Prandtl number, $v' = \sqrt{v^2}$ the intensity of the vertical component of fluctuation velocity, and λ_v is a characteristic length for the temperature fluctuations. Analogous to the definition of microscale λ for the velocity fluctuations [7], the thermal microscale [8] is a logical choice for λ_v. Thus the expression for the eddy diffusivity for heat with the correction of the size of eddies,

$$\frac{\epsilon_H}{lv'} = \left(\frac{lv'}{\alpha}\right)\left\{\frac{1}{30} - \frac{3}{\pi^4}\left(\frac{l}{\alpha}\right)\sum_{n=1}^{\infty}\frac{1}{n^5}\left[1 - \exp\left(-\frac{4n^2\pi^2\alpha}{lv'}\right)\right]\right\} \tag{2}$$

is subjected to the following condition:

$$\mathrm{Pr}\left(\frac{v'\lambda_v}{\nu}\right) \ll 1 \tag{3}$$

where l in (2) is the mixing length.

No experimental measurement, to the writer's knowledge, has been obtained for λ_v in turbulent pipe flow. For isotropic turbulence, λ_v can be expressed as [8]

$$\lambda_v = (\mathrm{Pr})^{-1/2}\lambda \tag{4}$$

If this relation is accepted as a legitimate approximation for turbulent pipe flow, (3) may be written as

$$(\mathrm{Pr})^{1/2}\,\mathrm{Re}\left(\frac{v'}{U_0}\right)\left(\frac{\lambda}{D}\right) \ll 1 \tag{5}$$

---

[1] Assistant Professor of Mechanical Engineering, University of California, Berkeley, Calif.

[2] Numbers in brackets designate References at end of paper.

Contributed by the Heat Transfer Division of THE AMERICAN SOCIETY OF MECHANICAL ENGINEERS. Manuscript received at ASME Headquarters, March 30, 1961.

where Re is the Reynolds number $\left(\frac{U_0 D}{\nu}\right)$, U_0 is the mean velocity at center of the pipe, and D is the diameter of the pipe. For turbulent air flow in pipes experimental measurements [9] indicate that (5) does not hold. For instance, when Re = 30,000, $\left(\frac{v'}{U_0}\right) = 0.03$, $\left(\frac{\lambda}{D}\right) = 0.024$, and Pr = 0.72, the left-hand side of (5) yields a value of 18. The lack of experimental measurements about the structure of turbulence in the liquid metal region prevents a check on the validity of (5). The small Prandtl number of liquid metals, however, offers a possibility that (5) may be valid in this range.

The analogous expression for the eddy diffusivity for momentum proposed by Jenkins implies a momentum equation of the form:

$$\frac{\partial u_i}{\partial t} = \nu \nabla^2 u_i \tag{6}$$

which in turn is the simplified form of the equation

$$\frac{\partial u_i}{\partial t} + u_j \frac{\partial u_i}{\partial x_j} = -\frac{1}{\rho} \frac{\partial p}{\partial x_i} + \nu \nabla^2 u_i \tag{7}$$

under the condition:

$$\left(\frac{v'\lambda}{\nu}\right) \ll 1 \tag{8}$$

where ρ and p in (7) are the density and the pressure, respectively. A check with the experimental data [9] shows that (8) does not hold for turbulent flow in pipes and channels.

References

1 C. L. Tien, "On the Eddy Diffusivities for Momentum and Heat," *Applied Scientific Research*, section A, vol. 8, 1959, p. 345.

2 R. Jenkins, "Variation of the Eddy Conductivity and Prandtl Modulus and Its Use in Prediction of Turbulent Heat Transfer Coefficient," Heat Transfer and Fluid Mechanics Institute, Stanford University, Stanford, Calif., 1951, p. 147.

3 C. A. Sleicher, Jr., "Experimental Velocity and Temperature Profiles for Air in Turbulent Flow," TRANS. ASME, vol. 80, 1958, p. 693.

4 J. A. Businger, "A Generalization of the Mixing-Length Concept," *Journal of Meteorology*, vol. 16, 1959, p. 516.

5 H. Schlichting, "Boundary Layer Theory," English translation by J. Kestin, McGraw-Hill Book Company, Inc., New York, N. Y., 1960, p. 510.

6 G. K. Batchelor, "Kolmogoroff's Theory of Locally Isotropic Turbulence," *Proceedings of the Cambridge Philosophical Society*, vol. 43, 1947, p. 533.

7 G. I. Taylor, "Statistical Theory of Turbulence," *Proceedings of the Royal Society* (London), vol. 151, 1935, p. 421.

8 S. Corrsin, "Heat Transfer in Isotropic Turbulence," *Journal of Applied Physics*, vol. 23, 1952, p. 113.

9 J. Laufer, "Investigation of Turbulent Flow in a Two-Dimensional Channel," NACA Report 1053, 1951.

Journal of HEAT TRANSFER

Information for Authors

• Manuscripts should be submitted in final form to the Editor. Each manuscript must be accompanied by a statement that it has not been published elsewhere nor has it been submitted for publication elsewhere. A paper which would occupy more than 8 pages of the Journal may be returned to the author for abridgment.

• The author should state his business connection, the title of his position, and his mailing address. A short abstract (50 to 100 words) should be included on the first page immediately preceding the introductory paragraph of the paper.

Three copies of the manuscript are required. One of these must be a carefully prepared printer's copy, typed in double spacing, on one side of the page only, with wide margins, on $8^1/_2$ by 11-in. opaque white paper. Mimeographed manuscripts, if prepared with exceptional care, can be accepted provided they are completely edited.

• As far as possible, all mathematical expressions should be typewritten. Greek letters and other symbols not available on the typewriter should be carefully inserted in ink. Care should be taken to distinguish between capital and lowercase letter, between zero (0) and the letter (*O*), between the numeral (1) and the letter (*l*), etc. A letter representing a vector cannot be printed with an arrow above or below it. The letter should be underscored with a single wavy line, wherever it appears in the text, to designate boldface type.

• A list of symbols carefully marked for the use of the editor (thus: κ, Greek l.c. kappa), if it has not been included in the body of the paper, should accompany the manuscript on a separate page.

• Before preparing a manuscript the author should study printed articles in the Journal, with special attention to the form and style of mathematical expressions, tables, footnotes, references, and abstract. Numbers that identify mathematical expressions should be enclosed in parentheses. Numbers that identify references at the end of the paper should be enclosed in brackets. Care should be taken to arrange all tables and mathematical expressions in such a way that they will fit into a single column when set in type. Equations that might extend beyond the width of one column (fractions that should not be broken or long expressions enclosed in parentheses) should be rephrased to go on two or more lines within column width. Fractional powers are preferred to root signs and should always be used in more elaborate formulas. The solidus should be used instead of the horizontal line for fractions wherever possible.

• A normal paper should not exceed 8 pages in the Journal. It is about 8000 words or 20 double-spaced typewritten pages exclusive of drawings. A Technical Brief should not exceed 750 words or about one page in the Journal inclusive of drawings.

• Originals and two copies of figures must accompany the manuscript. Line drawings should not be larger than $8^1/_2 \times 11$ in. and should be planned for reduction to column width. Lettering should be large enough to be clearly legible when the illustration is reduced. The originals of line drawings must be in India ink on white or pale blue tracing paper or tracing cloth. Photographs of equipment or test specimens must be glossy prints and should be used sparingly. Captions for figures should be typed double-spaced and included as the last page of the manuscript. The figure number and author's name should be written in the margin or on the back of each illustration.

• Titles of papers should be brief.

• Authors can obtain copies of the ASME Manual MS-4, "An ASME Paper," from the Editor and are urged to do so before drafting their papers in final form.

• Papers published in Journals of the Transactions of the ASME must be presented at a Meeting, either in person or by title.

• An author is entitled to 25 preprints free of charge (in the case of two authors, 15 each; three or more authors, 10 each). Larger quantities of preprints or reprints can be ordered from Editorial Department, The American Society of Mechanical Engineers, 29 West 39th Street, New York 18, N. Y. Quotations will be sent on request.

ASME Publications Committee

Please address all communications to:

Editor, ASME,

29 West 39th Street,

New York 18, N. Y.

Papers of Conference on

INTERNATIONAL DEVELOPMENTS IN HEAT TRANSFER

Just published

The Institution of Mechanical Engineers and the ASME have organized and sponsored the conference which will be held in Boulder, Colorado, August 28–September 1, 1961, for the purpose of reviewing a decade's development in heat transfer and in the design of heat transfer equipment.

The 124 papers to be presented at the conference are now available in five paper-bound books. Part I of these includes the contributions on heat conduction and thermoelectric effects, and on heat transfer in equipment. Part II contains the articles on boiling and burnout, condensation and two-phase flow, high speed flows, aspects of external convection, vibrations, and pulsating flows. Papers on internal and duct flow are in Part III. Problems associated with mass transfer, packed and fluidized beds, radiation, thermal properties, and instrumentation are dealt with in Part IV. Additional papers on heat transfer in equipment and the articles on free convection are in Part V.

$22.00 for all five parts to ASME members and nonmembers

This conference will be repeated in London, England, in January, 1962. Later in the year the papers, discussions, and four general lectures covering progress in engineering heat-transfer science, research during the past decade on forced convection heat transfer, heat transfer by natural convection, and problems in radiative transport will be published in bound form.

THE THEORY OF ELASTIC THIN SHELLS

To be published in September

Here is a monograph that presents with sufficient rigor the mathematical foundations of shell theory and discusses in detail the approximate methods of solution. Although originally published in the Russian language in 1953, it is today the only book that formulates as completely as possible the different sets of basic equations and various approximate methods of shell analysis emphasizing asymptotic integration. This English translation has been brought up to date by including a considerable number of additional and recent references, and a supplement, supplied by the author—Dr. Gol'denveizer, which embodies the most recent advances of the method of asymptotic integration. The presentation is arranged in such a manner that each part of the book represents a complete entity.

Partial contents: In Part I the general formulation and equations of the theory of shells are deduced which are based on the well-known hypothesis of the preservation of the normal element, and a brief survey of certain notions of the theory of shells is presented. Part II is devoted to the membrane theory. Part III considers methods of analysis of circular, cylindrical shells with the aid of trigonometric series. Part IV is essentially mathematical in character and its purpose is to justify the approximate methods of shell analysis. In Part V approximate methods of analysis of shells are formulated which are based upon the results obtained earlier. **$15.00***

THERMODYNAMIC AND TRANSPORTATION PROPERTIES OF GASES, LIQUIDS, AND SOLIDS

In this book world-wide authorities discuss today's experimental and theoretical techniques in thermal properties research, and give practical data on thermodynamic and transportation properties of gases, liquids, and solids. The papers in this volume were originally presented at an ASME-sponsored Symposium on Thermal Properties.

Contents: Theoretical Estimation of Transport Properties. Review of Recent Work on Transport Properties. Thermodynamic Properties: Gases and Liquids. PVT Data and Equation of State. Thermodynamic Properties of Boron Compounds. Transport Properties: Experimental. High Temperature Transport Properties of Metals and Ceramics. High Temperature Thermodynamic Properties of Gases.

Published, 1959 **$12.50***

*** 20% discount to ASME members**

THE AMERICAN SOCIETY OF MECHANICAL ENGINEERS

Current address:
29 W. 39th St., N. Y. 18, N. Y.

Address after September 1:
345 E. 47th St., N. Y. 17, N. Y.